WILEY-VCH

Edited by Jyotishkumar Parameswaranpillai, Harikrishnan Pulikkalparambil, Sanjay M. Rangappa, and Suchart Siengchin

Epoxy Composites

Fabrication, Characterization and Applications

Epoxy Composites

Epoxy Composites

Fabrication, Characterization and Applications

Edited by

Jyotishkumar Parameswaranpillai
Harikrishnan Pulikkalparambil
Sanjay M. Rangappa
Suchart Siengchin

WILEY-VCH

Editors

Dr. Jyotishkumar Parameswaranpillai
King Mongkut's University of
Technology North Bangkok (KMUTNB)
Department of Materials and Production
Engineering
1518 Pracharaj 1
Wongsawang Road, Bangsue
10800 Bangkok
Thailand

Mr. Harikrishnan Pulikkalparambil
King Mongkut's University of
Technology North Bangkok (KMUTNB)
Department of Materials and Production
Engineering
1518 Pracharaj 1
Wongsawang Road, Bangsue
10800 Bangkok
Thailand

Dr. Sanjay M. Rangappa
King Mongkut's University of
Technology North Bangkok
Department of Materials and Production
Engineering
1518 Pracharaj 1
Wongsawang Road, Bangsue
10800 Bangkok
Thailand

Prof. Suchart Siengchin
King Mongkut's University of
Technology North Bangkok
Department of Materials and Production
Engineering
1518 Pracharaj 1
Wongsawang Road, Bangsue
10800 Bangkok
Thailand

Cover Image: © Igor Krutov/Alamy Stock Photo

Library of Congress Card No.:
applied for

British Library Cataloguing-in-Publication Data
A catalogue record for this book is available from the British Library.

Bibliographic information published by the Deutsche Nationalbibliothek
The Deutsche Nationalbibliothek lists this publication in the Deutsche Nationalbibliografie; detailed bibliographic data are available on the Internet at <http://dnb.d-nb.de>.

Print ISBN: 978-3-527-34678-3
ePDF ISBN: 978-3-527-82406-9
ePub ISBN: 978-3-527-82407-6
oBook ISBN: 978-3-527-82408-3

Typesetting SPi Global, Chennai, India

Printed on acid-free paper

10 9 8 7 6 5 4 3 2 1

Contents

1

Introduction to Epoxy Composites

Harikrishnan Pulikkalparambil[1], Sanjay Mavinkere Rangappa[1], Suchart Siengchin[1], and Jyotishkumar Parameswaranpillai[2]

[1]King Mongkut's University of Technology North Bangkok, Department of Mechanical and Process Engineering, The Sirindhorn International Thai-German Graduate School of Engineering (TGGS), 1518 Pracharat 1, Wongsawang Road, Bangsue, Bangkok 10800, Thailand
[2]King Mongkut's University of Technology North Bangkok, Center of Innovation in Design and Engineering for Manufacturing, 1518 Pracharat 1, Wongsawang Road, Bangsue, Bangkok 10800, Thailand

1.1 Introduction

In the last two decades, one can observe a great increase in the replacement of traditional materials with polymer composites in high-strength and lightweight applications [1–3]. This is due to its high strength/weight ratio, toughness, and thermal stability [4]. Several factors are associated with the composite performance, such as filler properties, filler geometry, matrix properties, filler–matrix interactions, filler orientation in the matrix, and the volume fraction of the filler [5]. The matrix component of the composites can be thermoplastic, thermoset, or rubber. Thermosetting polymers are widely used over others in engineering applications due to their versatility and high performance. The epoxy resin was marketed in the late 1940s, since then it is widely used for several industrial and commercial applications. Its low shrinkage, better rigidity, good chemical and corrosion resistance, remarkable adhesion properties, good thermomechanical properties, good dielectric strength, etc., make it widely useful in engineering applications [6, 7]. Unlike polyester resins, epoxy can retain its mechanical and physical properties under the influence of aggressive solvents. Also, epoxy resin will bond with almost all materials such as stone, wood, glass, plastics, ceramics, and metals [8].

Epoxy resins are low-molecular weight materials that comprise oxirane/epoxide rings as functional groups attached to their main chain [9]. The characteristics of the epoxy resin make it suitable for reactivity against a wide range of curing agents. Different types of epoxy resins are available such as diglycidyl ether of bisphenol-A (DGEBA), cycloaliphatic epoxy resin, triglycidyl *p*-amino phenol, tetraglycidyl diamino diphenyl methane, and novolac epoxy resins [10]. In addition, other modified epoxy systems are available such as biobased epoxy, fluorine-containing

Epoxy Composites: Fabrication, Characterization and Applications,
First Edition. Edited by Jyotishkumar Parameswaranpillai, Harikrishnan Pulikkalparambil, Sanjay M. Rangappa, and Suchart Siengchin.

epoxy, phosphorus-containing epoxy, and silicon-containing epoxy. While the curing agents are mainly catalysts or hardeners, the catalysts are tertiary amines or Lewis acids, and their function is to initiate polymerization of the epoxy resin to produce polyether structures [11]. The role of epoxy resin in the composite is to transfer the force uniformly onto the filler and protect the integrity of the entire composite system [12].

Epoxy resin with natural fibers, synthetic fibers, and other reinforced particles has been extensively studied in recent decades [13]. Synthetic fiber-reinforced epoxy composites are made of synthetic fibers such as glass, carbon, kevlar, and aramid. Due to their lightweight, good strength, and good modulus, synthetic fiber-reinforced epoxy composites are generally used in automobile and construction applications. However, the recyclability of the synthetic fibers from the composites after use is a concern. Recently, natural fibers are used in automotive and construction industries due to their advantages, such as biodegradability, easy availability, lightweight, cheap, simple processing, and good thermomechanical properties. Extensive study has been done on epoxy composites based on natural fibers such as kenaf, banana, jute, bamboo, and cotton [14–16]. Studies have shown that they can replace glass and carbon fiber (CF) in epoxy composites for semi-structural applications [14–17]. Furthermore, epoxy is the best resin that can be used with either synthetic fiber or natural fiber [16, 18–22]. On the other hand, the addition of micro- or nanofillers shows different behavior. For example, the addition of clay fillers limits the plastic behavior of epoxy due to the rigid clay behavior. Abdellaoui et al. [23] discussed the effect of clay loading on the deformation of epoxy composites. The strength of the composites decreased with the incorporation of clay. It was observed that at lower clay loading (5% and 10%), the epoxy–clay interactions are weak owing to poor distribution. On the other hand, at higher loading of 20 wt%, the clay particles agglomerate forming high-stress concentration zones, which further weaken the composite strength. Thus, they concluded that the incorporation of clay particles weakens the epoxy ductility and degrades mechanical properties. Similarly, carbon nanotubes (CNTs) in epoxy were reported to show poor dispersion with an increase in specific surface area. However, the dispersion of CNTs in the epoxy matrix can be improved by chemical functionalization, especially functionalization with amino group improved dispersion to a large extent [24].

1.2 Manufacturing Methods for Fabrication of Epoxy Composites

For the manufacture of epoxy-based composites, several methods were used in different fields of application with the requirement of the final shape and size of the components. Some of the most important methods used for the manufacturing of epoxy composites are hand layup, vacuum bagging, vacuum-assisted resin transfer molding, autoclave, compression molding, pultrusion, and filament winding. All these methods have their own advantages and disadvantages. The best selection of the

method gives the best result in any manufacturing industry. Different manufacturing techniques used for the preparation of epoxy composites are given in Table 1.1.

1.3 Experimental Techniques for the Characterization of Epoxy Composites

The detailed understanding of the epoxy composites is necessary for its effective utilization in various application areas. Several characterization techniques have been used to study the reinforcement effect of different fillers in epoxy matrices. Some of the characterization techniques used for the characterization of epoxy composites are universal testing machine, dynamic mechanical analysis (DMA), differential scanning calorimetry (DSC), rheology, thermogravimetry analysis (TGA), electron microscopy, contact angle, and water absorption studies [47–50].

The rheological measurement is very helpful in analyzing the state of dispersion and interfacial interaction of the nanoparticles with the epoxy matrix [51, 52]. Song et al. [52] studied the impact of dispersion of multi-walled carbon nanotubes (MWCNTs) on the rheological properties of the epoxy composites. The authors reported increased storage modulus, loss modulus, and complex viscosity with the incorporation of MWCNTs. This implies that the MWCNT-based composite exhibits a solid-like behavior. Kim et al. [53] studied the rheological properties of surface-modified MWCNTs in the epoxy composite. The rheological studies revealed that the modified MWCNTs in the epoxy matrix show higher storage modulus, loss modulus, and shear viscosity when compared with the untreated MWCNTs. This is because MWCNTs treated with acid, plasma, and amine introduce functional groups onto the surface that imparts good dispersion and strong adhesion between the MWCNTs and epoxy matrix. The least modulus and viscosity were observed for the neat epoxy system. Park et al. [54] studied the rheological properties of the acid-treated MWCNT-reinforced epoxy matrix composites. They reported that the surface-treated MWCNTs composite showed good dispersion and faster gel time. In another work, Zhu et al. [55] studied the fiber distribution and interfacial interaction of 3-aminopropyltriethoxysilane (APTES)-modified carbon nanofiber (CNF) in the epoxy composite. They observed a sharp increase in complex viscosity and storage modulus at high temperatures due to the in situ reaction of amine groups present in APTES with epoxy resin.

The DMA is used to study the viscoelastic properties of composites. Here, the change in viscoelastic property of a material with respect to temperature or frequency is measured to study the material behavior under dynamic conditions. The storage modulus, loss modulus, and tan delta are the parameters observed from the DMA measurements. These parameters are used to study the viscoelastic behavior of the composite material [56]. The transition of the material from glassy to rubbery, i.e. glass transition temperature, can also be measured using DMA. In a recent work, Yorseng et al. [50] studied the dynamic mechanical behavior of neat bioepoxy and kenaf/sisal fiber fabric-reinforced epoxy composites. The authors observed a rapid drop in the storage modulus at the T_g of the bioepoxy matrix. However, for

Table 1.1 Manufacturing techniques used in composite fabrication.

S. No.	Manufacturing methods	Remarks	References
1.	Hand layup	The advantages of using hand layup are design freedom and least expensive. The disadvantages are the need for a greater number of cycles for fabrication, skilled labor cost, risk of placement errors, molding of complex parts with thickness variation, and poor surface finish.	[25–28]
2.	Vacuum bagging	The advantages of vacuum bag molding are better finish, void free, and, possibility of using a heated oven to accelerated consolidation. The disadvantages include more complex and expensive compared to hand layup, need to design the vacuum bag according to component dimensions, and finally, the size of the final component is limited to mold size.	[29]
3.	Vacuum-assisted resin transfer molding	The advantages of VARTM are the ability to manufacture large complex parts, can be used to produce different component geometries, resin and hardener can be stored separately and mixed just before infusion, and low volatile organic compound emission. The disadvantages of the VARTM process are the difficulty in the reuse of bag, tube, sealing tapes, and other consumables after one cycle, pressure (both injection pressure and compressive pressure) is limited in between vacuum pressure and atmospheric pressure, leakage problems, less robustness, etc.	[30–32]
4.	Solvent casting	The advantages of solvent casting are simple fabrication process and no need for specialized equipment. This technique limits the use of any mechanical stress or high thermal processes to avoid any degradation or side reactions. However, the limitation of the solvent casting method is the use of an external solvent that may affect environment-friendliness and costs.	[33]
5.	Autoclave	The advantage is that it produces composites with closer control of thickness and lower void content. The limitation of this process is that the component size may be limited to the autoclave size.	[34]
6.	Compression molding	The advantages of compression molding are easy processing, low cost, and minimum waste. The disadvantage of using compression molding is it is limited to small-scale industries due to the time-consuming process. Also, the compression molding technique requires highly trained manpower to operate the processes.	[35, 36]
7.	Pultrusion	The advantages of pultrusion are the unlimited length of the products, smooth surface, and continuous production. The disadvantages include limited size in the transverse direction, reinforcement in only one direction, and expensive.	[37, 38]

(Continued)

Table 1.1 (Continued)

S. No.	Manufacturing methods	Remarks	References
8.	Filament winding	The advantages of filament winding are higher reinforcement levels (up to 70% or more to improve mechanical strength), tailoring orientation of fibers, and large component fabrication is possible. The disadvantages are heavy investments and limited design and shape.	[39, 40]
9.	Low shear liquid batch mixer	These are batch-type mixers that are versatile to be suitable for all types of processing conditions such as mixing sequence, mixing temperature, and mixing time. However, the limitation of these mixers is time consumption.	[41]
10.	Internal mixer		
11.	Rheo mixer (RMX)		
12.	Extrusion	The advantages of using extruders are low cost, good heat transfer, good mixing, high production, and good surface finish. The disadvantages are size variance and product limitations.	[42]
13.	Three-roll mill	The main advantage of the three-roll mill is good dispersion. The fillers can achieve highly intercalated or exfoliated structure.	[43–45]
14.	Resonant acoustic mixer	The main advantage of RAM mixers is uniform mixing, unlike the batch and continuous mixers where localized mixing near the region of mixing blade tip is observed.	[46]

the composites, the drop in storage modulus at the T_g is marginal due to reinforcement of sisal and kenaf fibers with bioepoxy matrix. Matykiewicz et al. [57] studied the thermomechanical properties of epoxy composites filled with glass fiber. The authors reported an improvement in the storage modulus of the epoxy composite with the incorporation of glass fiber, due to better dispersion of glass fiber in the epoxy matrix. In another work, Chateauminois et al. [58] studied the plasticization of unreinforced and epoxy/glass fiber-reinforced unidirectional composites using DMA. The samples of reinforced and unreinforced composites were both unaged and aged by immersion in water. The composite samples were dried in an air oven immediately after immersion. The results of the samples were compared for change in plasticization after aging. The authors observed a change in plasticization for reinforced composites after aging. This is due to the trapping of water in the voids generated at the fiber/matrix interface because of hygrothermal aging. In a similar work, Xian and Karbhari [59] investigated the moisture uptake and aging of a room temperature cured epoxy system using DMA. The plasticization was observed in the aged samples.

The DSC is mostly used for the measurement of T_g and the cure kinetics of the epoxy thermoset [60]. The cure kinetics of epoxy composites and the degree of cure

is dependent on the curing temperature [61, 62]. High cure temperature accelerates the curing reaction and hence decreases the cure time. The T_g behavior of composites with different filler loadings may be used to understand the interaction between the polymer and fibers. The addition of fillers in epoxy composites may have strong effects on the T_g [61]. Gojny and Schulte [63] reported that the T_g of the composites may vary with the addition of CNT, and the change is more noticeable with functionalization. Also, the composites with a strong filler polymer interface show improved T_g. Kang et al. [64] studied the DSC of functionalized nanosilica particles obtained using the sol–gel process in epoxy composites. An improvement in the T_g was observed for the composites with strong interfacial interactions.

The thermal stability of epoxy composites plays an important role in determining the maximum temperature up to which the material is safe for practical applications. In TGA, the mass of a sample is monitored against temperature using a thermo-balance [65]. The weight loss at a specific temperature determines the amount of degradation, and the temperature at which maximum weight loss is observed shows maximum degradation temperature. Also, TGA is useful for determining the composition of lignocellulosic biomass such as lignin, α-cellulose, and hemicellulose contents [66, 67]. TGA is also used for the fiber and void content analysis in composites. Yee and Stephens [68] showed a fast and precise method to study the graphite fiber content in epoxy composites using TGA. Nowadays, hydrogen fuel in automotive has attracted most of the people due to the depletion of fossil fuels. However, the storage of hydrogen fuel needs to be taken care of due to its very high pressure and flammability. Very recently, Zhang et al. investigated the thermal stability of CF-reinforced epoxy composites taken from the outer material of hydrogen fuel storage tank [69]. TGA and Fourier transform infrared analysis (FTIR) can be used to study the pyrolysis of epoxy composites. The TGA is used to analyze the weight loss at elevated temperatures, while FTIR is used to measure constituents and functional groups in the produced gases. They reported that the decomposition of epoxy composite takes place between 277 and 477 °C [70, 71].

FTIR spectroscopy is a form of the vibrational spectroscopic technique commonly used to determine the functional groups present in the composites [72]. FTIR is also used to measure the curing reaction, phase separation, and aging with the assessment of bands [73]. The FTIR peaks are obtained in the range between 4000 and 400 cm^{-1}. The oxirane ring in the epoxy resin is observed at 915 cm^{-1}, which corresponds to C–O deformation, and the peaks at 3050 cm^{-1} correspond to stretching of methylene groups in the epoxy ring. Table 1.2 shows characteristic FTIR peaks of DGEBA epoxy resin.

1.4 Properties of Epoxy Composites

1.4.1 Mechanical Properties

The mechanical properties of epoxy composites are an important topic in shaping its efficient use in any application area. The factors that affect the mechanical properties

Table 1.2 Characteristic bands of DGEBA.

Band (cm^{-1})	FTIR peak assignment
≈3500	O–H stretching
3057	C–H stretching vibrations of the oxirane ring
2965–2873	C–H stretching vibrations in epoxy resin
1608	C=C stretching vibrations of aromatic rings
1509	C–C stretching vibrations of aromatic rings
1036	C–O–C stretching vibrations of ethers
915	C–O stretching vibrations of oxirane group
831	C–O–C stretching vibrations of oxirane group
772	CH_2 rocking

Source: María González et al. [73]. IntechOpen. CC BY 3.0.

of filler-reinforced epoxy composites are volume fraction of filler, filler aspect ratio, filler orientation, and filler–matrix interfacial adhesion [74]. The mechanical properties of natural fiber composites can be improved when it is used along with synthetic fibers [75]. In other words, the hybridization of natural fiber and synthetic fiber leads to improved mechanical properties due to the synergetic effects of both the fibers. Fiore et al. [76] studied the effect of alkali (NaOH) treatment on kenaf fibers. They reported that the alkali treatment resulted in improved mechanical strength by reducing the polymer chain mobility and enhancing the stress transfer. However, the immersion time in NaOH had an unfavorable effect on the mechanical properties. The particle size of fillers may also affect the mechanical properties. For example, Wang et al. [77] showed the effect of particle size of graphene nanoplatelets on the mechanical properties of epoxy composites. Moderate increase in strength and modulus is observed when smaller particles are used. On the other hand, larger particles improve the modulus remarkably but reduce the strength. This is due to the reinforcement effect of larger particles, but they have poor interfacial interaction with the epoxy matrix. In an interesting work, Gojny et al. [24] schematically described several mechanisms during the failure of CNT-modified epoxy matrix as shown in Figure 1.1. The different failures occurring on the CNTs during the application of tensile force are pullout, breakage, pullout of inner tube, and bridging or partial debonding at the interfaces.

The impact strength/resistance of a composite is the energy needed to break any material. In other words, the impact strength of a material is its ability to resist the applied stress at high speed. Many factors such as voids, sharp edges of fillers, filler agglomeration, and weak filler–epoxy interface may lead to stress concentrated areas that may cause failures in the form of cracks by the application of applied stress [78, 79]. One way to improve the impact strength is by the addition of dispersants or coupling agents [80]. The addition of dispersants reduces filler agglomeration that could otherwise act as a stress concentration point. Devendra and Rangaswamy [81]

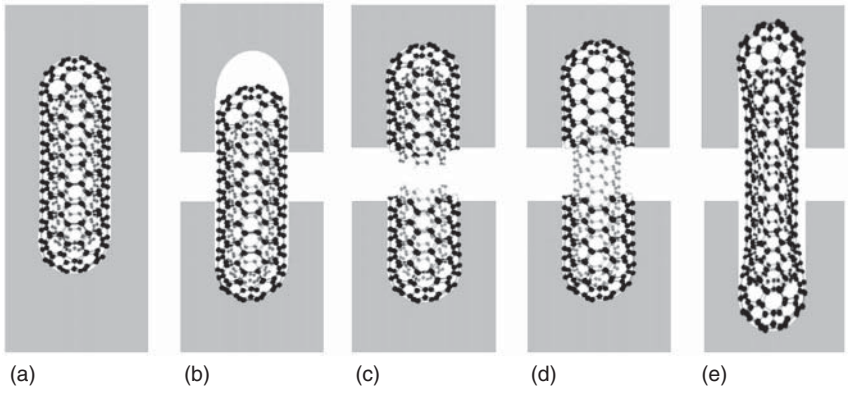

Figure 1.1 Schematic representation of failure types in epoxy/CNT composites: (a) undamaged CNT, (b) CNT pullout, (c) CNT breakage (very good CNT–epoxy interaction), (d) telescopic pullout damaging outer tube and pullout damaging inner tube, and (e) bridging and partial debonding at interface. Source: Gojny et al. [24]. © 2005, Elsevier.

reported that the filler content higher than optimum has an adverse effect on the impact resistance of a composite due to agglomeration of fillers.

The interfacial shear stress (IFSS) measures the degree of interfacial strength between the filler and the epoxy matrix. Wang et al. [82] studied IFSS measurements of Ag nanoparticles and graphene oxide (GO)-deposited CF-reinforced epoxy composites. The authors reported that the IFSS improved from 46.8 to 87.1 MPa for the epoxy composites. The presence of Ag nanoparticles was observed to increase the surface roughness of the fiber and the matrix, which provides better interlocking between the fiber and the matrix. While the incorporation of GO greatly improves the wettability and interfacial adhesion between the CF and polymer matrix that leads to improved shear strength (Figure 1.2). Godara et al. [83] studied the effect of CNTs on the IFSS of glass fiber-reinforced epoxy composites. It was observed that CNTs improve the IFSS irrespective of its location in the composites. However, as

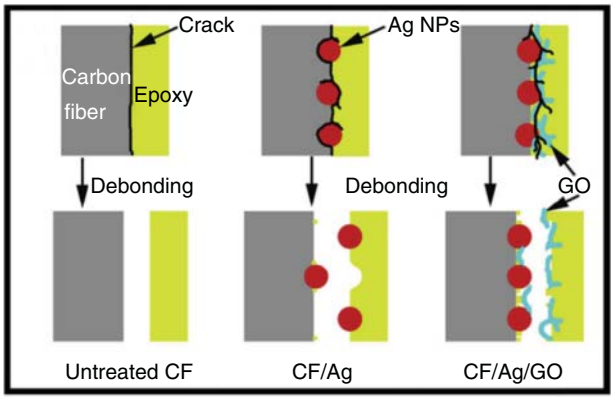

Figure 1.2 Scheme showing failure mode of untreated CF-modified epoxy, CF/Ag-modified epoxy, and CF/Ag/GO-modified epoxy. Source: Wang et al. [82]. © 2017, Elsevier.

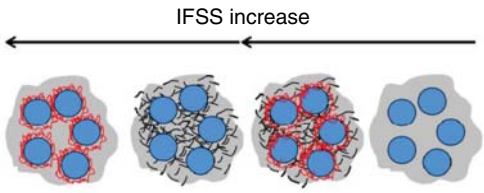

Figure 1.3 Schematic representation of CNTs on different locations in the composite and its effect on IFSS. Source: Godara et al. [83]. © 2010, Elsevier.

shown in Figure 1.3, the maximum improvement of IFSS is observed for composites with CNTs on the surface of the glass fiber.

1.4.2 Dielectric Properties

The dielectric constant and the dissipation factor are the two important parameters in measuring the dielectric properties [84]. The dielectric constant measures the ability of the material to store charge, while the dissipation factor is the energy dissipated by a dielectric. These are measured as a function of frequency of alternating current by placing the composite material between the plates of a condenser and measuring the impedance [85, 86]. The dielectric constant of epoxy resin is very low (<10) to be useful in practical applications [87]. Incorporating an adequate amount of fillers may improve the dielectric properties to some extent. However, higher loading may affect the mechanical properties of the composite [88–90]. In an interesting work, Singha and Thomas [91] studied the dielectric properties of inorganic filler (TiO_2, ZnO, and AI_2O_3)-incorporated epoxy composites. It was observed that the permittivity and tan delta values of the nanocomposites were lower than those of the micro-composites and unfilled composites. In another work, Kuo et al. [92] prepared epoxy composites using self-synthesized barium titanate ($BaTiO_3$), commercial $BaTiO_3$, and $Pb(Mg_{1/3}Nb_{2/3})O_3$ ceramic particles. It was observed that the self-synthesized ceramic particle $BaTiO_3$ exhibits a dielectric constant of 44 compared to 27 and 24 for commercial $BaTiO_3$ and $Pb(Mg_{1/3}Nb_{2/3})O_3$ composites. This is due to the large ceramic aggregates formed in the epoxy composites by self-synthesized $BaTiO_3$. In another study, Wan et al. [93] reported the dielectric properties of DGEBA–RGO/epoxy composites, where DGEBA–RGO was prepared by grafting DGEBA molecules on reduced graphene oxide (RGO) sheets. The DGEBA–RGO/epoxy composites showed an improved dielectric constant of ~32. This was attributed to better compatibility arising due to grafting of DGEBA and the better contact of RGO sheets making a pathway for suppressing the dielectric loss effectively. In one of the works, Jlassi et al. [94] reported that a very small amount of diazonium-modified clay-polyaniline nanofiller (B-DPA/PANI) in the epoxy matrix can improve the tensile strength (0.1 wt%) and dielectric constant with the incorporation as low as 0.5 wt%. This is due to the good dispersion of the nanofiller in the epoxy matrix.

1.4.3 Water/Moisture Absorption

Water absorption of a material maybe defined as the percentage of water uptake in a given unit time at a specific temperature. It is calculated by measuring the change

in weight with respect to its original weight after a given time. The weight gained at saturation is the final weight.

$$\text{Water uptake}\,(\%) = \frac{\text{Initial weight of sample-Final weight of sample}}{\text{Initial weight of sample}} \times 100$$

The rate of water uptake can be measured by calculating the diffusion coefficient of the composites [95]. The following equation can be used to calculate the coefficient of diffusion:

$$D = \pi\left(\frac{\text{kh}}{4\text{Mn}}\right)^2$$

One of the main limitations of epoxy resin and its composites is its high water absorption. The water uptake may adversely affect the T_g, modulus, strength, and toughness due to the degradation of the epoxy thermoset [73]. It also generates internal stresses due to swelling and causes delamination of the filler or other defects in composites. In general, the main concern with natural fiber composites is their high moisture intake due to the presence of hydroxyl groups in the fiber, which reduces the compatibility between the fiber and the epoxy matrix [96]. In fact, the fiber–matrix interfacial strength may be reduced, which in turn will decrease the mechanical performances of the composites. In few studies, it was observed that the hybridization of fibers in the composite may improve the mechanical and water absorption properties [97–99]. For example, Maslinda et al. [100] studied the effect of water absorption on the mechanical properties of woven kenaf, jute, and hemp fiber-based hybrid epoxy composites. The authors reported that the mechanical and water-resistant properties of the composites were improved with hybridization.

The water absorption is observed to be higher for natural fiber-reinforced composites when compared to synthetic fiber-reinforced composites [101, 102]. Therefore, the hybridization of natural fiber and synthetic fiber reduces the water uptake tremendously. Sanjay and Yogesha [102] studied the water absorption behavior of jute, kenaf, and E-glass woven fiber-reinforced epoxy composites with different layering sequences. The authors reported a reduction in water absorption behavior with the hybridization of natural and synthetic fibers. Venkateshwaran et al. [103] studied the water absorption rate of sisal and banana fiber composites. They observed a reduction in the rate of water absorption after hybridizing the sisal fiber (50%) with banana fiber.

The wetting of fibers or fillers plays an important role in reducing the water absorption because wetting improves the adhesion of the filler with matrix [104, 105]. The addition of a small amount of nanoclay (c. 3–5 wt%) in epoxy composites exhibits improved barrier properties [106, 107]. Becker et al. [108] studied water absorption in nanoclay-filled tetrafunctional tetraglycidyldiamino diphenylmethane (TGDDM) and DGEBA resin systems. It was evident from the results that nanoclay-filled composites showed lower water absorption when compared to neat epoxy resin. However, the rate of diffusion with the change in nanoclay concentration is observed to be unaffected. In an interesting work, Mohan and Kanny [109] reported the water barrier properties of sisal fiber-modified epoxy composites and nanoclay-filled sisal fiber-reinforced epoxy composites. After water

absorption, the tensile and wear properties of sisal fiber composites detrimentally decreased. However, after the addition of nanoclay to sisal fiber composites, the tensile and wear properties are least affected. This is due to the barrier property of nanoclay that stops the water from entering the composites.

1.4.4 Morphology

The morphology of composites plays an important role in identifying the failure mechanisms. For example, electron microscope is used to analyze the existence of voids, agglomeration, and dispersion of fillers [110, 111]. In an interesting study, Saba et al. [111] prepared hybrid epoxy composites containing kenaf and oil palm empty fruit bunch fiber (OPEFB) fillers that showed improved mechanical properties. The morphology study revealed that the addition of 3% OPEFB filler into epoxy/kenaf composites was observed to improve the interfacial bonding between the fiber and matrix. Also, the addition of OPEFB fiber reduces void contents, fiber pullout, and fiber protruding and tearing on the composites. Oksman et al. [112] studied the morphology of unidirectional sisal/epoxy composites. Figure 1.4a,b shows scanning electron microscopy (SEM) images of fractured surface of sisal/epoxy composites. Here, the fiber pullout and imprints are visible. Figure 1.4c,d shows the optical microscopy images of the composites. The figures show fiber distribution and horseshoe-shaped technical fibers. Atomic force microscopy (AFM) is also a powerful tool to characterize surface morphology and

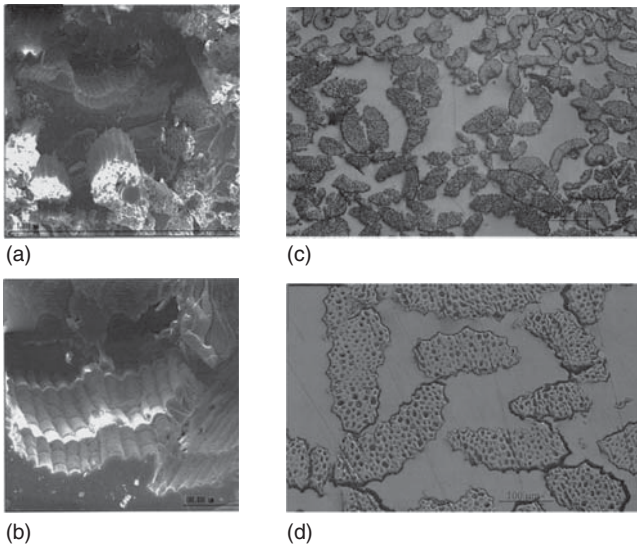

Figure 1.4 (a and b) SEM image of sisal/epoxy fracture surface shows fiber pullouts and imprint of the fiber on epoxy surface, (c and d) optical microscopy of sisal/epoxy composites shows horseshoe structure and voids in the fiber–epoxy interface. Source: Oksman et al. [112], Reproduced with permission from Wiley, License Number:4847180686936.

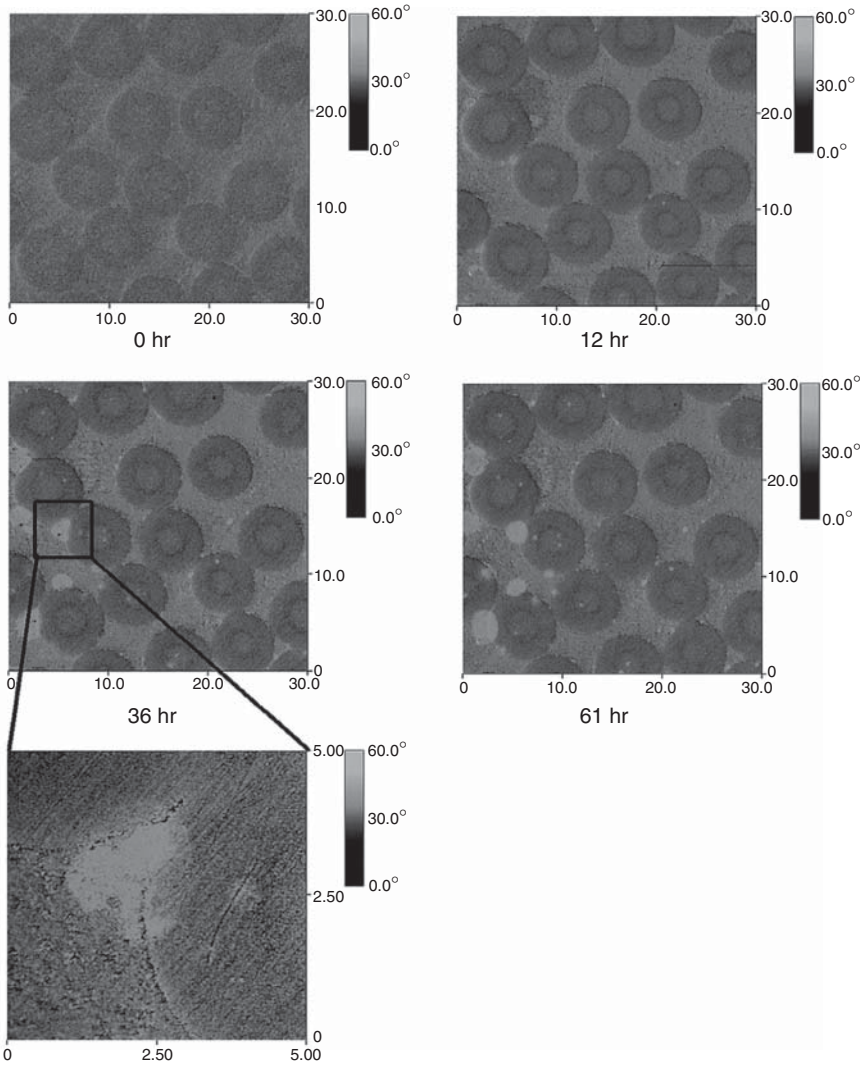

Figure 1.5 AFM image showing debonding occurred during hygroscopic treatments of carbon fiber-reinforced composite. Source: Wang and Hahn [114], Reproduced with permission from Elsevier, License Number:4847180982493.

thickness of nanosized fillers in epoxy composites. George and Verpoest [113] characterized the untreated and silane-treated fiber using AFM and observed that the surface of the treated fibers is rougher than that of the untreated fibers. In another work, Wang and Hahn [114] studied the effect of hygrothermal processes on the interfacial properties of CF-reinforced epoxy composites. The AFM was used to investigate the debonding of fibers. Figure 1.5 shows the AFM image of debonding in hygroscopic treated composites at different time intervals.

1.5 Conclusion

In this chapter, an overview of the manufacturing, characterization, and properties of the epoxy composites is briefly discussed. It is worth to point out that the applications of epoxy composites are widely accepted in all areas of manufacturing industries such as automotive, aerospace, construction, oil and gas, and marine owing to their excellent heat and solvent resistance, high thermomechanical properties, high specific strength, good adhesiveness, lightweight, and low cost. Epoxy composites also find applications in printed circuit boards (PCBs), electromagnetic shielding (EMI), supercapacitors, etc. The high performance of the composites is generally achieved by the incorporation of fibers, organic fillers, and inorganic fillers. Furthermore, the addition of thermoplastic copolymers may phase separate into different phase morphologies which may tailor the performance of the epoxy composites.

References

1 Basheer, B.V., George, J.J., Siengchin, S., and Parameswaranpillai, J. (2020). Polymer grafted carbon nanotubes – synthesis, properties, and applications: a review. *Nano-Structures & Nano-Objects* 22: 100429.

2 Masuelli, M.A. (2013). Introduction of fibre-reinforced polymers – polymers and composites: concepts, properties and processes. In: *Fiber Reinforced Polymers – The Technology Applied for Concrete Repair*. Rijeka, Croatia: IntechOpen.

3 Campbell, F.C. (2010). Introduction to composite materials. *Structural Composite Materials* 1: 1–29.

4 Cantwell, W.J. and Morton, J. (1991). The impact resistance of composite materials – a review. *Composites* 22 (5): 347–362.

5 Rahman, R. and Putra, S.Z. (2019). Tensile properties of natural and synthetic fiber-reinforced polymer composites. In: *Mechanical and Physical Testing of Biocomposites, Fibre-Reinforced Composites and Hybrid Composites*, 81–102. Woodhead Publishing, Cambridge, UK.

6 Jin, F.L., Li, X., and Park, S.J. (2015). Synthesis and application of epoxy resins: a review. *Journal of Industrial and Engineering Chemistry* 29: 1–1.

7 Gu, H., Ma, C., Gu, J. et al. (2016). An overview of multifunctional epoxy nanocomposites. *Journal of Materials Chemistry C* 4 (25): 5890–5906.

8 Stenko, M.S. and Chawalwala, A.J. (2001). Thin polysulfide epoxy bridge deck overlays. *Transportation Rresearch Rrecord* 1749 (1): 64–67.

9 Vijayan, P.P., Puglia, D., Jyotishkumar, P. et al. (2012). Effect of nanoclay and carboxyl-terminated (butadiene-*co*-acrylonitrile) (CTBN) rubber on the reaction induced phase separation and cure kinetics of an epoxy/cyclic anhydride system. *Journal of Materials Science* 47 (13): 5241–5253.

10 Kausar, A. (2017). Polyurethane/epoxy interpenetrating polymer network. In: *Aspects of Polyurethanes*, 27. Rijeka, Croatia: IntechOpen.

11 Hodd, K. (1989). Epoxy resins. In: *Comprehensive Polymer Science and Supplements*, vol. 5 (eds. V. Percec and C. Pugh), 667–699. Oxford: Pergamon Press.

12 Abdellaoui, H., Raji, M., Bouhfid, R., and el kacem Qaiss, A. (2019 Jan 1). Investigation of the deformation behavior of epoxy-based composite materials. In: *Failure Analysis in Biocomposites, Fibre-Reinforced Composites and Hybrid Composites*, 29–49. Cambridge, UK: Woodhead Publishing.

13 Paluvai, N.R., Mohanty, S., and Nayak, S.K. (2014). Synthesis and modifications of epoxy resins and their composites: a review. *Polymer-Plastics Technology and Engineering* 53 (16): 1723–1758.

14 Satyanarayana, K.G., Sukumaran, K., Mukherjee, P.S. et al. (1990). Natural fibre-polymer composites. *Cement and Concrete Composites* 12 (2): 117–136.

15 Satyanarayana, K.G., Sukumaran, K., Kulkarni, A.G. et al. (1986). Fabrication and properties of natural fibre-reinforced polyester composites. *Composites* 17 (4): 329–333.

16 Gowda, T.M., Naidu, A.C., and Chhaya, R. (1999). Some mechanical properties of untreated jute fabric-reinforced polyester composites. *Composites Part A: Applied Science and Manufacturing* 30 (3): 277–284.

17 Ashik, K.P. and Sharma, R.S. (2015). A review on mechanical properties of natural fiber reinforced hybrid polymer composites. *Journal of Minerals and Materials Characterization and Engineering* 3 (05): 420.

18 Vijay, R., Singaravelu, D.L., Vinod, A. et al. (2019). Characterization of raw and alkali treated new natural cellulosic fibers from Tridax procumbens. *International Journal of Biological Macromolecules* 125: 99–108.

19 Yorseng, K., Sanjay, M.R., Tengsuthiwat, J. et al. (2019). Information in United States Patents on works related to 'Natural Fibers': 2000–2018. Current Materials Science: Formerly: Recent Patents on. *Materials Science* 12 (1): 4–76.

20 Sanjay, M.R., Siengchin, S., Parameswaranpillai, J. et al. (2019). A comprehensive review of techniques for natural fibers as reinforcement in composites: preparation, processing and characterization. *Carbohydrate Polymers* 207: 108–121.

21 Khan, A., Vijay, R., Singaravelu, D.L. et al. (2020). Extraction and characterization of vetiver grass (*Chrysopogon zizanioides*) and kenaf fiber (*Hibiscus cannabinus*) as reinforcement materials for epoxy based composite structures. *Journal of Materials Research and Technology* 9 (1): 773–778.

22 Madhu, P., Sanjay, M.R., Senthamaraikannan, P. et al. (2019). Yogesha B. A review on synthesis and characterization of commercially available natural fibers: Part-I. *Journal of Natural Fibers* 16 (8): 1132–1144.

23 Abdellaoui, H., Bouhfid, R., and el Kacem Qaiss, A. (2016). Clay, natural fibers and thermoset resin based hybrid composites: preparation, characterization and mechanical properties. In: *Nanoclay reinforced polymer composites*, 225–246. Singapore: Springer.

24 Gojny, F.H., Wichmann, M.H., Fiedler, B., and Schulte, K. (2005). Influence of different carbon nanotubes on the mechanical properties of epoxy matrix

composites–a comparative study. *Composites Science and Technology* 65 (15–16): 2300–2313.

25 Fiore, V., Scalici, T., Di Bella, G., and Valenza, A. (2015). A review on basalt fibre and its composites. *Composites Part B: Engineering* 74: 74–94.

26 Summerscales, J., Virk, A., and Hall, W. (2013). A review of bast fibres and their composites: Part 3–Modelling. *Composites Part A: Applied Science and Manufacturing* 44: 132–139.

27 Mishra, V. and Biswas, S. (2013). Physical and mechanical properties of bi-directional jute fiber epoxy composites. *Procedia Engineering.* 51: 561–566.

28 Ramesh, M., Atreya, T.S., Aswin, U.S. et al. (2014). Processing and mechanical property evaluation of banana fiber reinforced polymer composites. *Procedia Engineering* 97: 563–572.

29 Harshe, R. (2015). A review on advanced out-of-autoclave composites processing. *Journal of the Indian Institute of Science* 95 (3): 207–220.

30 Hsiao, K.T. and Heider, D. (2012 Jan 1). Vacuum assisted resin transfer molding (VARTM) in polymer matrix composites. In: *Manufacturing Techniques for Polymer Matrix Composites (PMCs)*, 310–347. Cambridge, UK: Woodhead Publishing.

31 Schmachtenberg, E., Zur Heide, J.S., and Töpker, J. (2005). Application of ultrasonics for the process control of resin transfer moulding (RTM). *Polymer Testing* 24 (3): 330–338.

32 Ouarhim, W., Zari, N., Bouhfid, R., and el kacem Qaiss, A. (2019 Jan 1). Mechanical performance of natural fibers–based thermosetting composites. In: *Mechanical and Physical Testing of Biocomposites, Fibre-Reinforced Composites and Hybrid Composites*, 43–60. Cambridge, UK: Woodhead Publishing.

33 Kong, I., Tshai, K.Y., and Hoque, M.E. (2015). Manufacturing of natural fibre-reinforced polymer composites by solvent casting method. In: *Manufacturing of natural Fibre Reinforced Polymer Composites*, 331–349. Cham: Springer.

34 Eckold, G.C. (1994). Design and manufacture of composite structures. *Woodhead Publishing Series in Composites Science and Engineering*: 251–304.

35 de Andrade Silva, F., Chawla, N., and de Toledo Filho, R.D. (2008). Tensile behavior of high performance natural (sisal) fibers. *Composites Science and Technology* 68 (15-16): 3438–3443.

36 Rong, M.Z., Zhang, M.Q., Liu, Y. et al. (2001). The effect of fiber treatment on the mechanical properties of unidirectional sisal-reinforced epoxy composites. *Composites Science and Technology* 61 (10): 1437–1447.

37 Chachad, Y.R., Roux, J.A., Vaughan, J.G., and Arafat, E. (1995). Three-dimensional characterization of pultruded fiberglass-epoxy composite materials. *Journal of Reinforced Plastics and Composites* 14 (5): 495–512.

38 Santos, L.S., Biscaia, E.C. Jr.,, Pagano, R.L., and Calado, V.M. (2012). CFD-optimization algorithm to optimize the energy transport in pultruded polymer composites. *Brazilian Journal of Chemical Engineering* 29 (3): 559–566.

39 Belaadi, A., Bezazi, A., Maache, M., and Scarpa, F. (2014). Fatigue in sisal fiber reinforced polyester composites: hysteresis and energy dissipation. *Procedia Engineering* 74: 325–328.

40 Shen, F.C. (1995). A filament-wound structure technology overview. *Materials Chemistry and Physics* 42 (2): 96–100.

41 Cheng, X. and Wiggins, J.S. (2017). Novel techniques for the preparation of different epoxy/thermoplastic blends. In: *Handbook of Epoxy Blends* (eds. J. Parameswaranpillai, N. Hameed, J. Pionteck and E. Woo), 459–486. Cham: Springer.

42 Fenouillot, F. and Perier-Camby, H. (2004). Formation of a fibrillar morphology of crosslinked epoxy in a polystyrene continuous phase by reactive extrusion. *Polymer Engineering and Science* 44 (4): 625–637.

43 Olowojoba, G.B. and Fraunhofer, P. (2013). *Assessment of Dispersion Evolution of Carbon Nanotubes in Shear-mixed Epoxy Suspensions by Interfacial Polarization Measurement*. Fraunhofer Verlag: Stuttgart, Germany.

44 Chang, L., Friedrich, K., Ye, L., and Toro, P. (2009). Evaluation and visualization of the percolating networks in multi-wall carbon nanotube/epoxy composites. *Journal of Materials Science* 44 (15): 4003–4012.

45 Gojny, F.H., Wichmann, M.H., Köpke, U. et al. (2004). Carbon nanotube-reinforced epoxy-composites: enhanced stiffness and fracture toughness at low nanotube content. *Composites Science and Technology* 64 (15): 2363–2371.

46 Rumeau, N., Threlfall, D., and Wilmet, A. (2009). *ResonantAcoustic® Mixing–Processing and Formulation Challenges for Cost Effective Manufacturing*. France, Saint-Médard-en-Jalles: ROXEL.

47 Parameswaranpillai, J., George, A., Pionteck, J., and Thomas, S. (2013). Investigation of cure reaction, rheology, volume shrinkage and thermomechanical properties of nano-TiO_2 filled epoxy/DDS composites. *Journal of Polymers* 5: 2013.

48 Jyotishkumar, P., Logakis, E., George, S.M. et al. (2013). Preparation and properties of multiwalled carbon nanotube/epoxy-amine composites. *Journal of Applied Polymer Science* 127 (4): 3063–3073.

49 Hameed, N., Dumée, L.F., Allioux, F.M. et al. (2018). Graphene based room temperature flexible nanocomposites from permanently cross-linked networks. *Scientific Reports* 8 (1): 1–8.

50 Yorseng, K., Rangappa, S.M., Pulikkalparambil, H. et al. (2020). Accelerated weathering studies of kenaf/sisal fiber fabric reinforced fully biobased hybrid bioepoxy composites for semi-structural applications: morphology, thermo-mechanical, water absorption behavior and surface hydrophobicity. *Construction and Building Materials* 235: 117464.

51 Ivanov, E., Kotsilkova, R., Krusteva, E. et al. (2011). Effects of processing conditions on rheological, thermal, and electrical properties of multiwall carbon nanotube/epoxy resin composites. *Journal of Polymer Science Part B: Polymer Physics* 49 (6): 431–442.

52 Song, Y.S. and Youn, J.R. (2005). Influence of dispersion states of carbon nanotubes on physical properties of epoxy nanocomposites. *Carbon* 43 (7): 1378–1385.

53 Kim, J.A., Seong, D.G., Kang, T.J., and Youn, J.R. (2006). Effects of surface modification on rheological and mechanical properties of CNT/epoxy composites. *Carbon* 44 (10): 1898–1905.

54 Park, S.J., Bae, K.M., and Seo, M.K. (2010). A study on rheological behavior of MWCNTs/epoxy composites. *Journal of Industrial and Engineering Chemistry* 16 (3): 337–339.

55 Zhu, J., Wei, S., Yadav, A., and Guo, Z. (2010). Rheological behaviors and electrical conductivity of epoxy resin nanocomposites suspended with in-situ stabilized carbon nanofibers. *Polymer* 51 (12): 2643–2651.

56 Ferry, J.D. (1980). *Viscoelastic Properties of Polymers*. New York: John Wiley & Sons.

57 Matykiewicz, D., Barczewski, M., and Sterzyński, T. (2015 Oct 1). Morphology and thermomechanical properties of epoxy composites highly filled with waste bulk molding compounds (BMC). *Journal of Polymer Engineering* 35 (8): 805–811.

58 Chateauminois, A., Chabert, B., Soulier, J.P., and Vincent, L. (1995 Aug). Dynamic mechanical analysis of epoxy composites plasticized by water: artifact and reality. *Polymer Composites* 16 (4): 288–296.

59 Xian, G. and Karbhari, V.M. (2007). DMTA based investigation of hygrothermal ageing of an epoxy system used in rehabilitation. *Journal of Applied Polymer Science* 104 (2): 1084–1094.

60 Groenewoud, W.M. (2001). Differential scanning calorimetry. In: *Characterisation of Polymers by Thermal Analysis*, 10–60. Amsterdam, Netherlands: Elsevier Science.

61 Xie, H., Liu, B., Sun, Q. et al. (2005). Cure kinetic study of carbon nanofibers/epoxy composites by isothermal DSC. *Journal of Applied Polymer Science* 96 (2): 329–335.

62 Ricky, H., Jessop, J.L.P., Peters, F.E., and Kessler, M.R. (2013). Cure kinetics characterization and monitoring of an epoxy resin using DSC, Raman spectroscopy, and DEA. *Composites Part A: Applied Science and Manufacturing* 49: 100–108.

63 Gojny, F.H. and Schulte, K. (2004). Functionalisation effect on the thermo-mechanical behaviour of multi-wall carbon nanotube/epoxy-composites. *Composites Science and Technology* 64 (15): 2303–2308.

64 Kang, S., Hong, S.I., Choe, C.R. et al. (2001). Preparation and characterization of epoxy composites filled with functionalized nanosilica particles obtained via sol–gel process. *Polymer* 42 (3): 879–887.

65 Groenewoud, W.M. (2001). Thermogravimetry. In: *Characterisation of Polymers by Thermal Analysis*, 61–76. Amsterdam, Netherlands: Science.

66 Carrier, M., Loppinet-Serani, A., Denux, D. et al. (2011). Thermogravimetric analysis as a new method to determine the lignocellulosic composition of biomass. *Biomass and Bioenergy* 35: 298–307.

67 Lupoi, J.S., Singh, S., Parthasarathi, R. et al. (2015). Recent innovations in analytical methods for the qualitative and quantitative assessment of lignin. *Renewable and Sustainable Energy Reviews* 49: 871–906.

68 Yee, R.Y. and Stephens, T.S. (1996). A TGA technique for determining graphite fiber content in epoxy composites. *Thermochimica Acta* 272: 191–199.

69 Zhang, Z., Wang, C., Huang, G. et al. (2018). Thermal degradation behaviors and reaction mechanism of carbon fibre-epoxy composite from hydrogen tank by TG-FTIR. *Journal of Hazardous Materials* 357: 73–80.

70 Chen, Z., Zhu, Q., Wang, X. et al. (2015). Pyrolysis behaviors and kinetic studies on Eucalyptus residues using thermogravimetric analysis. *Energy Conversion and Management* 105: 251–259.

71 Gao, N., Li, A., Quan, C. et al. (2013). TG–FTIR and Py– GC/MS analysis on pyrolysis and combustion of pine sawdust. *Journal of Analytical and Applied Pyrolysis* 100: 26–32.

72 Zhao, S., Zhu, L., Gao, L., and Li, D. (2018). Limitations for microplastic quantification in the ocean and recommendations for improvement and standardization. In: *Microplastic contamination in aquatic environments*, 27–49. Amsterdam: Elsevier Inc.

73 González, G.M., Cabanelas, J.C., and Baselga, J. (2012). Applications of FTIR on epoxy resins-identification, monitoring the curing process, phase separation and water uptake. In: *Infrared Spectroscopy-Materials Science, Engineering and Technology*, 261–284. IntechOpen.

74 Kahraman, R., Abbasi, S., and Abu-Sharkh, B. (2005). Influence of epolene G-3003 as a coupling agent on the mechanical behavior of pal-fiber polypropylene composites. *International Journal of Polymeric Materials* 54 (6): 483–503.

75 Sanjay, M.R., Arpitha, G.R., and Yogesha, B. (2015). Study on mechanical properties of natural-glass fibre reinforced polymer hybrid composites: a review. *Materials Today: Proceedings* 2 (4–5): 2959–2967.

76 Fiore, V., Di Bella, G., and Valenza, A. (2015). The effect of alkaline treatment on mechanical properties of kenaf fibers and their epoxy composites. *Composites Part B: Engineering* 68: 14–21.

77 Wang, F., Drzal, L.T., Qin, Y., and Huang, Z. (2015). Mechanical properties and thermal conductivity of graphene nanoplatelet/epoxy composites. *Journal of Materials Science* 50 (3): 1082–1093.

78 DeArmitt, C. (2011 Jan 1). Functional fillers for plastics. In: *Applied Plastics Engineering Handbook*, 455–468. Waltham, USA: William Andrew Publishing.

79 Jyotishkumar, P., Pionteck, J., Moldenaers, P., and Thomas, S. (2013). Preparation and properties of TiO_2-filled poly(acrylonitrile-butadiene-styrene)/epoxy hybrid composites. *Journal of Applied Polymer Science* 127 (4): 3159–3168.

80 DeArmitt, C. and Rothon, R. (2017 Jan 1). Dispersants and coupling agents. In: *Applied Plastics Engineering Handbook*, 501–516. Waltham, USA: William Andrew Publishing.

81 Devendra, K. and Rangaswamy, T. (2013). Strength characterization of E-glass fiber reinforced epoxy composites with filler materials. *Journal of Minerals and Materials Characterization and Engineering* 1 (6): 353–357.

82 Wang, C., Zhao, M., Li, J. et al. (2017). Silver nanoparticles/graphene oxide decorated carbon fiber synergistic reinforcement in epoxy-based composites. *Polymer* 131: 263–271.

83 Godara, A., Gorbatikh, L., Kalinka, G. et al. (2010). Interfacial shear strength of a glass fiber/epoxy bonding in composites modified with carbon nanotubes. *Composites Science and Technology* 70 (9): 1346–1352.

84 Qing-Hua, L. and Zheng, F. (2018). Polyimides for electronic applications. In: *Advanced Polyimide Materials: Synthesis, Characterization and Applications* (ed. S. Yang), 195–255. Amsterdam: Elsevier.

85 Varshneya, A.K. and Mauro, J.C. Dielectric properties. In: *Fundamentals of Inorganic Glasses*, 3e, vol. 2019, 425–442. Amsterdam: Elsevier.

86 Morton, W.E. and Hearle, J.W.S. Dielectric properties. In: *Physical Properties of Textile Fibres*, 4e, vol. 2008, 625–642. Cambridge, UK: Woodhead Publishing Series in Textiles.

87 Zhang, L.B., Wang, J.Q., Wang, H.G. et al. (2012). Preparation, mechanical and thermal properties of functionalized graphene/polyimide nanocomposites. *Composites Part A: Applied Science and Manufacturing* 43 (9): 1537–1545.

88 Wang, Z., Zhou, W., Sui, X. et al. (2018). Dielectric studies of Al nanoparticle reinforced epoxy resin composites. *Polymer Composites* 39 (3): 887–894.

89 Shang, J., Zhang, Y., Yu, L. et al. (2013). Fabrication and enhanced dielectric properties of graphene–polyvinylidene fluoride functional hybrid films with a polyaniline interlayer. *Journal of Materials Chemistry A* 1 (3): 884–890.

90 Xie, P., Li, Y., and Qiu, J. (2014). Preparation and dielectric behavior of polyvinylidene fluoride composite filled with modified graphite nanoplatelet. *Journal of Applied Polymer Science* 131 (24): 40229.

91 Singha, S. and Thomas, M.J. (2008). Dielectric properties of epoxy nanocomposites. *IEEE Transactions on Dielectrics and Electrical Insulation* 15 (1): 12–23.

92 Kuo, D.H., Chang, C.C., Su, T.Y. et al. (2004). Dielectric properties of three ceramic/epoxy composites. *Materials Chemistry and Physics* 85 (1): 201–206.

93 Wan, Y.J., Yang, W.H., Yu, S.H. et al. (2016). Covalent polymer functionalization of graphene for improved dielectric properties and thermal stability of epoxy composites. *Composites Science and Technology* 122: 27–35.

94 Jlassi, K., Chandran, S., Poothanari, M.A. et al. (2016). Clay/polyaniline hybrid through diazonium chemistry: conductive nanofiller with unusual effects on interfacial properties of epoxy nanocomposites. *Langmuir* 32 (14): 3514–3524.

95 Pulikkalparambil, H., Parameswaranpillai, J., George, J.J. et al. (2017). Physical and thermo-mechanical properties of bionano reinforced poly(butylene adipate-*co*-terephthalate), hemp/CNF/Ag-NPs composites. AIMS. *Materials Science* 4 (3): 814–831.

96 JA, M.H., Majid, M.A., Afendi, M. et al. (2016). Effects of water absorption on Napier grass fibre/polyester composites. *Composite Structures* 144: 138–146.

97 Braga, R.A. and Magalhaes, P.A. Jr., (2015). Analysis of the mechanical and thermal properties of jute and glass fiber as reinforcement epoxy hybrid composites. *Materials Science and Engineering: C* 56: 269–273.

98 Ridzuan, M.J., Majid, M.A., Afendi, M. et al. (2016). Moisture absorption and mechanical degradation of hybrid *Pennisetum purpureum*/glass–epoxy composites. *Composite Structures* 141: 110–116.

99 Athijayamani, A., Thiruchitrambalam, M., Natarajan, U., and Pazhanivel, B. (2009). Effect of moisture absorption on the mechanical properties of randomly oriented natural fibers/polyester hybrid composite. *Materials Science and Engineering A* 517 (1–2): 344–353.

100 Maslinda, A.B., Majid, M.A., Ridzuan, M.J. et al. (2017). Effect of water absorption on the mechanical properties of hybrid interwoven cellulosic–cellulosic fibre reinforced epoxy composites. *Composite Structures* 167: 227–237.

101 Sanjay, M.R., Madhu, P., Jawaid, M. et al. (2018). Characterization and properties of natural fiber polymer composites: a comprehensive review. *Journal of Cleaner Production* 172: 566–581.

102 Sanjay, M.R. and Yogesha, B. (2016). Study on water absorption behaviour of jute and kenaf fabric reinforced epoxy composites: hybridization effect of e-glass fabric. *International Journal of Composite Materials* 6 (2): 55–62.

103 Venkateshwaran, N., ElayaPerumal, A., Alavudeen, A., and Thiruchitrambalam, M. (2011). Mechanical and water absorption behaviour of banana/sisal reinforced hybrid composites. *Materials and Design* 32 (7): 4017–4021.

104 Thakur, V.K., Singha, A.S., Kaur, I. et al. (2010). Silane functionalization of *Saccaharum cilliare* fibers: thermal, morphological, and physicochemical study. *International Journal of Polymer Analysis and Characterization* 15 (7): 397–414.

105 Anbukarasi, K. and Kalaiselvam, S. (2015). Study of effect of fibre volume and dimension on mechanical, thermal, and water absorption behaviour of luffa reinforced epoxy composites. *Materials & Design* 66: 321–330.

106 Utracki, L.A., Sepehr, M., and Boccaleri, E. (2007). Synthetic, layered nanoparticles for polymeric nanocomposites (PNCs). *Polymers for Advanced Technologies* 18 (1): 1–37.

107 Pavlidou, S. and Papaspyrides, C.D. (2008). A review on polymer–layered silicate nanocomposites. *Progress in Polymer Science* 33 (12): 1119–1198.

108 Becker, O., Varley, R.J., and Simon, G.P. (2004). Thermal stability and water uptake of high performance epoxy layered silicate nanocomposites. *European Polymer Journal* 40 (1): 187–195.

109 Mohan, T.P. and Kanny, K. (2011). Water barrier properties of nanoclay filled sisal fibre reinforced epoxy composites. *Composites Part A: Applied Science and Manufacturing* 42 (4): 385–393.

110 Saba, N., Mohammad, F., Pervaiz, M. et al. (2017). Mechanical, morphological and structural properties of cellulose nanofibers reinforced epoxy composites. *International Journal of Biological Macromolecules* 97: 190–200.

111 Saba, N., Paridah, M.T., Abdan, K., and Ibrahim, N.A. (2016). Effect of oil palm nano filler on mechanical and morphological properties of kenaf reinforced epoxy composites. *Construction and Building Materials* 123: 15–26.

112 Oksman, K., Wallström, L., Berglund, L.A., and Filho, R.D. (2002). Morphology and mechanical properties of unidirectional sisal–epoxy composites. *Journal of Applied Polymer Science* 84 (13): 2358–2365.

113 George, J. and Verpoest, J.I. (1999). Mechanical properties of flax fibre reinforced epoxy composites. *Die Angewandte Makromolekulare Chemie* 272 (1): 41–45.

114 Wang, Y. and Hahn, T.H. (2007). AFM characterization of the interfacial properties of carbon fiber reinforced polymer composites subjected to hygrothermal treatments. *Composites Science and Technology* 67 (1): 92–101.

2

Synthesis and Manufacturing of Epoxy Composites

Turup P. Mohan and K. Kanny

Durban University of Technology, Composite Research Group, Department of Mechanical Engineering, Steve Biko Campus, Steve Biko Road, Berea, Durban 4000, South Africa

2.1 Introduction

Epoxy resins are a thermosetting synthetic polymer which are basically composed of two substances known as resin and hardener. The main purpose of epoxy is to be used as an adhesive due to its high durability. Epoxy resin adhesive forms an excellent bonding agent. The bonding of the resin can be developed to yield several different products, each with its own unique application. Epoxies are typically used to fabricate high-performance composites with superior mechanical properties, resistance to corrosive liquids, and environments. Epoxies are also used to achieve good electrical properties, good performance at high temperature, and good adhesion to the substrate.

2.2 History of Epoxy Resin

The first commercial possibilities for epoxy resins were realized in Switzerland by Pierre Castan of De Trey Freres and in the Unites States by Sylvan Greenlee of DeVoe and Raynolds. In 1936, Castan produced a bisphenol-A-based epoxy resin via reaction with epichlorohydrin and subsequently prepared a thermoset composition after reaction of the resin with phthalic anhydride. The use of the hardened resin was foreseen in dental products, but initial attempts to market the resin were unsuccessful. The patents were licensed to CIBA AG of Basel, Switzerland (now CIBA-GEIGY), and in 1946, the first epoxy adhesive was shown at the Swiss Industries Fair [1]. During 1939, Sylvan Greenlee produced a high molecular weight resin from bisphenol-A and epichlorohydrin which was subsequently esterified with unsaturated fatty acids to provide an air-drying coating. His first patent was issued in 1948 [2]. In 1949, production of very high molecular weight thermoplastic polymers from bisphenol-A and epichlorohydrin was reported in 1949 using a one-step or two-step synthesis route, i.e. starting with epichlorohydrin and bisphenol-A in

Epoxy Composites: Fabrication, Characterization and Applications,
First Edition. Edited by Jyotishkumar Parameswaranpillai, Harikrishnan Pulikkalparambil, Sanjay M. Rangappa, and Suchart Siengchin.

a 1 : 1 mole ratio or utilizing a purified diglycidyl ether of bisphenol-A resin and a stoichiometric quantity of bisphenol-A in a solution polymerization [3]. Aerospace was the first commercial field that epoxies could penetrate within the early 1950s. It took more than two decades for epoxies to get its exposure [4]. Epoxies have made their way to residential applications and as a flooring option for parking lots during 1970s. This as a flooring substitution has shown prolonged longevity, ease of clean, and scratch proof properties. Epoxy is now a global compound with a dozen of breakthroughs that have occurred over the century and has now become the world's best and most used compounds [5]. Today epoxy adhesives are sold in local hardware stores, usually used as a binder under countertops or floor coatings [6].

2.3 Types of Epoxy Resins

2.3.1 Bisphenol-A Epoxy Resin

Production of epoxy resins is achieved by fusing epichlorohydrin and bisphenol to get bisphenol-A diglycidyl ethers, to produce polyethers together with glycidyl end groups that at room temperature have semi-crystalline materials. It is processed by increasing the ratio of bisphenol-A:epichlorohydrin [7]. Figure 2.1 shows the final product of bisphenol-A epoxy resin (chemical reaction of bisphenol-A and epichlorohydrin).

Raw materials: Materials that are used to make bisphenol-A epoxy resin are epichlorohydrin and bisphenol-A [8].

Production: Bisphenol-A epoxy resin is produced by condensation of acetone with 2 equiv of phenol. Hydrochloric acid or a sulfonated polystyrene resin is used to speed up the reaction. When acid is used as a catalyst, condensation of phenol with acetone happens [9].

2.3.2 Bisphenol-F Epoxy Resin

In this type of resin, viscosity is low and mean epoxy content per gram is high than bisphenol-A and chemical resistance increases once cured. Bisphenol-F undergoes

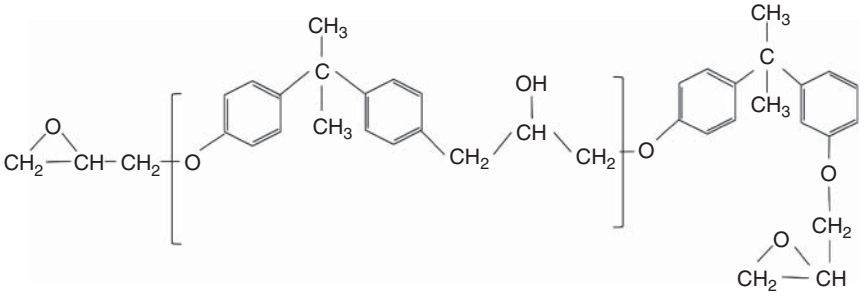

Figure 2.1 Chemical structure of bisphenol-A type epoxy resin.

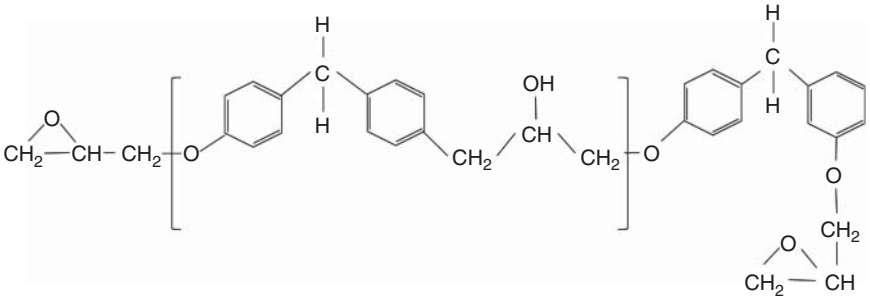

Figure 2.2 Chemical structure of bisphenol-F epoxy.

epoxy resin formation similar to bisphenol-A. Figure 2.2 shows the chemical structure of bisphenol-F epoxy resin.

Raw materials: Phenol, formaldehyde, and phenol paraben methanol dehydration catalyst [10].

Production: This epoxy resin is produced by reacting phenol and formaldehyde. This reaction takes place in the presence of a catalyst which is acid plus water and the unreacted phenol from the product to give a crude bisphenol-F and removing the acid catalyst. A part of the crude bisphenol-F is distilled to give a highly pure bisphenol-F. A distillate has a binuclear moiety content that is not <95% by weight and a novolac phenol resin, as a still-bottom product, having a binuclear moiety content that is not more than 15% by area. To give bisphenol-F for general use, highly pure bisphenol-F is mixed with the remaining crude bisphenol-F [9].

2.3.3 Phenol Novolac Epoxy Resin

Yielding epoxidized novolacs is achieved by the phenol reaction among subsequent glycidylation and formaldehyde, along with epichlorohydrin, like epoxy cresol novolacs (ECN) and epoxy phenol novolacs (EPN). The following resins compared to solid resins are exceptionally viscous and normal including epoxide functionality. When there is high epoxide functionality, an exceptionally cross-linked polymer network leading to chemical resistance and high temperature with low pliability is produced [11, 12]. Figure 2.3 shows the chemical structure during the response of phenols among subsequent glycidylation and formaldehyde, along with epichlorohydrin to produce phenol novolac epoxy resin.

Raw materials: Phenolic novolac resin and epichlorohydrin [13].

Production: Novolac epoxy resin is formed as a result of the reaction between phenolic novolac resin and epichlorohydrin. A highly cross-linked polymer network is formed by the high epoxide functionality of these resins showing high temperature and chemical resistance with low flexibility [8]. Novolac resins prepared by reacting phenolic novolac resin and epichlorohydrin are then reacted with epichlorohydrin and 30% NaOH solution and then later added to the reaction vessel over a period of 2.5 hours to conduct the epoxidation process; a 2 l glass reactor equipped with a thermometer, reflux condenser, and stirrer is required [13].

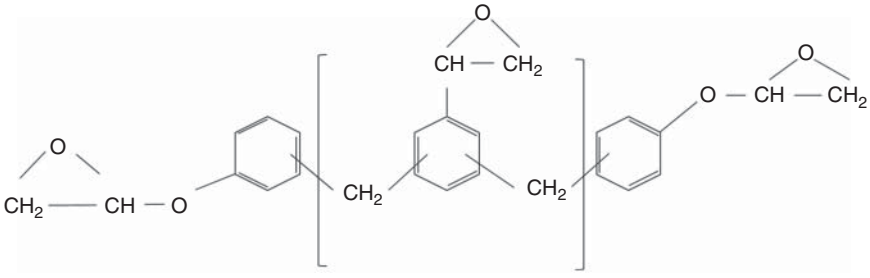

Figure 2.3 Chemical structure of phenol novolac epoxy.

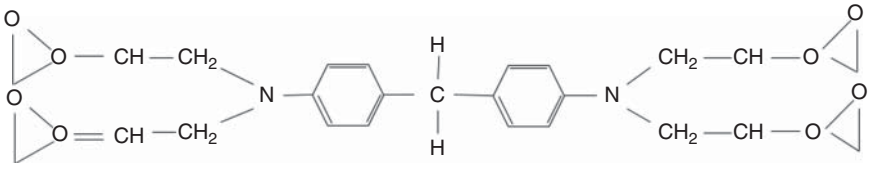

Figure 2.4 Cycloaliphatic epoxy resin structure.

2.3.4 Cycloaliphatic Epoxy Resin

This class of resin epoxy at room temperature displays low viscosity and offers relatively much higher temperature resistance than the aliphatic epoxy diluents. A class applicable is cycloaliphatic epoxy resin, containing the molecule about a single or more cycloaliphatic rings (e.g. 3,4-epoxycyclohexylmethyl-3,4-epoxycyclohexane carboxylate). However, the rate of reaction is less corresponding to the other classes of epoxy resins, and it is required to normally cure with high temperatures using suitable accelerators. The ultraviolet (UV) stability is improved since aromaticity is not in these materials [11, 14]. Figure 2.4 shows the chemical reaction that produces cycloaliphatic epoxy resin.

Raw materials: Cyclohexenylmethyl and peracetic acid.

Production: Cycloaliphatic epoxy resin is formed by reacting 30-cyclohexenylmethyl 3-cyclohexenecarboxylate with peracetic acid. This epoxy resin has an aliphatic backbone and a fully saturated molecular structure [8].

2.3.5 Epoxy Resin Diluents

Formation of resin diluents is made with polyols or glycidylation of aliphatic alcohol. Creating materials could be difunctional (e.g. butanediol diglycidyl ether), monofunctional (e.g. dodecanol glycidyl ether), or with greater functionality (e.g. trimethylolpropane triglycidyl ether). At room temperature, these resins show typically low viscosity (10–200 mPa s) and they are termed "reactive diluents." They are not usually used alone but instead used to reduce or increase the viscosity of other epoxy resins. This gives rise to the term "modified epoxy resin" to categorize those containing viscosity-lowering reactive diluents [15, 16].

Raw materials: Glycidylation of aliphatic alcohols or polyols.

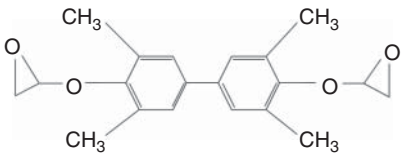

Figure 2.5 Glycidylamine epoxy resin structure.

Production: Epoxy resin diluents are obtained from glycidylation [8]. Mono-epoxy compounds and di/polyfunctional epoxies are epoxy resin diluents. Non-reactive diluents compounds are not chemically bound into the cross-linked network; these cured formulations that contain such materials usually show less chemical resistance. In both classes, the existence of the epoxide group(s) permits the diluent to interact with the resin and curing agent, to allow the diluent to form a chemical cross-linked network structure [17].

2.3.6 Glycidylamine Epoxy Resin

Reaction between aromatic amines and epichlorohydrin results in glycidylamine epoxy resins which are higher functional epoxies. The important grades of industrial epoxies are triglycidyl-*p*-aminophenol (functionality 3) and *N*,*N*,*N*′,*N*′-tetraglycidyl-bis-(4-aminophenyl)-methane (functionality 4). At room temperature, the resins range from low to medium functionalities thereby making it easier to process when compared to ECN or EPN resins. The combination of higher reactivity, high-temperature resistance, and mechanical properties of the cured network structure results them an important material for aerospace composite materials [18]. Figure 2.5 shows the glycidylamine epoxy resin chemical structure.

Raw materials: Glycidylamine is composed of aromatic amine and epichlorohydrin.

Production: This epoxy resin is formed due to the reaction of two raw materials, aromatic amine and epichlorohydrin [8]. Glycidyl epoxy resins are created using bisphenol-A and are reacted with epichlorohydrin.

2.4 Curing

Epoxy resins may be cured using a variety of curing agents. Generally, any compound that has a reactive hydrogen atom or hydroxyl group can react with the epoxide groups of the epoxy resin. These curing agents could be amines, polyamides, carboxylic acids, anhydrides, imidazoles, or amide-amines [19]. It is possible to control the cure rates to match processors through proper selection of hardeners and catalysts. Since epoxy has a higher viscosity than resin, a post cure at higher temperature is suggested to achieve superior mechanical properties.

2.4.1 Curing Agents

Curing agents or hardeners play a significant role in the curing kinetics, gel time, extent of curing (crosslinking), viscosity, the characteristics of the curing products,

and curing processors [20, 21]. In general, there consists of three different types of curing agents. Compounds containing hydrogen and their derivatives are the first type. Anionic and cationic initiators are included in the second type of curing agents. They are used to catalyze the homopolymerization of epoxy resins. The third would be latent curing agents [22]. The curing agents are discussed in detail.

2.4.1.1 Polyaddition Reactions (Active Hydrogen Compounds)

Active hydrogen-based compounds are the most widely used, and these undergo polyadditions through a compound that contains active elements of epoxy group which are hydrogen and the terminal carbon, with the epoxide being stabilized into a hydroxyl group.

Amines

Some of the factors required that affects the gel time of amine-based hardeners are the loading of amine and the type of amine of epoxy resin used. Glycidyl ether is a type of resin that is most popular, which can easily cure at room temperature. Glycidyl-ester type cures faster compared to glycidyl ether type. Figure 2.6 shows the different chemical constitutions of the different types of amines. Aliphatic and aromatic amines are the classification groups of amines, due to the types of hydrocarbons involved. Figure 2.6 shows the chemical structure of aliphatic amines.

Aliphatic Amine

This type of amine commonly has the following properties:

- Cures at room temperature.
- Final product has a strong and good bonding properties.
- Heat resistance of about 100 °C.
- Curing at high temperatures can improve the properties of aliphatic amines. 120 °C is the maximum heat deformation temperature of cured product.
- Aliphatic amine contains a stronger basicity than aromatic amine.

Aromatic Amine

- They are highly resistant to heat and chemicals compared to that of aliphatic amine which only ranges up to 100–150 °C.
- Aromatic amine has strong mechanical and electrical properties.
- They have a strong resistance against chemicals, especially alkalis. This property makes them to be highly resistant to solvents and also a good curing agent.
- With the help of steric hindrance by the aromatic ring, it can cure at slow rate at room temperature.
- Figure 2.7 shows the chemical structure of a typical aromatic amine.

2.4.1.2 Polyamide and Polyamine

Polyamine is an organic compound which is composed of amino functional groups; especially such compounds are formed by decomposition of proteins. Figure 2.8 shows the chemical structure of polyamide.

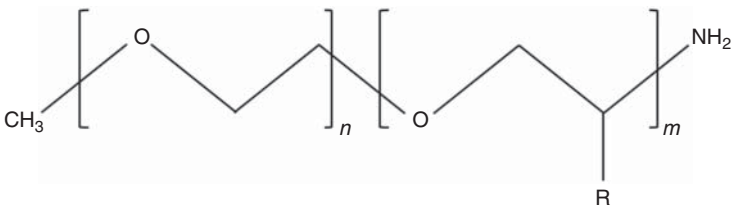

Diamine:

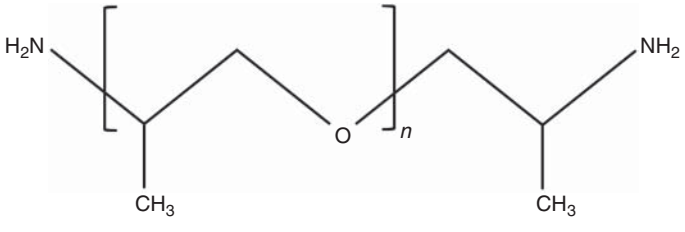

Triamine:

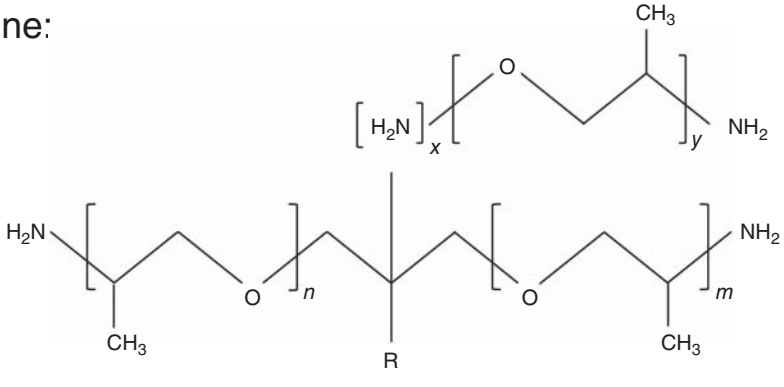

Polyamine:

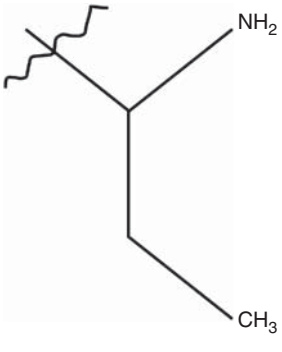

Figure 2.6 Chemical structure of amines.

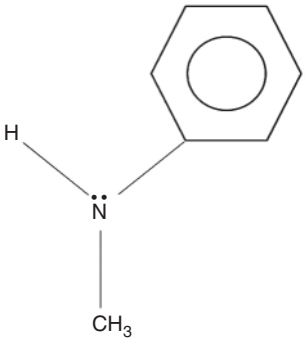

Figure 2.7 The chemical structure of aromatic amine.

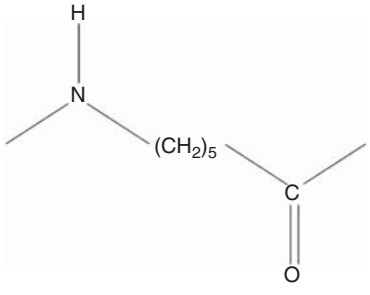

Figure 2.8 Chemical structure of polyamide.

- The chemical reaction between dimer acid and polyamine forms polyamide.
- Primary and secondary amines are used to build up their molecules. Average heat generation and base temperature allow the curing of polyamide amine and bisphenol-A type epoxy resin when they react together.
- Pot life is relatively long due to its slow curing process. The molecules of polyamide develop immense hydrocarbon moiety, a rigid thermosetting polymer that is highly plasticized when cured in the epoxy resin.
- Excellent in shock resistance, with high compressive, bending, and tensile strengths while being rigid and strong.

2.4.1.3 Secondary and Tertiary Amines

Tertiary amine is a polymerization catalyst, and it does not form any additional reaction with resin. The types of curing agents dictate the loading during the curing process (i.e. loading of these amines is not constant) [23]. Figure 2.9 shows the chemical structure of secondary and tertiary amines.

- Some of the factors that are influenced by the curing temperature are heat generation, properties of the cured resin, and curing speed.
- Paints and adhesives are of tertiary amines.
- It is used as an accelerator for polyamide and polyamine curing agents but is not useful as a curing agent itself.

Figure 2.9 Chemical structure of (a) secondary amine and (b) tertiary amine.

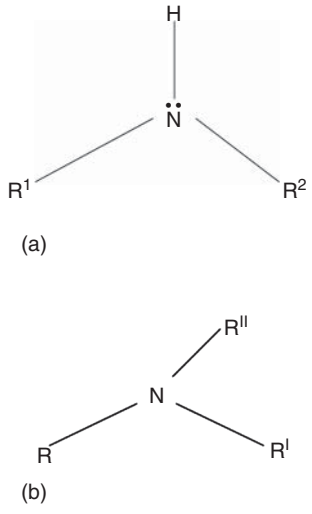

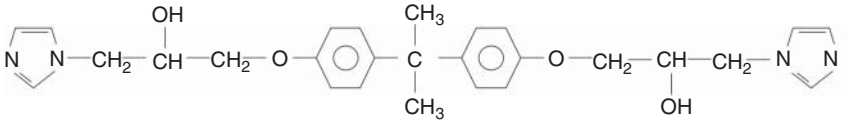

Figure 2.10 Chemical structure of imidazole.

2.4.2 Anionic and Cationic Initiators

Anionic polymerization of epoxides is reduced by metal hydroxides, secondary and amines. The molecular weight of the polymer increases as the polymerization progresses; this is called stepwise polymerization. Figure 2.10 shows the chemical reaction that produces imidazole.

Type of agent categorized under anionic and cationic initiators is:

2.4.2.1 Imidazole (Anionic Polymerizing)

- Are well known as a good curing catalyst or agent.
- It has application in compositions of resin such as casting materials and filling materials in one-part thermosetting coating adhesives.
- They have a longer pot life.
- Higher heat resistance and cure faster.

2.4.2.2 Polymercaptan

This type of curing agent functions at a low temperature (0 to −20 °C) range. Sometimes, tertiary amine is added as an accelerator. Polymercaptan rapidly cures and attains average strength in 10–30 minutes while having a life span of 2–10 minutes [24]. Figure 2.11 shows the chemical formula of liquid polymercaptan curing agent.

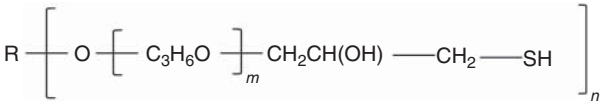

Figure 2.11 Chemical formula of liquid polymercaptan curing agent.

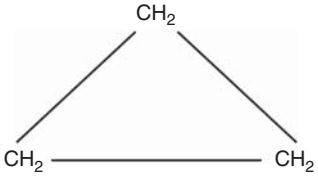

Figure 2.12 Chemical structure of alicyclic anhydrides.

2.4.2.3 Anhydrides

While producing a small quantity of heat, these cured resins also emit controlled mechanical, electrical, and chemical properties. Insolating coating for condensers and casting uses solutions in a liquid anhydride.

2.4.2.4 Canhydrides

These are generally solid. This is popular in powder paints for uses in powder molding. Canhydrides are used for insulating the coating of condensers and casting. They are the solution in liquid anhydrides.

2.4.2.5 Alicyclic Anhydrides

Most commonly used anhydrides fall into this section. Tetrahydrophthalic anhydride, methyltetrahydrophthalic anhydride, hexahydrophthalic anhydride, methyl nadic anhydride, and methylhexahydrophthalic anhydride are the principal curing agents. Figure 2.12 illustrates the chemical structure of alicyclic anhydrides [25].

2.4.2.6 Aliphatic Anhydrides

The reaction between aliphatic dibasic acid molecules is known as dehydration condensation which forms polycarboxylic anhydrides [23]. It can be used alone or with other anhydrides in casting resin and curing agents known as powder paints because it produces amazing thermal shock resistance and flexibility. Aliphatic dibasic molecules react together by dehydration condensation. Tertiary amine is curing accelerators which are boric acid ester, organic metal compounds, Lewis acid, organic metal salts, or imidazole. The chemical structure of aliphatic anhydride is shown in Figure 2.13.

2.4.3 Latent Curing Agents

Epoxy resin compositions which have outstanding storage stability at atmospheric conditions are brought by latent curing agents, resulting curing at common and sublime temperatures. Other elements used to cure are light, pressure, and heat which cures others rapidly.

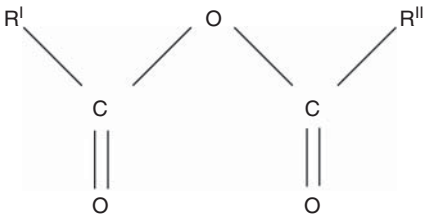

Figure 2.13 Chemical structure of aliphatic anhydride.

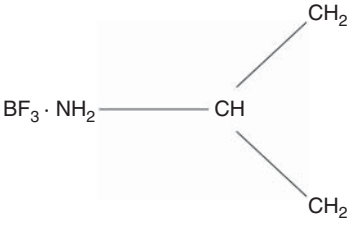

Figure 2.14 Chemical structure of boron trifluoride–amine complex.

2.4.3.1 Light-Curing and Ultraviolet-Curing Agents

The exposure of light or UV is used to cure resin and decomposes epoxy resin by the stability of light- or UV-curing agents. The main advantage of these agents is they are non-polluting paints and printing inks. The liquid with no solvent is added to cause the agents to dissolve.

2.4.3.2 Boron Trifluoride–Amine Complex

Boron trifluoride (BF_3) is a well-known catalyst for several chemical reactions. Leepoxy's LEECURE B series of epoxy curatives is a family of boron trifluoride-based accelerators. These accelerators span a broad reactivity range and are useful in the formulation of epoxy systems [26, 27]. Figure 2.14 shows the chemical structure of boron trifluoride–amine complex.

2.4.3.3 Dicyandiamide

Dicyandiamide (also referred to as DICY) is an alkaline and water-soluble crystalline compound that is scientifically known as cyanoguanidine. The chemical consists of two identical cyanamide or cyanoguanidine molecules mixed together, that is generally used in the making of melamine. Melamine is typically produced by this method. Laminates for powder coatings, adhesives, and a curing agent for epoxy resins are some of the many uses of PICY. It can dissolve in diethyl ether, water, and alcohol. The carbide method is used to prepare it commercially from the carbonate gotten from limestone or through the desulfurization of thiourea when a catalyst is introduced (mercuric oxide). Cyanamide can also be prepared by the interaction of ammonia with cyanogene halides. Cyanamide polymerizes to dicyandiamide (DCY) when it is heated to a temperature over 150 °C and to tricyantriamide or to melamine [28, 29]. Figure 2.15 shows the chemical structure of DCY.

2.4.3.4 Organic-Acid Hydrazide

Hydrazides are a category of organic compounds distinguished by a nitrogen to nitrogen covalent bond made up of four substituents with a minimum of one

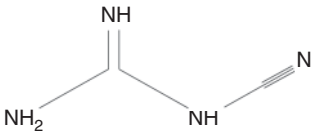

Figure 2.15 Chemical structure of dicyandiamide. Source: Yue et al. [29].

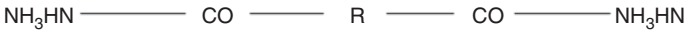

Figure 2.16 Chemical structure of organic acid hydrazide.

being an acyl group. The making of new hydrazide spin-offs is inspired by the hydrazine group of compounds that have antioxidant, analgesic, anticonvulsant, hormone antagonist, antiplatelet, antiviral, vasodilator, antitrypanosomal, anti-inflammatory, antimalarial, antimycobacterial, antimicrobial, and antitumor properties [30]. Figure 2.16 shows the chemical structure of organic acid hydrazide.

2.4.4 Curing Conditions

2.4.4.1 Bisphenol-A Epoxy Resin

This type of epoxy resin cures at room temperature which is scientifically considered to be 20–25 °C and also under heated conditions [31, 32].

2.4.4.2 Bisphenol-F Epoxy Resin

This type of epoxy resin cures at room temperature and also under heat conditions [31, 32].

2.4.4.3 Phenol Novolac Epoxy Resin

This type of epoxy resin cures at room temperature and also under heat conditions [31, 32].

2.4.4.4 Cycloaliphatic Epoxy Resin

This type of epoxy resin cures under UV light and under heat conditions [31].

2.4.4.5 Glycidylamine Epoxy Resin

Though some epoxy/hardener mixtures curate at room temperature (i.e. the air temperature of the environment), glycidylamine resin needs heat to cure. Commonly, temperatures reaching 150 °C are used but some special set-ups will use up to 200 °C. If not enough heat is added during the curing process, incomplete polymerization will occur which will result in reduced mechanical, chemical, and heat resistance [33].

2.5 Reaction Mechanisms

2.5.1 Bisphenol-A Epoxy Resin

Curing reaction of this type of resin based on the experiment that was conducted indicated that the structure was profound when a ratio of 10 : 3 of bisphenol-A

epoxy resin (DER331) to the curing agent (DEH622) and the reactional heat was 358.53 J/g which is four times to nine greater than the heat released by other different ratios. The minimum curing temperature was 36.35 °C which is lesser than the other different ratios; maximum curing temperature was 10–40 °C lower than other proportion [34].

2.5.2 Bisphenol-F Epoxy Resin

This type of resin undergoes a similar epoxy resin formation as bisphenol-A. By observation from these resins, the mean epoxy content is higher with lower viscosity per gram than bisphenol-A category of resins, which increases their chemical resistance [14].

If it is synthesized from phenol formaldehyde and epichlorohydrin, oxalic acid is used as a catalyst. Commonly, resin had epoxide number of 0.65–0.68 mol/100 g and viscosity of 1.3 Pa s [35].

2.5.3 Phenol Novolac Epoxy Resin

By combination of formaldehyde and phenols with subsequent epichlorohydrin, glycidylation results in epoxidised novolacs. This includes EPN and ECN which in many instances are highly viscous to solid resins, generally has same mean epoxide functionality of around two to six. A polymer network that is highly cross-linked can be formed showing high chemical resistance and temperature from the high epoxide functionality of these resins.This however has low flexibility [14].

Epoxy novolac resins are described as multifunctional epoxy resins because it has two or more epoxy groups per molecule; by chemical reacting a phenolic novolac resin with epichlorohydrin, polyepoxides are obtained. Upon processing, a high cross-link density can be achieved because of the increased functionality in epoxies.

This is generally recommended for appliactions requiring high performance which in turn require the best resistence to chemical, resistance to solvents, and outstanding temperature in high application resistance compared to the standard bisphenol-A epoxy. Epoxy novolac resins in most instances can also be applied in blend formulas to upgrade the performance produced by bisphenol-A and bisphenol-F epoxy resins [36].

2.5.4 Cycloaliphatic Epoxy Resin

Glycidyl ethers are base reactive and are principally reactive with polyamine hardener, while acidic hardeners, such as anhydrides of dibasic acids, cause cycloaliphatic epoxides. Recently, a vast variety of studies on different kind of catalysts called the latent catalysts which can produce reactive species to initiate polymerization by suitable stimulation, e.g. over irradiation or heating, were carried out [37].

2.5.5 Epoxy Resin Diluents

At room temperature, these resins actually display low viscosity (10–200 MPa s) and they are regularly alluded to as reactive diluents. Most of the time they are usually mixed and are used to decrease the viscosity of other epoxy resins. They may be reactive or non-reactive, but the reactive is preferable since they combine chemically with the main resin during curing [14].

2.6 Safety and Environmental Factors of Epoxy Resins

A specially selected blend of chemicals that gives each system its desired characteristics is often referred to as epoxy resin. Health hazardous is a buzz if you misuse or handle it in a manner not deemed for a professional or trained personnel since it is a chemical. Accidents and injuries can be minimized if one follows protocol and abide by the rules and regulation set forth. It is highly advisable that those who handle epoxies are trained adequately and apprehend all measures to be taken when handling this delicate chemical.

2.6.1 Bisphenol-A Epoxy Resin, Bisphenol-F Epoxy Resin, Glycidylamine Epoxy Resin, Epoxy Resin Diluents

2.6.1.1 Health Risks [38]

- They cause an irritation to the skin, which could cause toxic eczema or sensitizer, which could lead to a serious allergic contact of dermatitis.
- Most of the curing agents being used nowadays have a certain toxicity. But it would take quite a large volume of harm occurring due precisely to toxicity.

2.6.1.2 Environmental Issues [38]

- Cured agents and essentially most uncured epoxies are generally harmful and toxic to sea life which has a negative impact on the environment.
- In aquatic environment, it may cause long-term harmful effects for long time.

2.6.2 Phenol Novolac Epoxy Resin

2.6.2.1 Health Risks [39]

- Can cause skin irritation and allergic skin reaction which is a medical condition and needs medical attention.
- Serious eye damage/eye irritation and can also cause slight eye irritation

2.6.2.2 Environmental Issues [39]

Prevent from entering soil, ditches, sewers, waterways, and/or groundwater as they may cause contamination.

2.6.3 Cycloaliphatic Epoxy Resin

2.6.3.1 Health Risks [40]

- As some of these resins are adhesive and sticky and therefore will readily adhere to and stay on any surface, even the skin of the individual using it.
- Since some of the resins and many other curing agents do cause irritation of the skin and may cause sensitization.
- Vapor, droplets, and dusts of some of the materials can be very irritating to the eyes of the user and respiratory passages.

2.6.3.2 Environmental Issues [40]

Considering the harmful impact that uncured epoxies and curing agents have on the aquatic environment, it is therefore of the utmost importance that users remember to never dispose uncured epoxies by throwing them in domestic refuse.

2.7 Manufacturing of Epoxy Composites

A composite material is a material composed of the combination of two or more materials, a reinforcing material and a compatible binder. The reinforcing material is a discontinuous phase, while the matrix phase is a continuous phase. The matrix serves as a binder to the reinforcement and provides the shape of the material. Reinforcement, such as fibers, laminates in composites to provide strength and stiffness of the material and to overall improve its mechanical properties. Composites are generally developed for applications where lightweight is required with high specific stiffness, easy bonding, low electrical conductivity, and good fatigue resistance. There are different types of composites, such as long strand reinforced composites, short strand reinforced composites, and particulate reinforced composites. Composite materials have a wide range of applications amongst various industries such as automobile, aeronautics, boats, sport, and medical equipment.

Epoxy composites can be manufactured in various ways; the optimum manufacturing method depends on the desired final surface finish and the required properties of epoxy composites. Three main types of epoxy resin composite manufacturing processes exist, namely, closed molding, cast polymer molding, and open molding. Each of these main processes has several methods within that has its own benefits [41].

2.7.1 Open Molding

Raw composite materials (resin and fibers) are put into an open mold; they are left to cure and harden due to being exposed to air. Tooling cost for this method is not expensive. Therefore, it is possible to use this technique for prototypes and short production of composite materials. Open molding utilizes various processes which include hand lay-up, filament winding, and spray-up techniques [42].

2.7.1.1 Hand Lay-Up

This process is one of the simplest composite molding methods. This method is well suited for a lot of composite products of all sizes (small or large). Production volume per mold in this molding method is very low; however, production can be increased by the utilization of multiple molds. This method offers simpler processing and lower tooling costs for all different part sizes with less money spent on equipment. Fiberglass composites make use of single cavity molds which come in a variety of sizes dependent on the requirements. The molds are available from the smallest of sizes to larger ones [43].

Hand Lay-Up Process

Figure 2.17 shows the layout of a hand lay-up process. In this process, the first step is to clean and coat the mold surface with a non-stick gel. After curing of gel coat, fiberglass reinforcement stock is accurately laid on the mold. Then, laminating resin is applied (in many ways) either by paint roller or brushing. Any form of squeeze or compression tool can be utilized to consolidate thorough wetting of reinforcement to eliminate trapped air. In order to increase the laminate thickness, consecutive sheets of fiberglass reinforcement were layered on top of each other. Materials with lower density are utilized in stiffening the laminate. Some materials that are used are foam and honeycomb. This construction is known to be called a sandwich panel composite [43].

Advantages [44]

- No complicated equipment and tools required during processing.
- Production technology is easily mastered after only a short training.

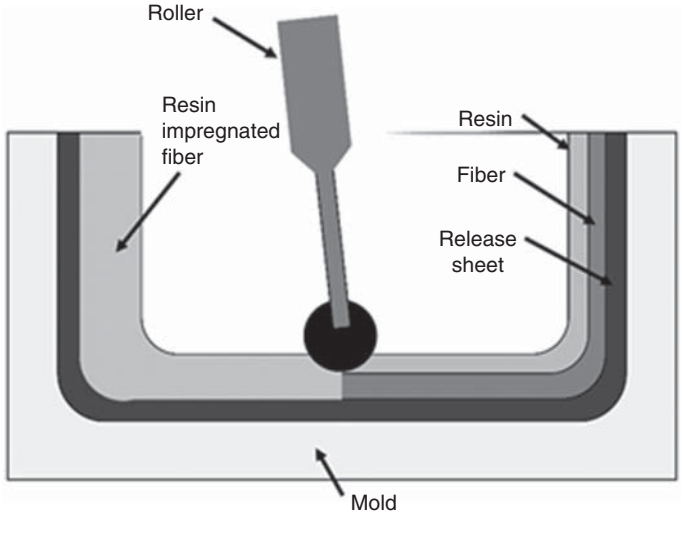

Figure 2.17 A schematic layout of a hand lay-up process.

- A large variety of products can be manufactured using this method.
- Composition can also include materials such as foam, metal, and wood in conjunction with the base composite.

Disadvantages [44]

- Production efficiency is lowered when compared to other open molding processes.
- Product quality is lowered when compared to other open molding processes.

2.7.1.2 Spray-Up

The spray-up process, also referred to as chopping, is an old open molding process which is suitable for producing products like oats, transportation components, and tanks in a plethora of shapes and sizes. The advantages of a chopped laminate include its comfortability and its rapid production of more complex shapes when molding. Similarly, to hand lay-up method, the volume production can be increased by using more molds. The molds used in this process are the same as those used in the hand lay-up process [45].

Spray-Up Process

Figure 2.18 shows a basic layout of a spray-up process. The step followed in this process is applying a gel coat to the mold surface and then allowing it to cure. A continuous feed of chopped strand fiberglass and resin is fed to the mold, and the laminate is then rolled to compact the chop. For getting more thickness, additional layers of chopped strands are added. Low-density materials are used and easily fit in with the method [45].

Advantages [46]

- It is compatible with medium to low manufacturing parts.
- It is inexpensive when compared to other processes when it comes to the production of little to big parts.
- Utilizes cheaper tools and materials.

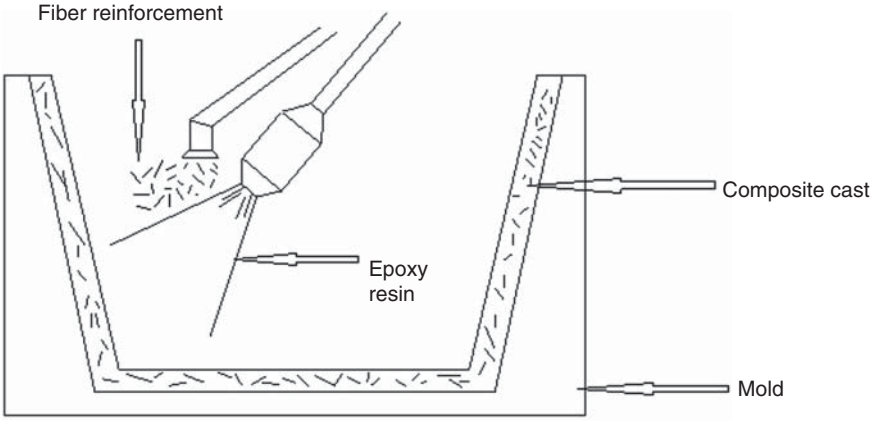

Figure 2.18 A schematic layout of a spray-up process.

Disadvantages [46]

- This process is not suited for the production of products that have high structural requirements.
- Control of the fiber volume and thickness is difficult.
- Styrene emission is a concern when using this process because of its open mold nature.
- This process results in a product that has one smooth side and one rough side.
- Where dimensional accuracy and process repeatability are the prime concerns, this process is not suitable as it is difficult to control the dimensional accuracy.
- Cores must be manually inserted when required.
- Due to pressurized resin being used, laminates do tend to be very rich in resin.
- Resin must be of low viscosity in this type of process.

2.7.1.3 Filament Winding

Filament winding is an open molding process that is automated in which a rotating mandrel is used as the mold. The configuration of the mold produces a smooth surface finish on the inside and on the outside of a laminate. This process yields high tensile strength products due to that it uses a high degree of fiber loading during the manufacturing of hollow cylindrical products such as stack, rocket motor cases, and chemical storage tanks. Laminates produced using this process have added benefits such as having a large strength to weight ratio and give a degree of control with a consistent fiber alignment. This method is used when manufacturing engineering structures that require strict tolerances. The labor factor in this process is lower than other open molding processes because it is fully automated and controlled by a computer. The molds are made of steel or aluminum, and the mandrels are used to produce different shapes and sizes and are collapsible for part removal [47].

Figure 2.19 shows a schematic layout of a filament winding process. A constant strand roving is inserted into a resin bath and onto a mandrel which is spinning. This roving feed works using a trolley system which travels the mandrel's length.

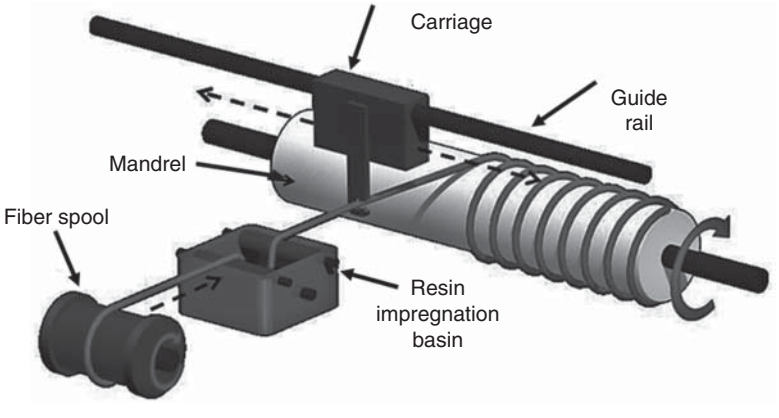

Figure 2.19 A schematic layout of a filament winding process.

The filament is then placed on an encoded symmetrical pattern in order to produce the maximum possible strength in the direction needed. The laminate is cured when enough layers are applied. After which, the molded part is then removed from the mandrel. The required tools are always available for the filament winding process [47].

Advantages [48]

- It is cost-effective as well as a quick method.
- Easier to control the resin content by measuring the required amount of resin on each die.
- The cost of fiber is reduced since this is a second process, where changes fiber to fabric before use is not needed.
- Laminates produced possess great structural properties because the linear fibers can be shaped into complex patterns to match a given load.

Disadvantages [48]

- Use is restricted to components in convex shapes.
- It is difficult to lay the fiber accurately along the component length.
- For large components, the cost of mandrel tends to be expensive.
- Can be cosmetically unattractive because the external surface comes out unmolded.
- This process uses low viscosity resin which in turn can lead to low mechanical properties of components

2.7.2 Closed Molding

The closed-molding process uses fibers and resin (raw materials), which are cured within a mold or in a vacuum bag (not exposed to air). The closed-molding process is typically automated, requiring special equipment, leading them being used majorly in plants that produce large quantity of substances. They are many different processing methods of closed mold manufacturing, such as [45]:

- Reinforced reaction injection molding (RRIM)
- Vacuum-assisted resin transfer molding (VARTM) process
- Light resin transfer molding (LRTM)
- Vacuum infusion process (VIP)
- Pultrusion process

2.7.2.1 Reinforced Reaction Injection Molding (RRIM)

RRIM is a processing method in which two or more reactive resins are metered and mixed using an impingement method with high pressure to produce a thermosetting polymer, impregnated within the mold, after which it is cured. RRIM composites have several advantages such as fast sequence period, little labor, very little mold clamping, and produces less excess scrap. Because of the use on reinforcements, polymerization shrinking is reduced, thermal growth is minimal, and properties

such as stiffness, tensile strength, and tensile elongation get normally better. Before the reaction takes place, pounded fibers and flakes can be added to the resin in the mixing head. The usage of pressure pumps and injection cylinders achieves metering. A mixing chamber used is usually a smaller one. The RRIM process requires unique types of resins, which include epoxy resins and polyurethanes. Currently, polyurethane is the dominating resin in RRIM processing. Reinforcements are cute (short fibers) or hit milled glass fiber and glass flake in RRIM. There are many different variations to this process, but it follows a similar theme [49].

RRIM Process

The streams of the two resins are introduced using injection from different sides of the mixing chamber whilst under high pressure. The clash of the two resins produces energy which results in the mixture of the resins. Even though the resins are mixed at high pressure, it results in always a little viscous fluid. The resulting liquid resin is then impregnated in a mold at a low pressure (~345 kPa). Polymerization occurs fast in the mold cavity with less or no added heat needed [49].

Figure 2.20 shows a schematic layout of a RRIM process.

Advantages [50]

- Reaction injection molding can produce strong, flexible, lightweight parts which can easily be painted.
- The mixture of two components that is injected into the mold has a lower viscosity than the viscosity of the molten thermoplastic polymers.
- Big, lightweight, as well as thin-walled items are able to be RRIM processed.
- The thinner mixture needs less clamping forces, resulting in a lower amount of equipment and lower cost.
- High-density skin is created with a low-density core.

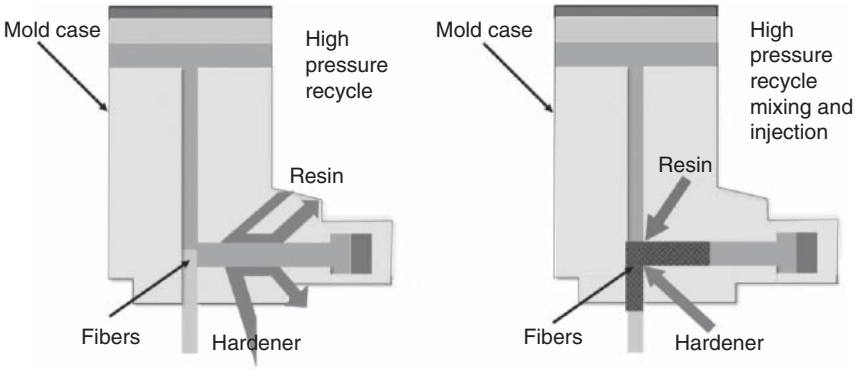

Figure 2.20 A layout of a RRIM process. (a) High pressure recycle. (b) High pressure recycle mixing and injection.

Disadvantages [50]

- Slow cycle times.
- Expensive raw materials.

Applications of RRIM

There are many different applications for RRIM products, mainly in transportation industries. Automotive applications for RRIM parts consist of Class A body panels, fascia, bumper beams, spare tire covers, floor pans, and further comparable products [49].

2.7.2.2 Vacuum-Assisted Resin Transfer Molding Process (VARTM)

In VARTM, a flexible vacuum bag is used to create a closed mold manufacturing process, a tool removed from a top part of a mold. Using a flexible vacuum bag and vacuum is to assist and facilitate the resin flow into a fiber lay-up contained within a mold tool covered by a vacuum bag. The part thickness under full vacuum dictates the material thickness. After composite part has been impregnated, it cures at room temperature (Figure 2.21).

Advantages [51, 52]

- This process does not need an autoclave while still being able to produce complex and big parts.
- The capability of creating large and complex components allows it to minimize manufacturing expenses when used to make parts that are constructed for small components.

Disadvantage

- Air leakages may occur which can cause defects on the final product.

Applications [51, 52]

Products created using this method can differ in their usage with components used in transportation, wind energy, marine, infrastructure, and aerospace applications.

Figure 2.21 A schematic layout of the VARTM process.

2.7.2.3 Light Resin Transfer Molding (LRTM)

Resin transfer molding is a composite manufacturing process that requires resin to be put under higher pressure into a mold cavity. This method manufactures components with two completed surfaces. It requires any stitched material together with epoxy and any core except honeycomb as the resin would fill into the cells, and due to the pressure being applied, some foams are not suited as the pressure could crush it [52, 53].

LRTM Process

This process requires that the mold is gel coated; the mold can be either soft tooling made of either polyester or epoxy or hard tooling made of cast machined aluminum or steel. The dry fibers and core material are situated within the mold, and the mold is full closed and well fastened using either a perimeter clamp or press clamp. By the aid of a mix/meter injector, the resin is injected under pressure. The part is then cured within the mold. This process can be done at room temperature yet need that the molds be heated in order to get fast cycle times together with product consistency. Figure 2.22 shows the schematic layout of the LRTM process.

Advantages [54]

- The process is efficient and suitable for complex shapes.
- Laminates with a high fiber volume can also be produced using lower void contents.
- With the resin being closed, it ensures good health and is safer.
- Reductions to labor are possible.
- Final product has superior surface finish.
- Better reproducibility.
- Low clamping pressure.
- Ability to induce inserts.

Disadvantages [54]

- Costly tooling and power.
- Restricted to small parts.

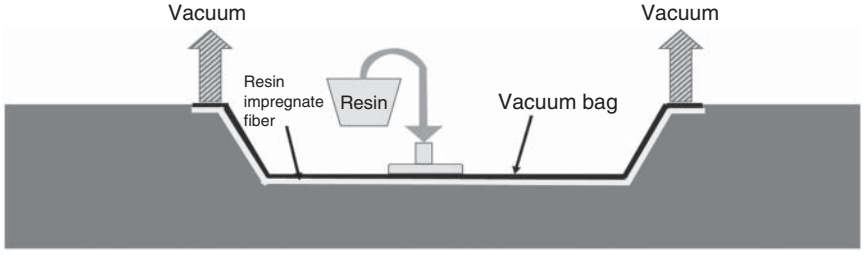

Figure 2.22 A layout of the LRTM process.

Applications

This manufacturing process can be used to manufacture small complex aircraft structures, automotive components, and train seats.

2.7.2.4 Vacuum Infusion Process (VIP)

This method of composite production requires the backup as well as core materials are laid dry into the mold; this then provides the chance to place the reinforcement. Once the resin is taken into the mold, the laminate is compact hence eliminating room for surplus resin. Vacuum infusion gives very high resin-to-glass ratios with superior mechanical properties of the laminate. Vacuum infusion is compatible for molding huge structures and is taken as a low volume molding method. Vacuum infusion method can be used to manufacture composites consisting of fiberglass, continuous strand mats, carbon fiber, or Kevlar together with epoxy, and any core can be used except honeycomb [55, 56].

Process

It is a process in which resin is infused into a dry fiber laminate by using a vacuum and tubing to draw resin into a mold. The mold can be gel covered, and when this gel coat cures, the dry fiber laminate may be placed into the mold. A release film with holes is placed over the dry fiber laminate, followed by a flow media consisting of a coarse mesh. The vacuum bag is then positioned and sealed around the periphery of the mold. A tube is connected between the vacuum bag and the resin container very carefully. A vacuum is applied to consolidate the laminate, and the resin is pulled into the mold. Figure 2.23 shows a layout of LRTM process.

Advantages [57]

- Consistent exfoliation of resin with process control (this limits human error).
- Diminishes part shrinkage.
- Provides satisfactory surfaces.
- Laminates complex fiber layers in an efficient manner.
- The process is much cleaner with not just limited by efficient, but no air pollution.
- The cycle period is much faster.

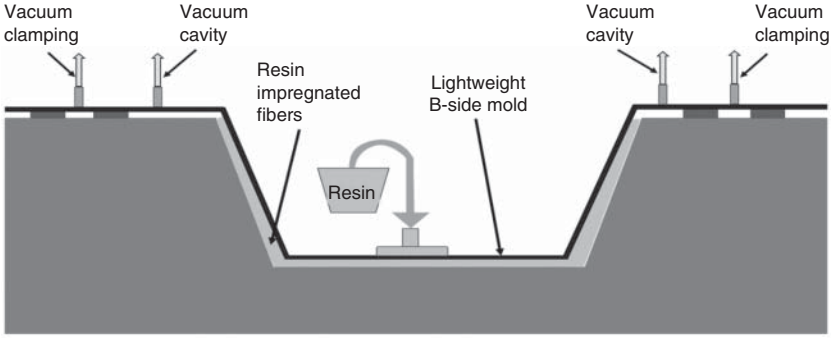

Figure 2.23 A schematic layout of LRTM process.

- Higher fiber-to-resin ratio.
- High strength and stiffness.
- No resin entrapment and presence of very low voids.

Disadvantages [57]

- Complicated set-up.
- If a vacuum leak is present, scrapping of the part is necessary.
- Open mold process is much better than cosmetic finish.
- The cost is more expensive.
- Standard materials cost less than VIP materials and consume some disposable supplies.

Applications

This method is used to manufacture composites that are suited for small yachts and the body panels of trucks and trains.

2.7.2.5 Pultrusion Process

Pultrusion is a process that makes use of any fiber together with epoxy and does not require a core; therefore, there is no sandwich construction.

It is a process that requires glass fiber, carbon fiber, or basalt fiber coming in the form of mat or cloth must be soaked in a resin bath and then pulled through a heated die, the layout of the fibers within the fiber reinforcement may be axial or multidirectional. For high demanding applications, hybrid fiber reinforcements can be incorporated. The die sets the shape of the stock and aids in controlling the fiber-to-resin ratio; a heated die is used to cure the resin. The required components for this process are a non-stop roller of fiber reinforcement, a resin bath, preform plate, heated die, puller, and a cut of saw [57, 58]. Figure 2.24 shows a layout of pultrusion process.

Applications

Manufactured components from a pultrusion process are used in beams and girders that are incorporated into roof structures, bridges, ladders, and frameworks. It is

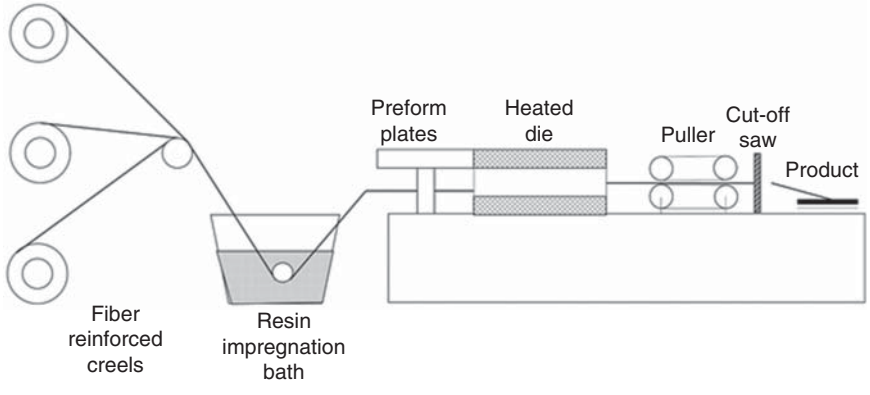

Figure 2.24 Layout of pultrusion process.

also used to manufacture channels, pipes, tubing, fishing rods, and golf club shafts. The products from this method can also be used in the automotive industry and to manufacture electrical components.

Advantages [59]

- Pultruded composite profiles are composed of high-performance fibers individually or in combination.
- Considered to be one of the highest performing composite materials.

Disadvantages [8]

- Technique limits the shape of materials that can be made.
- Can only produce materials of a consistent thickness.
- Complex shapes or varying diameters over their length cannot be made using this process.
- Limited to materials that can be pulled through in strands, such as polyester and epoxy.

2.7.2.6 Vacuum Bag Molding (Wet Bagging)

Vacuum bag molding is a technique that works on the principle of applying pressure to a laminate to remove any entrapped air that may be infused within the layers. It compacts the fiber layers and prevents shifting of the fibers during the cure, and it subsequently optimizes the fiber-to-resin ratio in a composite material. The use of pressure results in a greater concentration of fiber and provides better adhesion between layers of sandwich construction. It is the best technique to ensure that the outer laminate is bonded adequately to the core. Phenolic or epoxy can also be used to wet out a variety of heavy fibers or fabrics with any respective core.

Process

The vacuum bag molding process makes use of a vacuum to eliminate entrapped air and excess resin, after the wet lay-up is situated inside the well-shaped mold from pre-cut layers of glass mat or fabric and resin, a non-absorbent film of polyvinyl liquor or nylon is arranged over the lay-up and closed at the mold flange. A vacuum is drawn on the sack shaped by the film, whereas the composite is cured at room or elevated temperatures, as this happens at atmospheric pressure. Compared to hand lay-up, the vacuum method provides higher reinforcement concentrations, better adhesion between layers, and more control over resin/glass ratios [58]. Figure 2.25 shows the layout of the vacuum bagging process.

Advantages [57]

- Laminates that have a high content of fiber can be achieved.
- Low void contents.
- Better fiber wet-out due to pressure and resin flow.
- *Health and safety*: The vacuum bag method reduces the number of volatiles emitted during cure.

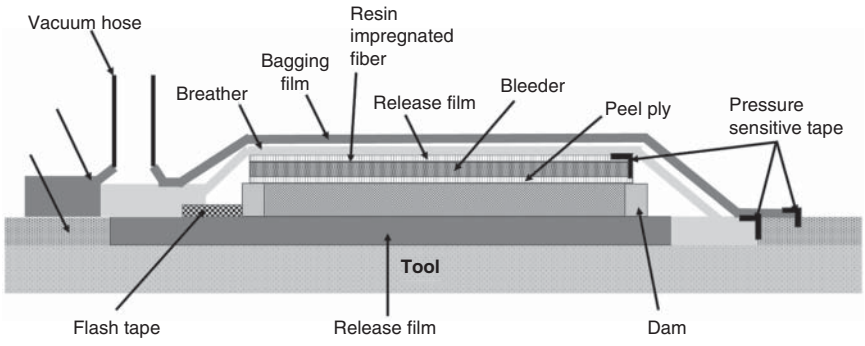

Figure 2.25 A schematic layout of vacuum bagging process.

Disadvantages [57]

- Extra process adds cost.
- Professionally and highly skilled personnel required.
- The operator is the sole determiner of the mixing and resin control.

Applications

This composite manufacturing procedure can be used to manufacture large components for cruise boats, race cars, aircrafts, and for building constructions [60].

2.7.2.7 Centrifugal Casting

In this process, reinforcements and resin are dropped against the inside surface of a rotating mold. The centrifugal force grips the materials in place until the part is cured. In this process, the outside surface of the part, which is cured against the inside surface of the mold, denotes the finished surface. The inside surface of centrifugal cast parts can be given an additional coating of pure resin to improve surface appearance and provide chemical resistance. Large composite tanks and pipes are commercially produced by this process. Figure 2.26 shows the layout of a centrifugal casting process.

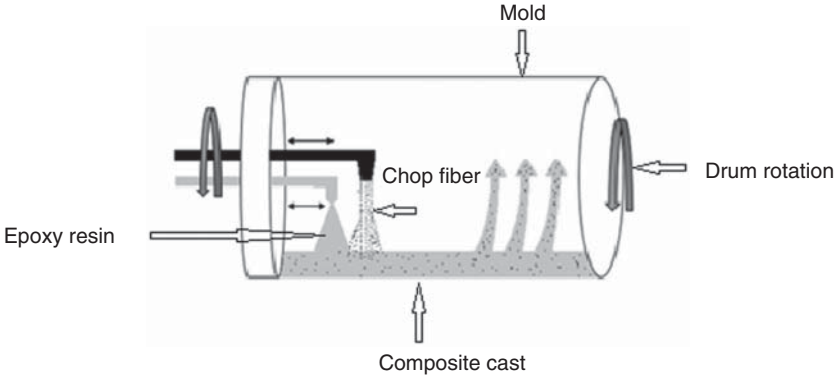

Figure 2.26 Layout of a centrifugal casting process.

Advantages [61]

- Suitable for small hollow cylindrical products.
- Economical for small production.

Disadvantages [61]

- Complex-shaped products cannot be made.
- Low-viscosity resin is needed.
- The finish of the product is not good.
- The structural properties may not be good.

2.7.3 Natural Fiber Reinforced Epoxy Composites

Natural fiber composites are lightweight, cost-effective, eco-friendly, and environmentally friendly material than glass fiber composites. The fact that they are biodegradable and abundant makes them environmentally superior to most composites in most cases for the following reasons [62]:

- Less energy is emitted in the production of natural fiber composite compared to the production of glass fiber composite.
- The fiber content to polymer content is high in natural fiber composite for equivalent performance.
- Natural fiber composites are light in weight and thus are used in auto application to reduce fuel emission and also to improve fuel efficiency.
- Natural fiber composites are biodegradable, and energy can be recovered as it degrades.

The application of natural fiber material is an ever-growing field from automotive, commercial construction, aerospace and particularly in preserving water, energy, air, and reducing waste. In recent, hybrid composite epoxy matrix was reinforced with tamarind fruit fibers, areca nut fruit husk fibers (treated with NaOH), and other plant fibers (banana, kenaf, coir, etc.) prepared using the hand lay-up method. The fiber concentration was 10, 20, 30, 40, and 50 wt%. A tensile test was conducted to measure the mechanical properties of the hybrid composite, and it was discovered that as the fiber content increases, the strength also increased, but in some cases as the fiber content increases, strength is decreased [63].

2.7.3.1 Manufacturing of Natural Fiber Reinforced Epoxy Composites

First, an epoxy (commonly bisphenol) is used as the matrix in the composite fabricating process. It is then mixed with a hardener (commonly 2-aminoethylethane-1,2-diamin). The epoxy resin and hardener are mixed to a weight ratio of generally 10 : 1. Natural fiber (plant, fruit, leaves, etc.) is cut to the desired length which depends on the application of the composite and is then used as a reinforcing agent in the composite preparation. The epoxy is formed by constantly stirring the resin and harder mixture until it is clear and has no swirl lines. The biofiber is then laid out on the mold surface to form a laminate material.

The epoxy resin is then added to the biofiber to complete the process of reinforcing the matrix. Once the reinforcement is complete, the laminate is then folded over to make a square panel in which the outer faces are laminated and inner structure is a combination of biofiber and epoxy resin. To achieve the final product, the reinforced composite is laid on a flat-bed which is then hard pressed to fuse the two constituents together. Figure 2.27 shows schematic sequence of epoxy natural fiber composites.

Manufacturing process of epoxy natural fiber composites (maximize fiber content):

- Figure 2.27a shows the short strand cut fiber to be used.
- Figure 2.27b shows the short strand fiber being dipped in the epoxy resin mixture.
- Figure 2.27c shows the excess epoxy being squeezed from the fibers.

Figure 2.27 The manufacturing process of natural fiber reinforced epoxy composite (a) Chopped short fibers, (b) Fiber dipping in epoxy hardener resin mixture, (c) Squeezing process to remove excess resin, and (d) Cured natural fiber reinforced epoxy composite. Source: Jyotishkumar Parameswaranpillai.

Figure 2.28 Epoxy natural fiber composite panel. Source: Jyotishkumar Parameswaranpillai.

- Figure 2.27d shows the random arrangement of the short strand fibers into a square/rectangular panel.
- Figure 2.28 shows the fully cured and solid epoxy natural fiber composite panel formed with pressure (2 bar) induced processing.

2.8 Preparing of Particulate Filled Epoxy Composites

2.8.1 Particle Reinforced Epoxy Composites

Particle reinforced composites are materials that consist of two or more constituents. The composite is constructed in a way by adding a reinforcing constituent to the matrix. There are many types of particulate reinforced composites. In all types, the particulates provide necessary material properties and the matrix acts as a binding medium necessary for applications. Nanoparticle-reinforced epoxy composites are a commonly used particulate composites.

2.8.2 Nanoparticle-Filled Epoxy Composite

This process aims to develop a relationship between nanoparticles and epoxy to form a strong and reliable composite. The presence of nanoparticles enhances the properties of the composite. Properties of such composites exceed the standard properties of other composites in terms of tensile strength, thermal properties, and flexural properties.

2.8.2.1 Method 1

In this process, montmorillonite (MMT) nano-clay particles will be used as the nano-filler and will be incorporated together with epoxy in a liquid form, a product bisphenol-A (epoxide value 23) and epichlorohydrin (amine value 300 g [mg KOH/g]). The cycloaliphatic amine hardener (Jointmine 905-3S) has an equivalent weight of 95, while the epoxide equivalent weight is 190 per equiv [64].

Preparation

To prepare samples using this technique, 1 g of MMT nano-clay filler of 1 phr (parts per hundred) has to be sonicated in a solution concentration of 50 ml of acetone or in a ratio of proportionality for approximately two hours. One parts per hundred is being used to achieve the maximum mechanical properties, it is sonicated to disrupt the particles using sound waves, and this is done to speed up the dissolution and prepare a mixed solution faster. Once the sonication is complete, epoxy is heated at 80 °C, then the mixture of MMT (containing acetone) is poured into the epoxy. The mixture is stirred for a few hours to disperse the MMT in epoxy and to remove acetone; vacuum extraction is performed at 55 °C for 20 to remove air bubbles. Once the acetone is completely removed, the curing agent (the hardener) is added and the curing takes place at 110 °C for two hours; thereafter, the mixture is added into a mold and is further cured in an oven [64].

2.8.2.2 Method 2

In this process, epoxy serves as the matrix; it is usually a bisphenol-A diglycidyl ether-based resin with a polyaminoamide hardener that forms the epoxy and is incorporated with MMT nano-clay [65].

Preparation

To prepare samples, the clay needs to be completely dry; therefore, it is dried in an oven for eight hours at 80 °C. The epoxy and clay are combined and stirred for two hours using a mechanical stirrer at 75 °C. All the gas from the mixture needs to be removed using a vacuum oven, and the hardener needs to be added to the epoxy. The final mixture is then poured into a mold, the gas is removed, and it is cured in an oven for about two hours at 80 °C and then post cured at 150 °C for two hours [65]. Figure 2.29 shows the basic process of preparing nanoparticle filled epoxy composite.

2.9 Futuristic Processing of Epoxy-Based Composites

2.9.1 Fast Curing Powder Adhesive Epoxy Resin

Powder epoxy resins had recently gained considerable attention due to that it is non-toxic and high recycling rate and is ease of use. To study the structural characteristics, mechanical properties and thermal stability of fast curing powder epoxy adhesive, 2-methylimidazole (2-MI) in bisphenol-A epoxy resin (E-20), and hexamethylenetetramine (HMTA) are chosen.

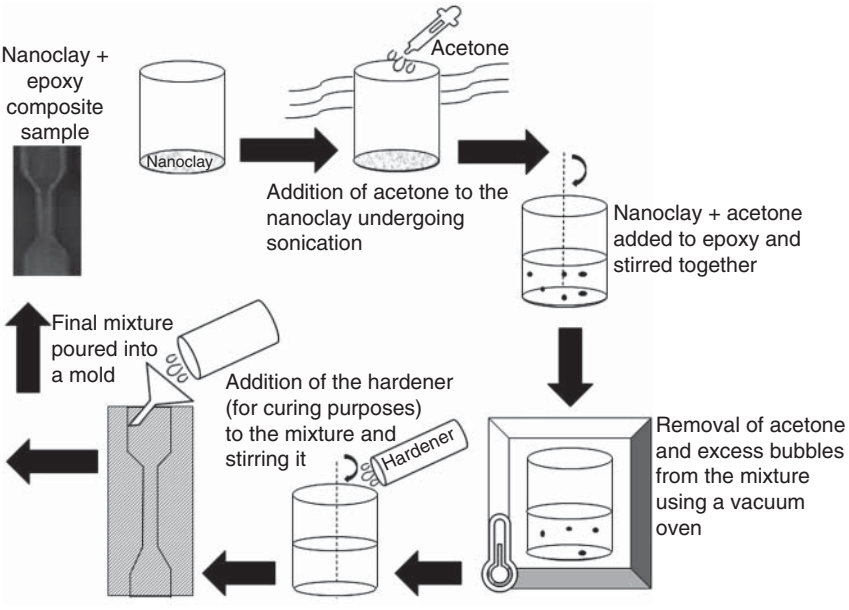

Figure 2.29 The basic process of preparing nanoparticle-filled epoxy composite. Source: Jyotishkumar Parameswaranpillai.

Powder epoxy adhesive has fast curing rate and thus is used as heat-resistant substrates. Adding a curing agent (HMTA), accelerant (2-MI) in bisphenol-A epoxy resin (E-20), resulted with a typical melt blending method. Decreasing the curing temperature of the powder epoxy adhesive widen its use to heat-sensitive substrates (such as plastic products, cardboard, and wood) [66].

2.9.2 3D Printing

This material based in epoxy opens a new channel for 3D printing. There has been epoxy resin that has been spiked with viscosity enhancing nano-clay platelets and a compound dimethyl methyl phosphonate combined with two types of fillers called silicon carbide and short carbon fibers. These new composites result in a composite stiffer than conventional processed composites. Currently, 3D printed polymer is also available on the market. This will allow a versatile ability to control the direction of the fillers for future use [67].

2.9.3 Adhesive Method

This is one of the most common processors that is used in batch processing using an oven. This however is a very time-consuming method; hence, an alternative is suggested. This being an in-line method which will allow a single line process from application to inspection. This will result in energy saving as well as a reduction in cost of over 90% [68].

2.9.4 Ultrasonic Fabrication Method for Epoxy Resin/SbSI Nanowire Composites

The new production is the use of ultrasound irradiation where antimony sulfo-iodide (SbSI) nanowires, with horizontal measurements of 10–100 nm and lengths up to a few micrometers, are orchestrated and imbued in epoxy resin/SbSI nanowire composites. The mass proportion is 1 : 4 for SbSI nanowires bound with epoxy tar, the blend experiences ultrasound light for the homogenization of the blend. The manufactured epoxy resin/SbSI nanowire composites, due to the piezoelectric properties of SbSI (electromechanical coefficient $k_{33} = 0.9$, and piezoelectric coefficient of $dV = 0.9 \times 10^{-9}$ C/N), possibly utilized as a dynamic layer in nano-sensors and nanogenerators [69].

2.9.5 Electron-Beam (E-Beam) Curing

In this process, a composite lay-up is uncovered to a stream of electrons which is deemed to be one of the methods of efficient curing of thin laminates. Introducing a stream of electron produces ionizing radiation, responsible for cross-linking in radiation-sensitive resins and polymerization. X-ray and the microwave curing technologies work in a similar way. UV radiation is used to activate a photo-initiator in UV curing, where it is included to a thermoset resin, which, when enacted, sets off a cross-linking response which requires light-permeable resin and fortifications UV curing [70].

2.9.6 Automated Fiber Placement (AFP) Epoxy Resin Composite

This is a method of manufacturing composites that is used mostly in materials having lightweight and same or greater strength compared to metals. This method involves compacting and heating resin pre-impregnated non-metallic fibers on tooling mandrels. Fiber comes as tows, meaning a bundle of carbon fiber soaked with epoxy resin. The tows are given to a heater and compaction roller on the fiber placement machine and then places in lines across tool surface. All these functions are performed with machine language using software program tools. This method is used to make complex structures and it increases the rate of deposition and precision [70].

2.10 Conclusion

This chapter discussed about the origin of epoxy and various types of epoxy polymer. A wide range of resins, hardeners, curing methods, and processing techniques were covered. The advantage and disadvantage of various types of epoxy resins were discussed. Following that, the epoxy-based composites were discussed. Composites include a wide range of products of different applications from construction to automobile components that is made from different fibers where growth has been seen in

the production of natural fibers composite and there are more future developments as discussed which can increase the composite production.

There have been several innovative methods in which epoxies are being processed. The improved methods are seen to be increasing the use of epoxies in manufacturing and industries in ways that have not been seen before. Such examples, as powder adhesive epoxy resins are opening the door to numerous points of interest such as non-toxicity and the ability of recycling. The boom of 3D printing also shows improvements in epoxy filaments with that of fillers that improve properties of materials being printed leading to increased options of printing materials based on material expectations. The use of ultrasonic fabrication methods has allowed for the use of SbSI nanowires being infused into epoxies, used in the production of active layers in nanosensors and nanogenerators. Advancements in the curing process with the introduction of electron-beam (E-beam) curing presents a proficient curing strategy for lean covers. Advancements can be seen all the way down to the placement of fibers with automated fiber placement (AFP) epoxy resin composites; the availability of high-speed robotics has allowed for fibers to be sized and orientated in multiple orientations with precision, reduced material scrap and lower labor costs.

As the bio-economy slowly gains interest to the researchers and in industries, the focus is shifting to the synthesis of bio-based epoxy resin extracted from inexpensive and renewable natural resources, such as lignin, vegetable oil, rosin, sugars, furan, and itaconic acid. Recent bio-based materials showed similar or greater properties than commercial petroleum-based product.

References

1 Guchhait, P.K., Pradhan, S., Kumar, K.D. et al. (2010). Influence of nanoclay on the morphology, adhesive and mechanical properties of polysulfide modified epoxy resin. *Polymers and Polymer Composites* 18: 123.

2 Chikhi, N., Fellahi, S., and Bakar, M. (2002). Modification of epoxy resin using reactive liquid (ATBN) rubber. *European Polymer Journal* 38: 251.

3 Shackelford, J.F. (1988). *Polymers Introduction to Materials Science for Engineers*, 2e, 403–449. New York, NY: MacMillan.

4 Garcĭa-Lopera, R., Figueruelo, J.E., Abad, C., and Campos, A. (2009). Miscibility of a DGEBA based epoxy resin blended with thermoplastic mixtures of poly(styrene) and block copolymers: influence of the copolymer content and chemical nature. *Journal of Macromolecular Science Part B Polymer Physics* 48: 128.

5 Astruc, A., Joliff, E., Chailan, J.F. et al. (2009). Incorporation of kaolin fillers into an epoxy/polyamidoamine matrix for coatings. *Progress in Organic Coatings* 65: 158.

6 Spangberg, L.S. (1982). Endodontic filling materials. In: *Biocompatibility of Dental Materials*, 10e, vol. 3 (eds. D.C. Smith and D.F. Williams), 161–222. Boca Raton, FL: CRC Press.

7 Luft, J.H. (1961). Improvements in epoxy resin embedding methods. *The Journal of Biophysical and Biochemical Cytology* 9 (2): 409.

8 Jin, F., Li, X., and Park, S. (2015). Synthesis and application of epoxy resins: a review. *Journal of Industrial and Engineering Chemistry* 29: 1–11.

9 Jin, N.J., Yeon, J., Seung, I., and Yeon, K.-S. (2017). Effects of curing temperature and hardener type on the mechanical properties of bisphenol F-type epoxy resin concrete. *Construction and Building Materials* 156: 933.

10 Ruth, R.J. and Louise, B.A. (2015). Bisphenol S and F: a systematic review and comparison of the hormonal activity of bisphenol a substitutes. *Environmental Health Perspectives* 123 (7): 643–650.

11 Jin, F.L. and Park, S.J. (2008). Fracture toughness of difunctional epoxy resin/thermally latent initiator system modified with polyesters. *Journal of Industrial and Engineering Chemistry* 14: 564.

12 Bu, Z., Hu, J., and Li, B. (2014). Novel silicon-modified phenolic novolac resins: non-isothermal curing kinetics, and mechanical and thermal properties of their biofiber-reinforced composites. *Thermochimica Acta* 575: 244–253.

13 Ahmed, M., Nasri, N., Mohsin, R. et al. (2014). Preparation of epoxy-novolac resin binder using phenolic rich fractions of biomass pyrolytic oil as partial substitute of phenol. *Applied Mechanics and Materials* 554: 101–105.

14 Ma, S., Liu, W., Zhao, Y. et al. (2012). Curing behavior and thermal properties of autocatalytic cycloaliphatic epoxy. *Journal of Macromolecular Science Part A* 49 (1): 81–84.

15 Bakar, M., Szymańska, J., Rudecka, J., and Fitas, J. (2010). Effect of reactive diluents and kaolin on the fracture toughness of epoxy resin. *Polymers and Polymer Composites* 18: 469.

16 Luft, J. (1961). Improvements in epoxy resin embedding methods. *The Journal of Cell Biology* 9 (2): 409–414.

17 Ellis, B. (1993). *Chemistry and Technology of Epoxy Resins*, 117–118. Dordrecht, Netherlands: Springer.

18 Bayliss, D.A. and Deacon, D.H. (2002). *Steelwork Corrosion Control*, 2e. London: Spon. ISBN: 978-0-415-26101-2.

19 Agag, T., Ishida, H., and Geiger, S. (2011). Thermal properties enhancement of polybenzoxazines: the role of additional non-benzoxazine polymerizing groups. In: *Handbook of Benzoxazine Resins* (eds. T. Agag and H. Ishida), 263–286. Amsterdam: Elsevier.

20 Woo, E.M. (2017). *Handbook of Epoxy Blends*. Springer International Publishing AG.

21 Pepper, J.E., Huneault, J., Rahmat, M. et al. The effect of curing agent on the dynamic tensile failure of an epoxy subjected to plate impact. *International Journal of Impact Engineering* 113: 203–211.

22 Yang, B., Mao, Y., Zhang, Y. et al. (2019). A novel liquid imidazole–copper (II) complex as a thermal latent curing agent for epoxy resins. *Polymer* 178: 121586.

23 Walker, D., Jones, R.M., and Wright, P. (2010). Chapter 4: Primary secondary and tertiary amines and their isosteres. In: *RSC Drug Discovery Series*, vol. 1 (ed. D.A. Smith), 168–209. Royal Society of Chemistry (RSC) Publishing.

24 Hara, O. (1990). Curing agents for epoxy resin. *Three Bond Technical News,* 20 December, 1990, p. 321-10.

25 Straka, P., Buryan, P., and Bičáková, O. (2018). The formation of quasi-alicyclic rings in alkyl-aromatic compounds. *Journal of Molecular Structure* 1154: 455–462.

26 Baraiya, R. and Thakkar, J. (1997). Epoxy resin based polyamides as epoxy curing agents. *International Journal of Polymeric Materials and Polymeric Biomaterials* 36: 189–196.

27 Chen, C.S. and Pearce, E.M. The boron trifluoride monoethyl amine complex cured epoxy resins. *Journal of Applied Polymer Science* 37 (4): 1105–1124.

28 Cheng, J., Hu, Z., Lv, K. et al. (2018). Drastic promoting the visible photo reactivity by polymerization of dicyandiamide at high pressure. *Applied Catalyst B: Environmental* 232: 330–339.

29 Yue, Y., Zhao, S., Liu, J. et al. (2017). Probing the binding properties of dicyandiamide with pepsin by spectroscopy and docking methods. *Chemosphere* 185: 1056–1062.

30 Bartazatt, R., Sule, P., Galbadage, D., and Cirillo, J. (2020). Aromatic hydrazide compounds that inhibit the growth of Mycobacteria tuberculosis. *Journal of Advances in Medical Sciences* 31: 1–11.

31 Masterbond®. *Resins and Curing Agents: Formulating Epoxy Systems*. Hackensack, NJ, USA: Master Bond.

32 Kotynia, R., Adamczewska, K., Strakowska, A. et al. (2017). Effect of accelerated curing conditions on shear strength and glass transition temperature of epoxy adhesives. *Procedia Engineering* 193: 423–430.

33 May, C.A. (1987). *Epoxy Resins: Chemistry and Technology*, 2e, 794. New York, NY: Marcel Dekker Inc.

34 Juan, Z. and Ye, L.G. (2015). Research on curing mechanism of bisphenol-A epoxy resin by DSC. In: *International Conference on Advances in Energy and Environmental Science*, 276–279. Atlantis Press.

35 Takeichi, T. and Furukwa, N. (2012). *Polymer Science: A Comprehensive Reference*, Material Science and Materials Engineering, vol. 5, 723–751.

36 Wang, M., Xu, X., Ji, J. et al. (2016). The hygrothermal aging process and mechanism of the novolac epoxy resin. *Composites Part B: Engineering* 107: 1–8.

37 Liu, J., Sun, Y., Wang, C. et al. (2019, 2019). Fabrication of monodisperse poly (allyl glycidyl ether-co-divinyl benzene) microspheres and their application in anion-exchange stationary phase. *Journal of Chromatography A* 1595: 91–96.

38 Chen, D., Kannan, K., Tan, H. et al. (2016). Bisphenol analogues other than BPA: environmental occurrence, human exposure, and toxicity – a review. *Environmental Science & Technology* 50: 5438–5453.

39 Bianchini, G. and Oldring, P.K.T. (1997). *Waterborne and Solvent Based Epoxies and Their End User Applications*. Chichester: Wiley.

40 May, C.A. (1988). *Epoxy Resins: Chemistry and Technology*, 2e. New York, NY: M. Dekker.

41 Petrie, E.M. (2006). *Epoxy Adhesive Formulations*, McGraw-Hill Chemical Engineering Series. New York, NY: McGraw-Hill.

42 Stevens, E.S. (2002). *Green Plastics: An Introduction to the New Science of Biodegradable Plastics*. Princeton, NJ: Princeton University Press.

43 American Chemistry Council (2015). *US Resin Production & Sales*. American Chemistry Council (ACC).

44 Nick, D.P. (2003). *The World of Epoxy Adhesives*. Philadelphia, PA: DPNA International Inc.

45 Kesarwani, P., Jahan, S., and Kesarwani, K. (2015). Composites: classification and its manufacturing process. *International Journal of Applied Research* 1 (9): 352–358.

46 Jahan, S., Kesarwani, K., and Kesarwani, P. (2015). Composites: classification and its manufacturing process. *Journal of Applied Research* 1: 352–358.

47 Kesarwani, K. (2015). Composites: classification and its manufacturing process. *Journal of Applied Research* 1: 352–358.

48 Rosato, D.V., Rosato, D.V., and Rosato, M.V. (2004). *Plastic Product Material and Process Selection Handbook*, 1e, 406–427. Kidlington, Oxford, UK: Elsevier.

49 Torres, M.V.L. (2014). *An Experimental Procedure for Reaction Injection Moulding – RIM – Materials Formulation Design*, 11–12. Universidad do Porto, Laboratory of Separation and Reaction Engineering.

50 Mason, K.F. (2006). Autoclave quality outside the autoclave. *Journal of High-Performance Composites* 14: 44–49.

51 Parnas, R. and Walsh, S. (2005). Vacuum assisted resin transfer molding model. *Journal of Polymer Composites* 26: 477–485.

52 Lund, J.Y. and Byrne, J.P. (2001). Leonardo Da Vinci's tensile strength tests-Implications for the discovery of engineering mechanics. *Journal of Civil Engineering and Environmental System* 18: 243–250.

53 Hindersmann, A. (2019). Confusion about infusion: an overview of infusion processes. *Composites Part A: Applied Science and Manufacturing* 126: 105583.

54 Beck, R.A.S., Arnold, J.O., Gasch, M.J., et al. (2012). Conformal ablative thermal protection system for planetary and human exploration missions. *9th International Planetary Probe Workshop*, Toulouse, France, 18–22 June.

55 Panerai, F., Ferguson, J.C., Lachaud, J. et al. (2017). Micro-tomography-based analysis of thermal conductivity, difusivity and oxidation behaviour of rigid and flexible-brous insulators. *International Journal of Heat and Mass Transfer* 108: 801–811.

56 Salonitis, K., Pandremenos, J., Paralikas, J., and Chryssolouris, G. (2010). Multifunctional materials engineering applications and processing challenges. *The International Journal of Advanced Manufacturing Technology* 49: 803–826.

57 Schubel, P.J., Crossley, R.J., Boateng, E., and Hutchinson, J.R. (2013). Review of structural health and cure monitoring techniques for large wind turbine blades. *Journal of Renewable Energy* 51: 113–123.

58 Konstantopoulos, S., Tonejc, M., Maier, A., and Schledjewski, R. (2015). Exploiting temperature measurements for cure monitoring of FRP composites – applications with thermocouples and infrared thermography. *Journal of Reinforcing Plastic Composites* 34: 1015–1026.

59 Srinivasagupta, D., Kardos, J., and Joseph, B. (2003). Rigorous dynamic model-based economic design of the injected pultrusion process with controllability considerations. *Journal of Composite Materials* 37: 1851–1880.

60 Shirude, S.R., Shambharkar, S.Y., Bhosale, H.B. et al. (2017). A survey on epoxy resins. *International Journal of Innovative Research and Science* 7 (6): 14861–14867.

61 Parbin, S., Waghmare, N.K., Sign, S.K., and Khan, S. (2019). Mechanical properties of natural fibre reinforced epoxy composites: a review. *Procedia Computer Science* 152: 375–379.

62 Alsagayar, Z., Rahmat, A., Arsad, A., and Mustapha, S.N.H. (2015). Tensile and flexural properties of montmorillonite nanoclay reinforced epoxy resin composites. *Advanced Materials Research* 1112: 373–376.

63 Kusmono, Wildan, M.W., and Mohd Ishak, Z.A. (2013). Preparation and properties of clay-reinforced epoxy nanocomposites. *International Journal of Polymer Science* 2013: 1–7.

64 Shokrieh, M.M., Kefayati, A.R., and Chitsazzadeh, M. (2012). Fabrication and mechanical properties of clay/epoxy nanocomposite and its polymer concrete. *Materials and Design* 40: 443–452.

65 Mirzataheri, M., Atai, M., and Mahdavian, A.R. (2010). Physical and mechanical properties of nanocomposite barrier film containing encapsulated nanoclay. *Journal of Applied Polymer Science* 118: 3284–3291.

66 Hesabi, M., Salimi, A., and Beheshty, M.H. (2019). Development of amine-based latent accelerator for one-pot epoxy system with low curing temperature and high shelf life. *European Polymer Journal* 112: 736–748.

67 Bekas, D.G., Hou, Y., Liu, Y., and Panesar, A. (2019). 3D printing to enable multifunctionality in polymer-based composites: a review. *Composites Part B: Engineering* 179: 107540.

68 Kasraie, S., Azarsina, M., Khamverdi, Z., and Shokraneh, F. (2012). Microleakage of dual-cured adhesive systems in class V composite resin restorations. *Journal of Dentistry* 9: 99–106.

69 Sugumar, S., Ghosh, V., Nirmala, M.J. et al. (2014). Ultrasonic emulsification of eucalyptus oil nanoemulsion: antibacterial activity against *Staphylococcus aureus* and wound healing activity in Wistar rats. *Ultrasonics Sonochemistry Journal* 21: 1044–1049.

70 Raghavan, J. (2009). Evolution of cure, mechanical properties, and residual stress during electron beam curing of a polymer composite. *Composites Part A: Applied Science and Manufacturing* 40 (3): 300–308.

3

Micro- and Nanoscale Structure Formation in Epoxy-Clay Nanocomposites

Seno Jose[1], V. K. Smitha[1], Sanjay M. Rangappa[2], Senthilkumar Krishnasamy[2], Debabrata Nandi[2], Suchart Siengchin[2], and Jyotishkumar Parameswaranpillai[3]

[1]Government College Kottayam, Department of Chemistry, Nattakom P O, Kottayam, Kerala 686 013, India
[2]Department of Mechanical and Process Engineering, The Sirindhorn International Thai–German Graduate School of Engineering (TGGS), King Mongkut's University of Technology North Bangkok, 1518 Pracharat 1 Road, Bangsue, Bangkok 10800, Thailand
[3]Center of Innovation in Design and Engineering for Manufacturing, King Mongkut's University of Technology North Bangkok, Bangkok, Thailand

3.1 Introduction

Epoxy resin is the most widely used thermosetting polymer matrix for the development of high-performance composites for structural applications in aerospace, automotive, and construction [1–3]. However, the inherent brittleness and poor damage tolerance of cured epoxy resins restrict their wide range applications. The toughness can be improved by conventional blending with functionalized liquid rubbers [4–6] or thermoplastics [7–9], or by creating nanoscale structural inhomogeneities through self-assembly [10–15] and reaction-induced phase separation [16–21] by the incorporation of block copolymers, but in most cases, compromising the strength and/or modulus.

The discovery of lightweight nylon 6/clay nanocomposites with excellent tensile strength and modulus by researchers at Toyota Central Research and Development Laboratories in 1993 inspired scientists to develop polymer matrix nanocomposites for advanced engineering applications [22, 23]. In the following year, Lan and Pinnavaia [24], in their pioneering work on clay-reinforced epoxy nanocomposites, reported that the mechanical properties of the composites depend on the nature, amount, and alignment of the nanoparticles. Other researchers also reported similar improvements in mechanical properties in epoxy-clay composites in the same year [25–27]. For the last two decades, extensive studies have been conducted by researchers to develop epoxy-based polymer nanocomposites for advanced structural applications.

The type, size, shape, amount, functionalization, and other properties of reinforcements, in addition to the inherent properties of the resin, curing agent, the

Epoxy Composites: Fabrication, Characterization and Applications,
First Edition. Edited by Jyotishkumar Parameswaranpillai, Harikrishnan Pulikkalparambil, Sanjay M. Rangappa, and Suchart Siengchin.

modifier, processing variables, have a decisive impact on the micro-and nanoscale structures, and thereby the ultimate properties of the developed composites. This offers the researchers a huge opportunity to tailor-specific properties of the reinforcements to meet required applications and therefore to develop different price/performance characteristics and the maximum diversification of properties of the final products. This instigates tremendous academic and industrial interests worldwide among researchers, and epoxy-based polymer nanocomposites gained significant commercial growth in the last decade. Moreover, lightweight, good strength, cost-effectiveness, and easy processability make epoxy-based nanocomposites a potential candidate for several industrial applications. Furthermore, the epoxy-based polymer nanocomposites could meet the needs of a wide range of demanding forms of applications in aerospace, automobile, marine, electronic, construction, coating, packaging, and biomedical industries [28–43].

This chapter reviews the highlights of important research findings of recent investigations on the development of micro- and nanoscale structural features of epoxy-based polymer nanocomposites. Although there is a large volume of published studies on epoxy-based polymer nanocomposites, to make this chapter concise and comprehensive, we restrict our focus mainly on epoxy-based nanocomposites containing nanoclays. Furthermore, the chapter seeks to elucidate the proposed mechanism of exfoliation of nanoclays in the epoxy matrix.

3.2 Micro and Nanoscale Structures of Polymer/Clay Nanocomposites

The clay particles retain their aggregated state in the matrix, if the polymer chains cannot diffuse into the intra-gallery space. This leads to a conventional composite (Figure 3.1a). However, depending on the interaction of polymer chains and silicate layers, either intercalated or exfoliated nanocomposites are generated [46]. The interaction may be visualized in terms of the degree of separation of the clay layers, known as d spacing. The intercalated nanocomposite, where the polymer molecules are inserted in a crystallographically regular manner into the clay structure, has a d spacing of 2–3 nm [47, 48]. The hydroxylated edge–edge interactions of silicate layers sometimes result in the intercalated and flocculated nanocomposite, where the d spacing is between 3 and 8 nm [49, 50]. In the exfoliated or delaminated

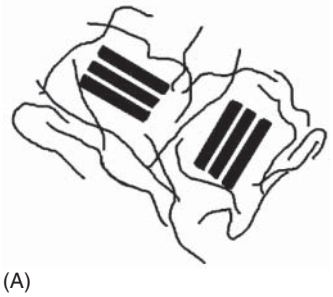

(A)

Figure 3.1 Different types of polymer clay composites [44, 45]. (A) Phase separated microcomposite. (B) Schematic of intercalated, intercalated-and-flocculated and exfoliated clay nanocomposites. Source: Suprakas Sinha et al. [44]. Copyright 2003, American Chemical Society. (C) Schematic of completely exfoliated and homogeneously dispersed clay platelets in the polymer matrix. Source: Fischer [45]. © 2003, Elsevier.

(a) Intercalated (b) Intercalated-and-flocculated (c) Exfoliated

(B)

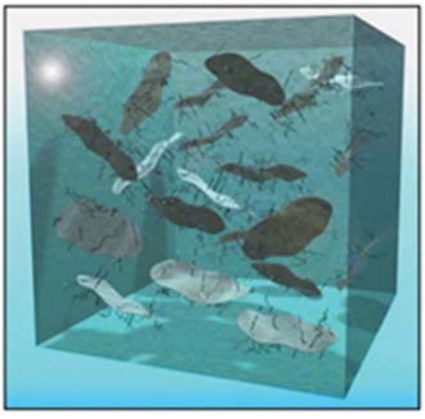

(C)

Figure 3.1 (*Continued*)

nanocomposite, the individual clay layers are separated and have a d spacing greater than 8 nm [46–51]. Figure 3.1b displays the different types of polymer nanocomposites – intercalated, intercalated and flocculated, and exfoliated nanocomposites [44, 46, 52]. Figure 3.1c displays the schematic representation completely exfoliated and homogeneously dispersed clay platelets in the polymer matrix [45].

Microscopic techniques (scanning electron microscopy (SEM), transmission electron microscopy (TEM), atomic force microscopy (AFM) and X-ray powder diffraction (XRD)) are used to study the distribution of nanoclay in the polymer matrix [53–59]. Optimization of the intensity, position, and shape of the basal reflection resulting from the clay nanoparticles dispersed in the polymer matrix helps to analyze the structure of the nanocomposites by XRD. In the intercalated structure, a shift in (001) peak to a lower 2θ is observed. On the other hand, in the exfoliated structure, a complete disappearance of (001) peak is observed. However, attention should be paid to the fact that the disappearance of the (001) peak may be attributed to the misalignment of sample holders, wrong slit setting or orientation, or by the resolution limitations of XRD instrument [55]. Figure 3.2 shows the XRD pattern of (a) microcomposite, (b) intercalated, and (c) exfoliated nanocomposite [54]

The TEM can provide an insight into the distribution of nanoclay layers. The TEM images of the interacted nanocomposites contain randomly distributed ordered stalks of layers, whereas the exfoliated nanocomposites exhibit homogeneously

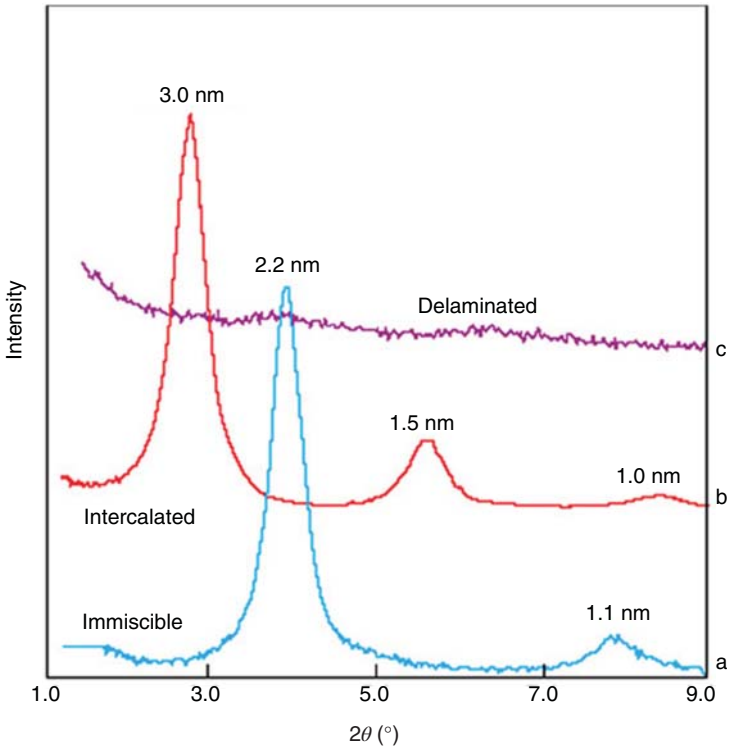

Figure 3.2 The XRD pattern of micro and nanocomposites. Source: Giannelis et al. [54]. © 1999, Springer Nature.

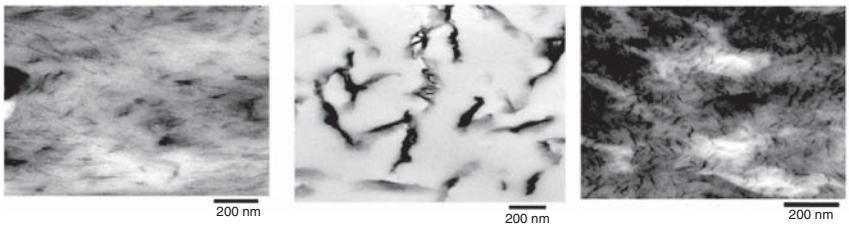

Figure 3.3 The TEM images of (a) intercalated (b) intercalated-and-flocculated, (c) and exfoliated polymer nanocomposites. Source: Delogu et al. [59]. © 2017, Elsevier.

dispersed clay layers in the polymer matrix. However, in most cases, nanocomposites show a mixture of intercalated and exfoliated structures. Figure 3.3 shows the TEM images of intercalated, intercalated and flocculated, and exfoliated nanocomposites [59].

The Fourier-transform infrared spectroscopy (FTIR) and NMR spectroscopic techniques too have been used by researchers to elucidate the structure of nanocomposites [60–63]. The former has been used to explain the bonding

characteristics such as hydrogen bonding and non-bonding interactions, whereas the latter provides an insight into the morphology and the exfoliation dynamics of the nanocomposites. In addition, the differential scanning calorimetry (DSC), the dynamic mechanical thermal analysis (DMTA), and the small-angle X-ray scattering (SAXS) could be used to evaluate the structure and performance of the nanocomposites [64–67]. Rao and Pochan [66] reported that the strong interfacial interactions between the polymer chains and the nanoclay reduce the polymer matrix mobility so that the structure of clay nanocomposites becomes analogous to that of semi-crystalline polymers, where the intercalated clay phase may act as a crystalline phase. This will enhance mechanical and thermal properties. Drummy et al. [67] studied the morphology of clay particles in an epoxy matrix by combining the SAXS and electron tomography.

3.3 Evolution of Epoxy-Clay Nanocomposite Structure

The cost-effectiveness, transparency, and strength make the 2D layered silicate clays an excellent nanoreinforcement for polymer matrices [68]. Among the different types of clay, montmorillonite, a soft layered clay silicate with an average particle size of 1 μm, the specific surface area of c. 800 m^2/g, and the interlamellar gallery thickness of c. 0.80 nm, is the most popular one [48, 49, 69, 70]. Belonging to a 2 : 1 phyllosilicate family, its ability to exhibit extensive interlayer expansion in conjunction with low cost makes it special among the clays belonging to the trimorphic smectite family [35]. However, due to its intrinsic hydrophilicity, the use of compatibilizing agents such as alkyl ammonium ions [71, 72] or silane coupling agents [73–76] is preferred. The compatibilizing agents create a hydrophobic surface and cause the expansion of interlayer distance which enables the diffusion of polymer chain into the intra-galleries and is indispensable to overcome its natural propensity for agglomeration, to achieve a better dispersion [77], and to facilitate favorable interfacial interactions [78, 79] for optimum reinforcement. The interlayer distance depends on the orientation of onium ions between the clay layers. It is the charge density of the clay that determines the orientation of onium ions – which may be a monolayer parallel to the clay surface, a lateral bilayer, a pseudo-trilayer, or paraffin structure [53, 80]. Figure 3.4 displays the different types of orientation of onium ions between the clay layers.

The preparation of epoxy-clay nanocomposites involves the dispersion of modified layered silicate in the epoxy matrix in the absence or presence of an appropriate solvent, followed by the cure reaction. In this approach, the modified nanoclay is swollen by the resin molecules that migrate into the silicate galleries where curing happens. This is technically referred to as “in situ intercalative polymerization.” The mechanical stirring [81, 82], ultrasonication [72, 83–87], high shear mixing [88, 89], ball milling [90, 91], and high-pressure mixing [92–94] are the most commonly employed dispersion methods. Many researchers used the slurry compounding technique for the preparation of epoxy-based clay-containing nanocomposites [95–99]. The frontal polymerization process is another effective method for the

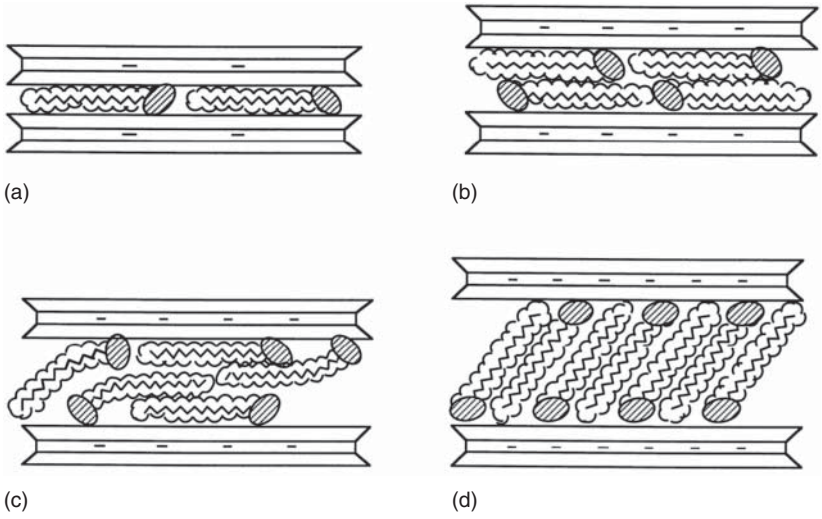

Figure 3.4 Different types of orientation of onium ions between clay layers: (a) monolayer, (b) bilayer, (c) pseudo-trilayer, and (d) paraffin structure. Source: Reprinted with permission from LeBaron et al. [53]. © 1999, Elsevier.

preparation of epoxy-clay nanocomposites [100, 101]. Li et al. [102, 103] proposed a method known as "nanodisassembling" for the preparation of exfoliated clay epoxy nanocomposites.

Numerous studies have shown that the type of curing agents, the nature of clay modifier, the resin type, nanoclay content, processing techniques, and several other factors independently or concomitantly affect the phase structure of epoxy-clay nanocomposites. For instance, the exfoliation ability of the organoclay depends on its catalytic effect on the curing, miscibility with the curing agent, cation exchange capacity (CEC), and the penetrability of the curing agent into the clay layers. Researchers have shown that the use of an amine-based curing agent results in an intercalated morphology, whereas an anhydride-based curing agent leads to an exfoliated phase structure [104, 105]. The diffusion rate and reactivity of curing agents are also critical parameters [106, 107].

The CEC, which determines the amount of surfactant that can be intercalated between the silicate layers, is another crucial parameter. For instance, Kornmann et al. [108] have reported that the clay modifier with a low CEC tends to increase the rate of intra-gallery polymerization of epoxy molecules and thus favors the formation of exfoliated clay structure. They opined that the large amount of space available between the silicate layers causes the diffusion of epoxy molecules into the clay galleries to undergo homopolymerization during the swelling phase. It is found that primary and secondary alkyl ammonium ions have greater Bronsted acidity which favors a greater rate of epoxy polymerization at intra-gallery space, which in turn favors the generation of exfoliated phase structure. The tendency of protonated or functionalized compatibilizer to catalyse intra-gallery polymerization of epoxy molecules enhances the d spacing [109].

Messersmith and Giannelis [25] have shown that at room temperature, a mix of intercalated and unintercalated structure is obtained for epoxy-clay nanocomposites, and as the curing temperature increased to 90 °C, the extent of intercalation improved. Moreover, these authors observed intercalated structures with diamine curing agents and exfoliated structures with other curing agents. Ratna et al. [110] have reported that the polarity of the epoxy/hardener mixture plays a vital role in the development of microstructures and thereby has remarkable impact on the ultimate properties of epoxy-clay nanocomposites. Pinnavaia and coworkers [111–113] reported that the greater chain length of the modifier favors exfoliation. It is observed that the catalytic influence of alkyl ammonium ion modifier on the curing of epoxy has an impact on the nanocomposite structure [112]. These authors opined that alkyl chains shorter than eight carbon atoms in the modifier leads to intercalated nanocomposites. Similarly, although an increase in clay content may increase the d spacing until exfoliation happens, it may change an exfoliated structure to the intercalated.

Several researchers have reported on the effects of processing techniques and variables on the micro- and nanoscale structures of the epoxy-clay composites [87, 92, 93, 95, 96, 114–120]. For instance, Liu et al. [92] have demonstrated that a better dispersion has been achieved by using "high-pressure process" in the presence of a solvent, whereas Vaia and coworkers [117] have reported that high shear forces facilitate homogenization of the nanoclay. Bashar et al. [120] have found that the nanoclay dispersion technique has significant impact on the nanocomposite structure – the ultrasonication leads to partially exfoliated structure, whereas the mechanical dispersion leads to intercalated and phase-separated structure. In the light of these studies, it is conceivable that high shear mixing, ultrasonication or combination of both, and slurry compounding predominantly favor exfoliated phase structure. Furthermore, the studies established that the processing variables and the nanoclay concentration should be optimized to accomplish an exfoliated nanocomposite structure with balanced end-use property. In a recent study, Gajjela et al. [121] have reported that the aspect ratio, shape, interphase thickness, and stiffness of clay particles have significant impact on the properties of nanocomposites. Very recently, Tomic et al. [122] have used a commercial multifunctional fatty acid both as a curing agent and clay modifier for epoxy-clay nanocomposites.

Hackman and Hollaway [123] reported that although resins with lower viscosity favor faster pre-intercalation, the resin component has no appreciable effect on the exfoliation of clay. Le Pluart et al. [124] argued that the quality of clay dispersion could be improved by the curing of epoxy resin. Thus, the evolution of nanocomposite structure involves a complex interplay of several parameters such as method of preparation, processing techniques, inherent properties of resin, curing agent, and nanoclay modifier. Even the slight variation in any of these factors reflect the developed morphology of the composites.

3.4 Mechanism of Nanocomposite Formation

Over the past few decades, there have been a number of research findings and conceptual evolutions to explore the molecular-level mechanism of polymer/clay

nanocomposite formation. In the light of these studies, it can be argued that the most crucial step during the development of polymer/clay nanocomposites is the process of exfoliation of nanoclay in the polymer matrix. Very recently, Zhu et al. [125] have reviewed the recent scientific advances in the methods of exfoliation such as in situ exfoliation, solution exfoliation, and melt exfoliation. The epoxy-clay nanocomposite formation involves the in situ polymerization where the nanocomposite formation occurs by the diffusion of the monomers and/or polymer chains into interlayer galleries of the layered silicate. It is important to consider the enthalpic (ΔH) and entropic (ΔS) contributions toward the negative free energy change (ΔG) associated with the spontaneous intercalation of polymer chains which leads to nano dispersion. Note that the entropic loss due to the polymer confinement is more or less compensated by an entropic increase of the desorbed molecules in the clay galleries. It turns out that the enthalpic contribution is the decisive part.

Pinnavaia and coworker [126] have shown that alkyl primary ammonium ion modifier, with the catalytic ability, due to availability of hydrogen on the ammonium groups, could effectively enhanced the intra-gallery reaction rate whereas alkyl quaternary ammonium ions could not. Brown et al. [127], on the other hand, have demonstrated that hydroxyl-substituted quaternary ammonium modifier has both catalytic functionalities and improves the miscibility with epoxy system. Balazs et al. [128, 129] have predicted that a large degree of polymerization and a negative value for the Flory–Huggins interaction parameter between the polymer and the clay would result in an intercalated nanocomposite. On the other hand, since exfoliation occurs by the complete separation of clay platelets by the polymer chains, it is desirable for the polymer to possess a segment that has affinity to the clay surface. It turns out that the polarity of the resin molecules tends them to diffuse in to the interlayer galleries where the surface energy is high. However, the curing that occurs outside the clay galleries increases the viscous forces and inhibits the migration of resin molecules into the interlayer galleries.

Lan et al. [112] used alkyl ammonium ions adequately acidic to catalyze the polymerization reaction and to regulate the balance and observed that the chain length and Bronsted acidity of onium ions, cure temperature, and the clay layer charge density have significant effects. They opined that the swelling of the clay by the resin molecules initially controls the polymerization, and the presence of long-chain onium ions provides a hydrophobic environment to migrate the curing agent and facilitate intergallery polymerization at a faster rate. This expands the intergallery space and realize the exfoliation. However, the lower or higher cure temperature tends to decrease the rate of intergallery reaction, and consequently the intercalation process, which leads to an intercalated nanocomposite. This signifies the optimum cure conditions that balance the rates of intra- and extra-gallery reactions. The authors also found that short chain onium ions fail to create the so-called "balance" of reactions as they restrict the migration of curing agent. Another critical parameter, according to the authors, is the Bronsted acidity of the onium ions. For achieving the same rate for initial swelling (as C_{18}), keeping the chain length constant, they used onium ions of different Bronsted acidity and found

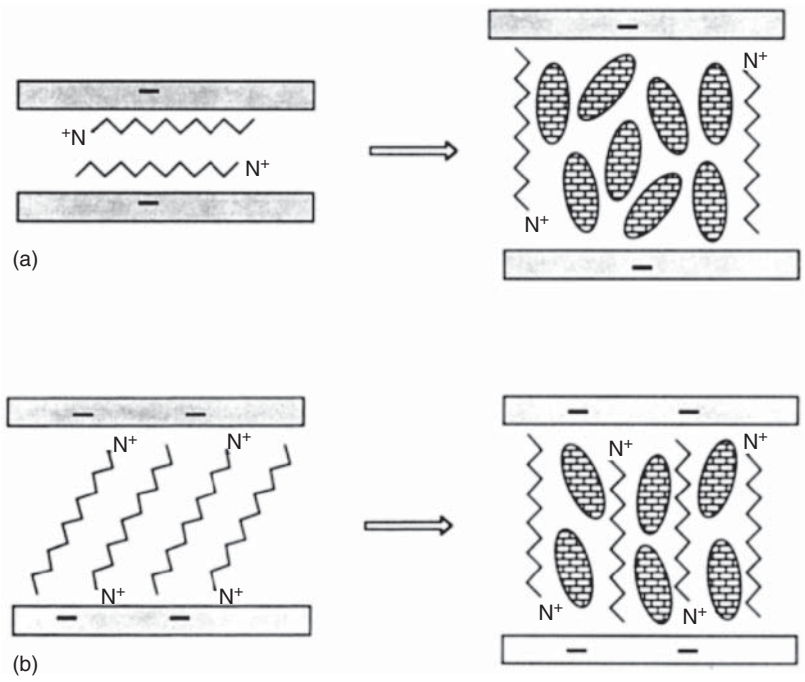

Figure 3.5 Mechanism of swelling of alkyl ammonium exchanged clay system by epoxy resins (a) low charge density clay with a bilayer structure and (b) high charge density clay with a paraffin structure. Source: Lan et al. [112]. Copyright 2002 American Chemical Society.

that primary and secondary onium ions ($C_{18}H_{37}NH_3^+$ and $C_{18}H_{37}(CH_3)NH_2^+$) generate exfoliate nanocomposite, whereas tertiary and quaternary onium ions ($C_{18}H_{37}(CH_3)_2NH^+$ and $C_{18}H_{37}(CH_3)_3N^+$) produce intercalated nanocomposite. Besides that, they claimed that irrespective of the initial charge density and orientation of the gallery onium ions, upon solvation with resin molecules, adopt a vertical orientation with epoxy resin molecules inserted between the onium ions as schematically represented in Figure 3.5. It turns out that there should be sufficient resin molecules and curing agents to realize the intra-gallery polymerization which leads to exfoliation.

Chen et al. [130] proposed a three-stage mechanism for the exfoliation clay layers in epoxy/organoclay nanocomposites. The first stage is the "intra-gallery polymerization induced interlayer expansion." The second stage is the steady increase in the interlayer spacing. The third stage is the cessation of the interlayer expansion. This happens when the modulus of the extra-gallery polymer slowly exceeds the modulus of the intra-gallery polymer. Recently, Ying et al. [131] have investigated the highly exfoliated structure of epoxy-clay nanocomposites prepared by "acetone-clay slurry compounding" and proposed a five-stage exfoliation process of nanoclay in epoxy composites as shown in Figure 3.6. The authors observed that the exfoliation had occurred prior to curing and argued that the significant increase of the

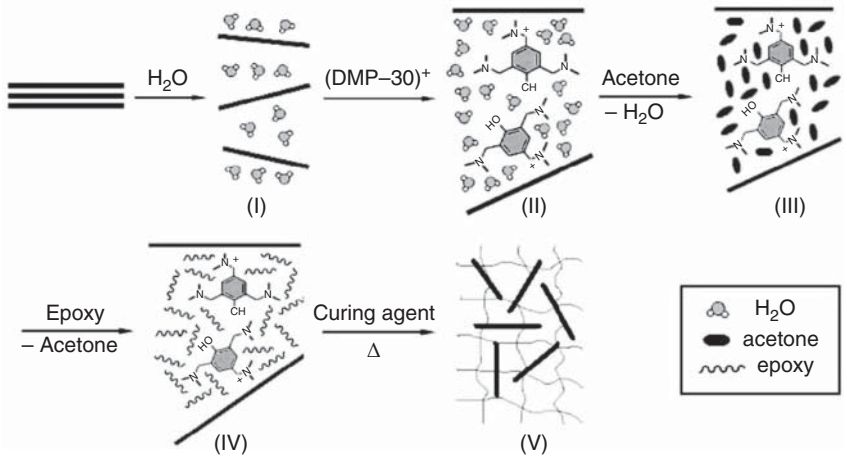

Figure 3.6 The schematic illustration of exfoliation of nanoclay in epoxy matrix. Source: Ying et al. [131]. © 2015, Elsevier.

glass transition temperature of the nanocomposite in comparison to the neat resin is attributed to the highly exfoliated structure and the strong interfacial interactions between the clay platelets and the epoxy matrix.

Camino et al. [132] have shown that the generation of intercalated or exfoliated structures depends on the competition between extra-gallery and intra-gallery polymerization, which in turn depends on the catalytic polymerization activity of the organic modifier rather than the diffusion of the resin molecules into the interlayer space. Generally, an exfoliated epoxy-clay nanocomposite can be created in two steps: loading the clay gallery with onium ions and expanding the gallery region with a mixture of resin and curing agent. Pinnavaia and coworkers [133] have also shown that the homostructured mixed inorganic–organic-ion clays prepared by substituting a fraction of the organic cation exchange sites with inorganic cations can dramatically reduce the amount of organic modifier and are a potential candidate for the preparation of polymer-exfoliated clay nanocomposites.

Park and Jana [134] proposed a mechanism of exfoliation on the basis of two countering forces generated during the intra- and extra-gallery polymerizations of epoxy molecules. During curing, due to entropic reasons, the cross-linked epoxy polymers have an inherent tendency for recoiling. However, the adjacent layers of clay particles, holding the growing polymer chains within them, have a natural tendency to resist the recoiling process. During fast curing, the polymer chains get little time for stress relaxation, and consequently store more elastic energy. This elastic force tends to push the clay layers apart, which leads to an exfoliated structure. The viscous force developed due to extra-gallery polymerization of epoxy molecules, on the other hand, tends to counter the "elastic force induced pushing" of the clay layers. In short, according to these authors, a competition between two simultaneously operating opposing forces – the combined viscous force and attractive forces, and the elastic force – determines the exfoliation. If the elastic force outweighs the former, exfoliation happens. But, if the former wins the battle, the result is intercalated

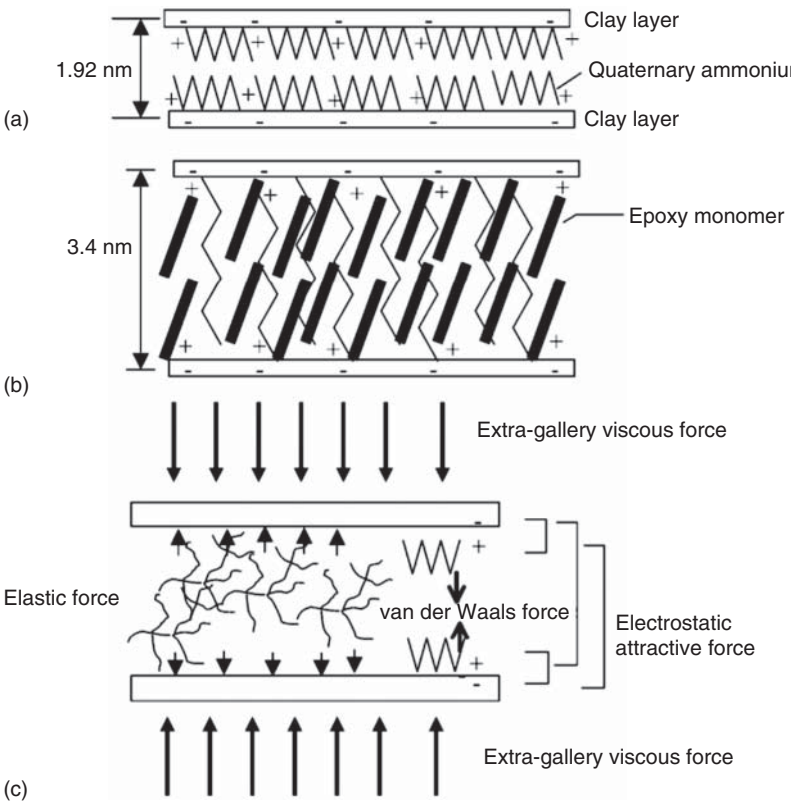

Figure 3.7 Mechanism of intercalation and exfoliation process (a) organically modified clay, (b) epoxy intercalated state, and (c) forces acting on a two-particle tactoid. Source: Park and Jana [134]. Copyright 2003 American Chemical Society.

nanocomposite. The proposed mechanism of developing nanocomposite structures is shown in Figure 3.7.

Tolle and Anderson [135] have shown that the interaction between the modified nanoclay and the resin prior to polymerization may play a crucial role in the development of nanocomposite structure. These authors, by performing in situ synchrotron SAXS studies, have demonstrated that the mixing of clay with epoxy resin, before adding the curing agent (pre-conditioning process), changes the intercalated structure to exfoliated and less exfoliated structure to more expanded exfoliated structure. Hutchinson et al. [136] confirmed this observation by adopting different methods for the preparation of epoxy resin/clay mixtures, before adding the curing agent.

Lin and coworkers [137] have investigated the mechanism of "organo-clay initiated silicate platelet self-organization" and observed that the resin molecules in the intra-gallery space underwent a synchronized mechanism involving clay-tethered epoxy self-polymerization, silicate pushing, and end cross-linking. These processes helped the clay layers to increase the d spacing beyond the XRD detection limit. The lamellar structure with d spacing of 36–96 nm was observed from the TEM image. Figure 3.8 shows randomly distributed clay platelets.

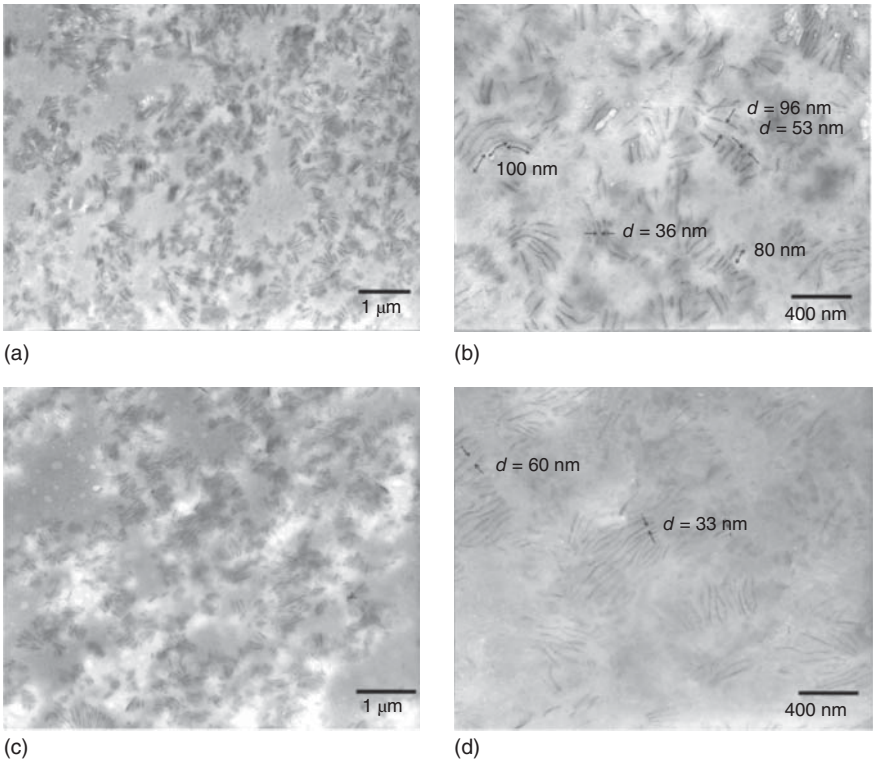

Figure 3.8 TEM images of epoxy/MMT (montmorillonite) nanocomposites with different clay content ((a, b) 3 wt% and (c, d) 10 wt% of MMT). Source: Reprinted with permission from Chan et al. [137].

3.5 Conclusion and Future Outlook

The discovery of lightweight high-performance polymer–clay nanocomposites by researchers at Toyota Central Research and Development Laboratories in 1993 instigates scientists to develop polymer matrix nanocomposites suitable for advanced engineering applications. Subsequently, there have been extensive research explorations on the nanoscale structural features and the conceptual evolution of the mechanism of polymer nanocomposites. The in situ intercalative polymerization is the most important method for the fabrication of epoxy-clay nanocomposites. The generation of final nanocomposite structure depends on a number of factors from the nature of the resin, the curing agent, the clay, and the modifier to the processing techniques and conditions. These factors independently or concomitantly influence the structure of nanocomposites. Since a complex interplay of several parameters and energy and entropic contributions simultaneously operating, it is extremely difficult to propose a generalized molecular level mechanism for the evolution of final nanocomposite structure. In the light of numerous research findings, it is conceivable that the most crucial step during the development of epoxy-clay nanocomposites is the process of exfoliation of nanoclay in the polymer matrix.

A balance of intra- and extra-gallery polymerizations and judiciously optimized cure conditions are the most important factors that determine the exfoliation and homogenous dispersion of nanoclay in the epoxy matrix, and even slight variations in the interface and interphase regions may change this balance, and thereby cause the differences in final nanocomposite structure.

Though the literature provides numerous research findings in this direction, there remains a number of unresolved and unsettled issues. A complete exfoliation with homogeneous dispersion of nanoclay in the epoxy matrix is challenging. A perfect correlation between the nanostructure and the end-use properties has not yet been achieved. A generalized mechanism by unifying various structural features of the resin, the curing agent, the nanoclay and the modifier, and the important molecular and thermodynamic parameters involved in the process of exfoliation is desirable. Finally, the motto, "progress through protecting the environment" is of great importance. The invention of "greener methods" for the exfoliation and nano dispersion of clay in the epoxy matrix and thereby the fabrication of "green epoxy-clay nanocomposites" is the need of the age and the responsibility of researchers.

References

1 Miracle, D.B. and Donaldson, S.L. (eds.) (2001). *ASM Handbook: Composites*, vol. 21. Materials Park, OH: ASM International.

2 Bagheri, R., Marouf, B.T., and Pearson, R.A. (2009). Rubber-toughened epoxies: a critical review. *Polymer Reviews* 49: 201–225.

3 Pethrick, R.A. (2014). Applications of toughened epoxy resins. In: *Micro and Nanostructured Epoxy/Rubber Blends*, Chapter 17 (eds. S. Thomas, C. Sinturel and R. Thomas), 339–362. Weinheim: Wiley.

4 Chikhi, N., Fellahi, S., and Bakar, M. (2002). Modification of epoxy resin using reactive liquid (ATBN) rubber. *European Polymer Journal* 38: 251–264.

5 Mathew, V.S., Jyotishkumar, P., George, S.C. et al. (2012). High performance HTLNR/epoxy blend – phase morphology and thermo-mechanical properties. *Journal of Applied Polymer Science* 125: 804–811.

6 Mathew, V.S., George, S.C., Parameswaranpillai, J., and Thomas, S. (2014). Epoxidized natural rubber/epoxy blends: phase morphology and thermomechanical properties. *Journal of Applied Polymer Science* 131 (4) https://doi.org/10.1002/app.39906.

7 Hourston, D.J. and Lane, J.M. (1992). The toughening of epoxy resins with thermoplastics: 1. Trifunctional epoxy resin-polyetherimide blends. *Polymer* 33: 1379–1383.

8 Hodgkin, J.H., Simon, G.P., and Varley, R.J. (1998). Thermoplastic toughening of epoxy resins: a critical review. *Polymers for Advanced Technologies* 9 (1): 3–10.

9 Pearson, R.A. and Yee, A.F. (1993). Toughening mechanisms in thermoplastic-modified epoxies: 1. Modification using poly(phenylene oxide). *Polymer* 34: 3658–3670.

10 Dean, J.M., Verghese, N.E., Pham, H.Q., and Bates, F.S. (2003). Nanostructure toughened epoxy resins. *Macromolecules* 36 (25): 9267–9270.

11 Thio, Y.S., Wu, J., and Bates, F.S. (2006). Epoxy toughening using low molecular weight poly(hexylene oxide)–poly(ethylene oxide) diblock copolymers. *Macromolecules* 39 (21): 7187–7189.

12 Liu, J., Thompson, Z.J., Sue, H.J. et al. (2010). Toughening of epoxies with block copolymer micelles of wormlike morphology. *Macromolecules* 43 (17): 7238–7243.

13 Wu, S., Guo, Q., Peng, S. et al. (2012). Toughening epoxy thermosets with block ionomer complexes: a nanostructure–mechanical property correlation. *Macromolecules* 45 (9): 3829–3840.

14 Cano, L., Builes, D.H., and Tercjak, A. (2014). Morphological and mechanical study of nanostructured epoxy systems modified with amphiphilic poly(ethylene oxide-b-propylene oxide-b-ethylene oxide) triblock copolymer. *Polymer* 55 (3): 738–745.

15 Jose, S., George, S.M., and Parameswaranpillai, J. (2016). Introduction to epoxy/block-copolymer blends. In: *Handbook of Epoxy Blends* (eds. J. Parameswaranpillai, N. Hameed, J. Pionteck and E. Woo), 827–839. Springer International Publishing. ISBN: 978-3-319-18158-5.

16 Xu, Z. and Zheng, S. (2007). Reaction-induced microphase separation in epoxy thermosets containing poly(ε-caprolactone)-*block*-poly(*n*-butyl acrylate) diblock copolymer. *Macromolecules* 40 (7): 2548–2558.

17 Yang, X., Yi, F., Xin, Z., and Zheng, S. (2009). Morphology and mechanical properties of nanostructured blends of epoxy resin with poly(ε-caprolactone)-block-poly(butadiene-co-acrylonitrile)-block-poly(ε-caprolactone) triblock copolymer. *Polymer* 50 (16): 4089–4100.

18 George, S.M., Puglia, D., Kenny, J.M. et al. (2013). Morphological and mechanical characterization of nanostructured thermosets from epoxy and styrene-block-butadiene-block-styrene triblock copolymer. *Industrial & Engineering Chemistry Research* 52 (26): 9121–9129.

19 Heng, Z., Chen, Y., Zou, H., and Liang, M. (2015). Simultaneously enhanced tensile strength and fracture toughness of epoxy resins by a poly(ethylene oxide)-block-carboxyl terminated butadiene-acrylonitrile rubber dilock copolymer. *RSC Advances* 5 (53): 42362–42368.

20 Parameswaranpillai, J., Sidhardhan, S.K., Harikrishnan, P. et al. (2017). Morphology, thermo-mechanical properties and surface hydrophobicity of nanostructured epoxy thermosets modified with PEO-PPO-PEO triblock copolymer. *Polymer Testing* 59: 168–176.

21 Parameswaranpillai, J., Krishnan Sidhardhan, S., Jose, S. et al. (2017). Reaction-induced phase separation and resulting thermomechanical and surface properties of epoxy resin/poly(ethylene oxide)–poly(propylene oxide)–poly(ethylene oxide) blends cured with 4,4′-diaminodiphenylsulfone. *Journal of Applied Polymer Science* 134 (4): 44406.

22 Usuki, A., Kojima, Y., Kawasumi, M. et al. (1993). Synthesis of nylon 6-clay hybrid. *Journal of Materials Research* 8 (5): 1179–1184.

23 Kawasumi, M. (2004). The discovery of polymer-clay hybrids. *Polymer Chemistry* 42: 819–824.

24 Lan, T. and Pinnavaia, T.J. (1994). Clay-reinforced epoxy nanocomposites. *Chemistry of Materials* 6: 2216–2219.

25 Messersmith, P.B. and Giannelis, E.P. (1994). Synthesis and characterization of layered silicate-epoxy nanocomposites. *Chemistry of Materials* 6 (10): 1719–1725.

26 Lan, T., Kaviratna, P.D., and Pinnavaia, T.J. (1994). Synthesis, characterization and mechanical properties of epoxy–clay nanocomposites. *Polymeric Materials Science and Engineering* 71: 527.

27 Kaviratna, P.D., Lan, T., and Pinnavaia, T.J. (1994). Synthesis of polyether - clay nanocomposites: kinetics of epoxy- self polymerization in acidic smectite clay. *Polymer Preprints* 35: 788–789.

28 Bhattacharya, S.K. and Tummala, R.R. (2001). Integral passives for next generation of electronic packaging: application of epoxy/ceramic nanocomposites as integral capacitors. *Microelectronics Journal* 32 (1): 11–19.

29 Yang, J.M., Shih, C.H., Chang, C.N. et al. (2003). Preparation of epoxy–SiO_2 hybrid sol–gel material for bone cement. *Journal of Biomedical Materials Research Part A* 64 (1): 138–146.

30 Campbell, S.G. and Johnston, C. (2004). Polymer/Silicate Nanocomposites Used to Manufacture Gas Storage Tanks with Reduced Permeability. *NASA Glenn's Research and Technology reports,* 20050192250.

31 Mittal, V. (2008). Epoxy—vermiculite nanocomposites as gas permeation barrier. *Journal of Composite Materials* 42 (26): 2829–2839.

32 Wang, X.F., Hu, Y.C., Li, Y.P., and Zhou, Q. (2010). Preparation of epoxy/montmorillonite nanocomposite coating and its application in the high-temperature oil–gas environment with H_2S. *Advanced Materials Research* 154–155: 508–514.

33 Wen, L.E., Tao, Y.A., Kao-jiang, W.A. et al. (2010). Preparation and characterization of bio-adhesive by modifying soy protein isolate with epoxy resin. *Soybean Science* 1.

34 Sancaktar, E. and Kuznicki, J. (2011). Nanocomposite adhesives: mechanical behavior with nanoclay. *International Journal of Adhesion and Adhesives* 31 (5): 286–300.

35 Azeez, A.A., Rhee, K.Y., Park, S.J., and Hui, D. (2013). Epoxy clay nanocomposites–processing, properties and applications: a review. *Composites Part B: Engineering* 45 (1): 308–320.

36 Mostafaei, A. and Nasirpouri, F. (2013). Preparation and characterization of a novel conducting nanocomposite blended with epoxy coating for antifouling and antibacterial applications. *Journal of Coatings Technology and Research* 10 (5): 679–694.

37 Guo, H., Sheng, H., Peng, X. et al. (2014). Preparation and mechanical properties of epoxy/diamond nanocomposites. *Polymer Composites* 35 (11): 2144–2149.

38 Barua, S., Dutta, N., Karmakar, S. et al. (2014). Biocompatible high performance hyperbranched epoxy/clay nanocomposite as an implantable material. *Biomedical Materials* 9 (2): 025006.

39 Monetta, T., Acquesta, A., and Bellucci, F. (2015). Graphene/epoxy coating as multifunctional material for aircraft structures. *Aerospace* 2 (3): 423–434.

40 Atta, A.M., El-Saeed, A.M., El-Mahdy, G.M., and Al-Lohedan, H.A. (2015). Application of magnetite nano-hybrid epoxy as protective marine coatings for steel. *RSC Advances* 5 (123): 101923–101931.

41 Jouyandeh, M., Moini Jazani, O., Navarchian, A.H., and Saeb, M.R. (2016). High-performance epoxy-based adhesives reinforced with alumina and silica for carbon fiber composite/steel bonded joints. *Journal of Reinforced Plastics and Composites* 35 (23): 1685–1695.

42 Vahabi, H., Gholami, F., Karaseva, V. et al. (2017). Novel nanocomposites based on poly(ethylene-co-vinyl acetate) for coating applications: the complementary actions of hydroxyapatite, MWCNTs and ammonium polyphosphate on flame retardancy. *Progress in Organic Coatings* 113: 207–217.

43 Aradhana, R., Mohanty, S., and Nayak, S.K. (2018). High performance epoxy nanocomposite adhesive: effect of nanofillers on adhesive strength, curing and degradation kinetics. *International Journal of Adhesion and Adhesives* 84: 238–249.

44 Sinha Ray, S., Okamoto, K., and Okamoto, M. (2003). Structure–property relationship in biodegradable poly(butylene succinate)/layered silicate nanocomposites. *Macromolecules* 36 (7): 2355–2367.

45 Fischer, H. (2003). Polymer nanocomposites: from fundamental research to specific applications. *Materials Science and Engineering: C* 23 (6–8): 763–772.

46 Alexandre, M. and Dubois, P. (2000). Polymer-layered silicate nanocomposites: preparation, properties and uses of a new class of materials. *Materials Science & Engineering R: Reports* 28 (1–2): 1–63.

47 Giannelis, E.P. (1996). Polymer layered silicate nanocomposites. *Advanced Materials* 8 (1): 29–35.

48 Pavlidou, S. and Papaspyrides, C.D. (2008). A review on polymer–layered silicate nanocomposites. *Progress in Polymer Science* 33 (12): 1119–1198.

49 Ray, S.S. and Okamoto, M. (2003). Polymer/layered silicate nanocomposites: a review from preparation to processing. *Progress in Polymer Science* 28 (11): 1539–1641.

50 Wu, D., Zhou, C., Yu, W., and Fan, X. (2005). Effect of flocculated structure on rheology of poly(butylene terephthalate)/clay nanocomposites. *Journal of Polymer Science Part B: Polymer Physics* 43 (19): 2807–2818.

51 Dennis, H., Hunter, D.L., Chang, D. et al. (2001). Effect of melt processing conditions on the extent of exfoliation in organoclay-based nanocomposites. *Polymer* 42 (23): 9513–9522.

52 Okamoto, M. (2003). *Polymer/Layered Silicate Nanocomposites*, 166. Shrewsbury: Rapra Technology Limited.

53 LeBaron, P.C., Wang, Z., and Pinnavaia, T.J. (1999). Polymer-layered silicate nanocomposites: an overview. *Applied Clay Science* 15 (1–2): 11–29.

54 Giannelis, E.P., Krishnamoorti, R., and Manias, E. (1999). Polymer-silicate nanocomposites: model systems for confined polymers and polymer brushes. In: *Polymers in Confined Environments*, Advances in Polymer Science, vol. 138 (eds. Granick, S., Binder, K., de Gennes, P.G. et al.), 107–147. Berlin, Heidelberg: Springer-Verlag.

55 Chen, B. (2004). Polymer–clay nanocomposites: an overview with emphasis on interaction mechanisms. *British Ceramic Transactions* 103 (6): 241–249.

56 Lingaiah, S., Sadler, R., Ibeh, C., and Shivakumar, K. (2008). A method of visualization of inorganic nanoparticles dispersion in nanocomposites. *Composites Part B Engineering* 39: 196–201.

57 Chen, D. and Zhao, Q. (2003). Effects of different kinds of clay and different vinyl acetate content on the morphology and properties of EVA/clay nanocomposites. *Polymer* 44 (26): 7953–7961.

58 Lv, S., Zhou, W., Li, S., and Shi, W. (2008). A novel method for preparation of exfoliated UV-curable polymer/clay nanocomposites. *European Polymer Journal* 44 (6): 1613–1619.

59 Delogu, F., Gorrasi, G., and Sorrentino, A. (2017). Fabrication of polymer nanocomposites via ball milling: present status and future perspectives. *Progress in Materials Science* 86: 75–126.

60 Ray, S.S. (2013). Structure and morphology characterization techniques. In: *Clay-Containing Polymer Nanocomposites: From Fundamentals to Real Applications*, Chapter 3, 53. Elsevier.

61 Wu, H.D., Tseng, C.R., and Chang, F.C. (2001). Chain conformation and crystallization behavior of the syndiotactic polystyrene nanocomposites studied using Fourier transform infrared analysis. *Macromolecules* 34 (9): 2992–2999.

62 Loo, L.S. and Gleason, K.K. (2003). Fourier transform infrared investigation of the deformation behavior of montmorillonite in nylon-6/nanoclay nanocomposite. *Macromolecules* 36 (8): 2587–2590.

63 Katti, K.S., Sikdar, D., Katti, D.R. et al. (2006). Molecular interactions in intercalated organically modified clay and clay–polycaprolactam nanocomposites: experiments and modeling. *Polymer* 47 (1): 403–414.

64 Zanetti, M., Lomakin, S., and Camino, G. (2000). Polymer layered silicate nanocomposites. *Macromolecular Materials and Engineering* 279 (1): 1–9.

65 Miltner, H.E., Rahier, H., Pozsgay, A. et al. (2005). Experimental evidence for reduced chain segment mobility in poly(amide)-6/clay nanocomposites. *Composite Interfaces* 12 (8–9): 787–803.

66 Rao, Y. and Pochan, J.M. (2007). Mechanics of polymer−clay nanocomposites. *Macromolecules* 40 (2): 290–296.

67 Drummy, L.F., Wang, Y.C., Schoenmakers, R. et al. (2008). Morphology of layered silicate (NanoClay) polymer nanocomposites by electron tomography and small-angle X-ray scattering. *Macromolecules* 41: 2135–2143.

68 Ianchis, R., Rosca, I., Ghiurea, M. et al. (2015). Synthesis and properties of new epoxy-organolayered silicate nanocomposites. *Applied Clay Science* 103: 28–33.

69 Shi, H., Lan, T., and Pinnavaia, T.J. (1996). Interfacial effects on the reinforcement properties of polymerorganoclay nanocomposites. *Chemistry of Materials* 8 (8): 1584–1587.

70 Kotal, M. and Bhowmick, A.K. (2015). Polymer nanocomposites from modified clays: recent advances and challenges. *Progress in Polymer Science* 51: 127–187.

71 Ginzburg, V.V., Singh, C., and Balazs, A.C. (2000). Theoretical phase diagrams of polymer/clay composites: the role of grafted organic modifiers. *Macromolecules* 33 (3): 1089–1099.

72 Jagtap, S.B., Rao, V.S., Barman, S., and Ratna, D. (2015). Nanocomposites based on epoxy resin and organoclay functionalized with a reactive modifier having structural similarity with the curing agent. *Polymer* 63: 41–51.

73 Xie, Y., Hill, C.A., Xiao, Z. et al. (2010). Silane coupling agents used for natural fiber/polymer composites: a review. *Composites Part A: Applied Science and Manufacturing* 41 (7): 806–819.

74 Bruce, A.N., Lieber, D., Hua, I., and Howarter, J.A. (2014). Rational interface design of epoxy–organoclay nanocomposites: role of structure-property relationship for silane modifiers. *Journal of Colloid and Interface Science* 419: 73–78.

75 Laghaei, M., Sadeghi, M., Ghalei, B., and Dinari, M. (2016). The effect of various types of post-synthetic modifications on the structure and properties of MCM-41 mesoporous silica. *Progress in Organic Coatings* 90: 163–170.

76 Laghaei, M., Sadeghi, M., Ghalei, B., and Shahrooz, M. (2016). The role of compatibility between polymeric matrix and silane coupling agents on the performance of mixed matrix membranes: polyethersulfone/MCM-41. *Journal of Membrane Science* 513: 20–32.

77 Calcagno, C.I., Mariani, C.M., Teixeira, S., and Mauler, R. (2007). The effect of organic modifier of the clay on morphology and crystallization properties of PET nanocomposites. *Polymer* 48 (4): 966–974.

78 Sikdar, D., Katti, D.R., and Katti, K.S. (2008). The role of interfacial interactions on the crystallinity and nanomechanical properties of clay–polymer nanocomposites: a molecular dynamics study. *Journal of Applied Polymer Science* 107 (5): 3137–3148.

79 Shah, K.J., Shukla, A.D., Shah, D.O., and Imae, T. (2016). Effect of organic modifiers on dispersion of organoclay in polymer nanocomposites to improve mechanical properties. *Polymer* 97: 525–532.

80 Hackett, E., Manias, E., and Giannelis, E.P. (1998). Molecular dynamics simulations of organically modified layered silicates. *The Journal of Chemical Physics* 108 (17): 7410–7415.

81 Agag, T., Koga, T., and Takeichi, T. (2001). Studies on thermal and mechanical properties of polyimide–clay nanocomposites. *Polymer* 42 (8): 3399–3408.

82 Miyagawa, H., Rich, M.J., and Drzal, L.T. (2004). Amine-cured epoxy/clay nanocomposites. I. Processing and chemical characterization. *Journal of Polymer Science Part B: Polymer Physics* 42 (23): 4384–4390.

83 Lee, E., Mielewski, D., and Baird, R. (2004). Exfoliation and dispersion enhancement in polypropylene nanocomposites by in-situ melt phase ultrasonication. *Polymer Engineering and Science* 44 (9): 1773–1782.

84 Lam, C.-k., Lau, K.-t., Cheung, H.-y., and Ling, H.-y. (2005). Effect of ultrasound sonication in nanoclay clusters of nanoclay/epoxy composites. *Materials Letters* 59 (11): 1369–1372.

85 Wang, R., Schuman, T., Vuppalapati, R.R., and Chandrashekhara, K. (2014). Fabrication of bio-based epoxy–clay nanocomposites. *Green Chemistry* 16 (4): 1871–1882.

86 Wang, J. and Qin, S. (2007). Study on the thermal and mechanical properties of epoxy–nanoclay composites: the effect of ultrasonic stirring time. *Materials Letters* 61: 4222.

87 Yasmin, A., Abot, J.L., and Daniel, I.M. (2003). Processing of clay/epoxy nanocomposites by shear mixing. *Scripta Materialia* 49 (1): 81–86.

88 Gupta, N., Lin, T.C., and Shapiro, M. (2007). Clay-epoxy nanocomposites: processing and properties. *Journal of Metals* 59 (3): 61–65.

89 Ngo, T.-D., Cole, K.C., That, T. et al. (2013). Epoxy/clay nanocomposites: preparation and performance improvement. *Plastics Research Online*: 1–3.

90 Lu, H.-j., Liang, G.-Z., Ma, X.-y. et al. (2004). Epoxy/clay nanocomposites: further exfoliation of newly modified clay induced by shearing force of ball milling. *Polymer International* 53 (10): 1545–1553.

91 Vertuccio, L., Gorrasi, G., Sorrentino, A., and Vittoria, V. (2009). Nano clay reinforced PCL/starch blends obtained by high energy ball milling. *Carbohydrate Polymers* 75 (1): 172–179.

92 Liu, W., Hoa, S.V., and Pugh, M. (2005). Organoclay-modified high performance epoxy nanocomposites. *Composites Science and Technology* 65 (2): 307–316.

93 Ngo, T.D., Ton-That, M.T., Hoa, S.V., and Cole, K.C. (2009). Effect of temperature, duration and speed of pre-mixing on the dispersion of clay/epoxy nanocomposites. *Composites Science and Technology* 69 (11–12): 1831–1840.

94 Al-Qadhi, M., Merah, N., and Gasem, Z.M. (2013). Mechanical properties and water uptake of epoxy–clay nanocomposites containing different clay loadings. *Journal of Materials Science* 48 (10): 3798–3804.

95 Wang, K., Wang, L., Wu, J. et al. (2005). Preparation of highly exfoliated epoxy/clay nanocomposites by "slurry compounding": process and mechanisms. *Langmuir* 21 (8): 3613–3618.

96 Wang, K., Chen, L., Wu, J. et al. (2005). Epoxy nanocomposites with highly exfoliated clay: mechanical properties and fracture mechanisms. *Macromolecules* 38: 788–800.

97 Wang, Y., Chen, F.B., Wu, K.C., and Wang, J.C. (2006). Shear rheology and melt compounding of compatibilized polypropylene nanocomposites: effect of compatibilizer molecular weight. *Polymer Engineering and Science* 46: 289–302.

98 Zaarei, D., Sarabi, A.A., Sharif, F. et al. (2010). Enhancement of nanoclay dispersion and exfoliation in epoxy using aminic hardener treated clay. *Journal of Dispersion Science and Technology* 31: 1350–1357.

99 Yang, L., Phua, S.L., Teo, J.K.H. et al. (2011). A biomimetic approach to enhancing interfacial interactions: polydopamine-coated clay as reinforcement for epoxy resin. *ACS Applied Materials & Interfaces* 3 (8): 3026–3032.

100 Mariani, A., Bidali, S., Caria, G. et al. (2007). Synthesis and characterization of epoxy resin-montmorillonite nanocomposites obtained by frontal polymerization. *Journal of Polymer Science Part A: Polymer Chemistry* 45 (11): 2204–2211.

101 Bitinis, N., Hernandez, M., Verdejo, R. et al. (2011). Recent advances in clay/polymer nanocomposites. *Advanced Materials* 23: 5229–5236.

102 Li, X., Zhan, Z., Peng, G., and Wang, W. (2011). A new method for preparing completely exfoliated epoxy/clay nanocomposites: nano-disassembling method. *Polymer Bulletin* 67 (4): 719–727.

103 Li, X., Zhan, Z.J., Peng, G.R., and Wang, W.K. (2012). Nano-disassembling method—a new method for preparing completely exfoliated epoxy/clay nanocomposites. *Applied Clay Science* 55: 168–172.

104 Jiankun, L., Yucai, K., Zongneng, Q., and Xiao-Su, Y. (2001). Study on intercalation and exfoliation behavior of organoclays in epoxy resin. *Journal of Polymer Science Part B: Polymer Physics* 39: 115.

105 Xu, W., Bao, S., and He, P. (2002). Intercalation and exfoliation behavior of epoxy resin/curing agent/montmorillonite nanocomposite. *Journal of Applied Polymer Science* 84: 842.

106 Chin, I.-J., Thurn-Albrecht, T., Kim, H.-C. et al. (2001). On exfoliation of montmorillonite in epoxy. *Polymer* 42: 5947–5952.

107 Kong, D. and Park, C.E. (2003). Real time exfoliation behavior of clay layers in epoxy-clay nanocomposites. *Chemistry of Materials* 15: 419–424.

108 Kornmann, X., Lindberg, H., and Berglund, L.A. (2001). Synthesis of epoxy-clay nanocomposites: influence of the nature of the clay on structure. *Polymer* 42: 1303–1310.

109 Ryznarova, B., Zelenka, J., Lednicky, F., and Baldrian, J. (2008). Epoxy-clay nanocomposites: influence of the clay surface modification on structure. *Journal of Applied Polymer Science* 109: 1492–1497.

110 Ratna, D., Manoj, N.R., Varley, R. et al. (2003). Clay-reinforced epoxy nanocomposites. *Polymer International* 52 (9): 1403–1407.

111 Wang, M.S. and Pinnavaia, T.J. (1994). Clay-polymer nanocomposites formed from acidic derivatives of montmorillonite and an epoxy resin. *Chemistry of Materials* 6 (4): 468–474.

112 Lan, T., Kaviratna, P.D., and Pinnavaia, T.J. (2002). Mechanism of clay tactoid exfoliation in epoxy-clay nanocomposites. *Chemistry of Materials* 7 (11): 2144–2150.

113 Lan, T., Kaviratna, P.D., and Pinnavaia, T.J. (1996). Epoxy self-polymerization in smectite clays. *Journal of Physics and Chemistry of Solids* 57 (6–8): 1005–1010.

114 Velumurugan, R. and Mohan, T.P. (2004). Room temperature processing of epoxy–clay nano composites. *Journal of Materials Science* 39: 7333.

115 Chen, C. and Tolle, T.B. (2004). Fully exfoliated layered silicate epoxy nanocomposites. *Journal of Polymer Science Part B: Polymer Physics* 42: 3981–3986.

116 Zunjarrao, S.C., Sriraman, R., and Singh, R.P. (2006). Effect of processing parameters and clay volume fraction on the mechanical properties of epoxy–clay nanocomposites. *Journal of Materials Science* 41: 2219–2228.

117 Koerner, H., Misra, D., Tan, A. et al. (2006). Montmorillonite–thermoset nanocomposites via cryocompounding. *Polymer* 47: 3426–3435.

118 Samandari, S.S., Khatibi, A.A., and Basic, D. (2007). An experimental study on clay/epoxy. nanocomposites produced in a centrifuge. *Composites Part B Engineering* 38: 102–107.

119 Wang, J., Kong, X., Cheng, L., and He, Y. (2008). Influence of clay concentration on the morphology and properties of clay-epoxy nanocomposites prepared by insitu polymerization under ultrasonication. *Journal of University of Science and Technology Beijing* 15 (3): 320–323.

120 Bashar, M., Mertiny, P., and Sundararaj, U. (2014). Effect of nanocomposite structures on fracture behavior of epoxy-clay nanocomposites prepared by different dispersion methods. *Journal of Nanomaterials* 2014: 312813.

121 Gajjela, S., Ramachandran, V., and Somasekharan, J. (2016). Influence of interphase material and clay particle shape on the effective properties of epoxy-clay nanocomposites. *Composites Part B: Engineering* 88: 11–18.

122 Tomić, M., Dunjić, B., Nikolić, M.S. et al. (2019). Polyamidoamine as a clay modifier and curing agent in preparation of epoxy nanocomposites. *Progress in Organic Coatings* 131: 311–321.

123 Hackman, I. and Hollaway, L. (2006). Epoxy-layered silicate nanocomposites in civil engineering. *Composites Part A: Applied Science and Manufacturing* 37 (8): 1161–1170.

124 Le Pluart, L., Duchet, J., and Sautereau, H. (2005). Epoxy/montmorillonite nanocomposites: influence of organophilic treatment on reactivity, morphology and fracture properties. *Polymer* 46 (26): 12267–12278.

125 Zhu, T.T., Zhou, C.H., Kabwe, F.B. et al. (2019). Exfoliation of montmorillonite and related properties of clay/polymer nanocomposites. *Applied Clay Science* 169: 48–66.

126 Wang, Z. and Pinnavaia, T.J. (1998). Hybrid organic–inorganic nanocomposites: exfoliation of magadiite nanolayers in an elastomeric epoxy polymer. *Chemistry of Materials* 10 (7): 1820–1826.

127 Brown, J.M., Curliss, D., and Vaia, R.A. (2000). Thermoset-layered silicate nanocomposites. Quaternary ammonium montmorillonite with primary diamine cured epoxies. *Chemistry of Materials* 12 (11): 3376–3384.

128 Balazs, A.C., Singh, C., and Zhulina, E. (1998). Modeling the interactions between polymers and clay surfaces through self-consistent field theory. *Macromolecules* 31: 8370–8381.

129 Balazs, A.C., Singh, C., Zhulina, E., and Lyatskaya, Y. (1999). Modeling the phase behavior of polymer/clay nanocomposites. *Accounts of Chemical Research* 32: 651–657.

130 Chen, J.S., Poliks, M.D., Ober, C.K. et al. (2002). Study of the interlayer expansion mechanism and thermal–mechanical properties of surface-initiated epoxy nanocomposites. *Polymer* 43 (18): 4895–4904.

131 Ying, Z., Xianggao, L., Bin, C. et al. (2015). Highly exfoliated epoxy/clay nanocomposites: mechanism of exfoliation and thermal/mechanical properties. *Composite Structures* 132: 44–49.

132 Camino, G., Tartaglione, G., Frache, A. et al. (2005). Thermal and combustion behaviour of layered silicate–epoxy nanocomposites. *Polymer Degradation and Stability* 90 (2): 354–362.

133 Triantafillidis, C.S., LeBaron, P.C., and Pinnavaia, T.J. (2002). Homostructured mixed inorganic–organic ion clays: a new approach to epoxy polymer–exfoliated clay nanocomposites with a reduced organic modifier content. *Chemistry of Materials* 14 (10): 4088–4095.

134 Park, J.H. and Jana, S.C. (2003). Mechanism of exfoliation of nanoclay particles in epoxy–clay nanocomposites. *Macromolecules* 36 (8): 2758–2768.

135 Tolle, T.B. and Anderson, D.P. (2004). The role of preconditioning on morphology development in layered silicate thermoset nanocomposites. *Journal of Applied Polymer Science* 91 (1): 89–100.

136 Hutchinson, J.M., Montserrat, S., Román, F. et al. (2006). Intercalation of epoxy resin in organically modified montmorillonite. *Journal of Applied Polymer Science* 102 (4): 3751–3763.

137 Chan, Y.N., Hsu, R.S., and Lin, J.J. (2010). Mechanism of silicate platelet self-organization during clay-initiated epoxy polymerization. *The Journal of Physical Chemistry C* 114 (23): 10373–10378.

4

Long Fiber-Reinforced Epoxy Composites

Ayesha Kausar

National Center For Physics, Quaid-i-Azam University Campus, Nanosciences Division, Islamabad, Pakistan

4.1 Introduction

Epoxy resins are also recognized as polyepoxides. Epoxy resins form a class of reactive prepolymers [1, 2]. Crosslinking of epoxy resins may be carried out through polyfunctional alcohols, amines, acids, or anhydrides. The low molecular weight polyfunctional compounds are often termed as hardeners. Epoxy may react with itself or other epoxies via catalytic homopolymerization. In this way, thermosetting epoxy polymer is obtained through the reaction of polyepoxides with polyfunctional hardeners or epoxies. Fiber-reinforced polymer composite is made up of polymeric matrix reinforced with fibrous filler. The fibrous filler may be of different types such as glass fiber, carbon fiber, aramid, or basalt [3, 4]. Fiber-reinforced polymer composites have gained attention for structural components [5, 6]. Among fibrous composite, long fiber-reinforced polymer (LFRP) composites have gained significant research interest [7, 8]. The LFRP composites own lightweight, strength, fatigue resistance, and anticorrosion properties. The LFRP composites have been employed in aerospace, automotive, construction, and sports industries [9–12]. Processing of LFRP composites has been found difficult owing to the presence of long hard fibers [13]. Moreover, LFRP composites may have the problems of matrix thermal degradation, fiber pullout, and failure during handling [14]. Usually, modified machining processes including milling, drilling, or trimming are needed for efficient cutting or processing of LFRP composites [5, 15]. Durability and structure of long glass fiber polymer composites or composites reinforced with continuous glass fiber have been explored for technical and infrastructure applications [16]. Development of LCFs of 75-mm long or longer has been focused [17, 18].The LCF polymer composites have been used to enhance the blasts and impact resistance. The flexural properties of these structural composites were also found superior [19]. Lengthened natural or bio-fiber-reinforced composites have also been studied for tensile, flexural, and impact strength [20]. Interfacial bonding between matrix and fibers has led to better durability and water absorption of these materials.

Epoxy Composites: Fabrication, Characterization and Applications,
First Edition. Edited by Jyotishkumar Parameswaranpillai, Harikrishnan Pulikkalparambil, Sanjay M. Rangappa, and Suchart Siengchin.

This chapter highlights the viability and current state of LFRP composites. Three categories of LFRP composites have been essentially stressed here: (i) epoxy and long glass fiber composite; (ii) epoxy and LCF composite; and (iii) epoxy and natural fiber composite. Toward the end, applications, challenges, and future prospects of these composites have been deliberated.

4.2 Long Fiber Fillers

Long glass fibers are cost-effective, strong, tough, and lightweight. Glass fiber is made up of a pure polymer $(SiO_2)_n$. Glass fiber has no true melting point; however, it may softens up to 1200 °C. Long glass fibers may enhance the mechanical properties of polypropylene, polyether ether ketone, and epoxy matrices [21]. Long glass fiber-based materials have been used in thermal insulating materials. Long glass fibers have been employed in mats and fabrics for heat insulation, electrical insulation, sound insulation, and corrosion resistance. Long glass fibers have been impregnated with epoxy resin. Thermoplastic matrices have also been reinforced with long glass fiber through pultrusion process, injection molding, or extrusion method [5, 22]. Epoxy–glass fiber composite has been prepared in the form of membrane with thickness of 4–5 mm. The glass fabric has been developed using 25 mm to several μm long fibers. The glass fiber laminates have been smeared with epoxy resin using *wet-in-wet* process and cured. E-glass fiber is an alumino-borosilicate fiber. E-glass refers to electric glass which is an electrical insulating material. E-glass fiber does not melt, but it softens. E-glass fiber has 0.55–0.77 mm diameter and length of 235 mm to few μm [23]. E-glass fiber can be further elongated, when it is heated. Carbon fibers have advantageous characteristics such as low weight, high tensile strength, high stiffness, high strength-to-weight ratio, chemical resistance, temperature lenience, and low thermal expansion. LCF may often segregate within the matrix and decrease its workability [24]. Sometimes, coatings are applied to carbon fiber yarns to attain stiff material. The coated CF has been used to enhance the properties of composite mixtures [18, 25]. Contrary to glass fibers, carbon fiber cannot undergo elongation and breaks. LCFs have been employed in blast-resistant materials. Other applications of CF are related to aerospace, automotive, military, civil engineering, and sports equipment. Essential properties of long glass fiber and carbon fiber are summarized in Table 4.1.

4.3 Long Fiber-Reinforced Epoxy Composite

4.3.1 Epoxy and Long Glass Fiber Composite

Epoxy and long glass fiber-reinforced composite (GFRC) have been extensively employed in advance aerospace structures [26]. GFRC has also been employed as metal replacement in aircraft, automobiles, military gears, and sporting goods. However, the fatigue phenomena of GFRC laminates is intricate to understand. In

Table 4.1 Characteristics of materials used in simulations.

Mechanical properties	GFRC	CFRP
Longitudinal tensile strength (MPa)	1200	1950
Longitudinal compressive strength (MPa)	800	1480
Transverse tensile strength (MPa)	59	48
Transverse compressive strength (MPa)	128	200
Shear strength (MPa)	25	79
Longitudinal modulus (GPa)	48	126
Transverse modulus (GPa)	12	11

Source: Soden et al. [21]. © 2004, Elsevier.

Table 4.2 Mechanical properties of E-glass fibers and epoxy resin.

E-glass fiber	
Average diameter (μm)	10
Young's modulus (MPa)	73 000
Ultimate tensile strength (MPa)	3400
Strain (%)	4.8
Epoxy	
Density (g/ml)	1.14–1.16
Young's modulus (MPa)	2900–3100
Ultimate tensile strength (MPa)	75–80
Strain (%)	8.5–9

Source: Giancane et al. [31]. © 2010, Elsevier.

this composite, the presence of various epoxy–glass interfaces may cause continuous stress redistributions [27, 28]. The damaged zones may cause loss of stiffness and decrease in material properties. Glass aluminum-reinforced epoxy (GLARE) is a special type of long glass fiber metal laminate. GLARE is usually prepared by means of alternating layers of glass–epoxy composite and aluminum metal sheets [29, 30]. Giancane et al. [31] prepared epoxy and long glass fiber-based composite using lay-up technique. Table 4.2 illustrates properties of continuous and unidirectional E-glass fiber and epoxy matrix. The mentioned factors were related to the damage state of composite material. During damage characterization, damage was evaluated using stiffness and dissipated energy per cycle.

Park et al. [32] designed glass/epoxy and GLARE laminates. Both the composite samples were prepared with different void content (0.5%–2.0%). The varying void levels were attained using three different magnitudes of autoclave pressures (304, 402, and 500 kPa). In GLARE samples, autoclave pressure was found to enhance the interfacial bonding and reduce void contents. Figure 4.1 illustrates photograph of

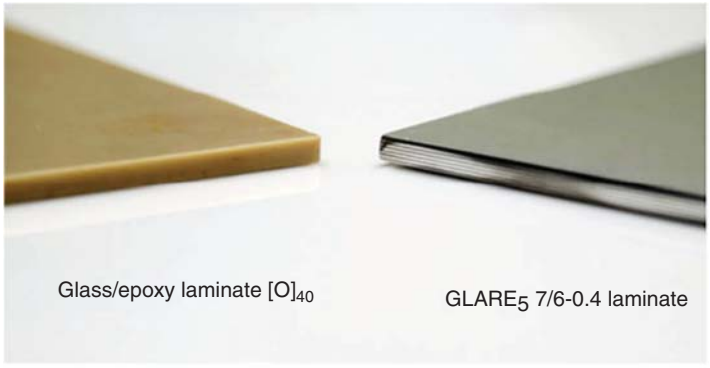

Figure 4.1 Photograph of glass/epoxy and GLARE laminates. Source: Park et al. [32].

Table 4.3 Measured properties of glass/epoxy and GLARE cured by different autoclave pressures (± standard deviation).

Void level	Fiber content (%)	Total thickness (mm)	Metal volume fraction (MVF)	Interlaminar shear strength (ILSS)
Epoxy/glass-1	46.82 ± 1.12	4.31 ± 0.28	—	45.56 ± 1.10
Epoxy/glass-2	56.42 ± 0.92	4.25 ± 0.12	—	57.56 ± 2.60
Epoxy/glass-3	57.35 ± 1.03	4.09 ± 0.45	—	57.76 ± 1.80
GLARE-1	49.56 ± 0.85	4.29 ± 0.35	0.66	40.70 ± 1.73
GLARE-2	56.49 ± 1.65	3.95 ± 0.95	0.72	54.14 ± 3.18
GLARE-3	57.61 ± 1.02	3.89 ± 0.16	0.73	59.61 ± 1.19

Source: Park et al. [32]. © 2010, Elsevier.

glass/epoxy and GLARE laminates. Table 4.3 shows physical and mechanical properties of glass/epoxy and GLARE. With the reducing void content, interlaminar shear strength (ILSS) was found to enhance in composites.

González-Benito [33] developed silane-coated long glass fiber and epoxy composite. The curing process was explored at the interface of silane-coated long glass fiber and epoxy matrix. Figure 4.2 shows amine : epoxy absorbance ratio variation from bulk epoxide mixture to interface for (a) the coated glass fiber, (b) the uncoated glass fiber, and (c) the poly(aminopropylsiloxane). Curing time was five minutes. With the increase in active amine concentration, the curing rate was increased. The amine : epoxy absorbance ratio was attained by dividing the amino group absorbance by phenyl C–H bending absorbance ($1604\,cm^{-1}$). It was observed that the amount of active amine declined near the glass fiber. Chabert et al. [34] also prepared long glass fiber-filled epoxy composite. The composite consisted of 50 vol% of reinforcing fibers. The epoxy–long glass fiber composite exhibited substantial bond strength and repeated welding capability. The composite developed chemical bonding between the matrix and filler at the joint interface [35].

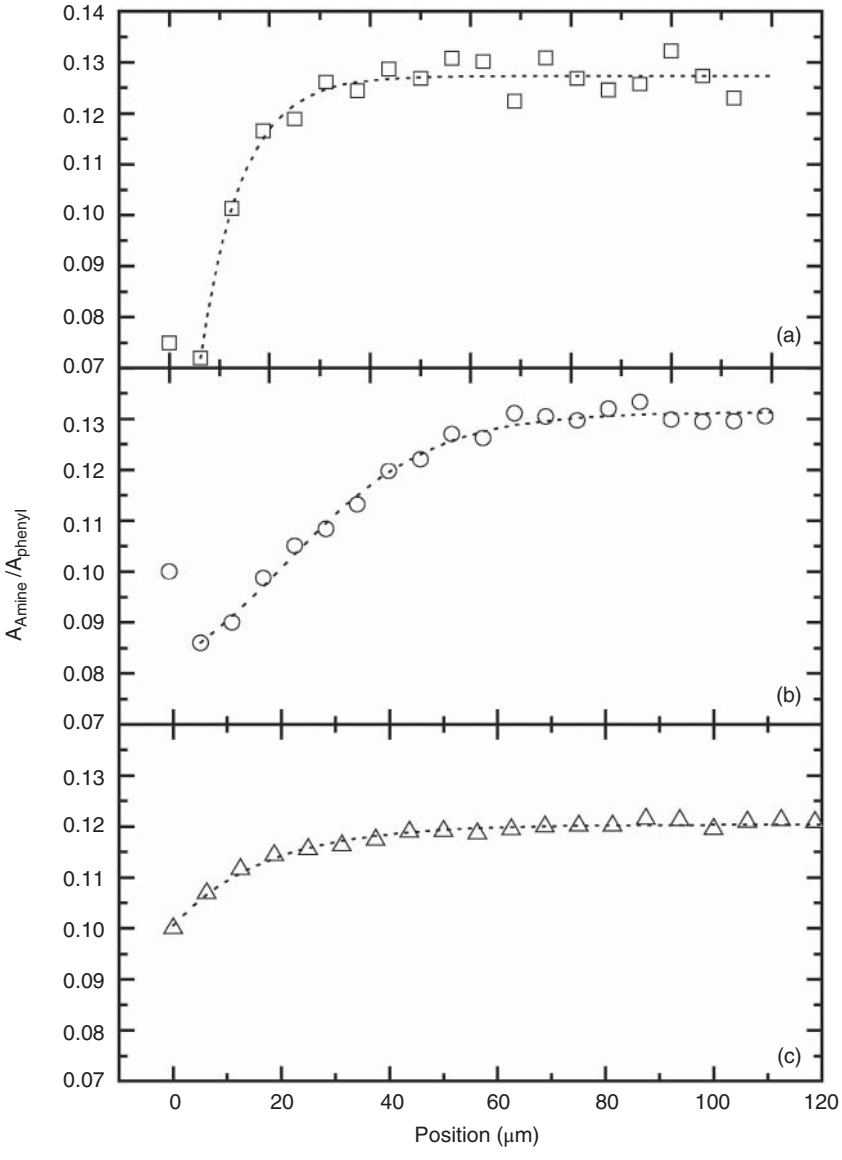

Figure 4.2 Amine : epoxy absorbance ratio variation from bulk epoxide mixture to interface for (a) coated glass fiber, (b) uncoated glass fiber, and (c) poly(aminopropylsiloxane) at curing time of five minutes. Source: González-Benito [33]. © 2003, Elsevier.

4.3.2 Epoxy and Long Carbon Fiber Composite

Carbon fiber-reinforced polymer (CFRP) composite has been widely employed in structural materials. CFRP composite possesses range of unique properties including high strength, stiffness, dimensional stability, heat constancy, and corrosion resistance. However, fatigue is a major cause of failure in CFRP composites

Table 4.4 Values of parameters used in fiber contact model.

Parameter	SCF	MCF	LCF
Electrical conductivity (Scm^{-1})	67	67	100
Critical volume fraction (%)	19.8	8	5.3
Saturated volume fraction (%)	35.1	22	9.8
Fiber diameter (μm)	14.5	18	13
Average fiber length (μm)	82	145	325
Orientation parameter (l)	0.61	0.62	0.52

Source: Tsotra and Friedrich [42]. © 2003, Elsevier.

[36, 37]. Carbon fibers of various forms have been used such as short carbon fiber (SCF), LCF, and medium carbon fiber (MCF). Fatigue may cause deprivation of mechanical and structural performance of the composite. In CFRP, fatigue damage modes are due to matrix cracking, delamination, fiber breakage, and interfacial matrix–fiber debonding. The orientation of laminates and lay-up sequence also affect the fatigue damage of the composite. In unidirectional CFRP laminates, high degree of fatigue resistance has been observed [38]. However, highly loaded laminates with off-axis fiber orientations may have multiple failure mechanisms [39–41]. In this case, the damage states depend on anisotropy and heterogeneity of the system. Tsotra et al. [42] prepared epoxy–carbon fiber composite using centrifugation technique for fiber distribution. The SCF, MCF, and LCF were used as filler in the matrix. Table 4.4 illustrates microstructural parameters used for modeling electrical conductivity of epoxy–carbon fiber composites. The epoxy–SCF, epoxy–MCF, and epoxy–LCF composites were reinforced with 14, 12.5, and 6 vol% content. The experimentally measured values were not in agreement with the theoretical parameters. Two-point probe method was used to measure the electrical conductivity. Electrical conductivity and volume content of fibers were directly related. Figure 4.3 shows transmission electron microscopy (TEM) images of SCF, MCF, and LCF. The fibers were found to have random orientation in the matrix. Zafar et al. [43] prepared LCF-based epoxy composite. Influence of moisture on the

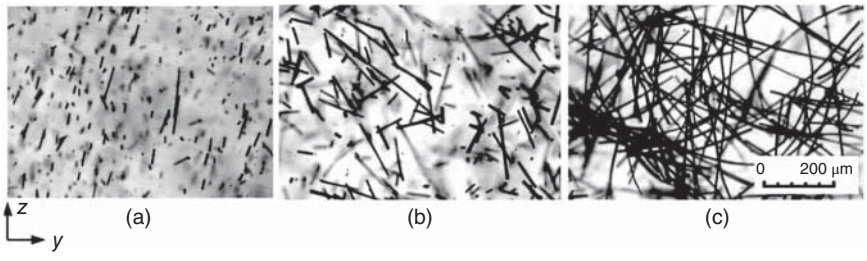

Figure 4.3 Transmission electron microscopy images: (a) SCF, (b) MCF, and (c) LCF. Source: Tsotra and Friedrich [42].

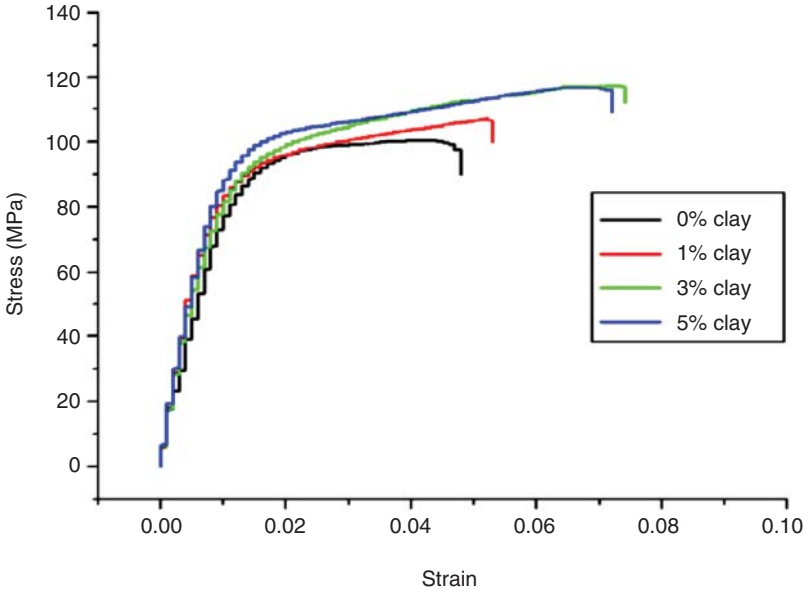

Figure 4.4 Representative stress–strain curves of clay-filled CFRP hybrid composites. Source: Khan et al. [45]. © 2010, Elsevier.

epoxy–carbon fiber interface has been studied. The epoxy–carbon fiber composite was immersed in seawater to study the moisture uptake. The moisture was found to reduce the glass transition temperature (T_g) and thermal stability of the composite. Mechanical and interfacial properties of the composites were also decreased under seawater immersion.

Wolfrum et al. [44] also studied LCF-reinforced epoxy composite. Effect of heat above maximum operational temperature of the composite was studied. Strength characteristics were found to decrease with increased heating temperatures. Khan et al. [45] designed LCF-reinforced composite and loaded with nanoclay. Figure 4.4 shows stress–strain curves of clay-reinforced CFRP hybrid.

The materials had bilinear stress–strain curve behavior [46, 47]. Involvement of polymer matrix caused nonlinear curves. The yield strength and failure strain of CFRR were found to upsurge with clay loading. The nanoclay improved the fiber–matrix interfacial bonding, so delaying the delamination damage in CFRP. Montesano et al. [48] investigated fatigue behavior of braided carbon fiber-based composite. Figure 4.5 shows surface temperature as a function of number of loading cycles for epoxy and long CF-based composites. The plot also depicts maximum stress magnitude for each sample. The cycle fatigue strength was determined using energy dissipation. The energy dissipation was found related to the number of cycles to failure. Thus, LCF-filled epoxy composites were found to have enhanced thermal stability, tensile strength, fatigue resistance, cycle fatigue strength, and electrical conductivity. However, the property enhancement depends on fiber content, orientation, interfacial interaction, and matrix–CF bonding.

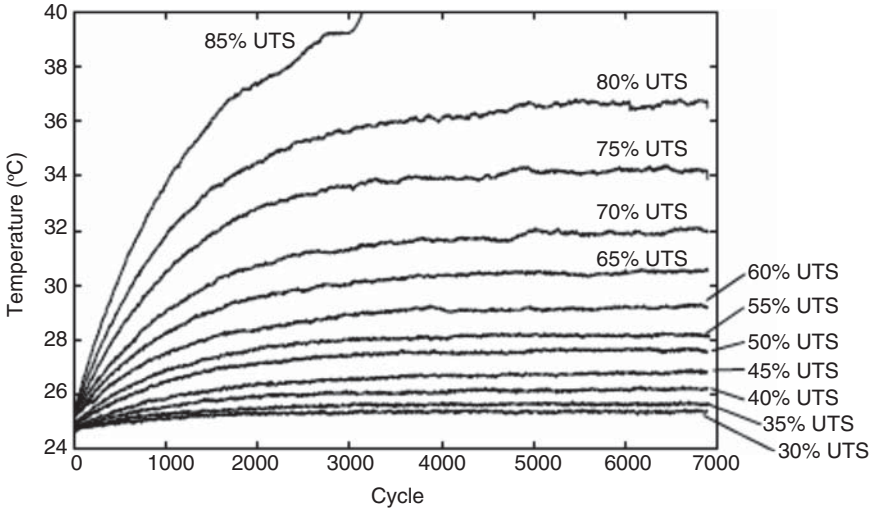

Figure 4.5 Temperature profile vs. cycle for indicated maximum stress magnitudes, ultimate tensile strength (UTS). Source: Montesano et al. [48]. © 2013, Elsevier.

4.3.3 Epoxy and Natural Fiber Composite

Natural fibers generally possess several advantageous features such as eco-friendliness and biodegradability [49]. Natural fibers are also lighter than the synthetic fibers such as carbon or glass fibers. They also have renewable nature and form strengthened polymeric composites [50, 51]. Boopalan et al. [52] prepared jute and banana fiber-reinforced epoxy composites. The tensile, flexural, impact, and thermal properties of epoxy resin with 50 wt% banana fiber were enhanced [53]. Sastra et al. [54] used Arenga pinnata fiber as natural fiber in epoxy resin. The woven Arenga pinnata fiber was used in 10–20 wt% content. Hand lay-up process was employed to form epoxy–Arenga pinnata composite. The 10 wt% loaded composite had high tensile strength and Young's modulus of 51.725 and 1255.825 MPa, respectively. Scanning electron microscopy (SEM) revealed better bonding between the matrix and fibers. Mahjoub et al. [55] reinforced continuous unidirectional kenaf fiber in epoxy matrix. The composites were obtained using hand lay-up method. Increase in fiber volume fraction caused enhancement in the tensile properties of epoxy matrix. The 40 vol% fiber in epoxy matrix led to tensile strength and tensile modulus of 164 and 18 150 MPa, respectively. Figure 4.6 shows that the tensile strength of 40 vol% composite was 180% higher than that of 10 vol% material. Figure 4.7 also reveals enhancement in tensile modulus of composite with kenaf fiber loading. Based on the studies, the epoxy–natural fiber composites may carry load perfectly till its ultimate strength or modulus. Advance fabrication processes need to be utilized to produce better interfacial bonding between natural fiber and the matrix.

4.4 Applications, Future Prospective, and Summary

Epoxy is a thermosetting resin widely used to form thermoset composite [56, 57]. Due to high crosslinking density, cured epoxies possess brittle nature [58]. They

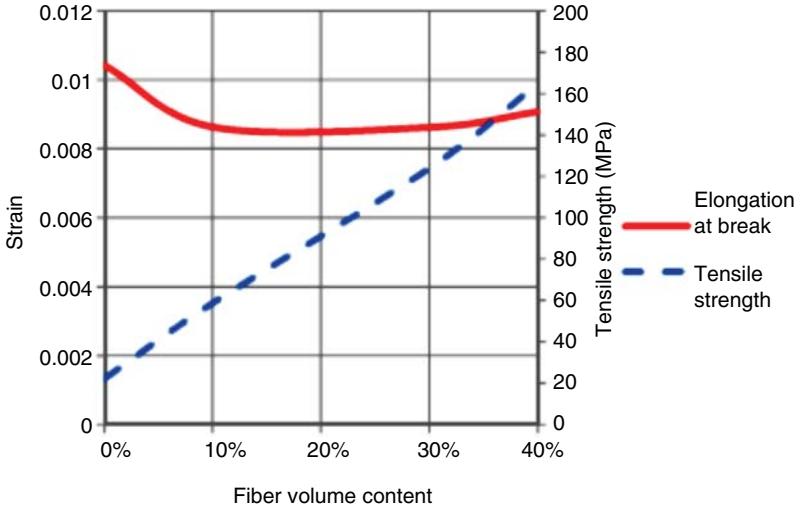

Figure 4.6 The effect of kenaf fiber volume content on the tensile strength and maximum strain of composites. Source: Mahjoub et al. [55]. © 2014, Elsevier.

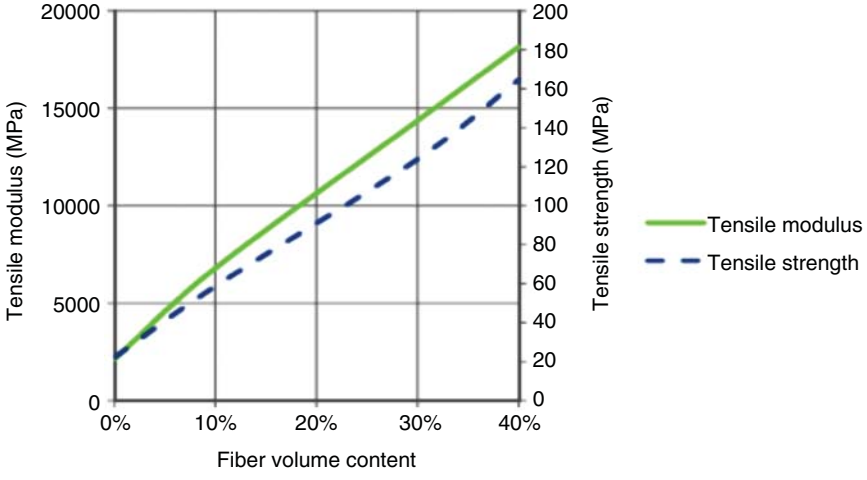

Figure 4.7 The effect of kenaf fiber volume content on the tensile strength and tensile modulus of composite. Source: Mahjoub et al. [55]. © 2014, Elsevier.

also have low impact resistance, delamination, and fracture toughness behavior. To attain high performance with flexibility, high strength, modulus, toughness, durability, and thermal and chemical resistance, modification and compositing of epoxies are needed [58, 59]. Epoxy and its derivatives have found potential for coatings, adhesives, electronic components, and composite materials [60, 61]. Consequently, limitations of epoxy resins have been overcome through fiber incorporation to attain broad spectrum of industrial applications. Long glass and carbon fiber-filled epoxy composite are attractive for engineering applications owing to low cost, lightweight, high strength-to-weight ratio, non-flammability, and corrosion resistance properties. Long fiber-reinforced epoxy composites have

been successfully employed in aerospace, automotive, defense, civil construction, sports, and oil and gas industries. To further broaden the application span of LFRP composite, several technical and implementation issues need to be resolved. LFRP composites are often hard to cut, which is time-consuming and expensive. In this regard, the mechanisms of chip formation of epoxy–long glass fiber and epoxy–LCF composites have been studied [7]. During orthogonal cutting of long fiber composites, machining caused damage to both the materials. Thus, LRFP composites have low machinability. To attain desired product, sufficient dimensional tolerance of LRFP composites is necessary. In LFRP composites machining, fiber inhalation may also cause serious health hazards to lungs and harm the skin in contact. Modified epoxy resin and natural fiber-reinforced composite may yield better matrix–filler bonding escorting superior mechanical, thermal, and electrical properties. Nowadays, bio-epoxy resin has also been developed for better interaction with bio-fibers. Future of these LFRP composite materials for advance applications relies on the development of advance cutting or machining tools. Efficient designing of products from LRFP may also minimize the risk of health hazards.

Hence, this is an original article dealing with cutting-edge research, application, and issues of LFRP composites. This is a comprehensive source of literature on recent advances in glass fiber, carbon fiber, and natural fiber-based epoxy composites. Additionally, it covers versatile characteristic properties, manufacturing techniques, and industrial relevance of these composites. The restricted use of LFRP composites in many high-performance fields is due to poor processing techniques and health risks in using these materials.

References

1 Jin, F.-L., Li, X., and Park, S.-J. (2015). *Synthesis and application of epoxy resins: A review*. *Journal of Industrial and Engineering Chemistry* 29: 1–11.

2 Baroncini, E.A., Kumar Yadav, S., Palmese, G.R. et al. (2016). *Recent advances in bio-based epoxy resins and bio-based epoxy curing agents*. *Journal of Applied Polymer Science* 133 (45).

3 Senthil Kumar, K., Bhatnagar, N., and Ghosh, A.K. (2007). *Development of long glass fiber reinforced polypropylene composites: mechanical and morphological characteristics*. *Journal of Reinforced Plastics and Composites* 26 (3): 239–249.

4 Wang, J., Nguyen, B.N., Mathur, R. et al. (2015). *Fiber orientation in injection molded long carbon fiber thermoplastic composites*. *Composites* 6 (8): 1–5.

5 Santiuste, C., Miguélez, H., and Soldani, X. (2011). *Out-of-plane failure mechanisms in LFRP composite cutting*. *Composite Structures* 93 (11): 2706–2713.

6 Joshi, P. and Bedi, K. (2019). *Strengthening of conventional beams using fibre reinforced polymer composite: an literature review*. *International Journal of Research* 6 (2): 1047–1051.

7 Santiuste, C., Soldani, X., and Miguélez, M.H. (2010). *Machining FEM model of long fiber composites for aeronautical components*. *Composite Structures* 92 (3): 691–698.

8 Soldani, X., Santiuste, C., Muñoz-Sánchez, A. et al. (2011). *Influence of tool geometry and numerical parameters when modeling orthogonal cutting of LFRP composites. Composites Part A: Applied Science and Manufacturing* 42 (9): 1205–1216.

9 Holbery, J. and Houston, D. (2006). *Natural-fiber-reinforced polymer composites in automotive applications. JOM* 58 (11): 80–86.

10 Freilich, M.A., Karmaker, A.C., Burstone, C.J. et al. (1998). *Development and clinical applications of a light-polymerized fiber-reinforced composite. The Journal of Prosthetic Dentistry* 80 (3): 311–318.

11 Friedrich, K. and Almajid, A.A. (2013). *Manufacturing aspects of advanced polymer composites for automotive applications. Applied Composite Materials* 20 (2): 107–128.

12 Yoo, D.-Y., Banthia, N., Gupta, R. et al. (2019). *Polymer-Based Construction Materials for Civil Engineering. International Journal of Polymer Science* 2019: 1–2.

13 Gadow, R., Weichand, P., and Jiménez, M. (2019). *Process technology, applications and thermal resistivity of basalt fiber reinforced SiOC composites. Ceramics* 2 (2): 298–307.

14 Nayak, D., Bhatnagar, N., and Mahajan, P. (2005). *Machining studies of uni-directional glass fiber reinforced plastic (UD-GFRP) composites part 1: effect of geometrical and process parameters. Machining Science and Technology* 9 (4): 481–501.

15 Cousin, P., Hassan, M., Vijay, P.V. et al. (2019). *Chemical resistance of carbon, basalt, and glass fibers used in FRP reinforcing bars. Journal of Composite Materials*: 0021998319844306.

16 Heshmati, M., Haghani, R., and Al-Emrani, M. (2015). *Environmental durability of adhesively bonded FRP/steel joints in civil engineering applications: state of the art. Composites Part B: Engineering* 81: 259–275.

17 Feito, N., López-Puente, J., Santiuste, C. et al. (2014). *Numerical prediction of delamination in CFRP drilling. Composite Structures* 108: 677–683.

18 Tabatabaei, Z.S., Volz, J.S., Gliha, B.P. et al. (2012). *Development of long carbon fiber-reinforced concrete for dynamic strengthening. Journal of Materials in Civil Engineering* 25 (10): 1446–1455.

19 Antonovič, V., Witek, J., Mačiulaitis, R. et al. (2017). *The effect of carbon and polypropylene fibers on thermal shock resistance of the refractory castable. Journal of Civil Engineering and Management* 23 (5): 672–678.

20 Xie, Y., Hill, C.A., Xiao, Z. et al. (2010). *Silane coupling agents used for natural fiber/polymer composites: a review. Composites Part A: Applied Science and Manufacturing* 41 (7): 806–819.

21 Soden, P., Hinton, M., and Kaddour, A. (2004). *Lamina properties, lay-up configurations and loading conditions for a range of fibre reinforced composite laminates*. In: *Failure Criteria in Fibre-Reinforced-Polymer Composites*, 30–51. UK: Elsevier.

22 Mkaddem, A. and El Mansori, M. (2009). *Finite element analysis when machining UGF-reinforced PMCs plates: Chip formation, crack propagation and induced-damage. Materials & Design* 30 (8): 3295–3302.

23 Krieger, R.E. (1970). *Handbook of Fiberglass and Advanced Plastic Composites.* New York: Huntingdon.

24 Tabatabaei, Z.S., Volz, J.S., Keener, D.I. et al. (2014). *Comparative impact behavior of four long carbon fiber reinforced concretes. Materials & Design* 55: 212–223.

25 Li, M., Yang, Y., Liu, M. et al. (2015). *Hybrid effect of calcium carbonate whisker and carbon fiber on the mechanical properties and microstructure of oil well cement. Construction and Building Materials* 93: 995–1002.

26 Kauffman, J. (2001). *A successful failure: NASA's crisis communications regarding Apollo 13. Public Relations Review* 27 (4): 437–448.

27 Talreja, R. (2006). *Multi-scale modeling in damage mechanics of composite materials. Journal of Materials Science* 41 (20): 6800–6812.

28 Talreja, R. (2008). *Damage and fatigue in composites–a personal account. Composites Science and Technology* 68 (13): 2585–2591.

29 Cepeda-Jiménez, C., Alderliesten, R.C., Ruano, O.A. et al. (2009). *Damage tolerance assessment by bend and shear tests of two multilayer composites: glass fibre reinforced metal laminate and aluminium roll-bonded laminate. Composites Science and Technology* 69 (3-4): 343–348.

30 Sinmazçelik, T., Avcu, E., Bora, M.Ö. et al. (2011). *A review: Fibre metal laminates, background, bonding types and applied test methods. Materials & Design* 32 (7): 3671–3685.

31 Giancane, S., Panella, F.W., and Dattoma, V. (2010). *Characterization of fatigue damage in long fiber epoxy composite laminates. International Journal of Fatigue* 32 (1): 46–53.

32 Park, S.Y., Choi, W.J., and Choi, H.S. (2010). *The effects of void contents on the long-term hygrothermal behaviors of glass/epoxy and GLARE laminates. Composite Structures* 92 (1): 18–24.

33 González-Benito, J. (2003). *The nature of the structural gradient in epoxy curing at a glass fiber/epoxy matrix interface using FTIR imaging. Journal of Colloid and Interface Science* 267 (2): 326–332.

34 Chabert, E., Vial, J., Cauchois, J.P. et al. (2016). *Multiple welding of long fiber epoxy vitrimer composites. Soft Matter* 12 (21): 4838–4845.

35 Legrand, A.l. and Soulié-Ziakovic, C. (2016). *Silica–epoxy vitrimer nanocomposites. Macromolecules* 49 (16): 5893–5902.

36 Zhang, W., Picu, R., and Koratkar, N. (2008). *The effect of carbon nanotube dimensions and dispersion on the fatigue behavior of epoxy nanocomposites. Nanotechnology* 19 (28): 285709.

37 Bortz, D.R., Merino, C., and Martin-Gullon, I. (2011). *Carbon nanofibers enhance the fracture toughness and fatigue performance of a structural epoxy system. Composites Science and Technology* 71 (1): 31–38.

38 Yang, Y. and Wu, G. (2018). *Evaluation of fatigue performance of ballastless track slabs reinforced with basalt-FRP and steel-FRP composite bars. Magazine of Concrete Research*: 1–12.

39 Kawai, M., Yajima, S., Hachinohe, A. et al. (2001). *Off-axis fatigue behavior of unidirectional carbon fiber-reinforced composites at room and high temperatures. Journal of Composite Materials* 35 (7): 545–576.

40 Quaresimin, M., Susmel, L., and Talreja, R. (2010). *Fatigue behaviour and life assessment of composite laminates under multiaxial loadings. International Journal of Fatigue* 32 (1): 2–16.

41 Carraro, P. and Quaresimin, M. (2014). *A damage based model for crack initiation in unidirectional composites under multiaxial cyclic loading. Composites Science and Technology* 99: 154–163.

42 Tsotra, P. and Friedrich, K. (2003). *Electrical and mechanical properties of functionally graded epoxy-resin/carbon fibre composites. Composites Part A: Applied Science and Manufacturing* 34 (1): 75–82.

43 Zafar, A., Bertocco, F., Schjødt-Thomsen, J. et al. (2012). *Investigation of the long term effects of moisture on carbon fibre and epoxy matrix composites. Composites Science and Technology* 72 (6): 656–666.

44 Wolfrum, J., Eibl, S., and Lietch, L. (2009). *Rapid evaluation of long-term thermal degradation of carbon fibre epoxy composites. Composites Science and Technology* 69 (3-4): 523–530.

45 Khan, S.U., Munir, A., Hussain, R. et al. (2010). *Fatigue damage behaviors of carbon fiber-reinforced epoxy composites containing nanoclay. Composites Science and Technology* 70 (14): 2077–2085.

46 Vergani, L., Colombo, C., and Libonati, F. (2014). *A review of thermographic techniques for damage investigation in composites. Fracture and Structural Integrity Ann* 8.

47 Aidi, B., Philen, M.K., and Case, S.W. (2015). *Progressive damage assessment of centrally notched composite specimens in fatigue. Composites Part A: Applied Science and Manufacturing* 74: 47–59.

48 Montesano, J., Fawaz, Z., and Bougherara, H. (2013). *Use of infrared thermography to investigate the fatigue behavior of a carbon fiber reinforced polymer composite. Composite Structures* 97: 76–83.

49 Ramesh, M., Palanikumar, K., and Reddy, K.H. (2017). *Plant fibre based bio-composites: sustainable and renewable green materials. Renewable and Sustainable Energy Reviews* 79: 558–584.

50 Pickering, K.L., Efendy, M.A., and Le, T.M. (2016). *A review of recent developments in natural fibre composites and their mechanical performance. Composites Part A: Applied Science and Manufacturing* 83: 98–112.

51 Väisänen, T., Das, O., and Tomppo, L. (2017). *A review on new bio-based constituents for natural fiber-polymer composites. Journal of Cleaner Production* 149: 582–596.

52 Boopalan, M., Niranjanaa, M., and Umapathy, M. (2013). *Study on the mechanical properties and thermal properties of jute and banana fiber reinforced epoxy hybrid composites. Composites Part B: Engineering* 51: 54–57.

53 Maleque, M., Belal, F., and Sapuan, S. (2007). *Mechanical properties study of pseudo-stem banana fiber reinforced epoxy composite. The Arabian Journal for Science and Engineering* 32 (2B): 359–364.

54 Sastra, H., Siregar, J.P., Sapuan, S. et al. (2006). *Tensile properties of Arenga pinnata fiber-reinforced epoxy composites. Polymer-Plastics Technology and Engineering* 45 (1): 149–155.

55 Mahjoub, R., Yatim, J.M., Sam, A.R.M. et al. (2014). *Characteristics of continuous unidirectional kenaf fiber reinforced epoxy composites. Materials & Design* 64: 640–649.

56 Abdellaoui, H., Bensalah, H., Echaabi, J. et al. (2015). *Fabrication, characterization and modelling of laminated composites based on woven jute fibres reinforced epoxy resin. Materials & Design* 68: 104–113.

57 Yousefi, A., Lafleur, P., and Gauvin, R. (1997). *Kinetic studies of thermoset cure reactions: a review. Polymer Composites* 18 (2): 157–168.

58 Raquez, J.-M., Deléglise, M., Lacrampe, M.F. et al. (2010). *Thermosetting (bio) materials derived from renewable resources: a critical review. Progress in Polymer Science* 35 (4): 487–509.

59 Guilleminot, J., Comas-Cardona, S., Kondo, D. et al. (2008). *Multiscale modelling of the composite reinforced foam core of a 3D sandwich structure. Composites Science and Technology* 68 (7-8): 1777–1786.

60 Saba, N., Jawaid, M., Alothman, O.Y. et al. (2016). *Recent advances in epoxy resin, natural fiber-reinforced epoxy composites and their applications. Journal of Reinforced Plastics and Composites* 35 (6): 447–470.

61 Saba, N., Paridah, M.T., Abdan, K. et al. (2016). *Effect of oil palm nano filler on mechanical and morphological properties of kenaf reinforced epoxy composites. Construction and Building Materials* 123: 15–26.

5

Eco-Friendly Epoxy-Based Composites

Vivek Mishra[1] *and Alok Agrawal*[2]

[1] *Department of Mechanical Engineering, Indore Institute of Science and Technology, Rau - Pithampur Road, Indore, Madhya Pradesh 453331, India*
[2] *Department of Mechanical Engineering, Sagar Institute of Research and Technology Excellence, Ayodhya Bypass Road, Bhopal, Madhya Pradesh 462041, India*

5.1 Introduction

Composite material is known to mankind since hundreds of years ago and they applied this innovation for improving the standard of life. Though composite is not a human invention, wood is an example of naturally available composite exists right from the beginning. Bricks made of clay which are incorporated with straw made by Israelites are an ancient example of composites developed by human [1]. From a huge research all over the world in the last few decades, contemporary composites progressed to glass fiber used in the body of automobiles and in aerospace where particulate composites are in use to many other applications. It has been observed that with the advancement in recent technologies, monolithic materials will not be able to meet the demand and the requirement will be fulfilled only by combining two or more than two materials together and named as composite material [2]. Further, a combination of material is said to be composite only if the identity of the combined constituent will be retained. In other words, composite can be explained as, if the combining constituent will not merge into each other or if they do not dissolve among themselves, they act as concert. Usually, the components which are combined should be identified physically with an interface between them. In the combination, one phase is generally continuous and is called matrix phase and the rest phase, which may be one or more are discontinuous phase, is known as reinforcing phase. Both the phases has their defined function, i.e. matrix phase will transfer stresses between the reinforcing phase. Matrix phase also protects the counterpart from various damages like mechanical or environmental. On contrary to that, reinforcing or discontinuous phase in the form of fibers or particles improves the different properties. It is very important to design the composite system properly so as to extract proper advantage of both the phases (strength from discontinuous phase and toughness from continuous phase) which is not available in conventional material.

Epoxy Composites: Fabrication, Characterization and Applications,
First Edition. Edited by Jyotishkumar Parameswaranpillai, Harikrishnan Pulikkalparambil, Sanjay M. Rangappa, and Suchart Siengchin.

Composite materials are commonly classified as metal matrix composites (MMCs), ceramic matrix composites (CMCs), and polymer matrix composites (PMCs) on the basis of continuous phase. PMCs have various advantages over the metal and ceramic counterparts such as often ductile nature, chemical inertness, low density, low cost, and ease of processing [2]. Because of all these unique characteristics of polymers, their everyday application in our daily life is more. Thermoplastic and thermoset are the two broad classifications of polymers. On the basis of their molecular structure, they have different chemical characteristics. The thermoset polymer is distinguished from thermoplastic polymer mainly by their makeover process from prepolymer to finished polymer. Thermoset polymers are not recyclable as they have undergone chemical reaction which originates either by the presence of heat and/or catalyst. It is not recyclable because it will not remelt once it gets cured. During its curing process, small monomers will combine to form network structure which is interconnected through complex link. The line diagram of such structure is shown in Figure 5.1a. With this complex and cross-linking structure, the chain will not slip over one another, which makes the thermoset polymer relatively strong and rigid. Against this, thermoplastic polymers are recyclable as it will melt upon heating and solidify once the temperature decreases. Contrary to the chemical changes occur during curing of thermoset, changes occur in thermoplastic are physical. In thermoplastics, monomers are joined end to end with no cross-link between layers as shown in Figure 5.1b. These polymers can be reinforced with either fibers or particles and named accordingly as fiber-reinforced polymer composites or particle-reinforced polymer composites. Further, the reinforcement may be either synthetic fiber/filler, i.e. man-made, or natural fiber/filler, i.e. derived from natural resources.

Natural fibers are eco-friendly and biodegradable substance. Government regulations and environment awareness pushed the world toward materials that are attuned with environment as well as do not produce any harmful effect on human. Nowadays, natural fiber-based composites are attracting the scientist as a new hope in lieu of synthetic fiber for the safeguards of environment. With an expensive and ecological alternative over petroleum-based materials, natural fiber-reinforced

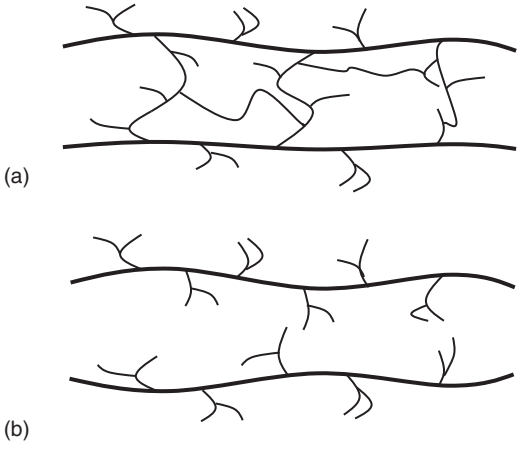

Figure 5.1 Molecular structures: (a) thermoset polymer and (b) thermoplastics polymer. Source: Agrawal [3].

Table 5.1 Pros and cons of natural fiber composites (NFCs).

Pros	Cons
Density is low and specific strength is high	Low durability
Obtained from renewable resource	High moisture absorption
Little energy is required for production	Greater variability of properties
Less abrasive damage to machines	Low strength against synthetic fiber
Low toxic fumes when subjected to heat	Inconsistent properties
Less hazardous	

Source: Modified from Pickering et al. [4].

polymeric composites found its usage in a wide variety of applications. Natural fiber polymer composites (NFPCs) have various advantages as well as disadvantages over synthetic fiber which is summarized in Table 5.1.

Natural fibers are commonly categorized based on the source from which they are available, i.e. plant, animal, or minerals. Cellulose is the major structural constituent of all kinds of plant fibers, whereas protein is the major constituent of animal fiber. The use of mineral fiber was diminished which was earlier used because of its hazardous nature. Among plant and animal fibers, plant fibers are more suitable to be used as reinforcement as it fulfills the structural requirement of composites and also can be artificially grown and harvested according to the need.

Matrix act as an important part of natural fiber-reinforced composites. For this, polymer matrix is most suitable because of its very low-density and low-temperature processing, so that plant fiber does undergo any thermal damage. Polymers have a high toughness value which prevents the fiber from mechanical damage and nicely distributes the load. Both the categories of polymers can be used in the combination with plant fibers to develop composite material. Thermoset has certain advantages over thermoplastic in terms of resistant to temperature, dimensional stability, flexibility in design, and cost-effectiveness. Epoxy, vinyl ester, and polyester are the often used thermosetting plastics. All thermosets require at least one more component to be mixed to cure it. In polyester and vinyl ester, it is called accelerator and for epoxy it is called hardener. Among all thermoset polymers, the most feasible polymer is epoxy resin. It is most frequently used because of its good mechanical strength, worthy toughness, and considerable resilience. Epoxy has appreciable resistance foreign hindrance which includes chemical and moisture outbreak. It also possesses excellent insulating properties [5]. Most importantly, it can be cured at normal temperature with appropriate curing agent without any external pressure by the source of heating. Also, they are acceptable to almost all materials which make them feasible as continuous phase in composite body [6]. The main aim of this chapter is to present a report related to the performance of various natural fiber-reinforced epoxy composites. This helps the scientific community to get a benchmark and fundamental basis to perform further work in the similar area, so that natural fiber-reinforced epoxy composites can grow its potential application in industries.

5.2 Physical Behavior of Natural Fiber/Filler-Reinforced Epoxy Composites

Apart from renewable, sustainable, and eco-friendly, polymeric composites with natural fibers as reinforcement have received a lot of attention as possible alternative replacement for synthetic fibers mainly because of its high specific strength at very low density. The density of the composites depends on the relative fraction of continuous and discontinuous phase. Some natural fibers have density more than epoxy matrix and some have less than epoxy matrix. So it is difficult to say that with the inclusion of natural fiber in epoxy, density of epoxy-based composites decreases or increases. Generally, most of the natural fibers are slightly denser as compared to epoxy, so generally, with natural fiber content density of epoxy composites increases, though the increase is very little. There are various methods of measuring the density of composites which include Archimedean principle, buoyancy method, and displacement method. Theoretically, density is evaluated using the rule of mixture model. Equations 5.1 and 5.2 were used for evaluating the density for single-filler composites and hybrid filler composites, respectively [7, 8]. It is generally found that experimentally evaluated densities are not equal to theoretically calculated values of density which is mainly because of the presence of voids. Also, voids present usually alter the expected properties of the developed composites. This is the reason that density is considered to be as vital factor determining most of the other properties of developed material. The generated voids can be evaluated using Equation (5.3):

$$\rho_{ct} = \frac{1}{\left(\frac{W_{f1}}{\rho_{f1}} + \frac{W_m}{\rho_m}\right)} \tag{5.1}$$

$$\rho_{ct} = \frac{1}{\left(\frac{W_{f1}}{\rho_{f1}} + \frac{W_{f2}}{\rho_{f2}} + \frac{W_m}{\rho_m}\right)} \tag{5.2}$$

$$V_v = \frac{\rho_{ct} - \rho_{ce}}{\rho_{ct}} \tag{5.3}$$

where $W_{f1,}$ W_{f2}, and W_m are the weight fraction of filler 1, filler 2, and matrix, respectively. $\rho_{f1,}$ ρ_{f2}, and ρ_m are the densities of filler 1, filler 2, and matrix, respectively. ρ_{ct} and ρ_{ce} are the theoretical and experimentally measured densities.

When natural fibers are incorporated in epoxy matrix, certain amount of void gets generated. It is mainly because of the natural structure of such fiber. As natural fiber consists of lumen in its cellulose structure, it acts as voids. It signifies that natural fiber contains natural voids within it and results in the increase in voids with increase in fiber content. Thus, fiber with less lumen results in less voids generation and fiber with more lumen results in more voids generation. A study performed by Devireaddy and Biswas [7] shows that, with banana fiber in epoxy matrix, void content is more whereas with jute fiber in epoxy matrix, void content is less. The reason is smaller lumen in jute fiber as compared to banana fiber. Voids generation also attributed to poor bonding between fiber and matrix. Poor bonding results in incomplete wetting of fiber and the gap originated gives rise to voids [8]. Apart from

the content of fiber, density and void content vary with the length of fiber used as well. Bhagat et al. [9] reported that with an increase in the length of fiber reinforced with matrix, the density of composite decreases linearly. In their study, they incorporated coir fiber and luffa fiber in epoxy matrix by varying length from 15 to 35 mm and observed the linear decrement in density. Also, with an increase in fiber length, void content increases which is mainly because of the decrease in packaging with increase in fiber length. This may also lead to the disruption of fiber distribution and generate more voids. Density and porosity of natural fiber-reinforced epoxy composites also get influenced by the fiber treatment and the duration of such treatment. Yusup et al. [10] used oil palm empty fruit bunch as reinforcement material in epoxy matrix. They performed alkali treatment over fiber for two different durations, i.e. 12 and 24 hours and fabricated different sets of composite with similar fiber content. These sets also include one set of composite with untreated fiber. Later, they compared the results obtained during density and porosity measurement and found that density of composite is minimum when untreated fiber is used and increases with increase in duration of alkali treatment. Further, they observed that porosity of 12-hours-treated composite has the higher percentage which is 2.02% followed by the untreated fiber treatment of 1.98% and 24-hours fiber treatment of 1.57%.

Another very important physical property is water absorption rate which is the major drawback in natural fiber-reinforced composites. Natural fibers are hydrophilic in nature and because of this, moisture absorption occurs more in such composites. Natural fibers mainly comprise of cellulose, hemicellulose, and lignin. Among them, cellulose and hemicellulose have high –OH to carbon ratio and hence absorb more moisture, whereas lignin has low –OH to carbon ratio and hence hydrophobic in nature.

When the molecules of water enter the natural fiber, they generally swell up as these water molecules capture the space between microfibrils. The absorption of water by natural fiber given by various factors includes fiber content, ambient temperature, nature of fiber, diffusivity, and the response between water and the polymer [11]. Among various factors, diffusivity is the major factor which governs the absorption of water molecules into such polymeric composites. The swelling of fibers results in the formation of microcrack which further transforms to debonding of fiber–polymer interface. This debonding results in poor transfer efficiency of load applied and reduces the mechanical properties of composites [12]. Water absorption test was generally carried out as per the ASTM D 570-98 standard. According to this standard, the samples were immersed in water at ambient temperature for the study of water absorption kinetics. The specimens were taken out on a regular interval of time weighted without any delay. Precise balance is used to evaluate the amount of absorbed water. The amount of water absorption is given as:

$$\text{Water absorption } (\%) = \frac{W_2 - W_1}{W_1} \times 100 \tag{5.4}$$

where W_1 is the weight of sample before immersion into water (g) and W_2 is the weight of sample after immersion into water (g).

It is a common experience regarding water absorption test that water absorption rate increases with fiber content and immersion time. The same was reported by

Reddy et al. [13] in their work. They fabricated cordia dichotoma epoxy composite using different fiber contents and performed the test for the duration of 240 hours. They found that with an increase in the fiber content, the absorption rate increases. Also, a sharp increase in the absorption rate is observed for the first 72 hours of duration, and after that, absorption rate reduces and saturation point is attained once the 192 hours of test duration is completed. Later, no further absorption of water is reported. They found the maximum water absorption of 6.07% for maximum fiber content. The amount of water absorption follows Fickian diffusion law, where rapid water absorption takes place at the beginning of the contact of matter to water; subsequently, a saturation point is reached. Further, when normal fiber was replaced by alkali-treated fiber, water absorption rate decreases and maximum absorption of 5.13% is registered. Alkaline-treated natural fiber-reinforced epoxy composite has low rate of water absorption. This is mainly because in treated fibers, the number of hydrophilic hydroxyl groups reduces by reacting with 5% NaOH and results in prohibiting the water from the substrate of composite. Figure 5.2 shows the graphical representation of water absorption rate. UF stands for untreated fiber, AF stands for alkali-treated fiber, and 0, 10, 15, 20, and 25 represent fiber content. The water absorption rate also depends on the type of fiber used as observed by Chaudhary et al. [14] where they fabricated composites with different combinations of fiber keeping other parameters same and reported different absorption rate for different combinations.

The attainment of saturation time depends on the test environment as well. Bera et al. [15] provided three different environment of distilled water, sea water, and subzero temperature water to epoxy/luffa fiber composites and evaluate water absorption rate. They reported that saturation time is least for subzero temperature environment, i.e. 84 hours which increases to 108 hours for distilled water and

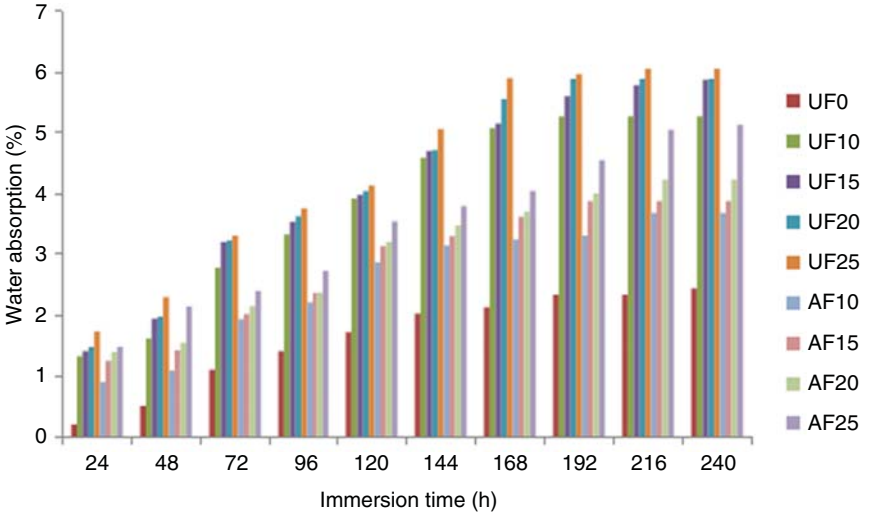

Figure 5.2 Water absorption characteristics of untreated and treated fiber epoxy composites. Source: Reddy et al. [13].

further increases to 120 hours for salt water. Water absorption rate also depends on the temperature of the environment as studied by Anand et al. [16]. They performed the test with distilled water at ambient temperature and with boiling distilled water. In their analysis, they found that in boiling water environment, water absorption rate is high as compared to room temperature water. Also saturation time gets affected by the temperature of water. With boiling water as an environment for composite, saturation time is less, i.e. water absorption ceases early as compared to the room temperature water.

Water absorption is an undesirable phenomenon as it greatly affects the mechanical properties of the fabricated composites. As reported by Habibi et al. [17], tensile modulus of the epoxy composites reinforced with flax fiber reduces immersion time drastically. The rate of decrement is more in the initial phase of immersion and once it reaches the saturation phase, the rate of decrement reduces. A decrement of 30% in the tensile modulus is registered. Similarly, other mechanical properties were also deteriorated with immersion time as reason behind them is common. Actually, diffusion of water inside the composite causes plasticization of body which decreases mechanical properties. Against that, mechanical properties increase due to induced post-cross-linking. In most of the cases, the significance of water uptake is quite high so that plasticization was predominant, leading to a significant decline in the different mechanical properties. A lot of work has been reported to reduce water absorption rate of such cellulose-based composites. Among them, surface modification of fiber [13] and hybridization of composite body [18, 19] are common which significantly reduced the water absorption rate. During hybridization, filler is combined with fiber and reinforced with epoxy matrix. It is supposed that incorporation of filler particles in epoxy matrix clogged the pores and microcracks within the complete surface of the composite, causing a restricted percentage in water absorption. Addition of filler develops the effective interface bond with fiber and matrix which reduces the water uptake by reducing the affinity to absorb water through capillary action. Though, reduction in water absorption occurs when filler is thoroughly encapsulated by the matrix body. This happens only when limited amount of filler is added, as beyond a prescribed limit, volume fraction of entrapped voids increases because the high content of filler particle gives rise to agglomeration.

5.3 Mechanical Properties of the Epoxy-Based Composites

The reinforcement of fibers with high strength in polymer matrix can substantially enhance different mechanical properties like hardness, tensile strength, flexural modulus, and impact strength. Mechanical properties of natural fiber-reinforced composites are mainly dependent on the different factors which include type of material used, quantity of fiber being reinforced, distribution of fiber in the matrix body, and the processing technique. Apart from these factors, the bonding strength and the load transfer mechanism at the fiber–matrix interface also play an important role [20].

5.3.1 Tensile Properties

The acceptance of the composites for the engineering application could be well judged with the tensile behavior of these materials. With tensile test, the various data that can be evaluated are modulus of elasticity, ultimate tensile strength, and elongation at break. The effect of the crosshead speed and variation of the fiber content on the mechanical properties of the composite sample can be determined. It is well accepted that the addition of the reinforcement material to the matrix will improve the tensile properties [21].

Sarikaya et al. [22] studied the effect of different natural fibers reinforcement on epoxy matrix. The composites were prepared by combining two different techniques, i.e. molded fiber production technique and resin transfer molding technique. The fabricated samples when undergone tensile test, different values of tensile strength were obtained. For birch/epoxy composites, 29.52 MPa of tensile strength is recorded. Likewise for palm/epoxy and eucalyptus/epoxy composites, the tensile strengths obtained were 42.24 and 45.28 MPa, respectively.

When epoxy matrix is reinforced with sisal fiber, the tensile properties of the composites were found to be increased with the increase in fiber content of up to 30 wt.%. The maximum values obtained is due to a strong adhesion between the fiber and matrix which led to uniform transfer of stress from epoxy to sisal fibers [23]. The tensile loading behavior for the combination of 25 wt. % of kenaf fiber and 75 wt.% of epoxy matrix composites fabricated by both resin casting (RC) and vacuum-assisted resin infusion (VARIM) methods with different fiber lengths was performed by Mohan and Kanny [24]. In their analysis, they found that with variation in the fiber length of kenaf fiber, the tensile strength, tensile modulus, and elongation at break vary. This value reaches to maximum with the increase in fiber length of up to critical length of fiber and thereafter reduces with the increase in fiber length. From the result, it was found that the superior tensile value is obtained for 30-mm fiber length. An optimized and stable network of the composite structure can be obtained at critical fiber length. The fiber–matrix interface, stress transfer, and adhesion properties might be optimum for 30-mm fiber length. Fiber length more than the critical fiber length could result in bending and the entanglement of fibers, which decreases effective fiber–matrix stress transfer, whereas low fiber length (<critical length) might not have sufficient length to withstand the load.

Some authors [25] compared the tensile properties of woven fabric-reinforced epoxy composites (aloe vera, sisal and its hybrid). The study revealed that the woven sisal-reinforced composite exhibits higher strength compared to others. This may be due to the higher specific properties of sisal fiber in comparison to the aloe vera fiber. The woven mat composites have extra features like interlace gap or spacing, interlace point, and unit cell. It has balanced properties by the interlock of fiber arrangement which in turn increases the strength. The tensile properties can be further enhanced if the fiber undergoes various chemical treatment processes, such as silane treatment, benzoylation, and mercerization, before processing for the composite fabrication. The chemical treatment process increases the adhesive bonding capacity of the fibers with the matrix material.

Another important mechanical property is flexural strength which is the combination of tensile and compression strength. During the flexural test, different mechanisms take place simultaneously. The different mechanisms include tension on outer layer, compression on inner layer, and shearing on transverse axis. As fiber-reinforced polymer composites have increasing application in the different industries, they are prone to such loading situation in which terrible failure may take place as foreign load increases. Thus, the understanding of flexural properties of the composite materials is of importance [26]. The flexural properties of the composites can be determined under three-point bending in a universal testing machine as per the ASTM D790 standards.

The flexural strength of short kenaf epoxy composites decreases with increase in fiber content. The decrease in the flexural property may be due to the agglomeration of the short fibers as the fiber content increases. This agglomeration could cause the stress transfer to the reinforcement gets blocked and results in reduced flexural strength and modulus [27].

The three-point bending test carried out on jute fabric-reinforced epoxy composites exhibited some interesting results, as shown in Figure 5.3. It is observed that the composite with 10% of fabric content exhibits reduction in flexural properties when compared to neat epoxy. The reduction may be due to a weak interfacial bonding and the presence of voids in the fabricated epoxy. It is also found that the flexural properties increase after 10% of fabric and maximum flexural strength and modulus are obtained in jute fabric composites having 50% of fabric reinforcement [28].

The variation in flexural strength with jute fiber content in epoxy matrix is presented in Table 5.2. In their investigation, they worked for untreated and

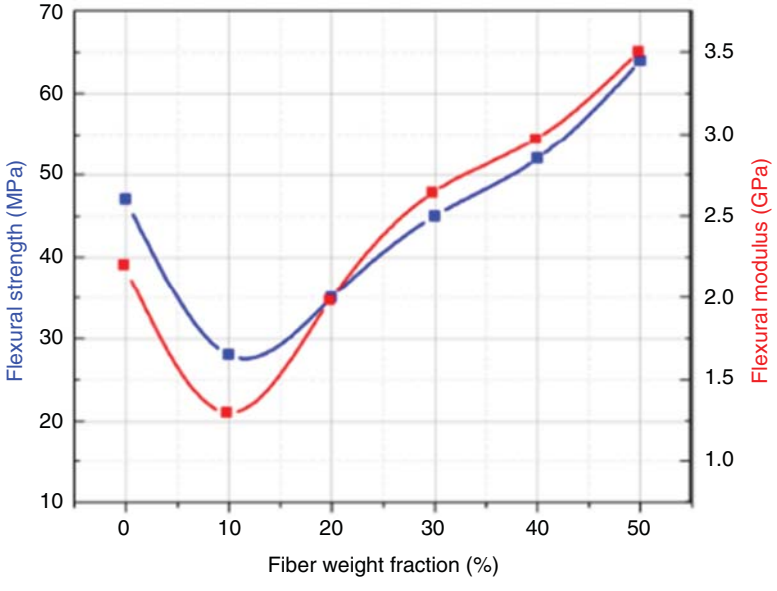

Figure 5.3 Effect of fiber weight fraction on flexural properties of composites. Source: Ikbal et al. [28]. © 2017, Textile Focus.

Table 5.2 Flexural properties of epoxy/jute composites.

Sample	Flexural strength (MPa)	Increase (%)	Flexural modulus (GPa)	Increase (%)
C-fiber	87.0	—	36.8	—
A-fiber	101.1	16.6	47.5	29.1
S-fiber	107.8	23.8	50.5	37.4
AS-fiber	128.5	47.6	70.1	90.6

Source: Dilfi et al. [29]. © 2018, John Wiley & Sons.

surface-treated fiber. C-fiber is for untreated fiber, A-fiber is for alkali-treated fiber, S-fiber is for silane-treated fiber, and AS-fiber is for alkali/silane-treated fiber. The combination of alkali and silane when used for the treatment exhibits highest improvement in flexural properties when compared to untreated fiber, alkali-treated, and silane-treated composites. The improvement in the flexural behavior is due to the strong interfacial bonding between fiber and matrix. In C-fiber composites, due to the weak interfacial bonding, the flexural property reduces. Another reason for enhanced properties shown by the treated fiber is mainly due to the reduction in the hydrophilicity of the treated fibers [29].

5.3.2 Impact Properties

In spite of numerous advantages of natural fiber composites, impact strength of such composites is comparatively low with respect to synthetic fiber-reinforced composites. Impact strength is defined as the capability of a material to bear shock load. It is actually an energy absorbed by the material during impact loading situation. Impact strength depends on the number of parameters like elastic modulus, strength, orientation and length of fibers, and fiber–matrix interfacial bond strength. Impact energy also depends on the procedure and type of test performed on the specimen. Charpy and Izod tests are the fast and easy methods that permit to generate large quantity of data. These test methods are economical as they can simply set up to test a large number of samples and obtain a large quantity of data in very short span [30]. Izod and Charpy impact tests are performed in accordance with ASTM D256 and ASTM A370 test standards, respectively.

Impact behavior of sisal fiber-reinforced epoxy composites was analyzed. It is noted that the impact toughness of the composite is directly proportional to the fiber content. The sisal fiber used in this investigation is raw sisal fiber and surface-modified treated fiber and their comparison is the prime aim of the work. The results obtained during experimentation are shown in Table 5.3. The scanning electron microscopic image of the tested composite revealed that there were higher occurrence of fiber pullout in untreated fiber composites in comparison to treated fiber composites as observed in Figure 5.4. As the number of fiber pullout is more with untreated fiber, it may be concluded that untreated fiber has low bonding strength with epoxy matrix. If the bonding between fiber and matrix is poor, major

Table 5.3 Impact energy of epoxy/sisal fiber composites.

Fiber content in composite (wt.%)	Average impact energy of untreated sisal fiber-reinforced epoxy composites (J)	Average impact energy of treated sisal fiber-reinforced epoxy composites (J)
0	**0.84 ± 0.24**	**0.84 ± 0.24**
5	1.14 ± 0.29	2.14 ± 0.29
10	2.50 ± 0.12	2.96 ± 0.93
15	3.47 ± 0.86	3.96 ± 0.84
30	6.54 ± 0.67	7.55 ± 0.67
50	10.34 ± 0.74	12.65 ± 0.82

Source: Modified from Webo et al. [31].

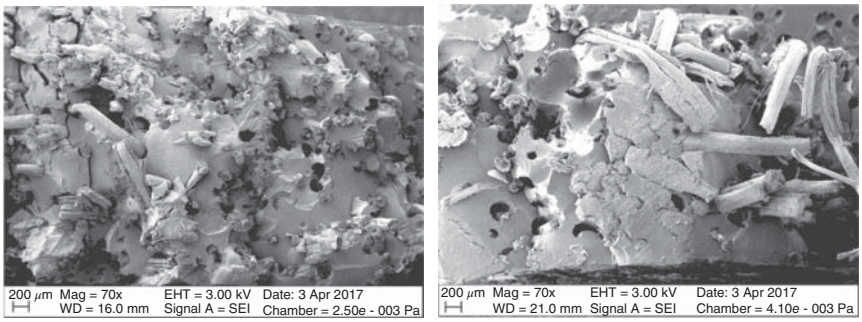

(a) (b)

Figure 5.4 (a) Raw sisal fiber-reinforced epoxy composite and (b) treated sisal fiber-reinforced epoxy composite. Source: Webo et al. [31]. Licensed under CC BY 4.0.

portion of the total energy exerted on composites has to be absorbed by matrix. As we know, matrix has lower fracture toughness as compared to fiber, and the impact energy absorbing capability will be low in that case. But when the bonding between them is good, fiber plays a major role in absorbing the energy. It has been seen that treated fibers show good bonding between the fiber and matrix. The increased impact energy with treated fiber can also be attributed to the enhanced mechanical interlocking due to the presence of rough surface of treated fibers and better interfacial adhesion [31].

The impact strength of bamboo fiber/epoxy composites was also determined. The change in impact strength with varying fiber content (0–40 wt.%) is represented in Figure 5.5. The impact strength of the bamboo-reinforced composite increased up to 30 wt.% of fiber and decreased on further addition of fiber. The drop in impact strength at higher fiber content may be due to the presence of microspaces between bamboo fiber and epoxy matrix, and it results in several microcracks when impact takes place, which further leads to crack propagation and ultimately decreases the impact strength of the composite material [32].

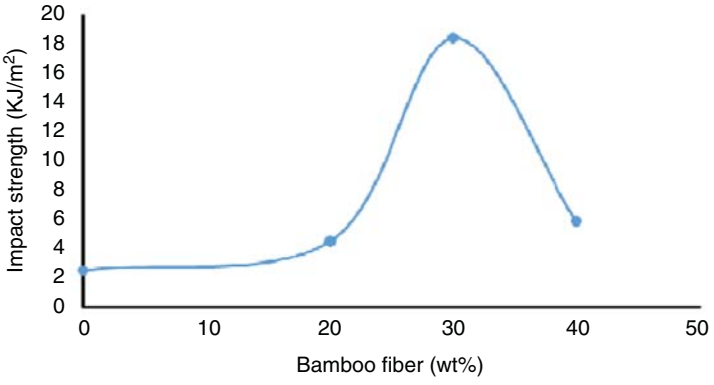

Figure 5.5 Impact energy of epoxy/bamboo fiber composites. Source: Banga et al. [32]. CC BY 3.0.

5.4 Thermal Behavior of Natural Fiber/Filler-Reinforced Epoxy Composites

Unlike synthetic fibers with excellent thermal properties, plant fibers show poor thermal stability. Incorporation of natural fiber in epoxy alters the thermal property of the combination. Hence, evaluating the thermal behavior of natural fiber-reinforced epoxy composites has become a common practice. Thermal stability is an important parameter to decide the future of natural fibers as reinforcement for composites product; therefore, for any developed composites, its thermal stability is of interest. Thermal stability is commonly evaluated using thermogravimetric analyzer (TGA) generally as per the ASTM E1131-03 standard. The TGA analysis is a measure of weight loss of material as a function of temperature. For performing TGA analysis, nitrogen atmosphere is preferred. Analysis is performed generally between temperature range of 30 °C and 700/800 °C which further depends on the type of fiber incorporated. The heating range in almost every case is fixed in between 10 and 20 °C per minute. From the TGA analysis, it can be concluded that the material with higher decomposition temperatures possesses greater thermal stability. During TGA, there are four different and important parameters registered to study the thermal stability of natural fiber-reinforced epoxy composites. Among them, the first is the initial degradation temperature followed by major degradation temperature and final degradation temperature and at the end the amount of char formation during the complete range of temperature. So, each curve of TGA for natural fiber polymer composites consists of three different degrading regions [33].

The first degradation is attributed to the conversion of water molecules to vapor molecules from the composite surface. It also comprises of moisture loss due to thermal degradation of reinforced natural plant fiber. Temperature for the first degradation is generally ranged from 100 to 200 °C. The second degradation occurs between 300 and 450 °C temperatures. Second degradation comprises degradation of both epoxy matrix and natural fiber. In epoxy matrix, degradation is attributed to the pyrolysis and decomposition of aromatic group of epoxy network formed during curing of epoxy from hardener. This leads to the substantial loss of weight, whereas

weight loss in almost all natural fibers is due to the decomposition of pectin, lignin, hemicellulose, and glycosidic linkages of cellulose constituents in the similar range of temperature. Around 700 °C, the third thermal degradation stage of the cured epoxy took place. Here, the volatilization of epoxy network starts forming during curing which finally results in complete degradation. Later, at higher temperature, the formation of char took place by the remaining segment of the composite which is nonvolatile in nature [34].

As it is known that cellulose, which is present in natural fiber, attracts water from the atmosphere and because of this, the thermal stability of the natural fiber-reinforced polymeric composites was higher. From the TGA curve obtained (shown in Figure 5.6) by Gheith et al. [35], it has been observed that when TGA analysis was performed in neat epoxy, 65.11% of weight loss is observed at a temperature of 305 °C. Also epoxy gives the final residue of 9.58%. Against that, with 50% date palm fiber in epoxy, the thermal degradation temperature increases to 316.9 °C with final remaining residue of 19.8%. The increase in residue content is mainly because of the lignin content present in the fiber. Incorporation of fiber in epoxy not only improves thermal degradation but also enhances the residue content which improves the flame resistance behavior of the composites.

When nanocellulose is added to epoxy matrix, slight improvement in thermal stability is observed by Ayrilmis et al. [36]. Against that, substantial improvement in remaining residue was obtained in their analysis when maximum fiber was reinforced. Again it is because of the presence of cellulose. Similar trend was obtained by Saba et al. [37] when cellulose nanofibers were incorporated in epoxy composites, as shown in Figure 5.7.

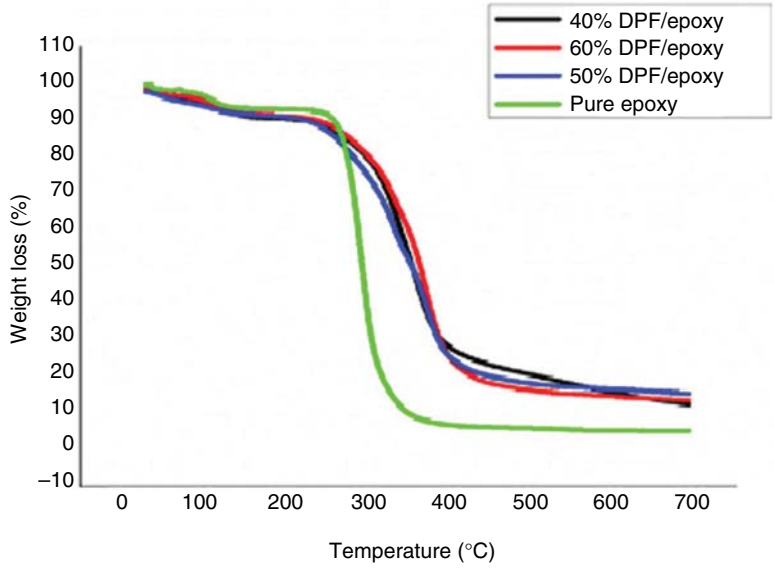

Figure 5.6 TGA plot for epoxy and date palm fiber/epoxy composites. Source: Gheith et al. [35]. © 2019, Elsevier.

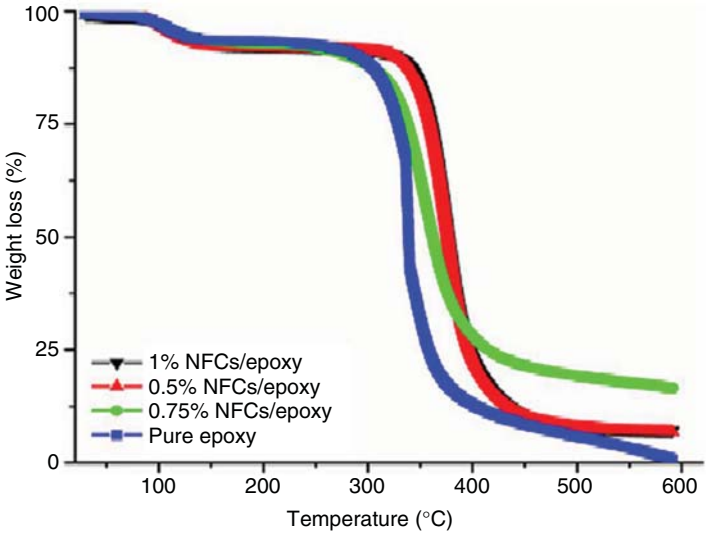

Figure 5.7 TGA graph of epoxy/carbon nano fibers (CNFs) composites. Source: Saba et al. [37]. © 2017, Elsevier.

In their study, they also performed analysis on the advanced stage of degradation and char formation during that stage. The formed char will provide an insulating layer over the material and this layer restricts further formation of char. During the formation of char, mass release of volatile which is combustible reduces rapidly which improves the thermal resistance of the filler polymer. Also, a barrier to the gases which are generated during degradation of polymer is generated which does not allow the fresh oxygen to make proper contact with the polymer surface.

Apart from fiber, cellulose-based filler also delivered increased thermal stability when reinforced with epoxy. A study reveals that when Calotropis gigantea powder was added to jute fiber-reinforced epoxy composites, it produced better result. It is purely attributed to good intrinsic thermal stability of incorporated powder over jute fiber. The residual char left is exceptional when filler was added to fiber in epoxy matrix [38]. Incorporation of filler results in reduction in the amount of epoxy matrix in the composite. It is known that degradation in epoxy occurs due to random chain scission and radical chain mechanism. Once the content of epoxy decreases, the major degradation happened primarily due to reinforcing material and thus enhancing the thermal stability. Another biodegradable Acacia Catechu particle was reinforced with epoxy matrix and thermal stability studied was performed by Shah et al. [39]. The improved thermal stability is obtained when Acacia Catechu particles were added to epoxy matrix. The improvement in thermal stability is attributed due to the formation of chemical cross-link between backbone of epoxy and AC particles' peculiar phenolic structure. The improvement confirms that the blends formed were homogeneous in nature and hydrogen bonds facilitate the formation of cross-links. The detailed thermal behavior of epoxy and epoxy/AC composites can be seen in Table 5.4.

Table 5.4 TGA for neat epoxy, AC particles, and AC/epoxy composites.

Sample	$T_{5\%}$ (°C)	$T_{10\%}$ (°C)	$T_{20\%}$ (°C)	$T_{50\%}$ (°C)	Y_e (%) at 800 °C	Derivative thermogravimetry (DTG) peak (°C)
AC powder	311	428	—	—	81.9	305
Neat	360	374	387	410	10.8	403
AC 0.5%	364	379	392	424	11.6	414
AC 1.0%	365	380	395	435	11.2	424
AC 1.5%	367	383	400	445	12.3	435
AC 2.0%	370	386	404	450	11.4	442

Source: Shah et al. [39]. © 2019, Elsevier.

It is further observed that thermal stability of composites improved once the surface-modified fibers were incorporated in matrix body. With treated fiber, temperature resistance is increased and weight loss is reduced over an unchanged range of temperature. Mittal and Sinha [40] performed alkali treatment over wheat straw fiber and found appreciable enhancement in thermal stability as compared to untreated fiber. For 10 wt.% fiber and epoxy matrix, it was seen that degradation rate with untreated fiber was around 1.01 mg/min and reduced to 0.95 mg/min when treated with alkali. Similar trend was also observed for other filler content as well. The improvement is obvious as treated fiber established good bonding with matrix and takes a major portion of heat, thus preventing the epoxy matrix to get overheated for a longer duration of time. It also provides effective barrier to the volatile product originated during the process of epoxy decomposition in a much more effective manner.

Surface of coir fiber was treated with eco-friendly sodium bicarbonate, and similar enhancement in thermal stability is observed. It is also observed that the time of treatment also effect the thermal stability of the fibers. With an increase in treatment time, fiber thermal stability reduces and hence the degradation temperature reduces [41].

Glass transition temperature (T_g) is another property of natural fiber-reinforced epoxy composites which is of interest among the scientific community. It is defined as the temperature after which material changes its behavior from brittle state to a rubbery state. Generally, glass transition temperature can be evaluated by differential scanning calorimetry (DSC) analysis or by dynamic mechanical analysis (DMA).

For DSC analysis, a sample of around 20 mg is required to be kept on aluminum pan, and the analysis is performed under nitrogen atmosphere with rate of heating varies from 10 to 20 °C/min. The range of temperature for polymeric composites is fixed to around 30 to 600 °C. Generally, DSC is performed in a controlled environment. When the material is heated over a wide range of temperature, endothermic and exothermic process occur, and the main function of DSC is to measure the heat flow during this process. During this analysis, different peaks were observed in temperature/heat flow curve. These are exothermic and endothermic peaks and

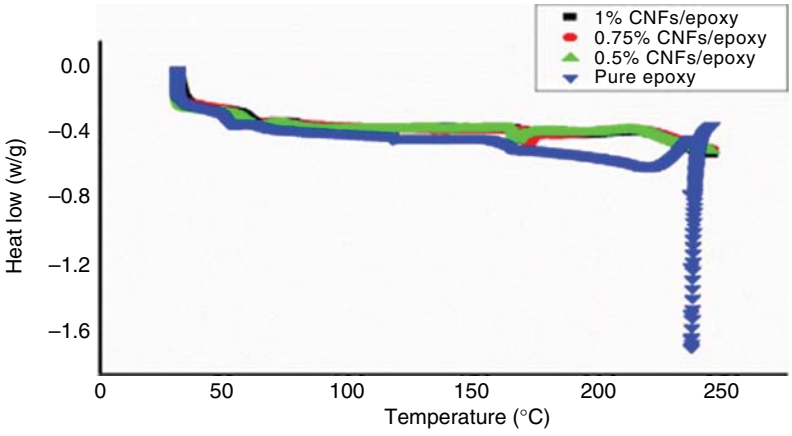

Figure 5.8 DSC analysis for epoxy-based composites. Source: Saba et al. [37]. © 2017, Elsevier.

its magnitude and location provide the thermal phase transformation of the material under observation. Heat is absorbed during endothermic process which provides information like melting, phase transition, evaporation, and dehydration, whereas heat is evolved during exothermic process which provides information like crystallization, oxidation, combustion, and decomposition [42]. The transition took place during endothermic process gives information regarding glass transition temperature and ultimate decomposition temperature [33]. A typical curve obtained during DSC analysis is shown in Figure 5.8.

DMA was performed as per the ASTM D4065-01 or ASTM D7028 standard to evaluate the viscoelastic behavior of polymeric composites. The complete analysis took place as a function of varied temperature. DMA was performed under a mechanical loading situation, i.e. three-point bend mode. The applied load is at an oscillating frequency of around 1 Hz. The temperature is varied over a range from 20–30 °C to 170–200 °C. The heating rate followed for complete analysis varies between 3 and 5 °C/min. The rectangular shape specimen is required to perform this analysis [37]. The DMA analysis provides information regarding storage modulus, loss modulus, and tan δ of the composites. The generalized graphs obtained during DMA analysis for a combination of epoxy with kenaf fiber were shown in Figure 5.9 [43]. Glass transition value can be obtained from storage modulus curve as well as from tan δ curve. Though, it has been seen that the value of glass transition temperature is more convincing when evaluated from storage modulus curve [42]. A typical graph of storage modulus and tan δ was shown in Figure 5.10. The output generated from DMA is used for determining glass transition temperature. The parameters obtained from the graph are shown in Table 5.5 [44]. The glass transition temperature is a measure of attainment of maximum value of damping or loss modulus.

Storage modulus obtained from DMA provides the deformation of specimen when predefined load is applied. Bonding or adhesion between the two different phases of composites is determined by the damping factor, i.e. tan δ curve. It is seen in figure

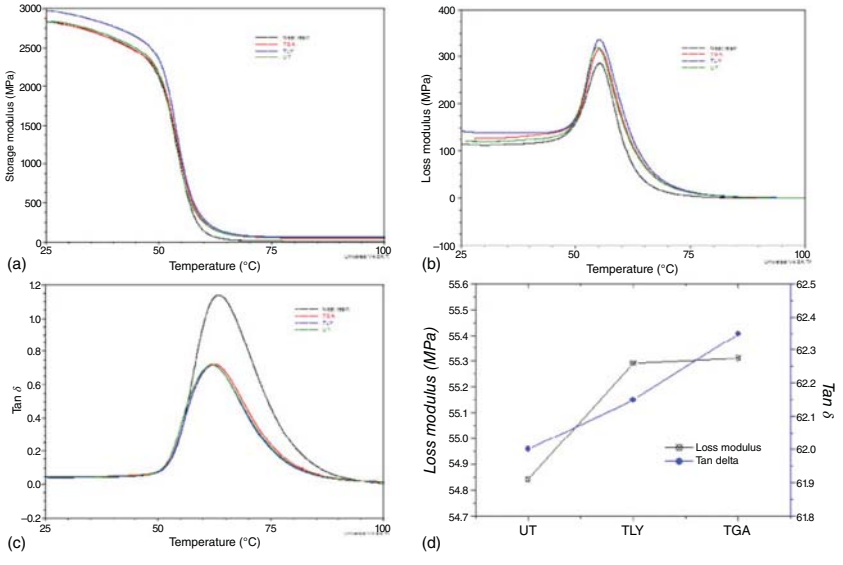

Figure 5.9 Dynamic mechanical analysis: (a) storage modulus, (b) loss modulus, (c) tan δ, and (d) peak maximum value of loss modulus and tan δ. Source: Krishna and Kanny [43]. © 2016, Elsevier.

Table 5.5 DMA of epoxy resin and its composites.

Sample	DMA Storage modulus (MPa)	T_g (°C)
Epoxy	1927	76.1
Epoxy/TF2.5	2126	80.1
Epoxy/TF5	2925	85.2
Epoxy/TF7.5	3225	90.1
Epoxy/TF10	3762	93.5

Source: Xu et al. [44]. © 2018, Elsevier.

that with an increase in fiber content in epoxy, the peak value of curve decreases and also the curve tends to widen. Increase in adhesion between the different phases is represented by this decrease in peak value [44]. Apart from good adhesion, an increase in fiber content increases the glass transition temperature of the developed material. Epoxy has low glass transition temperature. It is because epoxy has some flexible and movable polymer chain within its structure. With incorporation of fiber, cross-linked structure of epoxy gets hindrance which increases the heterogeneous behavior of the combination. With all this, the availability of free space reduces to the great extent and mobility of polymer chain gets limited. Because of this restriction in mobility of epoxy chain, it requires more energy to change its behavior from rubbery to glassy state and increases the glass transition temperature [37].

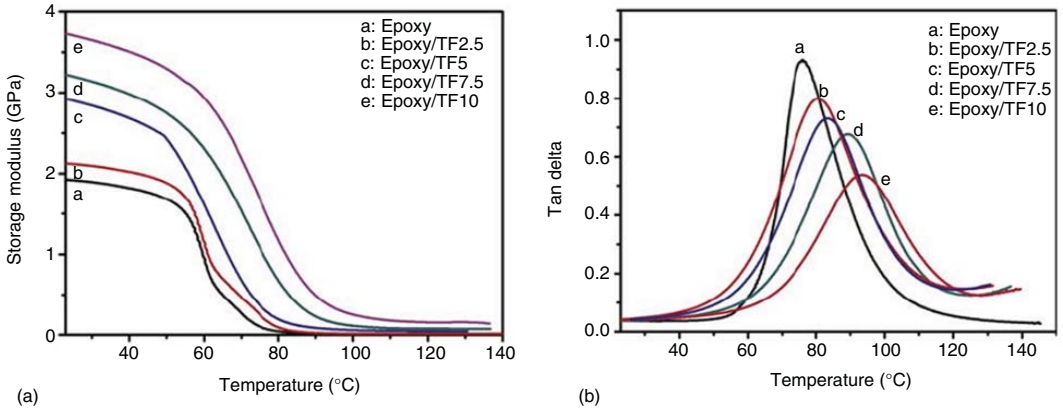

Figure 5.10 The thermomechanical properties of TF-filled composites: (a) storage modulus and (b) tan δ. Source: Xu et al. [44]. © 2018, Elsevier.

5.5 Wear Behavior of Natural Fiber/Filler-Reinforced Epoxy Composites

The impact of wear on the performance of components is widely recognized and the cost associated with the wear has also considered being high. In the 1960s, industrial countries begin their systematic effort to address wear problems. The real problems related with wear in everyday business and work are the direct cost of failures, i.e. loss of productivity, wear part replacement, and increased time and work, as well as increased environmental burden and indirect loss of energy. In case of sudden failure, there is a risk of human loss also. Though wear has been largely studied scientifically, still wear problem exists in industrial application in the twenty-first century. This in reality tells the complication in the wear [45]. Wear is a progressive loss of material due to the contact of two bodies when relative motion between them takes place. In most of the situations, wear can be induced in three major ways, namely erosion, adhesion, or abrasion.

5.5.1 Erosive Wear

Erosive wear occurs due to repeated impact of high-velocity particles over the surface of the material. This kind of wear takes place in numerous situations, such as helicopter blades, pipeline carrying sand slurries in petroleum refining, high-speed vehicles, pump impeller blades, and aircraft working in desert, surfing boats, radomes, and many more [46]. Erosion comprises various wear mechanisms which are mostly controlled by different parameters like particle material, particle size, impact velocity, and angle of impingement. The solid particle tests are conducted as per the ASTM G76 standards. When maximum erosion rate is observed at low impingement angles, then the "ductile mode" of erosive wear is assumed. On the other hand, when maximum erosion rate is observed at high impingement angle, it is assumed that the "brittle mode of erosion" occurs.

Figure 5.11 shows the result of study conducted, and it is observed that the angle of impingement has significant effect on erosion rate and maximum erosive wear takes place at impingement angle of 60°–75° for all the fabricated bamboo fiber composites irrespective of fiber content. This indicates that the erosion mode is neither brittle nor ductile in nature, and it is considered as a semibrittle/semiductile mode of erosive wear [47]. Raghavendra et al. [48] compared the erosion resistance of glass fiber-reinforced epoxy composite with virgin epoxy and also with jute fiber-reinforced composite. Authors reported that the incorporation of fiber in the epoxy results in improved erosion resistance. It was observed that jute fiber-reinforced epoxy composite exhibits higher erosion resistance among the fabricated composites.

5.5.2 Adhesive Wear

Adhesive wear is the category of wear that occurs because of localized bonding generated between two solid surfaces when they come in contact. In this category of

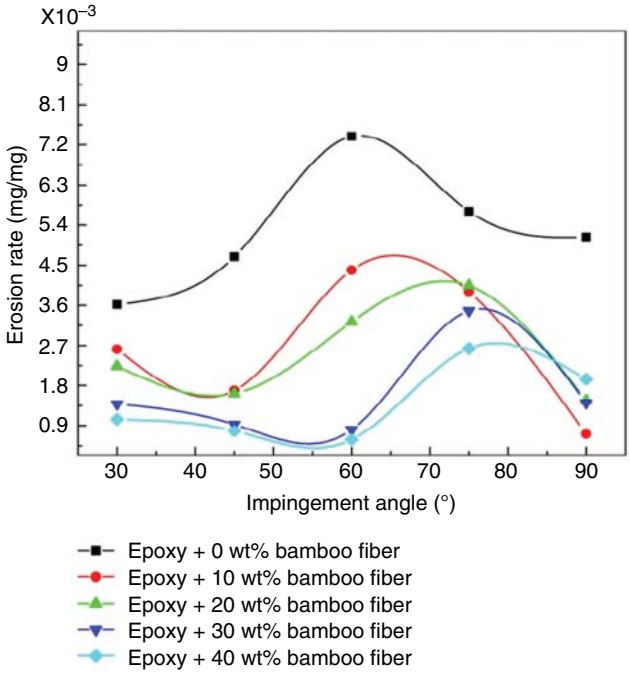

Figure 5.11 Impingement angle effect on the erosion rate. Source: Gupta et al. [47]. CC BY 3.0.

wear, exchange of material takes place. In this wear, material loss occurs from either of the surfaces. Polymer composites based on natural fibers are increasingly considered in several applications like bushing, bearing, linkages, and panels. In general, it is believed that adhesive wear of polymers has been affected by various issues like high material removal, stick-slip behavior, and high coefficient of friction. Also, the adhesive wear performance of such green composites depends on parameters like fiber orientation, applied load, and sliding velocity [49]. Adhesive wear tests are usually performed as per the ASTM G77 test standards using block-on-ring configuration.

Investigation to analyze the frictional and adhesive wear behavior of bamboo fiber-reinforced epoxy composites is performed. Bamboo composites with three different orientations of fibers were tested. A greater improvement in the specific wear rate of the material was observed when the fibers orientation was antiparallel relative to direction of sliding. The past studies also confirmed the similar behavior [50].

5.5.3 Abrasive Wear

In abrasive wear displacement of material occurs from the surfaces which are in relative motion caused by the existence of hard protrusions on both or any of the surfaces, or by the existence of hard particles either in between the surfaces or embedded on any one of them. The first part of the definition is related to

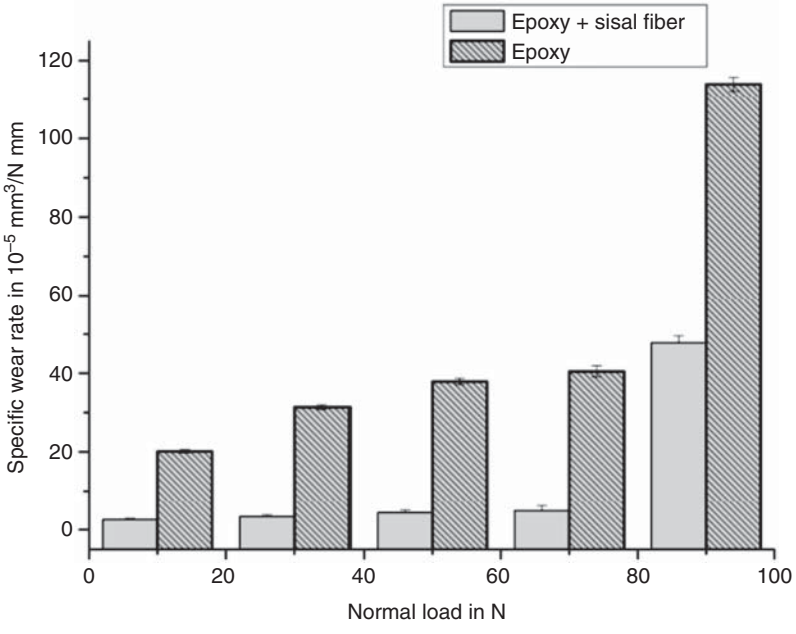

Figure 5.12 Effect of normal load on specific wear rate of sisal fiber-reinforced epoxy composite and neat epoxy. Source: Panda [53]. © 2016, Rajesh Panda.

two-body abrasion, in which the material under testing slides against rougher and harder counterface material, whereas the second part is related to three- and two-body abrasive wear, respectively [51]. Majority of the problems in agricultural and industrial apparatus is connected with three-body abrasion, while two-body abrasion mainly takes place during material removal operation [52]. Two-body and three-body abrasive wear tests are performed as per the ASTM G99 and ASTM G65 standards, respectively.

An analysis was carried out to understand the two-body abrasive wear behavior of sisal fiber-reinforced epoxy composites using pin-on-disk apparatus. The specific wear rate of the sisal fiber composites with respect to different applied loads (10–90 N) at constant velocity was determined as shown in Figure 5.12. All the test samples exhibited increase in specific wear rate as the applied load increases. The surface deformation of the composite material was caused by the asperities and at higher load the real area of contact increases which ultimately accelerates the wear rate. The plain epoxy test pieces showed brittle fracture, whereas the sisal fiber composites showed a decrease in fragmentation. It is further seen that wear rate reduces with sisal fiber incorporation and such behavior is because of the reinforcing effect which improved the mechanical property and results in enhanced wear resistance of composites [53].

Three-body abrasive wear study was performed and its effect on fiber treatment was studied [54]. The fibers used were jute fiber and matrix is epoxy. The main focus of the study is on the effect of normal load on wear. The result indicates that there

is no specific trend of specific wear rate with increase in normal load. When the fiber contents in composites are less, wear rate is more which is mainly attributed to the limited support provided by fiber to the matrix body. Because of this, abrading material of small size makes large depth grooves and probably severe cutting mode of abrasion is a governing mechanism. Wedge formation and ploughing are the reasons for low wear of the specimens. The study also revealed that, with increase in sliding distance, there is a decrement in the specific wear rate of jute fiber-reinforced epoxy composites. When the sliding distance is less, particles used for abrading come in contact with matrix with low modulus, i.e. low hardness, whereas at higher sliding distance, less specific wear rate was observed because of the wear resistance offered by high modulus fibers.

5.6 Bioepoxy Composites

In recent years, biocomposites are getting wide attention because of its eco-friendly nature, fair design flexibility, high strength to weight ratios, and excellent heat and chemical impact resistance, which makes them superior over the other conventional materials. The incorporation of natural reinforcing material in biopolymers significantly enhances the mechanical properties like impact and tensile strengths of the obtained composites. Natural fibers are obtained from plants, animals, or minerals. On the other hand, biopolymers are derived from biological sources like animals, plants, microbes, fossils, and agriculture wastes or produced chemically from biological monomer units like amino acid, natural fats and oils, sugars, and nucleotides [55]. Biocomposites have variety of next-generation uses particularly in construction, electronics, automotive, medicine, and packaging sectors [56].

Johnson et al. [57] carried out a comparative study of bioepoxy with commercially available polyester and epoxy resins. The tensile, water absorption, and soil burial behavior of the resins were examined. Authors reported that bioepoxy resin exhibits higher tensile strength than other two resins. The bioepoxy resin showed better water resistivity in distill water. In soil burial test, it was also identified that bioepoxy resin starts to decompose after 30 days.

Chandramohan and Bharanichandar [58] used roselle, sisal, banana, sisal and banana (hybrid), roselle and banana (hybrid), and roselle and sisal (hybrid) as reinforcing material with bioepoxy to fabricate composite for automobile application. Tensile and hardness tests were performed to understand the behavior of the material.

Baghaei et al. [59] fabricated hybrid biocomposites using recycled denim and jute as reinforcement and bioepoxy as a matrix material. Authors also compared the fabricate composites with recycled denim and jute fiber-reinforced hybrid polyester composites. The tensile and flexural test results exhibit that the bioepoxy matrix composites have higher strength than the polyester matrix composites.

Wang et al. [60] studied the tensile and water absorption behavior of recycled jute fiber-reinforced bioepoxy composites. It was reported that the water absorption is more in case of bioepoxy-based composites in comparison to jute epoxy composites.

It was also reported that the tensile strength of the fabricated composites increases with the increase in fiber content.

Lincoln et al. [61] developed and analyzed the bioepoxy–flax composites for printed circuit board (PCB). The total of 18 key performance parameters were considered for the study, out of which 15 met the requirements and 3 parameters were failed by a close margin. It was reported that the prepared composites offer significant advantage in terms of biodegradability, toxicity, green house gas (GHG) emissions, economic costs, and energy consumption in comparison to petroleum-based glass–epoxy composite. The environmental footprint of the bioepoxy composites is considerably lower than the petroleum-based glass–epoxy PCB. The design of treated flax fiber-based PCB satisfied most of the characteristics essential for proper performance, which comprises thermal resistance, flammability, and electrical and mechanical properties.

5.7 Conclusion

The studies performed on epoxy composites reinforced with natural fiber as well as bioepoxy composites clearly indicated that this category of material exhibits better properties. Thus, it can always be motivating factor to use such material as an alternate to conventional materials for different practical applications. Biodegradable bioepoxy composites may even consider as a strong and feasible solution to environmental problems caused by other polymer matrix-based composites. It was already established that fiber-reinforced epoxy composites have wide range of applications such as aerospace components, aircraft parts, skate boards, skis and snowboards, circuit boards, bicycle frames, boats and ships, hockey sticks, insulator rods, wind turbine blades, pressure vessels, arrow shafts, rocket housings, pipes, recreational equipment, hard tissue applications (bone fracture repair, skull reconstruction, total ankle, hip, knee, and other joint replacements), and dental applications (dental posts, brackets, and orthodontic arch wires). Further study is always required to improve the performance of the existing material.

References

1 Harris, B. (1999). *Engineering Composites*. London: Institute of Materials.
2 Nijssen, R.P.L. (2015). *Composite Materials an introduction*. The Netherland: VKCN Publication.
3 Agrawal, A. (2015) Thermal and dielectric behaviour of polymer composites with hybrid fillers. Ph.D. thesis. National Institute of Technology Rourkela.
4 Pickering, K.L., Efendy, M.G.A., and Le, T.M. (2016). A review of recent developments in natural fibre composites and their mechanical performance. *Composites. Part A, Applied Science and Manufacturing* 83: 98–112.
5 Belaadi, A., Bezazi, A., Bourchak, M. et al. (2014). Thermochemical and statistical mechanical properties of natural sisal fibres. *Composites. Part B, Engineering* 67: 481–489.

6 Feng, J. and Guo, Z. (2016). Temperature-frequency-dependent mechanical properties model of epoxy resin and its composites. *Composites. Part B, Engineering* 85: 161–169.

7 Devireddy, S.B.R. and Biswas, S. (2016). Physical and thermal properties of unidirectional banana-jute hybrid fiber-reinforced epoxy composites. *Journal of Reinforced Plastics and Composites* 35 (15): 1157–1172.

8 Devireddy, S.B.R. and Biswas, S. (2017). Physical and mechanical behavior of unidirectional banana/jute fiber reinforced epoxy based hybrid composites. *Polymer Composites* 38: 1396–1403.

9 Bhagat, V.K., Prasad, A.K., and Srivastava, A.K.L. (2017). Physical and mechanical performance of luffa-coir fiber reinforced epoxy resin based hybrid composites. *International Journal of Civil Engineering and Technology* 8 (6): 722–731.

10 Yusup, E.M., Mahzan, S., and Kamaruddin, M.A.H. (2019). Natural fiber reinforced polymer for the application of sports equipment using mold casting method. *IOP Conference Series: Materials Science and Engineering* 494 (1).

11 Zhang, D., Milanovic, N.R., Zhang, Y. et al. (2014). Effects of humidity conditions at fabrication on the interfacial shear strength of flax/unsaturated polyester composites. *Composites. Part B, Engineering* 60: 186–192.

12 Mochane, M.J., Mokhena, T.C., Mokhothu, T.H. et al. (2019). Recent progress on natural fiber hybrid composites for advanced applications: a review. *Express Polymer Letters* 13 (2): 159–198.

13 Reddy, B.M., Reddy, Y.V.M., and Reddy, B.C.M. (2018). Effect of alkali treatment on mechanical, water absorption and chemical resistance properties of cordia-dichotoma fiber reinforced epoxy composites. *International Journal of Applied Engineering Research* 13 (6): 3709–3715.

14 Chaudhary, V., Bajpai, P.K., and Maheshwari, S. (2018). Effect of moisture absorption on the mechanical performance of natural fiber reinforced woven hybrid bio-composites. *Journal of Natural Fibers* 00 (00): 1–17.

15 Bera, T., Mohanta, N., Prakash, V. et al. (2019). Moisture absorption and thickness swelling behaviour of luffa fibre/epoxy composite. *Journal of Reinforced Plastics and Composites*.

16 Anand, P., Rajesh, D., Senthil Kumar, M., and Saran Raj, I. (2018). Investigations on the performances of treated jute/Kenaf hybrid natural fiber reinforced epoxy composite. *Journal of Polymer Research* 25 (4).

17 Habibi, M., Laperrière, L., and Hassanabadi, H.M. (2019). Effect of moisture absorption and temperature on quasi-static and fatigue behavior of nonwoven flax epoxy composite. *Composites. Part B, Engineering* 166: 31–40.

18 Nair, M.M., Shetty, N., Divakara Shetty, S., and Shambhavi Kamath, M. (2018). Effect of distilled and sea water absorption on mechanical behaviour of short coir fibre epoxy composite/sawdust filler. *Pertanika. Journal of Science and Technology* 26 (1): 261–282.

19 Prasad, V., Joseph, M.A., and Sekar, K. (2018). Investigation of mechanical, thermal and water absorption properties of flax fibre reinforced epoxy composite with nano TiO_2 addition. *Composites Part A: Applied Science and Manufacturing* 115: 360–370.

20 EL-Wazery, M.S., EL-Elamy, M.I., and Zoalfakar, S.H. (2017). Mechanical properties of glass fiber reinforced polyester composites. *International Journal of Advanced Engineering Technology* 14 (3): 121–131.

21 Ramesh, M. and Deepa, C. (2018). *Processing of Green Composites*. Singapore: Springer.

22 Sarikaya, E., Çallioğlu, H., and Demirel, H. (2019). Production of epoxy composites reinforced by different natural fibers and their mechanical properties. *Composites. Part B, Engineering* 167: 461–466.

23 Gupta, M.K. and Srivastava, R.K. (2016). Properties of sisal fibre reinforced epoxy composite. *Indian Journal of Fibre & Textile Research* 41 (3): 235–241.

24 Mohan, T.P. and Kanny, K. (2018). Mechanical properties and failure analysis of short kenaf fibre reinforced composites processed by resin casting and vacuum infusion methods. *Polymers and Polymer Composites* 26 (2): 189–204.

25 Sekaran, A.S.J., Kumar, K.P., and Pitchandi, K. (2015). Evaluation on mechanical properties of woven aloevera and sisal fibre. *Bulletin of Materials Science* 38 (5): 1183–1193.

26 Mishra, V. (2014). Physical, mechanical and abrasive wear behaviour of jute fiber reinforced polymer composites physical, mechanical and abrasive wear behaviour of jute fiber. PhD thesis, National Institute of Technology Rourkela, July.

27 Fauzi, F.A., Ghazalli, Z., and Siregar, J.P. (2017). Effect of various kenaf fiber content on the mechanical properties of composites. *Journal of Mechanical Engineering Science* 10 (3): 2226–2233.

28 Ikbal, M.H., Khan, A.N., Hasan, S.M.K., and Vincent, M. (2017). Study on effect of fiber weight fraction on physical and mechanical behaviour of jute-epoxy composite laminates. *Textile Focus* 2 (4): 40–45.

29 Dilfi, K.F., Balan, A., Bin, H. et al. (2018). Effect of surface modification of jute fiber on the mechanical properties and durability of jute fiber-reinforced epoxy composites. *Polymer Composites* 39: E2519–E2528.

30 Navaranjan, N. and Neitzert, T. (2017). Impact strength of natural fibre composites measured by different test methods: a review. *MATEC Web of Conferences* 109: 01003.

31 Webo, W., Masu, L., and Maringa, M. (2018). The impact toughness and hardness of treated and untreated sisal fibre-epoxy resin composites. *Advances in Materials Science and Engineering* 2018.

32 Banga, H., Singh, V.K., and Choudhary, S.K. (2015). Fabrication and study of mechanical properties of bamboo fibre reinforced bio-composites. *Innovations in Systems and Software Engineering* 6 (1): 84–98.

33 Naveen, J., Jawaid, M., Zainudin, E.S. et al. (2019). Thermal degradation and viscoelastic properties of Kevlar/Cocos nucifera sheath reinforced epoxy hybrid composites. *Composite Structures* 219: 194–202.

34 Saba, N., Alothman, O.Y., Almutairi, Z., and Jawaid, M. (2019). Magnesium hydroxide reinforced kenaf fibers/epoxy hybrid composites: mechanical and thermomechanical properties. *Construction and Building Materials* 201: 138–148.

35 Gheith, M.H., Aziz, M.A., Ghori, W. et al. (2019). Flexural, thermal and dynamic mechanical properties of date palm fibres reinforced epoxy composites. *Journal of Materials Research and Technology* 8 (1): 853–860.

36 Ayrilmis, N., Ozdemir, F., Nazarenko, O.B., and Visakh, P.M. (2019). Mechanical and thermal properties of Moringa oleifera cellulose-based epoxy nanocomposites. *Journal of Composite Materials* 53 (5): 669–675.

37 Saba, N., Safwan, A., Sanyang, M.L. et al. (2017). Thermal and dynamic mechanical properties of cellulose nanofibers reinforced epoxy composites. *International Journal of Biological Macromolecules* 102: 822–828.

38 Vinod, A., Vijay, R., and Singaravelu, D.L. (2018). Thermomechanical characterization of calotropis gigantea stem powder-filled jute fiber-reinforced epoxy composites. *Journal of Natural Fibers* 15 (5): 648–657.

39 Shah, A.H., Li, X., Xu, X. et al. (2019, 2018). Evaluation of mechanical and thermal properties of modified epoxy resin by using acacia catechu particles. *Materials Chemistry and Physics* 225: 239–246.

40 Mittal, V. and Sinha, S. (2017). Effect of alkali treatment on the thermal properties of wheat straw fiber reinforced epoxy composites. *Journal of Composite Materials* 51 (3): 323–331.

41 dos Santos, J.C., de Oliveira, L.Á., Vieira, L.M.G. et al. (2019). Eco-friendly sodium bicarbonate treatment and its effect on epoxy and polyester coir fibre composites. *Construction and Building Materials* 211: 427–436.

42 Neto, J.S.S., Lima, R.A.A., Cavalcanti, D.K.K. et al. (2019). Effect of chemical treatment on the thermal properties of hybrid natural fiber-reinforced composites. *Journal of Applied Polymer Science* 136 (10): 47154.

43 Krishna, K.V. and Kanny, K. (2016). The effect of treatment on kenaf fiber using green approach and their reinforced epoxy composites. *Composites. Part B, Engineering* 104: 111–117.

44 Xu, Y., Dayo, A.Q., Wang, J. et al. (2018). Mechanical and thermal properties of a room temperature curing epoxy resin and related hemp fibers reinforced composites using a novel in-situ generated curing agent. *Materials Chemistry and Physics* 203: 293–301.

45 Patnaik, A., Satapathy, A., Chand, N. et al. (2010). Solid particle erosion wear characteristics of fiber and particulate filled polymer composites: a review. *Wear* 268 (1): 249–263.

46 Mohanty, J.R., Das, S.N., Das, H.C. et al. (2014). Solid particle erosion of date palm leaf fiber reinforced polyvinyl alcohol composites. *Advances in Tribology* 2014.

47 Gupta, A., Kumar, A., Patnaik, A., and Biswas, S. (2011). Effect of different parameters on mechanical and erosion wear behavior of bamboo fiber reinforced epoxy composites. *International Journal of Polymer Science* 2011: 12–14.

48 Raghavendra, G., Ojha, S., Acharya, S.K., and Pal, S.K. (2014). Jute fiber reinforced epoxy composites and comparison with the glass and neat epoxy composites. *Journal of Composite Materials* 48 (20): 2537–2547.

49 Mehoub, G. (2013) Adhesive wear and frictional behaviour of glass fibre reinforced thermoset composites. Thesis-Master of Engineering Technology (METC)-2013, University of Southern Queensland.

50 Nirmal, U., Hashim, J., and Low, K.O. (2012). Adhesive wear and frictional performance of bamboo fibres reinforced epoxy composite. *Tribology International* 47: 122–133.

51 Vencl, A. (2013). Abrasive wear resistance of the iron - and WC - based hardfaced coatings evaluated with scratch test method tribology in industry. *Tribology in Industry* 35 (2): 123–127.

52 Mishra, V. and Biswas, S. (2014). Three-body abrasive wear behavior of needle-punch nonwoven jute fiber reinforced epoxy composites. *International Polymer Processing* 29 (3): 356–363.

53 Panda, R. (2016). Investigation of thermal, mechanical, and tribological behaviour of biobased-resin – crosslinked, sisal-fibre – reinforced epoxy. *Composites* 163.

54 Swain, P.T.R. and Biswas, S. (2017). Abrasive wear behaviour of surface modified jute fiber reinforced epoxy composites. *Materials Research* 20 (3): 661–671.

55 Sanchez-Vazquez, S.A., Hailes, H.C., and Evans, J.R.G. (2013). Hydrophobic polymers from food waste: resources and synthesis. *Polymer Reviews* 53 (4): 627–694.

56 Sadasivuni, K.K., Saha, P., Adhikari, J. et al. (2020). Recent advances in mechanical properties of biopolymer composites: a review. *Polymer Composites* 41 (1): 32–59.

57 Johnson, R.D.J., Arumugaprabu, V., Rajasekar, E. et al. (2018). Mechanical property studies on environmental friendly bio epoxy resin. *Materials Today: Proceedings.* 5 (2): 6815–6820.

58 Chandramohan, D. and Bharanichandar, J. (2013). Natural fiber reinforced polymer composites for automobile accessories. *American Journal of Environmental Sciences* 9 (6): 494–504.

59 Baghaei, B., Temmink, R., and Skrifvars, M. (2017). Recycling of end-of-life textile materials by fabrication of green composites. 21st International Conference on Composite Materials, Xi'an, China, 20–25 August, 2017.

60 Wang, S., Masoodi, R., Brady, J., and George, B.R. (2013). Tensile strength and water absorption behavior of recycled jute-epoxy composites. *Journal of Renewable Materials* 1 (4): 279–288.

61 Lincoln, J.D., Shapiro, A.A., Earthman, J.C. et al. (2008). Design and evaluation of bioepoxy-flax composites for printed circuit boards. *IEEE Transactions on Electronics Packaging Manufacturing* 31 (3): 211–220.

6

Processing of Epoxy Composites Based on Carbon Nanomaterials

Lourdes Ramos-Galicia[1], Juventino López-Barroso[1], Julio Alejandro Rodríguez-González[2], Carlos Velasco-Santos[1], Carlos Rubio-González[2], and Ana Laura Martínez-Hernández[1]

[1] Tecnológico Nacional de México, Instituto Tecnológico de Querétaro, División de Estudios de Posgrado e Investigación, S/N Avenida Tecnológico esquina General Mariano Escobedo, Colonia Centro Histórico, C.P. 76000, Santiago de Querétaro, Querétaro, México
[2] Centro de Ingeniería y Desarrollo Industrial, Departamento de Energía, Av. Pie de la Cuesta #702, Col. Desarrollo San Pablo, Querétaro, Querétaro C.P. 76125, México

6.1 Introduction

Epoxy polymers have diverse applications involving paints, seals, adhesives, coatings, electrical insulators, and fiber-reinforced plastic (FRP) materials. Therefore, the study of the structure, process, properties, and applications of this polymer type in different fields is needed, as this book aims to cover.

Epoxy resin is one of the main matrices used in the development of high-performance composites; these materials have been constantly studied in order to improve, diversify, and innovate their properties and applications. Since nanomaterials were suggested as possible reinforcements of these types of resins, several efforts have been focused to incorporate them in epoxy polymers, characterize, and understand the behavior of the new epoxy nanocomposites. One of the most studied nanoreinforcements in epoxy is carbon allotropes of one and two dimensions (1D and 2D), carbon nanotubes (CNTs) (1D), and graphene-related materials (2D). Both nanomaterials are known for possessing outstanding characteristics, and their carbon nature, which is conducive for the chemical functionalization, allows to diversify the carbon surface. Thus, possible interactions with polymer matrices could be generated depending on the chemical group inserted. Therefore, several options in modified epoxy resins have emerged with these nanomaterials.

CNTs are a special type of carbon-based nanostructure (1D) with intrinsically high mechanical ($E = \sim 1$ TPa), electrical ($\nu = 10^6$ S/m), and thermal ($\lambda = 3500$ (W/m) K^{-1}) properties as well as large surface area and high aspect ratio (AR > 500) [1]. Graphene-based materials are considered 2D nanostructures with a crystalline structure formed by covalent carbon–carbon bonds [2]. Graphene (GE) (single layer) can exhibit outstanding physical and mechanical properties that are superior

Epoxy Composites: Fabrication, Characterization and Applications,
First Edition. Edited by Jyotishkumar Parameswaranpillai, Harikrishnan Pulikkalparambil, Sanjay M. Rangappa, and Suchart Siengchin.

to those of any material currently known [2]. It has been shown that graphene can exhibit extremely high aspect ratio (AR = 10^4), large specific surface area (SA = 2600 m^2/g), and high intrinsic flexibility [3]. These remarkable properties are the result of their 2D topology, crystalline structure, and size.

The aforementioned properties of both 1D and 2D carbon allotropes have resulted in several researches focused to inquire several combinations of these materials with epoxy resin. This chapter review, discuss, and analyze the effect of both allotropes in the epoxies separately and together. The first part involves the influence of carbon nanomaterials in composite properties if reinforcement is added during cure reaction of epoxy, second part is focused to review the effects directly in curing reaction of epoxy, and therefore in this specific polymer, cross-linking is finally overviewed the incidence of CNTs and graphene-related materials in laminated epoxy composites.

The final analysis establishes the epoxy composites with carbon nanomaterials as one of the most outstanding fields for epoxy polymers for may render multiscale composites with multifunctional features.

6.2 Epoxy Nanocomposites Reinforced with 1D and 2D Carbon Materials, Mechanical and Thermomechanical Performance

Epoxy resins are one of the most employed engineering polymers due to a wide variety of applications in automotive, aerospace, construction, electronics, marine, adhesives, sport materials, paints and coatings, among others [4, 5]. Epoxy resins are considered as high-performance polymers which can replace diverse materials, but are susceptible to fracture due to their brittle character [4]. To overcome this limitation, numerous research papers have been published in order to improve the epoxy performance, changing mechanical and thermomechanical properties, mainly. Among all the proposals found in the literature, the use of nanometric reinforcement has showed excellent results and carbon nanomaterials are of special interest. The incorporation of CNTs, graphene-related materials, and a mix of them to obtain a synergic effect in the epoxy resins has produced a variety of tendencies. However, many researchers coincide with some remarks established: dispersion of carbon nanomaterials and the interfacial interaction with the epoxy resin have to be attended for transferring the unique nanoreinforcement features to the matrix. Therefore, numerous treatments to the carbon nanomaterials have been reported, which include covalent and noncovalent functionalization for improving the compatibility with the epoxy matrix. Also, in the last years, interesting results have been published referring to high mechanical and thermomechanical epoxy properties, and analysis about the surface characteristics is to enhance the wettability of the nanomaterials by the resin.

Ma et al. [6] employed functionalized CNTs, which were modified by UV/O_3 processing and a posterior attachment of amino groups using ethylenediamine (EDA). The surface energy of the CNTs and their compatibility with the epoxy resin (Epon 828) were evaluated. They found that the amino functionalization of

CNTs improves their wettability by the resin. This observation was supported by contact angle (CA) measurements of the pristine and modified CNTs. The Epon 828 resin formed a CA of 74.1° ± 2.6° over the CNTs without modifications. The amino functionalization produced a decrease in the CA value until 61.5° ± 3.2°, which means that the reinforcements were more wetted by the resin; therefore, the interfacial interaction between the components was enhanced. The authors calculated the energy of CNTs/Epon 828 resin interface, and the value reported for functionalized CNTs was 38.9 mJ/m^2, which was higher to that found for pristine CNTs (29.5 mJ/m^2). Besides producing a stronger interface, the chemical modification of CNTs promoted a good and stable dispersion in the epoxy resin, avoiding agglomerations which could affect the mechanical performance. They reported results obtained through flexural tests. The highest values of flexural modulus and strength on the reinforced epoxy were ~3.5 GPa and ~130 MPa, respectively, with only 0.5 wt% of amino-CNTs. Pristine CNTs produced slight increments but those were higher than the neat epoxy (~2.9 GPa and ~106 MPa of modulus and strength, respectively). Thermomechanical improvements were observed on the epoxy nanocomposites through dynamic mechanical analysis (DMA) results. Initial storage moduli of the nanocomposites were highly increased with the addition of modified CNTs (Figure 6.1), even they exhibited more thermal stability on the glassy region. The authors attributed this behavior to the strong adhesion between the CNTs and the epoxy matrix, where the polymer chains are hindered by the presence of the nanocarbons reducing their mobility.

In other works, epoxy resin has been reinforced with CNTs without functionalization, but mechanical dispersion was attended before the curing process [7, 8]. Because good dispersion of CNTs is crucial for the obtention of improved epoxy

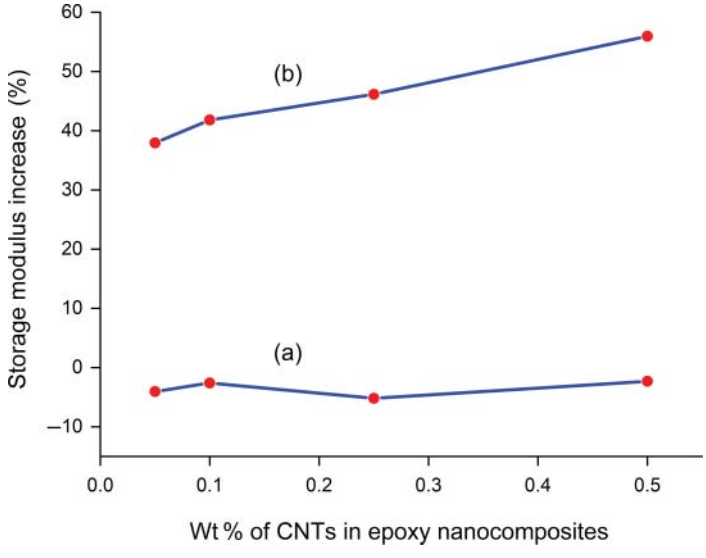

Figure 6.1 Initial storage modulus of nanocomposites reinforced with (a) pristine CNTs and (b) amino-CNTs. Source: Based on Ma et al. [6].

specimens, different techniques of mixing have been proposed. For example, Laurenzi et al. [7] incorporated multi-walled carbon nanotubes (MWCNTs) into pre-heated RTM6 epoxy resin for mechanical mixing during 20 minutes at 90 °C. Besides, the mix was sonicated by both, a sonication probe and an ultrasonic bath for 5 and 90 minutes, respectively, in order to enhance the dispersion of the nanomaterials. Tensile tests of epoxy nanocomposites indicated an increasing on Young's modulus of 42% and 23% respect to the reference (epoxy without MWCNTs), with the incorporation of 0.5 and 1.0 wt% of load, respectively. However, tensile strength values were lower than the specimens without reinforcements. Authors mentioned that decline in the tensile properties as the load increased was due to the manufacturing limits of the dispersion stage.

In an additional research [8], MWCNTs (0.05, 0.1, 0.25, and 0.5 wt%) were dispersed in ML-526 epoxy using a mechanical stirrer and a probe sonicator increasing the time as increases the load, until ~200 minutes. The highest tensile strength of the epoxy nanocomposites increases until 18.83% with respect to the specimens without CNTs, and the load was 0.1 wt%. Even when the Young's modulus showed an increment of 12% with 0.5% of load, the tensile strength declined due to the presence of stress concentration regions originated by the agglomeration of CNTs at higher loading. Therefore, the degree of dispersion reached with the sonicators, and pristine CNTs, produced moderated increments on the epoxy properties, even it has mentioned the brittle condition of some specimens at higher quantities of CNTs. To avoid the excessive agglomeration of the nanomaterials in the epoxy polymers, noncovalent functionalized CNTs have also been employed, owing to no defects are promoted on the graphitic lattice like in covalent functionalization [9, 10]. Different molecules are used in this kind of functionalization, but it is important to consider the affinity of the molecules with the epoxy matrices; otherwise, a weak interface will be formed [11]. Usually, the interaction between the adsorbed molecules and the surface CNTs is through π-bonds because of the presence of sp^2 hybridized carbon atoms in CNTs and the hexagonal rings founded in the additional molecules [12]. The molecules attached onto the CNTs are chosen by their compatibility with the epoxy resins, and some of them are capable to form covalent bonds with the matrix. Poly(4-aminostyrene) (PAS) and polystyrene sulfonate (PSS) were adsorbed onto CNTs for increasing dispersion and interfacial adhesion between CNTs and KFR-120 epoxy resin [11]. The noncovalent modification of CNTs was simple using a ball milling method. Authors reported the formation of covalent bonding between the matrix and the amino groups from PAS in contrast to PSS (which contains sulfonic groups), even when both molecules possess similar structure. Young's modulus and tensile strength of epoxy nanocomposites reinforced with PAS-CNTs were improved by 41% and 34%, respectively, using 1 wt% of loading. In regard to PSS-CNTs, the increments were lower, 25% and 13% for elastic modulus and tensile strength. It is discussed the higher affinity of PAS with the epoxy matrix compared to PSS, due to the kind of groups founded in each molecule: amino and sulfonic, respectively. The amino groups formed chemical bonding with epoxy resin, while sulfonic groups are not enough affined to the polymer.

Melamine also contains amine groups which may form chemical bonding with the epoxy resins. This molecule was noncovalently attached onto the CNT surface by ball milling method [12]. The integrity of the CNT structure was preserved through this modification, and the amino groups founded in melamine formed strong interactions with MY 0510-epoxy resin. Low and elevated loads of melamine-CNTs were evaluated in order to improve the properties of the epoxy matrix (0.1, 0.5, 1, 2, 3, and 5 wt%). Another reason for modifying CNTs is to prevent their agglomeration, which is observed while the load increases, usually around of 1 wt%, but this depends on the dispersion technique employed and the surface features of the CNTs. In the work mentioned, the best performance of epoxy nanocomposites was obtained at 2 wt% of melamine-CNTs, a quantity relatively high compared with other reports [13]. Young's modulus and tensile strength were 64% and 25% more than those observed for epoxy without reinforcements, respectively. At higher loading, the functionalized CNTs formed agglomerates, acting like defects which concentrate the stress. However, the amino groups could form chemical bonds with the matrix for a stronger adhesion between the components.

The works cited previously reported increments in mechanical properties, but even CNTs were chemically or physically modified, or only dispersion attended, the enhancement presented is moderated. A facile and rapid stage for improving the CNT dispersion was proposed, and the results obtained on epoxy nanocomposites were fascinating. Ramos-Galicia et al. [14] used oxidized CNTs (through a mix of sulfuric and nitric acids) to improve the properties of D-3415 epoxy resin. Dispersion of nanomaterials was handled by simple stages. Oxidized CNT agglomerates were grinded and sieved with a #325 mesh. Then, the nanomaterials were incorporated into the resin (0.1, 0.5, and 1 wt%) and sonicated for 1 hour. Epoxy specimens with 1 wt% of CNTs exhibited tensile strength until ~150% higher than the epoxy without reinforcements. Even Young's moduli of nanocomposites remained similar to the reference specimens, elongation at break increases until 150%; therefore, the tensile toughness obtained was 540% more than the simple epoxy. The tensile results of the nanocomposites in previous mentioned works exhibited lower elongation at break than the epoxy matrices without CNTs; therefore, their tensile toughness is not elevated. However, the high tensile properties reported by Ramos-Galicia et al. [14] were attributed to the good dispersion reached and the oxidized surface of CNTs, which probably formed chemical bonds with the epoxy matrix. Thermomechanical results showed an interesting tendency. Storage modulus and glass transition temperature (T_g) of nanocomposites were lower than the epoxy reference (Figure 6.2a). Authors mentioned that the presence of CNTs could hinder the cross-linking process and oxygen groups formed chemical bonds with the epoxy compounds, which affected the stoichiometric ratio between the epoxy resin and curing agent. Therefore, short polymer chains had higher degree of freedom facilitating their premature mobility. This explanation was supported by other recent work [15], where pristine CNTs were employed to reinforce the same epoxy matrix (D-3415) with similar loading (0.1, 0.3, 0.5, 0.7, 0.9, 1.0 wt%), and same process conditions. Epoxy nanocomposites with the ultimate tensile strength displayed 120% more than epoxy reference adding 0.7 wt% of nanomaterials,

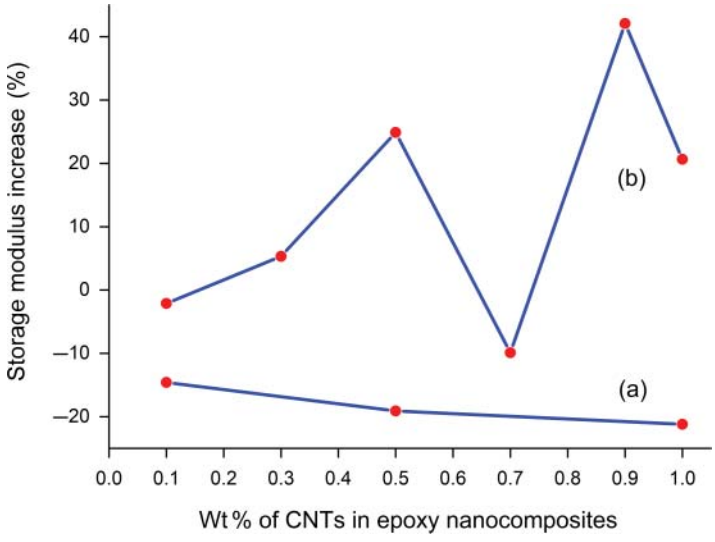

Figure 6.2 Initial storage modulus of nanocomposites reinforced with (a) oxidized CNTs. Source: Based on Ramos-Galicia et al. [14] and (b) pristine CNTs. Source: Based on Ramos-Galicia et al. [15].

which represents a slightly lower performance compared to that observed with oxidized CNTs, discussed at the beginning of this paragraph. Functionalization increases the tensile properties of the epoxy matrices due to a better compatibility between the components and the possibility to form chemical bonds at the interface [11–13]. However, DMA of nanocomposites with pristine CNTs, at almost all loads, showed higher storage moduli than that reported for pure epoxy (Figure 6.2b) [15]. Therefore, the presence of CNTs into the epoxy matrix did not impact, for almost all cases, on the cross-linking degree at those process conditions. Pristine CNTs did not contain oxygen groups to form covalent bonds with the resin or curing agent, but well dispersed, they were able to increase the mechanical and thermomechanical epoxy performance. Some specimens exhibited until ~43% of increments in storage modulus, even higher thermal stability on glassy regions, which means major usefulness as structural materials.

Results reported that for several years, CNT–epoxy systems have been used as a fundament for the study of the adding effect of a structurally similar nanomaterial: graphene. Even though CNTs and graphene are constituted by carbon atoms, the principal difference is their dimensionality: CNTs are 1D material and graphene is a 2D material [14], which can be observed in Figure 6.3.

Since the discovery of graphene in 2004, the attention was centered on its nanolayer [16] and different graphene-related materials emerged quickly [17]; then, some nomenclature proposals have been recommended, as the article published by the editorial team of the journal Carbon [17]. That suggestion was due to the general use of the term "graphene," but it may be referred to graphene oxide (GEO), reduced graphene oxide (RGO), graphene layer, few-layer graphene, multilayer graphene, graphite nanoplates, and exfoliated graphite, among others.

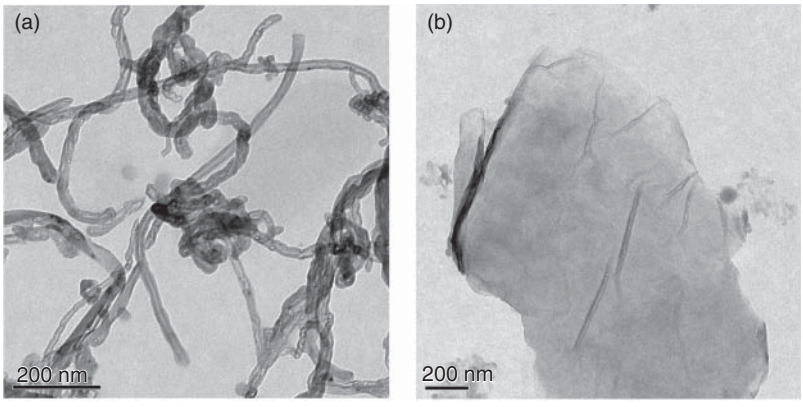

Figure 6.3 Transmission electron microscopy images of (a) 1D. Source: It was prepared by one of the authors, Ramos-Galicia L., and (b) 2D carbon nanomaterials. Source: It was prepared by one of the authors, Ramos-Galicia L.

However, the differences between these nanomaterials may influence on the epoxy nanocomposites; therefore, the 2D carbon nanomaterial used should be specified to consider its structural features. Actually, GEO and RGO have been widely used as reinforcement materials in epoxy matrices, due to their relatively easy production [18]. In the last years, works have been published comparing the epoxy performance of nanocomposites reinforced with CNTs and graphene-related materials, and most of them mentioned that graphene-related materials overcome CNTs in epoxy resins [14, 16, 19, 20]. Nevertheless, Ramos-Galicia et al. [15] found that pristine CNTs and RGO exhibited similar tensile properties, but in thermomechanical behavior, RGO showed lower values of storage moduli. Other publication reported attractive increments on epoxy nanocomposites when GEO was used as a reinforcement [14]. It was reported an ultimate tensile strength of ~180%, elongation at break of ~208%, and tensile toughness of ~760%, in contrast to those values reported for the epoxy reference, and adding only 0.5 wt% of GEO [14]. In this case, the enhancement was produced by the oxygen groups on each graphene layer, good dispersion, and the graphene wrinkled surface, factors that fomented the mechanical interlocking with the epoxy matrix [21]. Authors improved GEO dispersion through grinding and sieving the nanomaterial to avoid agglomeration, which can affect the performance of the nanocomposites (Figure 6.4).

The chemical structure of graphene-related materials affects their wettability by the epoxy resins, and if functional groups are attached to the layers, chemical bonds may be formed, producing strong interfacial surfaces. Besides, their elevated surface area and 2D geometry offer higher contact with the matrix [22]. Table 6.1 shows some works employing graphene-related materials and their performance on epoxy matrices, taking advantages of their unique features and chemical modifications.

Table 6.1 displays different results on mechanical and thermomechanical epoxy nanocomposites due to their physical and chemical structure, and the dispersion method employed for incorporating the 2D carbon materials into the epoxy matrices. Functionalization of graphene-related materials with distinct molecules was probed

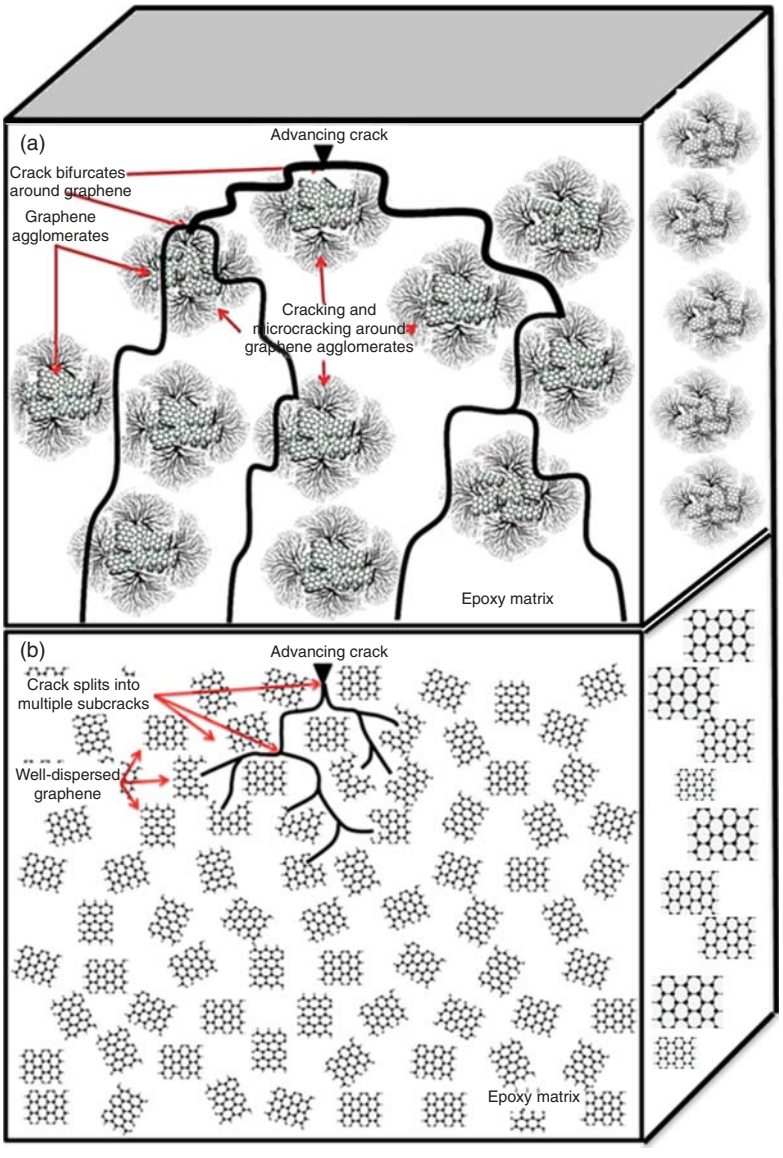

Figure 6.4 Representation of (a) agglomerated graphene and (b) well-dispersed graphene; illustration of crack propagation in a matrix. Source: Atif et al. [5]. CC BY 4.0.

to increase the compatibility between the components, through the major wettability and groups available to form chemical bonds. Actually, wettability is a key factor to improve the interfacial strength, and some authors expose that the surface energy of the graphenic layers must be greater than or equal to that measured for the polymer; therefore, a strong adhesion will be obtained between the components [22, 33]. Regarding additional molecules attached to the graphene-related materials, an interesting work reported the use of a hyperbranched polyamide-functionalized

Table 6.1 Mechanical and thermomechanical properties of epoxy nanocomposites reinforced with graphene-related materials.

Matrix	Graphene-related materials characteristics	Percentage of graphene-related materials	Mechanical properties, percentage of increase with respect to the epoxy reference	Thermomechanical properties, percentage of increase with respect to the epoxy reference	References
Araldite-F epoxy resin	Graphene platelets. 4,4′-methylene diphenyl diisocyanate grafted to graphene platelets	1, 2.5, 4, 5.5 wt%	Young's modulus, 1.6% at 4 wt% of modified graphene platelets Tensile strength under the epoxy reference	T_g, 8.1% with 2.5 wt% of graphene platelets, and 14.7% with modified graphene platelets	[23]
DGEBA type epoxy resin	Graphene nanosheets. 3-aminopropyltriethoxysilane-graphene nanosheets	1 wt%	Tensile strength, 36% and 45% with graphene nanosheets and modified graphene nanosheets, respectively	—	[24]
DER 331-epoxy resin	Different lateral-sized graphene oxide = 10.79, 1.72, and 0.70 μm	0.05, 0.1, 0.3, 0.6 wt%	Young's modulus, until ~12% at 0.05 and 0.3 wt%. Tensile strength was not reported	—	[25]
DGEBA epoxy resin	Thermally reduced graphene oxide	0.05, 0.10, 0.20 wt%	Tensile and flexural properties slightly improved	Storage modulus and T_g, until ~15% and 8%, respectively	[26]
DGEBA epoxy resin	Noncovalent functionalized reduced graphene oxide with polyoxyethylene octyl phenyl ether	0.05, 0.10, 0.15, 0.20 wt%	Tensile strength, 57% at 0.1 wt%	—	[27]
DGEBA epoxy resin	Graphene oxide, and DGEBA-graphene oxide	0.10, 0.25, 0.50 wt%	Tensile strength and modulus, ~13% and ~75%, respectively	T_g, until ~3%. Storage modulus until ~33% at 0.50 wt% of modified graphene oxide	[28]
DGEBA epoxy resin	Graphene nanoplatelets with thickness of 6 nm and 25 μm of lateral size	1.5, 2.0, 3.0, 5.0, 8.0 wt%	Tensile and flexural modulus remained similar to the reference; tensile and flexural strength decreased	Storage modulus, 38% at 8 wt%	[29]

(*continued*)

Table 6.1 (Continued)

Matrix	Graphene-related materials characteristics	Percentage of graphene-related materials	Mechanical properties, percentage of increase with respect to the epoxy reference	Thermomechanical properties, percentage of increase with respect to the epoxy reference	References
Clear epoxy resin	Graphene oxide	1.5, 3, 4.5, 6 vol%	Tensile strength and modulus, ~86% and ~79%, respectively. Impact strength, from 2.56 to 39.7 J/mm^2	—	[30]
Araldite LY1564 epoxy resin	Graphene nanoplatelets, graphene oxide, silane-modified graphene nanoplatelets, amino functionalized graphene nanoplatelets	0.25, 0.5, 1 wt%	Tensile strength and modulus, ~50% (0.5 wt% amino graphene nanoplatelets) and ~18% (1 wt% silane-graphene nanoplatelets), respectively	—	[31]
Epiran 6 epoxy resin	Methacrylate functionalized graphene oxide Poly(vinyl imidazole) (PVI) attached from methacrylate functionalized graphene oxide	0.10, 0.25, 0.50 wt%	Tensile strength and modulus, ~60% and ~46%, respectively, at 0.25 wt% of PVI-modified graphene oxide	—	[32]
YD-128 epoxy resin	Graphene oxide	0.25, 0.5, 1.0, 1.5, 2.0 wt%	Impact strength, ~80%; and critical stress intensity factor ~98% with 1 wt% of load	—	[33]
WSR618 epoxy resin	Hyperbranched polyamide functionalized graphene oxide	0.5 wt%	Tensile strength and modulus, ~24% and ~18%, respectively Fracture toughness and critical energy release rate, ~45% and 78%, respectively	—	[34]
5417A epoxy resin	Graphene oxide with five oxidation levels	0.2 wt%	Critical stress intensity factor, 56%. Critical strain energy release rate, 128% Tensile strength, 16%. Young's modulus, 6%	Storage modulus, ~9% T_g decreased until ~9.6%	[35]

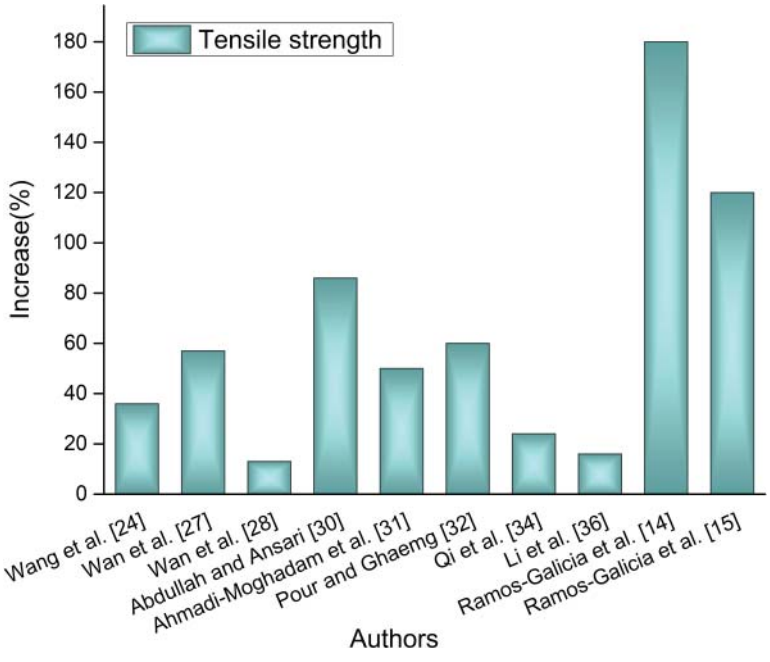

Figure 6.5 Percent enhancement in tensile strength of epoxy nanocomposites reinforced with graphene-related materials respect to the epoxy matrices without nanomaterials employed in each study.

GEO [34]. Hyperbranched polyamide acted like a cross-linker due to its abundant primary amine groups, which can form covalent bonds with the epoxy resin, even before adding the curing agent. Therefore, a strong interfacial adhesion between functionalized GEO and the matrix was obtained, and mechanical results can be observed in Table 6.1 and Figure 6.5. Further chemical modifications have been proposed by Wei et al. [35] like different oxidation levels of GEO achieving good mechanical improvement. Some groups such as epoxy, aliphatic hydroxyls, and ether were mainly found when the oxidation increased, which could form bonds with the curing agent. However, thermomechanical results exhibited lower values of T_g compared to that obtained for epoxy reference. In spite of some increments in storage modulus values, authors mentioned that T_g values under the epoxy reference were due to the lower cross-linking density of the matrix, disturbing the curing process.

Epoxy matrices have displayed good results incorporating CNTs or graphene-related materials; however, some researchers have proposed to use them together more than in separate way [36, 37]. The idea is to reach the best effect of reinforcement with a synergic mechanism between 1D and 2D carbon materials and producing epoxy nanocomposites with high mechanical and thermomechanical performance. It has been mentioned that the combination of graphene-related materials and CNTs produces a 3D hybrid structure; then, CNTs prevent the agglomerations of graphene materials [38]. Yang et al. [38] employed functionalized MWCNTs and multi-graphene platelets (MGPs) for taking advantage of the synergic

effect from these hybrid reinforcements. They commented that MWCNTs inhibit the MGP stacking due to their 1D structure and long and tortuous morphology. The intercalation of 1D and 2D carbon materials also increases the surface area available for the contact with the epoxy matrix. In the above-mentioned work, amine-MWCNTs acted like functional tentacles in the hybrid combination; then, 1D–2D reinforcements and epoxy chains resulted entangled, and the interaction was improved. As a result, the ultimate tensile strength was obtained for the epoxy composites reinforced with 1 wt% of the hybrid combination, reaching until ~36% more than the epoxy reference. The highest tensile modulus (27% more than epoxy) was obtained with the same combination over the performance of the nanocomposites reinforced with only MWCNTs, MGPs, or pristine MWCNTs–MGPs. Therefore, the synergic effect is possible when 1D and 2D carbon materials are combined. An additional work evaluated the 1D:2D ratio. Chatterjee et al. [39] utilized six mixture ratios of CNTs and graphene nanoplatelets (GNPs) in an EPIKOTE 828LVEL epoxy resin. They mentioned that the hybrid samples constructed an interconnected network taking advantages of the high aspect ratio of the 1D reinforcement and the elevated surface area of the 2D carbon material. Authors found that the best combination of CNTs:GNPs was 9 : 1 ratio, where CNTs have more contributions. The epoxy nanocomposites (at 0.5 wt% and the ratio mentioned) displayed a fracture toughness 77% higher than the epoxy reference, and a flexural modulus 17% more than the epoxy without nanomaterials. Similar results were reported by Yue et al. [40], where flexural properties of an epoxy matrix were enhanced by the incorporation of a hybrid combination of CNTs:GNPs in a ratio 8 : 2. They also mentioned the effective formation of a 3D network which increases the interfacial adhesion with the epoxy matrix.

The proposal to improve the epoxy properties through a combination of two different dimensional nanomaterials still offers an area of opportunity. Several variables can be evaluated to find experimental conditions for producing high-performance epoxy nanocomposites. According to the previous researches cited, the use of CNTs and graphene-related materials may be a viable route to increase the epoxy properties; however, more simple, easy, and low-cost processes are required to produce feasible epoxy nanocomposites.

6.3 Tracing of Cure Reaction

The use of a wide range of reinforcements in composite materials requires strict control in the synthesis process. Epoxy resin, one of the most used polymers in the composite industry, cures (polymerizes and cross-links) when is stoichiometrically mixed with a curing agent [41–43]. In other words, in most of the cases, the initial state of precursors is liquid; after the addition of a hardener, they turn on to a solid vitrified material [42]. During this change, an irreversible time-dependent and progressive molecular reaction happens, which requires heat energy. The amount of energy necessary for curing depends on the process requirements and structural performance [42–44]. Epoxy nanocomposites find their applications in aerospace,

automobile industries, structural composites, or in high mechanical resistance together lightweight composites are required [45–48]. Also, protecting coating, equipment for the chemical industry, electrical laminates, and electronic packaging are some of many applications of epoxy resins [46, 49]. Due to these reasons, monitoring of the curing reaction is a vital task during the manufacturing process.

Nowadays, with the outstanding development of carbon allotropes and their application as reinforcement in similar ways of their predecessors, the carbon fibers, techniques such as infrared spectroscopy, Raman, and some analysis such as differential scanning calorimetry (DSC) or DMA have been reported for the characterization of the curing reaction of these nanocomposites. Other techniques such as dielectric spectroscopy or vibrational generation spectroscopy have been mentioned for monitoring changes in the curing reaction of nanocomposites based on epoxy resin and carbon nanomaterials [42, 50].

6.3.1 1D Carbon Nanostructures Influence over the Epoxy Cure Reaction

CNTs and CNT–epoxy nanocomposites have been studied in the last decade for structural and electrical applications [44, 51]. Notwithstanding, issues such as the excessive surface energy of CNTs, changes in physical properties of matrix-like viscosity, and reaction kinetics of curing are critical parameters for manufacturing CNT-reinforced nanocomposites which have not been totally solved yet.

The chemical functionalization is commonly used to get all the advantages that CNTs can transfer to the epoxy matrix [46]. This way of improving the compatibilization introduces functional groups along the CNT surface. According to the pendant groups formed in the CNTs, both better dispersion and the strengthening of interfacial adhesion happens[47, 52–54]. However, the presence of functional groups can change the kinetics of cure reaction because of the interaction between reinforcement hardener and hardener matrix. Chapartegui et al. [47] reported the acceleration of the epoxy curing by the presence of MWCNTs. They based their arguments and hypothesis on the (i) chemical reaction between epoxy–CNTs; (ii) the inherent good thermal conductivity of CNTs which increase the heat flux; and (iii) the presence of catalysts as a result of synthesis method. Hence, the design, analysis, and optimization of manufacturing of epoxy composites are heavily impacted by the modifications in cure reaction [46]. Consequently, different studies have emphasized the effect in cure reaction of nanocomposites by CNTs.

The DSC has been used as the preferred characterization technique to study the cure reaction between epoxy and CNTs [44, 45, 51, 55–73]. This technique provides information from the changes observed in nanocomposite starting as a "freshly sample" toward the final cured state, as Cividanes et al. [46] reported. During the different steps, the parameters obtained by this technique are cure enthalpy, temperature/time of each reaction step, activation energy and glass transition temperature (when more than a cycle is performed) [46, 74]. From DSC measures, it has been determined that features of CNTs like type (single-walled or multi-walled),

length, diameter, and purity affect the curing. Also, the concentration, dispersion degree, and other factors related to CNTs impact the cure reaction [54, 55].

For instance, the catalytic effect of MWCNTs at low concentrations was reported when 1 wt% was added to the epoxy/imidazole system. In this study, for the nanocomposites evaluated, authors attributed the shift to lower temperatures in the exothermic peak of DSC to the high thermal conductivity of CNTs and the presence of –OH groups in their surface. Thus, the presence of hydroxyl groups in the surface of CNTs exerts a catalytic effect in the opening of epoxide ring during the O^-/OH adducts stage of curing mechanism [57]. Other approaches evidenced the impact on the curing reaction of epoxy-based nanocomposites by different pendant groups produced in functionalization of CNTs (DSC measurements). The presence of amino-functionalized CNTs decreases the activation energy of the curing reaction and facilitates the epoxide ring-opening. Authors mentioned that the presence of amine-functionalized MWCNTs overcomes the steric hindrance present in nanocomposites reinforced with CNTs without functionalization; consequently, the cure reaction is accelerated [58, 59].

In contrast, Rahaman and Mohanty [60] reported that the addition of carboxylic-CNTs (COOH-MWCNT) delayed the polymerization process (at 0.1, 0.5, and 1.0 wt%), and increments in the activation energy were observed in comparison of pure epoxy (DSC evidenced) [60]. Other authors followed the cure reaction by DSC in fluorine-CNTs and carboxylated-MWCNTs epoxy nanocomposites. In both cases, the final cure degree was not altered. However, the energy of the reaction was similar for fluorine-CNT and epoxy, while COOH-MWCNTs required the highest value of activation energy [56, 61]. Also, it has reported the effects of some features of modified CNTs such as size and functionalization [62], and dispersion of CNTs [56, 61, 63, 75, 76] on curing reaction.

Liu et al. [64] reported the use of DSC measurements to evaluate the curing process of MWCNTs–epoxy composites. In this research, two methods, the conventional thermal curing (CTM) and an alternative energy source as microwave (microwave curing [MWC] method), were applied in the cross-linking of epoxy composites. The basic kinetics parameters were calculated by some equations previously reported [70, 77]. These parameters exhibited notable differences, for example, the curing rate was approximately 0.08 min^{-1} for MWC method in contrast to 0.03 min^{-1} for CTM. The presence of COOH-MWCNTs in the epoxy produces quick heating as a result of superheating effect of microwaves. Moreover, the presence of COOH in MWCNTs favors strengthened interfacial bonding. Consequently, the curing activity was enhanced.

Another important technique used in the monitoring of epoxy nanocomposites' cure reaction is the DMA. This technique provides the glass transition temperature (T_g), which is related to cure extension of epoxy resin also to the interfacial interaction of epoxy CNTs [45, 46, 64, 65, 67, 70, 78–86]. Generally, samples analyzed in DMA are solid in the cured state.

Li et al. [79] reported the synthesis of COOH-MWCNTs modified by a series of hyperbranched polyesters (HBPs). DMA analysis evidenced the influence of the branching degree over the T_g of nanocomposites. Hence, an increment in the

branching degree provokes an increment in the T_g of nanocomposites. These results in T_g are related to good compatibility, higher homogeneity, and chemical bonding force between hyperbranched polymers and epoxy resin matrix.

It is known that a drop in the T_g values points an unfavorable interaction among CNT–epoxy. Frank and Wiggins [80] mentioned that lower cross-link density in epoxies is related to less restriction on the long-range coordinated molecular motion at lower temperatures; therefore, the T_g diminishes. Ling et al. [81] reported the synthesis of polydopamine (PDA)–MWCNT/epoxy systems. In this research, the interface created between CNTs and matrix was not enough to increase the T_g even with the presence of amino groups in PDA; consequently, immobile domains formed in PDA–MWCNTs/epoxy-based nanocomposite provoke a drop in the T_g. In contrast, Luo et al. [82] reported increments on the T_g values for MWCNT functionalized with phenylbiguanide, a rich amino-organic substance. Authors attributed those results to the accurate dispersion, homogeneity, good adhesion between matrix and reinforcements, and the higher restriction in chains mobility [63, 82]. Also, T_g obtained from tan δ maximum in DMA has been used as a reference of effective cross-linking on CNT–epoxy composites; T_g values were sensible to the stoichiometric amine/epoxy ratio; thus, the highest temperature was reached only at ratio = 1, contrary at different hardener (amine)/epoxy ratios, T_g values tended to diminish, indicating incomplete curing reactions [87].

Spectroscopy techniques, such as Raman, luminescence, and Fourier transform infrared analysis (FTIR), have been applied to the study of cure reaction in carbon-reinforced epoxy nanocomposites. Raman and luminescence spectroscopy showed a good correlation in the results [88]. Raman spectroscopy detects vibrational transitions in molecules and can be applied to detect changes in chemical bonds during a reaction [88]. In this research, some peaks of the Raman spectrum were used as a reference to know the state of cure. First, for the Raman technique, a relation between intensities of specific peaks is related to the cure degree in the nanocomposite. Second, in the case of the luminescence spectroscopy by monitoring changes in the peak related to the epoxy ring, the cure degree state can be known. The decrease in the intensity peak point means an increase in the cure degree. Hence, the α parameter which can be used to trace a curve of cure degree can be plotted [89]. Other authors [90] reported the use of Raman spectroscopy to assess indirectly the analysis of the behavior of cure reaction in epoxy-CNT nanocomposites which show the versatility of this technique. On the other hand, FTIR had reported as a tool for monitoring the evolution of signal related to the epoxy ring, while cure reaction is getting done. In this case, the signal corresponding to the oxirane ring in the spectrum is compared before and after the reaction of curing [91].

6.3.2 Influence of 2D Carbon Nanostructures Over the Cure Reaction

As the 1D carbon nanostructures, 2D carbon nanostructures like graphene (G), GNP, expanded graphite (EG), GEO, and RGO have been used broadly in carbon nanocomposites [92–96]. In these materials, improvement on their final properties depends

strongly on the formation of the cross-linked molecular network which is influenced by the mechanism and kinetics of epoxy cure reaction [97]. Additionally, the dispersion plays another essential role in the improvement of nanocomposites as a result of the incorporation of 2D carbon nanoreinforcements [4, 98].

DSC have been used as an important tool for the study of cure reaction in graphene–epoxy nanocomposites [97–116]. In the DSC measurements, conversion, reaction rate, and activation energy parameters are revealed [117]. Besides, the measurements in the DSC evidence the different behaviors such as acceleration or slows down the cure reaction in 2D carbon nanoreinforcements epoxy composites. Wei et al. [35] reported the curing behavior by DSC in a non-isothermal mode of epoxy/isophorone diamine blends reinforced with GEO. The authors reported a decrease in the onset and peak temperature (T_{peak}) of curing reactions. This response can be attributed to the reactivity of hydrogen present in the GEO surface, which can accelerate the curing reactions in the epoxy–amine system evaluated. In this research, GEO was prepared with the same procedure except for the oxidation time. Particularly, for the case of GEO oxidized during six hours exhibited the most notorious accelerating effect; the exothermic peak falls from 459.3 J g^{-1} for neat epoxy to 378.2 J g^{-1} for the nanocomposite with 0.2 wt% of GEO.

Wang et al. [117] reported measurements of DSC to evaluate the effect of the size of GEO sheets. This work follows the curing kinetics in DSC highlighting the importance of the suitable relation between the precursors oxirane-oligomers, hardener, functional groups present in reinforcements and the size of GEO sheets used to prepare GEO–epoxy nanocomposites. Three average sizes of the graphite flakes were reported as 150, 7, and 4 μm for samples named G-1, G-2, and G-3, respectively. Quasi-isothermal analysis exhibited a high heat flux at the beginning of the curing reaction, indicating a rapid process onset among epoxy and hardener. The addition of GEO boosted this behavior as the parameter α (α represents the degree of reaction at the particular temperature). The explanation provided involves competing reactions. In this case, the etherification prevails when the concentration of unreacted epoxide rings tends to a lower level, the GEO reacted with the pendant hydroxyl group, creating ether link after dehydration.

Another essential parameter obtained by DSC measurements in epoxy–2D carbon nanocomposites is the T_g. The reduction on T_g has been attributed to the plasticizer effect from 2D carbon nanomaterials to the epoxy matrix. Liu et al. [116] reported the addition of amino-G functionalized in the epoxy composite, improving flexibility of the network. The phenomena were explained from strong interfacial interactions between reinforcement and matrix. The amino functionalities attached in the G surface reacted covalently with the epoxy matrix. Therefore, not only the reaction was accelerated but also graphene flakes had a hinder effect on the mobility of the epoxy chains. Prolongo et al. [108] synthesized bisphenol A diglycidyl ether (DGEBA) and 4,4′-diaminodiphenylmethane (DDM) system reinforced by GNP, observing a shift to lower values of T_g in comparison of neat epoxy. This reduction is attributed to both: the hysteric hindrance of GNP, avoiding the molecular mobility of reactants reflected in the T_{peak}, and the high thermal conductivity of GNP reinforcements. These features impact negatively in the heat reaction (ΔH), suggesting that the GNP

hinders the cure reaction; consequently, a less perfect network is obtained in comparison to the polymeric matrix.

Although some researches have reported diminishing on T_g values, other authors have found extraordinary shifts to high temperatures of T_g in comparison of epoxy matrix analyzed. For instance, Ribeiro et al. [105] reported a shift approximately of 20 °C by the addition of graphene nanosheets covalently functionalized with triethylenetetramine (TETA). The improvements were attributed to the strong interface created between the nanoreinforcements and epoxy, overcoming the disruption in the network produced by the addition of 2D carbon nanoreinforcement as was aforementioned. These results agree to that reported by Sahoo et al. [111]. They reported a slight increase in the T_g after the incorporation of "in-house" functionalized graphene. DSC measurements were conducted to know the T_g; this parameter depends on the heat capacity of materials. In other words, "the higher the polymeric crosslinking density in the composite structure, the higher T_g" [111].

DMA measurements have been used [35, 45, 100, 104, 118–131] to monitoring the cure state of graphene 2D reinforcement–epoxy nanocomposites. As was mentioned, T_g is generally reported in researches because it is considered one of the most important characters to describe the thermal stability of carbon nanocomposites [4]. Chakraborty et al. [45] reported a slight decrease in the storage modulus (E') and tan δ curves for epoxy resin reinforced by two kinds of GEO. The first one used as the Hummers method produces and the second one with subsequent functionalization with amine groups (GEO-ButA). Both GEO and GEO-ButA showed soft E' and T_g curve transitions from glassy to a rubbery state; hence, these features are indicating a near-perfect network. Also, the authors mentioned that reduction in damping points hindrance to polymer chain movement in the presence of fillers, which can be interpreted as an improvement on the cross-link density (λ, mol/cm^3). The results evidenced good filler matrix interfacial interaction; also increment in λ was accompanied by a shift to high values of T_g. Notwithstanding, the improvements observed in DMA that test the fracture toughness of nanocomposites did not evidence better performance than the neat epoxy. In spite of the Tg shifts observed in DMA, other mechanical test (obtained by K_{IC}) such as the fracture toughness of nanocomposites in this research did not evidence better performance than the neat epoxy. The authors concluded that the fracture toughness is related to other factors such as internal stresses provoked during the cool down and the restricting shrinkage of nanocomposites.

Additionally, some authors [4, 74, 114, 117] have researched if functional groups on the 2D carbon surface react with the curing agent and epoxy resin, or graphene sheets covering the reactive sites in the resin due to their high surface area. Consequently, the λ diminishes and the polymer chains mobility increases drastically. Liu et al. observed shifts of T_g to lower temperatures [130]; in this research, the decline in T_g could be attributed to the incorporation of short flexible alkyl chains by the addition of imidazole-functionalized graphene (G-IMD) to epoxy and a subsequent reduction in the cross-linking density. They attributed to a broad range of relaxation temperatures in the nanocomposites reinforced with G-IMD. In other words, the G-IMD restrains the mobility of adjacent epoxy chains through strong

interface bonding; hence, different relaxation behaviors are shown with those chains far away from the interface. Similar to these results, Zhang et al. [132] reported that the addition of magnetic graphene nanoparticles interrupted the cross-linking network causing the appearance of lower T_g in comparison on neat epoxy.

It has also been reported that graphene-related materials enhance the T_g in epoxy-based nanocomposites [28, 45, 85, 104, 119, 121–124, 129, 131]. For example, Zhao et al. [128] reported the addition of GEO-functionalized bis-furan di-epoxide (BFDE). In this research, the authors attributed the reaction between the epoxy group of BFDE and the carboxyl groups of GEO to successful functionalization. The presence of epoxy groups in the BFDE–GEO sheets favors the thermal-mechanical performance because of the improvements on dispersion and exfoliation as well as strong interfacial bonding. For example, for the BFDE–GEO nanocomposites, the value of T_g increases as the amount of reinforcement. Mechanical properties of nanocomposites were improved insofar as the load transferred increased from the substrate to the lamellae, fomented by the chemical functionalization. In this case, the presence of epoxy groups in BFDE–GEO did not provoke an excessive consumption of curing agent, which can decrease λ, and therefore, diminishing the mechanical properties [133]. These results agree with that reported by Galpaya et al. [74], who mentioned the relevance of both the sensitivity to the detailed chemistry of the epoxy resin system (also the nature of curing agent) and the functional groups on the surface of carbon nanomaterials.

Other techniques used for monitoring the curing reaction of epoxy and 2D carbon nanomaterials have been the spectroscopies such as infrared and Raman. Galpaya et al. [74] reported the study of the curing process of epoxy–2D carbon nanocomposites by Fourier transform infrared emission spectroscopy (FT-IES). In this study, the spectral signals during cure reveal the chemical changes, allowing to verify cure kinetics in progress. The authors investigated the influence of two types of 2D carbon nanoreinforcements, as-produced GEO and autoclaved GEO (acGEO). From the spectra, results of this research can be inferred that the presence of a high amount of functionalities in aGEO, slow down the rate of epoxy groups consumption, in contrast of the behavior of acGO where the consumption of epoxy was faster. This behavior conditioned the λ value because of T_g measured by DSC in parallel to the IR spectral analysis reflected lower and higher values of T_g for aGEO and acGEO, respectively. These results can be interpreted as less and more cross-linking density than in the neat epoxy.

Raman and infrared spectroscopy were used to differentiate between primary and secondary interactions of GEO and RGO and epoxy systems [134]. In this research, authors studied the possible mechanisms of interactions among epoxy and graphene-related materials. From these results obtained, it was concluded that epoxy and GEO interact primarily by non-covalent π–π stacking mechanism, whereas RGO-epoxy systems interact mainly covalent bonding. In spite of, Raman and infrared techniques do not provide a direct measurement of the curing reaction, the information provided indirectly, complementing the characterization. Hence, these techniques provide useful information in the study of 2D carbon

nanocomposites involving chemical functionalization and its impact on final properties of nanocomposites.

Rheological measurements (carried on by constant oscillation of plate–plate) were related to curing reaction of 2D carbon nanomaterials and epoxy by Wolk et al. [135]. The authors observed faster cure reaction in thermally reduced freeze-dried graphene oxide (TRfdGEO) than that observed for thermally reduced graphene oxide (TRGO). The differences in the surface functionality between TRGO and TRfdGEO lead to the influence of the time of gelation for 2D carbon nanomaterial–epoxy systems. The measurements evidenced the longest gelation time for neat epoxy (60.5 minutes), followed by TRGO and TRfgGEO with 53.25 and 51.25 minutes, respectively. The authors explained the formation of salt as a result of the presence of amine and GEO. Also "the reaction of graphene oxide and the amine leads to a higher linkage epoxy-amine, producing earlier gelation of the epoxy-amine matrix." Therefore, salt accumulation of the amine on the TRGO and TRfdGEO particles decreases the gel time. The lowest gel time was for TRGO due to their richer functionality than that presented on TRGO.

6.3.3 3D Hybrid Carbon Nanostructures over Cure Reaction of Epoxy Nanocomposites

Nowadays, the research regarding the hybrid carbon reinforcement-epoxy-based nanocomposites has raised significantly. In these novel materials, the synergistic effect obtained from the combination of carbon allotropes with different geometries results in new materials with higher and better performance [136–138]. Predominantly, the mechanical or electrical properties have been studied [137], and other aspects toward some applications of these nanocomposites [137, 139, 140]. In this section is included a brief review of the cure reaction and the impact of hybrid reinforcement on it. In contrast to the CNTs and graphene-related materials composites, there are a restricted number of researches about the kinetics of cure reaction in the case of hybrid epoxy nanocomposites. The monitoring of the curing was boarded from the characterization techniques such as DSC, rheological measurements, and FTIR for 1D and 2D carbon nanomaterials, as was mentioned.

Recently, Chiou et al. [141] prepared hybrid epoxy composites. In this research, GNPs and nanocarbon aerogel (NCA) were used to reinforce the epoxy matrix cured with dicyanamide. This work was focused on the mechanical performance of nanocomposite. Moreover, DSC analysis was developed to identify the cure reactions of epoxy after the addition of GNP/NCA reinforcements. In this case, the cure reaction was not affected by hybrid reinforcement, as T_g evidenced in DSC.

As it was aforementioned, rheological measurements provide useful information about the state of curing in epoxy nanocomposites. Yue et al. [40] reported the rheological analysis of hybrid epoxy nanocomposites. In this research, MWCNTs and GNP were used as a hybrid system of reinforcements. Authors mentioned that the use of carbon nanofillers with different geometric shapes is an effective way to improve mechanical, electrical, and thermal properties as a result of the synergetic effect among them [40]. The experiments carried out in oscillatory

shear mode using a parallel plate geometry evidenced polymer–reinforcement interactions. The epoxy-hybrid reinforced system showed an increment in viscosity and storage modulus; this was related to high cross-linking density in epoxy [142]. These results agree to that reported by Kim et al. [143], who reported a rheological study via oscillation and steady shear tests, at a frequency range of 0.01–100 Hz, for nanocomposites reinforced with MWCNTs–EG hybrid. They found a relation between the increases of MWCNTs in the system reflected as an increment in the shear-thinning behavior of nanocomposite. For the nanocomposites, both the storage modulus and loss modulus increase monotonically for all frequencies tested. Consequently, results indicate a strong interaction between the epoxy matrix and hybrid reinforcement system.

Shen et al. [133] reported a synergistic effect of MWCNTs–GEO hybrid reinforcements following the performance of thermomechanical properties by DMA. The research studied epoxy nanocomposites reinforced with 3D carbon nanomaterials in the cured state. The authors observed notable shifts on T_g from 126 °C for the neat epoxy until 160 °C for 0.5 phr (parts per hundred resin) MWCNTs 0.05 phr GO hybrid system. The drastic shift of T_g toward high temperatures was explained by the restricted molecular mobility acquired of epoxy after MWCNTs and GEO were added. Notwithstanding, this synergistic effect diminishes when the amount of GEO was raised. This behavior can be attributed to the excessive consumption of the curing agent from the epoxy groups present in GEO. The excessive consumption provokes modifications on the initial stoichiometric amount of epoxy-curing agent; thus, the λ diminishes.

On the other hand, Shukla and Sharma [144] used the FTIR technique to confirm the successful reaction, effective interfacial interaction, and modification between the epoxy resin and amine-functionalized 1D and 2D reinforcements. In this research, the effective intercalation of functional groups (NH_2) to the matrix was evaluated by the modification of sharp peak due to stretching vibration in the region of 3400–3500 cm^{-1}. They attributed the best performance of nanocomposites to both aspects the increment in the specific contact area between matrix-carbon reinforcement and the stronger inter-phase built by the chemical functionalization between the fillers and epoxy. Ji et al. [145] reported how the presence of NH_2 on the reinforcement nanomaterials influences the cure reaction of epoxy nanocomposites, as a result of their nucleophilic reaction. In this research, FTIR was used to monitoring the characteristic absorption peak in 913 cm^{-1} of epoxide groups in order to evaluate qualitatively the curing degree of the epoxy-based nanocomposite. They attributed the diminishing in the signal intensity of CNTs/MoS_2/graphene–epoxy nanocomposite to less presence of remnant epoxy rings in the cured nanocomposite. The nucleophilic reaction consumed surface amino groups present in reinforcements, promoting strong bonds between fillers and the polymeric matrix. Hence, the amino groups in the hybrid reinforcement system take an important role not only by the modification of cure reaction but also as a hybrid reinforcement material.

Table 6.2 shows some works related to the study of epoxies and epoxies reinforced with 1D, 2D, or a hybrid system of carbon nanomaterials cure reaction. As can be

Table 6.2 Methods used for cure reaction analysis in carbon 1D, 2D, and hybrid carbon nanostructures reinforced epoxy composites.

Dimension of reinforcement	Analysis technique	Reinforcements used
1D		
	DSC	Multi-walled carbon nanotubes [44, 46, 55–73]
		Double-walled carbon nanotubes [51, 70]
		Single-walled carbon nanotubes [62, 70]
	DMA	Multi-walled carbon nanotubes [6, 46, 65, 67, 70, 78–84]
		Single-walled carbon nanotubes [46, 70]
	Raman	Multi-walled carbon nanotubes [46, 89]
	Luminescence	Multi-walled carbon nanotubes [89]
	FTIR	Multi-walled carbon nanotubes [91]
2D		
	DSC	Graphene oxide [32, 35, 45, 100–106, 109, 110, 112, 115]
		Reduced graphene oxide [97]
		Graphene nanoplatelets [86, 98, 107, 108, 114]
		Graphene [25, 104, 111, 113]
	DMA	Graphene oxide [45, 100, 118–122, 125–128]
		Reduced graphene oxide [26, 118, 122, 124, 131]
		Graphene nanoplatelets [23, 86, 107, 123]
		Graphene [104]
	Raman	Graphene oxide [134]
	FTIR	Graphene oxide [74]
	Rheological	Graphene oxide [135]
3D		
	DSC	Graphene nanoplatelets–nanocarbon aerogel [141]
	DMA	Graphene oxide–multi-walled carbon nanotubes [133]
	FTIR	Graphene–multi-walled carbon nanotubes [144]
		Graphene oxide–multi-walled carbon nanotubes [145]
	Rheological	Multi-walled carbon nanotubes–graphene nanoplatelets [40, 143]

seen, different researches have been done for 1D and 2D reinforcements. However, hybrid reinforcement–epoxy nanocomposite study offers a wide field of study. The principal characterization techniques used to monitor the cure reaction in epoxies have been DSC and DMA techniques, followed by the spectroscopic and rheological techniques. However, some new methods and characterization techniques have been developed for this goal, but they have not been used for the study of epoxy–carbon nanocomposites yet.

6.4 Improved Mechanical Properties of Carbon Fiber Reinforced Polymers (Epoxy) through the Incorporation of Carbon Nanostructures

The development of a new generation of composite materials with better physical and mechanical properties has gained substantial importance in recent years due to the increasing demand of advanced composite structures in high-tech industries. Owing to their easy manufacturing, excellent specific mechanical properties, and good chemical resistance, FRPs have become the adequate choice for design purposes of composite structures in many engineering applications [146], being epoxy resins one of the most used polymer matrices. For instance, in marine and aircraft manufacturing industries, naval ships and airplanes are designed and manufactured by using FRPs for almost 50% of their structural weight [147, 148]. Recent designs of wind turbine blades are also employing FRPs in order to provide lightweight structures combined with high stiffness and strength [149]. However, the recent technological advance of modern devices and lightweight structures has shown that the physical and mechanical properties of FRPs are not sufficiently high for specific applications in which an effective combination of properties (thermal, electrical, mechanical, etc.) are necessarily required. Furthermore, it has been shown that the brittle nature of thermoset matrices typically used to produce FRPs can simultaneously improve their mechanical properties but also increase the risk of damages when they are subjected to loading conditions during their service life [150]. For FRPs, matrix cracking, fiber/matrix debonding, fiber breakage, and delamination are the four main mechanisms of damage [150]. Among these damage mechanisms, delamination is one of the most common failure modes of FRPs which is usually driven by the formation of cracks in the interfacial region between bonded layers, defects in the polymer matrix, and poor out-of-plane properties [151]. From the mechanical point of view, delamination causes a significant reduction on the effective mechanical properties of the composite structures and may therefore reduce their service life [151]. Consequently, there is a deep necessity to develop new strategies that allow the possibility of improving the physical and mechanical properties of FRPs and thus lessen the risk of catastrophic failure. In this regard, recent studies in the field of advanced composite materials have showed that the incorporation of carbon-based nanostructures into FRPs can enhance their overall properties [152]. In particular, the addition of CNTs and graphene-based materials has shown their potential for improving the electrical, thermal, and mechanical properties of polymer-based composites [153]. Thus, this approach provides an opportunity for the development of a new class of advanced composite materials, in which different types of materials at different dimensional scales are combined to produce multiscale hierarchical composites with multifunctional properties for a broad range of structural applications, as shown in Figure 6.6.

Keeping this context in mind, this section presents a brief overview of improved mechanical properties of carbon fiber-reinforced polymers (CFRPs), based on epoxy matrix, through the effective incorporation of carbon-based nanostructures such

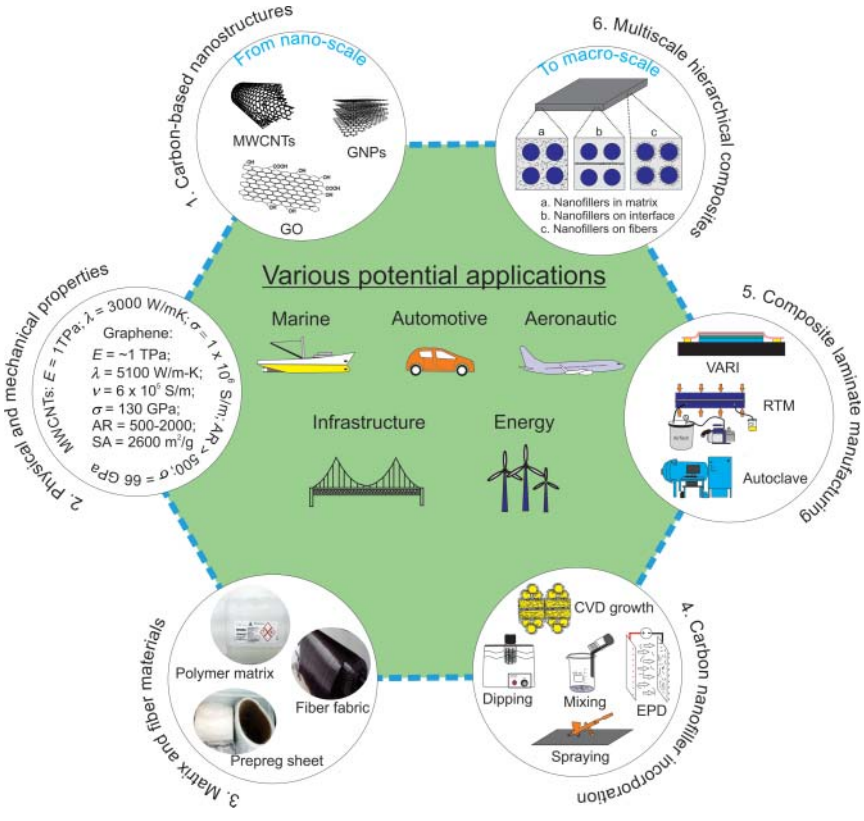

Figure 6.6 Schematic overview of multiscale hierarchical composites and their potential applications. Source: It was prepared by one of the authors, Rodríguez-González J.A.

as CNTs, GEO, RGO, GNPs, and the hybrid combinations of them. The improved mechanical properties of CFRPs comprise mainly mode I and mode II interlaminar fracture toughness, but also include interlaminar shear strength (ILSS), tensile strength, stiffness, and interfacial shear strength (IFSS), among others.

6.4.1 CFRPs (Based Epoxy) Modified with Carbon Nanotubes

The use of carbon-based nanostructures has also attracted considerable interest in recent years as reinforcement of CFRPs, for improving their physical properties. Several types of nanostructured materials have been explored in their ability to increase the mechanical properties of CFRPs. In this respect, CNTs have proven to be an excellent nanofiller reinforcement for enhancing the mechanical, electrical, and thermal properties of polymer-based composites [154]. The aforementioned characteristics of CNTs make them ideal candidates for achieving multifunctional properties in CFRPs. Recent research studies have reported the possibility of obtaining larger improvements in mechanical properties of CFRPs, based on epoxy matrices mainly, through the effective incorporation of CNTs onto their fibers,

matrix, and both of them [152]. Table 6.3 summarizes the most relevant mechanical properties of CFRPs modified with CNTs by using different types of nanofiller incorporation.

As seen in Table 6.3, one simple way of obtaining multiscale hierarchical composites is by using vacuum-assisted resin infusion process with a previous addition of CNTs within the polymer matrix [172, 176, 183]. Using this method, Borowski et al. [176] experimentally found enhanced mode I interlaminar fracture toughness (G_{IC}) by 25%, 20%, and 17% in CFRPs modified with 0.5, 1.0, and 1.5 wt% MWCNTs, respectively. Other authors have also reported improvements in G_{IC} and IFSS of CFRPs containing CNT-filled epoxy resin [173, 183]. Nevertheless, processing limitations related to CNT agglomeration, high resin viscosity, and filtration problems have motivated the development of innovative methods to deposit (or grow) CNTs on the fibers [187]. Some of those methods include in situ grown via chemical vapor deposition (CVD), electrophoresis deposition (EPD), dipping deposition, and spray coating technique [187]. For the case of in situ grown via CVD, Garcia et al. [156] developed an interlaminar reinforcement via aligned CNTs in the out-of-plane direction of the laminate and observed that this strategy significantly increased the interlaminar fracture toughness of CFRPs up to 1.5–2× in mode I and 3× in mode II. This approach has also been applied, for example, to transfer vertically aligned CNTs forest to prepreg surfaces and fabricate CFRPs with excellent interlaminar fracture properties [177]. Despite this method is useful for obtaining CFRPs with effective interlaminar reinforcement at their through-thickness direction, the complex experimental process and the requirement of equipment with a relatively high cost are important factors limiting its implementation at industrial scale. Another approach to deposit nanofillers onto the fibers is the EPD method; in this approach, the incorporation of nanofillers onto the fiber surface is applied by an electrical field [169, 184]. Carbon fiber/epoxy composites with successful deposition of MWCNTs on the fiber surface have been processed by this technique. Some authors have found improvement in shear strength and fracture toughness of CFRPs containing fibers coated with CNTs by EPD [169]. The above-mentioned techniques have in common the effective incorporation of CNTs either within the matrix or deposited onto the fibers, causing a positive effect on mechanical properties of CFRPs. However, the majority of the reported works show drawbacks related to long processing times, high cost, and complex processing; thus, their possible use at industrial scale is limited. To overcome these limitations, spray coating technique seems the most suitable to be implemented at industrial scale because of its simplicity and versatility. Recent researches have shown that the spray coating method is an effective strategy to deposit CNTs on the fibers for improving the interlaminar mechanical properties of CFRPs [160, 161, 163, 164, 170]. In particular, the spray coating technique has also been used for the addition of CNTs in prepreg-based CFRPs with the aim of improving their delamination resistance [166–168, 171, 175, 180–182, 185, 186]. Figure 6.7 presents an overview of previous research studies on the improved G_{IC} (left) and G_{IIC} (right) of CFRPs modified with CNTs by the spray coating technique.

As observed from Figure 6.7, there are many reports that explore the use of CNTs spray-coated in the interlaminar sites of prepreg-based CFRPs to increase

Table 6.3 Comparative studies regarding the effect of CNTs on mechanical properties of CFRPs (based epoxy).

Authors and year	Fiber/matrix	Laminate fabrication	Nanofiller (functionalization)	Nanofiller incorporation	Nanofiller content	Percentage increase (+)/ decrease (−) on mechanical properties
Kim et al. [155]	UD-CF/E (PRE)	Autoclave	MWCNTs (NF)	Filament winding method	0.2 wt%	G_{IC} (0%), G_{IC} at −150 °C (+20%)
					0.7 wt%	G_{IC} (+6.4%), G_{IC} at −150 °C (+30.8%)
Garcia et al. [156]	UD-CF/E (PRE)	Autoclave	Aligned CNTs (NF)	CVD	—	G_{IC} (+2×)
						G_{IIC} (+3×)
Romhány and Szebényi [157]	UD-CF/E (PRE)	HHP	MWCNTs (NF)	Three roll mill	0.1 wt%	G_{IC} (+13%)
					0.3 wt%	
					0.5 wt%	
					1.0 wt%	
Godara et al. [158]	UD-CF/E (PRE)	Autoclave	MWCNTs	High-shear calendaring	0.5 wt%	G_{IC} (+21%), G_{IR} (+17%)
			TMWCNTs			G_{IC} (+40%), G_{IR} (+25%)
			DWCNT (amine $-NH_2$)			G_{IC} (+33%), G_{IR} (+55%)
			MWCNT (modified)			G_{IC} (+75%), G_{IR} (+83%)
Karapappas et al. [159]	UD-CF/E	Autoclave	MWCNTs (NF)	Three roll mill	0.1 wt%	G_{IC} (−10%), G_{IIC} (−25%)
					0.5 wt%	G_{IC} (+43%), G_{IIC} (+75%)
					1.0 wt%	G_{IC} (+60%), G_{IIC} (+45%)
Davis et al. [160]	WO-CF/E	VARTM	SWCNTs/ DWCNTs/ MWCNTs (fluorine)	Spray coating (CNT/ethanol)	0.2 wt%	Tensile strength (+12%)
					0.3 wt%	Tensile strength (+14%)
					0.3 wt%	Tensile strength (+28%)
Davis and Whelan [161]	WO-CF/E	VARTM	SWCNTs/ DWCNTs/MWCNTs (fluorine)	Spray coating (CNT/ethanol)	0.5 wt%	G_{IIC} (+23%)

(Continued)

Table 6.3 (Continued)

Authors and year	Fiber/matrix	Laminate fabrication	Nanofiller (functionalization)	Nanofiller incorporation	Nanofiller content	Percentage increase (+)/ decrease (−) on mechanical properties
Wicks et al. [162]	WO-CF/E	Cured under vacuum	Aligned CNTs	CVD	—	G_{IC} (+76%)
Davis et al. [163]	WO-CF/E	H-VARTM	SWCNTs (amine)	Spray coating (CNT/ethanol)	0.2 wt%	Strength (+10%), stiffness (+19%)
					0.5 wt%	Strength (+7%), stiffness (+13%)
Thakre et al. [164]	WO-CF/E	VARTM	SWCNTs (NF) (silane)	Spray coating (CNT/ethanol)	0.1 wt%	G_{IC} (+6%)
					0.1 wt%	—
Ashrafi et al. [165]	UD-CF/E (PRE)	Autoclave	SWCNTs (NF)	Sonication and mechanical mixing of CNTs in resin	0.1 wt%	Area of impacted zone (−5%), residual compression strength (+3.5%), G_{IC} (+13%), G_{IIC} (+28%)
Kim and Hahn [166]	UD-CF/E (PRE)	Autoclave	SWCNTs (oxidized)	Spray/ethanol-coated process	0.5 wt%	Strength (+9%), G_{IC} (+6%)
					1.0 wt%	Strength (+7.3%), G_{IC} (0%)
Joshi and Dikshit [167]	WO-CF/E (PRE)	HHP	MWCNTs (NF)	Spray coating (CNT/ethanol)	~1.32 g/m^2	G_{IC} (+40%), G_{IR} (+32%)
						G_{IIC} (+140%)
Mujika et al. [168]	UD-CF/E (PRE)	HHP	MWCNTs (–NH_2 –S_2O_4)	Spray coating (CNT/ethanol)	0.1 wt%	G_{IIC} (+22%)
An et al. [169]	UD-CF/E	VARTM	MWCNTs (oxidized)	EPD process	0.5 wt%	ILSS (+18%), G_{IC} (+51%)
Shan et al. [170]	UD-CF/E	VARI	MWCNTs (–COOH)	Spray coating (CNT/E20)	0.6 wt%	ILLS (+12.6), G_{IC} (+24%), G_{IIC} (+11.7%)
Almuhammadi et al. [171]	UD-CF/E (PRE)	HHP	MWCNTs (–COOH)	Spray coating (CNT/ethanol)	0.5 wt%	G_{IC} (+17%)

Soliman et al. [172]	WO-CF/E	Vacuum-assisted hand lay-up technique	MWCNTs (–COOH)	Sonication and mechanical mixing of CNTs in resin	0.5 wt%	Flexure strength (+8%) and modulus (−6%), shear toughness (+15%)
					1.0 wt%	Flexure strength (+6%) and modulus (−10%), shear toughness (+23%)
					1.5 wt%	Flexure strength (+7%) and modulus (−6%), shear toughness (+33%)
Yu et al. [173]	WO-CF/E		MWCNTs (oxidized-silanized)	Mixing CNTs in resin	0.05 wt%	IFSS (26.3%)
					0.1 wt%	IFSS (18.1%)
Mirjalili et al. [174]	UD-CF/E	VARTM	MWCNTs (NF)	Three roll coater	0.3 wt%	G_{IC} (+33%), G_{IIC} (+23%)
Zhang et al. [175]	TW-CF/E (PRE)	VBM	MWCNTs (NF)	Spray coating (CNT/methanol)	0.02 wt%	G_{IC} (+22%)
					0.047 wt%	G_{IC} (+47%)
Borowski et al. [176]	UD-CF/E	VARTM	MWCNTs (NF)	Mixing CNTs in epoxy	0.5 wt%	G_{IC} (+25%)
					1.0 wt%	G_{IC} (+20%)
					1.5 wt%	G_{IC} (+17%)
Stahl et al. [177]	UD-CF/E (PRE)	Hot-pressed vacuum bag	Vertically aligned CNTs (–COOH)	CVD	—	Increasing G_{IC} by the factor 2–3 times
Guzmán de Villoria et al. [178]	UD-CF/E (PRE)	Autoclave	Aligned CNTs (NF)	Vertically aligned CNTs by CVD	~1.0% volume fraction	Tension-bearing strength (30%), open-hole compression strength (14%), L-section bending strength (25%)
Fogel et al. [179]	UD-CF/E	VARTM	MWCNTs (NF)	Three roll mill	0.75 wt%	ILSS (−10%), G_{IC} (−6.5%)
Guo et al. [180]	UD-CF/E (PRE)	Hot-press method	MWCNTs (–NH_2)	Spray-coated process	0.05 wt%	ILSS (+19%), ILSS (+21%)
			MWCNTs (butyl glycidyl ether [BGE])			
Rodríguez-González et al. [181]	UD-CF/E (PRE)	Autoclave	MWCNTs (–COOH)	Spray coating (CNT/ethanol)	0.05 wt%	G_{IC} (+52%)

Table 6.3 (Continued)

Authors and year	Fiber/matrix	Laminate fabrication	Nanofiller (functionalization)	Nanofiller incorporation	Nanofiller content	Percentage increase (+)/ decrease (−) on mechanical properties
Chaudhry et al. [182]	WO-CF/E (PRE)	Vacuum bag oven process	MWCNTs (NF)	Spray coating (CNT/ethanol)	~1.0 g/m^2	G_{IC} (+32%)
Srivastava et al. [183]	WO-CF/E	VARTM	MWCNTs (NF)	Mixing CNTs in resin	3.0 wt%	G_{IC} (+44.2%), G_{IIC} (+29.4%)
Sui et al. [184]	UD-CF/E	RTM process	MWCNTs (oxidized)	EPD process	0.3 mg/ml	IFSS (+33.3%), ILSS (+10.5%), flexural strength (+9.4%), and modulus (+15.4%)
Rodríguez-González et al. [185]	UD-CF/E (PRE)	Autoclave	MWCNTs (NF)	Spray coating (CNTs/ethanol)	0.25 wt%	ILSS (+3%), G_{IC} (+11%), G_{IIC} (+14%)
Rodríguez-González and Rubio-González [186]	UD-CF/E (PRE)	Autoclave	MWCNTs (NF)	Spray coating (CNTs/ethanol)	0.05 wt%	$G_{I/IIC}$ (+19%)
					0.1 wt%	$G_{I/IIC}$ (+17%)
					0.2 wt%	$G_{I/IIC}$ (+26%)
					0.5 wt%	$G_{I/IIC}$ (+9%)

CF, carbon fiber; CVD, chemical vapor deposition; DWCNTs, double-walled carbon nanotubes; E, epoxy; EPD, electrophoresis deposition; HHP, Hydraulic hot press; IFSS, interfacial shear strength; ILSS, interlaminar shear strength; NF, not functionalized; PRE, prepreg; RTM, resin transfer molding; SWCNTs, single-walled carbon nanotubes; TMWCNTs, thin-multiwalled carbon nanotubes; TW, twill; UD, unidirectional; VARI, vacuum assisted resin infusion; VARTM, vacuum-assisted resin transfer molding; WO, woven.

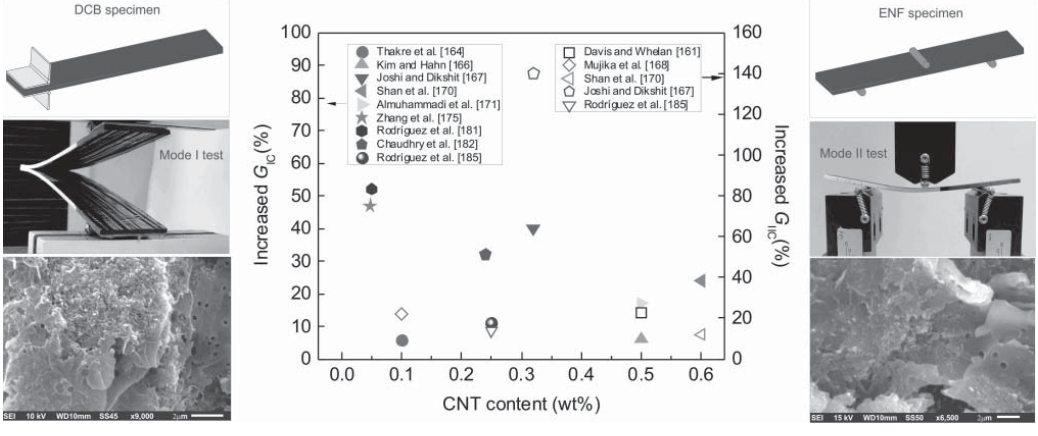

Figure 6.7 Interlaminar fracture toughness as a function of CNT content of CFRPs modified with CNTs by spraying coating technique. Solid symbols represent increased G_{IC} (left) and hollow symbols represent increased G_{IIC} (right). Schematics of double cantilever beam (DCB) (left) and end notched flexure (ENF) (right) specimens, photographs of mode I and mode II fracture tests and SEM images of fracture surface of tested specimens. Source: It was prepared by one of the authors, Rodríguez-González J.A.

their delamination resistance. Among the first studies reported to increase the interlaminar fracture properties of prepreg-based CFRPs using spray coating is probably the work of Joshi and Dikshit [167]; the technique was used to incorporate CNTs at the inter-ply interfaces of woven CFRPs. The presence of MWCNTs on the inter-ply interfaces of CFRPs increases the G_{IC} and G_{IIC} for about 40% and 140%, respectively, compared to the laminate without MWCNTs. These improvements strongly depend on the effective incorporation of CNTs into the composite and the generation of additional toughening mechanisms at the inter-ply interfaces of the laminate during the process of crack propagation [171]. These include CNTs pull-out, peeling, and bridging as depicted in the scanning electron microscopy (SEM) images from Figure 6.7. Furthermore, the possible strong bond interactions between CNTs and matrix provide an effective load transfer mechanism and as a consequence the generation of energy absorption mechanisms at microscopic level during the process of delamination even at extremely low contents of CNTs. Recent experimental investigations have also reported substantial improvements in the G_{IC} of prepreg-based CFRPs modified with spray-coated MWCNTs at very low concentrations (~0.02–0.05 wt%) [175, 181]. This trend to improve the interlaminar fracture toughness of CFRPs confirms that the spray coating technique is currently an effective strategy to produce multiscale hierarchical composites, with the potential for industrial scale-up.

6.4.2 CFRPs (Based Epoxy) Modified with Graphene-Based Materials

Given their excellent properties, graphene-based materials are also considered great candidates to develop a new generation of multifunctional composites for a variety of applications in industries as marine, automotive, aircraft, and energy (see Figure 6.6). Thus, graphene-based materials such as GEO [188–193], RGO [194–196], and GNP [197–202] as well have been used as nanoreinforcements to produce multiscale composite materials with superior mechanical properties. Table 6.4 enlists the mechanical properties of CFRPs containing graphene-based nanoscale materials either dispersed within the polymer matrix or deposited on the fibers.

In general, there is a trend to increase the mechanical properties of CFRPs by using graphene-based materials. For example, Du et al. [191] found that adding a small amount of GEO (0.5 wt%) into epoxy resin to produce interleaves for CFRPs, the G_{IC} of samples increases up to 95%. It has also been shown that GNPs promote improvements in the fracture toughness, flexural properties and ILSS of unidirectional CFRPs due to their strong adhesion with fibers and matrix. Mannov et al. [195] investigated the compression properties of composite laminates reinforced with thermally RGO. Their results shown a significant enhancement on compression strength of CFRPs by about 55%. Jiang et al. [193] deposited GEO into CFRPs and observed improvements up to 59% in the ILSS and 12% in strength under compression. Zhang et al. [188] fabricated GEO-modified carbon fiber composites and observed that by adding 2 wt% of GEO sheets in the sizing agent of carbon fibers, the IFSS of composites increased 20% with respect to composites with uncoated fibers. Other authors have also evaluated the mechanical properties

Table 6.4 Comparative studies regarding the effect of graphene-based materials on mechanical properties of CFRPs (based epoxy).

Authors and year	Fiber/matrix	Laminate fabrication	Nanofiller (functionalization)	Nanofiller incorporation	Nanofiller content	Percentage increase (+)/ decrease (−) on mechanical properties
Zhang et al. [188]	UD CF/E PRE	Autoclave	GEO	Sizing coating	1.0 wt%	IFSS (+21%), ILSS (+1%)
					2.5 wt%	IFSS (+29%), ILSS (+2%)
					5.0 wt%	IFSS (+35%), ILSS (+13%)
					7.5 wt%	IFSS (+36%), ILSS (+12%)
					10 wt%	IFSS (+36%), ILSS (+11%)
Lee et al. [194]	CF/E	VARTM	Partially reduced GEO	EPD process	7×10^{-5} wt%	ILSS (−2%)
					7×10^{-4} wt%	ILSS (+14%)
					7×10^{-3} wt%	ILSS (12%)
					7×10^{-2} wt%	ILSS (−23%)
Mannov et al. [195]	CF/E PRE (filament winding)	Autoclave	Thermally reduced GEO	Three-roll-mill	0.3 wt%	Residual compressive strength (+19%)
					0.5 wt%	Residual compressive strength (−0.5%)
He et al. [197]	WO CF/E PRE	Hand lay-up molding method	Graphene flakes	EPD process	0.5 mg/ml	Flexural strength (+14%), ILSS (+34%)
Hawkins and Haque [198]	UD CF/E	Hand lay-up method	Graphene nanoparticles	Graphene dispersed into matrix	0.1 wt%	G_{IC} (+8.3%)
Kostagiannakopoulou et al. [199]	UD-CF/E PRE	Autoclave	GEO	Three roll-mill	0.5 wt%	G_{IC} (+49%)
			GNP		0.5 wt%	G_{IC} (+51%)
Ning et al. [189]	UD-CF/E PRE	Hot press	GEO interleaf	Metallic roller	1.0 g/m^2	G_{IC} (+81%), G_{IR} (+39%)
					2.0 g/m^2	G_{IC} (+171%), G_{IR} (+108%)
					3.0 g/m^2	G_{IC} (+153%), G_{IR} (+99%)

(*continued*)

Table 6.4 (Continued)

Authors and year	Fiber/matrix	Laminate fabrication	Nanofiller (functionalization)	Nanofiller incorporation	Nanofiller content	Percentage increase (+)/ decrease (−) on mechanical properties
Pathak et al. [190]	CF/E	Hot plate hydraulic press	GEO	Epoxy-GEO mixture	0.3 wt%	Bending strength (+66%), elastic modulus (-70%), ILSS (+25%)
Qin et al. [200]	UD-CF/E PRE	Autoclave	GNP	GNP coated CF/epoxy composites	3.0 wt%	90° flexural strength (+52%), 0° flexural strength (+7%), ILSS (+19%)
Zhang et al. [203]	UD-CF/E	Compression molding method	GEO-NH_2	CF grafted with GEO-NH_2	—	ILSS (+34.7%)
			GEO-NH_2-POSS			ILSS (+53.0%)
Du et al. [191]	WO-CF/E	Hand lay-up	GEO	Graphene/epoxy as interleaves	0.5 wt%	G_{IC} (+95%)
					1.0 wt%	G_{IC} (+140%)
Han et al. [192]	UD-CF/E	Hot-pressed curing process	GEO	GEO dispersed into matrix	0.05 wt%	ILSS (+2.7%)
					0.1 wt%	ILSS (+8.0%)
	PRE				0.2 wt%	ILSS (−0.9%)
					0.4 wt%	ILSS (−5.3%)
Jiang et al. [193]	CF/E	VARTM	GEO	EPD process	0.25 g/l	ILSS (+59.4%), compressive strength (+12.8%)
Li et al. [202]	CF/E	VARI	GNP	GNP doped resin (three-roll milling)	5.0 wt%	ILSS (+18%), flexural modulus (+13%)

Li et al. [201]	CF/E	VARI	GNP	Spray coating	1.9 wt%	ILSS (−1.4%)
				Three-roll milling		ILSS (+6.8%)
Rodríguez-González et al. [185]	UD-CF/E	Autoclave	GEO	Spray coating	0.25 wt%	G_{IR} (+8%)
						G_{IIC_NPC} (+8%)
						G_{IIC_PC} (+8%)
Rodríguez-González et al. [196]	UD-CF/E	Autoclave	RGO	Spray coating	0.25 wt%	G_{IR} (+3%)
						G_{IIC_NPC} (+11%)
						G_{IIC_PC} (+1%)
Bhanuprakash et al. [204]	UD-CF/E	VARTM	GEO	EPD process	0.25 mg/ml	G_{IC} (+14.7%), G_{IR} (+13.8%)
			TRGO			G_{IC} (+11.6%), G_{IR} (+11.3%)
			REGO			G_{IC} (+7.8%), G_{IR} (+9.0%)

CF, carbon fiber; E, epoxy; EPD, electrophoresis deposition; IFSS, interfacial shear strength; ILSS, interlaminar shear strength; PRE, prepreg; UD, unidirectional; VARTM, vacuum-assisted resin transfer molding; WO, woven.

of CFRPs modified with functionalized GEO, reporting improvements on elastic modulus and fracture toughness. Ning et al. [189] reported that the addition of 2 g/m^2 of GEO interleaves in the middle interface of CFRP and the G_{IC} and mechanical strength increase by 171% and 108%, respectively. A similar positive effect with respect to interlaminar fracture toughness has been observed in CFRPs modified with graphene-based materials by spray coating deposition. For example, Rodríguez-González et al. [185] investigated the influence of GEO and RGO on interlaminar fracture toughness of prepreg-based CFRP laminates. Fracture characterization of the CFRP laminates containing 0.25 wt% of GEO and RGO yielded improvements on interlaminar fracture properties in the range of 8–11%. This is because the presence of graphene-based materials into the laminates generates additional energy dissipation mechanisms during the crack growth evolution.

6.4.3 CFRPs (Based Epoxy) Modified with Hybrids (Carbon Nanotubes and Graphene)

The use of hybrid combinations of carbon-based nanostructures to develop multiscale composite materials with superior mechanical properties is nowadays a topic of increasing interest. Recently, it has been shown that the hybrid combination of CNTs and graphene-based materials can be used to improve the mechanical and electrical properties of CFRPs [185, 196, 205–209]. The mixture of CNT and graphene (1D and 2D materials) can result in three-dimensional (3D) hybrid structures with synergistic effects on properties often superior to those of their individual form. Table 6.5 presents an overview of mechanical properties of CFRPs modified with the hybrid combination of CNTs and graphene-based materials, including hybrids such as CNT/GEO, CNT/RGO, and CNT/GNP.

The results showed in Table 6.5 confirm the hybrid combination of carbon-based nanofillers becomes suitable to produce CFRPs with enhanced mechanical properties. As for example, Kwon et al. [209] reported the use of a hybrid CNTs/GEO system (0.37 wt%) incorporated into woven CFRP to increase their ILSS (~11%). Other example is the incorporation of 0.3 wt% CNTs/GNP hybrids within the polymer matrix, where significant improvements in the tensile strength and elongation at breaking in CFRPs were obtained. Gao et al. [207] also obtained improvements in the IFSS and ILSS of composite laminates modified with CNTs/GEO hybrids chemically grafted onto the surface of carbon fibers. The inclusion of hybrid nanofillers to CFRPs for improving their interlaminar fracture toughness has been less investigated in comparison to carbon nanostructure in their individual form as discussed in Sections 6.4.1 and 6.4.2. Among these few reports, Wang et al. [205] reported an ~26% improvement in G_{IC} of CFRPs by using a hybrid combination of CNTs and GNPs. The authors argued the improvement to the synergistic effect of mechanical properties of carbon nanostructures combined with the formation of 3D hybrid structures. Recently, Kostagiannakopoulou et al. [208] developed a CFRP laminate modified with a hybrid combination of MWCNTs (1 wt%) and GNPs (0.5 wt%) and investigated their mode I and mode II fracture toughness. The authors found improvements in G_{IC} and G_{IIC} by 45% and 25% respectively,

Table 6.5 Comparative studies regarding the effect of the hybrid combination of carbon nanotubes and graphene-based materials on mechanical properties of CFRPs (based epoxy).

Authors and year	Fiber/matrix	Laminate fabrication	Nanofiller (functionalization)	Nanofiller incorporation	Nanofiller content	Percentage increase (+)/ decrease (—) on mechanical properties
Wang et al. [205]	UD-CF/E-(PRE)	Hot press molding	CNTs/GNP	Hybrids dispersed into matrix	CNTs:GNP 1 : 9	Flexural strength (+17.5%), flexural modulus (+7.7%), ILSS (+40.0%)
					1.0 wt%	G_{IC} (+84.9%)
Yu et al. [206]	CF/E	Hand-lay up	CNTs/GNP	Hybrids dispersed into matrix	0.3 wt%	Tensile strength (+53.7%), elongation breaking (+57.0%)
Gao et al. [207]	CF/E	Compression molding method	CNTs/GEO	Grafted coating	—	IFSS (+83.3%), ILSS (+48.1%)
Kostagiannakopoulou et al. [208]	UD-CF/E	Autoclave	CNTs/GNP	Nanofiller addition into epoxy	0.5/0.5 wt%	G_{IC} (+38.1%), G_{IIC} (+19.7%)
					0.5/1.0 wt%	G_{IC} (+45.4%), G_{IIC} (+25.4%)
Kwon et al. [209]	WO CF/E	VARTM	CNTs/GEO	EPD process	0.01 wt%	ILSS (+1.6%)
					0.37 wt%	ILSS (+11.2%)
					0.61 wt%	ILSS (+8.0%)
					0.65 wt%	ILSS (−11.2%)
Rodríguez-González et al. [196]	UD-CF/E-(PRE)	Autoclave	CNTs/RGO	Spray coating (hybrid/ethanol)	CNTs:RGO	G_{IC} (+1%), G_{IIC} (+8%)
					1 : 2	
					0.25 wt%	
Rodríguez-González et al. [185]	UD-CF/E-(PRE)	Autoclave	CNTs/GEO	Spray coating (hybrid/ethanol)	CNT:GEO	G_{IC} (+17%)
					1 : 2	G_{IIC} (+17%)
					0.25 wt%	

CF, carbon fiber; E, epoxy; EPD, electrophoresis deposition; IFSS, interfacial shear strength; ILSS, interlaminar shear strength; PRE, prepreg; UD, unidirectional; VARTM, vacuum assisted resin transfer molding; WO, woven.

compared to the composite without carbon nanostructures. This study also showed the presence of additional toughening mechanisms for the laminate due to the addition of MWCNT/GNP hybrids. In other studies, Rodríguez-González et al. [196] fabricated prepreg-based CFRPs reinforced with the hybrid combination of CNTs and GEO and investigated the effect on interlaminar fracture toughness. Results show that the use of hybrid carbon-based nanostructures enhances the G_{IC} and G_{IIC} of CFRPs due to the formation of 3D hybrid structures into the composite with better interaction between nanofiller and matrix. Other researches also highlighted a great synergistic effect of the GEO/CNT hybrids on interlaminar mechanical properties of prepreg-based CFRPs, as shown in Table 6.5. These improvements have been directly associated with the synergetic effect of different energy absorption mechanisms generated in the laminate during the crack propagation, which have the tendency to contribute to the increase of fracture toughness. The mechanical properties of multiscale hierarchical composites evaluated by researchers to date show the possibility to obtain improvements in the mechanical properties of CFRPs with the effective incorporation of CNTs and graphene-based materials individually and/or through their hybrid combination. Although, the topic is still immature and some aspects need to be improved to further exploit the potential of carbon nanostructures, the results presented herein motive and encourage developing of new types of composite materials with a great potential for their use in a large variety of engineering applications (see Figure 6.6).

6.5 Concluding Remarks

In this chapter, several reviewed researches gave enough evidence about the unique properties of 1D and 2D carbon nanomaterials to modify significantly epoxy resins structure and therefore properties. These researches demonstrated that the incorporation of low quantities of CNTs or graphene-related materials, covalently or noncovalently functionalized, and well dispersed, is able to increase the mechanical properties of the prepared epoxy nanocomposites. Also, the combination of these two nanomaterials contributes, effectively, to the dispersion of the reinforcements, which is reflected on the performance of their nanocomposites. Moreover, the effect of their addition over the curing reaction was discussed, and different characterization techniques were presented to analyze the reaction between epoxy and functionalized carbon nanomaterials, activation energy, cross-linking degree, gelation time, among other parameters. The reviewed and analyzed researches show important advances regarding the incorporation of carbon nanomaterials into the epoxy resins, which allow to continue with the development of materials with high mechanical requirements, such as carbon fiber-reinforced polymers. In this field, it was observed promising results with the 1D, 2D or as hybrid 1D–2D combination for one of the most important problems to solve in CFRPs: delamination between layers. The results obtained at present about properties, dispersion, and compatibility and functionalization of carbon nanomaterials can offer an excellent alternative for the production of a new generation of high-performance materials based on epoxy matrices.

References

1 Popov, V.N. (2004). Carbon nanotubes: properties and application. *Materials Science and Engineering R: Reports* 43: 61–102.

2 Novoselov, K.S., Geim, A.K., Morozov, S.V. et al. (2004). Electric field effect in atomically thin carbon films. *Science* 306: 666–669.

3 Huang, X.Q., Boeya, F., and Zhang, H. (2012). Graphene-based composites. *Chemical Society Reviews* 41: 666–686.

4 Wei, J., Vo, T., and Inam, F. (2015). Epoxy/graphene nanocomposites – processing and properties: a review. *Royal Society of Chemistry Advances* 5: 73510–73524.

5 Atif, R., Shyha, I., and Inam, F. (2016). Mechanical, thermal, and electrical properties of graphene-epoxy nanocomposites—a review. *Polymers* 8 (8): 281–318.

6 Ma, P.-C., Mo, S.-Y., Tang, B.-Z., and Kim, J.-K. (2010). Dispersion, interfacial interaction and re-agglomeration of functionalized carbon nanotubes in epoxy composites. *Carbon* 48: 1824–1834.

7 Laurenzi, S., Botti, S., Rufoloni, A., and Santonicola, M.G. (2014). Fracture mechanisms in epoxy composites reinforced with carbon nanotubes. *Procedia Engineering* 88: 157–164.

8 Vahedi, F., Shahverdi, H.R., Shokrieh, M.M., and Esmkhani, M. (2014). Effects of carbon nanotubes content on mechanical and electrical properties of epoxy-based composites. *New Carbon Materials* 29 (6): 419–425.

9 Zhang, A.B., Luan, J.F., Zheng, Y.P. et al. (2012). Effect of percolation on the electrical conductivity of amino molecules non-covalently coated multi-walled carbon nanotubes/epoxy composites. *Applied Surface Science* 258 (22): 8492–8497.

10 Sanes, J., Saurin, N., Carrion, F.J. et al. (2016). Synergy between single-walled carbon nanotubes and ionic liquid in epoxy resin nanocomposites. *Composites Part B Engineering* 105: 149–159.

11 Cha, J., Jin, S., Shim, J.H. et al. (2016). Functionalization of carbon nanotubes for fabrication of CNT/epoxy nanocomposites. *Materials and Design* 95: 1–8.

12 Cha, J., Jun, G.H., Park, J.K. et al. (2017). Improvement of modulus, strength and fracture toughness of CNT/epoxy nanocomposites through the functionalization of carbon nanotubes. *Composites Part B Engineering* 129: 169–179.

13 Gantayat, S., Rout, D., and Swain, S.K. (2017). Mechanical properties of functionalized multiwalled carbon nanotubes/epoxy nanocomposites. *Materials Today: Proceedings* 4: 4061–4064.

14 Ramos-Galicia, L., Martinez-Hernandez, A.L., Fuentes-Ramirez, R., and Velasco-Santos, C. (2017). 1D and 2D oxidized carbon nanomaterials on epoxy matrix: performance of composites over the same processing conditions. *Material Ressearch Express* 4: 115604.

15 Ramos-Galicia, L., Perez-Ramirez, E.E., Fuentes-Ramirez, R. et al. (2019). Carbon nanotubes and reduced graphene oxide's dimensionality effect on thermoset matrix performance. *Materials Performance and Characterization* 8: 434–447.

16 Zakaria, M.R., Kudus, M.H.A., Akil, H.M., and Thirmizir, M.Z.M. (2017). Comparative study of graphene nanoparticle and multiwall carbon nanotube filled epoxy nanocomposites based on mechanical, thermal and dielectric properties. *Composites Part B Engineering* 119: 57–66.

17 Bianco, A., Cheng, H.-M., Enoki, T. et al. (2013). All in the graphene family – a recommended nomenclature for two-dimensional carbon materials. *Carbon* 65: 1–6.

18 Ni, Y., Chen, L., Teng, K. et al. (2015). Superior mechanical properties of epoxy composites reinforced by 3D interconnected graphene skeleton. *ACS Applied Materials & Interfaces* 7: 11583–11591.

19 Cha, J., Kim, J., Ryu, S., and Hong, S.H. (2019). Comparison to mechanical properties of epoxy nanocomposites reinforced by functionalized carbon nanotubes and graphene nanoplatelets. *Composites Part B Engineering* 162: 283–288.

20 Martin-Gallego, M., Bernal, M.M., Hernandez, M. et al. (2013). Comparison of filler percolation and mechanical properties in graphene and carbon nanotubes filled epoxy nanocomposites. *European Polymer Journal* 49: 1347–1353.

21 Moriche, R., Prolongo, S.G., Sànchez, M. et al. (2015). Morphological changes on graphene nanoplatelets induced during dispersion into an epoxy resin by different methods. *Composites Part B Engineering* 72: 199–205.

22 Dai, J.F., Wang, G.J., Ma, L., and Wu, C.-K. (2015). Surface properties of graphene: relationship to graphene-polymer composites. *Reviews on Advanced Materials Science* 40: 60–71.

23 Zaman, I., Phan, T.T., Kuan, H.-C. et al. (2011). Epoxy/graphene platelets nanocomposites with two levels of interface strength. *Polymer* 52: 1603–1611.

24 Wang, X., Xing, W., Zhang, P. et al. (2012). Covalent functionalization of graphene with organosilane and its use as a reinforcement in epoxy composites. *Composites Science and Technology* 72: 737–743.

25 Wang, X., Jin, J., and Song, M. (2013). An investigation of the mechanism of graphene toughening epoxy. *Carbon* 65: 324–333.

26 Tang, L.-C., Wan, Y.-J., Yan, D. et al. (2013). The effect of graphene dispersion on the mechanical properties of graphene/epoxy composites. *Carbon* 60: 16–27.

27 Wan, Y.-J., Tang, L.-C., Yan, D. et al. (2013). Improved dispersion and interface in the graphene/epoxy composites via a facile surfactant-assisted process. *Composites Science and Technology* 82: 60–68.

28 Wan, Y.-J., Tang, L.-C., Gong, L.-X. et al. (2014). Grafting of epoxy chains onto graphene oxide for epoxy composites with improved mechanical and thermal properties. *Carbon* 69: 467–480.

29 Prolongo, S.G., Moriche, R., Jiménez-Suárez, A. et al. (2014). Advantages and disadvantages of the addition of graphene nanoplatelets to epoxy resins. *European Polymer Journal* 61: 206–214.

30 Abdullah, S.I. and Ansari, M.N.M. (2015). Mechanical properties of graphene oxide (GO)/epoxy composites. *HBRC Journal* 11: 151–156.

31 Ahmadi-Moghadam, B., Sharafimasooleh, M., Shadlou, S., and Taheri, F. (2015). Effect of functionalization of graphene nanoplatelets on the mechanical response of graphene/epoxy composites. *Materials and Design* 66: 142–149.

32 Pour, Z.S. and Ghaemy, M. (2016). Polymer grafted graphene oxide: for improved dispersion in epoxy resin and enhancement of mechanical properties of nanocomposite. *Composites Science and Technology* 136: 145–157.

33 Kang, W.-S., Rhee, K.Y., and Park, S.-J. (2017). Influence of surface energetics of graphene oxide on fracture toughness of epoxy nanocomposites. *Composites Part B Engineering* 114: 175–183.

34 Qi, Z., Tan, Y., Gao, L. et al. (2018). Effects of hyperbranched polyamide functionalized graphene oxide on curing behavior and mechanical properties of epoxy composites. *Polymer Testing* 71: 145–155.

35 Wei, Y., Hu, X., Jiang, Q. et al. (2018). Influence of graphene oxide with different oxidation levels on the properties of epoxy composites. *Composites Science and Technology* 161: 74–84.

36 Li, W., Dichiara, A., and Bai, J. (2013). Carbon nanotube–graphene nanoplatelet hybrids as high-performance multifunctional reinforcements in epoxy composites. *Composites Science and Technology* 74: 221–227.

37 Liang, X. and Cheng, Q. (2018). Synergistic reinforcing effect from graphene and carbon nanotubes. *Composites Communications* 10: 122–128.

38 Yang, S.-Y., Lin, W.-N., Huang, Y.-L. et al. (2011). Synergetic effects of graphene platelets and carbon nanotubes on the mechanical and thermal properties of epoxy composites. *Carbon* 49: 793–803.

39 Chatterjee, S., Nafezarefi, F., Tai, N.H. et al. (2012). Size and synergy effects of nanofiller hybrids including graphene nanoplatelets and carbon nanotube in mechanical properties of epoxy composites. *Carbon* 50: 5380–5386.

40 Yue, L., Pircheraghi, G., Monemian, S.A., and Manas-Zloczower, I. (2014). Epoxy composites with carbon nanotubes and graphene nanoplatelets – dispersion and synergy effects. *Carbon* 78: 268–278.

41 Janković, B. (2018). Kinetic and reactivity distribution behaviors during curing process of carbon/epoxy composite with thermoplastic interface coatings (T800/3900-2 Prepreg) under the nonisothermal conditions. *Polymer Composites* 39: 201–220.

42 Mgbemena, C., Li, D., Li, M. et al. (2018). Accelerated microwave curing of fire-reinforced thermoset polymer composites for structural applications: a review of scientific challenges. *Composites Part A Applied Science and Manufacturing* 115: 88–103.

43 Jin, F., Li, X., and Park, S. (2015). Synthesis and application of epoxy resins: a review. *Journal of Industrial and Engineering Chemistry* 29: 1–11.

44 Saeb, M., Rastin, H., Nohanal, M. et al. (2017). Cure kinetics of epoxy/MWCNTs nanocomposites: nonisothermal calorimetric and rheokinetic techiniques. *Journal of Applied Polymer Science* 134: 45221–45231.

45 Chakraborty, S., Chakraborty, A., Barbezat, M., and Terrasi, G.P. (2018). Interfacial interaction and the fracture toughness (KIC) trends in epoxy

nanocomposites filled with functionalized graphene-based fillers. *Polymer Composites* 39: 2356–2369.

46 Cividanes, L., Simonetti, E., Moraes, M. et al. (2014). Influence of carbon nanotubes on epoxy resin cure reaction using different techniques: a comprehensive review. *Polymer Engineering and Science* 54: 2–11.

47 Chapartegui, M., Markaide, N., Florez, S. et al. (2012). Curing of epoxy/carbon nanotues physical networks. *Polymer Engineeering and Science* 52: 663–670.

48 Ahmadi, Z. (2019). Epoxy in nanotechnology: a short review. *Progress in Organic Coatings* 132: 445–448.

49 Duemichen, E., Javdanitehran, M., Erdmann, M. et al. (2015). Analyzing the network formation and curing kinetics of epoxy resins by in situ near-infrared measurements with variable heating rates. *Thermochimica Acta* 616: 49–60.

50 Demleitner, M., Sanchez-Vazquez, S., Raps, D. et al. (2019). Dielectric analysis monitoring of thermoset curing with ionicliquids: from modeling to the prediction in the resin transfermolding process. *Polymer Composites* 40: 4500–4509.

51 El Sawi, I., Olivier, P., Demont, P., and Bougherara, H. (2012). Investigation of the effect of double-walled carbon nanotubes on the curing reaction kinetics and shear flow of an epoxy resin. *Journal of Applied Polymer Science* 126: 358–366.

52 Meng, H., Sui, G., Fang, P., and Yang, R. (2008). Effects of acid- and diamine-modified MWNTs on the mechanical properties and crystallization behavior of polyamide 6. *Polymer* 49: 610–620.

53 Shen, J., Huang, W., Wu, L. et al. (2007). The reinforcement role of different amino-functionalizedmulti-walled carbon nanotubes in epoxy nanocomposites. *Composites Science and Technology* 67: 3041–3050.

54 Sahoo, N., Rana, S., Cho, J. et al. (2010). Polymer nanocomposites based on functionalized carbon nanotubes. *Progress in Polymer Science* 35: 837–867.

55 Brando-Susin, S., Pistor, V., Campos-Amico, S. et al. (2014). Investigation of cure kinetics in epoxy/multiwalled carbon nanotube nanocomposites. *Journal of Applied Polymer Science* 131: 39857–39863.

56 Aguilar-Ventura, I., Rahaman, A., and Lubineau, G. (2013). The thermal properties of a carbon nanotube-enriched epoxy: thermal conductivity, curing and degradation kinetics. *Journal of Applied Polymer Science* 130: 2722–2733.

57 Zhou, T., Wang, X., Liu, X., and Xiong, D. (2009). Influence of multi-walled carbon nanotubes on the cure behavior of epoxy-imidazole system. *Carbon* 47: 1112–1118.

58 Yang, K., Gu, M., and Jin, Y. (2008). Cure behavior and thermal stability analysis of multiwalled carbon nanotube/epoxy resin nanocomposites. *Journal of Applied Polymer Science* 110: 2980–2988.

59 Vijayan, P., Puglia, D., Rastin, H. et al. (2017). Cure kinetics of epoxy/MWCNTs nanocomposites: isothermal calorimetric and rheological analyses. *Progress in Organic Coatings* 108: 75–83.

60 Rahaman, A. and Mohanty, A. (2014). Effect of carbon nanotubes on the curing and thermomechanical behavior of epoxy/carbon nanotubes composites. *Polymer Composites* 35: 441–449.

61 Abdalla, M., Dean, D., Robinson, P., and Nyairo, E. (2008). Cure behavior of epoxy/MWCNT nanocomposites: the effect of nanotube surface modification. *Polymer* 49: 3310–3317.

62 Qiu, J. and Wang, S. (2010). Reaction kinetics of functionalized carbon nanotubes reinforced polymer composites. *Materials Chemistry and Physics* 121: 295–301.

63 Wu, J., Guo, J., Zhang, Q. et al. (2016). Effect of different amino functionalized carbon nanotubes on curing behavior and mechanical properties of carbon fiber/epoxy composites. *Polymer Composites* 39: 733–744.

64 Liu, X., Luo, J., Fan, J. et al. (2019). Comprehensive enhancement in overall properties of MWCNTs-COOH/epoxy composites by microwave: an efficient approach to strengthen interfacial bonding via localized superheating effect. *Composites Part B Engineering* 174: 106909.

65 Cui, L., Wang, Y., Xiu, W. et al. (2013). Effect of functionalization of multi-walled carbon nanotube on the curing behavior and mechanical property of multi-walled carbon nanotube/epoxy composites. *Materials and Design* 49: 279–284.

66 Wang, Y., Chai, M., Zhao, H. et al. (2016). Improvement of dispersion of carbon nanotubes in epoxy resin through pyrogallol functionalization. *Plastics Engineering* 56: 1079–1085.

67 Ciecierska, E., Boczkowska, A., Jan Kurzydlowski, K. et al. (2013). The effect of carbon nanotubes on epoxy matrix nanocomposites. *Journal of Thermal Analysis and Calorimetry* 111: 1019–1024.

68 Fotiou, I., Baltopoulos, A., Vavouliotis, A., and Kostopoulos, V. (2013). Microwave curing of epoxy polymers reinforced with carbon nanotubes. *Journal of Applied Polymer Science* 129: 2754–2764.

69 Kim, S., Lee, W., and Park, J. (2009). Assessment of dispersion in carbon nanotube reinforced composites using differential scanning calorimetry. *Carbon* 47: 2699–2703.

70 Esmizadeh, E., Yousef, A., and Naderi, G. (2015). Effect of type and aspect ratio of different carbon nanotubes on cure behavior of epoxy-based nanocomposites. *Iranian Polymer Journal* 24: 1–12.

71 Patil, V., Dennis, R., Rout, T. et al. (2014). Graphene oxide and functionalized multi walled carbon nanotubes as epoxy curing agents: a novel synthetic approach to nanocomposites containing synthetic approach to nanocomposites containing. *Royal Society of Chemistry Advances* 4: 49264–49274.

72 Aradhana, R., Mohanty, S., and Nayak, S. (2018). High performance epoxy nanocomposite adhesive: effect of nanofillers on adhesive strength, curing and degradation kinetics. *International Journal of Adhesion and Adhesives* 84: 238–249.

73 Martone, A., Formicola, C., Piscitelli, F. et al. (2012). Thermo-mechanical characterization of epoxy nanocomposites with different carbon nanotube distributions obtained by solvent aided and direct mixing. *Express Polymer Letters* 6: 520–531.

74 Galpaya, D., Rintoul, L., Fernando, J. et al. (2015). The effect of graphene oxide and its oxidized debris on the cure chemistry and interphase structure of epoxy nanocomposites. *Polymer* 71: 122–134.

75 Saeb, M., Bakhshandeh, E., Ali Khonakdar, H. et al. (2013). Cure kinetics of epoxy nanocomposites affected by MWCNTs functionalization: a review. *The Scientific World Journal* 2013: 703708.

76 Zhao, Z., Teng, K., Li, N. et al. (2017). Mechanical, thermal and interfacial performances of carbon fiber reinforced composites flavored by carbon nanotube in matrix/interface. *Composite Structures* 159: 761–772.

77 Khan, S., Pothnis, J., and Kim, J. (2013). Effects of carbon nanotube alignment on electrical and mechanical properties of epoxy nanocomposites. *Composites Part A: Applied Science and Manufacturing* 49: 26–34.

78 López-Barroso, J., Mártinez-Hernández, A., Rivera-Armenta, J., and Velasco-Santos, C. (2018). Multidimensional nanocomposites of epoxy reinforced with 1D and 2D carbon nanostructures for improve fracture resistance. *Polymers* 10 (3): 281–300.

79 Li, L., Liao, X., Sheng, X. et al. (2019). Effect of structure regulation of hyper-branched polyester modified carbon nanotubes on toughening performance of epoxy/carbon nanotube nanocomposites. *Royal Society of Chemistry Advances* 9: 12864–12876.

80 Frank, K. and Wiggins, J. (2013). Effect of stoichiometry and cure prescription on fluid ingress in epoxy networks. *Journal of Applied Polymer Sicience* 130: 264–276.

81 Ling, Y., Li, W., Wang, B. et al. (2016). Epoxy resin reinforced with nanothin polydopamine-coated carbon nanotubes: a study of the interfacial polymer layer thickness. *Royal Society of Chemistry Advances* 6: 31037–31045.

82 Luo, Y., Zhao, Y., Cai, J. et al. (2012). Effect of amino-functionalization on the interfacial adhesion of multi-walled carbon nanotubes/epoxy nanocomposites. *Materials & Design* 33: 405–412.

83 Hsu, S., Wu, M., Chen, S. et al. (2012). Synthesis, morphology and physical properties of multi-walled carbon nanotube/biphenyl liquid crystalline epoxy composites. *Carbon* 50: 896–905.

84 Bisht, A., Dasgupta, K., and Lahiri, D. (2018). Effect of graphene and CNT reinforcement on mechanical and thermomechanical behavior of epoxy—a comparative study. *Journal of Applied Polymer Science* 135: 46101.

85 Chandrasekaran, S., Seidel, C., and Schulte, K. (2013). Preparation and characterization of graphite nano-platelet (GNP)/epoxy nano-composite: mechanical, electrical and thermal properties. *European Polymer Journal* 49: 3878–3888.

86 Prolongo, S., Jiménez-Suárez, A., Moriche, R., and Ureña, A. (2014). Graphene nanoplatelets thickness and lateral size influence on the morphology and behavior of epoxy composites. *European Polymer Journal* 53: 292–301.

87 Gude, M., Prolongo, S., and Ureña, A. (2012). Effect of the epoxy/amine stoichiometry on the properties of carbon nanotube/epoxy composites. *Journal of Thermal Analysis and Calorimetry* 108: 717–723.

88 Hardis, R., Jessop, J.L.P., Peters, F.E., and Kessler, M.R. (2013). Cure kinetics characterization and monitoring of an epoxy resin using DSC, Raman spectroscopy, and DEA. *Composites Part A: Applied Science and Manufacturing* 49: 100–108.

89 Cividanes, L., Brunelli, D., Antunes, E. et al. (2012). Cure study of epoxy resin reinforced with multiwalled carbon nanotubes by Raman and luminescence spectroscopy. *Journal of Applied Polymer Science* 127: 544–553.

90 de la Vega, A., Kovacs, J., Bauhofer, W., and Schulte, K. (2009). Combined Raman and dielectric spectroscopy on the curing behaviour and stress build up of carbon nanotube–epoxy composites. *Composites Science and Technology* 69: 1540–1546.

91 Yi, X., Mishra, A., Kim, N. et al. (2013). Synergistic effects of oxidized CNTs and reactive oligomer on the fracture toughness and mechanical properties of epoxy. *Composites Part A: Applied Science and Manufacturing* 49: 58–67.

92 Ferrari, A., Bonaccorso, F., Fal'ko, V. et al. (2015). Science and technology roadmap for graphene, related two-dimensional crystals, and hybrid systems. *Nanoscale* 7: 4587–5062.

93 Smith, A., LaChance, A., Zeng, S. et al. (2019). Synthesis, properties, and applications of graphene oxide/reduced graphene oxide and their nanocomposites. *Nano Materials Science* 1: 31–47.

94 Lawal, A. (2019). Graphene-based nano composites and their applications. A review. *Biosensors and Bioelectronics* 141: 111384.

95 Salzano de Luna, M., Wang, Y., Zhai, T. et al. (2019). Nanocomposite polymeric materials with 3D graphene-based nanocomposite polymeric materials with 3D graphene-based potential applications. *Progress in Polymer Science* 89: 213–249.

96 Li, Z., Wang, L., Li, Y. et al. (2019). Carbon-based functional nanomaterials: preparation, properties and applications. *Composites Science and Technology* 179: 10–40.

97 Monteserín, C., Blanco, M., Aranzabe, E. et al. (2017). Effects of graphene oxide and chemically reduced graphene oxide on the curing kinetics of epoxy amine composites. *Journal of Applied Polymer Science* 134: 44803–44817.

98 Park, J. and Kim, D. (2014). Effects of an amino silane and a tetra-functional epoxy on the physical properties of di-functional epoxy/graphene nanoplatelets nanocomposites. *Polymer Engineering & Science* 54: 969–976.

99 Nonahal, M., Saeb, M., Jafari, S. et al. (2018). Design, preparation, and characterization of fast cure epoxy/amine-functionalized graphene oxide nanocomposites. *Polymer Composites* 39: 2016–2027.

100 Bortz, D., Garcia Heras, E., and Martin-Gullon, I. (2012). Impressive fatigue life and fracture toughness improvements in graphene oxide/epoxy composites. *Macromolecules* 45: 238–245.

101 Lei, L., Shan, J., Hu, J. et al. (2016). Co-curin g effect of imidazole grafting graphene oxide synthesized by one-pot method to reinforce epoxy nanocomp osites. *Composites Science and Technology* 128: 161–168.

102 Li, L., Zeng, Z., Zou, H., and Liang, M. (2015). Curing characteristics of an epoxy resin in the presence of functional graphite oxide with amine-rich surface. *Thermochimica Acta* 614: 78–84.

103 Yarahmadi, E., Didehban, K., Sari, M. et al. (2018). Development and curing potential of epoxy/starch-functionalized graphene oxide nanocomposite coatings. *Progress in Organic Coatings* 119: 194–202.

104 Martin-Gallego, M., Verdejo, R., Lopez-Manchado, M.A., and Sangermano, M. (2011). Epoxy-graphene UV-cured nanocomposites. *Polymer* 52: 4664–4669.

105 Ribeiro, H., Silva, W., Rodrigues, M. et al. (2013). Glass transition improvement in epoxy/graphene composites. *Journal of Materials Science* 48: 7883–7892.

106 Acocella, M., Esposito Corcione, C., Giuri, A. et al. (2016). Graphene oxide as a catalyst for ring opening reactions in amine crosslinking of epoxy resins. *Royal Society of Chemistry Advances* 6: 23858.

107 Prolongo, S., Jimenez-Suarez, A., Moriche, R., and Ureña, A. (2013). In situ processing of epoxy composites reinforced with graphene nanoplatelets. *Composites Science and Technology* 86: 185–191.

108 Prolongo, M., Salom, C., Arribas, C. et al. (2016). Influence of graphene nanoplatelets on curing and mechanical properties of graphene/epoxy nanocomposites. *Journal of Thermal Analysis and Calorimetry* 125: 629–636.

109 Malik, P., Bhasha, B., and Jain, P. (2018). Influence of surface modified graphene oxide on mechanical and thermal properties of epoxy resin. *Oriental Journal of Chemistry* 34: 1597–1603.

110 Wang, Z., Liu, L., Cao, L. et al. (2019). Optimizing curing process of graphene oxide/waterborne epoxy blends by curing kinetics simulation considering the coupling of heat conduction and curing reaction. *Thermochimica Acta* 672: 60–69.

111 Sahoo, S., Ray, B., and Mallik, A. (2017). Role of electrochemically in-house synthesized and functionalized graphene nano-fillers on the structural performance of epoxy matrix composites. *Physical Chemistry Chemical Physics* 19: 16219.

112 Ryu, S., Sin, J., and Shanmugharaj, A. (2014). Study on the effect of hexamethylene diamine functionalized graphene oxide on the curing kinetics of epoxy nanocomposites. *European Polymer Journal* 52: 88–97.

113 Monetta, T., Acquesta, A., Carangelo, A., and Bellucci, F. (2017). The effect of graphene on the protective properties of water-based epoxy coatings on Al2024-T3. *International Journal of Corrosion* 2017: 1541267, 1–9.

114 Kim, K., Jeon, I., Ahn, S. et al. (2011). Edge-functionalized graphene-like platelets as a co-curing agent and a nanoscale additive to epoxy resin. *Journal of Materials Chemistry* 21: 7337–7342.

115 Liu, F., Wu, L., Song, Y. et al. (2015). Effect of molecular chain length on the properties of amine-functionalized graphene oxide nanosheets/epoxy resins nanocomposites. *Royal Society of Chemistry Advances* 5: 45987–45995.

116 Liu, K., Chen, S., Luo, Y. et al. (2013). Edge-functionalized graphene as reinforcement of epoxy-based conductive composite for electrical interconnects. *Composites Science and Technology* 88: 84–91.

117 Wang, X., Jin, J., Song, M., and Lin, Y. (2016). Effect of graphene oxide sheet size on the curing kinetics and thermal stability of epoxy resins. *Materials Research Express* 3: 105303–105303.

118 Aradhana, R., Mohanty, S., and Nayak, S. (2018). Comparison of mechanical, electrical and thermal properties in graphene oxide and reduced graphene oxide filled epoxy nanocomposites adhesives. *Polymer* 141: 109–123.

119 Yu, J.W., Jung, J., Choi, Y.-M. et al. (2016). Enhancement of the crosslink density, glass transition temperature, and strength of epoxy resin by using functionalized graphene oxide co-curing agents. *Polymer Chemistry* 7: 36–43.

120 Surnova, A., Balkaev, D., Musin, D. et al. (2019). Fully exfoliated graphene oxide accelerates epoxy resin curing, and results in dramatic improvement of the polymer mechanical properties. *Composites Part B Engineering* 162: 685–691.

121 Starkova, O., Chandrasekaran, S., Prado, L. et al. (2013). Hydrothermally resistant thermally reduced graphene oxide and multi-wall carbon nanotube based epoxy nanocomposites. *Polymer Degradation and Stability* 98: 519–526.

122 Silva, L.C.O., Silva, G.G., Ajayan, P.M., and Soares, B.G. (2015). Long-term behavior of epoxy/graphene-based composites determined by dynamic mechanical analysis. *Journal of Materials Science* 50: 6407–6419.

123 Naebe, M., Wang, J., Amini, A. et al. (2014). Mechanical property and structure of covalent functionalised graphene/epoxy nanocomposites. *Scientific Reports* 4: 4375.

124 Bindu-Sharmila, T., Nair, A., Abraham, B. et al. (2014). Microwave exfoliated reduced graphene oxide epoxy nanocomposites for high performance applications. *Polymer* 55: 3614–3627.

125 Tang, J., Zhou, H., Liang, Y. et al. (2014). Properties of graphene oxide/epoxy resins composites. *Journal of Nanomaterials* 2014: 696859, 1–5.

126 Shen, X.-J., Pei, X.-Q., Fu, S.-Y., and Friedrich, K. (2013). Significantly modified tribological performance of epoxy nanocomposites at very low graphene oxide content. *Polymer* 54: 1234–1242.

127 Li, W., Young, R., Wang, R. et al. (2013). The role of functional groups on graphene oxide in epoxy nanocomposites. *Polymer* 54: 5821–5829.

128 Zhao, H., Ding, J., and Yu, H. (2018). Variation of mechanical and thermal properties in sustainable graphene oxide/epoxy composites. *Scientific Reports* 8: 16560.

129 Deng, H., Wu, F., Chen, L. et al. (2014). Enhanced interfacial interaction of epoxy nanocomposites with activated graphene nanosheets. *Journal Applied of Polymer Science* 131: 41164.

130 Liu, W., Koh, K., Yang, L. et al. (2012). Simultaneous catalyzing and reinforcing effects of imidazole-functionalized graphene in anhydride-cured epoxies. *Journal of Materials Chemistry* 22: 18395–18402.

131 Dong, B., Yuan, Y., Luo, J. et al. (2018). Acryloyl-group functionalized graphene for enhancing thermal and mechanical properties of acrylated epoxidized soybean oil UV-curable based coatings. *Progress in Organic Coatings* 118: 57–65.

132 Zhang, X., Alloul, O., He, Q. et al. (2013). Strengthened magnetic epoxy nanocomposites with protruding nanoparticles on the graphene nanosheets. *Polymer* 54: 3594–3604.

133 Shen, X., Pei, X., and Fu, S. (2014). Tribological performance of carbon nanotube–graphene oxide hybrid/epoxy composites. *Composites Part B: Engineering* 57: 120–125.

134 Yousefi, N., Lin, X., Zheng, Q. et al. (2013). Simultaneous in situ reduction, self-alignment and covalent bonding in graphene oxide/epoxy composites. *Carbon* 59: 406–417.

135 Wolk, A., Rosenthal, M., Weiß, J. et al. (2018). Graphene oxide as flexibilizer for epoxy amine resins. *Progress in Organic Coatings* 122: 280–289.

136 Kumar, A., Sharma, K., and Dixit, A. (2019). A review of the mechanical and thermal properties of graphene and its hybrid polymer nanocomposites for structural applications. *Journal of Materials Science* 54: 5992–6026.

137 Szeluga, U., Kumanek, B., and Trzebicka, B. (2015). Synergy in hybrid polymer/nanocoarboncomposites. A review. *Composites Part A Applied Science and Manufacturing* 73: 204–231.

138 Schuster, M. and Coelho, L. (2019). Toughness and roughness in hybrid nanocomposites of an epoxy matrix. *Polymer Engineering and Science* 59: 1258–1269.

139 Damnalı, O. and Eskizeybek, V. (2019). Synergistic impact of graphene and carbon nanotubes synergistic impact of graphene and carbon nanotubes. *Cellulose* 26: 3935–3954.

140 Gu, H., Ma, C., Gu, J. et al. (2016). An overview of multifunctional epoxy nanocomposites. *Journal of Materials Chemistry C* 4: 5890–5906.

141 Chiou, Y., Chou, H., and Shen, M. (2019). Effects of adding graphene nanoplatelets and nanocarbon aerogels toepoxy resins and their carbon fiber composites. *Materials and Design* 178: 107869.

142 López-Barajas, F., Ramos-DeValle, L., Sánchez-Valdes, S. et al. (2019). Curing kinetics of diglycidyl ether of bisphenol-A epoxy system using a tertiary amine, through the study of its rheometric characteristics. *Polymer Testing* 73: 346–351.

143 Kim, K., Rhee, K., Byun, J. et al. (2010). Rheological behaviors and mechanical properties of graphite nanoplate/carbon nanotube-filled epoxy nanocomposites. *Journal of Industrial and Engineering Chemistry* 16: 572–576.

144 Shukla, M. and Sharma, K. (2019). Effect of functionalized graphene/CNT ratio on the synergetic enhancement of mechanical and thermal properties of epoxy hybrid composite. *Materials Research Express* 6: 085318.

145 Ji, C., Yan, C., Wang, Y. et al. (2019). Thermal conductivity enhancement of CNT/MoS_2/graphene–epoxy nanocomposites based on structural synergistic effects and interpenetrating network. *Composites Part B Engineering* 163: 363–370.

146 Taheri, F. (2013). *Advanced Fibre-Reinforced Polymer (FRP) Composites for Structural*. Cambridge: Woodhead Publishing Limited.

147 Soutis, S. (2005). Fibre reinforced composites in aircraft construction. *Progress in Aerospace Sciences* 41: 143–151.

148 Mouritz, A.P., Gellert, E., Burchill, P., and Challis, K. (2001). Review of advanced composite structures for naval ships and submarines. *Composite Structures* 53: 21–41.

149 Mishnaevsky, L. Jr., Branner, K., Petersen, H.N. et al. (2017). Materials for wind turbine blades: an overview. *Materials* 10: 1285.

150 Talreja, R. and Singh, C.V. (eds.) (2012). *Damage and Failure of Composite Materials*. New York: Cambridge University Press.

151 Sridharan, S. (2008). *Delamination Behaviour of Composites*. Boca Raton, FL: Woodhead Publishing Limited.

152 Rafiee, R. (2018). *Carbon Nanotube–Reinforced Polymers: From Nanoscale to Macroscale*. Amsterdam: Elsevier.

153 Punetha, V.D., Rana, S., Yoo, H.J. et al. (2017). Functionalization of carbon nanomaterials for advanced polymer nanocomposites: a comparison study between CNT and graphene. *Progress in Polymer Science* 67: 1–47.

154 Ma, P.-C. and Kim, J.-K. (2011). *Carbon Nanotubes for Polymer Reinforcement*. Boca Raton, FL: Taylor & Francis.

155 Kim, M.-G., Hong, J.-S., Kang, S.-G., and Kim, C.-G. (2008). Enhancement of the crack growth resistance of a carbon/epoxy composite by adding multi-walled carbon nanotubes at a cryogenic temperature. *Composites Part A: Applied Science and Manufacturing* 39: 647–654.

156 Garcia, E.J., Wardle, B.L., and Hart, J.A. (2008). Joining prepreg composite interfaces with aligned carbon nanotubes. *Composites Part A: Applied Science and Manufacturing* 39: 1065–1070.

157 Romhany, G. and Szebenyi, G. (2009). Interlaminar crack propagation in MWCNT/fiber reinforced hybrid composites. *Express Polymer Letters* 3: 145–151.

158 Godara, A., Mezzo, L., Luizi, F. et al. (2009). Influence of carbon nanotube reinforcement on the processing and the mechanical behaviour of carbon fiber/epoxy composites. *Carbon* 47: 2914–2923.

159 Karapappas, P., Vavouliotis, A., Tsotra, P. et al. (2009). Enhanced fracture properties of carbon reinforced composites by the addition of multi-wall carbon nanotubes. *Journal of Composite Materials* 43: 977–985.

160 Davis, D.C., Wilkerson, J.W., Zhu, J., and Ayewah, D.O.O. (2010). Improvements in mechanical properties of a carbon fiber epoxy composite using nanotube science and technology. *Composite Structures* 92: 2653–2662.

161 Davis, D.C. and Whelan, B. (2011). An experimental study of interlaminar shear fracture toughness of a nanotube reinforced composite. *Composites Part B: Engineering* 42: 105–116.

162 Wicks, S.S., de Villoria, R.G., and Wardle, B.L. (2010). Interlaminar and intralaminar reinforcement of composite laminates with aligned carbon nanotubes. *Composites Science and Technology* 70: 20–28.

163 Davis, D.C., Wilkerson, J.W., Zhu, J., and Hadjiev, V.G. (2011). A strategy for improving mechanical properties of a fiber reinforced epoxy composite using functionalized carbon nanotubes. *Composites Science and Technology* 71: 1089–1097.

164 Thakre, P.R., Lagoudas, D.C., Riddick, J.C. et al. (2011). Investigation of the effect of single wall carbon nanotubes on interlaminar fracture toughness of woven carbon fiber—epoxy composites. *Journal of Composite Materials* 45: 1091–1107.

165 Ashrafi, B., Guan, J., Mirjalili, V. et al. (2011). Enhancement of mechanical performance of epoxy/carbon fiber laminate composites using single-walled carbon nanotubes. *Composites Science and Technology* 71: 1569–1578.

166 Kim, H.S. and Hahn, H.T. (2011). Graphite fiber composites interlayered with single-walled carbon nanotubes. *Journal of Composite Materials* 45: 1109–1120.

167 Joshi, S.C. and Dikshit, V. (2012). Enhancing interlaminar fracture characteristics of woven CFRP prepreg composites through CNT dispersion. *Journal of Composite Materials* 46: 665–675.

168 Mujika, F., Vargas, G., Ibarretxe, J. et al. (2012). Influence of the modification with MWCNT on the interlaminar fracture properties of long carbon fiber composites. *Composites Part B: Engineering* 43: 1336–1340.

169 An, Q., Rider, A.N., and Thostenson, E.T. (2012). Electrophoretic deposition of carbon nanotubes onto carbon-fiber fabric for production of carbon/epoxy composites with improved mechanical properties. *Carbon* 50: 4130–4143.

170 Shan, F.L., Gu, Y.Z., Li, M. et al. (2013). Effect of deposited carbon nanotubes on interlaminar properties of carbon fiber-reinforced epoxy composites using a developed spraying processing. *Polymer Composites* 34: 41–50.

171 Almuhammadi, K., Alfano, M., Yang, Y., and Lubineau, G. (2014). Analysis of interlaminar fracture toughness and damage mechanisms in composite laminates reinforced with sprayed multi-walled carbon nanotubes. *Materials & Design* 53: 921–927.

172 Soliman, E., Kandil, U., and Taha, M.R. (2014). Improved strength and toughness of carbon woven fabric composites with functionalized MWCNTs. *Materials* 7: 4640–4657.

173 Yu, B., Jiang, Z., Tang, X.-Z. et al. (2014). Enhanced interphase between epoxy matrix and carbon fiber with carbon nanotube-modified silane coating. *Composites Science and Technology* 99: 131–140.

174 Mirjalili, V., Ramachandramoorthy, R., and Hubert, P. (2014). Enhancement of fracture toughness of carbon fiber laminated composites using multi wall carbon nanotubes. *Carbon* 79: 413–423.

175 Zhang, H., Liu, Y., Kuwata, M. et al. (2015). Improved fracture toughness and integrated damage sensing capability by spray coated CNTs on carbon fibre prepreg. *Composites Part A: Applied Science and Manufacturing* 70: 102–110.

176 Borowski, E., Soliman, E., Kandil, U., and Taha, M. (2015). Interlaminar fracture toughness of CFRP laminates incorporating multi-walled carbon nanotubes. *Polymers* 7: 1020–1045.

177 Stahl, J.J., Bogdanovich, A.E., and Bradford, P. (2016). Carbon nanotube shear-pressed sheet interleaves for mode I interlaminar fracture toughness enhancement. *Composites Part A: Applied Science and Manufacturing* 80: 127–137.

178 Guzman de Villoria, R., Hallander, P., Ydrefors, L. et al. (2016). In-plane strength enhancement of laminated composites via aligned carbon nanotube interlaminar reinforcement. *Composites Science and Technology* 133: 33–39.

179 Fogel, M., Parlevliet, P., Olivier, P., and Dantras, É. (2017). Manufacturing of conductive structural composites through spraying of CNTs/epoxy dispersions on dry carbon fiber plies. *Composites Part A: Applied Science and Manufacturing* 100: 40–47.

180 Guo, J., Zhang, Q., Gao, L. et al. (2017). Significantly improved electrical and interlaminar mechanical properties of carbon fiber laminated composites by using special carbon nanotube pre-dispersion mixture. *Composites Part A: Applied Science and Manufacturing* 95: 294–303.

181 Rodríguez-González, J.A., Rubio-González, C., Meneses-Nochebuena, C.A. et al. (2017). Enhanced interlaminar fracture toughness of unidirectional carbon fiber/epoxy composites modified with sprayed multi-walled carbon nanotubes. *Composite Interfaces* 24: 883–896.

182 Chaudhry, M.S., Czekanski, A., and Zhu, Z.H. (2017). Characterization of carbon nanotube enhanced interlaminar fracture toughness of woven carbon fiber reinforced polymer composites. *International Journal of Mechanical Sciences* 131–132: 480–489.

183 Srivastava, V.K., Gries, T., Veit, D. et al. (2017). Effect of nanomaterial on mode I and mode II interlaminar fracture toughness of woven carbon fabric reinforced polymer composites. *Engeneering Fracture Mechanics* 180: 73–86.

184 Sui, X., Shi, J., Yao, H. et al. (2017). Interfacial and fatigue-resistant synergetic enhancement of carbon fiber/epoxy hierarchical composites via an electrophoresis deposited carbon nanotube-toughened transition layer. *Composites Part A: Applied Science and Manufacturing* 92: 134–144.

185 Rodríguez-González, J.A., Rubio-González, C., Jiménez-Mora, M. et al. (2018). Influence of the hybrid combination of multiwalled carbon nanotubes and graphene oxide on interlaminar mechanical properties of carbon fiber/epoxy laminates. *Applied Composite Materials* 25: 1115–1131.

186 Rodríguez-González, J.A. and Rubio-González, C. (2018). Mixed-mode I/II interlaminar fracture toughness of carbon fiber/epoxy composites with the addition of multiwalled carbon nanotubes by spraying technique. *Journal of Composite Materials* 52: 3045–3052.

187 Avilés, F., Kú-Herrera, J.J., and Oliva-Avilés, A.I. (2018). Deposition of carbon nanotubes on fibers. In: *Carbon Nanotube-Reinforced Polymers* (ed. R. Rafiee), 117–144. Amsterdam: Elsevier.

188 Zhang, X., Fan, X., Yan, C. et al. (2012). Interfacial microstructure and properties of carbon fiber composites modified with graphene oxide. *ACS Applied Materials & Interfaces* 4: 1543–1552.

189 Ning, H., Li, J., Hu, N. et al. (2015). Interlaminar mechanical properties of carbon fiber reinforced plastic laminates modified with graphene oxide interleaf. *Carbon* 91: 224–233.

190 Pathak, A.K., Borah, M., Gupta, A. et al. (2016). Improved mechanical properties of carbon fiber/graphene oxide-epoxy hybrid composites. *Composites Science and Technology* 135: 28–38.

191 Du, X., Zhou, H., Sun, W. et al. (2017). Graphene/epoxy interleaves for delamination toughening and monitoring of crack damage in carbon fibre/epoxy composite laminates. *Composites Science and Technology* 140: 123–133.

192 Han, X., Zhao, Y., Sun, J.-M. et al. (2017). Effect of graphene oxide addition on the interlaminar shear property of carbon fiber-reinforced epoxy composites. *New Carbon Materials* 32: 48–55.

193 Jiang, J., Yao, X., Xu, C. et al. (2017). Influence of electrochemical oxidation of carbon fiber on the mechanical properties of carbon fiber/graphene oxide/epoxy composites. *Composites Part A: Applied Science and Manufacturing* 95: 248–256.

194 Lee, W., Lee, J.U., Cha, H.-J., and Byun, J.-H. (2013). Partially reduced graphene oxide as a multi-functional sizing agent for carbon fiber composites by electrophoretic deposition. *RSC Advances* 3: 25609.

195 Mannov, E., Schmutzler, H., Chandrasekaran, S. et al. (2013). Improvement of compressive strength after impact in fibre reinforced polymer composites by matrix modification with thermally reduced graphene oxide. *Composites Science and Technology* 87: 36–41.

196 Rodríguez-González, J.A., Rubio-González, C., Ku-Herrera, J.J. et al. (2018). Effect of seawater ageing on interlaminar fracture toughness of carbon fiber/epoxy composites containing carbon nanofillers. *Journal of Reinforced Plastics and Composites* 37: 1346–1359.

197 He, P., Huang, B., Liu, L. et al. (2016). Preparation of multiscale graphene oxide-carbon fabric and its effect on mechanical properties of hierarchical epoxy resin composite. *Polymer Composites* 37: 1515–1522.

198 Hawkins, D.A. and Haque, A. (2015). Strain energy release rate and mode-I delamination growth in carbon-graphene/epoxy hybrid nanocomposites. *Procedia Engineering* 105: 829–834.

199 Kostagiannakopoulou, C., Loutas, T.H., Sotiriadis, G. et al. (2015). On the interlaminar fracture toughness of carbon fiber composites enhanced with graphene nano-species. *Composites Science and Technology* 118: 217–225.

200 Qin, W., Vautard, F., Drzal, L.T., and Yu, J. (2015). Mechanical and electrical properties of carbon fiber composites with incorporation of graphene nanoplatelets at the fiber–matrix interphase. *Composites Part B: Engineering* 69: 335–341.

201 Li, Y., Zhang, H., Peijs, T., and Bilotti, E. (2016). Graphene delivery systems for hierarchical fiber reinforced composites. *MRS Advances* 1: 1339–1344.

202 Li, Y., Zhang, H., Huang, Z. et al. (2017). Graphite nanoplatelet modified epoxy resin for carbon fibre reinforced plastics with enhanced properties. *Journal of Nanomaterials* 2017: 1–10.

203 Zhang, R.L., Gao, B., Du, W.T. et al. (2016). Enhanced mechanical properties of multiscale carbon fiber/epoxy composites by fiber surface treatment with graphene oxide/polyhedral oligomeric silsesquioxane. *Composites Part A: Applied Science and Manufacturing* 84: 455–463.

204 Bhanuprakash, L., Parasuram, S., and Varghese, S. (2019). Experimental investigation on graphene oxides coated carbon fibre/epoxy hybrid composites: mechanical and electrical properties. *Composites Science and Technology* 179: 134–144.

205 Wang, P.N., Hsieh, T.H., Chiang, C.L. et al. (2015). Synergetic effects of mechanical properties on graphene nanoplatelet and multiwalled carbon nanotube hybrids reinforced epoxy/carbon fiber composites. *Journal of Nanomaterials* 2015: 838032, 1–9.

206 Yu, K., Wang, M., Wu, J. et al. (2016). Modification of the interfacial interaction between carbon fiber and epoxy with carbon hybrid materials. *Nanomaterials* 89: 1–11.

207 Gao, B., Zhang, R., He, M. et al. (2016). Effect of a multiscale reinforcement by carbon fiber surface treatment with graphene oxide/carbon nanotubes on the mechanical properties of reinforced carbon/carbon composites. *Composites Part A: Applied Science and Manufacturing* 90: 433–440.

208 Kostagiannakopoulou, C., Tsilimigkra, X., Sotiriadis, G., and Kostopoulos, V. (2017). Synergy effect of carbon nano-fillers on the fracture toughness of structural composites. *Composites Part B: Engineering* 129: 18–25.

209 Kwon, Y.J., Kim, Y., Jeon, H. et al. (2017). Graphene/carbon nanotube hybrid as a multi-functional interfacial reinforcement for carbon fiber-reinforced composites. *Composites Part B: Engineering* 122: 23–30.

7

Thermal Stability and Flame Retardancy of Epoxy Composites

Mohamedismail Fathima Rigana, Tharakan Simi Anne, Sadhasivam Balaji, Shanmugam Chandrasekar, and Muthusamy Sarojadevi

Anna University, Department of Chemistry, Sardar Patel Road, Chennai 600025, India

7.1 Introduction

Fiber reinforced plastic (FRP) composites are superior to traditional materials like metals and alloys because of their low density, high strength-to-weight ratio, corrosion resistance, tailorability, inherent dampness, and dimensional stability [1]. A variety of fibers and resins are used to manufacture composites. Both synthetic (glass, carbon, aramid, and boron) and natural fibers (jute, banana, sisal, cotton, hemp, silk, etc.) are used as reinforcement in FRP.

The processing of composites using metals like steel and aluminum as matrix has many drawbacks. Epoxy resins are the major class of organic matrix used for the fabrication of high-performance FRP products like lightweight structural panels in aircrafts and components for other automobiles. The major advantages of epoxy resin over unsaturated polyesters are that they impart excellent physicochemical properties (especially hot/wet mechanical properties) and low shrinkage on curing to the composite and they are lower in cost compared to polyimides. Though they have better heat resistance than unsaturated polyesters, at higher temperatures, it causes damage resulting in significant deterioration in their mechanical properties during and after thermal exposure [2]. Improvements in flame retardancy of the epoxy resins are given significant priority because of current stringent aviation and other legislation, to increase safety thereby increasing the market penetration. Enhancement of their char forming tendency and thermal stability was achieved by adding suitable additives [3].

During or after exposure to high temperature, the organic resin matrix in polymer-based composites undergoes thermo-oxidative degradation resulting in deterioration in strength and stiffness, thereby causing structural degradation leading to severe implications on the safety of vehicle/building occupants/fire fighters. Exposure of FRP composites, used as structural load-bearing members, to temperatures around the T_g of the matrix is likely to reduce the stiffness, strength, and creep resistance, thereby inducing these structures to distort and collapse,

Epoxy Composites: Fabrication, Characterization and Applications,
First Edition. Edited by Jyotishkumar Parameswaranpillai, Harikrishnan Pulikkalparambil, Sanjay M. Rangappa, and Suchart Siengchin.

long before they ignite and burn. Distorted structures may have larger ply surface areas that will be exposed directly to fire, causing accelerated ignition. Therefore, to improve the overall structural performance of FRP composites and to withstand the fire exposure, the thermo-mechanical properties and flammability resistance must be enhanced [4]. In the forthcoming sections, the important methodologies adopted to achieve the above said enhancements are discussed.

7.2 Effects of Micro Fillers on Thermal Properties of Epoxy Resin

7.2.1 Epoxy/Glass Fiber Composites

7.2.1.1 Bis(4-cyanato-3,5-dimethylphenyl) Naphthyl Methane/Epoxy/Glass Fiber Composites

Jayakumari et al. in 2008 prepared laminated composites from E-glass fiber (plain woven fabric [200 g/m^2]) and epoxy resin (LY556)/cyanate (3%, 6%, 9%)-modified epoxy resin by hand lay-up technique. The epoxy resin and 4,4′-diamino diphenyl methane (DDM) were obtained from Huntsman.

The differential scanning calorimetry (DSC) analysis reveals the cure characteristics of the dicyanate CDPNM (bis(4-cyanato-3,5-dimethylphenyl) naphthyl methane) and their 3%, 6%, and 9% blends with epoxy resin (Table 7.1). The decrease in peak maximum temperature for 3%, 6%, 9% blends (165, 154, 138 °C) with increasing cyanate ester concentration confirms the fact that addition of the cyanate ester, CDPNM, increases the cure reaction rate of the neat epoxy resin. Polycyclo trimerization of cyanate monomers, reaction of cyanate with amine, and the reaction of epoxy with cyanurate are responsible for the large exothermic peak obtained from cyanate ester epoxy systems.

The dynamic mechanical analysis (DMA) reveals that the T_g of all the cyanate/epoxy blend composites are higher than that of the neat epoxy (142.7 °C) composites. The T_g of CDPNM–LY556/DDM–glass fiber composites is 152, 157, and 145 °C for the 3%, 6%, 9% CDPNM content, respectively. With increasing cyanate

Table 7.1 DSC cure characteristics, glass transition temperature, and TGA data of epoxy and cyanate modified epoxy system-glass fiber composites.

Composition	T_i (°C)	T_p (°C)	T_f (°C)	T_g (°C)	$T_{10\%}$ (°C)	Charyield (%)
EP	—	—	—	142.7	358	18.2
CDPNM	185	227	285	—	—	—
3 CDPNM	125	165	231	152	393	25.7
6 CDPNM	115	154	214	157	395	27.0
9 CDPNM	102	138	180	145	398	29.0

Source: Jayakumari et al. [5] Reproduced with permission from John Wiley & Sons. © 2008, John Wiley & Sons.

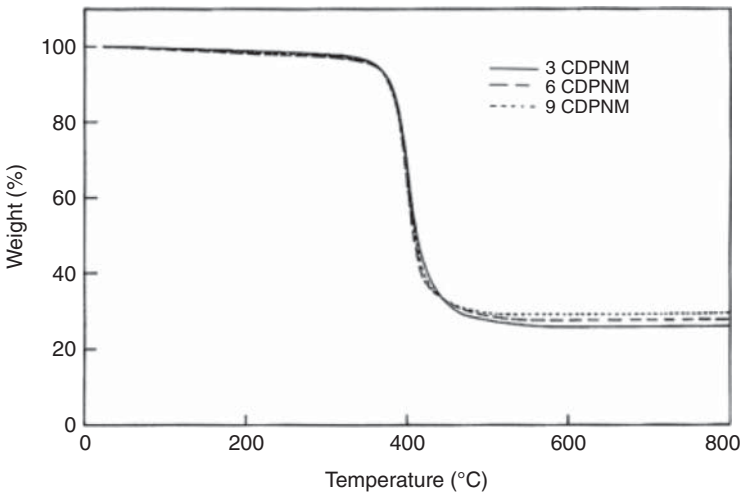

Figure 7.1 TGA curves of neat epoxy and cyanate-modified epoxy blends. Source: Jayakumari et al. [5]. © 2008, John Wiley & Sons.

content, the T_g increases upto 6%, due to the formation of oxazoline rings by the reaction of cyanate ester with epoxy resin (Table 7.1). But with 9% cyanate content, the T_g is decreased because of very high content of bulky naphthalene rings in the CDPNM leading to increased free volume and hence easy mobility of the polymer chains, thereby decreasing the T_g [5].

The $T_{10\%}$ values of the blends and hence composites of all compositions were found to be about 40 °C higher than that of the neat-cured LY556/DDM (Figure 7.1 and Table 7.1). This enhanced $T_{10\%}$ is due to the triazine rings formed by curing of cyanate ester resin. The char yield of 3%, 6%, 9% CDPNM/epoxy blends was found to be (25.7, 27.0, and 29.0) higher than that of neat-cured LY556/DDM (18.2%).

7.2.1.2 Epoxy (DGEBA) Resin + CSE (Chlorinated Soy Oil) – Based Epoxy/Glass Fiber Composites

Thulasiraman et al. in 2008 prepared the epoxy/glass fiber composites using epoxy (diglycidyl ether of bisphenol A)/CSE (chlorinated soy oil)-based epoxy, MPDA (*m*-phenylene diamine), and glass fiber (woven fabric-plain weave-biaxial [200 g/m^2]) at different compositions. The epoxy equivalent weight (EEW) of diglycidyl ether bisphenol-A (DGEBA) and the prepared CSE are 180 and 208, respectively. The commercial epoxy resin (DGEBA) was obtained from Huntsman, India.

It was observed from the DSC analysis that all the epoxy/CSE/MPDA systems (Figure 7.2 and Table 7.2) show a single exothermic peak in the temperature range of 155 ± 5 °C. The higher curing temperature for 100% CSE (188 °C) is because of the low reactivity of aliphatic epoxy group when compared with the aromatic epoxy system and also lower epoxide content as indicated by the higher EEW of the CSE (208). The heat of reaction values of 100% epoxy (EP), 5% CSE/95% epoxy, 10% CSE/90% epoxy, 15% CSE/85% epoxy, 20% CSE/80% epoxy and 100% CSE (360, 359, 359, 358, 357, and 354 J/g) confirm that all the epoxy groups in the resin cured with hardener

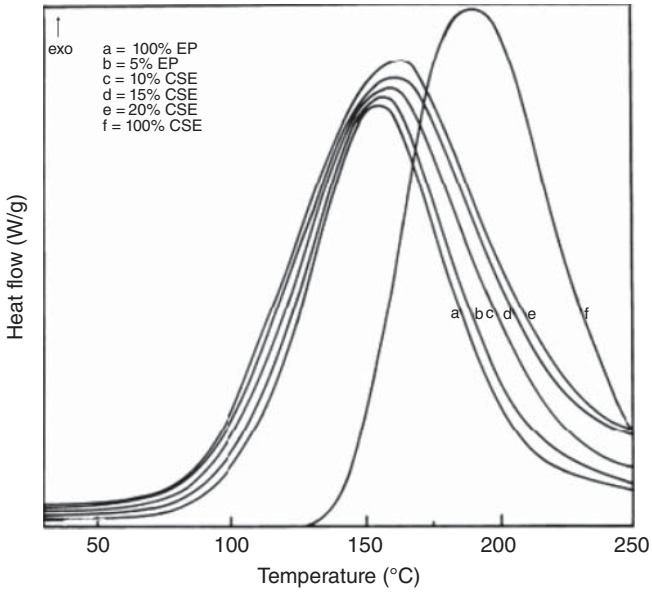

Figure 7.2 DSC cure curve of epoxy/CSE blends. Source: Thulasiraman et al. [6]. © 2008, John Wiley & Sons.

Table 7.2 DSC cure characteristics, glass transition temperature and TGA of neat epoxy and CSE modified resins/cyanate modified epoxy glass fiber composites.

Composition	Cure temperature at peak (°C)	Tan δ (post cured at 150 °C)	Tan δ (post cured at 225 °C)	$T_{10\%}$ value (°C)	Char yield (%)
100% EP	151.2	137.4	161	350	20.36
5% CSE/95% epoxy	153.4	131.9	156	348	18.15
10% CSE/10% epoxy	154.7	127.6	154.4	347	17.59
15% CSE/85% epoxy	157.1	122	152.2	344	13.68
20% CSE/80% epoxy	159.5	111	138.5	309	12.35
100% CSE	187.5	-	-	254	8.47

Source: Modified from Thulasiraman et al. [6].

completely. With increasing CSE content, the peak maximum shifted to higher temperature (151.2–159.5 °C) and hence the addition of CSE to commercial epoxy appears to decrease the rate of curing of the blend. This is due to the lower reactivity of CSE with epoxy because it has the long aliphatic chains and bulky groups.

The T_g obtained from DMA analysis of the composites postcured at 150 and 225 °C is given in Table 7.2. T_g value decreases with increasing CSE content in commercial epoxy resin due to the segmental motion of aliphatic chains being higher than

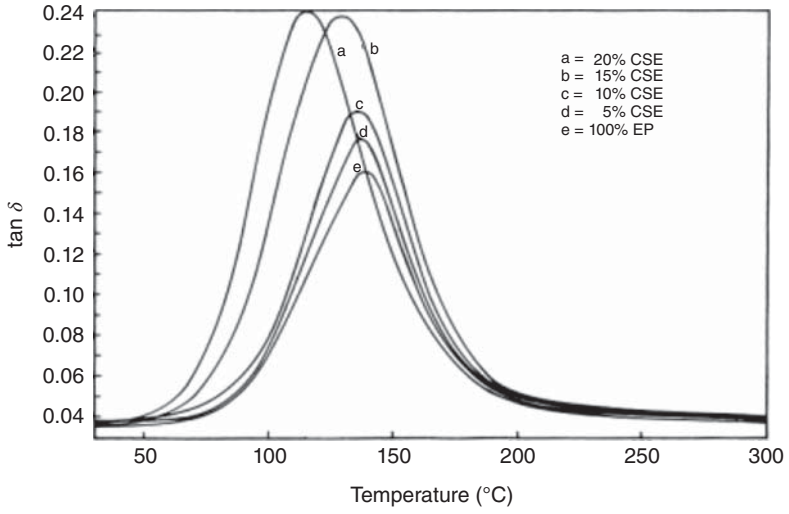

Figure 7.3 Tan δ curves of neat epoxy and CSE-modified epoxy composites post cured at 150 °C. Source: Thulasiraman et al. [6]. © 2008, John Wiley & Sons.

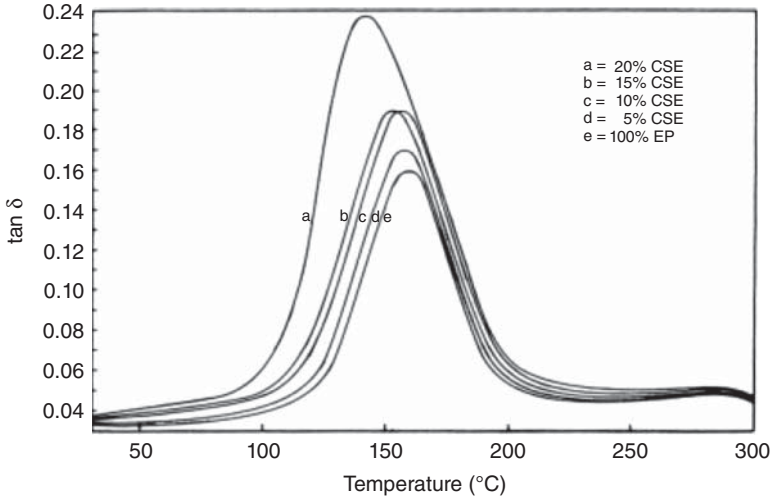

Figure 7.4 Tan δ curves of neat epoxy and CSE-modified epoxy composites post cured at 225 °C. Source: Thulasiraman et al. [6]. © 2008, John Wiley & Sons.

that of the aromatic groups. Figures 7.3 and 7.4 show the loss factor (tan δ) for the epoxy/MPDA/CSE composite with different compositions. The single loss factor peak indicates that the prepared blends possess a single glass transition temperature and hence a homogenous phase [6].

The $T_{10\%}$ of the cured resins is shown in Figure 7.5 and Table 7.2. From the thermograms, it is proved that the cured samples degrade in a single step and begin their decomposition at around 300 °C. Thermal stability of the resin decreases with increase in CSE content compared with epoxy toughening agents such as rubber

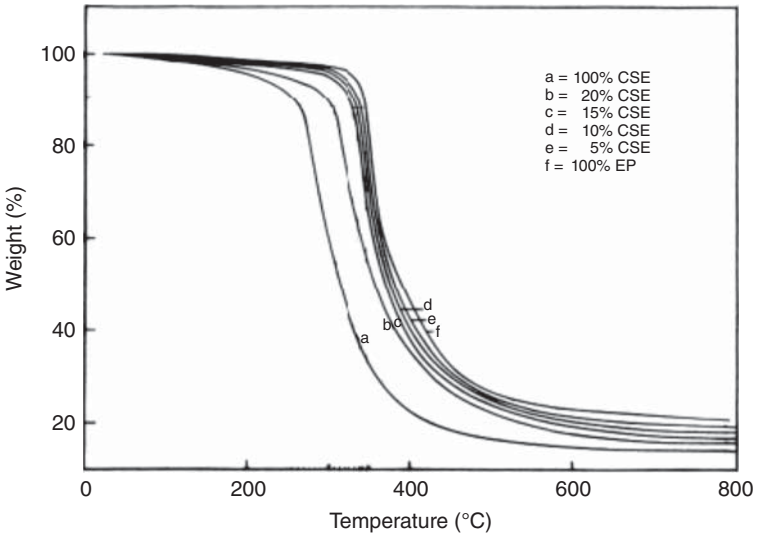

Figure 7.5 TGA curves of neat epoxy and CSE-modified epoxy blends. Source: Thulasiraman et al. [6]. © 2008, John Wiley & Sons.

and polyurethane [7]. The char yield of neat epoxy decreases with increasing CSE content (Table 7.2) because of the high aliphatic content. 100% CSE has the lowest char yield of 8.5% when compared to the other compositions. Since the corresponding LOIs will be lower, the flame-retardant character would also be decreased.

7.2.1.3 Novolac-Type Epoxy and Isocyanate-Modified Epoxy/Glass Fiber Composites

Shin et al. in 2015 prepared glass fiber (HM-345R) composites using novolac-type epoxy (YDPN-638, Kukdo chemical Co. Ltd., Korea)/isocyanate modified epoxy (SEY-5310, Shin A, TVC, Korea) with amine hardener (KH-100, Kukdo chemical Co. Ltd., Korea). Epoxy/glass fiber prepregs were made by coating a solution of epoxy (with amine hardener in acetone) on glass fiber (30 wt%). The prepregs were kept in an oven at 150 °C for seven minutes for solvent evaporation and precuring. The composites were then made by hot compression molding of the prepregs. The curing was carried out at 150 °C under a pressure of 220 kg(f)/cm^2 for one hour and at 170 °C for three hours [1].

The novolac-type epoxy resin shows (Figure 7.6) a higher T_g (169 °C) than the isocyanate-type epoxy composites (107.3 °C) and the 1:1 mixed epoxy (163 °C).

7.2.2 Epoxy/Natural Fiber Composites

7.2.2.1 Epoxy (DER 331)/Kenaf Fiber Composites

Azwa et al. reported the thermal stability of the epoxy (obtained by reacting epichlorohydrin with bisphenol A)/kenaf fiber (Malaysian Agricultural Research and Development Institute [treated and untreated]) composites. Jointmine 905-3S,

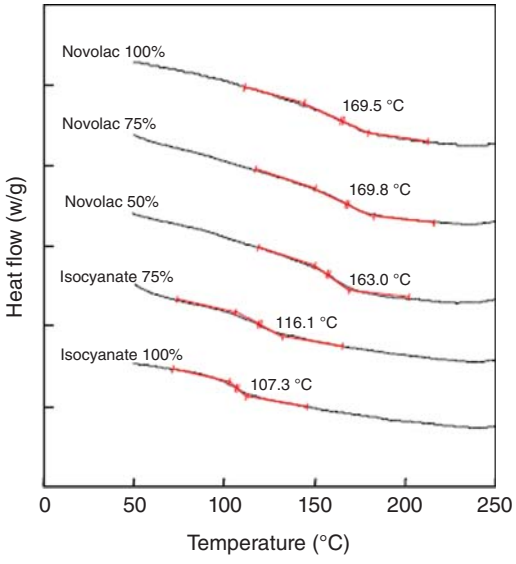

Figure 7.6 DSC curves of epoxy resins with different mixing ratios. Source: Shin et al. [1]. © 2015, Elsevier.

Table 7.3 Decomposition temperature and charring of samples.

	Epoxy	Glass fiber/epoxy	Treated kenaf-fiber/epoxy	Untreated kneaf-fiber/epoxy	Treated kneaf-fiber	Untreated kneaf-fiber
Decomposition temperature (°C)	372	380	373	378	350	346
Final weight after decomposition (%)	8.29	39.83	12.46	13.67	18.96	16.21
Increment in thermal stability from epoxy (%)	—	2.19	0.40	1.79	—	—
Increment in char production from epoxy (%)	—	380.46	50.30	64.90	—	—

Source: Azwa and Yousif [8]. © 2013, Elsevier.

a liquid cycloaliphatic amine, was used as a curing agent. For comparison, thermal property of epoxy/glass fiber (450 R-glass) was discussed. TGA (Figure 7.7) and differential thermal analysis (DTA) (Figure 7.8) analyses (Table 7.3) reveal that the untreated kenaf/epoxy composite starts to undergo weight loss earlier (80 °C) than the treated samples because of the presence of higher moisture content. The hydrophilic nature of the kenaf fibers can be observed for both treated and untreated fibers as they show a much higher early weight loss. Treated kenaf fiber/epoxy composite has lower char yield than the untreated kenaf/epoxy composite, due to the removal of lignin during treatment with alkali.

Lignin in natural fiber is the main cause for char; thus, the untreated fibers leave behind a high char. The DTA results, indicate that the neat epoxy and its composite

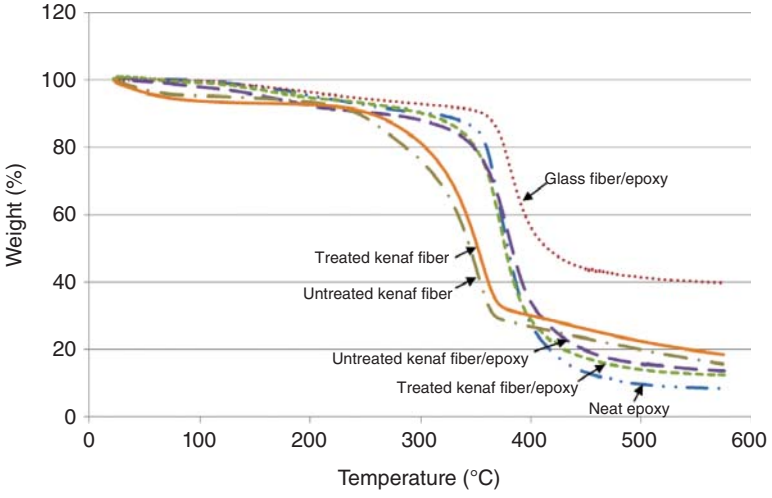

Figure 7.7 TGA curves of treated and untreated kenaf fiber/epoxy composites. Source: Azwa and Yousif [8]. © 2013, Elsevier.

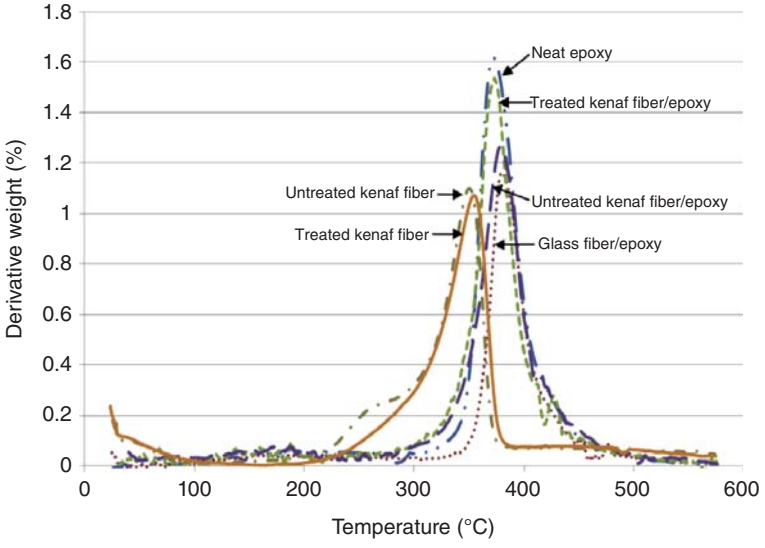

Figure 7.8 DTA curves of treated and untreated kenaf fiber/epoxy composites. Source: Azwa and Yousif [8]. © 2013, Elsevier.

with glass fiber have the highest decomposition temperatures at 372 and 382 °C while the other composites with treated and untreated kenaf fibers have lower decomposition temperatures. The peaks at 260 and 346 °C observed in the DTA curves of untreated kenaf fiber/epoxy composites are due to the decomposition of hemicelluloses and cellulose, respectively. The hemicelluloses are expected to be removed during treatment with NaOH as indicated by the increase in the temperature of first decomposition for the treated kenaf fibers. In the meanwhile,

the second decomposition temperature was found to increase to 350 °C. Compared to treated and untreated kenaf fiber/epoxy composites, glass fiber/epoxy composites have higher T_d and char yield as expected [8].

7.2.2.2 Epoxy (Ampreg 26)/*Phormium tenax* Composites

Epoxy/*Phormium tenax* fiber composites were made [9] using a low viscosity epoxy resin (SP systems ampreg 26), a slow reacting hardener (mixing ratios 100 : 33.3), and *Phormium tenax* fibers of length 20 mm and average diameter 151.3 ± 45.65 μm with a final fiber weight fraction of 0.20 ± 0.02. The composite was cured at room temperature and at 70 °C for 24 hours each.

Rose et al. reported that the *Phormium tenax* fibers undergo an initial weight loss of ~8% in the temperature range of 37–130 °C due to vaporization of water from the fibers (the thermogravimetry [TG] curve in Figure 7.9a). The fibers are stable upto 200 °C. The first- and second-stage decompositions occur in the temperature range of 200–305 °C and 305–370 °C (20% weight loss) (Table 7.4) due to the thermal depolymerization of hemicellulose and the cleavage of glycosidic linkages of cellulose (45.2% weight loss). The decomposition of lignin takes place slowly in the temperature range of 200–900 °C because of the complex branched aromatic

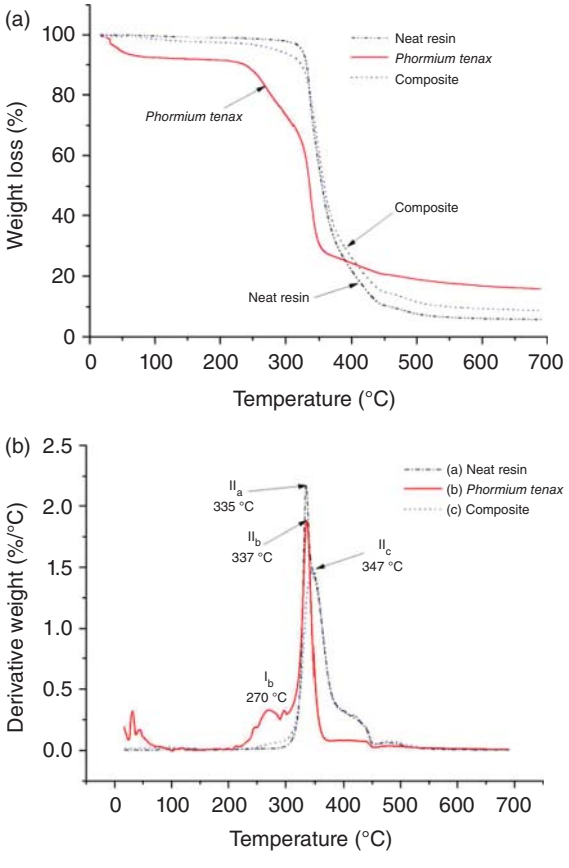

Figure 7.9 (a) TG and (b) DTG curves of neat resin, *Phormium tenax* fibers, and *Phormium tenax*-reinforced composites. Source: Rosa et al. [9]. © 2010, Elsevier.

Table 7.4 Thermal degradation data of *Phormium tenax* fibers at 5 °C/min in nitrogen atmosphere.

	Weight loss (%) below 130 °C	First degradation stage			Second degradation stage			Residual char
		T_1 (°C)	Weight loss (%)	T_{peak} (°C)	T_n (°C)	Weight loss (%)	T_{peak} (°C)	
Phorium tenax fibers	8.1	200-305	20.0	270	305–370	45.2	337	15.7

Source: Rosa et al. [9]. © 2010, Elsevier.

structure of lignin (Table 7.4). The derivative thermogravimetry (DTG) curves (Figure 7.9b) indicate that the fiber, neat resin and the composite decompose at 337, 335, and 347 °C, respectively, illustrating that the fiber-matrix system degrades at a higher temperature than the neat resin. This may be attributed to good fiber matrix interaction [9].

7.2.3 Epoxy/Natural Fiber Hybrid Composites

7.2.3.1 Epoxy (Araldite M)/Jute–Glass Fiber Hybrid Composites

In 2015, Braga et al. reported the analysis of the mechanical and thermal properties of jute (grammage 361.1 g/m^2) and glass fiber (grammage 194.4 g/m^2)-reinforced epoxy hybrid composites. Epoxy resin (Araldite M), jute, and glass fibers were laminated in three weight ratios (69/31/0, 68/25/7, and 64/18/19) to form composites, and they are denoted as E69-J31-V0, E68-J25-V7, E64-J18-V19, respectively. Thermogravimetric analysis reveals that while decreasing the jute fiber and epoxy resin content with increasing glass fiber content, there is a reduction in mass loss as a function of temperature. The thermogravimetric analysis (TGA) curves of E69-J31-V0 (Figure 7.10a), E68-J25-V7 (Figure 7.10b), and E64-J18-V19 (Figure 7.10c) show that the composites lose 1.95%, 1.52%, and 1.27% of weight, respectively, until the temperature of 100 °C and at 200 °C the weight loss is 9.00%, 7.76%, and 6.57% that corresponds to the removal of solvent in polymer matrix. Due to degradation and volatilization of the epoxy resin and jute fibers present in the composites, the weight loss was 70.70%, 68.97%, and 63.54%, respectively, between 200 and 450 °C. After that the composites maintain a linear mass loss up to 1000 °C, where the final residue is only 6.48%, 17.50%, 24.19% of the original mass for the three types of composites [10].

7.2.3.2 Epoxy/Flax and Sisal–Glass Fiber Composites

Meenakshi et al. studied the effect of surface modification on the mechanical and thermal behavior of flax, sisal, and glass fiber-reinforced epoxy hybrid composites. Hybrid composites were made using epoxy resin (LY 556) as matrix, hardener (HY-951) in the ratio of 10 : 1, flax (density – 1.45g/cm^3), sisal (density – 1.45 g/cm^3), and glass fiber (600 grams per square meter [GSM]) biaxial mats as reinforcements. Glass and flax fiber-reinforced epoxy was prepared by

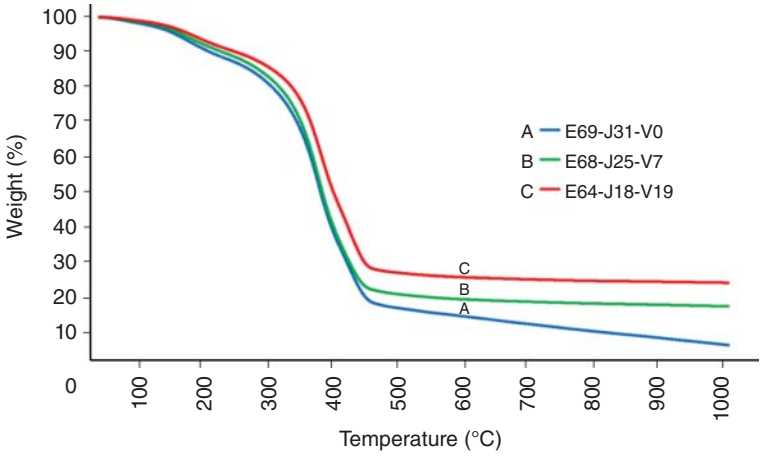

Figure 7.10 TGA curves of the epoxy/jute-glass fiber hybrid composites (a) E69-J31-V0, (b) E68-J25-V7 and (c) E64-J18-V19. Source: Braga and Magalhaes [10]. © 2015, Elsevier.

layering up fibers in a thin cleaned mold coated with mold-releasing agents and denoted as glass–flax–glass-treated (GFG-T) (alkali treated natural fiber mats) and glass–flax–glass-untreated (GFG-UT) (untreated fiber mats).

The interfacial bonding between the fiber and matrix is the major factor deciding the strength and modulus of the composites. Poor bonding will impart poor strength and modulus to the composites. The natural fiber-based composites have improved interfacial bonding after the fibers are subjected to mercerization, esterification, and ionized air treatment. The hemicelluloses present on the outer surface of the natural fibers make the bonding between fiber and matrix inferior. It has been reported that mercerization will remove the wax, pectin, lignin, and hemicelluloses leading to enhanced interfacial bonding. In this work, the jute and sisal fibers were subjected to mercerization by treatment with NaOH solution.

TGA analysis reveals that the hybrid composites with sisal, jute, and glass fibers are all thermally stable upto 300 °C and they decompose in the temperature range of 306–315 °C even on mercerization with NaOH [11].

7.2.3.3 Epoxy (DER 331)/MH (Magnesium Hydroxide)-Kenaf Fiber Composites

Magnesium hydroxide (MH) (10, 15, 20, 25 wt%)/kenaf fiber (40% by weight)/epoxy hybrid composites were fabricated by hand lay up technique by Saba et al., using a liquid epoxy resin (D.E.R. 331) and the modified aliphatic amine hardener jointmine 905-3S [12].

The TGA curves show the effect of inclusion of MH on the thermal stability and char content of pure kenaf fiber/epoxy composites (Figure 7.11). The TGA curves reveal that the pure kenaf/epoxy and all hybrid MH/kenaf/epoxy composites undergo three-stage degradation. The initial weight loss around 100–200 °C may be attributed to the moisture loss upon thermal degradation of the kenaf fibers. The second weight loss occurs in the range of 300–450 °C. The decomposition of the phenyl rings of the epoxy network, hemicellulose, lignin, pectin, and the glycosidic

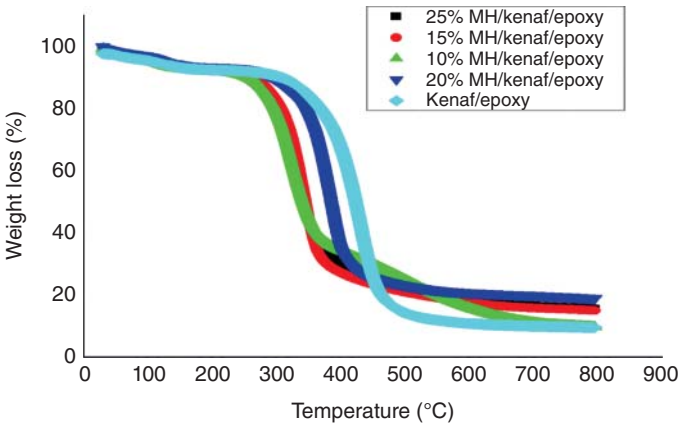

Figure 7.11 TGA curves of MH/kenaf/epoxy and kenaf/epoxy composites. Source: Saba et al. [12]. © 2019, Elsevier.

linkages of cellulosic constituents from kenaf fibers contribute to this weight loss. The third stage thermal degradation takes place at 700 °C due to the degradation of the cured epoxy network. In the case of MH/kenaf/epoxy hybrid composites, the decomposition of MH to MgO, with loss of water through endothermic dehydroxylation, leads to a sudden and significant weight loss around 300–400 °C. The MgO formed is extremely thermally stable acting as ceramic insulating material/heat sink for the kenaf fibers and the epoxy network protecting them from undergoing degradation, thereby making it extremely resistant to high temperature [13]. MH filler upto 20% enhanced the thermal stability and the char content, while beyond 20% loading, thermal stability gets reduced, which can be ascribed to the formation of agglomerates of MH within the matrix. The formation of high residual char content in MH filled kenaf/epoxy hybrid indicates their better flame retardancy character than kenaf/epoxy composites.

7.3 Effect of Nanofillers on Thermal Properties of Epoxy Resin

7.3.1 Epoxy/Clay Nanocomposites

7.3.1.1 Epoxy (DGEBA)/Clay Nanocomposites

Zaman et al. prepared epoxy/clay nanocomposites. DGEBA resin having EEW 182–196 g/equiv, Jeffamine J230 (hardener), clay [surface modified with surfactent ethanolamine (eth-clay), Jeffamine M2070 (m27-clay) and Jeffamine XTJ 502 (xtj-clay)] with a cation exchange capacity of 85 mequiv/100 g, were used for the preparation of the nanocomposites.

The peak maximum temperature of the tan δ curve shows that the added clay has enhanced the T_g of the neat epoxy matrix (Table 7.5). Furthermore, the T_g increases with increasing clay content with the exception observed at 1.16 vol% of

Table 7.5 Glass transition temperatures of epoxy/clay nanocomposites.

	Clay content (vol%)	T_g (°C)
Neat epoxy	0	93.7
eth-clay/epoxy	0.46	101.1
	1.16	92.8
	1.87	102.4
m27-clay/epoxy	0.46	96.6
	1.16	96.3
	1.87	100.9
xtj-clay/epoxy	0.46	97.2
	1.16	99.6
	1.87	100.4

Source: Zaman et al. [14]. © 2015, Elsevier.

eth – clay (modified with ethanolamine, eth) and the nanocomposite has reduced T_g. This may be caused by variations of curing condition, and excess surfactant left by modification although great care was paid in fabrication. This result indicates that the presence of the grafted long-chain molecules of the surfactants onto clay layers (*m*27 and *xtj*) does not compromise T_g at all. The strong interaction exerted by *xtj*-clay with epoxy matrix results in the restricted molecular motion in the resin, increasing the T_g values [14].

7.3.1.2 Epoxy (E51)/D-clay (Na^+-MMT) Nanocomposites

Epoxy/D-clay nanocomposites with varying content of D-clay (0%, 1%, 2%, 3%, and 4%) were prepared by Bin Chen et al. [15]. D-clay was prepared from (Na-MMT) pristine montmorillonite clay and dopamine hydrochloride (DOPA) by ion exchange reaction of DOPA with clay, when dopamine gets intercalated in the galleries of clay.

The DMA analysis shows that the storage modulus of the epoxy/D-clay nanocomposites is higher (1632 MPa [1% D-clay], 1971 MPa [2% D-clay], 2096 MPa [3% D-clay], and 2009 MPa [4% D-clay]) than that of pristine epoxy resin (1477 MPa). This enhanced storage modulus of the nanocomposite may be due to the efficient load transfer from the matrix to the homogeneously dispersed, high aspect ratio D-clay, due to the strong interfacial bonding leading to restricted polymer chain mobility. T_g (obtained from the peak temperature of the tan δ curves) of the neat epoxy was found to be enhanced significantly (from 86.0 to 89.9, 92.1, 96.3 and 96.0 °C for 1,2, 3 and 4% D-clay) in the epoxy/D-clay nano composites. The high surface area of the clay platelets, their homogeneous dispersion in the epoxy matrix, and the strong interfacial bond are reported to reduce the mobility of the polymer chains leading to longer relaxation time and hence enhanced T_g.

All the epoxy/D-clay nano composites have $T_{5\%}$ of around 351 °C, much lower than that of pure epoxy resin (360 °C) which may be attributed to degradation of small molecules in the intergallery space of clay. But $T_{85\%}$ of the nano composites was

found to be 436 °C (1% D-clay), 442 °C (2% D-clay), 447 °C (3% D-clay), and 450 °C (4% D-clay) indicating higher stability at higher temperatures. This is due to good adhesion of the clay platelets to the epoxy matrix. Also, since the polymer chains are entrapped in the intergallery space of the clay platelets, the latter hinders polymer degradation by acting as the heat shields [15].

7.3.1.3 Epoxy (DGEBA)/Cloisite Na+, Cloisite 10A, Cloisite 15, Cloisite 93A Nanocomposites

Salam et al. 2016 prepared the epoxy/clay nano composites with DGEBA resin and montmorillonite (MMT) clays [unmodified (Cloisite Na+) and organomodified (Cloisite 10A, Cloisite 15, and Cloisite 93A)] purchased from BYK-Chemie, GmbH, Germany.

The DSC thermogram suggests that the T_g values of epoxy/clay (all types used) nanocomposites are higher than that of the neat epoxy indicating that the rigid clay platelets restrict the mobility of epoxy polymer chains enhancing the T_g. The addition of 3 wt% clay for epoxy nanocomposites reinforced with Cloisite 10A, Cloisite Na^+, Cloisite 93A, and Cloisite 15 was found to consistently increase T_g by approximately 11%, 13%, 16%, and 23%, respectively. Eventhough T_g decreases slightly at the clay content from 3 to 5 wt% for epoxy nanocomposites reinforced with Cloisite Na+, Cloisite 93A, and Cloisite 15, associated values were still higher than that of neat epoxy. More remarkably, epoxy/Cloisite 15 nanocomposites exhibit a maximum increase of 28% in T_g (relative to neat epoxy) with 10 wt% clay inclusions [16].

7.3.1.4 Organo Phosphorus Epoxy/Clay Nanocomposite

Hussain et al. [17] prepared 3% organophosphorus – DGEBA/TGDDM epoxy resins by reacting the organo-phosphorus compound 9,10-dihydro-9-oxa-10-phosphaphenanthrene- 10-oxide (DOPO) with DGEBA (DER-331–Dow Chemical Company, Australia)/TGDDM (Araldite MY 720-vantico, Australia). Organophosphorus epoxy/clay nanocomposites were made using octadecyl ammonium ion- exchanged montmorillonite layered silicate clay (Nanomer 1.30E) with an initial interlayer d-space of 23 Å and the mixture of 3,5-diethyl toluene-2,4- diamine and 3,5-diethyltoluene-2,6-diamine (DETDA–Ethacure-100–Albemar Corporation) as the hardener [17].

DSC analysis of neat DGEBA/TGDDM + hardener, 3% phosphorus–DGEBA/TGDDM + hardener, 7.5% clay + DGEBA/TGDDM + hardener, and 7.5% clay + 3% phosphorus – DGEBA/TGDDM + hardener reactions reveals that the curing temperature of both the DGEBA and TGDDM decreases on adding the organically modified clay. This indicates that the latter acts as a catalyst and increases the rate of the curing reaction thereby decreasing the cure temperature. DGEBA seems to be more influenced by the catalytic effect than TGDDM. Jiankun et al. [18] reported that in the organo clay/epoxy system, the epoxy and the hardener molecules intercalate into the clay galleries causing swelling of the clay and hence exfoliation taking place during cure.

3% phosphorus–DGEBA system was found to cure at a lower curing temperature revealing a faster cure rate compared to neat DGEBA. But the 3% phosphorus–TGDDM undergoes curing at a higher temperature than neat TGDDM indicating slower cure reaction compared to neat TGDDM. The high reactivity

of a phosphorus-containing DGEBA epoxy with amine may be due to the P=O group acting as electron withdrawing group within the epoxy, reducing the electron density of oxirane rings facilitating nucleophilic attack by the amine species, thereby accelerating the reaction rate. In the case of phosphorus containing TGDDM epoxy, the molecule becomes very bulky by the incorporation of bulky 9,10-dihydro-9-oxo-10-phosphaphenantharene-10-oxide (DOPO) leading to decreased monomer mobility and hence decreased rate of curing.

Dynamic mechanical thermal analysis reveals that the T_g of DGEBA and TGDDM is decreased on adding organo clay. The influence of the addition of clay to the polymer on the T_g has been reported by several authors. Some researchers report an increase in T_g values, while others reported a decrease in T_g (attributed to the interference of the clay with the crosslink density, epoxy homopolymerization, and the alkyl ammonium ion in gallery space of the clay acting as plasticizers). The cured 3% phosphorus–DGEBA and 3% phosphorus–TGDDM also were found to have lower T_g compared to the respective neat-cured resins. The lower T_g is attributed to higher EEW leading to lower crosslink density. The bigger DOPO structure would be expected to hinder molecular mobility thereby increasing T_g. In this case, it can be seen clearly that the effect of decreased crosslink density decreasing T_g dominates over the effect of the size of the DOPO increasing the T_g.

For the neat cured DGEBA, the thermal degradation starts at around 420 °C with the maximum weight loss occurring around 450 °C and a char yield of 14% remaining at 600 °C. The initial degradation temperature occurs at a lower temperature of 340 °C on addition of 5% and 7.5% clay in DGEBA, and the maximum weight loss temperature increases to about 465 °C with the greater char yield of around 38–40% at 600 °C. The results indicate that the clay forms a barrier to degradation and stabilizes the char layer. For the 3% phosphorus DGEBA and its nanocomposite with 7.5% clay, the onset degradation temperature is 300 °C and the char yield is 42% and 28%, respectively. The decrease in onset degradation temperatures of 3% phosphorus–DGEBA or 3% phosphorus–DGEBA/clay nanocomposite when compared to neat epoxy is due to the decomposition of P=O=C bonds. Similar behavior was observed for the TGDDM epoxy system. The char yield of TGDDM was found to be 22% at 600 °C. The char yield was improved to 42% for the 3% phosphorus–TGDDM and to 48% for the 3% phosphorus–TGDDM/clay nanocomposite while the onset degradation temperature was decreased. The limiting oxygen index (LOI) calculated from char yield for neat DGEBA, phosphorus-modified DGEBA, 7.5% clay-modified DGEBA, phosphorus and 7.5% clay-modified DGEBA were found to be 25.0, 33.0, 34.5, and 28.7, respectively. Phosphorus-, clay-, and phosphorus + clay-modified DGEBA have higher fire retardance than pure DGEBA. Similarly, TGDDM system has LOI values of 26.3, 34.3, 35.1, 36.7, and 35.1 for neat TGDDM, phosphorus-modified TGDDM, 5% clay-modified TGDDM, 7.5% clay modified TGDDM and phosphorus–clay-modified TGDDM, respectively. Synergistic effects of clay and phosphorus addition on char formation were not observed.

7.3.1.5 Epoxy (DGEBA)/DNA-Modified MMT Clay Nanocomposites

Zabihi et al. in 2016 reported the preparation of epoxy/DNA modified MMT clay and epoxy/organoclay nanocomposites. The DGEBA epoxy resin (DER332), DNA modified clay (d-clay) and organoclay ([m-clay; Nanomer 1.28E; Nanocor Co., USA])

were used for the preparation of the nanocomposites. The nanocomposites were made by compression moulding process using d-clay and m-clay at 2.5% and 5 wt% and named as EP-D2.5, EP-M2.5, EP-D 5 and EP-M5.

Dynamic mechanical thermal analysis (DMTA) analysis shows that in the glassy region ($T < T_g$), the addition of 2.5% clay (m-clay or d-clay) increases the storage modulus of the neat epoxy resin, while in the rubbery region ($T > T_g$), the storage modulus of neat epoxy is greater than that of the epoxy/m-clay nanocomposite. This is because of the plasticizing effect of the m-clay on the epoxy matrix reducing the storage modulus leading to a reduction in the ability of load transfer from matrix to the m-clay, also causing lower T_g for the epoxy/m-clay nanocomposite compared to that of the neat epoxy resin.

The T_g of epoxy/2.5% d-clay was found to be 6 and 9 °C higher than that of pure-cured epoxy and cured epoxy/m-clay indicating the absence of plasticizing effect at the interface of the epoxy/d-clay nanocomposite, resulting in a strong interface leading to very high restriction to segmental mobility of the polymer chains. Another reason for the high T_g of the epoxy/2.5% d-clay nanocomposite is that it shows 0.35 mmol/m^3 increase in the crosslink density compared to neat-cured epoxy and epoxy/2.5% m-clay.

The TGA of the epoxy/m-clay (or d-clay)nanocomposite reveals that they undergo multistep degradation involving two main steps. On adding 2.5% d-clay, T_i, $T_{max\text{-}1}$, and $T_{max\text{-}2}$ of the neat epoxy-cured matrix increase by 16, 6, and 19 °C, respectively. The increase in char yield at 850 °C is more for the d-clay addition than for m-clay addition.

Cone calorimetry studies reveal that pure epoxy shows a high peak heat release rate (HRR) of (1542 kW/m^2) than epoxy/2.5% m-clay nanocomposite. Addition of 2.5% d-clay reduces the peak HRR of the pure epoxy by 322 kW/m^2.

The time of reaching peak of HRR (t_{PHRR}) increases from 71 to 87 seconds and 96 seconds for epoxy/2.5% m-clay and epoxy/2.5% d-clay, respectively, indicating that the d-clay nanocomposite requires nine seconds more to reach peak of heat release rate (PHRR) in comparsion to m-clay nanocomposite. This behavior is due to the inherent flame retardancy of the DNA having phosphate groups. These results demonstrate that the epoxy/d-clay has the highest flammability resistance [19].

7.3.2 Epoxy/CNF Nanocomposites

7.3.2.1 Epoxy (SC-15)/Carbon Nano Fiber (PR-24) Nanocomposites

Yuanxin Zhou et al. [20] synthesized the carbon nanofiber (CNF)/epoxy nanocomposites with commercially available SC-15 epoxy (Applied Poleramic, Inc., 6166 Egret Court, Benicia, CA, USA). It is a low-viscosity, two-phase toughened epoxy resin system consisting of part A (mixture of diglycidylether of bisphenl A 60–70%, aliphatic diglycidylether 10–20%, and epoxy toughener 10–20%) and part B (hardener, cycloaliphatic amine 70–90%, and polyoxylalkylamine10–30%). The CNF (PR-24) is two dimensional and plain weave and has a diameter of 60–200 nm and fiber length of 30–100 μm (Applied Science, Inc., 154W Xenia Avenue, Cedarville, OH, USA).

DMA curves (Figure 7.12a) of rectangular specimens (1.7 mm × 30 mm × 8 mm) indicate that the storage modulus increases with increasing CNF content with 3% of CNF, enhancing the storage modulus by 65% at 30 °C. The tan δ (Figure 7.12b) curves indicate that the T_g of the epoxy/CNF nanocomposites also increase with increasing CNF content though the peak height decreased. There is broadening of the peak due to the unconstrained segments of the polymer molecules which retained the original

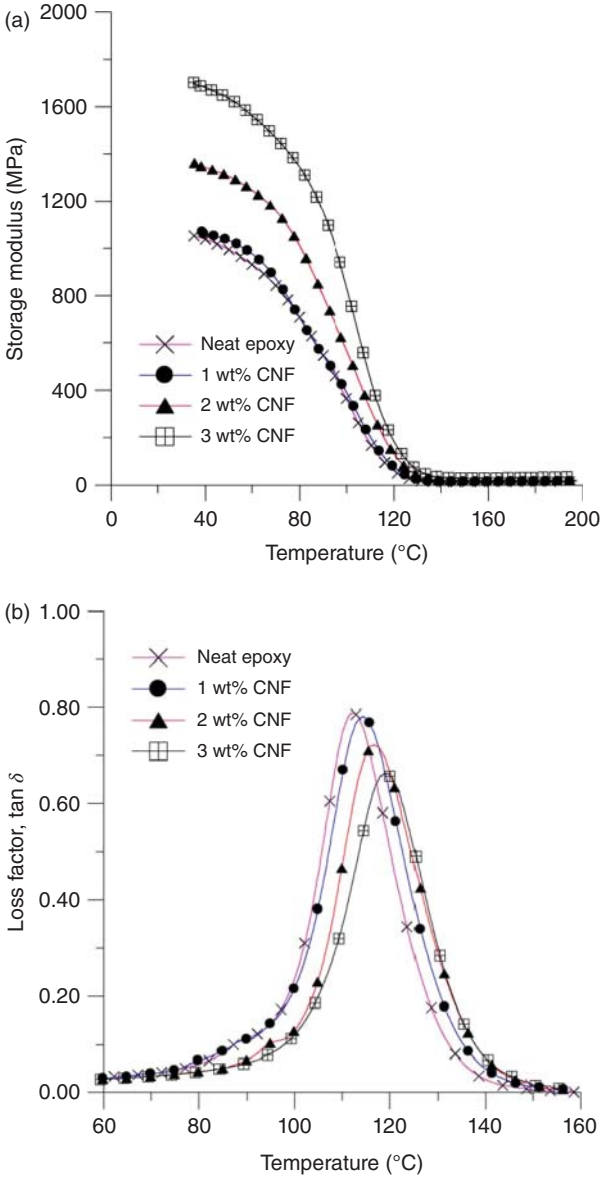

Figure 7.12 (a) Storage modulus vs. temperature of CNFs-modified epoxy. (b) Loss factor vs. temperature of CNFs-modified epoxy. Source: Zhou et al. [20]. © 2006, Elsevier.

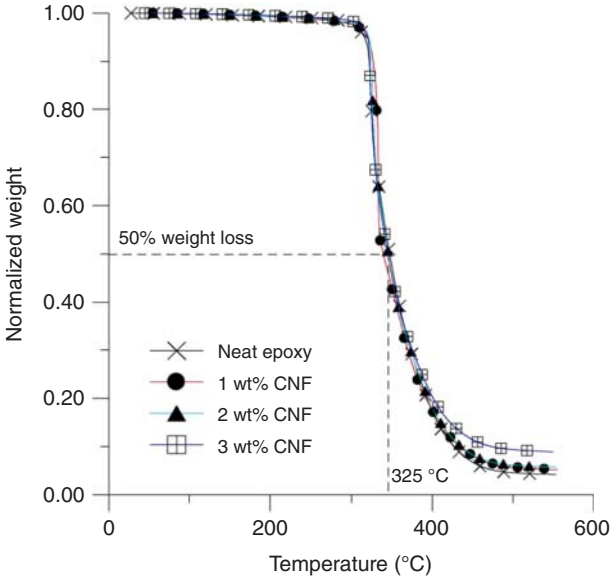

Figure 7.13 TGA curves of CNFs/epoxy nanocomposites. Source: Zhou et al. [20]. © 2006, Elsevier.

T_g. But those segments of the polymer chain which are close to the nanofiller surface should have hindered mobility leading to an increased T_g.

The decomposition temperature of the epoxy matrix remained the same (Figure 7.13) irrespective of the CNF content as evidenced from the TGA curves. The reason is that at lower temperatures the interfacial bonding is strong where the molecular chains are holding the CNF strongly in the nanocomposite. But this bond becomes weaker at higher temperatures and the polymer chains can move freely. So CNFs in epoxy matrix cannot increase decomposition temperature though they can increase the tensile strength and T_g.

Laminated composite panels were manufactured by using plain weave carbon fiber (CF) and 2 wt% CNF-modified epoxy. Carbon/neat epoxy laminated composite panels were also fabricated. The CNF (2%) epoxy nanocomposites, carbon/neat epoxy composites, and carbon/2%CNF-modified epoxy composites are reported to have the decomposition temperatures of 325, 351, and 353 °C, respectively (Figures 7.14 and 7.15). CNF has little effect on thermal stability of carbon/epoxy composite. But the decomposition temperature of carbon/2% CNF-modified epoxy composite is 28 °C higher than that of 2% CNF/epoxy nanocomposites [20].

7.3.3 Epoxy/CNT Nanocomposites

7.3.3.1 CNT/Epoxy Nanocomposites

Tao et al. in 2006 studied the effect of carbon nanotube fillers on the curing processes of bisphenol F-based epoxy resin (EPIKOTE™ resin 862). The nanocomposite material was prepared using EPIKOTE resin 862, EPIKURE™ W curing agent, and carbon nanotubes. Three kinds of carbon nanotubes, namely short SWNT

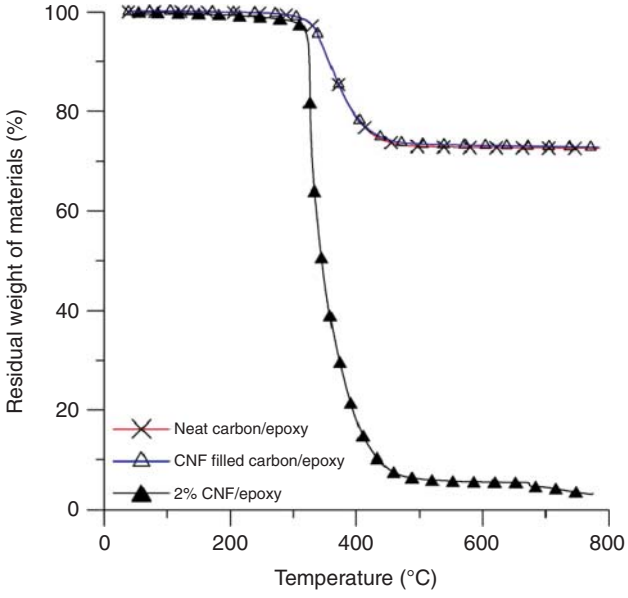

Figure 7.14 Residual weight vs. temperature curves of CNF/epoxy, CF/epoxy, and CF/CNF/epoxy. Source: Zhou et al. [20]. © 2006, Elsevier.

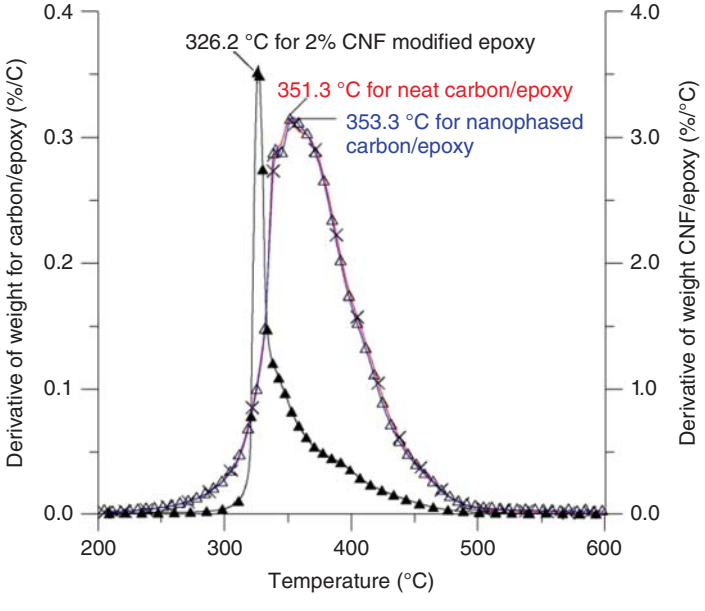

Figure 7.15 Thermo gravimetric traces of CNF-modified epoxy and carbon/epoxy composite. Source: Zhou et al. [20]. © 2006, Elsevier.

(S_SWNT, 96.3% carbon content), HiPco SWNT, and XD-grade carbon nanotube (XD-CNT), were used for making the nanocomposites. The cure behavior of the epoxy–hardener mixture was studied using DSC. The broad exothermic peak ranging from 80 to 310 °C is due to the curing reaction. At higher temperatures another exotherm was observed which may be due to thermal degradation. The exothermic peak for the CNT/epoxy-hardener mixture is smaller than that of the neat epoxy indicating decreased rate of curing in the epoxy on addition of CNT.

DSC thermograms of the cured epoxy nanocomposites show that all the CNT-embedded nanocomposites exhibited lower T_g irrespective of the stiffness of CNT, which is a strong signal of less curing compared to neat epoxy resin. DSC thermograms of the neat epoxy and single-walled carbon nanotubes (S_SWNT) embedded epoxy nanocomposites cured for 2.5 and 24 hours reveal that the 24 hours cured composites (862 + W = 159; 862 + W + S_SWNT = 135; 862 + W + HiPco-SWNT = 148; 862 + W + XD-CNT = 143 °C) showed higher T_g than 2.5 hours (862 + W = 144; 862 + W + S_SWNT = 115; 862 + W + HiPco-SWNT = 133; 862 + W + XD-CNT = 130 °C) cured samples. The S_SWNT-epoxy composites exhibited lower T_g than the neat epoxy material. Addition of even very low amount (1 wt%) of CNT also lowered the T_g of epoxy nanocomposites by 10–30 °C. This may be attributed to weakly bonded CNT within the epoxy matrix, which increased the distance between polymeric chains, resulting in a decrease in intermolecular forces hence lowering the T_g of the composite material. The finding of lowering the T_g of composite is highly essential for the applications where CNTs are expected to improve the thermal properties of the composite materials [21].

7.3.4 Epoxy/Cellulose Nanofiber Nanocomposites

7.3.4.1 Epoxy (D.E.R. 331)/Cellulose Nanofiber Nanocomposites

Saba et al. prepared epoxy/cellulose nanofiber (CNF: 0.5%, 0.75%, and 1%) filler nanocomposites by casting technique using D.E.R. 331, DGEBA epoxy resin, and jointmine 905-3S (a modified cycloaliphatic amine curing agent) [22].

TGA curves (Figure 7.16) reveal that the epoxy/CNF nanocomposites have higher degradation temperature compared to epoxy composites, due to char formation in the advanced stages of degradation. The char act as an insulating layer against further thermal degradation. The decomposition temperature of the epoxy resin at 330 °C shifts to relatively higher temperature 400 °C by the incorporation of CNFs in epoxy composites as seen from DTG curves (Figure 7.16b). The DMA curves (Figure 7.16c) reveal that the tan δ values of the epoxy resin (0.78) decrease (0.70–0.74) by adding CNFs indicating better dispersion in the matrix inhibiting the polymer movement and increasing the T_g of the epoxy resin (from 60 to 61–62 °C).

7.3.5 Epoxy/Spherical Metal Oxide Nanocomposites

7.3.5.1 Epoxy (Epon 862)/Coreshell Fe@FeO Nanocomposites

In 2010, Zhu et al. reported the preparation of the nanocomposite using the epoxy resin, Epon 862 (bisphenol F diglycidyl ether) and the curing agent Epicure W purchased from Miller-Stephenson Chemical Company, Inc. and core shell structured

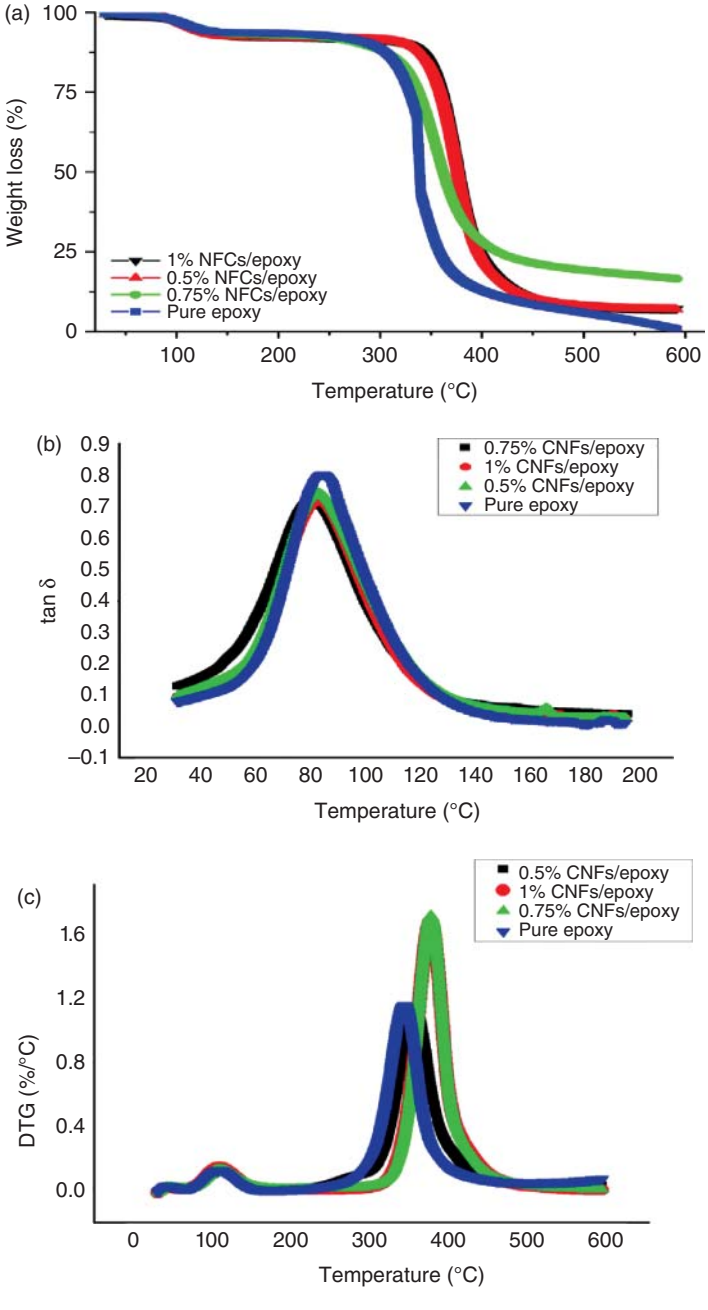

Figure 7.16 (a) Effect of CNFs filler loadings on TGA graph of epoxy composites. (b) DTG curves for the epoxy composites and epoxy nanocomposites. (c) Effect of CNFs filler loadings on the tan δ value of epoxy composites. Source: Saba et al. [22]. © 2017, Elsevier.

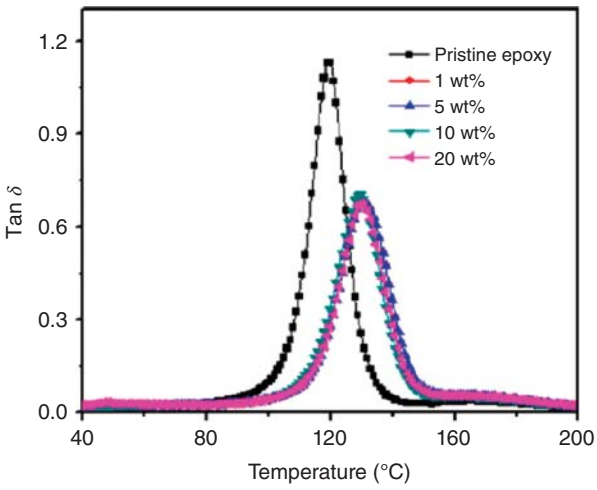

Figure 7.17 Tan δ curves for nanocomposites with different Fe@FeO loadings. Source: Zhu et al. [23]. Copyright 2010 American Chemical Society.

Fe(core)@FeO(shell) nanoparticles 1, 5, 10, 20 wt%, with a particle size of 15–25 nm and oxide thickness of 0.5 nm, QuantumSphere, Inc.

The G' (storage modulus which is measure of elastic modulus) of the pristine epoxy (1.06 GPa) shows 4% increase on adding 20% Fe@FeO nanoparticles ($G' = 1.7$ GPa) in the glassy plateau at 60 °C and 82.4% increase (14.3 MPa) in the rubbery plateau at 160 °C. This increase in storage modulus is attributed to the presence of rigid homogeneously dispersed nano particles. The G'', loss modulus, was also found to exhibit a similar trend. The tan δ (ratio of the loss modulus to the storage modulus) peak temperature was found to be about 10 °C higher compared to that of the neat epoxy (Figure 7.17) [23].

Thermal analysis by TGA indicates two-stage decomposition with similar decomposition behavior for both the neat epoxy and the nanocomposites. The addition of 5% Fe@FeO nanoparticles seems to decrease (Figure 7.18) the first

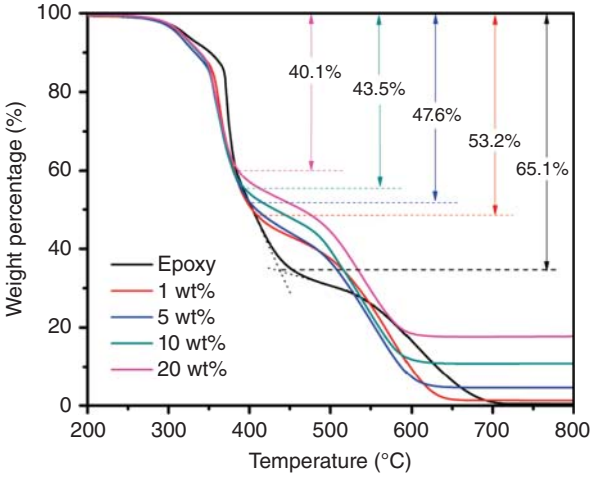

Figure 7.18 TGA curves of pristine epoxy and nanocomposites. Source: Zhu et al. [23]. Copyright 2010 American Chemical Society.

Table 7.6 TGA data of pristine epoxy and nanocomposites.

Samples	T_1 onset (°C)	T_2 onset (°C)	$T_{5\%}$ (°C)
Epoxy	364.5	549.8	319.0
1 wt% Fe@FeO/epoxy	345.4	509.6	314.7
5 wt% Fe@FeO/epoxy	338.9	500.8	314.6
10 wt% Fe@FeO/epoxy	339.1	499.1	315.5
20 wt% Fe@FeO/epoxy	338.0	497.9	315.7

Source: Zhu et al. [23]. Copyright 2010 American chemical society.

decomposition temperature, second decomposition temperature, and the 5% weight loss temperature by about 20, 50, and 5 °C, respectively, (Table 7.6).

7.3.5.2 Epoxy (Epon 862)/Polyaniline-Stabilized Silica Nano Composites

Gu et al. [24] reported the preparation of flame-retardant epoxy resin/polyaniline (PANI)-stabilized silica nanoparticles nanocomposites. The Epon 862 , a bisphenol F-based epoxy resin, was used as the matrix. EpiCure W procured from Miller-Stephenson Chemical Company, Inc. was used as the curing agent. Ninety-eight percentage amorphous silica nanoparticles with an average diameter of 60–70 nm, specific surface area of 160–800 m^2/g obtained from US Research Nanomaterials Inc. was functionalized with PANI using a facile surface-initiated polymerization method. 1.0, 3.0, 5.0, and 7.0 wt% of the untreated silica (u-silica) and functionalized silica (f-silica) were used for the preparation of the nanocomposites.

The ΔH of the reaction between u-silica and epoxy is 1.234 J/g while that for f-silica with epoxy is 6.431 J/g indicating that the reaction of u-silica with epoxy is very much insignificant compared to that of f-silica (Figure 7.19).

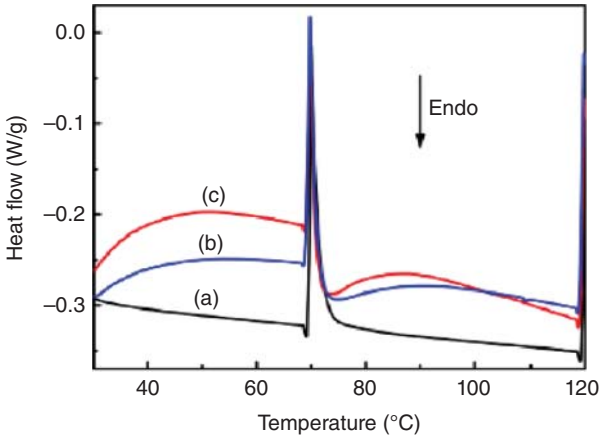

Figure 7.19 DSC curves of (a) Epon monomers, (b) Epon suspension with 7.0 wt% loading of f-silica nanoparticles, (c) Epon nanosuspension with 7.0 wt% u-silica nanoparticles. Source: Gu et al. [24]. Copyright 2013 American Chemical Society.

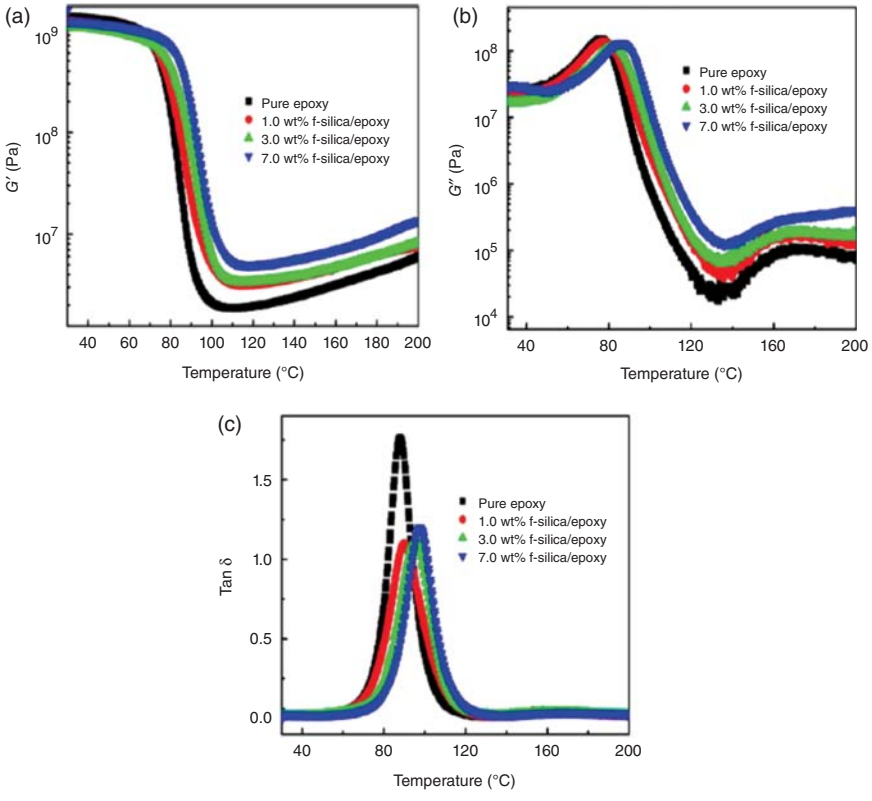

Figure 7.20 (a) G', (b) G'', (c) tan δ vs. temperature curves for the cured pure epoxy and its polymer nanocomposites (PNCs) with different f-silica nanoparticle loadings. Source: Gu et al. [24]. Copyright 2013 American Chemical Society.

The peak maximum temperature of the tan δ curves indicates an increase in T_g with increasing f-silica content. The cured f-silica/epoxy nanocomposites have T_g 2–10 °C (Figure 7.20) higher than that of the cured pure epoxy (87.5 °C). This is attributed to the fact that the added f-silica particles are dispersed well due to the covalent bonding (increased crosslink density) with the epoxy resin which restricts the segmental movement of the polymer chains and also increase in the free volume. The storage modulus (G') and loss modulus (G'') of 7% f-silica/epoxy nanocomposites (86 and 87) are observed to be higher than those of the u-silica/epoxy nanocomposites (84 and 82) (Figure 7.21) indicating that the f-silica increases the crosslinking density of the epoxy matrix [24].

TGA curves of pure epoxy and u-silica (5.0 wt%)/epoxy, f-silica doped with H_3PO_4 (5.0 wt%)/epoxy, and f-silica doped with H_2SO_4 (5.0 wt%)/epoxy nanocomposites (Figure 7.22) under air and nitrogen conditions show that the main degradation takes place in two stages. The small weight loss around 250–320 °C in the nanocomposites is due to the homolytic scission of chemical bonds in the epoxy network. The first weight loss takes place around 350–430 °C because of the elimination of water molecules from oxypropylene groups (–CH_2–CH(OH)–) and the breakdown

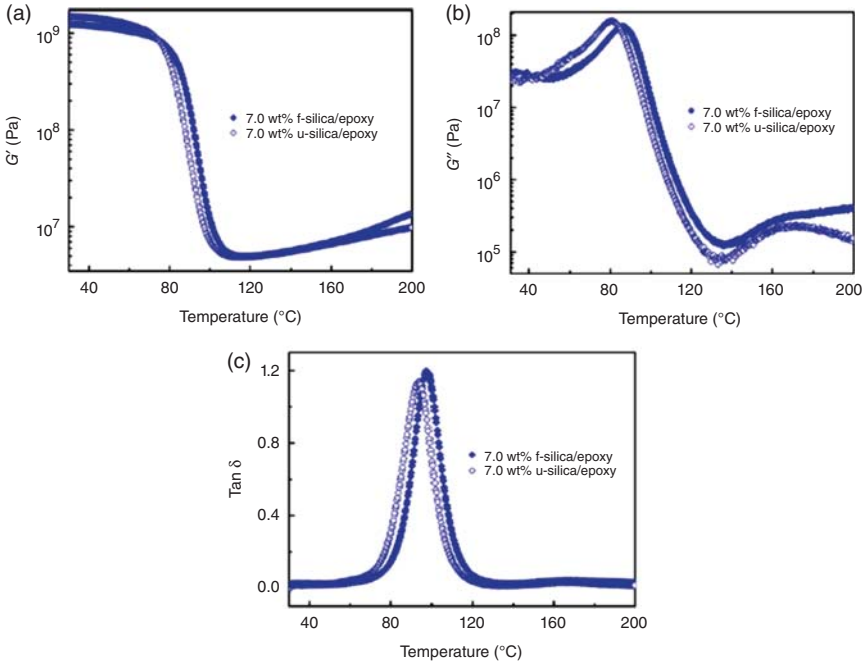

Figure 7.21 (a) G', (b) G'', (c) tan δ vs. temperature curves for the PNCs filled with 7.0 wt% u-silica and f-silica nanoparticles, respectively. Source: Reprinted with permission from Gu et al. [24]. Copyright 2013 American Chemical Society.

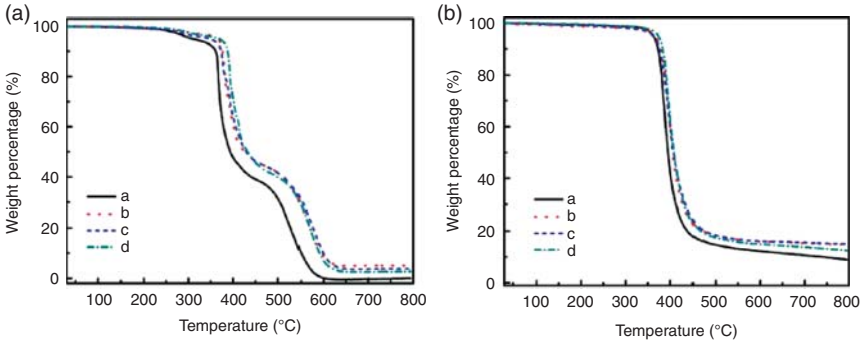

Figure 7.22 TGA curves of the (a) cured pure epoxy, (b) epoxy filled with 5.0 wt% u-silica. Source: Gu et al. [24]. Copyright 2013 American Chemical Society.

of the epoxy network. The second weight loss (at about 450–600 °C) corresponds to the degradation of benzene rings of the cured epoxy.

7.3.6 Epoxy Based Hybrid Nanocomposites

7.3.6.1 Epoxy (DGEBA)/CNT/OMPOSS/APP Hybrid Nanocomposite

Caroline Gerard et al. prepared epoxy (DGEBA, EEW = 172–176)/octamethyl polyhedral oligomeric silsesquioxane (OMPOSS)/ammonia polyphosphate (APP) CNT

(Nanocyl 7000, 90% purity) nanocomposites by casting technique after mixing the fillers with epoxy resin and hardener (diethylene triamine).

TGA shows that the degradation of virgin epoxy occurs in two stages: the first one is between 200 and 430 °C and the second one is between 430 and 610 °C, which corresponds to decomposition resulting in char and volatilization of the char, respectively. The incorporation of OMPOSS alone in the epoxy slightly modifies the degradation path, the main volatilization begins at lower temperatures (~160 °C), and the intermediate residue is 20 wt% lower than that of virgin epoxy. However, the maximum volatilization rate is slightly shifted toward higher temperatures. It seems that after the initial decomposition at a lower temperature, the OMPOSS partially shields the epoxy resin. When APP is incorporated into the resin, the main volatilization starts at lower temperature and the intermediate residue is 10% higher than that of virgin material. However, the second stage (460–600 °C) does not lead to complete volatilization of the resin, and a more stable (20 wt%) residue is produced. In addition to these, a third stage was also observed in between 580 and 750 °C due to final volatilization of the char. Incorporation of CNT does not show any distinct features in the first degradation step of epoxy/APP, except that the intermediate residue is 5% lower. However, the second step takes place at somewhat higher temperatures, and the final residue observed in the last step was slightly lower than that of epoxy/APP. In the case of incorporation of OMPOSS, the first stage leads to a 10% higher intermediate residue and the second stage was observed in the same temperature range as epoxy/APP with lower residual weight in the last degradation step [25].

7.3.6.2 Acrylonitrile–Butadiene–Styrene/Brominated Epoxy–Antimony Oxide/Organo Montmorillonite (ABS/BER-AO/OMT) Nanocomposites

Haiyun Ma et al. prepared ABS/OMT and ABS/BER-AO (2–5 μm)/OMT nanocomposites by melt compounding followed by hot compression molding process (at a pressure of 14 MPa). The Na^+-montmorillonite was modified with octadecyl trimethyl ammonium bromide (C_{18}) before use. The brominated epoxy (BER) (F-2100H) having molecular weight of 2.5×10^4, density of 1.8 g/cm^3, and bromine content of 53% was used for making the nanocomposites.

From TGA and DTG thermograms of acrylonitrile–butadiene–styrene/brominated epoxy–antimony oxide/organo montmorillonite (ABS/BER-AO/OMT) hybrids, pure ABS, ABS/OMT, and ABS/BER-AO systems, ABS/OMT nanocomposites have a lower T_{onset} (361.1 °C) than pure ABS resin (368.2 °C), due to the thermal decomposition of organic modifiers of the clay, but have a higher $T_{50\%}$ temperature (424.4 °C) and a higher char residue showing an enhanced thermal stability at higher temperatures due to the barrier properties of clay layers. The TGA/DTG curves show that the thermal degradation of ABS/BER-AO and ABS/BER-AO/OMT takes place in three independent steps. In the first step, the T_{onset} of ABS/BER-AO (335.5 °C) is much lower than that of pure ABS resin because of the pyrolysis of BER. Isomerization of epoxy group, formation of hydrogen bromide, and the reactions between HBr and AO all occur in the first step. The thermal degradation of ABS resin occurs in the second step (350–500 °C). The degradation of the protective char residue occurs during the third step. The T_{onset} and $T_{50\%}$ of the ABS/BER-AO/OMT

nanocomposites (339.3 and 411.4 °C) are higher than that of the ABS/BER-AO composites (335.5 and 408.8 °C). The above results indicate that the addition of organoclay enhances the thermal stability of the ABS/BER-AO composites. It is noted that the LOI value of ABS/BER-AO/OMT nanocomposites (31.4) is higher than that of ABS/BER-AO (29.2) composites. The results indicate that synergistic effect does exist between BER-AO and organoclay in the combustion [26].

7.3.6.3 Epoxy/Ag@Cu–Ag@rGO Nanocomposite-Based Conductive Adhesives

Conductive adhesives were prepared by Peighambardoust et al. using amine-cured (Y441) epoxy resin, silver-coated copper particles, and silver-coated rGO (reduced graphene oxide). The cured neat epoxy and the cured epoxy filled with conductive fillers like Ag-coated Cu particles/Ag-coated rGO, undergo initial decomposition at 200 °C. But the final weight loss rate of epoxy resin (88.71%) is reduced to 23.69% by the addition of silver-coated copper particles indicating improved thermal stability. The addition of Ag-coated rGO enhances the rate of weight loss to 30.54%. This may be because of the aggregation of the particles leading to heterogeneity in the heating of the different parts of the sample thereby reducing the thermal stability of the adhesive [27].

7.3.6.4 Epoxy/HM-SiO_2@CeO_2/NiO Nanocomposites

Huang et al. [28] synthesized hollow mesoporous silica (HM-SiO_2)-based ternary HM-SiO_2@CeO_2/NiO hybrid-incorporated bisphenol A epoxy nano composites using DDM as hardner for fire safety applications. The same procedure was employed for the preparation of neat EP, EP/HM-SiO_2, and EP/CeO_2/NiO nanocomposites. The TGA and DTG curves indicate that the EP/HM-SiO_2 nanocomposite has lower thermal stability ($T_{10\%}$) (374.7 °C) compared to neat EP (375.1 °C). This could be due to the presence of silanol groups on the surface of HM-SiO_2, which may act as bronsted acid and activate the catalytic degradation process. However, at higher temperatures, the EP/HM-SiO_2 shows high stability owing to the barrier effect of the mesoporous structure of the silica walls, which delays the degradation of the EP. Since transition metals are known to cause catalytic degradation of the polymer, the addition of CeO_2/NiO or HM-SiO_2@CeO_2/NiO promotes degradation of EP. However, in comparison with EP/CeO_2/NiO, the EP/HM-SiO_2@CeO_2/NiO has improved thermal properties due to the barrier effect. Also, the incorporation of CeO_2/NiO or HM-SiO_2@CeO_2/NiO into EP results in slight increase in the char residue at 700 °C; this is because CeO_2/NiO could catalyze the progress of carbonization. In addition to this, the peak maximum temperature of DTG curves of EP/HM-SiO_2, EP/CeO_2/NiO and EP/HM-SiO_2@CeO_2/NiO composites was lower than that of pure EP, which implies the increase in weight loss rate due to the catalytic effect of the additives on the degradation process. HRR curves showed that in comparison to EP, the addition of HM-SiO_2@CeO_2/NiO nanohybrid obviously reduced the values of PHRR, effective heat combustion (EHC), total heat released (THR), maximum average rate of heat emission (MARHE), and total smoke released (TSR) by 23.4, 15.3, 24.9, 16.7, and 22.2%, respectively. From these results, it can be

concluded that the EP/HM-SiO_2@CeO_2/NiO nanocomposite has the highest flame retardancy among all the nanocomposites [28].

7.3.6.5 Epoxy (Araldite)/Microsilica/Nanoalumina Nanocomposites

The SiO_2/Al_2O_3/epoxy micro nano composites were prepared by vacuum casting process using araldite CY 228 epoxy resin (Huntsman Germany), alumina particles ([0, 1, 2, 3 and 10%] [average size 40 nm; average surface area 40 m^2/g]), hardener (dicarboxylic anhydride HY 918), 65% silica flour (16 μm), and accelerator (tertiary amine, DY 062) by casting in a mold under vacuum and cured at 140 °C for 16 hours [29].

The DSC curves show that as the amount of nanoalumina is increased in the EP, the T_g of micro/nano composites decreased. The reduction in T_g may be due to the reduction in degree of crosslink density in the micro nano composites as a result of the presence of nanoalumina in the epoxy resin. The TGA curves of the micro nano composites with varying contents of nanoalumina indicate major weight loss in the temperature range of 370–420 °C, which relates to the degradation of bisphenol A. The thermal stability and char yield at 600 °C of nanocomposites with 1%, 3%, 5%, and 10% alumina are higher than that without alumina. The initial decomposition temperature of the micro nano composites (360 °C) increases with increasing concentration of alumina. Also the % weight loss during the intial decomposition was found to be high for the 1–10% alumina filled micronanocomposites; this may be due to the decrease in crosslink density with increasing alumina content. Low degree of crosslink density induces free volume and provides paths for diffusion of volatile components. However, the improved thermal stability of micro nanocomposites compared to the controls should be due to the alumina absorbing heat and acting as heat sink prohibiting thermal degradation in the system [29].

7.4 Epoxy-Based Hybrid Micro and Nanocomposites

7.4.1 Epoxy (LY556)–Closite 25A OMMT/Glassfiber Micro Nano Composite

DGEBA–LY556-epoxy resin, triethylene tetraamine–HY951 hardener (resin hardener ratio 100 : 10 by weight) Cloisite 25A MMT nanoclay modified with the quarternary ammonium salt (hydrogenated tallow alkyl methyl-2-ethylhexyl ammonium salt), and plain woven E-Glass fiber mat with an aerial density of 200 g/m^2 (Saint Gobain) were used for making the nanoclay-modified epoxy/glass fiber composite laminates.

TGA in nitrogen atmosphere reveals that all the organically modified MMT filled glass fiber reinforced plastic (GFRP) nanocomposites show only upto 3% weight loss upto 300 °C and loose weight rapidly beyond 400 °C. About 45% and 61% weight loss was observed in the temperature range of 500–550 °C and 600–800 °C indicating complete decomposition of the samples. The $T_{10\%}$ and $T_{50\%}$ values indicate that the 6% (366 and 756 °C) and 10% clay (366 and 743 °C) filled composites are thermally more stable than the others [30].

7.4.2 Epoxy/Glass Fiber (GE) Composites, Epoxy/Glass Fiber/FGO Nanocomposites

Ashori et al. prepared epoxy/glass fiber (GE) composites, GO-epoxy/glass fiber (GO/GE), and functionalized GO-epoxy/glass fiber micro-nanocomposites (DA-GO/GE and IL-GO/GE). Chopped strand mat (E-glass) with a thickness of 0.8 mm and areal density of 300 g/m^2 was used as the reinforcement. Bisphenol A-based epoxy resin (EM 500) with EEW of 180–190 and an aromatic amine hardener (H 917) were used. GO was prepared by oxidizing graphite powder by a modified Staudenmeier method and functionalized using dodecylamine (DA-GO) and 1-(3-aminopropyl) imidazole (IL-GO).

On addition of GO, DA-GO, IL-GO nanofillers, the storage modulus of the GE composite increased. This may be due to the hindered segmental mobility of the polymer chains in the epoxy network around the nanofillers, as a result of a very strong interfacial interaction and large interface area between the nanofillers and polymer. Among all, the DA-DO/GE composite shows highest increase in the storage modulus because the functionalization should have enhanced the interfacial interaction to the greatest level. The T_g of the GE composite shifts to higher temperature on adding GO/DA-GO/IL-GO into GE composites. The TGA thermograms show that the onset of main degradation starts around 260–320 °C and ends at ~600 °C, which is attributed to the decomposition of epoxy resin. The thermal stability of the composites increases (50–110 °C) upon addition of GO/DA-GO/IL-GO. This may be attributed to the uniform dispersion of GO/functionalized graphene oxides (FGOs,) which act as physical barrier for the diffusion of small gaseous molecules, causing delay in the decomposition rate of the composites. The highest enhancement in the thermal stability was achieved for FGO (DA-GO and IL-GO). The higher heat capacity of GO/FGOs as compared to neat epoxy can also account for the enhanced thermal stability of the micro-nanocomposites [31].

7.4.3 Epoxy/Glass Fiber (GE) Composites and Epoxy/Glassfiber/Nano Al_2O_3 Nanocomposites

Epoxy nano composites were made by Kishore Kumar Mahato et al. Nano alumina particles 0.1%, 0.30%, and 0.5% (diameter 50 nm), 3K plain weave glass fiber (diameter of 15 μm), DGEBA-type epoxy resin, and TETA hardener were used for making the composites/nanocomposites.

The DSC curves (Figure 7.23a) for the first heating cycle of glass fiber/epoxy (GE) and nano-Al_2O_3 GE composites reveal that the T_g of the GE composites is decreased by the addition of nano-Al_2O_3. With increasing Al_2O_3 content, the T_g decreases upto 0.3% and then increases slightly at 0.5% Al_2O_3 (Figure 7.23b). In the DSC curves for the second heating of GE and nano alumina GE, the T_g was found to be enhanced by about 5–6 °C (Figure 7.23c). A similar trend of T_g with increasing nano-Al_2O_3 was observed in the second heating cycle also though for all the composites the T_g values are higher than that observed for the first heating cycles (Figure 7.23d).

The T_g measured by DMTA for the control GE composite is 112.8 °C (Figure 7.24). With the addition of 0.1 wt% of nano-Al_2O_3, it is decreased by about 10.6 °C. At

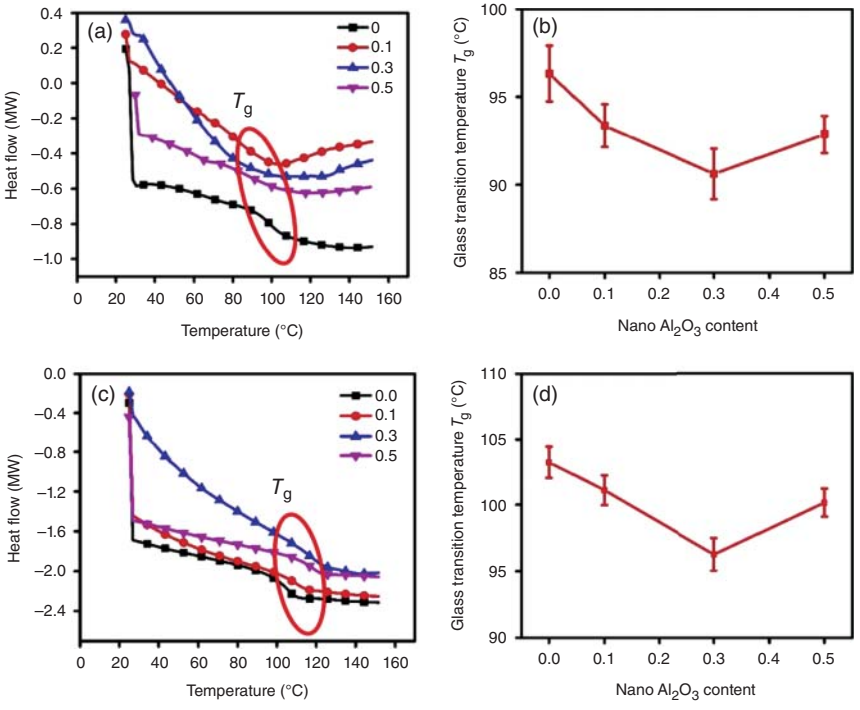

Figure 7.23 DSC analysis of GE and nano-Al_2O_3 enhanced GE composites (a) DSC curves of first heating cycle, (b) T_g vs. nano-Al_2O_3 content of first heating cycle, (c) DSC curves of second heating cycle, (d) T_g vs. nano-Al_2O_3 content of second heating cycle. Source: Mahato et al. [32]. © 2019, Elsevier.

0.3 wt% nano-Al_2O_3 the T_g continues to decrease but at a lower rate. This may be due to the diffusion of the isolated and well- dispersed nano-Al_2O_3 particles between the polymeric interchain spacing leading to decreased crosslink density and reduced T_g [32].

7.4.4 Epoxy/CF/DWCNT-NH_2 Micro-Nanocomposites

Inam et al. in 2010 reported epoxy/carbon fiber (CF)/amino-functionalized double-walled carbon nanotubes (DWCNT-NH_2) micro-nanocomposites. The micronanocomposites were prepared using DWCNT-NH_2 (Nanocyl 2152; 0.025, 0.05 and 0.1 wt%), six layers of plain weave carbon fiber fabric (P1726, 0°/90°), with an areal density of 0.445 kg/m^2, resin transfer molding (RTM) grade liquid epoxy resin (CYCOM 823), and aromatic anhydride hardener by vacuum infusion technique. Epoxy/CF microcomposites were made by the same procedure. For comparison, DWCNT-NH_2/epoxy nanocomposites were made by casting technique.

DMA data are shown in Figure 7.25 and Table 7.7. The storage modulus (Figure 7.25a,b) of the epoxy/DWCNT-NH_2 nano composites increased tremendously on incorporating carbon fibers. While increasing the concentration of double-walled carbon nanotubes (DWCNT), the loss modulus of nanocomposites

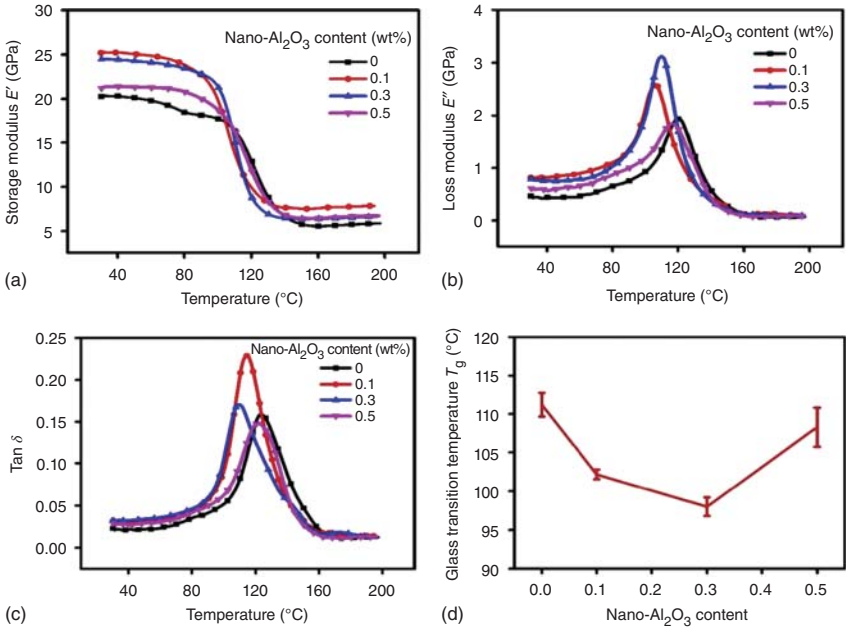

Figure 7.24 DMTA results for the GE composites with different nano-Al_2O_3 content (a) storage modulus curve, (b) loss modulus curve, (c) tan δ curve, and (d) glass transition temperature vs nano Al_2O_3 content. Source: Mahato et al. [32]. © 2019, Elsevier.

and hybrid micro-nanocomposites decreased and shifted the T_g peak (tan δ peak) downward (Figure 7.25c,d). Higher concentrations lead to lower-energy dissipation ability as well, this effect is very clear above 90 °C. Hence, it can be concluded that dampening characteristics (tan δ) of nanocomposites and hybrid micro-nanocomposites start to improve above 90–100 °C because of increased energy dissipation ability of the matrix. Based on the tan δ peak, the T_g for all composites is given in Table 7.7. Table 7.7 shows that DWCNTs enhanced the T_g of epoxy nanocomposites up to 6 °C ($T_g = 122$ °C). However, DWCNT-NH_2/CF/epoxy hybrid micro-nanocomposites did not show much increase in T_g instead of having a positive effect on T_g in the absence of carbon fiber. This could be due to nonuniform distribution of CNT's in the carbon fiber-reinforced plastics (CFRP) laminates as a result of filtering effects by the carbon fabrics [33].

7.4.5 Epoxy/Carbon Fiber Composites, Epoxy/Carbon Nanotube Membrane/Carbon Nanofiber (CNF) Paper Micro-Nanocomposites

Epoxy/carbon [34] fiber composites were made using the diglycidyl ether of bisphenol F-based epoxy resin (Epon 862), diethylene toluene diamine (curing agent; EPICURE W), and six layers of carbon fiber fabric (IM7-Style 4178, 5HS weave, 400 g/m^2, Textile Products Inc.) by hand lay-up followed by vacuum bagging with the cure schedule of two hours each at 121 and 177 °C. The epoxy/IM-7 composites with buckypaper skins (one layer of buckypaper was placed at the top and two

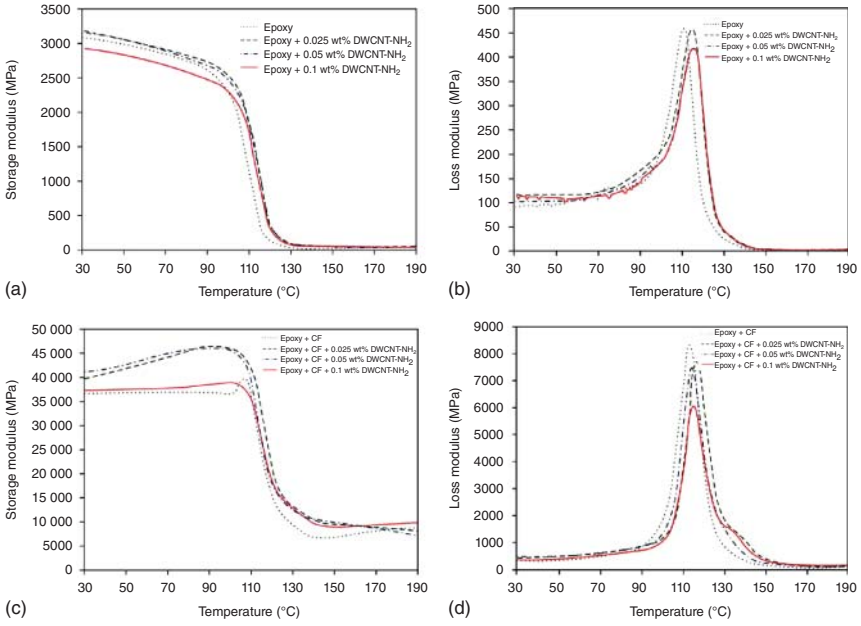

Figure 7.25 Dynamic mechanical analysis of nanocomposites: (a,b) storage and loss modulus of neat epoxy and nanocomposites and (c,d) storage and loss modulus of CFRP and hybrid micro-nanocomposites. Source: Inam et al. [33]. CC BY 3.0.

Table 7.7 Effect of DWCNTs on T_g and tan δ for nanocomposites and hybrid micro/nanocomposites.

Samples	T_g	Tan δ (at rt)
Neat epoxy	116 ± 3	34 ± 2
0.025 wt% DWCNT-NH_2 + epoxy	122 ± 4	27 ± 3
0.05 wt% DWCNT-NH_2 + epoxy	122 ± 5	31 ± 4
0.1 wt% DWCNT-NH_2 + epoxy	122 ± 3	26 ± 4
CF + epoxy	188 ± 3	108 ± 4
0.025 wt% DWCNT-NH_2 + CF + epoxy	188 ± 6	89 ± 3
0.05 wt% DWCNT-NH_2 + CF + epoxy	188 ± 4	84 ± 4
0.1 wt% DWCNT-NH_2 + CF + epoxy	188 ± 4	100 ± 3

Source: Inam et al. [33]. CC BY 3.0.

layers at the bottom of the laminate) were fabricated by the same technique. The epoxy/IM-7 composites with CNF paper (one layer of CNF paper was placed at each side of the composite) were also made.

Buckypapers were prepared by filtering a suspension of single walled carbon nanotube (SWCNT)/multiwalled carbon nanotube (MWCNT) (ground in a mortar, diluted with 0.4 wt% Triton X-100/-deionized H_2O solution and sonicated) through

Table 7.8 Main parameters from cone calorimeter measurements.

Sample	TTI(s)	Peak HRR (kW/m^2)	Time to peak HRR(s)	THR (MJ/m^2)	TSR (m^2/m^2)	MAHRE	Total mass loss (g)	Sample weight (g)
Epoxy/IM-7	46 ± 2	568 ± 6	84 ± 2	23.2 ± 1.1	1123.7 ± 53	179 ± 4	10.6 ± 0.2	36.6 ± 0.3
Epoxy/IM-7/SWCNT-BP	50 ± 4	526 ± 7	95 ± 3	24.5 ± 1.3	1180.1 ± 42	152 ± 4	10.8 ± 0.2	37.4 ± 0.4
Epoxy/IM-7/MWCNT-BP	64 ± 4	258 ± 5	90 ± 3	13.2 ± 0.9	526.1 ± 26	82 ± 6	6.2 ± 0.1	37.2 ± 0.3
Epoxy/IM-7/CNFpaper	59 ± 3	508 ± 5	96 ± 3	24.8 ± 1.3	1165.3 ± 37	158 ± 6	10.8 ± 0.2	38.0 ± 0.4

Source: Wu et al. [34]. © 2006, Elsevier.

a similar nylon membrane. CNF papers were prepared by filtering a CNF suspension in isopropanol through a nylon membrane on a homemade 9×9 in funnel under vacuum. The bucky/CNF papers were then peeled off from the nylon membrane [34].

The combustion behavior of materials on exposure to fire can be predicted by studies using cone calorimetry [35, 36]. Time to ignition (TTIs) for epoxy/IM-7/buckypaper or CNF paper micro-nanocomposites appear to be longer compared to epoxy/IM-7 composite, and a remarkable delay is observed for epoxy/IM-7/MWCNT buckypaper (Table 7.8). When the temperature of a polymer is increased beyond the critical value, combustion starts with bond breaking. The volatile fraction of the resulting combustion products diffuses into the air and creates a combustible gaseous mixture. This gaseous mixture ignites when the critical concentration and the auto-ignition temperature are reached. The buckypaper or CNF paper can act as barrier to the release of the volatile combustion products from the matrix underneath into the air, leading to an increase in the time required to reach the critical concentration of the combustible gases required for ignition to start. The TTI data obtained from cone calorimetry predict that the bucky/CNF papers have a very good shielding effect.

A similar trend was observed in the HRR also. The HRR of the epoxy/IM-7/SWCNT-buckypaper and epoxy/IM-7/CNF paper micro-nanocomposites (Figure 7.26a) slightly lower than that of the epoxy/IM-7 composite, whereas the epoxy/IM-7/MWCNT-buckypaper micro-nanocomposite shows a significant reduction in HRR. The fire behavior is also evaluated from the value of the PHRR over time. The PHRR of the epoxy/IM-7/MWCNT-buckypaper micro-nanocomposite is only about 45% of that of the epoxy/IM-7 composite. Heat release rate curves also show increase in the time to peak HRR for epoxy/IM-7/buckypaper or CNF paper micro-nanocomposites compared to epoxy/IM-7 composites.

The average rate of heat emission (AHRE; the ratio of cumulative heat emission to time) is shown in Figure 7.26b. The maximum average rate of heat emission (MAHRE) is a measure of the ability of a material for fire development in reality. MAHRE of epoxy/IM-7/MWCNT-buckypaper (Table 7.8) is

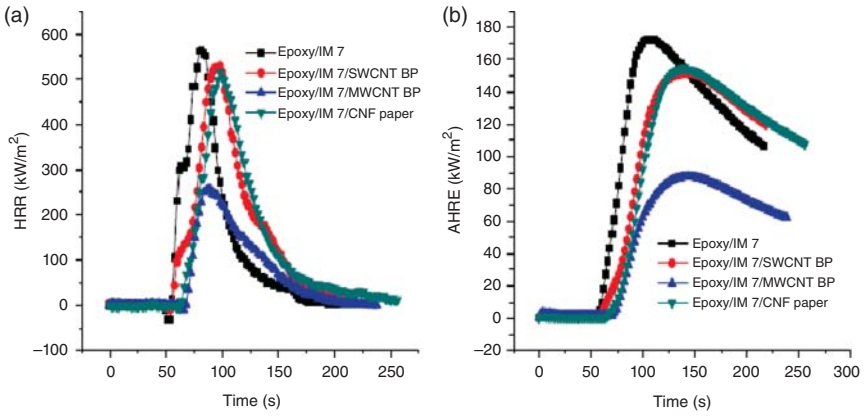

Figure 7.26 Comparison of heat release rate curves (a) and average heat emission rate curves (b) for epoxy/IM-7, epoxy/IM-7/SWCNT-buckypaper, epoxy/IM-7/MWCNT-buckypaper, and epoxy/IM-7/CNF paper. Source: Wu et al. [34]. © 2006, Elsevier.

very low (50% lower) compared to the control sample (Epoxy/IM-7 composite) indicating that the former has excellent fire-retardant property compared to the later. But the epoxy/IM-7/SWCNT-buckypaper and epoxy/IM-7/CNF paper micro-nanocomposites show only 15% reduction proving that the former two have only marginal improvement in fire retardancy.

THR given in Table 7.8 is the integral of heat release rate curves over the duration of the experiment. The THR of the epoxy/IM-7/MWCNT-buckypaper composite is only 60% of that of the epoxy/IM-7 composite (Table 7.8). The reduction of THR values indicates that the presence of MWCNT buckypaper can restrict fire development or even extinguish a fire. But the THR of the epoxy/IM-7/SWCNT-bucky paper and epoxy/IM-7/CNF paper micro-nanocomposites is close to that of the epoxy/IM-7 composite indicating that the former have comparable fire-retardant properties to that of the later.

The total mass loss of epoxy/IM-7/SWCNT-buckypaper and epoxy/IM-7/CNF paper micro-nanocomposites is around 80 wt% of epoxy (Table 7.8) in the original composite epoxy/IM-7, whereas in the case of epoxy/IM-7/MWCNT-buckypaper micro-nanocomposites, only 50% mass of epoxy was lost during the test. The mass loss is mainly from the epoxy decomposition. The presence of MWCNT buckypaper accumulated the polyaromatic hydrocarbons in the network and prevented the epoxy resin from pyrolysis/oxidation/combustion. MWCNT buckypaper reduces the mass loss during the combustion, which is directly dependent on the THR values.

Smoke and toxic gases generated during combustion (fire) are the other two important factors concerning fire safety: heavy smoke can hinder escape and toxic gases act as the killer during the fire hazard. The smoke production parameters are given in Figure 7.27 and Table 7.8. Figure 7.27a shows that the CO production and hence the mass loss is significantly decreased due to the MWCNT buckypaper skin. The lower the mass lost during a fire test, the lower will be the heat released and hence

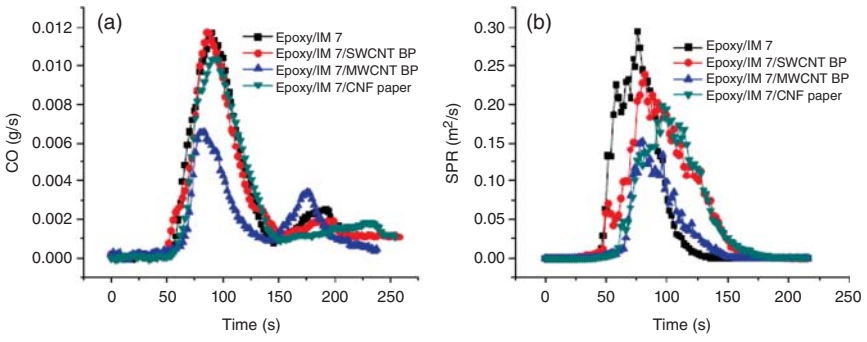

Figure 7.27 Comparison of CO production rate (a) and smoke production rate (b) during combustion. Source: Wu et al. [34]. © 2006, Elsevier.

the less smoke and CO will be generated. The values of the smoke production rate (SPR) (Figure 7.27b) and total smoke released (TSR) of the epoxy/IM-7/MWCNT buckypaper micro-nanocomposite were reduced by more than 50% compared to the epoxy/IM-7 composite. The smoke production is ascribed to the thermal decomposition of the aromatic rings in the resins, which leads to volatiles in the flame with increased soot. An increase in time required to achieve the peak of the SPR of the micro-nanocomposite with CNF paper was observed, which means that the CNF paper can act as a physical barrier to limit soot transfer.

The different flame-retardant efficiencies of SWCNT, MWCNT buckypapers, and CNF paper can be attributed to their specific properties. The median pore diameter of CNF paper determined by mercury intrusion porosimetry is around 900 nm, which is responsible for its high gas permeability. The CNF paper on the micro-nanocomposite surface cannot resist the release of gas formed during combustion efficiently. In the case of the micro-nanocomposite with SWCNT buckypaper, it can be found the SWCNT buckypaper was burnt away after combustion, and there is only red iron catalyst residue left on the fiber surface after the cone calorimetry test. The thermal stability of SWCNT is not good enough to survive during this fire test; therefore, SWCNT buckypaper cannot act as fire shield to protect the epoxy/IM-7 composite underneath. By combining high thermal stability and resistance to gas flow, MWCNT buckypaper reduced the fire hazard of epoxy/IM-7 composite by acting as a fire shield, which makes it a promising novel material to improve flame retardancy of polymeric composites.

7.5 Conclusions

This chapter deals with the thermal and flame-retardant properties of micro and nano fiber/filler-reinforced epoxy hybrid composites. The addition of fibers into the epoxy composites especially when the micro and nanofibers are well dispersed into the epoxy matrix improves the thermal stability of the composites as well as its charring capability. Addition of cyanate esters and glass fibers to the epoxy

resin enhanced the thermal stability. But a reverse trend was observed on adding CSE-based epoxy to the epoxy/glass fiber composites. Epoxy/clay nanocomposites exhibit good thermal properties. The high surface area of the clay platelets, their homogeneous dispersion in the epoxy matrix, and the strong interfacial bond are reported to reduce the mobility of the polymer chains leading to longer relaxation time and hence enhanced T_g. While some researchers reported an increase in T_g on adding clay to the epoxy, others have reported a decrease in T_g, attributed to the interference of the clay with the crosslink density. T_g of the epoxy/CNF nanocomposites also increases with increasing CNF content is due to the segments of the polymer chain which are close to the nanofiller surface should have hindered mobility leading to an increased T_g. Epoxy/CNT nanocomposites exhibited lower T_g is due to the stiffness of CNT. Cellulose nanofibers with better dispersion in the matrix inhibit the polymer movement and increase the T_g of the epoxy resin. While adding spherical nanoparticles into the epoxy resin, sometimes it increases the thermal properties and some researchers reported a decrease in thermal properties. The MWCNT buckypaper increases the fire resistance of the epoxy significantly.

Acknowledgments

The authors are grateful to Ms. R. Sindu, Mrs. D. Brinda devi, Mr. K. Lakshmanan, and Mr. A. Karunanidhi research scholars for their help in the preparation of the manuscript.

References

1 Shin, P.-S., Wang, Z.-J., Kwon, D.-J. et al. (2015). Optimum mixing ratio of epoxy for glass fibre reinforced composites with high therma stability. *Composites Part B: Engineering* 79: 132–137.
2 Kandare, E., Kandola, B.K., and Myler, P. (2013). Evaluating the influence of varied fire-retardant surface coatings on post-heaat flexural properties of glass/epoxy composites. *Fire Saftey Journal* 58: 112–120.
3 Kandola, B.K., Horrocks, R.A., Myler, P., and Blair, D. (2003). New developments in flame retardancy of glass-reinforced epoxy composites. *Journal of Applied Polymer Science* 88: 2511–2521.
4 Katsoulis, C., Kandola, B.K., Myler, P., and Kandare, E. (2012). Post-fire flexural performance of epoxy-nanocomposite matrix glass fibre composites containing conventional flame retardants. *Composites Part A: Applied Science and Manufacturing* 43: 1389–1399.
5 Jayakumari, L.S., Thulasiraman, V., and Sarojadevi, M. (2008). Synthesis and characterization of bis(4-cyanato-3,5-dimethylphenyl) naphthyl methane/epoxy/glass fibre composites. *Polymer Composites* 29: 709–716.

6 Thulasiraman, V., Rakesh, S., and Sarojadevi, M. (2008). Synthesis and characterization of chlorinated soy oil based epoxy resin/glass fiber composites. *Polymer Composites* 30: 49–58.

7 Raymond, M.-P. and Bui, V.T. (1998). Epoxy/castor oil graft interpenetrating polymer networks. *Journal of Applied Polymer Science* 70: 1649–1659.

8 Azwa, Z.N. and Yousif, B.F. (2013). Characteristics of kenaf fibre/epoxy composites subjected to thermal degradation. *Polymer Degradation and Stability* 98: 2752–2759.

9 Rosa, I.M.D., Santulli, C., and Sarasini, F. (2010). Mechanical and thermal characterization of epoxy composites reinforced with random and quasi-unidirectional untreated *Phormium tenax* leaf fibers. *Materials and Design* 31: 2397–2405.

10 Braga, R.A. and Magalhaes, P.A.A. Jr., (2015). Analysis of the mechanical and thermal properties of jute and glass fiber as reinforcement epoxy hybrid composites. *Materials Science and Engineering C* 56: 269–273.

11 Meenakshi, C.M. and Krishnamoorthy, A. (2019). Study on the effect of surface modification on the mechanical and thermal behaviour of flax, sisal and glass fiber-reinforced epoxy hybrid composites. *Journal of Renewable Materials* 7: 153–169.

12 Saba, N., Alothman, O.Y., Almutairi, Z., and Jawaid, M. (2019). Magnesium hydroxide reinforced kenaf fibers/epoxy hybrid composites: mechanical and thermomechanical properties. *Construction and Building Materials* 201: 138–148.

13 Li, X., Zhang, K., Shi, R. et al. (2017). Enhanced flame-retardant properties of cellulose fibers by incorporation of acid-resistant magnesium-oxide microcapsules. *Carbohydrate Polymers* 176: 246–256.

14 Zaman, I., Nor, F.M., Manshoor, B. et al. (2015). Influence of interface on epoxy/clay nanocomposites: 2. Mechanical and thermal dynamic properties. *Procedia Manufacturing* 2: 23–27.

15 Chen, B., Li, J., Li, X. et al. (2017). Achieving high thermal and mechanical properties of epoxy nanocomposites via incorporation of dopamine interfaced clay. *Polymer Composites* 39: E2407–E2414.

16 Salam, H., Dong, Y., Davies, I.J., and Pramanik, A. (2016). The effects of material formulation and manufacturing process on mechanical and thermal properties of epoxy/clay nanocomposites. *The International Journal of Advanced Manufacturing Technology* 87: 1999–2012.

17 Hussain, M., Varley, R.J., Mathys, Z. et al. (2004). Effect of organo-phosphorus and nano-clay materials on the thermal and fire performance of epoxy resins. *Journal of Applied Polymer Science* 91: 1233–1253.

18 Jiankun, L., Yucai, K., Zongneng, Q., and Xiao-Su, Y.J. (2001). Study on intercalation and exfoliation behavior of organoclays in epoxy resin. *Journal of Polymer Science Part B: Polymer Physics* 39: 115.

19 Zabihi, O., MojtabaAhmadi, H.K., and Naebe, M. (2016). Fish DNA-modified clays: towards highly flame retardant polymer nanocomposite with improved interfacial and mechanical performance. *Scientific Reports* 6: 1–17. https://doi.org/10.1038/srep38194.

20 Zhou, Y., Pervin, F., Vijaya, K., and Rangari, J.S. (2006). Fabrication and evaluation of carbon nano fiber filled carbon/epoxy composite. *Materials Science and Engineering A* 426: 221–228.

21 Tao, K., Yang, S., Grunlan, J.C. et al. (2006). Effects of carbon nanotube fillers on the curing processes of epoxy resin-based composites. *Journal of Applied Polymer Science* 102: 5248–5254.

22 Saba, S.A., Sanyang, M.L., Mohammad, F. et al. (2017). Thermal and dynamic mechanical properties of cellulose nanofibers reinforced epoxy composites. *International Journal of Biological Macromolecules* 102: 822–828.

23 Zhu, J., Wei, S., Ryu, J. et al. (2010). Magnetic epoxy resin nanocomposites reinforced with core–shell structured Fe@FeO nanoparticles: fabrication and property analysis. *ACS Applied Materials & Interfaces* 2: 2100–2107.

24 Gu, H., Guo, J., He, Q. et al. (2013). Flame-retardant epoxy resin nanocomposites reinforced with polyaniline-stabilized silica nanoparticles. *Industrial & Engineering Chemistry Research* 52: 7718–7728.

25 Gérard, C., Fontaine, G., and Bourbigot, S. (2011). Synergistic and antagonistic effects in flame retardancy of an intumescent epoxy resin. *Polymers for Advanced Technologies* 22: 1085–1090.

26 Ma, H., Fang, Z., and Tong, L. (2006). Preferential melt intercalation of clay in ABS/brominated epoxy resine antimony oxide (BEReAO) nanocomposites and its synergistic effect on thermal degradation and combustion behavior. *Polymer Degradation and Stability* 91: 1972–1979.

27 Peighambardoust, S.J., Rikhtegar, H., Pakdel, P.M., and Mirmohseni, A. (2019). Electrically conductive epoxy-based nanocomposite adhesives loaded with silver-coated copper and silver-coated reduced graphene oxide nanoparticles. *Polymers for Advanced Technologies* 30: 1996–2004.

28 Huang, Z.Q., Jiang, S.D., Hong, N.N. et al. (2017). Synthesis of highly active HM-SiO_2@CeO_2/NiO hybrids for fire safety applications of epoxy resins. *Composites Part A: Applied Science and Manufacturing* 95: 337–345.

29 Farhadinejad, Z., Ehsani, M., Moemenbellah, S. et al. (2012). An investigation of thermal, physical, and electrical properties and morphological behavior on nanoepoxy composite insulation. *IEEE Transactions on Nanotechnology* 11: 957–963.

30 Senthil Kumar, S.M.S., Raju, M.-S.N., Sampath, P.S., and Selvan, C.-P.M. (2018). Influence of nanoclay on mechanical and thermal properties of glass fiber reinforced polymer nanocomposites. *Polymer Composites* 39 (6): 1862–1868.

31 Ashori, A., Ghiyasi, M., and Fallah, A. (2019). Glass fiber-reinforced epoxy composite with surface modified graphene oxide:enhancement of interlaminar fracture toughness and thermo mechanical performance. *Polymer Bulletin* 76: 259–270.

32 Mahato, K.K., Dutta, K., and Ray, B.C. (2019). Assessment of mechanical, thermal and morphological behavior of nano-Al_2O_3 embedded glass fiber/epoxy composites at in-situ elevated temperatures. *Composites Part B: Engineering* 166: 688–700.

33 Inam, F., Wong, D.W.S., Kuwata, M., and Peijs, T. (2010). Multiscale hybridmicro-nanocomposites based on carbon nanotubes and carbon fibers. *Journal of Nanomaterials* 2010: 1, 453420–12, 12 pages doi:https://doi.org/10.1155/2010/453420.

34 Wu, Q., Zhu, W., Zhang, C. et al. (2010). Study of fire retardant behavior of carbon nanotube membranes and carbon nanofiber paper in carbon fiber reinforced epoxy composites. *Carbon* 48: 1799–1806.

35 Schartel, B., Bartholmai, M., and Knoll, U. (2005). Some comments on the use of cone calorimter data. *Polymer Degradation and Stability* 88: 540–547.

36 Lopez-Cuesta, J.M. (2009). New prospects in flame retardant polymer material: from fundamental to nanocomposites. *Materials Science and Engineering* 63: 100–125.

8

Spectroscopy and X-ray Scattering Studies of Epoxy Composites

P. Poornima Vijayan

Sree Narayana College for Women (Affiliated to University of Kerala), Department of Chemistry, College Junction, Kollam, 691001, Kerala, India

8.1 Introduction

The demand for epoxy-based composites in aerospace, automobile, construction, electronics, energy, and coating industries leads the material scientists to focus on advanced epoxy composites to satisfy variety of needs [1]. Fiber-reinforced epoxy composites are popular lightweight structural material in aircrafts and automobiles [2]. Also, huge and complicated structures from fiber-reinforced epoxy composites are used in wind turbine blade structure [3]. Carbon fiber (CF), glass fiber, aramid fibers, and natural fibers are commonly used to reinforce the epoxy matrix. Both surface-treated and untreated fibers are employed for this purpose. In the last two decades, nanocomposites have been developed to overcome the compromised performance of epoxy and fiber-reinforced epoxy composites [4–6]. Both nanocomposites of epoxy and fiber-reinforced epoxy were reported for the pending requirements for future aircraft, automobile designs as well as for coating, adhesive applications. The most successful nanofillers in epoxy matrix include layered clay, various inorganic nanoparticles, carbon nanotubes (CNTs), and graphene derivatives.

The structural integrity and performance of epoxy composites depend on various factors such as cure parameters, fiber/matrix interfacial strength, nature of nanofiller and microfillers, filler dispersion methods, etc. Primarily, precise monitoring and control of the cure reaction are needed to fabricate high-quality composite materials for specific application. The cure reaction between epoxy resin and curing agent determines the resulting cross-link structure. The cure reaction could be well controlled by chemical nature of curing agent, temperature, time, heating rate, presence of additives and fillers, etc. Thermal analysis (differential scanning calorimetry [DSC]) is the practiced industry-standard method for evaluating the cure process in epoxy resins [7]. Thermal analysis of cure process is a labor-intensive method. Spectroscopic techniques, such as Fourier transform infrared (FTIR) and Raman, provide best confirmatory support for DSC. These spectroscopic techniques have the advantage over the thermal analysis that in situ

Epoxy Composites: Fabrication, Characterization and Applications,
First Edition. Edited by Jyotishkumar Parameswaranpillai, Harikrishnan Pulikkalparambil, Sanjay M. Rangappa, and Suchart Siengchin.

monitoring of cure process is possible. These non-invasive and non-destructive methods offer real-time information about the cure reaction [7].

The evaluation of fiber–matrix interaction, nano- or microfiller–matrix interaction, and the role of nanofillers in strengthening fiber–matrix interaction in epoxy composites is of great importance in designing structural materials. The chemical interactions established at the interface between surface-treated fibers or filler and the epoxy polymer have been explored using spectroscopic techniques [8, 9]. It is also important to evaluate the morphological feature of epoxy composite materials to evaluate their fitness for a specific application. The morphological feature involves dispersion state of the filler, the orientation of fibers or CNTs, the exfoliation of layer structured fillers (such as nanoclay, graphene derivatives), the localization of filler along fiber/matrix interface, and many more. Here, for these purpose, both spectroscopic and X-ray scattering techniques have been proved as suitable tools [10, 11]. Apart from evaluating the cure state and morphological features, these techniques are also used to study the stress transmission and moisture uptake through the composite matrix.

Advanced options in IR spectroscopy such as FTIR-attenuated total reflection (FTIR-ATR), two-dimensional (2D) IR spectroscopy, etc. have been used by many researchers to carryout studies on epoxy composites. ATR sampling technique requires no sample preparation stage to acquire the infrared spectra [12]. Hence, it is a suitable probing tool for diffusion of water into the polymer interface [13]. Further, the ability of 2D IR spectroscopy to probe the temperature-dependent and time-dependent spectral changes could be effectively used to follow cure reaction and water diffusion in epoxy [14]. Technical details and application of spectroscopic techniques and X-ray scattering for the in-depth analysis of epoxy composites are discussed in the current chapter.

8.2 In situ Cure Monitoring

Monitoring of chemical changes during processing of epoxy composites would be helpful for proper designing of the final product. Real-time FTIR has been used to monitor the cure reactions and to predict the mechanism of epoxy in the presence of different curing agents and catalysts [15]. It has been useful in validating the reaction kinetics in epoxy cure process [16]. During the reaction between the epoxy and curing agent, the epoxy rings open up to form a three-dimensional network. The quantitative evaluation of consumption of epoxide rings or functional group present in the curing agent could be done with FTIR spectroscopy. The cure reaction in epoxy resin can be followed through changes in bands associated with epoxide, hydroxyl, ether, and amine groups. The formation of cross-linked epoxy network using different curing agents such as amine, anhydride, carboxylic acid, and phenol could be successfully monitored. While all these reactions result in disappearance of epoxide band, depending on the curing agent and cure conditions, appearance of new band for ester group, hydroxyl group, and ether groups is detected in the IR spectrum. Reaction of epoxy with primary amine, secondary amine, anhydride, and homopolymerization

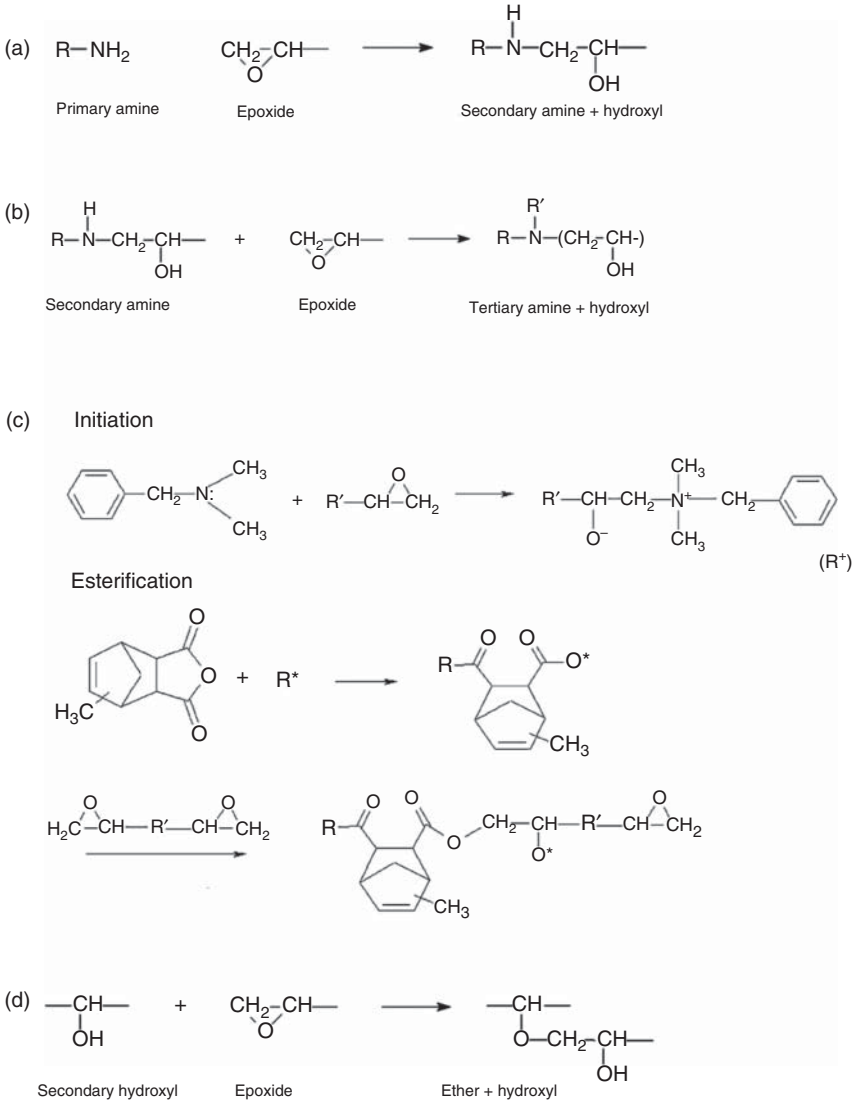

Scheme 8.1 Reactions of epoxy with (a) primary amine, (b) secondary amine, (c) anhydride, and (d) etherification reaction.

is shown in Scheme 8.1. Primary amine open ups epoxide ring to form secondary amine; further, this secondary amine open ups another epoxide ring to form tertiary amine (Scheme 8.1a,b). For the reaction of epoxy with anhydride, the reaction is initiated by tertiary amine catalyst. The obtained quaternary ammonium (R^*) starts to react with the anhydride to continue the cross-linking reaction (Scheme 8.1c). The formed hydroxyl groups during above-described cure reactions may react with epoxide ring to form ether linkages which is shown in Scheme 8.1d. Apart from direct epoxy-curing agent reaction, the chance of homopolymerization via

Table 8.1 The IR bands corresponding to groups under goes changes during cure reaction of epoxy.

Sl. No.	Bands (cm^{-1}) approximate	Assignation	Characteristics	References
1	915	Stretching C–O of oxirane group	Consumed during cure reaction	[15]
2	3056	Stretching of C–H of the oxirane ring	Consumed during cure reaction	[17]
3	1638	–OH bend	Appeared during cure reaction	[17]
4	3427	–OH Stretch	Appeared during cure reaction	[17]
5	1072	Stretching C–O–C of ethers	Appeared if homo-polymerization happens	[15]
6	5056	$–NH_2$ combination band (stretching and bending vibrations)	Consumption of primary amine curing agent during reaction	[18]
7	1858 and 1779	C=O stretch of anhydride	Consumed during cure reaction	[19]
8	1774	Ester carbonyl	New band appeared as a result of epoxy/anhydride reaction	[19]
9	1510	C–C stretching of aromatic ring	No change during cure reaction and is used as a reference peak	[15]
10	1190	C–O aromatic ring stretching	No change during cure reaction and is used as a reference peak	[15]

The band values may vary with chemical nature of epoxy resin, amine, and anhydride used.

etherification reaction adversely affects the cross-link density. The IR bands which are significant in monitoring the epoxy cure reaction are tabulated in Table 8.1. The bands given in table is for epoxy resin cured with amine or anhydride curing agent.

There are bands, which remain unchanged during cure reaction are taken as the quantitative reference. For example, band at 1510 cm^{-1} corresponding to C–C stretch in aromatic ring, which is not participating in cure reaction, is a taken as a reference band. The cure conversion can be calculated by normalizing the epoxy bands (or bands from curing agents) with reference bands according to Eq. (8.1). The normalizing process cancels out background and instrument noise, including shifts in the spectral baseline over time.

$$\alpha = 1 - \frac{(A_{et})(A_{r0})}{(A_{rt})(A_{e0})} \tag{8.1}$$

where α is the epoxy conversion, A_{r0} is the area under reference peak at cure time = 0, A_{rt} represents the area under reference peak at cure time t, A_{e0} represents the area

under the epoxy peak at cure time = 0, and A_{et} represents the area under the epoxy peak at cure time t.

In epoxy amine, a much studied system due to its extensive use, the chance of homopolymerization has been studied with FTIR spectroscopy. The nature of amine curing agent predicts the type of cross-linking reactions. While the chance of homopolymerization is less with aliphatic diamine, the use of aromatic diamine as a curing agent leads to etherification reaction due to less reactivity and high temperature required for the reaction [20, 21]. For instance, Riccardi and Williams [22] reported that a significant etherification reaction was evident in the reaction of diglycidylether of bisphenol A (DGEBA)-type epoxy resin with 4,4′-diamino diphenyl sulfone (DDS) below 150 °C. FTIR is also useful in studying the effect of solvent on epoxy curing process. Hong and Wu [23] studied the role of different solvents on the cure reaction of epoxy with dicyandiamide (DICY). The change in intensities of bands near 2210 cm^{-1} (cyano group from DICY), 915 cm^{-1} (epoxide), 1650 cm^{-1} (imino group formed by the intermolecular addition of hydroxyl to the DICY cyano functionality), and 1750 and 1690 cm^{-1} (carbonyls formed by the structural rearrangement of the imino esters) was mainly used to evaluate the curing kinetics and the mechanism of cure in the presence of different solvents. Figure 8.1 shows the FTIR spectra of cured epoxy/DICY system with acetone, tetrahydrofuran (THF), and toluene as solvents. The system with toluene left with highest content of unreacted epoxide and DICY functional groups as reflected from highest intensity of bands at 915 and 2180 cm^{-1}. The band at 2180 cm^{-1} was due to the shifting of the band at 2210 cm^{-1} as a result of the formation of alkylated DICY. The different amounts of functional groups formed in different solvent systems as indicated by changes in band intensities concluded a solvent-affected curing mechanism in the epoxy–DICY system.

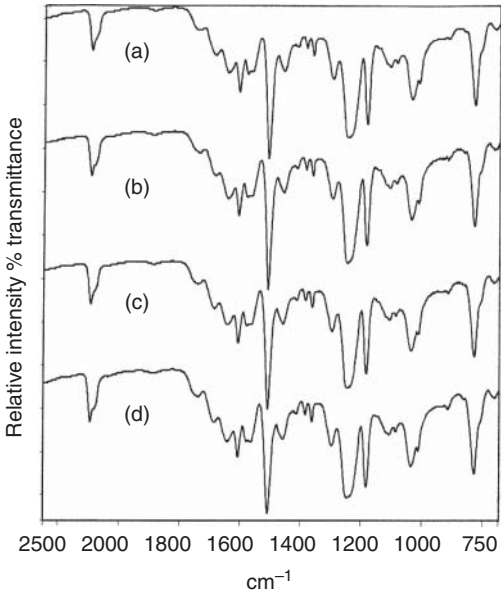

Figure 8.1 The representative FTIR spectra obtained from the specimens epoxy/DCIY system (a) without solvent, (b) with acetone, (c) with THF, and (d) with toluene after 150 °C cure. Source: Hong et al. [23]. © 1998, Elsevier.

The cure reaction in epoxy with various curing agents can be analyzed quantitatively and in real time by FTIR spectroscopy. The role of various micro- and nanofillers on the curing process has been explored.

The cure kinetics of DGEBA-type epoxy and nadic methyl anhydride were studied by Poornima Vijayan et al. [19]. The spectral changes associated with cure reaction between DGEBA and nadic methyl anhydride at 100 °C are given in Figure 8.2. The reported spectral transitions are the decrease of epoxy band at 913 cm^{-1} and anhydride carbonyl bands at 1858 and 1779 cm^{-1} with the formation of a new ester carbonyl band at 1774 cm^{-1}. This epoxy/anhydride matrix was modified with nanoclay and microphase-separated liquid rubber so as to increase both the toughness

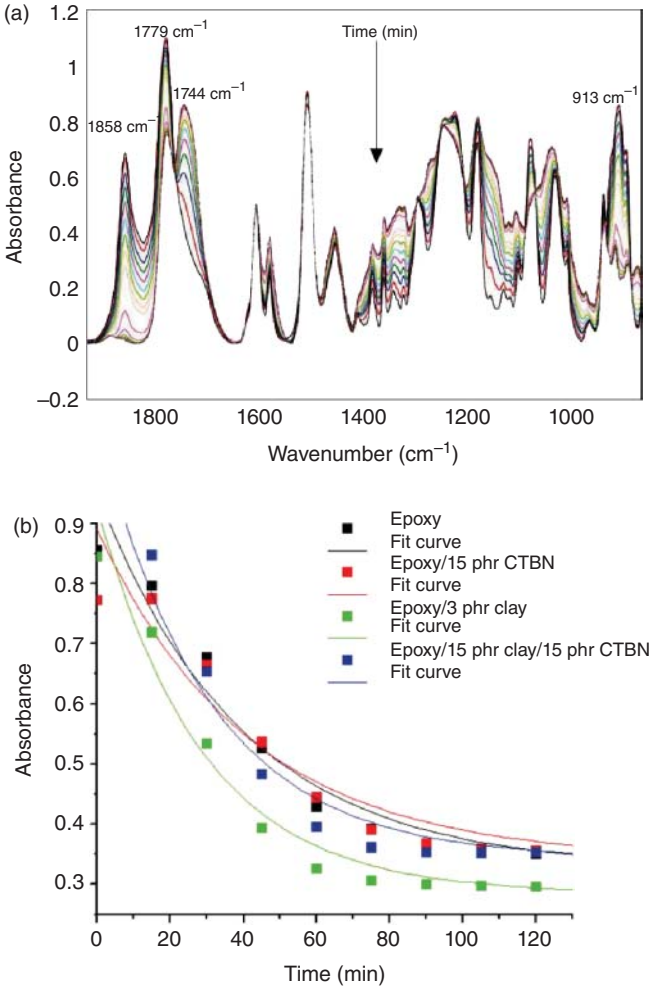

Figure 8.2 (a) FTIR spectral changes for the epoxy/anhydride cure at 100 °C and (b) exponential decay behavior of epoxy band in epoxy, epoxy/15 phr CTBN, epoxy/3 phr clay, and epoxy/3 phr clay/15 phr CTBN systems. Source: Pionteck et al. [19]. © 2015, Elsevier.

and thermal properties of the final product. FTIR was successfully used to evaluate the role of these modifiers on the cure process and cross-linking density. The consumption of epoxy band at 913 cm^{-1} with cure time for epoxy and modified epoxies was simulated with Maxwell's equation (Eq. (8.2))

$$y = y_o + A_1 \exp(-x/t_1) \tag{8.2}$$

where A_1 is the magnifier and t_1 is the cure time. From the obtained t_1 values, the role of fillers on cure process was predicted. While the nanoclay accelerated the epoxy/anhydride cure reaction with lower t_1, the phase-separated microparticle of liquid rubber retarded the cure process with higher t_1 value. The epoxy anhydride system simultaneously modified with nanoclay and liquid rubber, the decay time is lower than that of unmodified epoxy but higher than that of nanoclay-modified system. The spectral observations confirms that the effect of nanoclay dominates in the cure reaction; however, in the late stage of cure, the micro-sized liquid rubber particles retardes the cure reaction.

UV-initiated cure reactions which proceed within a fraction of a second were successfully followed using FTIR spectroscopy [24]. Various epoxy composites have been investigated for the role of filler in UV-initiated curing process by real-time FTIR. In general, the consumption of epoxide group as a function of irradiation time has been used to find out the extent of the reaction. The conversion curves can be calculated from the normalized absorbance of the epoxy. Martin-Gallego et al. [25] studied the role of graphene on UV-curing process of epoxy. The kinetics of photopolymerization of bis-cycloaliphatic diepoxy resin 3,4-epoxycyclohexylmethyl 3′,4′-epoxycyclohexyl carboxylate (CE) with triphenylsulfonium hexafluoroantimonate as a photoinitiator and functionalized graphene sheets (FGSs) as a reinforcing filler was studied in real time. Figure 8.3a shows FTIR spectra for both pristine and 1.5 wt% FGS filled epoxy. Here, the band centered around 750 cm^{-1} due to the presence of epoxide group was decreased as a function of photo-irradiation time, and from this, the conversion curves were drawn. The conversion curves were calculated from the normalized absorbance of the epoxy by the carbonyl band. The conversion curves for epoxy with various contents of FGS obtained from real time Fourier transform infrared spectroscopy (RT-FTIR) are shown in Figure 8.3b, where the slope of curves represents the rate of polymerization (R_p) and the plateau value represents the final epoxy group conversion. It was found that the UV-shielding effect of graphene sheets decreased both polymerization rate and final cure conversion.

Parallel to FTIR, Raman spectroscopy has also been used to monitor the cure process in epoxy. Merad et al. [7] studied the cure reaction in DGEBA-type epoxy and DDS using Raman spectroscopy. The consumption of peak corresponding to epoxide vibration at 1275 cm^{-1} has been used to evaluate the cure rate. Figure 8.4 shows the reduction in epoxide peak as a function of time in Raman spectra obtained at 135 °C. The peak at 1275 cm^{-1} was normalized with peak corresponding to the phenyl ring (internal reference) at 1160 cm^{-1}. The percentage of reticulation was calculated according to Eq. (8.3)

$$\%\text{reticulation} = 100\frac{I^0_{1275} - I^t_{1275}}{I^0_{1275}} \tag{8.3}$$

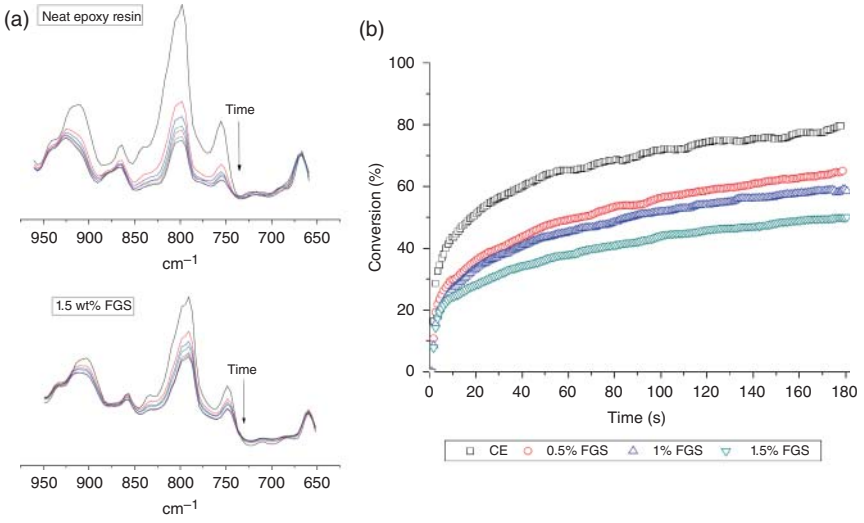

Figure 8.3 (a) FTIR spectra in the region between 950 and 650 cm^{-1} for the neat epoxy and the formulation containing 1.5% FGS. (b) Real-time FTIR conversion curves as a function of irradiation time for the pristine epoxy resin (CE) and for the epoxy resin formulations containing 0.5 wt% FGS, 1 wt% FGS, and 1.5 wt% FGS. Source: Martin-Gallego et al. [25]. © 2011, Elsevier.

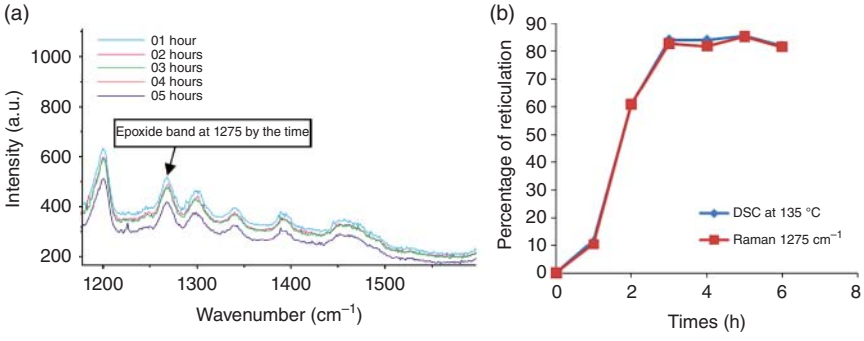

Figure 8.4 (a) Raman spectra as function of time; (b) comparison between percentage of reticulation obtained from Raman and DSC for DGEBA/DDS mixture at 135 °C. Source: Merad et al. [7]. © 2009, Elsevier.

where I^0_{1275} is the normalized intensity of the 1275 cm^{-1} peak at cure time $t = 0$ and I^t_{1275} is the normalized intensity of the same peak at cure time t.

The percentage of reticulation vs. time measured from DSC using heat of reaction (ΔH) and that measured by Raman using normalized intensity of epoxide vibration peak showed a close correlation. Figure 8.4b shows a comparison between the percentage of reticulation calculated from Raman and DSC for DGEBA/DDS mixture at 135 °C.

Depending on the type of epoxy and curing agent used, the peak for epoxide vibration slightly varies. Hardis et al. [3] find out the degree of cure (α) between

DGEBA-type epoxy and a modified aliphatic amine, where the epoxide peak appeared at 1255 cm^{-1}, using the following equation.

$$\alpha(t) = 1 - \frac{I_{1255}(t)/I_{ref}(t)}{I_{1255}(0)/I_{ref}(0)} \tag{8.4}$$

where $I_{1255}(t)$ and $I_{1255}(0)$ correspond to the intensity of peak at 1255 cm^{-1} at time t and $t = 0$, respectively; $I_{ref}(t)$ and $I_{ref}(0)$ correspond to the intensity of reference peak at time t and $t = 0$, respectively. Here, the peak at 1609 cm^{-1}, corresponding to stretching of phenyl ring, was taken as the reference. Thus, the calculated degree of cure showed a good agreement with that calculated from heat of reaction obtained using DSC.

8.3 Characterization of Interface in Fiber-Reinforced Epoxy Composites

Raman spectroscopy has been recognized as a powerful technique to probe the vibrational modes and the structure in popular carbonaceous fillers such as carbon fibers (CFs), CNT, graphene, and graphene oxides. In addition to the main G band (around 1580 cm^{-1}) in first-order Raman scattering from a graphite crystal, carbonaceous materials in general (and carbon fibers in particular) present a D band at lower wavelength (around 1350 cm^{-1}) which is associated with structural disorder [26–28]. Width and position of both of these bands and D to G band intensity ratio (I_D/I_G) are the generally used parameters to quantify the degree of disorder in carbonaceous materials [9, 28, 29]. An increase in I_D/I_G represents a higher degree of disorder in the fiber surface. In addition to these two main bands, other second-order bands are also assigned (D′ and G′). The G′ (sometimes quoted as D^*) band (at around 2600 cm^{-1}) is assigned as overtone of the D band.

Raman spectroscopy was used by researchers to detect changes in structural order in carbon fibers and CNTs after various surface treatments. Montes-Morán and Young [9] studied the effect of oxygen plasma treatment on the surface structure of high-modulus (HM) carbon fibers. It was found that the plasma treatment did not affect the position and width of the main Raman bands. However, high intensity ratio of D and G for the plasma-treated carbon fibers than untreated one (Figure 8.5) indicates an increased structural disorder in the surface of treated fibers due to the presence of higher proportion of edge planes.

The chemical functionalization of CNTs was effectively characterized using Raman spectroscopy [30]. Figure 8.6 shows the changes in the intensity and width of G, D, and D^* bands upon different functionalization of multi-walled carbon nanotube (MWCNT). Unmodified MWCNT has the least I_D/I_G value showing less degree of disorder in the structure. The highest I_D/I_G value for fluorinated MWCNT (F-MWCNT) suggests that the functional groups are along the surface of the MWCNT structure inducing higher degree of disorder.

Most importantly, Raman spectroscopy has been effectively used to characterize the fiber–epoxy matrix interface [31, 32]. Load transfer depends on the interfacial shear stress (IFSS) between the fiber and the matrix. There are three mainly accepted

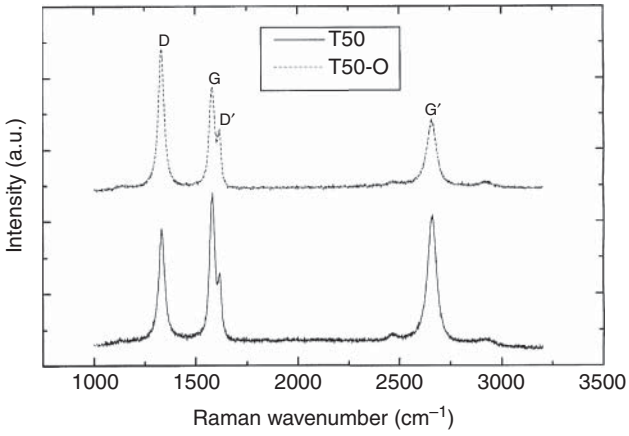

Figure 8.5 Raman spectra, untreated (T50), and plasma-treated (T50-O) carbon fibers. Source: Montes-Morán et al. [9]. © 2002, Elsevier.

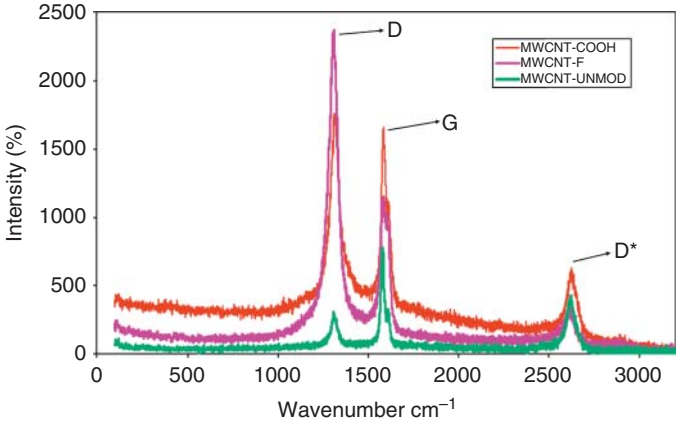

Figure 8.6 Raman spectroscopy image of unmodified and functionalized MWCNTs. Source: Theodore et al. [30]. © 2011, Elsevier.

mechanisms of load transfer from a matrix to fiber [32, 33]. They are micromechanical interlocking, the chemical bonding between the fiber and the matrix and weak van der Waals bonding between the fiber and the matrix. Researchers used Raman spectroscopy to study the process of load transfer in carbonaceous fiber-reinforced epoxy composites.

Graphite fibers are deformed; vibrational frequencies of some of the normal modes change to cause Raman peak shift [34]. This phenomenon of strain-induced Raman band shifts is the basis of mapping of stress transfer from the matrix to the fibers during fragmentation. The G′ band of graphite fiber shifts with uniaxial strain or hydrostatic compression. G′ band moves toward lower wavenumbers when the fiber is in tension and shift to higher wavenumber while in compression [35, 36]. Figure 8.7a shows the shift in G′ ($\sim$2660 cm^{-1}) Raman band peak under tensile strain along with significant broadening of peaks. There is linear relationship

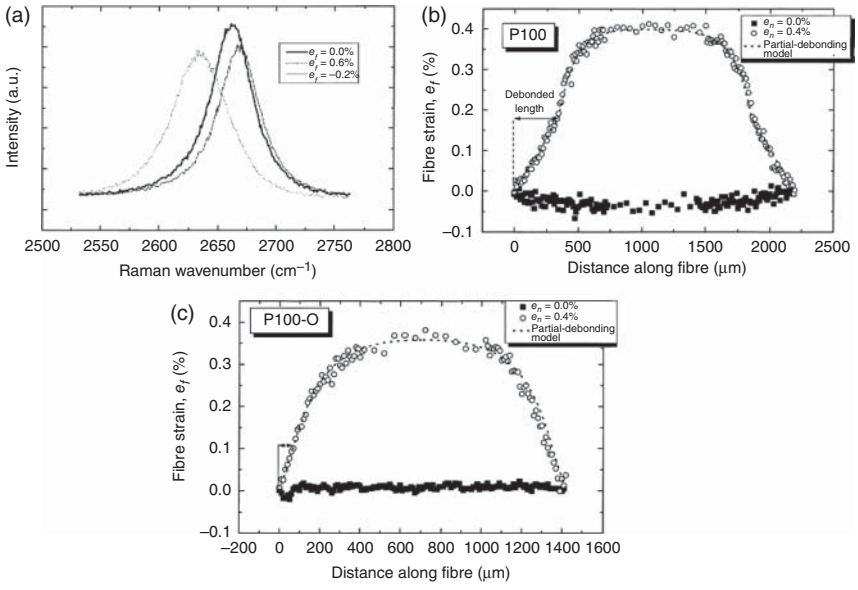

Figure 8.7 (a) Shift of the G′ (~2660 cm^{-1}) band under tensile strain for P100 carbon fiber. Fiber strain distributions determined from strain-induced Raman band shifts at 0.4% of matrix strain of (b) an untreated P100 fiber–epoxy composite; (c) a plasma-treated P100-O fiber–epoxy composite. Source: Montes-Morán et al. [36]. © 2002, Elsevier.

between the peak shift and the applied strain. The slope corresponding to the linear fit of Raman band shift vs. strain graph is commonly known as strain calibration factor (SCF) of the fiber. Using these values of the SCF, the G′ band positions are converted into axial fiber strain. Montes-Morán and Young [36] studied the interfacial properties of oxygen plasma-treated carbon fibers–epoxy composite. The strain distribution curve (Figure 8.7b,c), showed that the oxygen plasma-treated carbon–carbon filament (P100-O) is almost perfectly bonded at matrix deformation $e_m = 0.4\%$. However, in the untreated carbon fiber composite (P100) (Figure 8.7b) at the same level of matrix deformation, debonding of the interface along a 350 μm distance from both fiber ends is evident. This results reflected the improved interface quality of plasma-treated carbon fiber–epoxy matrix as evident from their high IFSS.

Epoxy/CNT composites come under the category of fiber-reinforced composites within which the fibers are oriented randomly. Hence, different from carbon fiber-reinforced polymer composites, it is important to consider Raman band shift rate (per unit strain) for a fiber not parallel to the deformation axis (off-axis loading) and for a fiber not parallel to the axis of laser polarization. Also, Raman band shift needs to be related to the stress on the nanotubes [37]. MWCNT-reinforced epoxy cured with triethylene tetraamine was subjected to load transfer test in both tension and compression mode using Raman peak shift [33]. Figure 8.8 shows the shift in the Raman peak (second-order peak – G′ at 2700 cm^{-1}) both in compression and tension mode. It was reported that the large shift in compression compared to tension was due more strain carried by the nanotubes in compression than in tension. According to Ajayan and coworkers, during the load transfer to MWCNT,

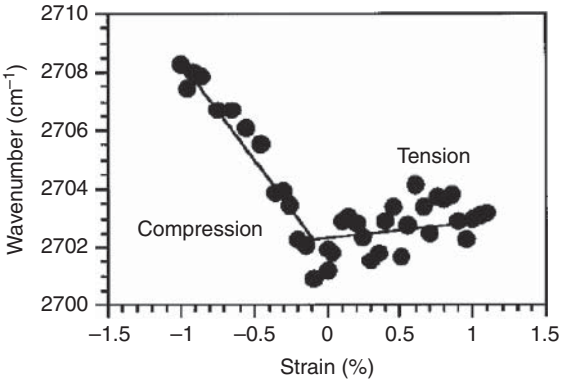

Figure 8.8 Nanotube Raman peak shift as a function of applied strain showing the large shift in the Raman peak ~second order peak at 2700 cm^{-1} in compression compared to tensile loading. Source: Schadler et al. [33]. © 1998, AIP Publishing.

only the outer layers were stressed in tension, whereas all the layers responded in compression.

Later, the low-frequency part of the Raman spectra was used to study the strain effects on the intensity of the radial breathing modes (RBMs) in epoxy/MWCNT composites [38, 39]. RBM bands in CNT directly give the core nanotube diameter values. Lucas and Young [39] reported that the RBM intensity values depend on strain and the nanotube structure and large intensity variations were observed due to variation in the nanotube structure.

8.4 Determination of Residual Stress Developed During Cure

The processing of thermosetting resin is always accompanied by volume shrinkage which produce undesirable residual stresses in the cured material [19, 40]. During cure of the thermosetting resins, the volumetric shrinkage occurs from two different sources: chemical shrinkage and thermal shrinkage. Chemical shrinkage accounts for volume decrease due to cross-linking reaction. At the same time, thermal shrinkage accounts for thermal expansion and contraction accompanied by initial ramp to the cure temperature and cool down to room temperature after cure completion, respectively. When compared with other thermosets, epoxy has the advantage of low shrinkage during cure (4–6%) [41]. Still, this small percentage of shrinkage produces significant residual stress which leads to early product failure. Raman spectroscopy has been effectively used to trace out the residual stress in epoxy composites filled with CNT by virtue of sensitivity of G′ band of CNT to the pressure exerted by different liquid and viscous media [42, 43]. The micro- and nanoscale sensing ability of CNTs enable the detection of the development of residual stresses during epoxy cure [44]. de la Vega et al. [44] carried out a detailed study on stress build up during cure reaction in epoxy/single-walled carbon nanotube (SWCNT) composites using Raman spectroscopy in combination with dielectric spectroscopy. They investigated the effect of chemical nature of cross-link, the viscosity of the resin, and the cure schedule on the developed residual stress in epoxy/SWCNT composites. Figure 8.9. shows the Raman and dielectric in situ curing experiment for two hot

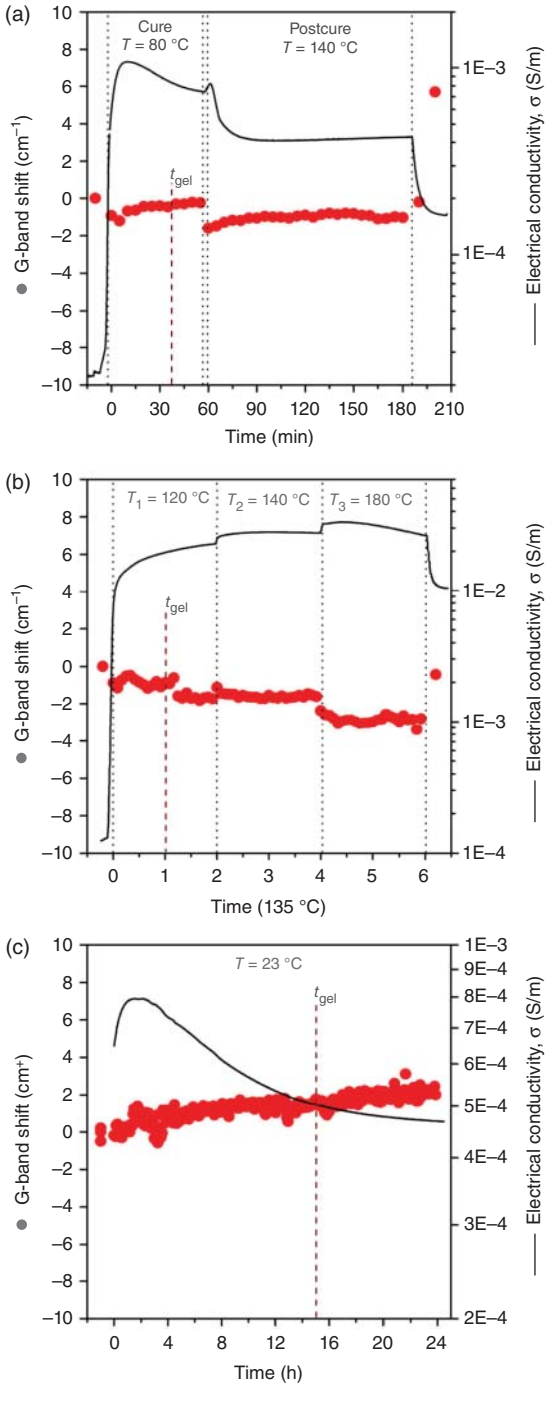

Figure 8.9 Raman and impedance in situ curing experiment for (a) the low viscous epoxy/cyclo aliphatic amine system, (b) the epoxy/aromatic amine system, and (c) the epoxy/linear aliphatic amine system, each with 0.2 wt% SWCNT filler concentration. The time regions before the first isotherm and after the second (a) or third (b) isotherm show the band positions at room temperature before and after the curing cycle, respectively. Source: de la Vega et al. [44]. © 2009, Elsevier.

cure epoxy–amine systems and a room-temperature cure epoxy–amine system containing 0.2 wt% of SWCNT. For a hot cure epoxy–cyclo aliphatic amine system without post curing (Figure 8.9a), upon increasing the temperature during cure cycle, a band shift of ~6 cm^{-1} is recorded at the end of the curing period. This observation was an indication of absence of chemical shrinkage or at least undetectable with Raman spectroscopy. Different from this observation, for a hot cure epoxy–aromatic amine system undergone post curing (Figure 8.9b), there is no significant difference in band shift values between these two cure stages due to the post cure treatment as an annealing effect to relief internal stresses and a lower stress transfer efficiency of a weaker interface between aromatic polymeric cross-link and nanotubes. In order to investigate the contribution of chemical shrinkage toward residual stresses independently of thermal shrinkage, they compare the in situ Raman shift during cure reaction of hot cure epoxy resins with a room-temperature cure epoxy resin (epoxy/linear aliphatic amine system). Raman shift of ~2 cm^{-1} at the end of the curing period for the room-temperature cure epoxy resin is negligible when compared with that of hot cure epoxy system (~6 cm^{-1}). This observation rules out the contribution of

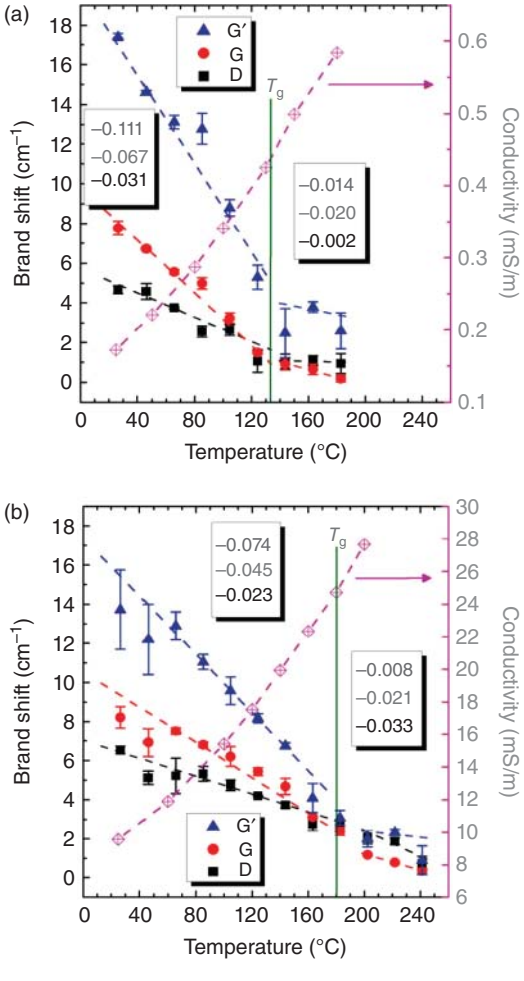

Figure 8.10 Temperature dependence of the Raman bands of (a) the low viscous epoxy/cycloaliphatic amine system, (b) the epoxy/aromatic amine system filled with 0.2 wt% SWCNT. The inset display the slopes (in cm^{-1} K^{-1}) of this dependence below (left inset) and above (right inset) T_g. The laser intensity was kept constant at 1%. Source: de la Vega et al. [44]. © 2009, Elsevier.

chemical shrinkage toward the overall residual stress state of the epoxy/SWCNT composites, which is mostly thermal-induced stress.

The hot-cured epoxy/SWCNT composites were re-heated stepwise, and the band shift with respect to temperature has been studied. Figure 8.10 represents the variation band shift and conductivity with temperature for the two cured epoxy systems. The slope change at T_g indicated a "stress releasing" effect above T_g arises from the free mobility of the molecular chains. However, the electrical conductivity recorded using dielectric spectroscopy showed no such deflection indicating the less affected CNT network by the buildup of residual stresses. The higher Raman shift rate was reported for low viscous epoxy than for the high viscous epoxy due to the high interfacial strength in low viscous epoxy/SWCNT composite.

8.5 Stress Transmission Studies in Particulate Filled Epoxy Composite

When a stress is applied to a particulate-filled epoxy composite, the stress is transmitted to the particles through epoxy matrix. Due to this stress, the crystal lattice of the particles get strained and it appears as a shift in diffraction angle 2θ in X-ray diffraction pattern [45]. The crystal strain (ε) can be calculated using Eq. (8.5)

$$\varepsilon = \frac{\Delta d}{d_o} \tag{8.5}$$

where d_o is the initial lattice spacing of the particle crystal, d is the change in the lattice spacing induced by the applied stress. Thus, calculated strain in the crystal, the stress (σ_f) subjected to particles can be calculated using Eq. (8.6)

$$\sigma_f = E\varepsilon \tag{8.6}$$

where E is the elastic modulus of the crystal lattice for a specific plane. Elastic modulus for all planes can be calculated from the experimental values of the elastic stiffness constants [46, 47].

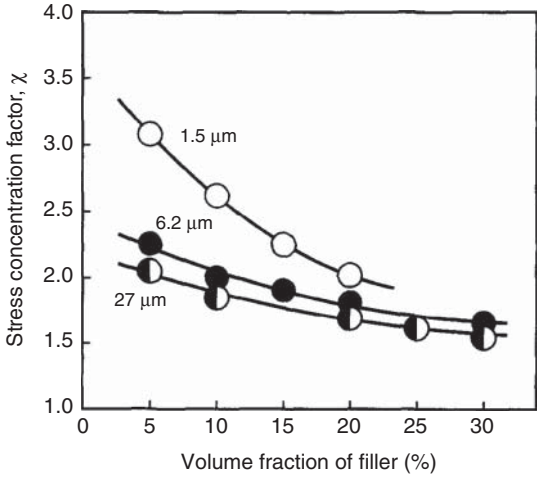

Figure 8.11 Relationship between the stress concentration factor χ and the volume fraction of filler for silica particulate epoxy composites. Source: Xu et al. [45]. © 1992, Elsevier.

Stress transmission studies in different particle-filled epoxy composites were reported using X-ray diffraction technique [45, 48]. The stress transmission in silica-filled epoxy composites showed that the stress on particles was several times larger than the applied stress [45]. This indicates that the stress concentrated on silica particles facilitates expected mechanical reinforcement of the composite. Also, the ratio of stress to the applied stress (χ) was found to decrease with the size of the filler and on the other hand increased with filler content as shown in Figure 8.11.

8.6 Water Diffusion Studies

The water diffusion through epoxy is a serious concern over several decades as it causes the deterioration of excellent performance of epoxy-based materials used in various industries [49, 50]. FTIR is useful to probe the diffusion of water through the epoxy matrix in terms of changes of frequency, intensity, and shapes of bands corresponding to water. The three IR bands used for this purpose are the normal vibrational modes ν_a(OH·) (antisymmetric) and ν_s(OH) (symmetric), bands and the bending band, δ(HOH) in isolated water molecule. Upon diffusion into solid polymer matrix, the vibrational bands ν_a(OH·) and ν_s(OH) gradually shift to lower frequencies, while the δ(HOH) band shifts to higher frequency [51]. The different states of water inside epoxy network such as bound and free water, water clustering, orientation, and networking could be confirmed from FTIR band shifts and band splitting. Cotugno et al. [52] investigated the water diffusion through tetraglycidyl 4,4′-diamino diphenylmethane (TGDDM) type epoxy film cured with 4,4′-diamino diphenyl sulfone by using in situ FTIR spectroscopy. The spectroscopic region between 3800 and 2800 cm^{-1}, where the fundamental stretching vibration of the water molecule is located, has been examined in detail. Figure 8.12 represents the spectra of sorbed water as a function of sorption time. By using curve resolving algorithm, the individual peak in this unresolved multicomponent band was

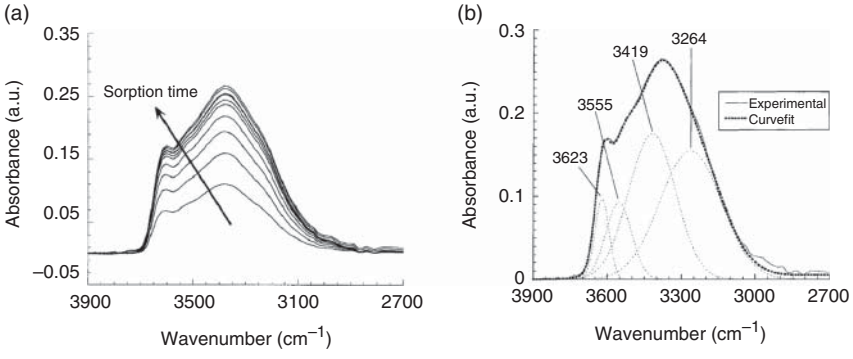

Figure 8.12 (a) Subtraction FTIR spectra collected at different sorption time in TGDDM thin film cured with DDS and (b) curve fitting analysis of subtraction spectra corresponding to water absorbed at equilibrium, displays four resolved components, the simulated profile and the experimental line shape. Source: Cotugno et al. [52]. © 2001, Elsevier.

separated and four resolved peaks are shown in Figure 8.3b. The four resolved peaks correspond to unassociated water (3623 cm^{-1}), weakly hydrogen-bonded water (3555 cm^{-1}), and strongly hydrogen-bonded water molecules (3419 and 3264 cm^{-1}). The unassociated water confined into free volume (microvoids), at the same time weakly hydrogen-bonded water, was molecularly dispersed (bulk dissolved). The third one is firmly bound to specific sites in the epoxy network via strong hydrogen bonding. These less mobile bound water sometime exists as clusters, and their plasticizing efficiency is very high resulting in poor mechanical performance [53, 54].

FTIR-ATR has been used for water diffusion studies in polymer matrix in order to get saturation artifacts free spectra [55]. Liu et al. study the nature of water in novolac epoxy resins cured with phenol novolac resin (epoxy [EP]) and phenol novolac acetate resin (EPA) by using 2D ATR-FTIR spectroscopy [14, 56]. It was found that the amount of bound water depends on the nature of polymer network as it is more in EP than that in EPA. They proposed the sequential steps in water diffusion, initially, the water molecules bind with specific hydrophilic groups in the epoxy network and thereafter diffuse into free volume (microvoids) or molecularly dispersed with less hydrogen bonding (bulk dissolved).

The effect of saline solutions in carbon–epoxy composite was studied using both Raman and universal attenuated total reflectance (UATR)/FTIR spectroscopy [57]. Raman and FTIR spectra of carbon–epoxy composites submitted to saline vapor at various time intervals were examined. Raman spectra during saline vapor exposure at different temperatures showed a decrease of the relative intensity of the bands at 1610 and 1511 cm^{-1} (associated with aromatic rings) due to the enhanced conformational freedom of the polymeric chains due to the plasticization effect. Increase in temperature promoted the moisture absorption in the carbon–epoxy composite. In the FTIR spectrum, the bands associated with hydroxyl and carbonyl groups showed an increase in half-width due to hydrogen bonds established with bound water.

8.7 Morphological Analysis in Epoxy Composites

Morphological characterization of epoxy composites with layer structured fillers is usually done with X-ray diffraction (XRD). The state of dispersion, i.e. exfoliation/intercalation of layered structures such as graphite [58], graphene [59], graphene oxide [60], and nanoclay [61], could be explored well with the help of XRD patterns. Both wide-angle X-ray scattering (WAXS) and small-angle X-ray scattering (SAXS) techniques were used to find the basal spacing of these layered nanostructures in epoxy composites.

XRD is a well-established technique to study the state of dispersion of organically montmorillonite clay nanoplatelets in the polymeric matrix. XRD patterns help to get an idea of whether the clay layers intercalate or exfoliate upon interaction with polymer [62, 63]. The pristine clay is usually modified with suitable long-chain alkyl moiety to make them compatible with polymeric matrix. For instance, Ha et al. [64] modified the pristine clay with 3-amonopropyltriethoxysilane, which increases the d-spacing between the clay layers by about 8.0 Å (Figure 8.13a). The basal spacing

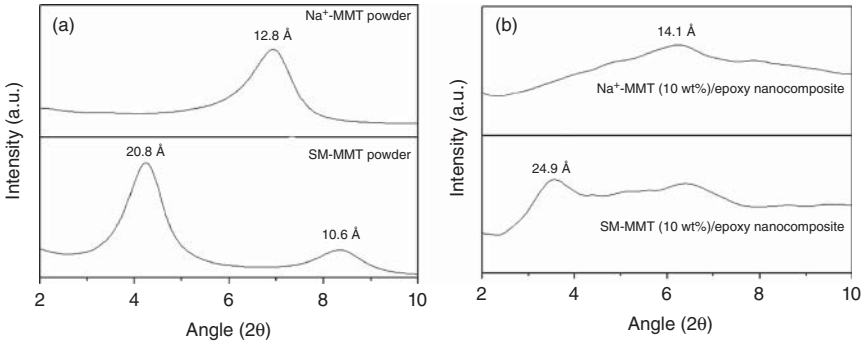

Figure 8.13 X-ray diffraction patterns of the (a) pristine clay (Na^+-MMT) and surface-modified clay (surface-modified clay [SM-MMT]) powders, (b) epoxy/Na^+-MMT and epoxy/SM-MMT composites with 10 wt% clay concentration. Source: Ha et al. [64]. © 2007, Elsevier.

of organically modified clay layers further get expanded in the epoxy matrix due to the penetration of epoxy chains into the clay galleries. A higher "d" spacing of clay layers in epoxy/clay nanocomposites than organoclay was recorded for a intercalated clay layers (Figure 8.13a,b). At the same time, the characteristic diffraction peaks were absent in epoxy/clay nanocomposite with exfoliated clay layers. The role of processing technique, curing agent, processing parameters, etc. on the exfoliation/intercalation of clay layers was studied by different scientists [61, 65].

It was reported that the telechelic liquid rubbers such as carboxyl terminated butadiene-acrylonitrile copolymer (CTBN) and hydroxyl-terminated polybutadiene (HTPB) could directly exfoliate organoclays as their low molecular weight polymeric chains easily penetrate into clay layers [66]. Poornima Vijayan et al. [67, 68] studied the preferential interpenetration of telechelic liquid rubbers into clay galleries than epoxy chains in epoxy/CTBN/clay hybrid nanocomposite with the help of XRD patterns (Figure 8.14). The [001] diffraction of the used organoclay was recorded at 2θ value of 3.64 corresponding to the basal spacing 24.5 Å. However, in epoxy/3 phr clay nanocomposite and epoxy/10 phr CTBN/3 phr clay nanocomposites, the recorded basal spacings are 35.94 and 39.57 Å, respectively. As the content of liquid rubber increased in the hybrid composite, the d spacing also increased.

Yasmin et al. [69] compared the ability of processing technique in dispersing the graphite sheets in epoxy matrix using WAXD. Figure 8.11a shows the WAXD patterns of epoxy composite with 1 wt% expanded graphite (EG) processed with different techniques. The characteristic peak of pure graphite is generally observed at 2θ value of ~26°, diffraction from (002) plane corresponding to a d spacing of 3.37 Å. In Figure 8.15a, it can be seen that the broad peak in the pattern is characteristics of epoxy and the sharp peaks at 2θ value of 26.38° are for pure graphite. This concluded that the applied processing techniques were unable to exfoliate or separate the graphite layers. The epoxy/1 wt% EG composites processed via shear mixing, sonication, and combination of shear and sonication showed less intense peak when compared with composites obtained via direct mixing. The effect of content of graphite on the dispersion state has also been explored for a fixed processing

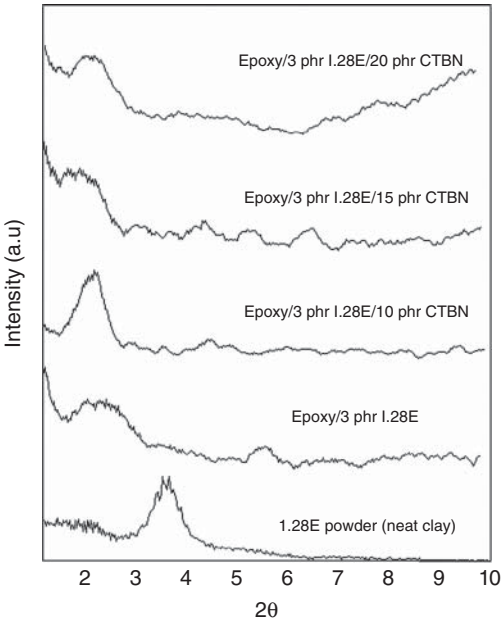

Figure 8.14 XRD plots for organically modified clay (I.28E), epoxy/3 phr I.28E nanocomposite, and epoxy/3 phr I.28E/10–20 phr CTBN ternary nanocomposites. Source: Vijayan et al. [67].

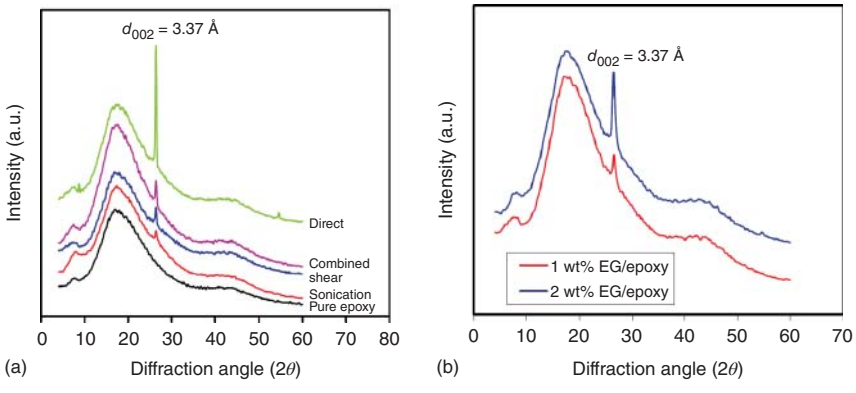

Figure 8.15 (a) WAXD patterns of epoxy/1 wt% EG nanocomposites processed by different techniques. (b) WAXD patterns of nanocomposites processed by shear mixing with varying graphite content. Source: Yasmin et al. [69]. © 2006, Elsevier.

technique. It was observed that the peak at 26.38° recorded with a higher intensity for epoxy/2 wt% EG composite than for epoxy/1 wt% EG nanocomposite (Figure 8.15b). It is due to the presence of higher number of graphite layers that exist in composites with high EG content. Wajid et al. [59] used XRD to find out the dispersion of polyvinyl pyrrolidone (PVP) stabilized graphene in the epoxy prepared via freeze dry and solution processing. XRD pattern of epoxy/graphene composites has no characteristic peak for diffraction from graphitic plane, which confirmed the exfoliation of graphene in the epoxy matrix.

8.8 Conclusion

It is important to optimize cure parameters in developing epoxy and fiber-reinforced epoxy composites for various applications. Real-time FTIR and Raman spectroscopy quantitatively collect the cure data, which are in excellent agreement with that collected from heat of reaction measured using DSC. The efficiency of spectroscopic methods in real-time monitoring of cure process in epoxy supports the future use for in-plant monitoring. Implementation plan for in-plant monitoring will be developed for real-time cure monitoring using Raman spectroscopy as a non-invasive and non-destructive method. The phenomena of strain-induced Raman band shift have been successfully used to trace out the stress transfer from matrix to fiber during fragmentation and residual stress developed during cure in epoxy/graphitic fiber composites. Both Raman spectroscopy and XRD are non-destructive techniques in measuring the residual stress and stress transfer in epoxy composites without causing any permanent damages in the product. Spectroscopic techniques are effective in monitoring the diffusion of water and predicting the diffusion mechanism. Above all, XRD has been proved as an excellent supporting technique for the morphological evaluation in epoxy composites with layered fillers. The scope of spectroscopic techniques and XRD is numerous in characterizing epoxy composites and needs to explore more.

References

1 Jin, F.-L., Li, X., and Park, S.-J. (2015). Synthesis and application of epoxy resins: a review. *Journal of Industrial and Engineering Chemistry* 29: 1–11.

2 Xu, Y. and Hoa, S.V. (2008). Mechanical properties of carbon fiber reinforced epoxy/clay nanocomposites. *Composites Science and Technology* 68 (3): 854–861.

3 Hardis, R., Jessop, J.L.P., Peters, F.E., and Kessler, M.R. (2013). Cure kinetics characterization and monitoring of an epoxy resin using DSC, Raman spectroscopy, and DEA. *Composites Part A: Applied Science and Manufacturing* 49: 100–108.

4 Hussain, M., Nakahira, A., and Niihara, K. (1996). Mechanical property improvement of carbon fiber reinforced epoxy composites by Al_2O_3 filler dispersion. *Materials Letters* 26 (3): 185–191.

5 Davis, D.C., Wilkerson, J.W., Zhu, J., and Hadjiev, V.G. (2011). A strategy for improving mechanical properties of a fiber reinforced epoxy composite using functionalized carbon nanotubes. *Composites Science and Technology* 71 (8): 1089–1097.

6 Khan, S.U., Munir, A., Hussain, R., and Kim, J.-K. (2010). Fatigue damage behaviors of carbon fiber-reinforced epoxy composites containing nanoclay. *Composites Science and Technology* 70 (14): 2077–2085.

7 Merad, L., Cochez, M., Margueron, S. et al. (2009). In-situ monitoring of the curing of epoxy resins by Raman spectroscopy. *Polymer Testing* 28 (1): 42–45.

8 Chiang, C.-.H. and Koenig, J.L. (1982). Spectroscopic characterization of the matrix–silane coupling agent interface in fiber-reinforced composites. *Journal of Polymer Science: Polymer Physics Edition* 20: 2135–2143.

9 Montes-Morán, M.A. and Young, R.J. (2002). Raman spectroscopy study of HM carbon fibres: effect of plasma treatment on the interfacial properties of single fibre/epoxy composites. *Carbon* 40 (6): 845–855.

10 Abdalla, M., Dean, D., Theodore, M. et al. (2010). Magnetically processed carbon nanotube/epoxy nanocomposites: morphology, thermal, and mechanical properties. *Polymer* 51 (7): 1614–1620.

11 Prolongo, S.G., Jiménez-Suárez, A., Moriche, R., and Ureña, A. (2014). Graphene nanoplatelets thickness and lateral size influence on the morphology and behavior of epoxy composites. *European Polymer Journal* 53: 292–301.

12 Schuttlefield, J.D. and Grassian, V.H. (2008). ATR-FTIR spectroscopy in the undergraduate chemistry laboratory. Part I: Fundamentals and examples. *Journal of Chemical Education* 85 (2): 279.

13 Murphy, D. and de Pinho, M.N. (1995). An ATR-FTIR study of water in cellulose acetate membranes prepared by phase inversion. *Journal of Membrane Science* 106 (3): 245–257.

14 . Two-dimensional (2D) ATR-FTIR spectroscopic study on water diffusion in cured epoxy resins. *Macromolecules*.

15 Smith, R.E., Larsen, F.N., and Long, C.L. (1984). Epoxy resin cure. II. FTIR analysis. *Journal of Applied Polymer Science* 29 (12): 3713–3726.

16 Heise, M.S. and Martin, G.C. (1990). Analysis of the cure kinetics of epoxy/imidazole resin systems. *Journal of Applied Polymer Science* 39: 721–738.

17 Nikolic, G., Zlatkovic, S., Cakic, M. et al. (2010). Fast Fourier transform IR characterization of epoxy GY systems crosslinked with aliphatic and cycloaliphatic EH polyamine adducts. *Sensors* 10 (1): 684–696.

18 Mijović, J., Andjelić, S., and Kenny, J.M. (1996). In situ real-time monitoring of epoxy/amine kinetics by remote near infrared spectroscopy. *Polymers for Advanced Technologies* 7 (1): 1–16.

19 Poornima Vijayan, Pionteck, J., and Thomas, S. (2015). Volume shrinkage and cure kinetics in carboxyl-terminated poly(butadiene-co-acrylonitrile) (CTBN) modified epoxy/clay nanocomposites. *Journal of Macromolecular Science Part A* 52 (5): 353–359.

20 Dušek, K., Ilavský, M., and Luňak, S. (1975). Curing of epoxy resins. I. Statistics of curing of diepoxides with diamines. *Journal of Polymer Science: Polymer Symposia* 53 (1): 29–44.

21 Luňák, S. and Dušek, K. (1975). Curing of epoxy resins. II. Curing of bisphenol a diglycidyl ether with diamines. *Journal of Polymer Science: Polymer Symposia* 53: 45–55.

22 Riccardi, C.C. and Williams, R.J.J. (1986). A kinetic scheme for an amine–epoxy reaction with simultaneous etherification. *Journal of Applied Polymer Science* 32 (2): 3445–3456.

23 Hong, S.-G. and Wu, C.-S. (1998). DSC and FTIR analysis of the curing behaviors of epoxy/DICY/solvent open systems. *Thermochimica Acta* 316 (2): 167–175.

24 Scherzer, T. and Decker, U. (1999). Real-time FTIR-ATR spectroscopy to study the kinetics of ultrafast photopolymerization reactions induced by monochromatic UV light. *Vibrational Spectroscopy* 19 (2): 385–398.

25 Martin-Gallego, M., Verdejo, R., Lopez-Manchado, M.A., and Sangermano, M. (2011). Epoxy-graphene UV-cured nanocomposites. *Polymer* 52 (21): 4664–4669.

26 Wang, Y., Alsmeyer, D.C., and McCreery, R.L. (1990). Raman spectroscopy of carbon materials: structural basis of observed spectra. *Chemistry of Materials* 2 (5): 557–563.

27 Roh, J.-S. (2008). Structural study of the activated carbon fiber using laser Raman spectroscopy. *Carbon Letters* 9 (2): 127–130.

28 Cuesta, A., Dhamelincourt, P., Laureyns, J. et al. (1994). Raman microprobe studies on carbon materials. *Carbon* 32 (8): 1523–1532.

29 Cuesta, A., Dhamelincourt, P., Laureyns, J. et al. (1998). Effect of various treatments on carbon fiber surfaces studied by Raman microprobe spectrometry. *Applied Spectroscopy* 52: 356–360.

30 Theodore, M., Hosur, M., Thomas, J., and Jeelani, S. (2011). Influence of functionalization on properties of MWCNT–epoxy nanocomposites. *Materials Science and Engineering A* 528 (3): 1192–1200.

31 Hughes, J.D.H. (1991). The carbon fibre/epoxy interface – a review. *Composites Science and Technology* 41 (1): 13–45.

32 Huang, Y. and Young, R.J. (1994). Analysis of the fragmentation test for carbon-fibre/epoxy model composites by means of Raman spectroscopy. *Composites Science and Technology* 52 (4): 505–517.

33 Schadler, L.S., Giannaris, S.C., and Ajayan, P.M. Load transfer in carbon nanotube epoxy composites. *Applied Physics Letters* 73 (26): 3842.

34 Mitra, V.K., Risen, W.M., and Baughman, R.H. (1977). A laser Raman study of the stress dependence of vibrational frequencies of a monocrystalline polydiacetylene. *The Journal of Chemical Physics* 66 (6): 2731–2736.

35 Young, R.J. (1996). Evaluation of composite interfaces using Raman spectroscopy. *Key Engineering Materials* 116–117: 173–192.

36 Montes-Morán, M.A. and Young, R.J. (2002). Raman spectroscopy study of high-modulus carbon fibres: effect of plasma-treatment on the interfacial properties of single-fibre–epoxy composites. Part II: Characterisation of the fibre–matrix interface. *Carbon* 40 (6): 857–875.

37 Cooper, C.A., Young, R.J., and Halsall, M. (2001). Investigation into the deformation of carbon nanotubes and their composites through the use of Raman spectroscopy. *Composites Part A: Applied Science and Manufacturing* 32 (3): 401–411.

38 Hadjiev, V.G., Iliev, M.N., Arepalli, S. et al. (2001). Raman scattering test of single-wall carbon nanotube composites. *Applied Physics Letters* 78 (21): 3193–3195.

39 Lucas, M. and Young, R.J. (2004). Raman spectroscopic study of the effect of strain on the radial breathing modes of carbon nanotubes in epoxy/SWNT composites. *Composites Science and Technology* 64 (15): 2297–2302.

40 Potter, K. (2012). Chapter 2 – Manufacturing defects as a cause of failure in polymer matrix composites. In: *Failure Mechanisms in Polymer Matrix Composites* (eds. P. Robinson, E. Greenhalgh and S. Pinho), 26–52. Woodhead Publishing.

41 Sangermano, M., Ortiz, R.A., Urbina, B.A.P. et al. (2008). Synthesis of an epoxy functionalized spiroorthocarbonate used as low shrinkage additive in cationic UV curing of an epoxy resin. *European Polymer Journal* 44 (4): 1046–1052.

42 Wood, J.R. and Wagner, H.D. (2000). Single-wall carbon nanotubes as molecular pressure sensors. *Applied Physics Letters* 76 (20): 2883–2885.

43 Zhao, Q., Wood, J.R., and Wagner, H.D. (2001). Stress fields around defects and fibers in a polymer using carbon nanotubes as sensors. *Applied Physics Letters* 78 (12): 1748–1750.

44 de la Vega, A., Kovacs, J.Z., Bauhofer, W., and Schulte, K. (2009). Combined Raman and dielectric spectroscopy on the curing behaviour and stress build up of carbon nanotube–epoxy composites. *Composites Science and Technology* 69 (10): 1540–1546.

45 Xu, A.-R., Nishino, T., and Nakamae, K. (1992). Stress transmission in silica particulate epoxy composite by X-ray diffraction. *Polymer* 33 (24): 5167–5172.

46 Bigg, D.M. (1976). A review of techniques for processing ultra-high modulus polymers. *Polymer Engineering & Science* 16 (11): 725–734.

47 Morgan, P.W. (1977). Synthesis and properties of aromatic and extended chain polyamides. *Macromolecules* 10 (6): 1381–1390.

48 Nakamae, K., Nishino, T., and Airu, X. (1992). Studies on mechanical properties of polymer composites by X-ray diffraction: 3. Mechanism of stress transmission in particulate epoxy composite by X-ray diffraction. *Polymer* 33 (13): 2720–2724.

49 Zhou, J. and Lucas, J.P. (1999). Hygrothermal effects of epoxy resin. Part I: The nature of water in epoxy. *Polymer* 40 (20): 5505–5512.

50 Núñez, L., Villanueva, M., Fraga, F., and Núñez, M.R. (1999). Influence of water absorption on the mechanical properties of a DGEBA ($n = 0$)/1, 2 DCH epoxy system. *Journal of Applied Polymer Science* 74: 353–358.

51 Kusanagi, H. and Yukawa, S. (1994). Fourier transform infra-red spectroscopic studies of water molecules sorbed in solid polymers. *Polymer* 35 (26): 5637–5640.

52 Cotugno, S., Larobina, D., Mensitieri, G. et al. (2001). A novel spectroscopic approach to investigate transport processes in polymers: the case of water–epoxy system. *Polymer* 42 (15): 6431–6438.

53 Musto, P., Ragosta, G., and Mascia, L. (2000). Vibrational spectroscopy evidence for the dual nature of water sorbed into epoxy resins. *Chemistry of Materials* 12 (5): 1331–1341.

54 Musto, P., Ragosta, G., Scarinzi, G., and Mascia, L. (2002). Probing the molecular interactions in the diffusion of water through epoxy and epoxy–bismaleimide networks. *Journal of Polymer Science Part B: Polymer Physics* 40 (10): 922–938.

55 Fieldson, G.T. and Barbari, T.A. (1993). The use of FTi.r.-a.t.r. spectroscopy to characterize penetrant diffusion in polymers. *Polymer* 34 (6): 1146–1153.

56 Wu, P. and Siesler, H.W. (2003). Water diffusion into epoxy resin: a 2D correlation ATR-FTIR investigation. *Chemical Physics Letters* 374 (1): 74–78.

57 Soares-Pozzi, A.C. and Dibbern-Brunelli, D. (2016). Study of the influence of saline solutions in carbon/epoxy composite by luminescence, Raman and UATR/FT-IR spectroscopy. *Journal of Materials Science* 51 (20): 9342–9355.

58 Yasmin, A. and Daniel, I.M. (2004). Mechanical and thermal properties of graphite platelet/epoxy composites. *Polymer* 45 (24): 8211–8219.

59 Wajid, A.S., Ahmed, H.S.T., Das, S. et al. (2013). High-performance pristine graphene/epoxy composites with enhanced mechanical and electrical properties. *Macromolecular Materials and Engineering* 298 (3): 339–347.

60 Abdullah, S.I. and Ansari, M.N.M. (2015). Mechanical properties of graphene oxide (GO)/epoxy composites. *HBRC Journal* 11 (2): 151–156.

61 Miyagawa, H., Drzal, L.T., and Carsello, J.A. (2006). Intercalation and exfoliation of clay nanoplatelets in epoxy-based nanocomposites: TEM and XRD observations. *Polymer Engineering & Science* 46: 452–463.

62 Ratna, D., Divekar, S., Samui, A.B. et al. (2006). Poly(ethylene oxide)/clay nanocomposite: thermomechanical properties and morphology. *Polymer* 47 (11): 4068–4074.

63 Morgan, A.B. and Gilman, J.W. (2003). Characterization of polymer-layered silicate (clay) nanocomposites by transmission electron microscopy and X-ray diffraction: a comparative study. *Journal of Applied Polymer Science* 87: 1329–1338.

64 Ha, S.R., Ryu, S.H., Park, S.J., and Rhee, K.Y. (2007). Effect of clay surface modification and concentration on the tensile performance of clay/epoxy nanocomposites. *Materials Science and Engineering A* 448 (1): 264–268.

65 Kornmann, X., Lindberg, H., and Berglund, L.A. (2001). Synthesis of epoxy–clay nanocomposites. Influence of the nature of the curing agent on structure. *Polymer* 42 (10): 4493–4499.

66 Chen, T., Zhu, J., Li, B. et al. (2005). Exfoliation of organo-clay in telechelic liquid polybutadiene rubber. *Macromolecules* 38 (9): 4030–4033.

67 Poornima Vijayan, P., Puglia, D., Kenny, J.M., and Thomas, S. (2013). Effect of organically modified nanoclay on the miscibility, rheology, morphology and properties of epoxy/carboxyl-terminated (butadiene-co-acrylonitrile) blend. *Soft Matter* 9 (10): 2899–2911.

68 Poornima Vijayan, P., Puglia, D., Maria, H.J. et al. (2013). Clay nanostructure and its localisation in an epoxy/liquid rubber blend. *RSC Advances* 3 (46): 24634–24643.

69 Yasmin, A., Luo, J.-J., and Daniel, I.M. (2006). Processing of expanded graphite reinforced polymer nanocomposites. *Composites Science and Technology* 66 (9): 1182–1189.

9

Water Absorption Studies in Epoxy Nanocomposites

Bejoy Francis

St. Berchmans College, Department of Chemistry, Changanassery 686101, India

9.1 Introduction

Epoxy resins are the most versatile among the thermosetting polymers. Since its commercialization in 1946, they are accepted as workhorse raw materials among the various thermosetting polymers. They are used as adhesives, coatings and matrices for composite materials in microelectronic industry, aerospace industry, etc. The cured resins are characterized by high chemical and corrosion resistance, good mechanical and thermal properties, low shrinkage upon cure, and flexibility in processing [1]. Despite all these characteristics, epoxy resins have low impact strength and fracture toughness. The fracture toughness can be improved by blending with elastomers or thermoplastics [2–4]. Similar to other materials, epoxy resins are also susceptible to moisture absorption, which in turn decreases their physical properties. The extent of water uptake depends on several factors like the number of hydroxyl groups, glass transition temperature, and the presence of other dispersed materials.

Nanotechnology has gained much interest in the last few decades [5]. The properties of epoxy resins are influenced by the addition of nanoparticles. Carbon nanotubes (CNTs), nanosilica, nanoclay, graphene, graphene oxide, TiO_2, etc. have been used extensively to modify epoxy resins [6–10]. Among these, the most widely used nanoparticle is clay and its modifications. Since epoxy resins are exposed to atmosphere in a large number of applications, the effect of moisture absorption on its properties is very crucial. Therefore, the research on moisture absorption behavior in epoxy resins arose much interest. The moisture absorption in epoxy resin can be affected by the type of resin used, the nanomaterial used, the conditions prevailing at the time of moisture absorption, etc.

Epoxy Composites: Fabrication, Characterization and Applications,
First Edition. Edited by Jyotishkumar Parameswaranpillai, Harikrishnan Pulikkalparambil, Sanjay M. Rangappa, and Suchart Siengchin.

9.2 Factors Affecting Water Absorption

Epoxy resins are available as viscous liquids to tack free solids. The choice of the resin depends on the end use applications. The properties of the resin depends on the functionality of the resin. The equilibrium water uptake is dependent on the polarity of the epoxy resin rather than on the free volume in the neat resin. Therefore, the water absorption in nanocomposites may also vary with the type of resin used. Becker et al. [11] observed that the water absorption at 80 °C was maximum in octadecyl ammonium ion-modified montmorillonite/trifunctional resin followed by octadecyl ammonium ion-modified montmorillonite/tetrafunctional resin and the least by octadecyl ammonium ion-modified montmorillonite/diglycidyl ether bisphenol A (DGEBA) resin. These systems were cured with diethyltoluene diamine (DETDA) isomers, containing 74–80% 2,4-isomer and 18–24% 2,6-isomer. The extent of water uptake increased as the clay content increased but always less than the neat epoxy resin in the compositions investigated (up to 10%). However, a proportional change in water uptake with nanoclay content was not observed in the systems investigated.

Diaminodiphenyl sulfone-cured tetraglycidyl diaminodiphenyl methane (TGDDM) epoxy resin showed a different behavior, where the equilibrium uptake decreased with increase in the octadecyl ammonium ion-modified montmorillonite clay (up to 15 phr content) at 23, 50, and 80 °C. Liu et al. [12] attributed this to the low water absorption of clay (2.8%) compared to epoxy resin (7.5%). The decrease in moisture absorption was also due to the tortuosity effect imparted by nanoparticles. Clay platelets are impenetrable. Therefore, water molecules have to follow a tortuous pathway. Another peculiarity of this system is the difference in maximum uptake on changing the mixing method. Water absorption was found to be lower in a high-pressure mixing technique compared to a direct mixing technique. The difference in water absorption between the two methods decreased with increase in temperature due to high diffusion coefficient at high temperatures. Due to low diffusion coefficient, saturation point is not reached at low temperature, whereas saturation point is observed at high temperature. Decrease in water absorption with the addition of nanoclay was also observed in difunctional resin by Al-Qadhi et al. [13]. The increased uptake at higher clay loading was explained due to the presence of more voids at higher clay loading. Glaskova and Aniskevich [14] found that the diffusivity decreased by 6% in clay-modified epoxy resin. This is due to the high aspect ratio of clay platelets which increased the tortuosity of the path. The increase in moisture absorption with increase in clay content was due to the growth of interphase moisture content.

The morphology of the nanocomposite varies with the type of clay used to prepare the nanocomposites. Different types of clays namely quaternary alkylamine-modified montmorillonite (KH-MT), quaternary ammonium-modified montmorillonite (cloisite) and octadecylamine (ODA)-modified montmorillonite (I30P) were used to prepare nanocomposites with diamine-cured DGEBA epoxy resin [15, 16]. Saturation was obtained in the case of KH-MT clay, whereas cloisite and I30P systems did not show saturation even after 25 days. The I30P and cloisite systems

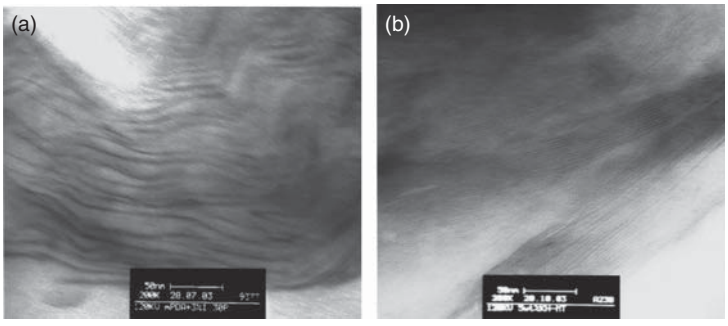

Figure 9.1 Transmission electron micrographs of nanocomposites containing (a) 5 wt% I30P and (b) 5 wt% KH-MT. Source: Hu and Kim [16].

showed better barrier properties compared to KH-MT system. The difference is due to the difference in the morphology of the nanocomposites. I30P system gave an exfoliated system with an interlayer distance of about 8 nm (Figure 9.1a), while KH-MT system gave an intercalated system with an interlayer distance of 3.3 nm (Figure 9.1b) and cloisite showed a morphology in between those of the two mentioned above. The small interlayer distance in the KH-MT system prevented the curing agent from entering the clay galleries and increased the local concentration of polar amine groups, which enhance moisture absorption [17]. In the other two systems, larger interlayer distance between the individual silicate layers resulted in better barrier properties. The moisture permeability decreased with increase in clay content due to tortuous path.

In contrast to the studies by Liu et al. [12], where equilibrium absorption was observed at high temperature in multifunctional resin, equilibrium absorption was not observed in montmorillonite (MMT) clay-modified bisphenol-A epoxy resin at 80 °C [18]. Also, the equilibrium water uptake increased with increase in clay content. The weight change with respect to temperature and clay content is shown in Figure 9.2.

According to Abacha et al. [18], the moisture absorption below T_g is assumed to occur in three stages. In the first stage, water occupies the free volume, then swelling, and in the final stage absorption in the highly cross-linked areas. The absorption showed Fickian behavior in the initial stages but deviated at a later stage and followed Langmuir path. Initially, water moves through the epoxy matrix and then it enters the clay galleries and starts to diffuse slowly. At this stage, clay platelets will absorb water and diffusion becomes slow. After complete saturation of platelets, water will diffuse further and follow a tortuous pathway. Based on the above description, the absorbed water is classified into free water and bound water.

Clay modification is an important factor in determining the extent of water absorption. But insufficient modification of clay will lead to unexpected results. Wang et al. [19] observed that the water absorption increased when a silane-modified clay was added to epoxy resin. According to them, insufficient amount of silane rendered the clay hydrophilic. As a consequence, the water absorption increased.

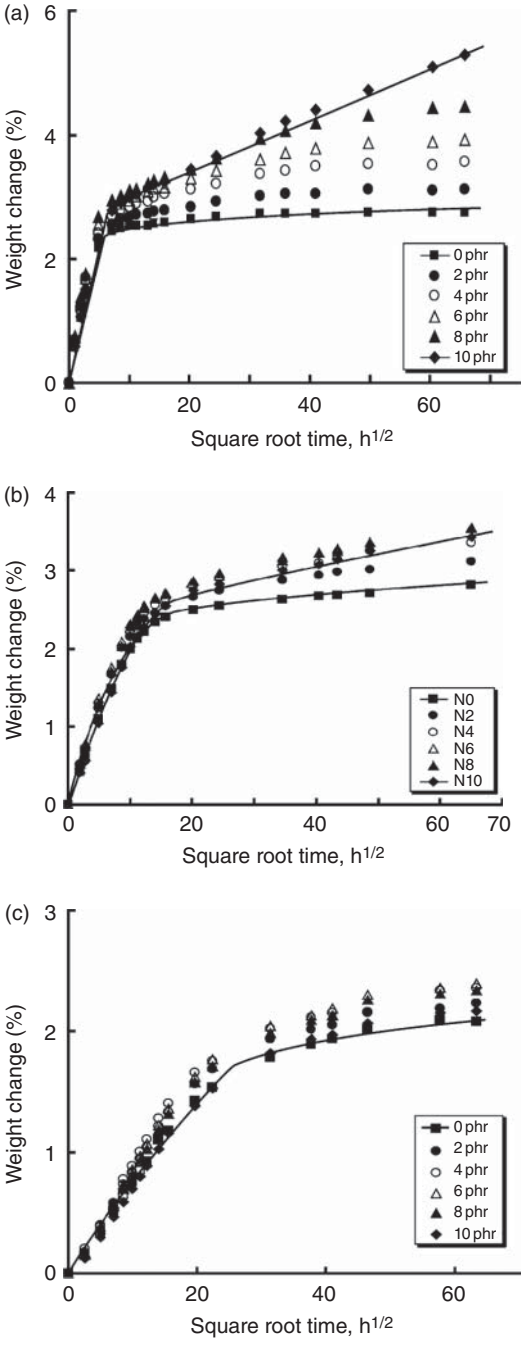

Figure 9.2 Weight change of epoxy organoclay nanocomposite in deionized water at (a) 80 °C, (b) 60 °C, and (c) 40 °C. Source: Abacha et al. [18]. © 2009, John Wiley & Sons.

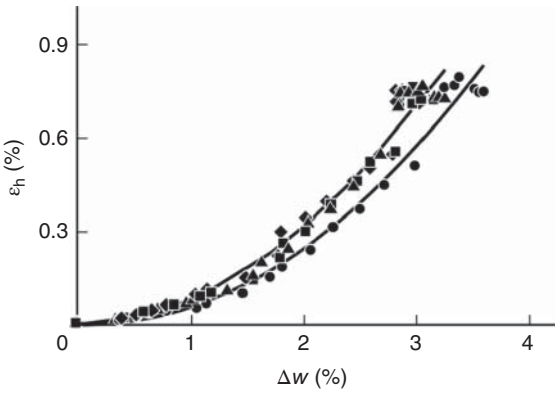

Figure 9.3 Swelling strain ε_h of NC specimen's vs. w at $\mu = 0$ (♦), 2 (■), 4 (▲), and 6 wt% (●). Source: Aniskevich et al. [21]. © 2011, Springer Nature.

Madhup et al. [20] used a mixture of (approximately 80 : 20 by weight) of sepiolite and smectite (hectorite, montmorillonite) to prepare nanocomposite with aliphatic amine-cured DGEBA epoxy resin. The improvement in the water vapor barrier properties is due to the platy and acicular shape and filling of spatial gaps due to particular shape and size of the mixed nanoparticles used.

Moisture absorption of epoxy resin as well as nanocomposites is followed by swelling. The swelling characteristics are represented in Figure 9.3 [21]. The swelling strain increased with moisture absorption, and for 2% and 4% nanocomposites, the strain is due to swelling of the epoxy matrix. The swelling strain in the nanocomposite with maximum clay loading (6%) was less than that of the neat resin, indicating that some water molecules are present in the layer bordering the filler particles or occurs in free volume.

Nanoparticles other than clay also influenced the water absorption in epoxy resin. It was found that multiwalled carbon nanotube (MWCNT) can act as an efficient barrier toward water absorption [7]. MWCNT and the oxidized and silanized multiwall carbon nanotubes (MWNTs) were used to prepare nanocomposite with DGEBA resin cured with polyamidoamine [22]. Saturation point was observed in all the systems unlike some clay/epoxy nanocomposites. The sea water absorption characteristics of the modified and unmodified nanomaterials showed similar absorption characteristics.

Prolongo et al. [23] found that MWNT and carbon nanofibers were efficient in decreasing the water absorption in diaminodiphenyl methane (DDM)-cured epoxy resin. Significant decrease (20–30%) in diffusion coefficient was observed in both cases. CNT was more efficient than nanofibers due to the strong chemical interaction between epoxy resin and amine functionality on CNT. In addition to this, the hydrophobic nature of carbon nanomaterials also contributed to the reduction in moisture absorption.

Addition of MWCNT caused a twofold decrease in diffusivity in amine-cured DGEBA epoxy resin. However, the equilibrium water uptake was similar to that of neat resin. Starkova et al. [24] explained this type of behavior by classifying water into two types Type I and II based on the interaction with the resin. The nanoparticles acted as a barrier and reduced the intermolecular movements of epoxy near

them resulting in a decrease in diffusivity, i.e. reduced Type I water associated with free volume. But with the addition of nanoparticles, new polar groups were created in the epoxy matrix. These polar groups will form H-bonds with water molecules. This increased the Type II water in the nanocomposite. Thus, the equilibrium water uptake in the nanocomposites became similar to that of neat resin.

Various carbon nanoparticles like CNTs, graphene nanoplatelets (GNPs), and single-walled carbon nanohorns (CNHs) reduced the water absorption of DGEBA epoxy resin due to a tortuous path as a result of nanoparticle addition. Epoxy GNP system showed the lowest value of diffusion coefficient [25].

Khoramishad and Alizadeh [26] compared the efficiency of MWCNT and silicon carbide (SiC) as modifier for triethylene tetra amine (TETA)-cured epoxy resin. Both the particles decreased the maximum uptake of water. The extent of decrease was different during the initial stages and saturation point, and due to the geometry difference between the nanoparticles, MWCNT has slightly better barrier properties than SiC. The diffusion coefficient decreased with the addition of nanoparticles. 58.4% decrease was observed at 0.5 wt% addition of MWCNT and 56.9% decrease was observed at 3 wt% SiC. However, due to the presence of bubbles, diffusion coefficient increased above 3 wt% SiC content.

Starkova et al. [8] compared the efficiency of thermally reduced graphene oxide (TRGO) and MWCNT in reducing the water absorption in epoxy resin. Although both the particles have good interfacial bonding and dispersion in epoxy resin, TRGO was more efficient in reducing water absorption than MWCNT. TRGO nanoparticles reduced the free volume content by hindering intermolecular movements in epoxy resulting in lower water absorption.

In an isophorone diamine-cured general purpose epoxy resin, organoclay platelets (cloisite 30B), halloysite nanotubes (HNTs), and nanosilicon carbide (n-SiC) particles reduced the water absorption and diffusion coefficient compared to the neat epoxy resin [27]. The characteristic properties are given in Table 9.1. The high aspect ratio nanofillers created a tortuous pathway for water molecules to diffuse into the composites. Among the various nanofillers used, SiC nanoparticles were found to be the most effective with a reduction of 33.3% water uptake. The extent of reduction increased with increase in nanoparticle loading in all the systems investigated.

Starkova et al. [28] reported the effect of carbon nanoparticles like MWCNTs, GnP, expanded graphite platelets, and carbon black on the water absorption in epoxy resin. The nanoparticles decreased the diffusion coefficient by 8–20%, but the equilibrium water uptake was higher in nanocomposites. This is due to the creation of voids and additional polar groups in epoxy resin, which favored water absorption.

Although nanoalumina reduced the water absorption in epoxy resin, it is not as effective as nanoclay due to its ineffectiveness to introduce tortuous paths [29]. In another study by Siegel and coworkers [9] on the addition of nano-TiO_2 in DGEBA epoxy cured with 1,3-phenylenediamine (MPDA), the extent of water absorption was less but the permeability was more than that of micron-sized particle. Here, also the nano-TiO_2 failed to produce a highly tortuous path.

Graphene nanoparticles absorbed water slowly than the cycloaliphatic resin cured with anhydride. The equilibrium water absorption was similar in both neat resin and nanocomposites [30]. When GNPs were used as a modifier in epoxy resin, the

Table 9.1 Maximum water uptake and diffusion coefficient (*D*) of epoxy-based nanocomposites filled with nanoclay, HNT, and n-SiC particles.

Sample	Maximum water uptake (%)	Diffusion coefficients (*D*) (10^{-7} mm^2/s)
Epoxy	2.34	11.75
Epoxy/nanoclay (1%)	2.01	9.98
Epoxy/nanoclay (3%)	1.92	10.1
Epoxy/nanoclay (5%)	1.76	8.23
Epoxy/HNT (1%)	2.09	10.87
Epoxy/HNT (3%)	1.90	8.47
Epoxy/HNT (5%)	1.87	8.03
Epoxy/SiC (1%)	1.83	11.35
Epoxy/SiC (3%)	1.67	13.84
Epoxy/SiC (5%)	1.56	7.48

Source: Alamri and Low [27]. © 2012, Elsevier.

geometry of the nanoplatelets played a crucial role in determining the barrier properties [31]. Graphene with different thicknesses was used to modify epoxy resin. The diffusion coefficient was lower than that of neat epoxy resin for all the systems investigated and remained very close to each other among the various GNP-modified systems. In general, the equilibrium water uptake decreased with the addition of graphene. However, the graphene with highest aspect ratio and specific area showed more equilibrium water uptake because of the phenomenon of weaving. Due to weaving, the effective surface area decreased and the interphase became weak and helped water molecules to diffuse through the system.

Voo et al. [10] studied the effect of boron nitride (BN), synthetic diamond (SD), and silicon nitride (Si_3N_4) on water absorption in epoxy resins. The nanocomposites were resistant to moisture uptake. The diffusivity and permeability of epoxy thin film filled with nanofillers were also found to be lower compared with the neat epoxy. In general, the hydrophobic nature of the nanofillers was responsible for the decrease in water absorption and the extent to which each particle changed the moisture absorption depends on the size and nature of the filler. The moisture absorption in cycloaliphatic resin and diglycidyl ether of bisphenol F (DGEBF) resins decreased with the inclusion of silica nanoparticles due to the increased surface contact between filler and epoxy resins [32]. Also, the diffusion coefficient became small with the addition of nanoparticles because the nanoparticles acted as obstacles for the diffusion of water molecules.

9.3 Effect of Water Absorption on Mechanical Properties

The extent of water absorption varied with the type of nanoparticle used. The absorbed water causes plasticization of the matrix. Hence, a change in mechanical properties is expected. The extent of variation depends on the property investigated.

The tensile strength and modulus decreased with moisture absorption in epoxy resin, but the addition of nanoclay lowered the deterioration in properties. The decrease in properties is due to moisture absorption and agglomeration of nanoparticles especially at high concentration [13]. The tensile strength of amine-modified clay/DGEBA epoxy resin decreased with water absorption [19]. The moisture will diffuse through the interface between clay and epoxy resin. This will destroy the interface and deteriorate the properties since the mechanical properties depend on the interfacial strength. The strain at break for the nanocomposites is lower than that of neat epoxy. Although it was lower than neat epoxy, the values increased initially with water absorption and then decreased around saturation. The absorbed water molecules formed clusters, and they acted as stress concentrators. The tensile modulus and fracture energy were not much affected by water absorption, although the nanocomposite absorbed more water than neat epoxy. This is because these properties are dominated by the polymer framework structure and the reinforcement and are not affected by plasticization. Kim and Kim [33] found that addition of nanoclay to epoxy resin prevented moisture absorption to the bulk epoxy and interface between epoxy adhesive and adherend steel and helped to prevent interfacial failure. In ODA-modified MMT-based organoclay, water absorption reduced the mechanical properties of epoxy resin [34]. Moisture absorption reduced tensile strength two times and one-third reduction in modulus. The decrease in properties is due to the absorption of moisture by the epoxy resin in the interplatelet region. The moisture in this region plasticized the composite.

Alamri and Low [27] investigated the flexural properties of amine-cured epoxy resin modified with various nanoparticles. The flexural strength increased with the addition of nanoparticles. Water absorption tends to decrease the flexural strength at all compositions, but the strength is always higher than the neat resin. The flexural modulus was not much affected by water absorption. The data are given in Table 9.2. The improvement in interfacial bonding resulted in high surface area of interaction and good stress transfer between matrix and filler. The flexural modulus of water absorbed nanocomposites was higher than that of neat epoxy but decreased with water absorption due to the plasticization of epoxy matrix by absorbed water. Nanoclay-modified epoxy showed the maximum decrease among the various nanoparticles. The fracture toughness and impact strength increased with water absorption (Table 9.3). This is due to the plasticization of the matrix, which will enhance the ductility of the epoxy chains.

The mechanical properties, tensile and fracture properties, were deteriorated by seawater absorption in MWCNT and modified MWCNT nanocomposites [22]. This is due to the weakening of interfacial bonding due to swelling of the matrix. NaCl in seawater may cause rapid degradation. The changes are due to debonding as a result of volume expansion between MWCNT and the epoxy matrix.

Khoramishad and Alizadeh [26] studied the effect of MWCNT and SiC on the mechanical properties of epoxy resin under various aging conditions. They observed that the degradation due to moisture absorption in neat epoxy resin was reduced by the addition of nanoparticles. MWCNT was found to be more effective in reducing the degradation than SiC because the tensile properties of aged samples at higher loading were low for SiC nanocomposites. The maximum improvement in

Table 9.2 Flexural strength and modulus of epoxy and its nanocomposites before and after water treatment.

Samples	Before placing in water		After placing in water	
	Flexural strength (MPa)	Flexural modulus (GPa)	Flexural strength (MPa)	Flexural modulus (GPa)
Epoxy	58.5 ± 2.6	0.9 ± 0.1	51.4 ± 3.1	0.7 ± 0.2
+1% nanoclay	85.2 ± 2.5	1.6 ± 0.4	52.6 ± 4.3	1.3 ± 0.2
+3% nanoclay	58.7 ± 3.9	1.5 ± 0.1	52.7 ± 4.3	1.3 ± 0.2
+5% nanoclay	61.2 ± 3.5	1.4 ± 0.2	53.0 ± 3.9	1.3 ± 0.2
+1% HNT	70.7 ± 6.2	1.5 ± 0.2	55.8 ± 6.5	1.4 ± 0.2
+3% HNT	68.2 ± 8.1	1.3 ± 0.1	52.5 ± 4.9	1.3 ± 0.2
+5% HNT	64.5 ± 4.7	1.4 ± 0.1	53.1 ± 3.5	1.4 ± 0.2
+1% n-SiC	71.1 ± 3.2	1.6 ± 0.3	59.8 ± 4.3	1.4 ± 0.3
+3% n-SiC	66.3 ± 2.9	1.4 ± 0.2	56.5 ± 5.8	1.3 ± 0.3
+5% n-SiC	61.9 ± 3.2	1.4 ± 0.1	54.5 ± 3.4	1.4 ± 0.3

Source: Alamri and Low [27]. © 2012, Elsevier.

Table 9.3 Fracture toughness and impact strength of epoxy and its nanocomposites before and after water treatment.

Samples	Before placing in water		After placing in water	
	Fracture toughness ($MPam^{1/2}$)	Impact strength (kJ/m^2)	Fracture toughness ($MPam^{1/2}$)	Impact strength (kJ/m^2)
Epoxy	0.9 ± 0.1	5.6 ± 0.7	1.3 ± 0.2	6.2 ± 1.4
+1% nanoclay	1.1 ± 0.1	6.1 ± 1.3	1.4 ± 0.3	7.4 ± 1.5
+3% nanoclay	0.9 ± 0.2	6.9 ± 1.4	1.4 ± 0.2	6.6 ± 1.5
+5% nanoclay	1.0 ± 0.2	7.8 ± 2.7	1.3 ± 0.3	7.3 ± 1.7
+1% HNT	1.3 ± 0.1	5.6 ± 1.1	1.7 ± 0.2	6.5 ± 1.8
+3% HNT	1.0 ± 0.1	6.4 ± 0.7	1.6 ± 0.5	6.3 ± 1.8
+5% HNT	1.2 ± 0.1	7.0 ± 0.9	1.3 ± 0.3	6.2 ± 1.5
+1% n-SiC	1.6 ± 0.3	7.5 ± 1.1	2.2 ± 0.3	9.1 ± 1.8
+3% n-SiC	1.2 ± 0.2	7.0 ± 0.8	2.1 ± 0.3	7.9 ± 2.2
+5% n-SiC	1.1 ± 0.1	7.6 ± 1.2	1.9 ± 0.3	8.2 ± 1.4

Source: Alamri and Low [27]. © 2012, Elsevier.

strength of the wet epoxy/MWCNT nanocomposites aged until saturation compared to the neat epoxy was 31.8%, while this was 16% for the epoxy/SiC nanocomposites (Figure 9.4). The elastic modulus decreased with moisture absorption, and the nanoparticles decreased the reduction in stiffness like tensile strength. This might be due to the less water absorption on addition of these nanoparticles.

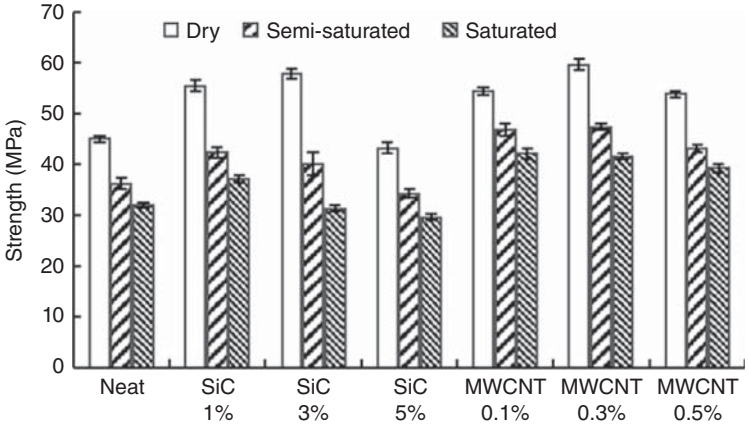

Figure 9.4 Comparison between the tensile strengths of the neat epoxy and nanocomposite samples at different moisture content conditions. Source: Khoramishad and Alizadeh [26]. © 2018, John Wiley & Sons.

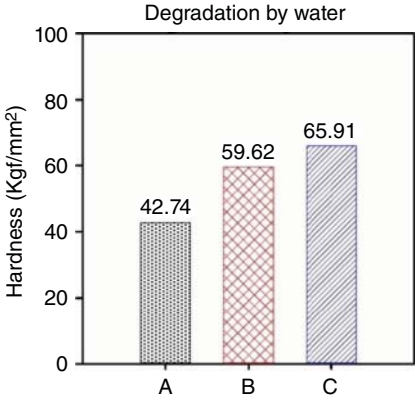

Figure 9.5 Effect of chemical degradation by various solvents on hardness of nanocomposites with 0.5 wt% filler loadings. A, B, and C are neat epoxy resin, GO/epoxy nanocomposite, and GO-ODA/epoxy nanocomposite, respectively. Source: Mousavi et al. [35]. © 2018, John Wiley & Sons.

The hardness of epoxy, epoxy/graphene oxide, and epoxy/ODA-modified graphene oxide nanocomposite is shown in Figure 9.5 [35]. The modification of GO with amine led to solvent resistance, and decrease in hardness is less than that in neat epoxy and epoxy/GO systems. In this case, neat epoxy resin and GO/epoxy nanocomposite showed 63.5%/57.3%/46.8% and 54.2%/46.2%/23.7% decrease in the hardness after seven days of exposure to the toluene/xylene/water solvent, respectively. While, under the same conditions, GO-ODA/epoxy nanocomposite presented 46.5%/37.0%/23.7% decrease in the final hardness, which is much lower than the other specimens.

DGEBF (epoxy equivalent weight equal to 320) and the TETA as hardener modified with modified and unmodified silica [36]. Water absorption increased with increase in time, and the T_g decreased with water absorption due to plasticization. The decrease in T_g was less for amino silane-treated particle that modified epoxy due to increase in cross-link density.

9.4 Effect of Water Absorption on Dynamic Mechanical Properties

Modification of epoxy resin by nanoparticles influenced the segmental mobility of the polymer chains. The extent of change depends on the type of nanoparticle used. It can be affected further by moisture absorption. The tan δ vs. temperature plots differed from system to system. In alumina/epoxy nanocomposite, the glass transition temperature decreased with water absorption due to the plasticization of epoxy matrix as a result of moisture absorption [37]. The tan δ plots in Figure 9.6 showed an additional peak due to the evaporation of water, which is not chemically bound to epoxy [29].

The storage modulus of the composite was improved by the addition of alumina nanoparticles (Figure 9.7). The extent of improvement was high above T_g in dry and wet samples. Rigid Al_2O_3 nanoparticles acted as physical cross-links for the epoxy chains below T_g, and above glass transition, the stiffening effect of alumina particles on the soft and rubbery epoxy chains becomes more pronounced, and therefore, the increase is more above T_g [38].

In the nanoclay-modified DGEBA/amine system, the storage modulus showed no significant change at low temperature (80 °C) but at higher temperature more change was observed [19]. Above 80 °C, the epoxy/clay nanocomposite suffered larger decrease (22%, from 1744 to 1361 MPa) compared to neat resin because of its higher water uptake (2.2%) as compared with the neat epoxy (Figure 9.8). The glass transition temperature decreased with the increase in water uptake. The tan δ peak broadened with increase in water uptake. Also, the intensity of the peak decreased. With increased exposure to water, a shoulder peak appeared and shifted further to lower temperature with immersion time. These effects are due to the uneven cross-link density in epoxy resin, which was further complicated by the presence of clay particles. Since clay can absorb more water, it will be present in regions of low cross-link density and near clay particles. The two peaks are due to the presence of more plasticized and less plasticized regions.

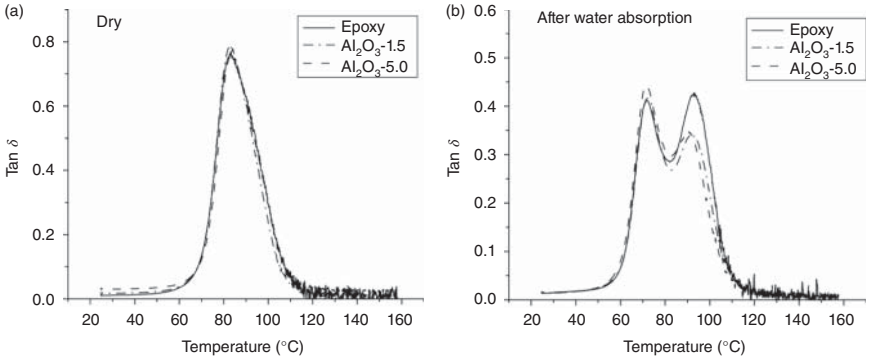

Figure 9.6 Dynamic mechanical analysis (DMA) results for epoxy, Al_2O_3-1.5 and Al_2O_3-5.0 nanocomposites: (a) tan δ for the dry samples and (b) tan δ for the water-treated samples. Source: Zhao and Li [29]. © 2008, Elsevier.

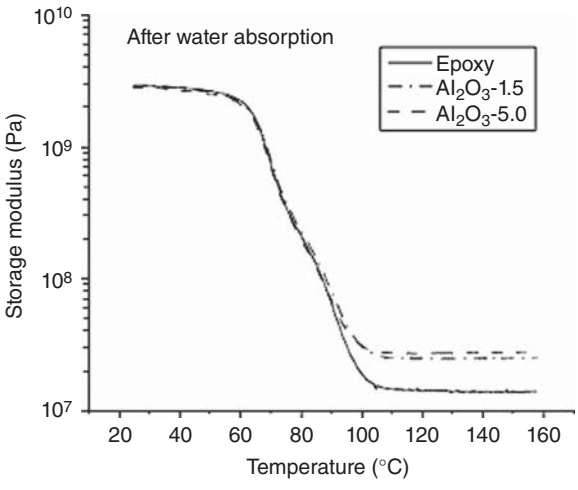

Figure 9.7 Storage modulus for the water-treated samples of epoxy, Al_2O_3-1.5 and Al_2O_3-5.0 nanocomposites. Source: Zhao and Li [29]. © 2008, Elsevier.

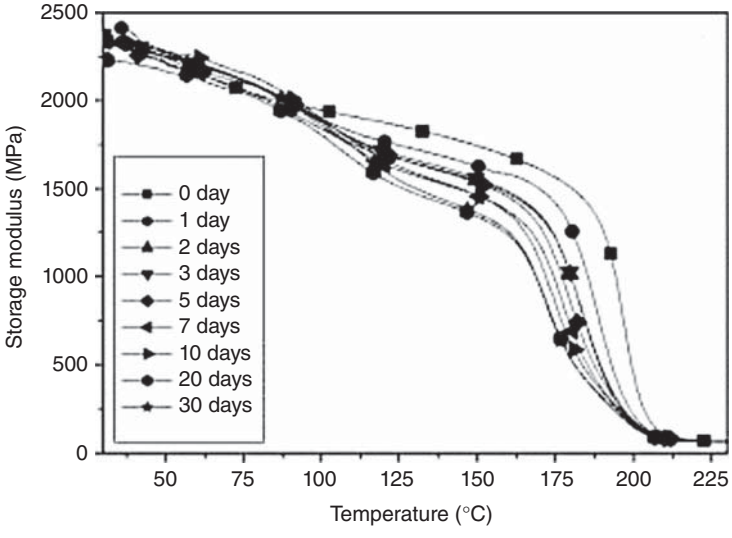

Figure 9.8 Variations of storage modulus on immersion time for nanocomposite with 2.5 wt% clay. Source: Wang et al. [19]. © 2006, John Wiley & Sons.

The difference in the behaviors of clay and alumina-modified epoxies is different because of the difference in the extent of water absorption. Alumina particles reduced water absorption, whereas clay increased absorption. In an amine-cured DGEBA epoxy/ODA-modified nanoclay, the T_g increased with increase in nanoclay but decreased with increase in moisture absorption but always higher than the T_g of the corresponding neat epoxy [15]. According to the authors, the change in T_g with moisture absorption in nanocomposites is indirectly due to the change in the permeability and diffusion behavior of the matrix by the nanoclay. In montmorillonite clay-modified bisphenol A epoxy resin cured with amine hardener Jeffamine

D400, increasing the nanoclay decreased the glass transition temperature from 45 to 35 °C. The decrease indicates that the absorbed water serves to decrease the intensity of interaction between polymer molecules raising the mobility of the segments and acceleration of relaxation process [21].

The tan δ curves of nanocomposites are broader compared to the water-absorbed DGEBA epoxy resin. Also, the secondary became more extensive on addition of MWCNT [24]. This is due to the contribution from Type II water. The storage modulus of the above system decreased with moisture absorption. However, the extent of decrease was less in the case of nanocomposite than water-absorbed epoxy resin. This is due to the lower plasticization of epoxy chains. The lower plasticization in nanocomposites is due to the decrease in the amount of Type I water in MWNT-modified epoxy resin.

In GNP-modified systems, the glass transition initially decreased and then remained almost same [31]. The initial decrease was due to the plasticization of the matrix. At a later stage, the water molecules formed H-bonds with the few remaining epoxy rings and enhanced the post-curing reaction, thereby increasing the cross-link density.

9.5 Effect of Water Absorption on Thermomechanical Properties

The results from thermomechanical analysis of epoxy/alumina nanocomposites revealed two linear regions above and below glass transition [29]. The glass transition temperature also decreased with moisture absorption. The coefficient of thermal expansion (CTE) showed some interesting characteristics. Below glass transition, the addition of alumina has no pronounced effect on the CTE of the composite. In the wet samples, CTE increased compared to unmodified epoxy resin due to the plasticization of molecular chains, which enhanced the segmental motions. Above glass transition, the CTE of dry samples decreased with increase in particle content due to the anchoring effect of nanoparticles. But above T_g, the CTE of wet sample is lower than dry sample due to the evaporation of absorbed water. The evaporation contributes to volume contraction and counterbalanced the normal thermal expansion (Figure 9.9).

In amine-cured epoxy resin with ODA-modified montmorillonite nanocomposites, the wet samples showed a sudden increase near the onset of glass transition. This was attributed to the onset of mobility of hydrogen-bonded water. According to Luo et al. [39], the H-bonded water molecules acted as side groups to the polymer chains.

The CTE decreased with increase in the amount of clay irrespective of dry or wet samples. However, the CTE of wet samples was slightly higher than that of dry samples below T_g, but CTE of dry samples was higher than wet samples above glass transition temperature as in the case of epoxy/alumina nanocomposites. This observation gives an indication of the segmental mobility of the polymer in the presence of water. When the polymer chains are rigid, the segmental mobility is not affected

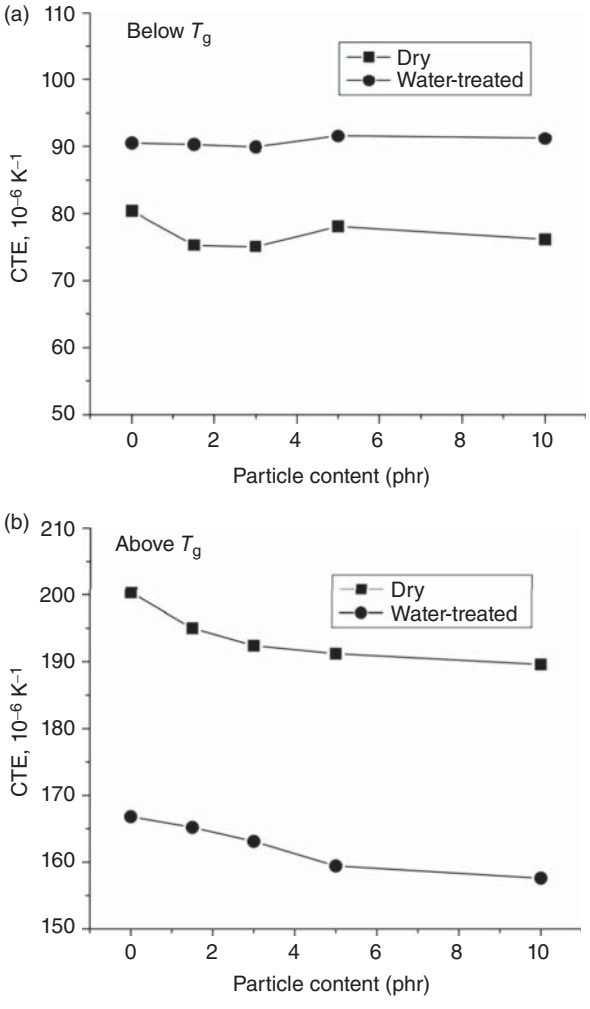

Figure 9.9 Coefficient of thermal expansion (CTE) for epoxy and nanoalumina-filled epoxy nanocomposites. (a) CTE values measured below T_g and (b) CTE values measured above T_g. Source: Zhao and Li [29]. © 2008, Elsevier.

by water absorption. Above glass transition, the hydrogen-bonded water disrupts the interchain H-bonding and gives rise to large thermal expansion.

9.6 Effect of Water Absorption on Dielectric Properties

The effect of water absorption on dielectric properties of epoxy/nanocomposites is a less explored area. The dielectric constant of an amine-cured DGEBA epoxy modified with silane-modified alumina was higher than that of the corresponding dry samples. One of the reasons for the increase is the strong dipoles of water. The other factors include the plasticization of the epoxy chains, increase in free volume, and breaking of weak bonds [40]. The dielectric loss factor of the wet samples increased continuously without showing a peak in contrast to the dry sample where a peak was observed near glass transition as shown in Figure 9.10. The exact reason for this observation is not known, but it could be due to the rapid increase in ε'' due to water absorption, which overlapped the glass transition peak.

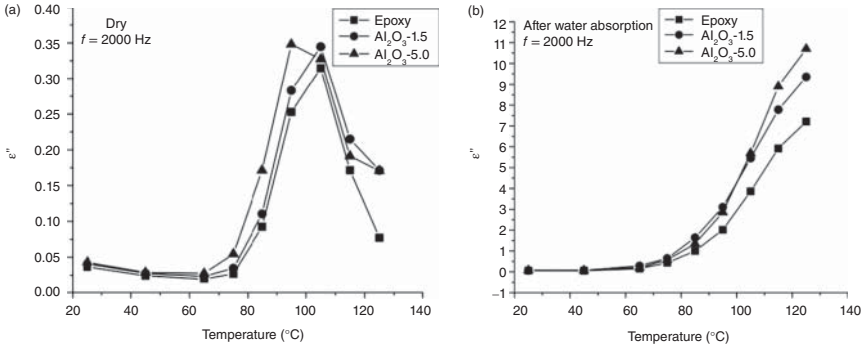

Figure 9.10 Effect of temperature on the dielectric loss ε'' of nanoalumina-filled epoxy nanocomposites in the: (a) dry and (b) water-treated samples. Source: Zhao and Li [29]. © 2008, Elsevier.

9.7 Conclusion

Nanocomposites of epoxy resin were prepared using a variety of nanoparticles. Difunctional as well as other multifunctional epoxy resins were used as the matrix. The moisture absorption in the nanocomposites varied with the nanoparticles used, its content, surface modification if any, and the hydrophilic or hydrophobic nature of the nanoparticle. Moisture absorption led to the destruction of the interfacial interaction between the nanoparticle and epoxy resin in some cases, whereas in some other cases, it promoted the post-curing process. Moisture absorption affected the mechanical, dynamic mechanical, and dielectric properties. In majority of the composites, the tensile strength decreased with moisture absorption. The fracture toughness and impact strength increased in several systems. The changes in mechanical properties are due to the plasticization of the epoxy matrix. The change in properties due to water absorption and extent of absorption could not be explained in full in all the cases. Some ambiguities still exist in the correlation between properties and moisture absorption and need further research.

References

1 May, C.A. (1973). *Epoxy Resins: Chemistry and Technology*, Chapter 1. New York, NY: Marcel Dekker.

2 Pethrick, R.A. (2014). Applications of toughened epoxy resins, Chapter 17. In: *Micro and Nanostructured Epoxy/Rubber Blends* (eds. S. Thomas, C. Sinturel and R. Thomas), 339–362. Weinheim: Wiley.

3 Francis, B., Thomas, S., Sadhana, R. et al. (2007). Diglycidyl ether of bisphenol-A epoxy resin modified using poly(ether ether ketone) with pendent *tert*-butyl groups. *Journal of Polymer Science Part B: Polymer Physics* 45: 2481–2496.

4 Francis, B., Rao, V.L., Poel, G.V. et al. (2006). Cure kinetics, morphological and dynamic mechanical analysis of diglycidyl ether of bisphenol-A epoxy resin modified with hydroxyl terminated poly(ether ether ketone) containing pendent tertiary butyl groups. *Polymer* 47: 5411–5419.

5 Monetta, T., Acquesta, A., and Bellucci, F. (2015). Graphene/epoxy coating as multifunctional material for aircraft structures. *Aerospace* 2: 423–434.

6 Azeez, A.A., Rhee, K.Y., Park, S.J., and Hui, D. (2013). Epoxy clay nanocomposites – processing, properties and applications: a review. *Composites Part B: Engineering* 45: 308–320.

7 Guadagno, L., Vertuccio, L., Sorrentino, A. et al. (2009). Mechanical and barrier properties of epoxy resin filled with multi-walled carbon nanotubes. *Carbon* 47: 2419–2430.

8 Starkova, O., Chandrasekaran, S., Prado, L.A.S.A. et al. (2013). Hydrothermally resistant thermally reduced graphene oxide and multi-wall carbon nanotube based epoxy nanocomposites. *Polymer Degradation and Stability* 98: 519–526.

9 Ng, C.B., Ash, B.J., Schadler, L.S., and Siegel, R.W. (2001). A study of the mechanical and permeability properties of nano- and micron-TiO_2 filled epoxy composites. *Advanced Composites Letters* 10: 101–111.

10 Voo, R., Mariatti, M., and Sim, L.C. (2012). Thermal properties and moisture absorption of nanofillers-filled epoxy composite thin film for electronic application. *Polymers for Advanced Technologies* 23: 1620–1627.

11 Becker, O., Varley, R.J., and Simon, G.P. (2004). Thermal stability and water uptake of high performance epoxy layered silicate nanocomposites. *European Polymer Journal* 40: 187–195.

12 Liu, W., Hoa, S.V., and Pugh, M. (2005). Fracture toughness and water uptake of high-performance epoxy/nanoclay nanocomposites. *Composites Science and Technology* 65: 2364–2373.

13 Al-Qadhi, M., Merah, N., Gasem, Z.M. et al. (2014). Effect of water and crude oil on mechanical and thermal properties of epoxy-clay nanocomposites. *Polymer Composites* 35: 318–326.

14 Glaskova, T. and Aniskevich, A. (2009). Moisture absorption by epoxy/montmorillonite nanocomposite. *Composites Science and Technology* 69: 2711–2715.

15 Kim, J.K., Hu, C., Ricky Woo, R.S.C., and Sham, M.L. (2005). Moisture barrier characteristics of organoclay–epoxy nanocomposites. *Composites Science and Technology* 65: 805–813.

16 Hu, C. and Kim, J.K. (2005). Epoxy-organoclay nanocomposites: morphology, moisture absorption behavior and thermo-mechanical properties. *Composite Interfaces* 12: 271–289.

17 Vanlandingham, M.R., Edduljee, R.F., and Gillespie, J.W. Jr. (1999). Moisture diffusion in epoxy systems. *Journal of Applied Polymer Science* 71: 787–798.

18 Abacha, N., Kubouchi, M., Sakai, T., and Tsuda, K. (2009). Diffusion behavior of water and sulfuric acid in epoxy/organoclay nanocomposites. *Journal of Applied Polymer Science* 112: 1021–1029.

19 Wang, L., Wang, K., Chen, L. et al. (2006). Hydrothermal effects on the thermomechanical properties of high performance epoxy/clay nanocomposites. *Polymer Engineering and Science* 46: 215–221.

20 Madhup, M.K., Shah, N.K., and Parekh, N.R. (2017). Investigation and improvement of abrasion resistance, water vapor barrier and anticorrosion properties of mixed clay epoxy nanocomposite coating. *Progress in Organic Coating* 102: 186–193.

21 Aniskevich, K.K., Glaskova, T.I., Aniskevich, A.N., and Faitelson, Y.A. (2011). Effect of moisture on the viscoelastic properties of an epoxy-clay nanocomposite. *Mechanics of Composite Materials* 46: 573–582.

22 Lee, J.H., Rhee, K.Y., and Lee, J.H. (2010). Effects of moisture absorption and surface modification using 3-aminopropyltriethoxysilane on the tensile and fracture characteristics of MWCNT/epoxy nanocomposites. *Applied Surface Science* 256: 7658–7667.

23 Prolongo, S.G., Gude, M.R., and Ureña, A. (2012). Water uptake of epoxy composites reinforced with carbon nanofillers. *Composites: Part A* 43: 2169–2175.

24 Starkova, O., Buschhorn, S.T., Mannov, E. et al. (2013). Water transport in epoxy/MWCNT composites. *European Polymer Journal* 49: 2138–2148.

25 Jojibabu, P., Janaki Ram, G.D., Deshpande, A.P., and Bakshi, S.R. (2017). Effect of carbon nano-filler addition on the degradation of epoxy, adhesive joints subjected to hygrothermal aging. *Polymer Degradation and Stability* 140: 84–94.

26 Khoramishad, H. and Alizadeh, O. (2018). Effects of silicon carbide nanoparticles and multi-walled carbon nanotubes on water uptake and resultant mechanical properties degradation of polymer nanocomposites immersed in hot water. *Polymer Composites* M39: E883–E890.

27 Alamri, H. and Low, I.M. (2012). Effect of water absorption on the mechanical properties of nano-filler reinforced epoxy nanocomposites. *Materials and Design* 42: 214–222.

28 Starkova, O., Chandrasekaran, S., Schnoor, T. et al. (2019). Anomalous water diffusion in epoxy/carbon nanoparticle composites. *Polymer Degradation and Stability* 164: 127–135.

29 Zhao, H. and Li, R.K.Y. (2008). Effect of water absorption on the mechanical and dielectric properties of nano-alumina filled epoxy nanocomposites. *Composites: Part A* 39: 602–611.

30 Tomasi, J.M., Helman, I.D., Pisani, W.A. et al. (2016). Accelerated hydrothermal aging of cycloaliphatic epoxy/graphene nanoparticle composite. *Polymer Degradation and Stability* 133: 131–135.

31 Prolongo, S.G., Suárez, A.J., Moriche, R., and Ureña, A. (2018). Influence of thickness and lateral size of graphene nanoplatelets on water uptake in epoxy/graphene nanocomposites. *Applied Sciences* 8: 1550–1559.

32 Dittanet, P., Pearson, R.A., and Kongkachuichay, P. (2017). Thermo-mechanical behaviors and moisture absorption of silica nanoparticle reinforcement in epoxy resins. *International Journal of Adhesion and Adhesives* 78: 74–82.

33 Kim, D.H. and Kim, H.S. (2013). Waterproof characteristics of nanoclay/epoxy nanocomposite in adhesively bonded joints. *Composites: Part B* 55: 86–95.

34 Glaskova, T. and Aniskevich, A. (2010). Moisture effect on deformability of epoxy/montmorillonite nanocomposite. *Journal of Applied Polymer Science* 116: 493–498.

35 Mousavi, S.M., Hashemi, S.A., Arjmand, M. et al. (2018). Octadecyl amine functionalized graphene oxide towards hydrophobic chemical resistant epoxy nanocomposites. *Chemistry Select* 3: 7200–7207.

36 Gholamian, F., Ghariban-Lavasani, S., Garshasbi, M.M. et al. (2013). The effects of water absorption and surface treatment on mechanical properties of epoxy nanocomposite using response surface methodology. *Polymer Bulletin* 70: 1677–1695.

37 De Neve, B. and Shanahan, M.E.R. (1993). Water-absorption by an epoxy-resin and its effect on the mechanical-properties and infrared-spectra. *Polymer* 34: 5099–5105.

38 Sue, H.J., Gam, K.T., Bestaoui, N. et al. (2004). Epoxy nanocomposites based on the synthetic α-zirconium phosphate layer structure. *Chemistry of Materials* 16: 242–249.

39 Luo, S.J., Lwlawn, J., and Wong, C.P. (2002). Study on mobility of water and polymer chain in epoxy and its influence on adhesion. *Journal of Applied Polymer Science* 85: 1–8.

40 Reid, J.D., Lawrence, W.H., and Buck, R.P. (1986). Dielectric-properties of an epoxy resin and its composite 1. Moisture effects on dipole relaxation. *Journal of Applied Polymer Science* 31: 1771–1784.

10

Fracture Surface and Mechanical Properties of Epoxy Composites

Mehdi Naderi[1] *and Farnaz Ebrahimi*[2]

[1] *POLYMAT and Department of Applied Chemistry, Faculty of Chemistry, University of the Basque Country UPV/EHU, Joxe Mari Korta Center, Avenida Tolosa 72, 20018 Donostia-San Sebastián, Spain*
[2] *University of Tehran, College of Engineering, Department of Polymer Engineering, School of Chemical Engineering, 16th Azar Street, Enghelab Square, 11155-4563 Tehran, Iran*

10.1 Introduction

Firstly commercialized in 1946, epoxy resins are known to be one of the most critical thermosetting materials, and due to their superior properties, they are placed among the most commonly used engineering materials. Epoxy resins are developed for numerous industries such as aerospace, automotive, marine, composites, sport materials, construction, electrical and electronic insulation, biomedical devices, thermal management systems, adhesives, paints and coatings, industrial tooling, and other consumption goods. The properties of cured epoxy systems mainly depend on the type and structure of used raw materials including epoxy resin and curing agent. In terms of application, mechanical properties, chemical resistance, thermal stability, electrical insulation, flame, and weathering resistance are considered as the chief qualities of epoxy resins. Epoxies possess superb mechanical properties compared to other thermoset polymers as a result of their highly cross-linked network. They show high tensile strength, modulus, flexural, and impact strength. Despite all mentioned characteristics as well as thriving industrial applications, epoxy resins suffer an outstanding drawback, which is their brittleness, because of their high degree of cross-linking. This issue needs to be addressed through practical measures in order to widen epoxy resins' applications as a critical industrial material. Using external modifiers such as rubbers, thermoplastic polymers, etc., chemical structure modification, and introducing structured reinforcements or functional fillers to epoxy composite systems are some of the offered feasible solutions to overcome epoxy brittleness. Furthermore, addition of fillers with specific structures and functionalities into epoxy composite systems would efficiently enhance various properties of epoxy resin such as mechanical properties, thermal stability, and corrosion resistance, as a means to exploit the properties of matrix to the full. In addition, development of novel epoxy-based composite materials has been considered in

Epoxy Composites: Fabrication, Characterization and Applications,
First Edition. Edited by Jyotishkumar Parameswaranpillai, Harikrishnan Pulikkalparambil, Sanjay M. Rangappa, and Suchart Siengchin.

frequent studies and projects in the past few years. Consequently, the various applications of epoxy-based composites have been spreading in different industries [1, 2].

Over the past few decades, numerous investigations announced the usage of fillers and nanomaterials acting as reinforcing agents for epoxy resins. In addition, utilization of fillers as reinforcement is not limited to epoxy resins, and they are frequently applied in a variety of polymeric matrices with different purposes. In several studies, it is claimed that applying reinforcing fillers, especially nanofillers, could dramatically augment the mechanical properties of epoxy system. Addition of fillers into epoxy resins with the aim of modifying mechanical as well as other vital properties like thermal stability and electrical conductivity has broaden the ultimate application of epoxy-based composites as practical materials in numerous industries. Recently, many reinforcing fillers and nanostructures are developed, and each of them provides different characteristics and properties based on their distinct structures.

The epoxy matrix considerably benefits from the specific properties of reinforcement. Take as an example, a filler with a high modulus as well as a perfect interaction with epoxy matrix would increase the stiffness of cured epoxy system. Eventually, novel composite systems could be designed based on characteristics of the fillers and desired properties of the final material. A basic knowledge of epoxy fillers and nanoreinforcements is of chief importance to further investigate the mechanical properties of epoxy composites. Ceramic nanoparticles like silica and alumina, fibers such as glass fibers and carbon fibers (CFs), and carbon nanofillers including carbon nanotubes (CNTs), graphene, carbon aerogels, etc. are the main suggested groups of fillers for epoxy resins with the aim of ameliorating their mechanical properties. Among all of the mentioned groups, nano-sized fillers have drawn huge attention, as they are the most effective group concerning mechanical properties improvement. This stems from their larger specific surface, causing a superior interaction between epoxy matrix and the fillers. Each filler provides the epoxy matrix with particular properties. Therefore, various fillers have distinct effect on mechanical properties, and each system should be studied separately [1–8].

Ceramic fillers are one of the common reinforcing agents for polymers. Silica nanoparticles are among the most important groups of ceramic fillers, represented in several past and novel studies from 1970s to 2010s [9–12]. Silica particles offer high mechanical properties and stiffness and could efficiently increase the mechanical properties of epoxy composites. Moreover, they can slightly ameliorate the fracture toughness of epoxy resins, showing no decreasing effect on modulus [13]. However, how nanofillers are dispersed in epoxy resin and their interaction with thermoset matrix are two critical factors in terms of mechanical properties improvement. A considerable enhancement in mechanical strength and modulus will not be achieved, if the dispersion and interaction of filler–matrix are low. Subsequently, the interaction enhancement between filler and matrix has been examined in various studies to increase the efficiency of reinforcement concerning mechanical properties improvements. It is claimed that interfacial modification of silica nanoparticles using functional groups and materials including active groups could effectively promote the dispersion and interaction of filler in/with epoxy matrix, leading to

an increase in mechanical performance of epoxy nanocomposites [14–16]. Another common group of ceramic fillers for epoxy is alumina. The researches of Lange and Radford [17] showed that using correct content of alumina at proper particle size ameliorates the fracture energy as well as tensile modulus and strength. Alumina as an inorganic filler possesses high stiffness and mechanical strength, which could provide these significant properties to its surrounding epoxy matrix. Moreover, the increment of mechanical properties, in particular modulus, strength, and toughness of epoxy using alumina as an inorganic filler depends on three crucial factors including filler loading, particle size, and filler–matrix interaction. Although the stiffness of final composite is highly influenced by filler loading, strength and toughness are affected by all three factors [18, 19]. Several studies on alumina-reinforced epoxy systems have declared that introducing alumina in epoxy matrix effectively augments different mechanical parameters such as tensile and flexural modulus, strength, fracture toughness, and glass transition temperature. However, the filler content should be controlled, since the high filler loadings may lead to particles agglomeration, and consequently a decline in mechanical properties [20–22]. Following inorganic fillers, clay is one of the most common inorganic reinforcements for a broad range of polymers because of its fascinating characteristics like high mechanical properties, thermal stability, barrier properties, etc. Additionally, there are several grades of modified and unmodified clay, each providing different properties. Clay in an exfoliated form was first introduced in polymeric matrix by Toyota for the purpose of ameliorating mechanical and thermal properties of nylon 6. Since then, researchers started using clay as a novel reinforcement in various polymeric composite systems. The form in which clay layers are dispersed in epoxy matrix along with the microstructure of clay-reinforced nanocomposites clearly affects their mechanical properties.

It could be inferred from several studies on clay–epoxy composites that clay has the potential to enhance the modulus and stiffness of epoxy resin. The way clay particles affect tensile modulus as reinforcing agents could be ascribed to their stiffness as well as high aspect ratio, which results in high interaction between clay layers and epoxy matrix [23, 24]. The influence of clay on mechanical strength and toughness, on the other hand, was variable. In some works, it has been concluded that adding clay to epoxy system causes reduction in tensile strength, elongation at break, and subsequent decrease in toughness. In other words, using clay as a reinforcing agent has made epoxy composites more stiff and brittle [25, 26]. In an investigation, Chan et al. [27] examined the reinforcing impact of clay on tensile properties of epoxy and it was observed that clay nanofillers improved both modulus and tensile strength. However, high loading of clay (9 wt%) reduced the modulus and tensile strength. Kusmono et al. [28] showed that the effect of clay on mechanical strength and fracture toughness of epoxy composite extremely depends on the weight fraction of added clay, and there is an optimum weight percentage of 3 wt%, giving the highest strength as well as fracture toughness. Furthermore, the epoxy composite containing 3 wt% of clay showed a more tough fracture behavior compared with neat epoxy.

One of the most practical forms of epoxy-based materials is fiber-reinforced epoxy composites, currently being applied in numerous areas of crucial industries

including construction, aerospace, marine, wind power, automotive, and transportation applications. With the advent of fiber-reinforced epoxy composites, various metal and heavy parts of airplanes, ships, automobiles, etc. have been replaced with epoxy composites because of their superior mechanical properties. The epoxy composite parts are mainly made out of glass and CFs impregnated with epoxy resin. The fibrous fillers, thanks to their special geometry, provide high aspect ratio, which bring about fine interaction with epoxy matrix. Furthermore, the mechanical properties of a fiber-reinforced epoxy composite depend on the fiber stiffness and strength and the interface bonding between the fiber and matrix in order to enable stress transfer. Glass fibers have been exceedingly used as an ideal mechanical reinforcement in polymer industries, in particular thermosetting polymers, and they are available in different grades with distinct properties [29–32]. Introducing glass fibers as mechanical reinforcement into epoxy matrix dramatically augments the modulus, flexural strength, and fracture toughness of epoxy [29]. It appears that reinforcing epoxy using glass fibers would be a practical measure to tackle the problem of brittleness in epoxy resins without any reduction in modulus. Moreover, the interfacial bonding modification using functional materials and nanostructures on the fiber structure could enhance the efficiency of glass fibers in mechanical properties improvement [31, 32]. Another fibrous structure, which has dominated the market of fiber-reinforced epoxy-based composites, is CF. CFs, known as practical engineering materials, possess high rigidity and strength as well as low density, which have drawn massive attention of researchers and industries for manufacturing epoxy-based materials. CF-reinforced epoxy systems show significant promotions in mechanical behavior, particularly modulus and hardness, flexural strength, and fracture toughness in comparison with neat cured epoxy [33]. The ultimate characterizations of a composite system are governed by both the properties of individual parts along with the bonding between the fibers and the resins in the interface. Numerous studies on interface modification of CF–epoxy systems are accomplished, since it is of great concerns for researchers. These works mostly focused on the modification of fibers using non-functionalized and functionalized nanofillers like CNTs and graphene oxide (GO). Owing to their extremely high surface area and possible functionalities, nanofillers could effectively improve the interaction between CF and epoxy matrix, leading to higher efficiency of CFs in terms of mechanical properties enhancement [34–36]. Moreover, adding both fibers and nanoparticles in an epoxy system could be another technique to increase the efficiency of fibers [37, 38]. Recently, cellulose nanofibers have been introduced as a novel bio-based reinforcement for polymeric matrices. In an epoxy system, applying cellulose nanofiber as a nanoreinforcement would result in mechanical and thermal properties improvement [39, 40]. It has been revealed that using insignificant amount of cellulose nanofibers (<1 wt%) could considerably raise the storage modulus and glass transition temperature.

Over recent years, a wide range of carbon nanomaterials, such as CNTs, carbon nanohorns, fullerene, graphene and its derivations, for instance graphene nanoplatelets (GNPs), nanoporous graphene (NPG's), and GO, have been vastly used as indispensable parts in several industries such as energy and fuel applications,

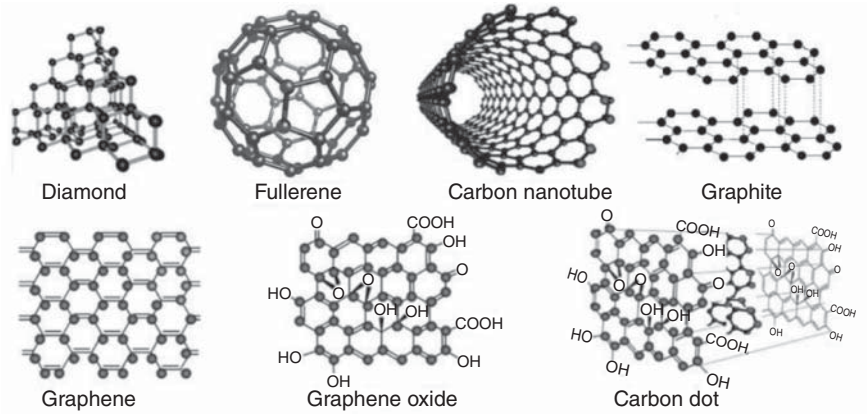

Figure 10.1 Different multidimensional structures of carbon-based nanofillers. Source: Yan et al. [41]. CC BY 3.0.

sensors, nanocomposites, and so on. Furthermore, some of these nanomaterials are widely used as a means to modify the mechanical properties and fracture toughness of epoxy-based nanocomposites. Carbon nanofillers are available in various structures of tube-like, platelet, and isodimensional nanofillers (Figure 10.1), providing distinct characteristics and properties such as superior mechanical properties, thermal resistance, electrical conductivity, barrier and anticorrosion properties in a polymeric matrix. Among carbon nanomaterials, graphene, a two-dimensional (2D) material composed of atom carbons bound in a hexagonal honeycomb lattice with high specific surface area, and CNT with its high aspect ratio and specific geometry have gained greater heed because of their magnificent properties, specifically high stiffness and mechanical strength. Moreover, graphene along with CNT has excellent physical interaction with epoxy matrix due to its extremely higher surface area, compared with other suggested organic and inorganic fillers. This characteristic makes graphene and CNT two perfect mechanical reinforcements, even at low filler loadings (<1 wt%) [41–46]. However, chemical interaction between carbon nanofillers is a crucial factor in carbon-reinforced polymer composites, which has been considered in many researches in order to exploit the maximum potential of nanoreinforcement in mechanical properties improvement [41, 44, 45]. In addition, graphene and CNT show supreme modulus and strength, comparing with other industrially applied fillers (Table 10.1), and the epoxy matrix could inherit this characteristic from carbon fillers, if good interfacial bonding and dispersion are achieved.

In recent years, graphene has been considered in numerous studies for various engineering fields, especially polymer nanocomposites with different purposes. Figure 10.2 illustrates the increasing trend in graphene–epoxy composites publications between 2006 and 2015. This is mainly because of the capability of graphene nanostructure in mechanical behavior modification of epoxy as well as improving other industrially crucial properties like thermal, electrical, and anticorrosion properties [47].

Table 10.1 Mechanical properties of different fillers applied as epoxy's reinforcements.

Filler	Young modulus (GPa)	Tensile strength (GPa)	References
Glass fiber (type E)	72.3	3.4	Sathishkumar et al. [30]
Carbon fiber	225.0	5.4	Feih and Mouritz [42]
Multi-walled carbon nanotube	200.0–950.0	11.0–150.0	Yu et al. [43]
Graphene	1000.0	130.0	Lee et al. [46]

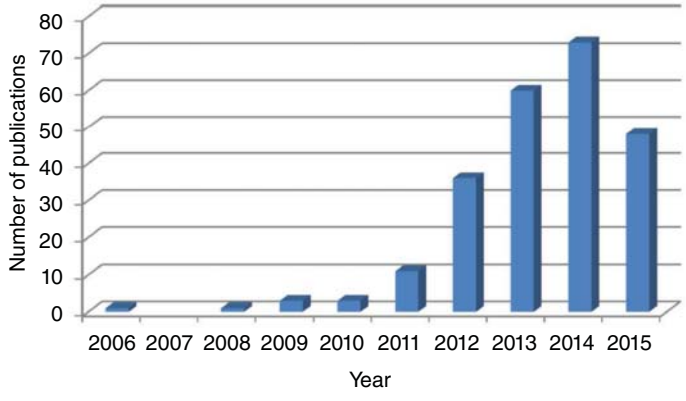

Figure 10.2 Diagram showing number of papers in Web of Science using the keywords "graphene epoxy" when titles were searched (By 30 June 2015). Source: Wei et al. [47]. CC BY 3.0.

Using graphene as nanoreinforcement in epoxy composite generally strengthens modulus and glass transition temperature, since nanoparticles cause movement restrictions in polymer molecules, particularly when nanoparticles are perfectly dispersed in epoxy matrix. However, there is often a decrease or no considerable change in tensile strength when GNPs are added. Furthermore, it has been shown that introducing graphene into epoxy promotes the fracture toughness and makes the fracture surface rougher and tougher with a disordered crack pattern, compared with the neat epoxy, which demonstrates a typical brittle fracture behavior. The mentioned phenomena are caused by the preventive effect of nanofillers in crack propagation and higher energy dissipation during the fracture process. As far as flexural properties are concerned, using graphene could enhance the flexural modulus and strength [48–53]. Naderi et al. [54] applied porous graphene as a novel nanoreinforcement with high porosity and specific surface area in the epoxy system. It was concluded that, although using porous graphene increases modulus and glass transition temperature, it curbs tensile strength, elongation at break, and impact strength, which means that the composite has become more rigid and brittle. Another graphene-based nanomaterial is GO providing various chemical functionalities including hydroxyl groups, carboxyl groups, and epoxy

bridges. Thanks to the mentioned functionalities, GO creates a perfect chemical interaction with epoxy groups of the epoxy resin, which brings about a superior interfacial adhesion between filler and matrix compared to reduced GO (graphene). Subsequently, GO has become a potential nanofiller for epoxy resins in terms of mechanical properties improvements. GO, as a functional reinforcement, could excellently enhance modulus, glass transition temperature, and fracture toughness. However, these functional groups can have both favorable and unfavorable consequences. In some systems, the mechanical properties like modulus and strength have declined because of the interference of nanofiller's functionalities in curing process [44, 55–58]. Considerable reinforcing potential of graphene is negatively affected by its incomplete specifications of interface bonding, caused by the robust van der Waals forces. Consequently, graphene particles form serious agglomerations which creates problems regarding their dispersion in epoxy matrix. These nanoparticles possess poor interfacial bonding with matrix, which may inversely influence the reinforcing effectiveness of graphene with the aim of strengthening mechanical properties. An advantageous method recommended for dominating over the nonmaterial dispersion and augmenting filler–matrix interaction in order to improve fillers' efficiency regarding mechanical properties enhancement is to modify the surface by grafting different functional groups like epoxy, hydroxyl, and ketones [58–61]. Furthermore, in some cases, the chemical modification of epoxies' reinforcement has been implemented with the aim of toughness and flexibility improvement, and also addressing the problem of epoxy brittleness by reacting functional groups with epoxy matrix and consequently creating a disturbance in its process of curing [44, 53, 62]. In a recent study, Naderi, Ebrahimi, and coworkers [44] investigated the effect of porous graphene (NPG) functionalized with different groups including carboxyl and amine. It was inferred that amine-functionalized NPG outperforms carboxylated NPG in mechanical properties (toughness, impact strength) modification, which could be due to the better reactivity of amine groups with epoxy, compared with carboxyl groups.

CNT has also been widely used as a nanoreinforcement in epoxy composites, mainly to ameliorate the mechanical and electrical properties. Adding low content of CNT (<1 wt%) to an epoxy-based composite could simultaneously strengthen the stiffness and fracture toughness, since CNT has outstanding mechanical properties and specific fibrous structure [63–65]. Similar to graphene derivatives, interface modification of CNT by active sites such as carboxyl and amine groups is of chief importance for improving the reinforcing effect of nanoparticles concerning mechanical behaviors as well as other critical properties. Moreover, many researches have been accomplished in the field of CNT chemical modification, revealing that functionalized CNT shows better performance in enhancing mechanical properties, in particular young modulus, fracture toughness, and impact strength, compared with unmodified CNT. The reason is that functionalized CNT disperses much better in epoxy resin and owns higher degree of filler–matrix interaction [63, 66–69]. Comparative studies on epoxy composites reinforced with graphene and CNT have shown variable results. Li et al. [70] used a molecular model and declared that graphene nanoparticles outperform CNT in mechanical properties improvement

through examination of young modulus, tensile strength, and fracture energy. In contrast, the experimental results of a study on epoxy composites by Zakaria et al. [71] showed that CNT is more effective than graphene in terms of mechanical properties improvement. There are also some works proposing hybrid nanomaterial systems for improving different properties of epoxy composites. In a hybrid system, for instance, graphene–CNT, carbon–graphene, graphite–ceramic, etc., each individual nanostructure could provide the epoxy matrix with distinct properties [72, 73]. As a new group of carbon-based nanomaterial, carbon aerogel has been introduced into epoxy composite systems recently. Carbon aerogel is widely applied in energy application for different purposes. Aghabararpour, Naderi, and coworkers [74], and Hsieh et al. [75] claimed that not only the carbon aerogels promote the modulus and tensile strength of epoxy composites, but also they considerably enhance toughness and impact strength. Moreover, adding carbon aerogel changes the fracture behavior of the virgin epoxy from a brittle fracture to a tougher fracture in the epoxy composite system, examined by fracture surface morphology.

10.2 Morphology

10.2.1 Dispersion and Interfacial Adhesion

The interface bonding between fillers and the matrix along with their dispersion have inevitably affected the final characterizations of epoxy-based composites. Achieving an ideal dispersion of fillers in epoxy matrix for exploiting the mechanical properties of reinforcement to the full is of great importance. In an investigation, Tang et al. [55] examined how the dispersion state of thermally reduced graphene oxide (RGO) impacts on the mechanical properties of epoxy composites. They employed two diverse mixing procedures to produce highly and poorly dispersed epoxy composites with and without using a high shear planetary ball mill mixer, respectively. It was found that the state of fillers' dispersion in epoxy has direct impact on fillers' efficiency in mechanical properties, in particular mechanical strength and fracture toughness (Figures 10.3 and 10.4). However, the effect of dispersion state on modulus is relatively insignificant. It is worth noting that poor dispersion could even inversely affect the mechanical properties and diminish the mechanical strength.

Researchers have implemented a number of different measures to ameliorate the degree of fillers' dispersion in the epoxy matrix. Take an example, using high shear and effective mixing techniques, matrix modification, and filler modification. The main process of epoxy composite consists of mixing fillers with one of the two key components of epoxy (epoxy resin and hardener), followed by adding and mixing the remaining component. In this state, the filler–resin/hardener mixing stage plays the most important role and should be methodized carefully. Over recent years, several studies have focused on promoting fillers' mixing in the viscous matrix of epoxy. These enhanced mixing methods mostly consist of high-shear or multistage mixing, normally in the presence of an external solvent for ease of processing and nanoparticles' exfoliation. Tomić et al. [76] used solution intercalation method for improving

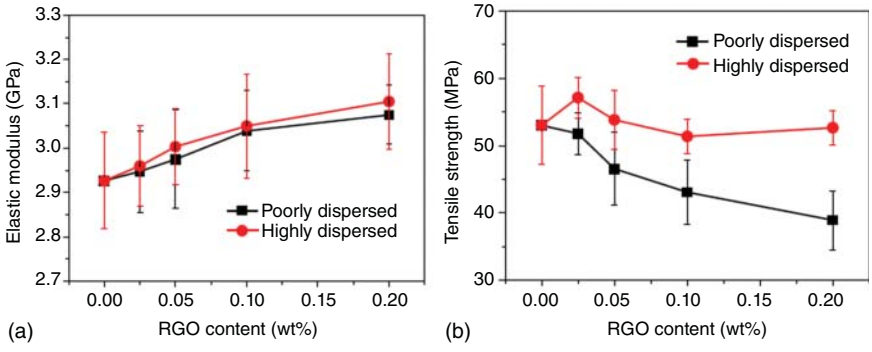

Figure 10.3 Diagrams showing tensile properties, (a) modulus and (b) strength, in cured epoxy composites reinforced with graphene. Source: Tang et al. [55]. © 2013, Elsevier.

Figure 10.4 Fracture toughness curves in cured epoxy composites based on the RGO content. Source: Tang et al. [55], Elsevier.

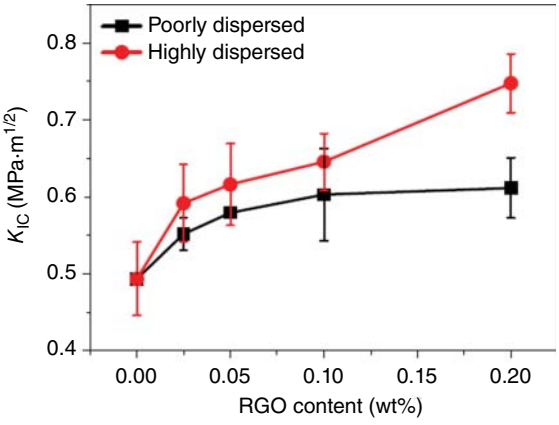

the dispersion of organoclay in epoxy matrix. In this method, before blending the filler with epoxy resin, organoclay (hexadecylamine-modified montmorillonite) is firstly swollen in a mixture of different solvents (79 wt% xylene, 10 wt% *n*-butanol, and 11 wt% methyl ethyl ketone [MEK]). This method causes the clay mineral layers to be delaminated, which enhance the dispersion of clay in the epoxy matrix, compared with a direct mixing method. In a recent study on single-walled carbon nanotube (SWCNT) and epoxy composite, Jamal-Omidi and ShayanMehr [77] incorporated a sonication-based multistage method in order to disperse SWCNT in the epoxy matrix. Figure 10.5 illustrates the schematic of this processing technique. Firstly, the SWCNT is treated using acid group to prepare carboxylated SWCNT (SWCNT-c), which provides better interaction with epoxy matrix. Secondly, a highly dispersed suspension of SWCNT-c in tetrahydrofuran (THF) is produced using mechanical stirring as well as high probe sonication. In the next stage, the resulted suspension is intensively mixed with epoxy resin through five cycles of alternative sonication and mechanical mixing. Finally, the mixture is ready to be blended with the hardener and be molded. The scanning electron microscopy (SEM) images (Figure 10.6) show the higher level of SWCNT dispersion in epoxy

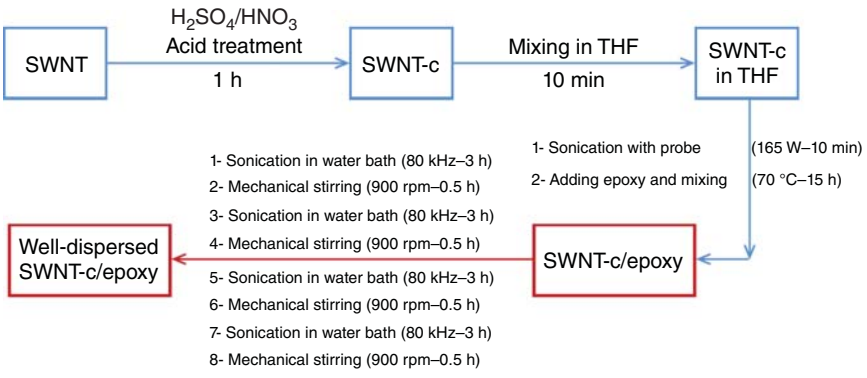

Figure 10.5 Sonication procedure of the suggested multistep technique to mix SWNT-c in epoxy resin. Source: Jamal-Omidi and ShayanMehr [77]. © 2019, Elsevier.

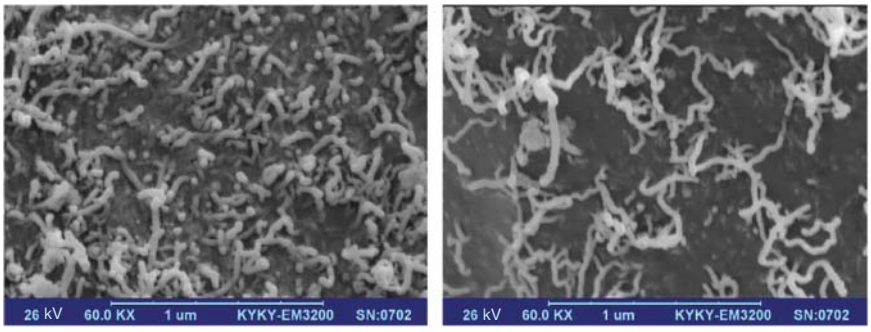

(a) (b)

Figure 10.6 SEM photographs illustrating the SWNTs dispersed in epoxy on account of (a) old technique using probe and (b) suggested multistep technique. Source: Jamal-Omidi and ShayanMehr [77].

matrix using multistep method, compared with a traditional mixing method, which only includes a 15-minute sonication of SWCNT-THF suspension with epoxy resin.

Kumar et al. [78] introduced a novel procedure for attaining a greater dispersion of multi-walled carbon nanotubes (MWCNTs) through the simultaneous incorporation of ultrasonic waves and shear force, produced by axial flow impeller in the presence of acetone as a solvent for ease of mixing (Figure 10.7). In another relevant studies, Tang et al. [55] used a planetary ball mill (PM 400, Retsch) equipped with four steel containers (125 ml) and three different types of zirconia balls (3, 6, and 11 mm in diameter and the corresponding 250, 50, and 10 in number) in order to disperse RGO sheets in epoxy matrix. First, they dispersed RGO in ethanol using sonication, and then they added epoxy to the final mixture and again mixed it by sonication. Finally, a ball mill mixer was used, and high shear force was generated by the milling impact, which could break up the RGO agglomerated layers, resulting in nanoparticles' exfoliation in order to achieve a highly dispersed RGO/epoxy mixture. Furthermore, Figure 10.8 demonstrates the effect of using high shear

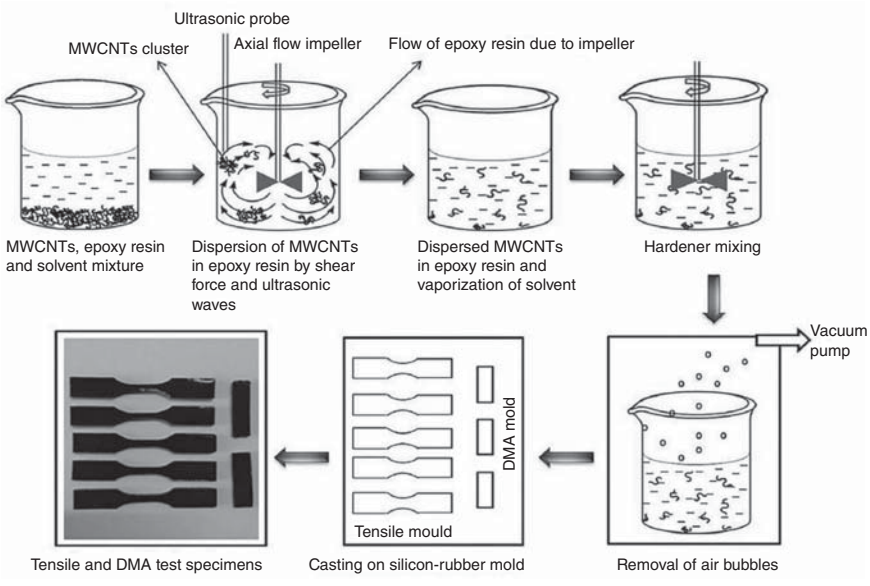

Figure 10.7 Schemes showing the process for fabricating MWCNT-reinforced epoxy composite by simultaneous application of ultrasonic waves and shear stress using axial flow impeller. Source: Kumar et al. [78]. © 2017, Elsevier.

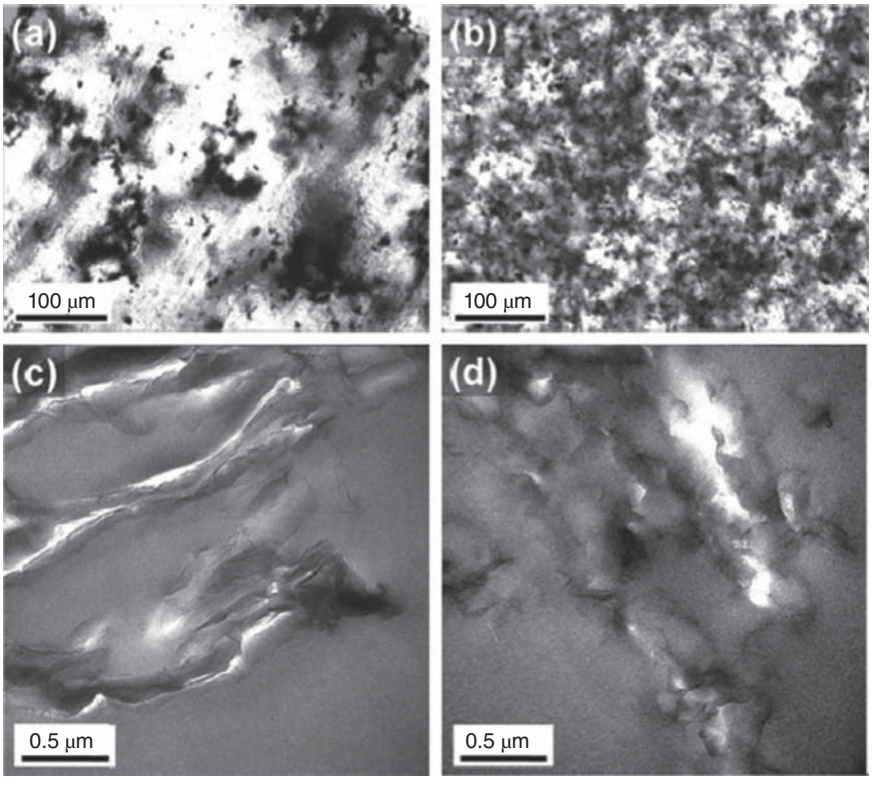

Figure 10.8 Optical microscopy and TEM photographs of epoxy composites containing 0.2 wt% RGO produced (a,c) without and (b,d) with using the ball mill technique. Source: Tang et al. [55].

technique on dispersion of RGO in epoxy matrix, examined by optical microscopy and transmission electron microscopy (TEM) images. It is evident that using ball mill has increased the level of RGO's dispersion, and the large-scale agglomerates of RGO created in the absence of ball mill have been disappeared. This phenomenon effectively led to superior efficiency of highly dispersed RGO in terms of enhancing the mechanical properties of epoxy, compared with poorly dispersed RGO.

Two main techniques are proposed in the category of matrix modification with the aim of promoting the processability and dispersion of fillers in epoxy matrix and enhance interfacial bonding between filler and matrix. The first technique for a superior dispersion is using an external diluent to reduce the viscosity of epoxy, and the second one is the addition of nanoparticles in epoxy matrix, which is mostly applied in epoxy-based composites reinforced with fiber to augment the interfacial adhesion between fibers and epoxy matrix. Ultimately, applying the mentioned techniques has an increasing effect on the effectiveness of fillers with the aim of strengthening the mechanical properties in epoxy-based composites. Due to its high viscosity, epoxy resin impedes the good dispersion of fillers, usually because the viscous forces of epoxy prevail over the adhesion forces in the nanomaterials/matrix system. Forming a fine dispersion of reinforcing agents in epoxy resin and consequently facilitating its processability could be reached by reducing the viscosity of epoxy resin through addition of a (reactive) diluent. Diluents containing epoxide groups in their structure have the ability to involve epoxy in a chemical reaction, creating ideal effects on properties of resin mixtures and its processing as well as being less damaging for the environment [44, 79–81]. For instance, the alternation in viscosity of epoxy through the addition of three types of reactive diluent has been examined by several researchers. According to results, a glycidylether C12–C14 alcohol outperforms ether-based diluents (i.e. 1,6-hexanediol diglycidylether and trimethylolpropane glycidylether) for the purpose of diminishing epoxy viscosity because of possessing a lower viscosity and molecular weight [79].

CFs suffer from poor interfacial bonding with polymeric matrices. It has been claimed that mechanical properties improvement by using fibers highly depends on the filler–matrix interface. In this regard, matrix modification using rigid nanomaterials such as graphite, silica, GO, etc. would substantially ameliorate the fiber–epoxy matrix interaction, leading to higher mechanical properties, compared with unmodified matrix [37, 38]. Figure 10.9 shows SEM images of epoxy composites reinforced with CFs which are modified and not modified with GO. Looking at the images, it is apparent that applying only 0.6 wt% of GO as a matrix modifier could enhance the interfacial adhesion, providing higher tensile and flexural properties. These interaction improvements are originated in the chemical reaction of functional groups of fiber with nanoparticle. In conclusion, the nanoparticles grafted on the fibers possess high physical and chemical interaction with epoxy matrix, since they own excellent surface area and frequent functional groups (Figure 10.10).

The last category of approaches to improve the dispersion of fillers along with interfacial adhesion in order to enhance mechanical properties is filler's modification, which has been intensively reported in various studies for epoxy composite reinforced with organic and inorganic fillers. It has been stated that surface

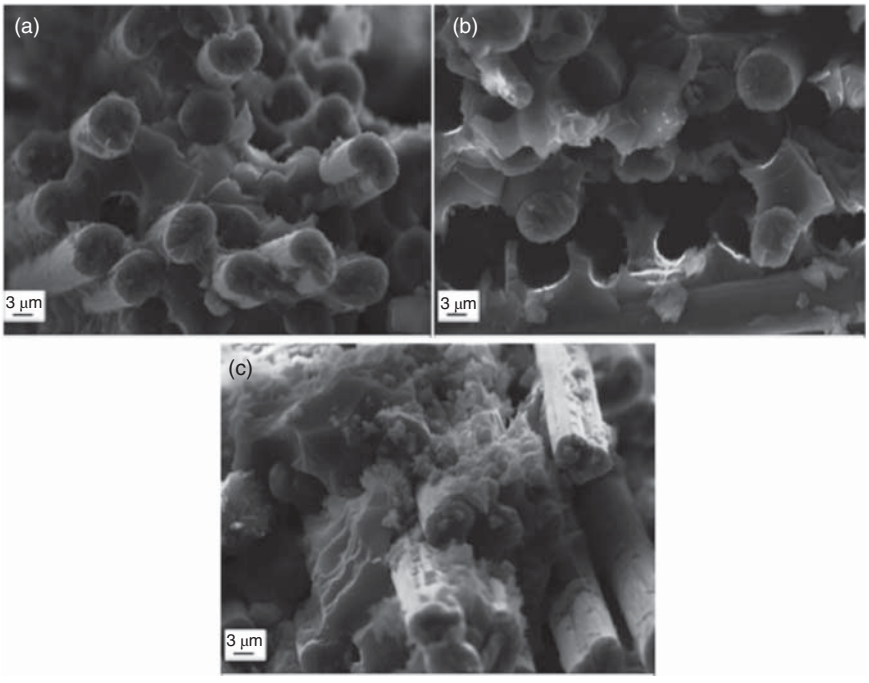

Figure 10.9 SEM photographs of epoxy/carbon fiber-reinforced composite (a) neat (b) with 0.3% of GO (c) with 0.6% of GO. Source: Pathak et al. [37].

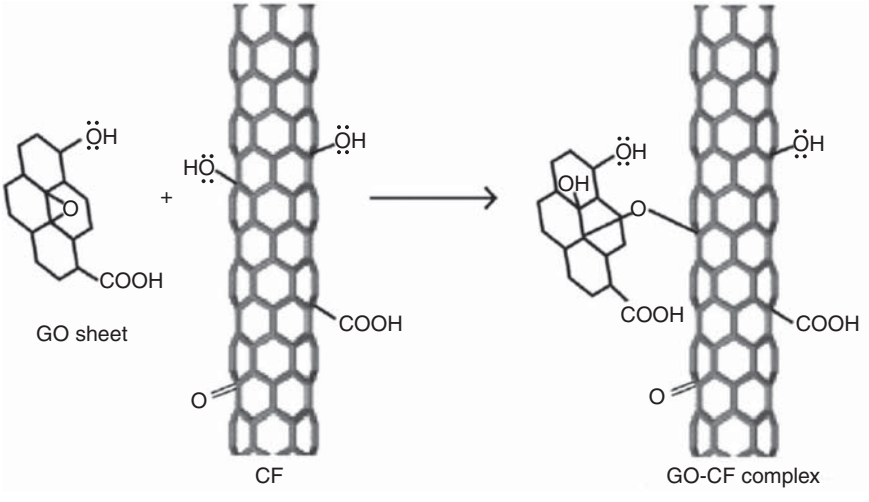

Figure 10.10 Scheme illustrating the mechanism of graphene oxide and carbon fibers reaction (led to linkage to ether bond). Source: Pathak et al. [37]. © 2016, Elsevier.

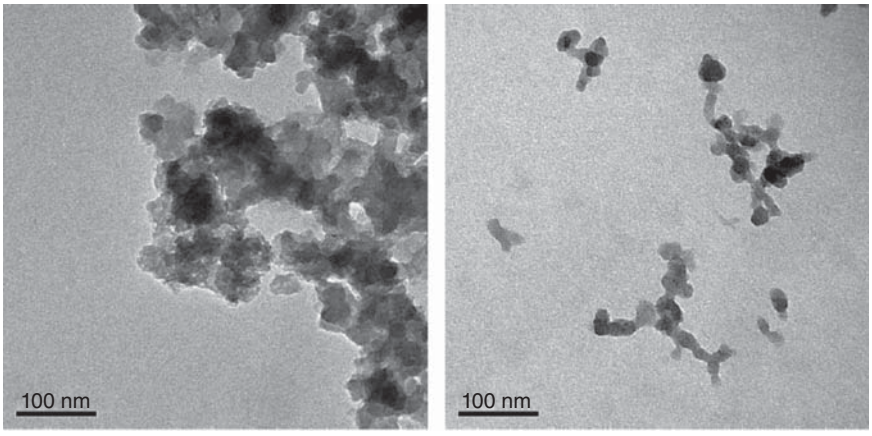

Figure 10.11 TEM photographs of (a) functionalized and (b) non-functionalized silica-reinforced epoxy composites. Source: Constantinescu et al. [16].

modification of silica is of vital importance to exploit its mechanical properties. This surface modification could be attained by coupling functional groups like silane and amine, or grafting another functional nanoparticle such as GO on the surface of silica. Consequently, an ideal chemical interaction between filler and epoxy matrix would be obtained, resulting in higher level of dispersion, modulus, tensile strength, and fracture toughness, compared with epoxy composites reinforced with unmodified silica [14, 16]. Figure 10.11 vividly illustrates the great effect of chemical functionalization of silica on its dispersion promotion. The unmodified particles, on the other hand, are extremely agglomerated which diminish their positive effect in improving mechanical properties to a great extent. As a result, the modified particles are more effective in mechanical properties improvement of final epoxy composite.

Interfacial treatment of fibers is of great benefit to augment the mechanical properties of the resulted composites to a greater degree, since the interaction between organic fibers and epoxy resin is weak. Moreover, the surface treatment of fibers could be examined through morphological studies. Grafting CNTs on CFs is a practical strategy for surface modification, which has been reported in several projects [36, 69]. Li et al. [36] studied the CNTs linkage to the outer area of CFs using SEM images. They incorporated two different grades of CFs. SEM images (Figure 10.12) illustrate a successful grafting of CNTs on the surface of CFs. The presence of CNTs on the surface of fibers provides a high fiber–matrix interaction, tackling the poor bonding of CFs with epoxy resin.

As mentioned before, the carbon-based nanoparticles show strong tendency to agglomeration, which curbs their efficiency with regard to improvement of mechanical properties of epoxy. In this case, chemical modification of nanoparticles would simultaneously simplify their dispersion in epoxy matrix and create chemical interaction between particles and resin. Naderi, Ebrahimi, and coworkers [44] used chemically modified porous graphene (NPG), using carboxyl and amine groups in order to efficiently disperse nanoparticles and solve the problem of brittleness in

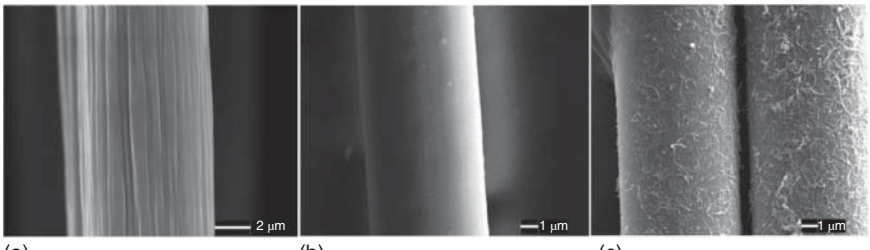

Figure 10.12 SEM photographs of different carbon fibers including: (a) T300B, (b) T700SC, and (c) CNT-modified. Source: Li et al. [36].

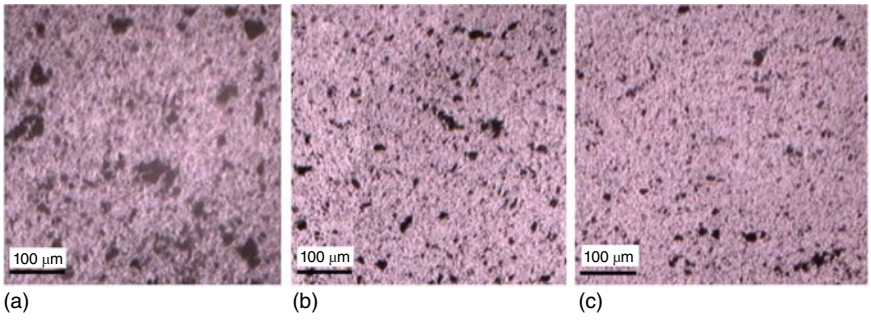

Figure 10.13 The optical microscopy photographs of epoxy nanocomposites filled with 2.0 wt% of (a) NPG, (b) carboxylated NPG, and (c) amine-functionalized NPG. Source: Naderi et al. [44].

cured epoxy, and evaluated the level of dispersion using optical microscopy images (Figure 10.13). It can be inferred from the results that better interfacial adhesion of chemically modified nanoparticles causes higher level of dispersion, which is a critical parameter in modification of mechanical properties. In another study, Guo et al. [66] used three types of CNTs containing different functionalities as reinforcing agents in epoxy matrix. It was concluded that amine-grafted CNT possesses the highest impact strength since it owns brilliant dispersion and interfacial bonding.

10.2.2 Fracture Surface Morphology

Morphological studies of fracture surface (fractographic studies) of epoxy composites are highly beneficial to examine the mechanical properties and fracture toughness. These studies are frequently implemented in addition to further mechanical tests like tensile and/or bending, fracture toughness, and impact to explore the mechanical behavior of epoxy composites profoundly. The fractographic behavior is mostly evaluated using SEM and scrutinizing the fractured surface of composite as well as its crack pattern. As a result of these studies and their relationship with mechanical characteristics, the fracture toughness and the mechanisms that might be contributed to the enhancement of toughness of epoxy composites could be identified. A cured epoxy resin which is not reinforced with fillers typically shows

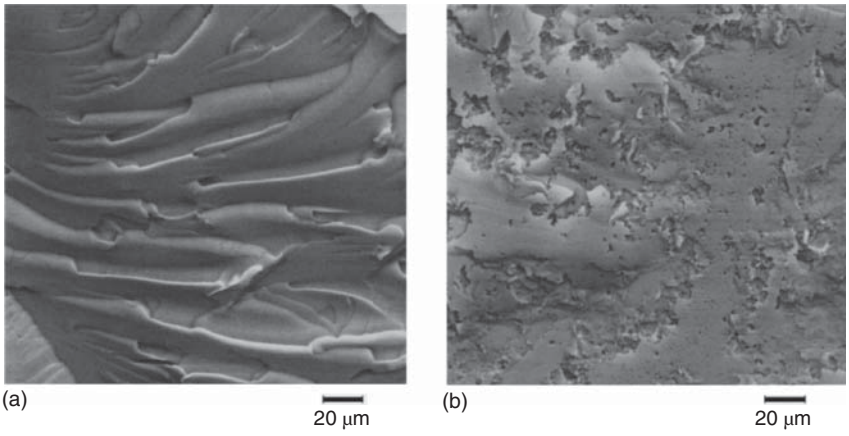

Figure 10.14 SEM photographs of the fracture surfaces in (a) an epoxy resin with no filler and (b) a composite reinforced by 2 wt% of carbon aerogel. Source: Aghabararpour et al. [74].

a brittle fracture behavior, identified by a smooth surface with long elongated and parallel fracture lines, shown in Figure 10.14a. The extended fracture lines are rooted in the highly cross-linked network and brittle behavior of cured epoxy network, representing poor resistance to crack initiation and growth. Using reinforcing fillers generally alters the brittle behavior of epoxy resin by restricting the crack propagation and dissipating the fracture energy. These phenomena proceed to a more rough fracture surface containing disordered crack pattern (Figure 10.14b). The changes in fracture behavior and crack patterns indicate that the epoxy became tougher in the presence of reinforcing agent, which brings about a higher fracture toughness of final composite, and more fracture energy is needed, compared with neat epoxy [13, 44, 54, 56, 74, 75].

Furthermore, the mechanisms of epoxy composites filled with reinforcements could be studied through the morphology of fracture surface. Hsieh et al. [75] studied the toughening mechanism of epoxy-based composites containing carbon aerogel as a reinforcing agent. To this end, they used SEM images of epoxy composite's fracture surface at high magnification (×2000). Crack pinning and crack deflection (bowing) are two possible toughening mechanisms occurring in the presence of filler's agglomerates (Figure 10.15). These two mechanisms efficiently lead to energy absorption, and subsequently, the toughness of epoxy composite would enhance. Using higher magnification of SEM images in the mentioned work, researchers found various voids on the fracture surface of epoxy composite, which are the signs of plastic void growth toughening mechanism. This is the key toughening mechanism regarding improvement of toughness in polymeric composites reinforced with nanoscale particles. The growth of a void in plastic includes the interfacial debonding between the filler particles and the epoxy matrix, and subsequently the plastic distortion of the polymer matrix. Carbon aerogel-reinforced composites may get tougher through the mentioned energy dissipative processes. In a recent study, Aghabararpour, Naderi , and coworkers [74] examined the toughness of

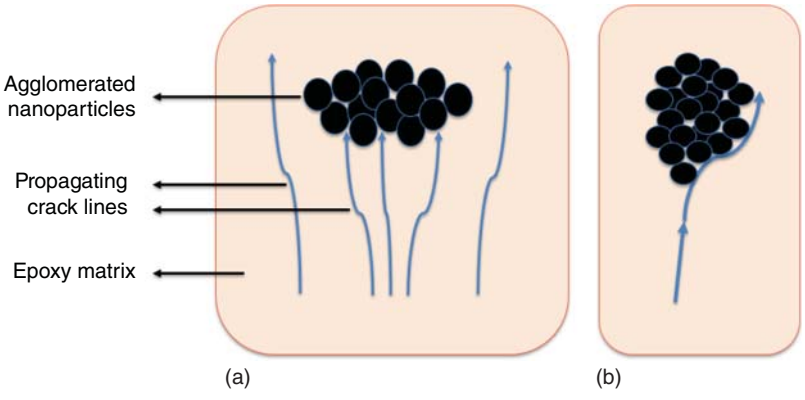

Figure 10.15 Schematics illustrating (a) crack pinning and (b) crack deflection mechanisms in the presence of nanoparticles agglomerates.

epoxy-based composites affected by carbon aerogel. It has been concluded that, in the presence of carbon aerogel particles, the fracture behavior completely changes from a brittle fracture for neat epoxy to a rougher and tougher fracture excluding frequent and elongated fracture lines. The observations were also well in line with the result of tensile analysis, indicating that epoxy composites exhibit larger area under the stress–strain curve (fracture energy in tensile test), in comparison with that of neat epoxy.

In one study, Hsieh et al. [13] investigated how silica nanoparticles influence on toughness of epoxy composites and the possible toughening mechanism. Figure 10.16 illustrates the fracture surfaces of virgin epoxy and the epoxy composite. Neat epoxy shows a smooth fracture surface. The silica-reinforced nanocomposite, however, exhibits a rough surface fracture including various voids around the silica particles. The toughening related to the incorporation of nanoparticles into epoxy matrix stems from the voids created by debonding of filler and matrix, which consequently could undergo the plastic void growth.

Several studies examined the fracture toughening of graphene-reinforced epoxy as one of the most practical fillers [44, 54, 56]. Naderi et al. [54] studied the fracture surface morphology of cured epoxy and its porous graphene-reinforced composite to further understand the fracture behavior and toughening mechanism. Like other epoxy systems, a typical brittle fracture behavior was observed for neat epoxy

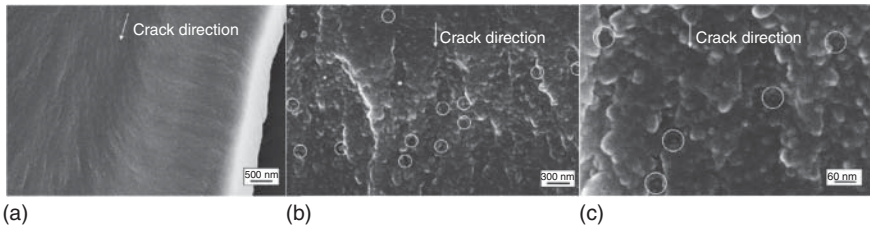

Figure 10.16 SEM photographs showing the fracture surface for (a) an unmodified epoxy, and (b,c) silica-reinforced epoxy. Source: Hsieh et al. [13].

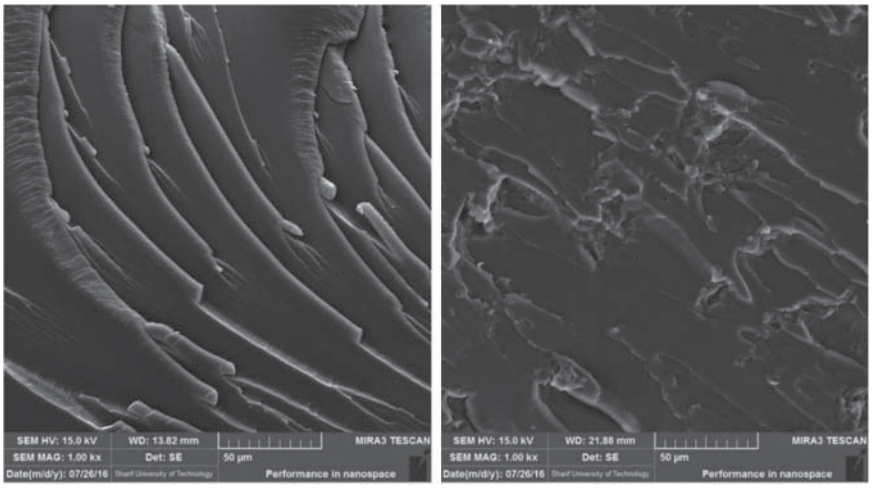

(a) (b)

Figure 10.17 SEM images in micro-scale illustrating the fracture surface for (a) pristine epoxy and (b) porous graphene/epoxy composite. Source: Naderi et al. [54].

(Figure 10.17a), indicating oriented fracture lines initialized from the crazes. The space between uniform fracture lines is highly smooth, representing a fast crack propagation. The graphene-reinforced epoxy composite, on the contrary, shows a coarse and wrinkled surface as well as an irregular and nonuniform crack pattern as a result of crack deflection in graphene-rich regions (Figure 10.17b). When a growing crack encounters a cluster of nanoparticles, it will bow and the crack propagation will be efficiently prevented. This process can lead to an increment in the overall fracture surface area, resulting in a more energy adsorption compared with the pristine epoxy.

Investigation of the fracture surface morphology of fiber-reinforced epoxy composites is a promising technique to study the interfacial adhesion of fibers to the epoxy matrix which is a decisive parameter in mechanical properties improvement of epoxy with fibers. Strong bonding in the interface between fibers and matrix is vital to achieve ideal mechanical properties in epoxy composites. Some recent studies put their emphasis on interfacial modification of CF in order to increase its efficiency as an industrial reinforcing filler for epoxy resin. In some studies, researchers applied CNTs on the surface of CFs to augment the interaction of fiber with the matrix [34–36]. Davis et al. [34] modified CFs with amine-functionalized CNT and studied the effect of CFs' modification on the toughness and interfacial bonding of epoxy composites through morphology of the surface fracture. For epoxy composite filled with non-modified fibers, a brittle fracture of epoxy in the area between fibers was observed (Figure 10.18a). The epoxy composite containing CNT-modified fibers, on the other hand, showed a rough surface and disordered crack pattern in the epoxy phase, representing a tougher fracture behavior (Figure 10.18c). Moreover, using higher magnification of SEM images declared that modified CFs possess higher adhesion to epoxy matrix compared

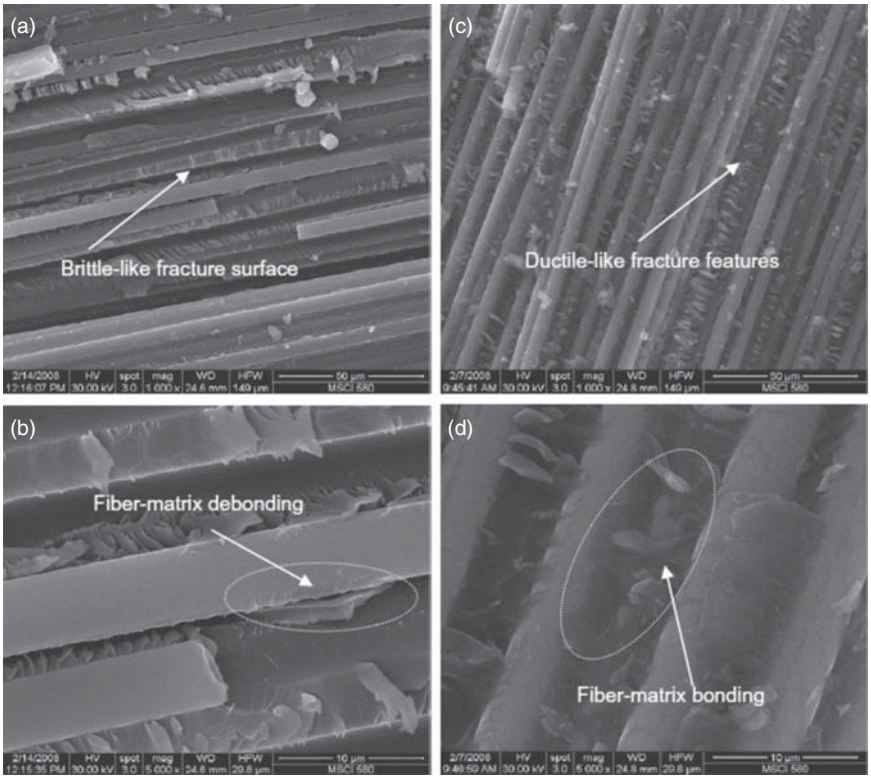

Figure 10.18 Fracture surfaces of specimens failed under tensile test; (a,b) epoxy reinforced with neat carbon fibers, (c,d) epoxy reinforced with modified carbon fibers. Source: Davis et al. [34].

with non-modified ones, due to the excellent physical and chemical interaction of functionalized CNTs on the surface of fibers with epoxy matrix (Figure 10.18b,d). This higher degree of interaction would result in a higher extent of enhancement in mechanical properties (tensile strength and modulus).

In some studies, the surface modification of glass fibers using nanostructures such as cellulose nanocrystal and CNTs has been considered to enhance the surface adhesion of glass fibers and consequently their efficiency in mechanical properties modification [31, 32]. Asadi et al. [32] used cellulose nanocrystals to coat the surface of glass fibers with the aim of increasing the fiber–matrix interaction. To investigate the influence of the surface modification, they performed morphological studies of fracture surfaces of epoxy composites. It could be inferred from the results (Figure 10.19) that modification of glass fibers leads to higher bonding between fibers and epoxy matrix. Figure 10.19 demonstrates the fracture behaviors of epoxy composites filled with modified fibers by simultaneous matrix cracking, fiber breakage, and interfacial debonding of fiber and matrix, implying a high adhesion between fibers and epoxy matrix. Although, the key failure mechanism in epoxy composites reinforced with uncoated glass fibers is fiber–matrix debonding, indicated by vivid pulled-out fibers. This phenomenon stems from the poor interaction between fiber and epoxy.

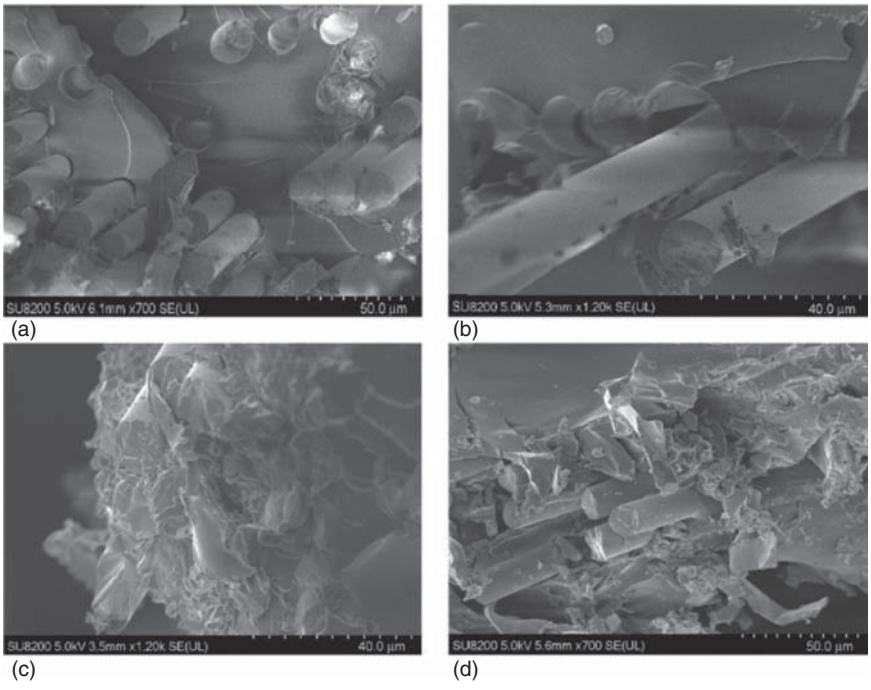

Figure 10.19 SEM photographs showing fracture surfaces of various epoxy-based composites; (a,b) epoxy reinforced with uncoated glass fibers (GF), (c,d) epoxy reinforced with coated GF. Source: Asadi et al. [32].

10.3 Mechanical Properties

10.3.1 Stress–Strain Behavior

The stress–strain properties of epoxy composites are frequently evaluated through tensile and bending tests to determine mechanical parameters including modulus, tensile and flexural strength, elongation at break, and toughness (the area under stress–strain curve). These parameters give valuable information about stiffness, strength, and ductility of the final composites, which are of vital importance in material selection in industrial applications. The slope of the small elastic deformation area in the stress–strain curve is defined as modulus, which describes the rigidity and resistance of material toward deformation. It is assumed that the incorporation of a rigid filler in epoxy matrix would effectively curb the movement of polymer chains and consequently increase the modulus and stiffness of epoxy. Tensile and flexural strength and deformation at break, on the other hand, demonstrate the resistance of material to breakage under tension or bending. The effect of rigid fillers on strength and elongation of epoxy composites is not precise and highly depends on surface interaction between filler and matrix. In several studies, conducted on epoxy composites containing rigid organic or inorganic fillers, it has been revealed that the incorporation of nanofillers, providing only physical

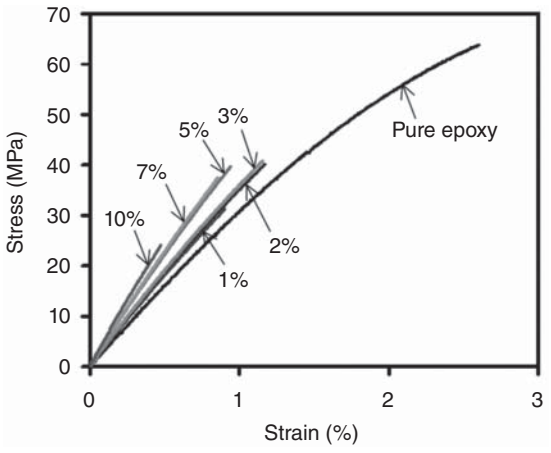

Figure 10.20 Stress–strain performance of nanocomposites containing clay. Source: Yasmin et al. [25]. © 2003, Elsevier.

interaction with epoxy matrix, results in a reduction in strength and elongation at break, or no significant changes were reported. In this case, the most outstanding change is the improvement of modulus and stiffness [21, 25, 33, 54]. Yasmin et al. [25] studied the effect of nanoclay on tensile properties of epoxy composites. The results, as shown in Figure 10.20, illustrate that the addition of nanoparticles considerably ameliorated the modulus. In contrast, the tensile strength as well as elongation at break decreased dramatically, which could be attributed to the poor interfacial adhesion of clay to epoxy matrix. Put differently, it could be affirmed that the composite became more rigid and brittle as a result of clay addition to the system. Same trend has been observed in the epoxy system reinforced with chopped CFs. Although a decrease was observed in tensile strength, tensile and flexural modulus increased substantially when using fibers [33].

The mechanical strength of epoxy nanocomposites is remarkably influenced by chemical bonding between fillers and epoxy matrix. Chemical modification of fillers has been proposed as a useful technique for enhancing the mechanical properties of epoxy nanocomposites because of the higher chemical interaction between fillers and epoxy, compared with non-modified fillers [14, 27, 60, 68, 69]. However, the influence of chemical modification of fillers on the modulus of epoxy composites is varying. Although the modulus of epoxy composite increases with the addition of both modified and unmodified particles, it has been reported that the functional groups of modified reinforcing particles may disturb the curing process of epoxy, resulting in lower efficiency of particles in modulus and stiffness enhancement [44]. In a comparative study, Chen et al. [14] incorporated different silica particles modified with GO and amine groups. Figure 10.21 illustrates the stress–strain plot of epoxy composite systems reinforced with various structures. It is apparent that using raw silica has no significant effect on the tensile strength, and there is just a slight increase in modulus. However, the elongation at break reduces by about 15%. Using modified silica particles, nevertheless, markedly improves the tensile strength as well as the efficiency of particles in enhancing the modulus. Additionally, the GO as a modifier outperforms the amine functionalities in mechanical

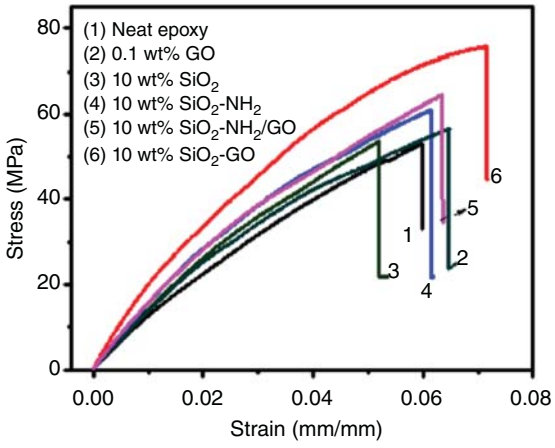

Figure 10.21 Tensile test diagram for pristine epoxy and epoxy-based composites. Source: Chen et al. [14]. © 2012, American Chemical Society.

properties improvement, which could be attributed to the presence of the GO covering the outer area of silica, and perfect placing of GO particles at the interface of silica and the matrix in order to reach utmost efficiency. Furthermore, the filler content should be controlled to gain the optimum mechanical properties. At higher loadings of nanofillers, the particle may become agglomerated, causing reduction in tensile properties [60]. Studies conducted by Cha et al. [68] and Roy et al. [69] have shown that chemical modification of CNTs using functional groups promotes the effectiveness of nanotubes in improving young modulus and tensile strength.

The ductility of epoxy composites could be investigated via stress–strain analysis. The energy required to break samples during the tensile test is defined as toughness which could be determined by the area under the stress–strain graph. Normally, lower toughness indicates higher brittleness, which brings about less breakage resistance [82]. Several studies devoted their attention to the toughness improvement of epoxy and tackling its remarkable drawback (brittleness) through the incorporation of functional fillers. Tensile analysis and the area under the stress–strain curve could successfully examine the effect of nanofillers on the toughness of epoxy. Naderi, Ebrahimi, and coworkers [44] incorporated functionalized porous graphene to ameliorate the toughness of epoxy through chemical reaction between functional groups of modified graphene with epoxy resin. Functionalized nanoparticles could have various influences on epoxy network such as movement limitation of polymer chains as a result of both physical and chemical interactions with epoxy matrix, higher degree of dispersion in the epoxy matrix, and interference in the curing process of epoxy by unbalancing the stoichiometry of the curing reaction, resulting in less cross-linking and higher free volume. There is always a rivalry between these possible effects, which determine the ultimate properties of produced nanocomposite. Table 10.2 gives information about the tensile properties as well as the toughness (area under stress–strain curve) of epoxy composites reinforced with raw and functionalized nanoparticles. The results declare that modified particles would effectively enhance the elongation (flexibility) and toughness of epoxy composites. However, the non-functionalized porous graphene diminishes the toughness and

Table 10.2 Table showing mechanical properties of the pristine epoxy and epoxy-based nanocomposites reinforced with porous graphene (NPG), carboxylated porous graphene (CNPG), and amine-functionalized porous graphene (ANPG).

Sample	Modulus (GPa)	Tensile strength (MPa)	Elongation (%)	Toughness (MPa)
ER-Neat	1.75	45.6	2.6	0.6113
ER-0.5% NPG	2.15	45.9	2.1	0.5026
ER-1% NPG	2.83	49.3	2.0	0.5538
ER-2% NPG	2.86	47.7	1.8	0.4597
ER-0.5% CNPG	2.14	46.8	4.43	1.3074
ER-1% CNPG	2.24	51.83	4.40	1.5471
ER-2% CNPG	2.43	61.76	3.69	1.2944
ER-0.5% ANPG	2.1	44.19	5.23	1.6944
ER-1% ANPG	2.12	47.41	5.61	1.9826
ER-2% ANPG	1.99	59.32	5.42	2.1882

Source: Naderi et al. [44]. © 2019, John Wiley & Sons.

efficiently enhances the modulus, making the composite stiffer and more brittle, which is rooted in restricting effect of graphene sheets on polymer chains movement. The toughness and flexibility improvement of epoxy composites reinforced with modified porous graphene could be ascribed to the high chemical linkage between filler and matrix, and disturbance in curing process, increasing the free volume and toughness of final composites.

10.3.2 Fracture Toughness

Fracture toughness indicates a material's potential of resistance to fracture in the presence of a crack, which is very essential to design the ultimate application of a material. Stress intensity factor (K) is exploited for determining the fracture toughness of a material (K_{Ic}) at the point of a crack propagation. The fracture energy (G_{Ic}) could also be calculated from K_{Ic} and modulus (E). It is frequently reported that introduction of a reinforcing filler in epoxy causes increment in fracture toughness and fracture energy values, resulting in the matrix to be toughened. There are different possible reasons to this toughness enhancement, known as toughening mechanisms. Crack pinning, crack deflection, and plastic void growth have been suggested as toughening mechanisms for epoxy composites. Ultimately, it is expected that the presence of filler particles prevents crack propagation and enhances fracture toughness. There are various studies conducted to explore the toughening effect of inorganic fillers on epoxy composites, reporting the effective fracture toughness improvement of composites by adding fillers [11, 13, 20, 21, 24]. Zhang et al. [21] studied the fracture toughness of epoxy composites based on alumina nanofillers' content. It was observed that addition of alumina would significantly promote both fracture toughness (K_{Ic}) and fracture energy (G_{Ic}), and

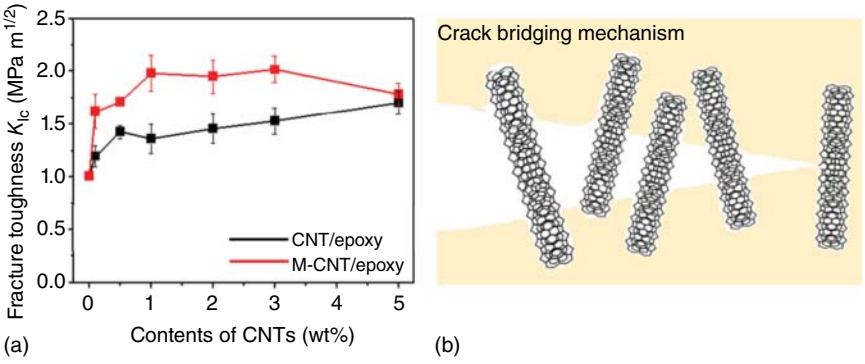

Figure 10.22 Fracture toughness of neat epoxy, CNT/epoxy, and M-CNT/epoxy composites and schematic of crack bridging toughening mechanism. (a) Fracture toughness of neat epoxy, CNT/epoxy, and M-CNT/epoxy composites. (b) Schematic of crack bridging toughening mechanism. Source: Cha et al. [68]. © 2017, Elsevier.

consequently the material became more ductile. It is also claimed that inorganic fillers would increase the fracture toughness more effectively, when an efficient mixing is achieved by using high shear mixing techniques [24].

Over past few years, researchers have studied the fracture toughness of epoxy composites reinforced with carbon-based fillers, implying the high efficiency of these fillers in fracture toughness improvement of epoxy composites, especially those providing functional groups in their nanostructures [55–57, 60, 68, 75]. Cha et al. [68] used raw CNT and melamine-treated carbon nanotube (M-CNT) as reinforcements to enhance the toughness of epoxy composites. Figure 10.22 obviously shows that both nanostructures have an increasing impact on fracture toughness, which is caused by nanoparticle agglomerates hindering the crack propagation. However, the modified CNT outperforms raw CNT in toughness improvement of epoxy resin, which could be due to the potential of functionalized nanotubes to undergo the crack bridging mechanism (schematically shown in Figure 10.22) along with other common mechanisms proposed for nanomaterials due to the amine groups' attachments to the surface of nanofillers, which can take part in chemical interaction with epoxy matrix. Hsieh et al. [75] and Chhetri et al. [60] used carbon aerogel and functionalized graphene, respectively, in order to improve the mechanical properties and toughness of epoxy composites. They reported dramatic enhancement of fracture toughness (more than 100%), which is highly vital to tackle the brittleness of epoxy resin.

10.3.3 Impact Properties

Impact strength is another critical mechanical characteristic of polymeric materials in industrial applications, which demonstrates the energy needed to fracture a sample by a sudden impact. Impact test of epoxy composites is performed to study the impact resistance and toughness, in other words, the ability of composite to absorb energy during plastic deformation. Cured epoxy resins typically have low

impact strength and toughness due to their highly cross-linked network and brittle nature. Application of reinforcing fillers including graphene, CNT, carbon aerogels, alumina, glass fibers, etc. is an efficient means to combat brittleness and improve the impact energy absorption as well as toughness of epoxy resin, which has been studied through impact analysis (mostly izod and charpy tests) in several studies [18, 30, 44, 66, 74]. It is worth mentioning that a perfect chemical interaction between filler and matrix is needed to exploit the impact properties of reinforcing agent efficiently. Instead, the rigid fillers which only provide physical interaction with epoxy matrix might make epoxy even more brittle, exhibiting lower impact strength. In two different studies, Naderi et al. [44, 54] showed that incorporation of nonfunctionalized porous graphene (NPG) makes epoxy-based composite more stiff and brittle and could decrease the impact strength. Despite this, they claimed that the chemical functionalization of porous graphene using carboxyl (CNPG) and amine groups (ANPG) results in the filler particles to act effectively as a toughener. As a result, the impact strength was promoted dramatically (Figure 10.23), implying the crucial importance of filler-matrix chemical interaction in toughness and impact strength improvement. Moreover, the results were well in accordance with the results obtained by tensile test and fracture surface morphology, in which the composites containing functionalized nanofillers exhibited high toughness (the area under stress-strain curve) and rough fracture surface. Khanbabaei et al. [26] also reported a reduction in impact energy for epoxy composites reinforced with clay particles with filler contents of 1, 2, and 3 wt%.

Guo et al. [66] also declared that CNTs containing amine groups could promote the impact strength of epoxy by about 300%. This astonishing enhancement in impact properties was assigned to the linkage between CNTs and epoxy resin through chemical reaction of epoxy and amine groups. As a consequence, the deformation ability

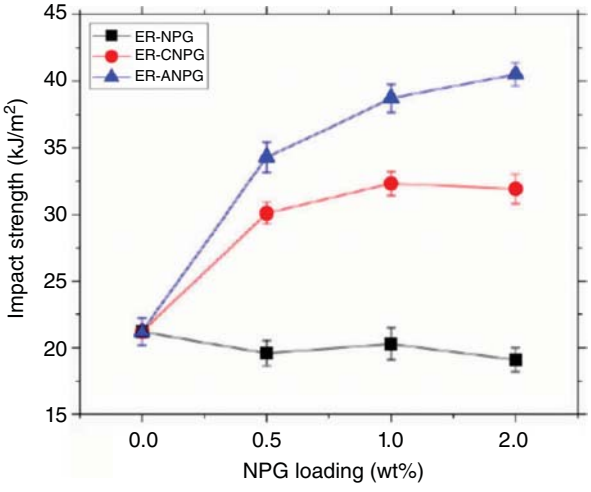

Figure 10.23 Curves of impact strength for virgin epoxy and epoxy-based nanocomposites containing various contents of NPGs, carboxylated NPGs, and amine-functionalized NPGs. Source: Naderi et al. [44]. © 2019, John Wiley & Sons.

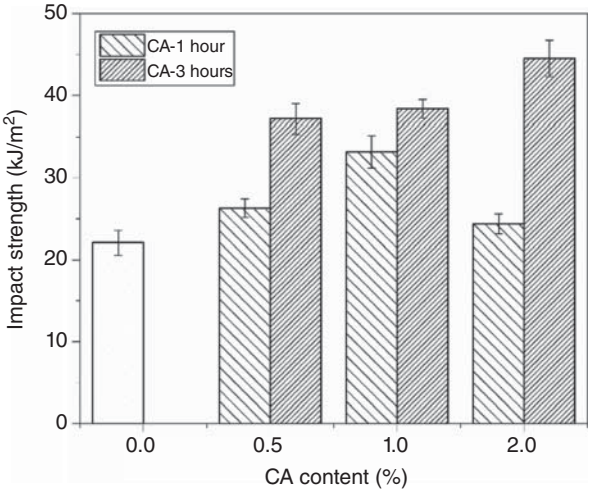

Figure 10.24 Chart of impact strength for epoxy resins reinforced with various contents of carbon aerogels. Source: Aghabararpour et al. [74]. © 2019, Springer Nature.

of matrix increased, resulted in an extremely higher impact strength in comparison with that of virgin epoxy. It is also claimed that carbon aerogels, due to their specific geometry, would act as a toughener for epoxy systems, which could promote the toughness and fracture resistance of epoxy [74, 75]. Figure 10.24 illustrates the effect of carbon aerogels with different pyrolysis times on the impact properties. The carbon aerogel with higher pyrolysis duration (three hours), named CA-3 h, shows higher efficiency in improving impact resistance, since it owns greater specific area, compared with carbon aerogel with one hour of pyrolysis (CA-1 h). It is also declared that CA-3 h considerably improves tensile strength and toughness of epoxy resin as well, making this structure a novel reinforcement in composite applications. In conclusion, physical interaction between filler and matrix, caused by the specific surface area of nanoparticles, is another factor affecting their effectiveness in mechanical properties improvement.

10.3.4 Dynamic Mechanical Properties

Characterization of epoxy composite through dynamic mechanical analysis (DMA) has been reported frequently. This is a frequently applied method for studying the viscoelastic behavior of polymers and polymer composites. In epoxy systems, DMA is of great help to study the stiffness and glass transition temperature of composites. Moreover, valuable information about the epoxy cured network including changes in cross-linking density and free volume could be obtained. The mentioned investigations are performed by the parameters achieved from DMA. The storage modulus (E') is a mechanical property that measures the recoverable stored strain energy, which indicates how much load a material could bear. E' shows a decreasing trend by temperature increment, experiencing a rapid drop near the glass transition region.

This phenomenon stems from the high molecular mobility of the polymer chains near glass transition temperature (T_g). The loss modulus (E'') is a measure of the energy dissipated under deformation, generally lost as heat, which is related to the viscous nature of the material. Tan δ or loss factor is defined as the ratio of the loss modulus to the storage modulus, representing the damping properties of material. Numerous techniques are used for measuring the glass transition temperature of polymers, though the dynamic mechanical testing is the most reliable technique since T_g could be estimated by the peak of tan δ or loss modulus. Tan δ peak is a good measure of leather-like midpoint between the glassy and rubbery states, which is mostly used by researchers to determine T_g. The higher the T_g, the more stiff and rigid a material will be. High T_g in epoxy resin is caused by its highly cross-linked network, and accordingly its low free volume.

Researchers have reported phenomenal findings regarding dynamic mechanical behavior of inorganic filler-reinforced epoxy-based composites. It has been shown that the incorporation of inorganic fillers like silica and alumina in epoxy composites increases the storage modulus, which could be predicted, since rigid fillers have the ability to restrict the motion of epoxy chains [14, 19, 21]. In some systems, the reduction of glass transition temperature is reported as a result of adding inorganic fillers into epoxy matrix, which seems to be contradictory and should be further investigated. Chen et al. [14] used different types of silica as reinforcing fillers including silica (SiO_2), amine-modified silica (SiO_2-NH_2), and GO-modified silica (SiO_2-GO) to investigate the mechanical properties of epoxy composites. All inorganic-based fillers improved the storage modulus and T_g as expected (Figure 10.25), and SiO_2-GO had the most efficiency in modulus enhancement due to its high physical and chemical interaction with epoxy matrix. On the other hand, the epoxy reinforced with SiO_2-GO had the lowest T_g among composites reinforced with inorganic fillers. This contrary result could be rooted in the participation of GO in curing process of epoxy resin. Although the GO sites on the SiO_2-GO as a rigid filler effectively curb the movements of epoxy chains and

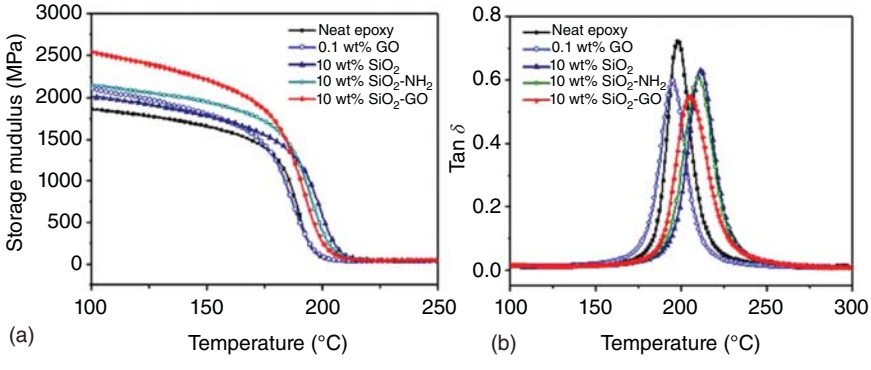

Figure 10.25 Curves illustrating dynamic mechanical properties of virgin epoxy and reinforced epoxy-based composites: (a) storage modulus, (b) damping spectra (tan δ). Source: Chen et al. [14]. © 2012, American Chemical Society.

increase the stiffness of composite due to its chemical interaction with epoxy resin, it can change the stoichiometry of curing process and alter the cured epoxy network at the GO–epoxy interface. Subsequently, the interference of GO in curing process could reduce the cross-linking density and increase the free volume of final epoxy network, leading to lower T_g of SiO_2-GO/epoxy composite, compared with that of SiO_2/epoxy composite. The reduction in T_g of epoxy using high loadings (13.1 and 18.4 wt%) of nanoalumina is also reported by Zhang et al. [21], despite the storage and young modulus enhancement. It is stated that at high nanofillers content, partial epoxy prepolymer is likely to be absorbed by the interface of nanofillers, causing the stoichiometric mismatching of epoxy and curing agent. Consequently, the cross-linking density would decline, lowering the T_g of final composite.

In numerous recent studies, various nanocarbons like graphene, GO, and CNTs are recommended as efficient modifiers to improve the dynamic mechanical properties of epoxy resin. Generally, the incorporation of these nanostructures limit epoxy chain movement, which brings about a rise in the storage modulus and glass transition temperature [54–56, 59, 69]. Naderi et al. [54] claimed that adding porous graphene as an innovative reinforcing agent with high specific surface area in epoxy matrix significantly increases the modulus and T_g of the final composite. Roy et al. [69] applied four types of CNT with different functionalities including raw CNT, CNT-OH, CNT-ODA, and CNT-COOH as modifiers in epoxy composite systems. It was concluded that different functionalities of CNT structure have diverse effects on the cross-linked network of epoxy, and various values of T_g are achieved for each individual system. Addition of raw CNT increased the T_g of epoxy by approximately 18 °C. CNT-OH promoted T_g even more efficiently, though the CNT-ODA and CNT-COOH were less effective in enhancing T_g. These findings are attained by the way functional groups interact with epoxy chains. Figure 10.26a demonstrates how CNT-OH could restrict the mobility of an epoxy chain. Besides, Figure 10.26(b–d) illustrate the chemical (Figure 10.26b and c) and physical (Figure 10.26d) interactions between epoxy chains and other CNT structures. The lower efficiency of CNT-ODA in improving T_g, despite its superior interaction between amine groups of CNT and epoxy, could be due to the existence of bulky $C_{18}H_{37}$ groups, which prevents the jammed packing of polymer chains, bring about higher free volume. In addition, the lower enhancement of T_g in the case of CNT-COOH is rooted in the fact that its acid groups adsorb the curing agent in a preferential manner, causing a non-stoichiometric balance in the curing reaction. This stoichiometric mismatching results in lower cross-linking density of final cure network. Naderi, Ebrahimi, and coworkers [44] also reported the same findings. They used functionalized nanoporous graphene with the aim of improving effective toughness without any decline in modulus and stiffness and applied DMA to study the cured epoxy network. It was observed that composites reinforced with carboxylated and amine-functionalized porous graphene exhibit less T_g as compared with composites containing raw porous graphene, implying the toughening effect of functionalized nanofillers on epoxy as a result of functional groups

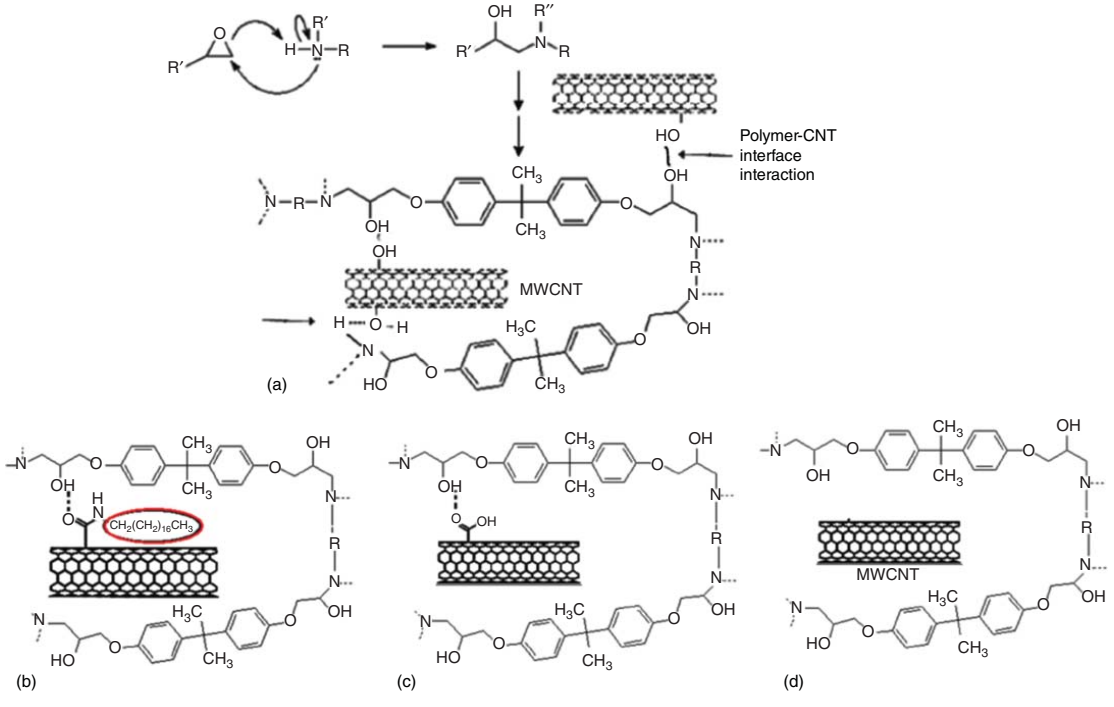

Figure 10.26 Schematic of nanoparticles' interactions with epoxy and curing agent. (a) CNT-OH, (b) CNT-ODA, (c) CNT-COOH, and (d) raw CNTs. Source: Roy et al. [69]. © 2018, De Gruyter.

interference in the curing process, and decreasing cross-linking density. Moreover, Ribeiro et al. [59] used GO and aminated graphene oxide (AGO) with the aim of promoting the mechanical properties of epoxy. They found that functionalized GO is more efficient to augment the T_g of epoxy, due to high chemical interaction between amine groups of filler with epoxy resin, which could further restrict the polymer chain movements. However, in some systems, the negative effect of using functionalized nanofillers on T_g (mismatching the stoichiometry of curing process) overcome their reinforcing effect [48, 61]. Ferreira et al. [61] showed that although using GO and AGO considerably increased the storage modulus of epoxy, it would diminish the T_g of composite as a result of functional groups' interference in curing process and enlarging free volume. In addition, damping values ($\tan\delta$) of epoxy composites reinforced with GO and AGO were lower than that of neat epoxy. The addition of nanofillers in epoxy system would change damping behavior, and a good adhesion between filler and matrix as well as mobility restriction of polymer chains by fillers could decrease the damping.

10.3.5 Lap Shear Properties

Epoxy resins have found extensive applications in adhesive and coating industries. Therefore, their adhesion to different surfaces is very important. Lap shear strength is another critical mechanical parameter of epoxy resin, which indicates the shear properties of epoxy as a measure of its adhesion to a surface. This issue should be carefully investigated regarding adhesive and coating application. Several researches have examined the effect of reinforcing fillers on the lap shear strength of epoxy composites [83–86]. The shear strength of adhesive joints is determined by using a simple tensile testing of two metal panels, which are jointed together with epoxy composites as adhesive. Figure 10.27. illustrates the schematic of an example sample in lap shear joint test. Jojibabu et al. [84] applied three different carbon-based fillers naming CNTs, GNPs, and carbon nanohorns to examine the rheological and lap shear properties of epoxy resins used as adhesives. The results showed an approximate increment of 50% in the lap shear strength of epoxy resin just by adding 0.5 wt% of these carbon-based fillers (Figure 10.28). The increase of joint strength properties could be ascribed to the reinforcing effect of nanofillers due to their perfect interaction with epoxy matrix, resulting in high shear properties. However, higher filler loadings diminish the lap shear strength, due to severe agglomeration of carbon fillers. Consequently, the filler content should be controlled to achieve optimum mechanical properties.

In an investigation, Mansourian-Tabaei et al. [83] incorporated nanoalumina and MWCNT to improve the lap shear properties of epoxy composites. The results illustrated that both mentioned nanostructures were efficiently able to promote the lap shear strength of epoxy resin because of their specific geometries and interactions with epoxy matrix.

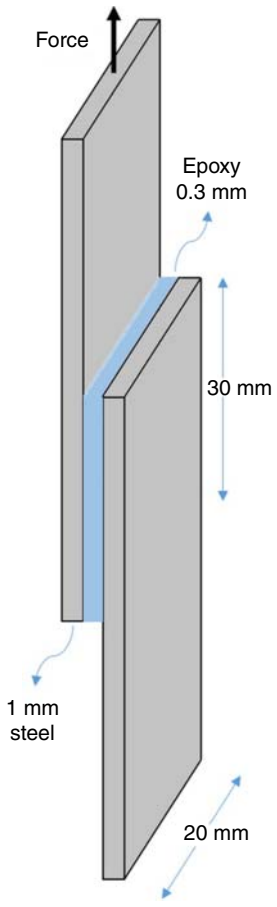

Figure 10.27 Schematic presentation of a regular sample used in lap shear joint test. Source: Naderi et al. [86]. © 2019, John Wiley & Sons.

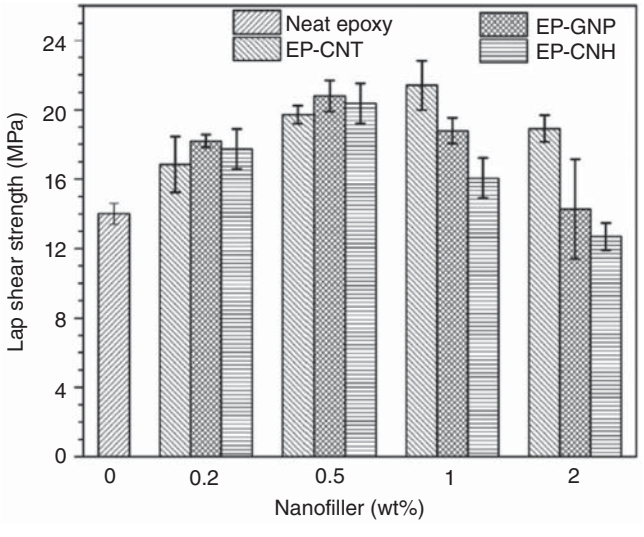

Figure 10.28 Lap shear strengths of epoxy adhesive joints with different weight percentages of nanocarbon. Source: Jojibabu et al. [84]. © 2016, Elsevier.

10.4 Conclusions and Outlooks

This chapter is aimed to discuss the morphological and mechanical properties of epoxy composites reinforced with various fillers. Epoxy resins, despite their fascinating mechanical, thermal, and anticorrosion properties, suffer high brittleness caused by highly cross-linked network of epoxy resin. Incorporation of reinforcing agents including inorganic fillers, fibers, and carbon-based nanomaterials into epoxy resin has been proposed to ameliorate the mechanical properties of epoxy in addition to its essential properties considering the industrial applications such as corrosion resistance, electrical and thermal conductivity, thermal stability, and so on. Consequently, the industrial application of epoxy composites has been developing at a staggering rate during past few decades. Moreover, the addition of functional fillers could successfully tackle high brittleness of epoxy and enhance its toughness without any reduction in its stiffness, which is of chief importance, industrially. Despite all superior characteristics of epoxy-based composites reinforced with various fillers, it is worth noting that numerous elements related to fillers considerably influence the ultimate properties of epoxy-based composite, and different fillers provide epoxy matrix with varying properties based on their individual characteristics. For instance, fillers' loading, geometry, specific surface area, and functional groups, etc. could precisely affect the ultimate properties of epoxy composites. Subsequently, the mentioned parameters should be considered intently in order to fully exploit the fillers' efficiency in mechanical properties improvement and achieve the optimum properties.

Fine dispersion of reinforcing fillers in epoxy resin and establishing high interaction with polymeric matrix are critical to effectively adjust the mechanical properties. In this direction, a number of techniques address poor processability of fillers in viscous matrices of epoxy, including application of high shear mixing techniques and novel scenarios, matrix modification using (reactive) diluents and rigid nanoparticles, and chemical modification of fillers. Researchers frequently have implemented chemical modification of different categories of fillers to augment the interfacial adhesion between fillers and matrix to achieve higher mechanical enhancement. Additionally, poor dispersion and filler–matrix interaction could also influence the mechanical properties inversely. In some systems, it has been found that poor dispersion of fillers in epoxy matrix results in lower mechanical properties in comparison with the neat epoxy. The fillers' dispersion as well as their interaction with matrix could be evaluated through morphological investigations. Also, comparative morphological studies of fracture surface of neat epoxy and epoxy nanocomposites have revealed that incorporation of nanofillers in epoxy matrix can effectively alter the fracture behavior of epoxy from a typical brittle behavior for neat epoxy, shown by a smooth fracture surface with elongated fracture lines, to a tougher fracture behavior, displaying rough fracture surface and disordered crack pattern. This toughening, which is a result of nanoparticles addition, is caused by different mechanisms including crack deflection, crack pinning, and plastic void growth induced by filler–matrix debonding. These energy dissipative processes increase the toughness and flexibility of epoxy composites. It is worth mentioning

that there is a relationship between morphology of the fracture surface and the results obtained by mechanical testing methods such as tensile and impact tests. It is reported in several studies that composites with a tougher fracture behavior show higher fracture toughness and impact resistance.

Looking through literatures, it has been found that the effect of reinforcing fillers on the mechanical properties of epoxy-based composites is often examined by different mechanical analyses such as tensile, bending, impact, fracture toughness, and dynamic mechanical tests. Introducing rigid fillers into epoxy matrix promotes the stiffness and rigidity of the epoxy composites, indicated by an increment in tensile modulus, storage modulus, and T_g. However, the effect of fillers on mechanical strength, elongation at break, impact resistance, and toughness of epoxy is not precise and mainly depends on the chemical interaction between fillers and epoxy matrix. As a promising technique, the chemical modification of reinforcing fillers using functional groups and nanoparticles has been suggested in numerous studies in order to improve the flexibility, toughness, and strength of epoxy composites, which are known as crucial factors in terms of industrial applications of epoxy resin. Epoxy groups, provided by epoxy resin, have the potential to react with several functional groups like amine, carboxyl, and hydroxyl groups. Accordingly, the chemical modification of fillers using mentioned groups effectively improves their interaction with epoxy matrix, which can lead to the improvement of modulus and stiffness as well as toughness and flexibility of epoxy composites, simultaneously.

Recently, the use of carbon-based nanomaterial in epoxy-based composite applications has been developing at a staggering rate because of their distinct characteristic such as superior specific surface area, special geometries, high filler–matrix interaction, electrical conductivity, thermal and barrier properties, and so on. The specific characteristics of carbon nanofillers make them more effective regarding mechanical properties enhancement compared with other conventional inorganic fillers. These nanostructures including graphene, GO, CNTs, and carbon aerogels can remarkably fulfill our expectations in mechanical properties improvement of epoxy, particularly when supreme degree of dispersion and high filler–matrix interaction are achieved. It is frequently reported that the functionalized carbon-based nanomaterials could considerably strengthen several mechanical properties of epoxy composites including tensile and flexural modulus, strength, fracture toughness, impact resistance, and glass transition temperature. Nevertheless, in some systems in which functionalized carbon nanomaterials were used as a toughener, reduction in T_g was obtained.

The reason for this phenomenon could be ascribed to the fillers' functional sites interfering in the process of epoxy curing, causing an unbalance in the stoichiometry of curing reaction, which proceeds to a lower cross-linking density and higher free volume. As a result, the epoxy composite becomes tougher and T_g diminishes.

It is expected that production of novel and cost-effective nanostructures with distinct functionalities and geometries will develop the industrial applications of epoxy composites in further high-tech fields. For instance, carbon aerogels as novel carbon-based nanomaterials have been recently introduced into epoxy composites. These cost-effective nanostructures are developed for energy-related

applications due to their high porosity. Not only the mechanical properties of epoxy will be increased through the addition of these novel nanomaterials which also fulfill the decent industrial mechanical properties, but also they can widen the application of epoxy composites in high-tech and energy-related fields, like coatings of state-of-the-art aircrafts, electronic fields, and so on.

References

1 Ellis, B. (1993). *Chemistry and Technology of Epoxy Resins*. Springer.
2 Ratna, D. (2009). *Handbook of Thermoset Resins*. Smithers Rapra Technology.
3 Pourhashem, S., Vaezi, M.R., Rashidi, A., and Bagherzadeh, M.R. (2016). Exploring corrosion protection properties of solvent based epoxy-graphene oxide nanocomposite coatings on mild steel. *Corrosion Science* [Internet] 115: 78–92. https://doi.org/10.1016/j.corsci.2016.11.008.
4 Liu, D., Zhao, W., Liu, S. et al. (2015). Comparative tribological and corrosion resistance properties of epoxy composite. *Surface and Coating Technology* [Internet] 286: 354–364. https://doi.org/10.1016/j.surfcoat.2015.12.056.
5 Li, P., Zheng, Y., Li, M. et al. (2016). Enhanced toughness and glass transition temperature of epoxy nanocomposites filled with solvent-free liquid-like nanocrystal-functionalized graphene oxide. *Materials & Design* 89: 653–659.
6 Wei, J., Vo, T., and Inam, F. (2015). Epoxy/graphene nanocomposites – processing and properties: a review. *RSC Advances* [Internet] 5: 73510–73524. http://pubs.rsc.org/en/content/articlelanding/2015/ra/c5ra13897c%5Cn; http://pubs.rsc.org/en/content/articlelanding/2015/ra/c5ra13897c#!divAbstract.
7 Liu, S., Yan, H., Fang, Z., and Wang, H. (2014). Effect of graphene nanosheets on morphology, thermal stability and flame retardancy of epoxy resin. *Composites Science and Technology* 90: 40–47.
8 Carolan, D., Ivankovic, A., Kinloch, A.J. et al. (2016). Toughening of epoxy-based hybrid nanocomposites. *Polymer (United Kingdom)* 97: 179–190.
9 Young, R.J. and Beaumont, P.W.R. (2004). Failure of brittle polymers by slow crack growth. *Journal of Materials Science* 10 (8): 1343–1350.
10 Nakamura, Y., Yamaguchi, M., Okubo, M., and Matsumoto, T. (1992). Effect of particle size on the fracture toughness of epoxy resin filled with spherical silica. *Polymer (Guildf).* 33 (16): 3415–3426.
11 Kinloch, A.J., Mohammed, R.D., Taylor, A.C. et al. (2006). Erratum to: the effect of silica nano particles and rubber particles on the toughness of multiphase thermosetting epoxy polymers. *Journal of Materials Science* 41 (4): 1293–1293.
12 Ahmad, T., Mamat, O., and Ahmad, R. (2013). Studying the effects of adding silica sand nanoparticles on epoxy based composites. *Journal of Nanoparticles* 2013: 1–5.
13 Hsieh, T.H., Kinloch, A.J., Masania, K. et al. (2010). The mechanisms and mechanics of the toughening of epoxy polymers modified with silica nanoparticles. *Polymer (Guildf).* 51 (26): 6284–6294.

14 Chen, L., Chai, S., Liu, K. et al. (2012). Enhanced epoxy/silica composites mechanical properties by introducing graphene oxide to the interface. *ACS Applied Materials & Interfaces* 4 (8): 4398–4404.

15 Antonelli, C., Serrano, B., Baselga, J. et al. (2015). Interfacial characterization of epoxy/silica nanocomposites measured by fluorescence. *European Polymer Journal* 62: 31–42.

16 Constantinescu, D.M., Apostol, D.A., Picu, C.R. et al. (2017). Mechanical properties of epoxy nanocomposites reinforced with functionalized silica nanoparticles. *Procedia Structural Integrity* [Internet] 5: 647–652. https://doi.org/10.1016/j.prostr.2017.07.034.

17 Lange, F.F. and Radford, K.C. (1971). Fracture energy of an epoxy composite system. *Journal of Materials Science* 6 (9): 1197–1203.

18 Fu, S.Y., Feng, X.Q., Lauke, B., and Mai, Y.W. (2008). Effects of particle size, particle/matrix interface adhesion and particle loading on mechanical properties of particulate-polymer composites. *Composites Part B: Engineering* 39 (6): 933–961.

19 Johnsen, B.B., Frømyr, T.R., Thorvaldsen, T., and Olsen, T. (2013). Preparation and characterisation of epoxy/alumina polymer nanocomposites. *Composite Interfaces* 20 (9): 721–740.

20 Wang, K., Ogier, P., Tjiu, C.W., and He, C. (2009). Morphology and mechanical properties of epoxy/alumina nanocomposites. *Key Engineering Materials* 312: 233–236.

21 Zhang, H., Zhang, H., Tang, L. et al. (2010). The effects of alumina nanofillers on mechanical properties of high-performance epoxy resin. *Journal of Nanoscience and Nanotechnology* 10 (11): 7526–7532.

22 Mishra, S.K., Shukla, D.K., and Patel, R.K. (2018). Flexural properties of functionally graded epoxy-alumina polymer nanocomposite. *Materials Today: Proceedings* [Internet] 5 (2): 8431–8435. https://doi.org/10.1016/j.matpr.2017.11.538.

23 Azeez, A.A., Rhee, K.Y., Park, S.J., and Hui, D. (2013). Epoxy clay nanocomposites – processing, properties and applications: a review. *Composites Part B: Engineering* [Internet] 45 (1): 308–320. https://doi.org/10.1016/j.compositesb.2012.04.012.

24 Zabihi, O., Ahmadi, M., Nikafshar, S. et al. (2018). A technical review on epoxy–clay nanocomposites: structure, properties, and their applications in fiber reinforced composites. *Composition Part B: Engineering* 135: 1–24.

25 Yasmin, A., Abot, J.L., and Daniel, I.M. (2003). Processing of clay/epoxy nanocomposites by shear mixing. *Scripta Materialia* 49, 81 (1 Special): –6.

26 Khanbabaei, G., Aalaie, J., Rahmatpour, A. et al. (2007). Preparation and properties of epoxy–clay nanocomposites. *Journal of Macromolecular Science, Part B: Physics* 46 (5): 975–986.

27 Chan, M.L., Lau, K.T., Wong, T.T. et al. (2011). Mechanism of reinforcement in a nanoclay/polymer composite. *Composites Part B: Engineering* 42 (6): 1708–1712. https://doi.org/10.1016/j.compositesb.2011.03.011.

28 Kusmono, Wildan, M.W., and Mohd Ishak, Z.A. (2013). Preparation and properties of clay-reinforced epoxy nanocomposites. *International Journal of Polymer Science* 2013: 1–7.

29 Gershon, B. and Marom, G. (1975). Fracture toughness and mechanical properties of glass fibre–epoxy composites. *Journal of Materials Science* 10 (9): 1549–1556.

30 Sathishkumar, T.P., Satheeshkumar, S., and Naveen, J. (2014). Glass fiber-reinforced polymer composites – a review. *Journal of Reinforced Plastics and Composites* 33 (13): 1258–1275.

31 Godara, A., Gorbatikh, L., Kalinka, G. et al. (2010). Interfacial shear strength of a glass fiber/epoxy bonding in composites modified with carbon nanotubes. *Composites Science and Technology* [Internet] 70 (9): 1346–1352. https://doi.org/10.1016/j.compscitech.2010.04.010.

32 Asadi, A., Miller, M., Moon, R.J., and Kalaitzidou, K. (2016). Improving the interfacial and mechanical properties of short glass fiber/epoxy composites by coating the glass fibers with cellulose nanocrystals. *Express Polymer Letters* 10 (7): 587–597.

33 Ozsoy, N., Ozsoy, M., and Mimaroglu, A. (2016). Mechanical properties of chopped carbon fiber reinforced epoxy composites. *Acta Physica Polonica A* 130 (1): 297–299.

34 Davis, D.C., Wilkerson, J.W., Zhu, J., and Hadjiev, V.G. (2011). A strategy for improving mechanical properties of a fiber reinforced epoxy composite using functionalized carbon nanotubes. *Composites Science and Technology* [Internet] 71 (8): 1089–1097. https://doi.org/10.1016/j.compscitech.2011.03.014.

35 An, F., Lu, C., Li, Y. et al. (2012). Preparation and characterization of carbon nanotube-hybridized carbon fiber to reinforce epoxy composite. *Materials and Design* [Internet] 33 (1): 197–202. https://doi.org/10.1016/j.matdes.2011.07.027.

36 Li, M., Gu, Y., Liu, Y. et al. (2013). Interfacial improvement of carbon fiber/epoxy composites using a simple process for depositing commercially functionalized carbon nanotubes on the fibers. *Carbon* [Internet] 52: 109–121. https://doi.org/10.1016/j.carbon.2012.09.011.

37 Pathak, A.K., Borah, M., Gupta, A. et al. (2016). Improved mechanical properties of carbon fiber/graphene oxide-epoxy hybrid composites. *Composites Science and Technology* [Internet] 135: 28–38. https://doi.org/10.1016/j.compscitech.2016.09.007.

38 Liu, F., Deng, S., and Zhang, J. (2017). Mechanical properties of epoxy and its carbon fiber composites modified by nanoparticles. *Journal of Nanomaterials* 2017: 1–9.

39 Shimazaki, Y., Miyazaki, Y., Takezawa, Y. et al. (2007). Excellent thermal conductivity of transparent cellulose nanofiber/epoxy resin nanocomposites. *Biomacromolecules* 8 (9): 2976–2978.

40 Pervaiz, M., Jawaid, M., Alothman, O.Y., and Sain, M. (2017). Thermal and dynamic mechanical properties of cellulose nanofibers reinforced epoxy composites. *International Journal of Biological Macromolecules* [Internet] https://doi.org/10.1016/j.ijbiomac.2017.04.074.

41 Yan, Q.L., Gozin, M., Zhao, F.Q. et al. (2016). Highly energetic compositions based on functionalized carbon nanomaterials. *Nanoscale* 8 (9): 4799–4851.

42 Feih, S. and Mouritz, A.P. (2012). Tensile properties of carbon fibres and carbon fibre-polymer composites in fire. *Composites Part A: Applied Science and Manufacturing* [Internet] 43 (5): 765–772. https://doi.org/10.1016/j.compositesa.2011.06.016.

43 Yu, M., Tang, L., Shah, S. et al. (2000). Strength and breaking mechanism of multiwalled carbon nanotubes under tensile load. *Science* 287 (5453): 637–640.

44 Naderi, M., Ebrahimi, F., Najafi, M., and Naderi, H. (2019). Reinforcing effect of amine-functionalized and carboxylated porous graphene on toughness, thermal stability, and electrical conductivity of epoxy-based nanocomposites. *Journal of Applied Polymer Science* 136 (19): 1–10.

45 Khan, Z.U., Kausar, A., and Ullah, H. (2016). A review on composite papers of graphene oxide, carbon nanotube, polymer/GO, and polymer/CNT: processing strategies, properties, and relevance. *Polymer-Plastics Technology and Engineering* 55 (6): 559–581.

46 Lee, C., Wei, X., Kysar, J.W., and Hone, J. (2008). Measurement of the elastic properties and intrinsic strength of monolayer graphene. *Science* 321 (5887): 385–388.

47 Wei, J., Vo, T., and Inam, F. (2015). Epoxy/graphene nanocomposites – processing and properties: a review. *RSC Advances* 5 (90): 73510–73524.

48 Tang, J., Zhou, H., Liang, Y. et al. (2014). Properties of graphene oxide/epoxy resin composites. *Journal of Nanomaterials* 2014: 1–5.

49 Shiu, S.C. and Tsai, J.L. (2014). Characterizing thermal and mechanical properties of graphene/epoxy nanocomposites. *Composites Part B: Engineering* 56: 691–697.

50 Shadlou, S., Ahmadi-Moghadam, B., and Taheri, F. (2014). The effect of strain-rate on the tensile and compressive behavior of graphene reinforced epoxy/nanocomposites. *Materials and Design* 59: 439–477.

51 Prolongo, S.G., Moriche, R., Jiménez-Suárez, A. et al. (2014). Advantages and disadvantages of the addition of graphene nanoplatelets to epoxy resins. *European Polymer Journal* 61: 206–214.

52 Zhang, Z., Zhang, W., Li, D. et al. (2015). Mechanical and anticorrosive properties of graphene/epoxy resin composites coating prepared by in situ method. *International Journal of Molecular Sciences* 16 (1): 2239–2251.

53 Meng, Q., Araby, S., and Ma, J. (2015). Toughening mechanisms in epoxy/graphene platelets composites. In: *Toughening Mechanisms in Composite Materials* (eds. Q. Qin and J. Ye), 73–112. Elsevier.

54 Naderi, M., Hoseinabadi, M., Motahari, S., and Shokri, M. (2018). Investigation of the mechanical , thermal , and anticorrosion properties of epoxy nanocomposite coatings: effect of synthetic hardener and nanoporous graphene. *Journal of Applied Polymer Science* 135: 46201–46211.

55 Tang, L.C., Wan, Y.J., Yan, D. et al. (2013). The effect of graphene dispersion on the mechanical properties of graphene/epoxy composites. *Carbon* [Internet] 60: 16–27. https://doi.org/10.1016/j.carbon.2013.03.050.

56 Wang, X., Jin, J., and Song, M. (2013). An investigation of the mechanism of graphene toughening epoxy. *Carbon* [Internet] 65: 324–333. https://doi.org/10.1016/j.carbon.2013.08.032.

57 Kausar, A., Rafique, I., Anwar, Z., and Muhammad, B. (2016). Perspectives of epoxy/graphene oxide composite: significant features and technical applications. *Polymer-Plastics Technology and Engineering* 55 (7): 704–722.

58 Yu, J.W., Jung, J., Choi, Y. et al. (2016). Enhancement of the crosslink density, glass transition temperature, and strength of epoxy resin by using functionalized graphene oxide co-curing agents. *Polymer Chemistry* 7: 36–43.

59 Ribeiro, H., Da Silva, W.M., Neves, J.C. et al. (2015). Multifunctional nanocomposites based on tetraethylenepentamine-modified graphene oxide/epoxy. *Polymer Testing* 43: 182–192.

60 Chhetri, S., Adak, N.C., Samanta, P. et al. (2017). Functionalized reduced graphene oxide/epoxy composites with enhanced mechanical properties and thermal stability. *Polymer Testing* 63: 1–11.

61 Ferreira, F.V., Brito, F.S., Franceschi, W. et al. (2018). Functionalized graphene oxide as reinforcement in epoxy based nanocomposites. *Surfaces and Interfaces* 10: 100–109.

62 Song, M. and Xu, J. (2013). Preparation of polyethylenimine-functionalized graphene oxide composite and its application in electrochemical ammonia sensors. *Electroanalysis* 25 (2): 523–530.

63 Gojny, F.H., Wichmann, M.H.G., Köpke, U. et al. (2004). Carbon nanotube-reinforced epoxy-composites: enhanced stiffness and fracture toughness at low nanotube content. *Composites Science and Technology* 64 (15 Special issue): 2363–2371.

64 Shalini, V. and Revathi, A. (2017). Tensile and viscoelastic properties of epoxy–carbon nanotube nanocomposites. *Indian Journal of Advances in Chemical Science* S2: 19–22.

65 Arash, B., Wang, Q., and Varadan, V.K. (2014). Mechanical properties of carbon nanotube/polymer composites. *Scientific Reports* [Internet] 4: 6479. doi: https://doi.org/10.1038/srep06479.

66 Guo, X., Yu, D., Wu, J. et al. (2012). Effects of nanotube modification on the dielectric behaviors and mechanical properties of multiwall carbon nanotubes/epoxy composites. *Polymer Engineering and Science* 53: 370–377.

67 Yoonessi, M., Lebroín-Coloín, M., Scheiman, D., and Meador, M.A. (2014). Carbon nanotube epoxy nanocomposites: the effects of interfacial modifications on the dynamic mechanical properties of the nanocomposites. *ACS Applied Materials & Interfaces* 6 (19): 16621–16630.

68 Cha, J., Jun, G.H., Park, J.K. et al. (2017). Improvement of modulus, strength and fracture toughness of CNT/epoxy nanocomposites through the functionalization of carbon nanotubes. *Composites Part B: Engineering* [Internet] 129: 169–179. https://doi.org/10.1016/j.compositesb.2017.07.070.

69 Roy, S., Petrova, R.S., and Mitra, S. (2018). Effect of carbon nanotube (CNT) functionalization in epoxy–CNT composites. *Nanotechnology Reviews* 7 (6): 475–485.

70 Li, Y., Wang, S., Wang, Q., and Xing, M. (2018). A comparison study on mechanical properties of polymer composites reinforced by carbon nanotubes and graphene sheet. *Composites Part B: Engineering* [Internet] 133: 35–41. https://doi.org/10.1016/j.compositesb.2017.09.024.

71 Zakaria, M.R., Helmi, M., Kudus, A. et al. (2017). Comparative study of graphene nanoparticle and multiwall carbon nanotube filled epoxy nanocomposites based on mechanical, thermal and dielectric properties. *Composites Part B: Engineering.* [Internet] https://doi.org/10.1016/j.compositesb.2017.03.023.

72 Hawkins, D.A. Jr. and Haque, A. (2014). Fracture toughness of carbon-graphene/epoxy hybrid nanocomposites. *Procedia Engineering* [Internet] 90: 176–181. https://doi.org/10.1016/j.proeng.2014.11.833.

73 Mun, S.Y., Lim, H.M., and Lee, S. (2017). Thermal and electrical properties of epoxy composite with expanded graphite-ceramic core-shell hybrids. *Materials Research Bulletin* [Internet] https://doi.org/10.1016/j.materresbull.2017.06.046.

74 Aghabararpour, M., Naderi, M., Motahari, S., and Najafi, M. (2019). A study on resorcinol formaldehyde carbon aerogel/epoxy nanocomposites: the effect of carbon aerogel pyrolysis time. *Journal of Polymer Research* 26 (3): 1–8.

75 Hsieh, T.H., Huang, Y.S., and Shen, M.Y. (2015). Mechanical properties and toughness of carbon aerogel/epoxy polymer composites. *Journal of Materials Science* 50 (8): 3258–3266.

76 Tomić, M., Dunjić, B., Nikolić, M.S. et al. (2018). Dispersion efficiency of montmorillonites in epoxy nanocomposites using solution intercalation and direct mixing methods. *Applied Clay Science* 154 (January 2017): 52–63.

77 Jamal-Omidi, M. and ShayanMehr, M. (2019). Improving the dispersion of SWNT in epoxy resin through a simple multi-stage method. *Journal of King Saud University – Science* 31 (2): 202–208.

78 Kumar, A., Ghosh, P.K., Yadav, K.L., and Kumar, K. (2017). Thermo-mechanical and anti-corrosive properties of MWCNT/epoxy nanocomposite fabricated by innovative dispersion technique. *Composites Part B: Engineering* 113: 291–299.

79 Ozgul, E.O. and Ozkul, M.H. (2018). Effects of epoxy, hardener, and diluent types on the workability of epoxy mixtures. *Construction and Building Materials* [Internet] 158: 369–377. https://doi.org/10.1016/j.conbuildmat.2017.10.008.

80 Gupta, N. and Ricci, W. (2007). Processing and compressive properties of aerogel/epoxy composites. *Polymer* 8: 178–182.

81 Monti, M., Rallini, M., Puglia, D. et al. (2013). Morphology and electrical properties of graphene–epoxy nanocomposites obtained by different solvent assisted processing methods. *Composites Part A: Applied Science and Manufacturing* 46 (1): 166–172.

82 Richardson, M.O.W. and Wisheart, M.J. (1996). Review of low-velocity impact properties of composite materials. *Composites Part A: Applied Science and Manufacturing* 27: 1123–1131.

83 Mansourian-Tabaei, M., Jafari, S.H., and Khonakdar, H.A. (2014). Lap shear strength and thermal stability of diglycidyl ether of bisphenol a/epoxy novolac adhesives with nanoreinforcing fillers. *Journal of Applied Polymer Science* 131 (6): 1–8.

84 Jojibabu, P., Jagannatham, M., Haridoss, P. et al. (2016). Effect of different carbon nano-fillers on rheological properties and lap shear strength of epoxy adhesive joints. *Composites Part A: Applied Science and Manufacturing* [Internet] 82: 53–64. https://doi.org/10.1016/j.compositesa.2015.12.003.

85 Moriche, R., Prolongo, S.G., Sánchez, M. et al. (2016). Thermal conductivity and lap shear strength of GNP/epoxy nanocomposites adhesives. *International Journal of Adhesion and Adhesives* [Internet] 68: 407–410. https://doi.org/10.1016/j.ijadhadh.2015.12.012.

86 Naderi, M., Aghabararpour, M., Najafi, M., and Motahari, S. (2019). An investigation into resorcinol formaldehyde carbon aerogel/epoxy coatings: exploring mechanical properties, ultraviolet stability, and corrosion resistance. *Polymer Composites* 41: 121–133. https://doi.org/10.1002/pc.25351.

11

Dielectric and Conductivity Studies of Epoxy Composites

Anastasios C. Patsidis and Georgios C. Psarras

University of Patras, School of Natural Sciences, Department of Materials Science, Smart Materials & Nanodielectrics Laboratory, Patras University Campus of Rion, Patras 26504, Greece

11.1 Introduction

Epoxy resins became commercially available after the Second World War and since then they are used in a vast number of technological applications. The term "epoxy resin" is used for both the prepolymer and the cured resin. Its origin is related to the epoxy groups of the prepolymer, which in a completely cured resin do not exist.

Composites are materials' systems consisting of two, or in sometimes more, distinct constituents or phases, which vary significantly in their physical and mechanical properties. The continuous phase, being also in the greater amount, is called matrix, while the dispersed or discontinuous constituent (or constituents) is called reinforcing phase or filler. Between matrix and reinforcing phase, an interface exists with properties different from those of the constituents and the composite. The main roles of the matrix are to connect the reinforcing phase, to provide protection to the composite from environmental or corrosive attacks, to maintain the configuration/orientation of the reinforcing phase, and to transfer applied mechanical load to the load members of the composite, which typically are long fibers. Composites could be natural or synthetic. Mankind produces synthetic composites for more than 7000 years, since ancient type of bricks consisted of mud and straw are classified as composite materials. The properties of composite materials differ notably from those of their constituents, and composites' performance at service is expected to be superior to the corresponding constituent phases [1, 2].

Polymers are by far the most commonly used matrices for the development of composite materials. Polymers fail to follow the high values of strength and stiffness exhibited by metals and ceramics and thus appear to be a material suitable for reinforcement. On the contrary, polymers are lightweight, due to their low density, can be formed easily to complex shapes without needing high temperature and pressure, and present enhanced resistance to chemical attacks and corrosive environments. A significant drawback of polymers is their low maximum working temperature. Thermosetting polymers (or thermosets) are amorphous polymers that

Epoxy Composites: Fabrication, Characterization and Applications,
First Edition. Edited by Jyotishkumar Parameswaranpillai, Harikrishnan Pulikkalparambil, Sanjay M. Rangappa, and Suchart Siengchin.

develop cross-links between macromolecular chains upon curing. Curing process is a reaction involving a catalyst known as curing agent or hardener and sometimes heating. The duration of heating varies depending on the employed resin and hardener. Often curing is followed by post-curing targeting to the completion of the chemical reaction and to the formation of an extensive cross-linking network. Curing and post-curing result in the endurance of the polymer since the weak van der Waals bonding between polymer chains is substituted by strong covalent bonds. Epoxy resins belong to this category of polymers, being widely used as matrices in composite materials [3, 4].

The properties of epoxy resins make them suitable materials to be employed as matrices for composites. Among others, their advantages include good flow characteristics, thermal stability, advanced mechanical properties with respect to other polymers used as composites' matrix, reduced absorption of moisture, low shrinkage, strong electrical insulating properties, high dielectric breakdown strength, low coefficient of thermal expansion-dimensional stability, environmental stability, and high resistance to chemical and corrosive attacks.

11.2 Experimental Techniques and Data Interpretation

11.2.1 Experimental Techniques

Electrical properties of epoxy-based composites can be experimentally examined via broadband dielectric spectroscopy (BDS) and direct current (dc) conductivity measurements. BDS has been proved as a very effective experimental technique for the investigation of molecular dynamics, molecular mobility, relaxation processes, polarization, conductivity mechanisms, interfacial phenomena, phase changes, and chemical and thermal events like polymerization, crystallization, and melting in polymers and complex systems. The range of applicability of BDS (depending upon the available devices) extends from 10^{-6} to 10^{12} Hz covering a very wide part of the electromagnetic spectrum, in which it provides information upon the interaction between electromagnetic waves and matter. Experimental setups vary with respect to the applied frequency range. Details upon the employed experimental setup can be found in [5–8].

Measurements of dc conductivity can be carried out through the sample's thickness (bulk properties) or on the surface of the sample. The latter are used in thin films and membranes for studying their surface conductance or in the case of surface leakage currents. In thick specimens, measurements through thickness are more reliable [9–11].

In both experimental techniques, BDS and dc conductivity measurements, the temperature of the sample is almost always an important parameter.

11.2.2 Dielectric and Conductivity Data Interpretation

Dielectric response under dc field can be described or studied via the relative dielectric constant (ε) or in other words the static value of dielectric permittivity, which

is a characteristic material property. Applied field (E), polarization (P), and relative dielectric constant are connected via Eqs. (11.1) and (11.2) [12]:

$$P = \varepsilon_0 (\varepsilon - 1) E \tag{11.1}$$

$$\varepsilon = 1 + \frac{1}{\varepsilon_0} \frac{P}{E} = 1 + \chi \tag{11.2}$$

The quantity χ is the electric susceptibility and expresses the amount of the produced polarization by the applied electric field.

Under the influence of an alternating field, polarization is not able to acquire its maximum value instantaneously because of the inertia of dipoles to orient themselves parallel to the time-varying field, thus giving rise to the occurrence of relaxation processes. This delay is related to the resistance of the medium in the dipole motion and to the occurring interactions in solid state. A rigorous analysis of dielectric theory in polymers and polymer composites can be found in [12]. By applying a time-varying field, such as the one expressed in Eq. (11.3), dielectric permittivity becomes a complex quantity defined via Eq. (11.4):

$$E = E_0 \exp i (\omega \cdot t) \tag{11.3}$$

$$\varepsilon^* (\omega) = \varepsilon' (\omega) - i\varepsilon'' (\omega) \tag{11.4}$$

where ε' is the real and ε'' the imaginary part of complex dielectric permittivity, ε'' is also referred as loss factor, loss index or simply dielectric loss of the material, and ω is the angular frequency of the field. The real part of dielectric permittivity represents the ability of the dielectric material to store energy, while the imaginary part denotes the dissipated energy as heat.

It is well known [12–15] that dielectric behavior and relaxation processes can be described and analyzed by means of equivalent formalisms. These are (i) dielectric permittivity, (ii) electric modulus, (iii) alternating current (ac) conductivity, and (iv) complex impedance. Dielectric response and relaxation effects can be interpreted by any of these four formalisms. However, under specific experimental conditions (applied field's frequency range, temperature, injection of charges by the dielectric cell electrodes, structure of the under test material, etc.), one of them could be more effective in the analysis of the physical effects, giving the opportunity to reveal a deeper insight of the material's dielectric behavior [14]. Dielectric permittivity is defined via Eq. (11.4), while electric modulus, ac conductivity, and complex impedance are defined via Eqs. (11.5)–(11.7), respectively. Equation (11.8) defines loss tangent delta ($\tan \delta$) or dissipating factor, which expresses the ratio of the dissipated energy upon the stored one per charging cycle.

$$M^* = \frac{1}{\varepsilon^*} = \frac{\varepsilon'}{\varepsilon'^2 + \varepsilon''^2} + i \frac{\varepsilon''}{\varepsilon'^2 + \varepsilon''^2} = M' + iM'' \tag{11.5}$$

where M' and M'' are the real and imaginary parts of electric modulus. Electric modulus has been proved very effective, in the low-frequency range and at high temperatures, since it neglects the parasitic effect of electrode polarization and stray capacitance. Its validity increases especially in the case of composites consisted of an insulating matrix and conductive inclusions [13, 16–19].

According to von Hippel [20], ac conductivity (σ_{ac}) sums all energy dissipative effects including actual ohmic conductivity caused by migrating charge carriers on isolated or adjacent conductive sites or clusters as well as frequency dielectric dispersions [20].

$$\sigma_{ac}(\omega) = \varepsilon_0 \omega \varepsilon'' \tag{11.6}$$

where $\varepsilon_0 = 8.85 \times 10^{-12}$ F/m is the permittivity of the free space.

$$Z^*(\omega) = Z'(\omega) - iZ''(\omega) \tag{11.7}$$

where Z' and Z'' are the real and imaginary parts of impedance.

$$\tan\delta = \frac{\varepsilon''}{\varepsilon'} = \frac{M''}{M'} \tag{11.8}$$

Conductivity under dc conditions (σ_{dc}) can be evaluated mostly by measuring the resistance (R) of the under test sample and the geometrical characteristics of the specimen. Important parameters are the applied voltage (or in other words the applied electric field) and the electrification time [9, 10]. Thus, dc conductivity can be determined via mathematical formulas of the type of Eq. (11.9):

$$\sigma_{dc} = \frac{1}{R} \cdot F(\text{dimensions}) \tag{11.9}$$

where F is a function of the sample's dimensions and changes according to the experimental configuration (for example four-point probe, bulk measurements through thickness, etc.). In bulk conductivity measurements, Eq. (11.9) takes the following form (Eq. (11.10)) [10]:

$$\sigma_{dc} = \frac{1}{R} \cdot \frac{t}{A} \tag{11.10}$$

where t and A are the thickness of the sample and the effective electrode area, respectively.

Furthermore, in many cases, dc conductivity is considered as the extrapolation of σ_{ac} at $\omega \to 0$.

11.3 Electrical Properties of Epoxy Resins

Although polymers with enhanced conductivity have been synthesized the last decades, the majority of the polymers remain insulating in nature. Epoxy resins belong to this class of materials with low conductivity because of the limited free charge carriers. For this reason, epoxy resins find applications as protective coatings in electrical circuit components in microelectronics, as insulating adhesives in multilayered capacitors, etc. Insulating materials are dielectrics, meaning that are materials able to be polarized under the influence of an external electric field. With the application of electric field, permanent and induced dipoles are forced to be aligned in the direction of field, although no macroscopic charge migration occurs. Polarization results in the development of a net positive and net negative surface charge at the edges of the dielectric material, which are in contact with the opposing charged electrodes of the capacitors.

Depending on the structure of the polymer and the frequency of the applied field, electronic, atomic/ionic, orientational, and interfacial polarization (IP) can be present in the dielectric spectra of the polymers. The large number of possible space configurations of macromolecular chains, branches, and side groups gives rise to distinct relaxation phenomena. These processes correspond to various dipoles and characterized by different relaxation times. Variation of relaxation times indicates differences in size and mass of dipoles, as well as the interactions with their environment. The existence of various types of dipoles in solid polymers complicates their dielectric response and the identification of each process. Relaxation processes are detected as "step-like" transitions in the spectra of the real part of permittivity (from high to low values) and electric modulus (from low to high values) or by the formation of loss peaks in all dielectric loss representations. Notably that relaxation times in some processes do not vary significantly resulting in overlapping of the effects in the dielectric spectra. The labeling of relaxations is given by using the lowercase letters of the Greek alphabet (α, β, γ) in the dielectric loss vs. temperature plots, at constant frequency, following the convention that the process recorded at the higher temperature is labeled with α, the right next one with β, and so on.

Figure 11.1 [21] shows a representative picture of the dielectric response of epoxy resins. Figure 11.1a,b depicts the variation of the real part of dielectric permittivity and loss tangent with frequency and temperature in three-dimensional (3D) plots. It is apparent that (ε') increases rapidly at low frequencies and high temperatures. At low frequencies, the alternation of the applied field is low, giving thus time to dipoles to be aligned with the field. Equation (11.1) indicates that polarization and dielectric permittivity are proportional quantities. Increase of temperature provides thermal agitation to dipoles, facilitating further their orientation. Thus, maximum polarization is expected to occur at the low-frequency and high-temperature edge. The "step-like" transition recorded in the intermediate frequencies is indicative of the presence of a relaxation process. Figure 11.1b gives a more comprehensive image of the recorded relaxations via the formation or the tendency for the formation of loss peaks. In the intermediate-frequency range, the recorded loss peak is attributed to the glass-to-rubber transition of epoxy. Epoxy resins as well as amorphous polymers undergo transition from the glassy state to the rubbery one at a characteristic temperature range. In most cases, this range is denoted by a single temperature, namely, the glass transition temperature (T_g). The value of glass transition temperature depends on the experimental method used for its determination (i.e. differential scanning calorimetry, dynamic mechanical analysis, BDS) and the data analysis conducted. Obviously, different values of T_g can be reported for the same polymer, corresponding to the onset, completion, or midpoint of the transition.

In the glassy state, at temperatures below T_g, macromolecular chains are frozen and stiff with cross-links between them. At temperatures close to T_g, thermal energy is offered to the system allowing the synergetic motion of large parts of the macromolecular chains. By these means, epoxy resin becomes softer and its stiffness decreases rapidly. The mechanical degradation can be detected easily by dynamic mechanical analysis tests, where storage modulus undergoes a significant transition to low values. In this temperature range, the enhanced mobility of the

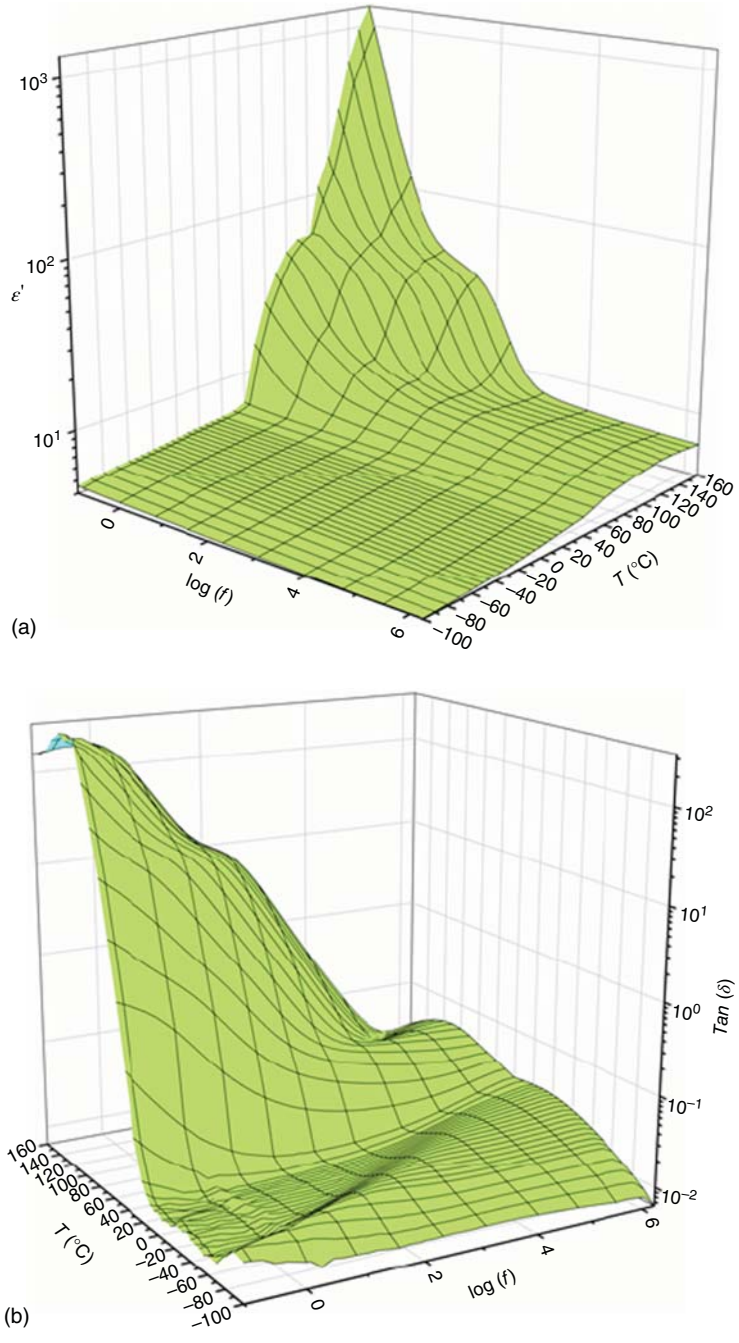

Figure 11.1 Variation of the real part of dielectric permittivity (a), loss tangent (b), and ac conductivity (c) with frequency and temperature for an epoxy resin. Source: Koufakis et al. [21].

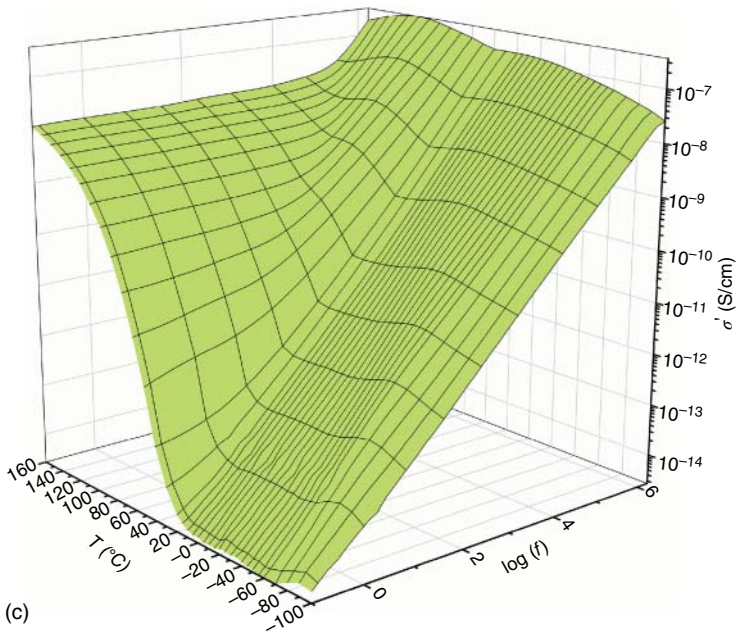

Figure 11.1 (*Continued*)

polymer chains facilitates the alignment of dipoles parallel to the applied field. Thus, the level of the achieved polarization increases in tandem with the real part of dielectric permittivity. The corresponding loss peak of glass-to-rubber transition is referred as α-relaxation. In the loss spectra of $\tan\delta$ (Figure 11.1b), additional peaks can be observed. Those recorded at low temperatures and high frequencies are assigned as secondary relaxations and are weak processes characterized by short relaxation times. The process recorded at the highest frequency range is attributed to "crankshaft-like" motion of the $(CH_2)_n$ units of the polymer chains involving sometimes the C–O polar groups [22, 23] and is denoted as γ-relaxation. At relatively lower frequencies, under constant temperature, the observed process is labeled as β-relaxation and results from the reorientation of small polar side groups (i.e. C=O, –OH, etc.). Both β- and γ-relaxations are considered as local processes and exhibit lower values of activation energy with respect to α-relaxation. In the low-frequency and high-temperature region, another relaxation process is present. This mechanism is related to space charges, originates from the system's heterogeneity, and is referred as IP. IP is also present in neat polymers because of the presence of plasticizers, additives, and so on [21]. IP effect will be analyzed in Section 11.6.

The variation of epoxy's ac conductivity vs. frequency and temperature is depicted in Figure 11.1c. Equation (11.6) is employed for the determination of ac conductivity. As expected, conductivity attains low values due to the insulating nature of the resin. Moreover, conductivity spectra exhibit strong dispersion with frequency and temperature [14]. The influence of temperature appears to be more pronounced at low frequencies. Under isothermal conditions, σ_{ac} acquires constant values approaching its dc value, while above a critical frequency ac conductivity exhibits an exponential

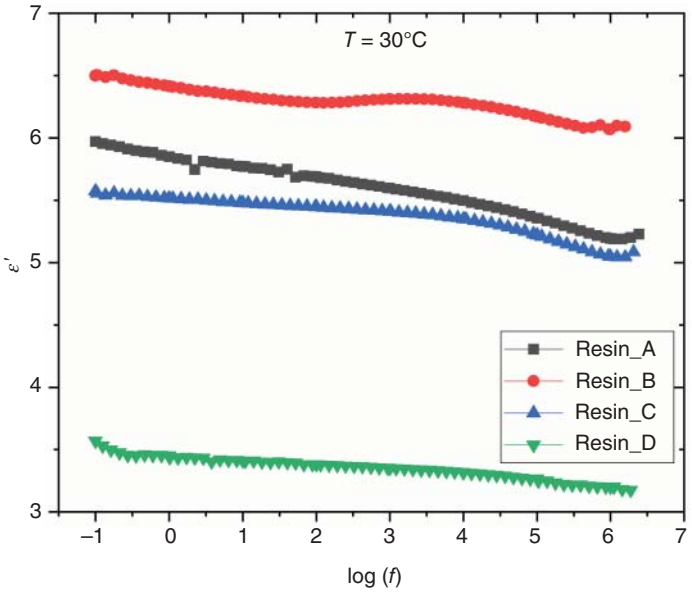

Figure 11.2 The real part of dielectric permittivity (ε') vs. frequency at 30 °C for four different epoxy resins. Epoxy resin providers: (A) Neotex SA. (B) RenLam, Huntsman. (C) Araldite, Huntsman. (D) Sintenco.

dependence on frequency. This behavior, which is common in disordered systems, is in accordance with the ac universality law, as expressed by Eq. (11.11) [24, 25]. It should be noted that the term disorder systems refers to nonmetallic materials with no perfect crystal lattice [26].

$$\sigma_{ac}(\omega) = \sigma_{dc} + A(\omega)^s \tag{11.11}$$

where σ_{dc} is the limiting value of σ_{ac} when frequency tends to zero and A, s parameters depending on the examined material and temperature [27, 28].

Figure 11.2 depicts values of ε' vs. frequency at 30 °C for four different epoxies. As it can be seen, values range between 4 and 6.5 revealing the insulating nature of the epoxies.

11.4 Epoxy/Nonconductive Reinforcing Phase Composites

The nonconductive reinforcing phase for epoxy resins could be organic, such as organic fibers, and inorganic like ceramic particles or fibers.

11.4.1 Epoxy/Nonconductive Filler Micro-composites

Typical nonconductive fillers for epoxy micro-composites are metal oxides (such as ZnO and TiO_2), complex metal oxides (such as $PbTiO_3$ and $BaTiO_3$), and organic

compounds like the aramid fibers. The selection of the employed reinforcement is related to the end-user application.

Obviously, the occurring relaxations are related to both constituents, that is, the epoxy matrix and the employed filler.

Ceramic inclusions exhibit values of dielectric permittivity much higher, in general, than the epoxy matrix, and thus, their presence within the epoxy results in altering the values of real part of dielectric permittivity. Figure 11.3 gives a representative example of the reinforcing ability of $BaTiO_3$ particles, varying the reinforcing phase content, at constant temperature. Filler content is expressed in parts per hundred resins per weight (phr). Permittivity increases steadily with filler content because of the higher values of (ε') of the inclusions and to the induced heterogeneity by the composite's constituents. The influence of heterogeneity enhances with temperature and will be discussed later.

Figure 11.4 presents the variation of the real part of dielectric permittivity with frequency at 30 (Figure 11.4a) and 120 °C (Figure 11.4b) of aramid fibers/epoxy composite systems with the fibers content as parameter. Employed aramid fibers are Kevlar® 49 pulp purchased by DuPont de Nemours, Inc., with aspect ratio $1/7 \times 10^3$, while the employed epoxy resin (Epicote 828) was supplied by Shell Chemicals. Values of neat matrix increase with the aramid content and temperature. Increase of temperature provides sufficient energy to dipoles to follow the alternation of the field, leading to higher values of polarization and permittivity. However, the electrical reinforcing ability of the aramid fibers is low, and the recorded values of (ε') do not vary significantly.

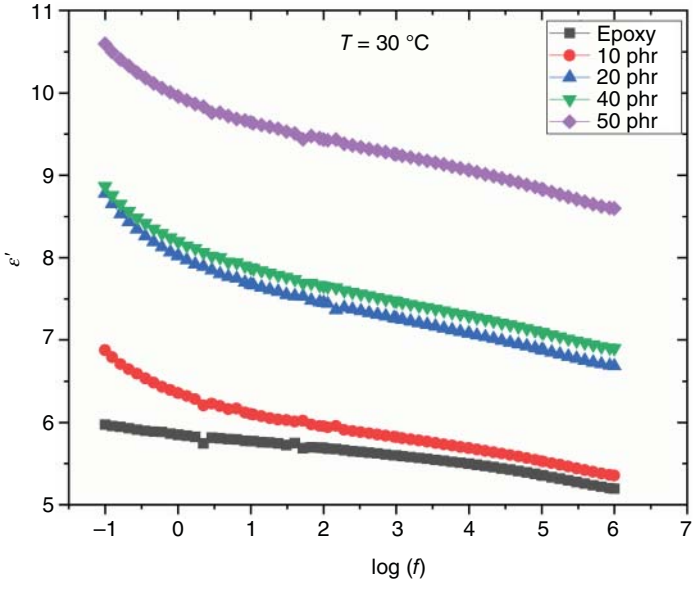

Figure 11.3 The real part of dielectric permittivity (ε') vs. frequency, at 30 °C, varying the content of $BaTiO_3$ microparticles.

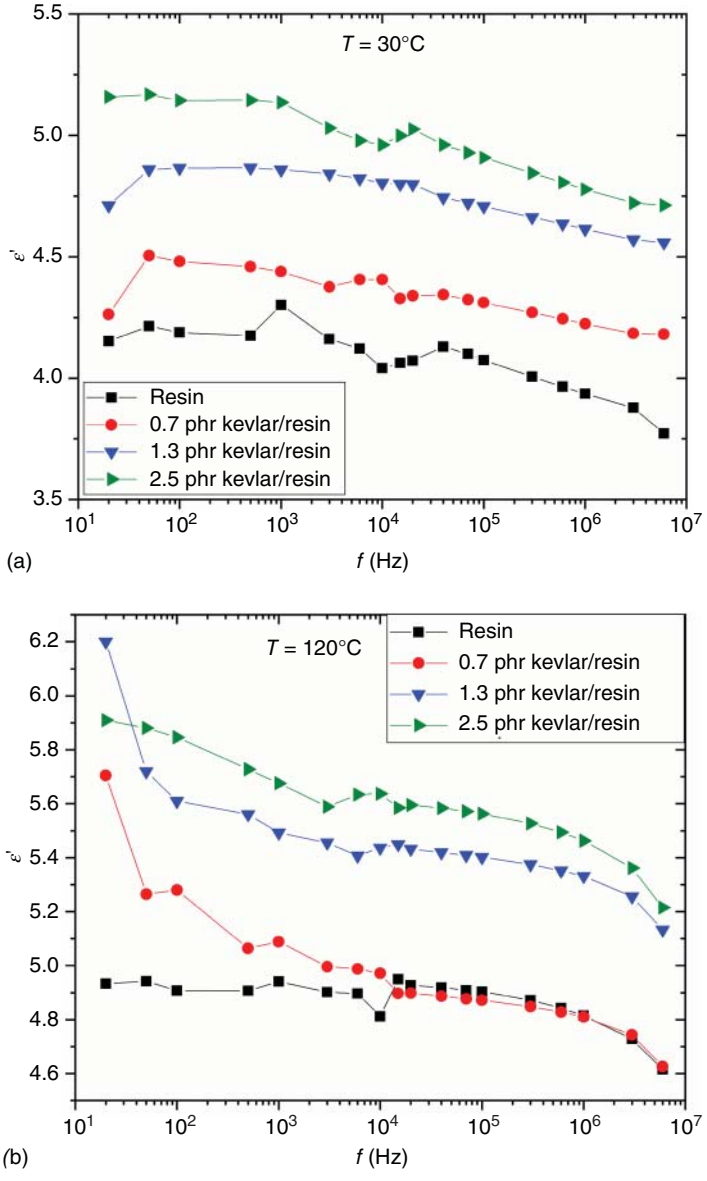

Figure 11.4 The real part of dielectric permittivity (ε') vs. frequency at (a) 30 °C and (b) 120 °C, for aramid fibers/epoxy resin composites, varying the filler content.

The real (M') and the imaginary (M'') part of electric modulus, as a function of frequency at various temperatures, for a 20 phr $PbTiO_3$ micro-particle-loaded resin is shown in Figure 11.5. Electric modulus is effective in analyzing dielectric data, when the parasitic effect of electrode polarization masks relaxation processes occurring at low frequencies and high temperatures, due to the significantly increased values of (ε') and (ε''). The normalized form of electric modulus (Eq. 11.5) neglects

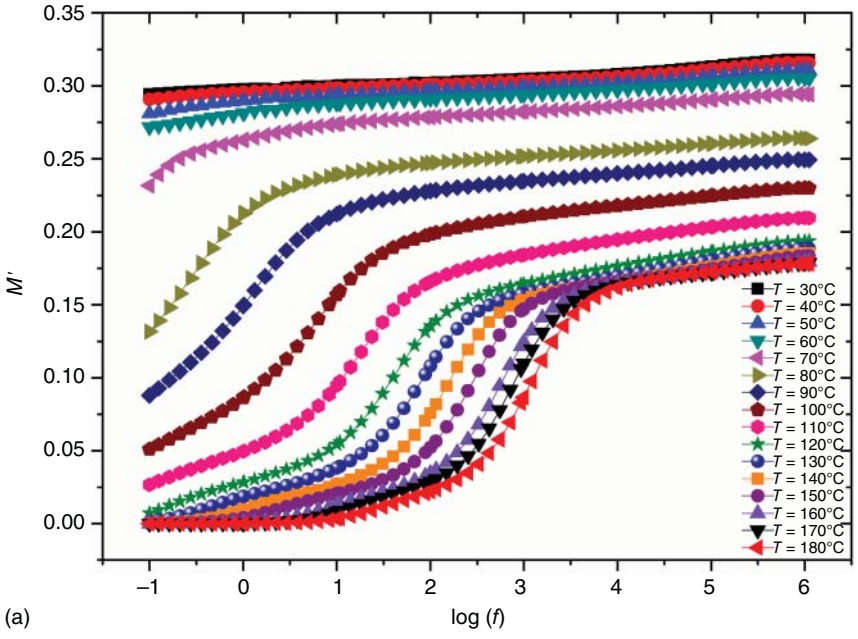

(a)

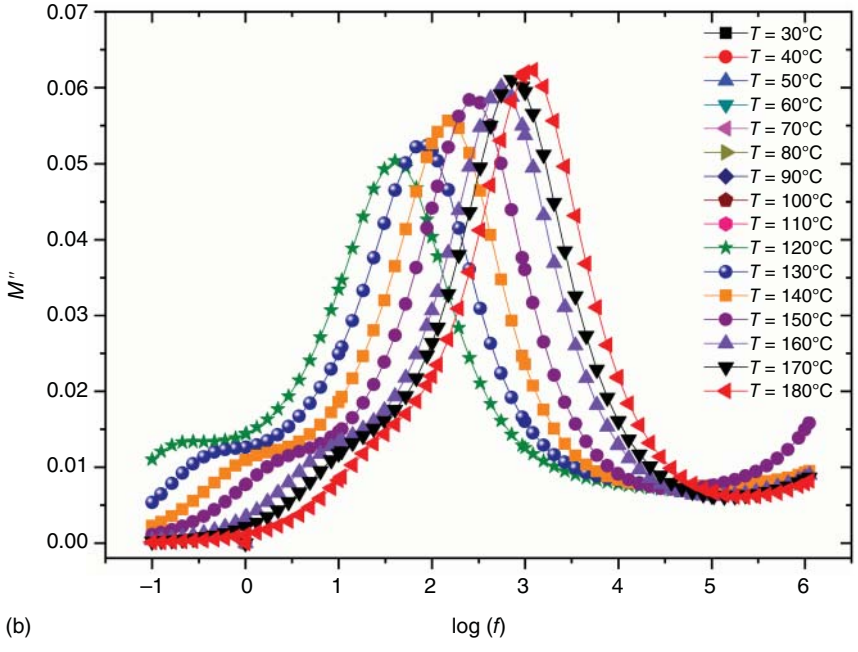

(b)

Figure 11.5 (a) The real (M') and (b) the imaginary (M'') part of electric modulus, as a function of frequency at various temperatures, for a 20 phr $PbTiO_3$ micro-particle-loaded epoxy resin.

the effect of electrode polarization, revealing completely the masked relaxations. Electric modulus formalism has been applied and tested in numerous polymeric systems and nowadays is considered as a powerful methodology for dielectric data analysis [13, 18, 29, 30]. Spectra of the real part of electric modulus (Figure 11.5a) form two "step-like" transitions from low to higher values, which shift to higher frequencies with the increase of temperature. The first and weaker one appears at low frequencies and high temperatures and is attributed to IP between the constituent phases of the composite. The second and more intense "step-like" transition is recorded at intermediate frequencies and temperatures and is assigned to glass-to-rubber transition of the epoxy. Relaxation processes are more evidently depicted in Figure 11.5b via the formed loss peaks of (M''). Recorded peaks shift to higher frequencies with the increase of temperature, since thermally activated dipoles are able to follow faster alternations of the applied field. However, the temperature-caused shifting rate appears to differ between the two processes implying different dynamics of each one. Relaxation dynamics can be studied by plotting the loss peak frequency position, at each examined temperature, as a function of reciprocal temperature. Figure 11.6 presents the frequency of the loss modulus peaks vs. reciprocal temperature for the data presented in Figure 11.5b. Relaxations follow a different dependence on temperature. The slowest process (IP) exhibit Arrhenius-type behavior expressed by Eq. (11.12):

$$f_{\max} = f_0 \exp\left(-\frac{E_A}{k_B T}\right) \tag{11.12}$$

where $f_{\max}$ is the loss peak frequency at specific temperature, f_0 a pre-exponential factor, E_A the activation energy of the process, k_B the Boltzmann constant,

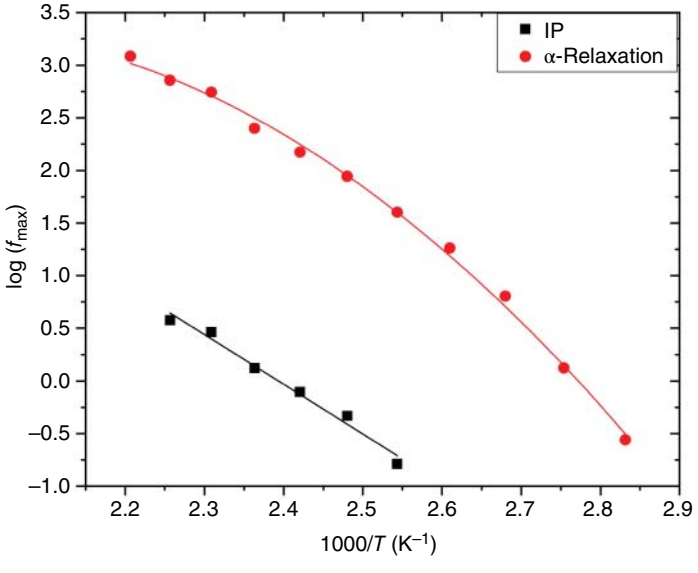

Figure 11.6 Frequency of the loss modulus peak position vs. reciprocal temperature for the data presented in Figure 11.5b.

and T the absolute temperature. The relaxation rate (loss peak frequency shift with temperature) of glass to rubber relaxation diminishes rapidly with temperature because of the reduction of free volume, thus α-relaxation follows the Vogel–Fulcher–Tammann (VFT) expression of Eq. (11.13):

$$f_{\max} = f_0 \exp\left(-\frac{B}{T - T_V}\right) \tag{11.13}$$

where B is a parameter being a measure of the activation energy of the process, f_0 is a pre-exponential factor, and T_V is the Vogel temperature or ideal glass transition temperature, a temperature varying approximately 40–50 K from the real T_g. Experimental data in Figure 11.6 are fitted via Eqs. (11.12) and (11.13). The determined values for their parameters are $E_A = 0.910$ eV, $B = 57.3$ K, and $T_V = 394.3$ K.

Results from $BaTiO_3$/epoxy composites are presented in Figure 11.7. The variation of (ε') with frequency, varying filler content, at 30 °C shown in Figure 11.3 is in agreement with the previously noted comments. Permittivity increases with filler content because of the higher value of (ε') for barium titanate, as well as due to the induced heterogeneity in the systems. Increase of frequency results in diminishing of permittivity because of the dipoles' inertia to follow the field. Figure 11.7 depicts the variation of the real part of dielectric permittivity with temperature, for the same set of composites, at 10 Hz. In linear dielectrics (at low applied field), polarization is proportional to permittivity (Eq. (11.1)) and the variation of (ε') reflects the variation of polarization [31–33]. Permittivity varies significantly in the temperature

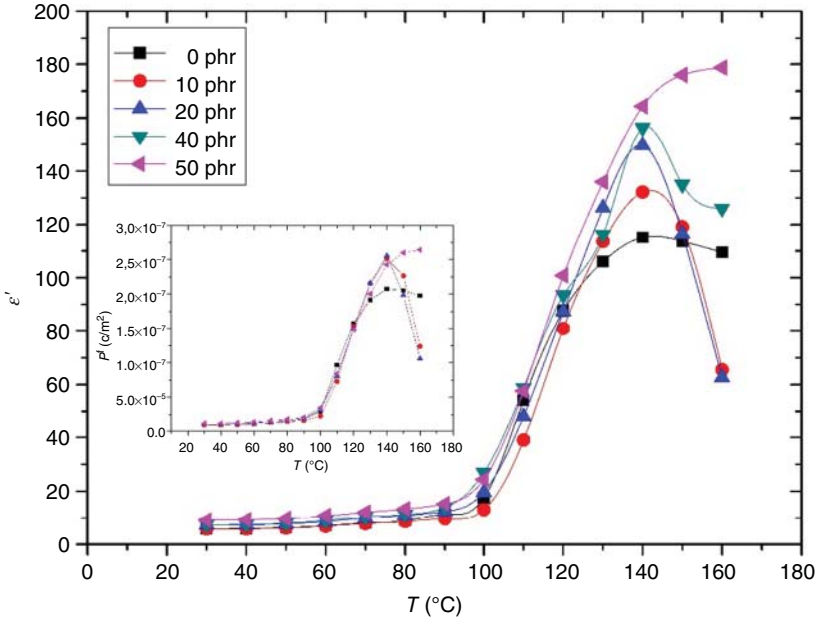

Figure 11.7 The real part of dielectric permittivity as a function of temperature, for the set of specimens presented in Figure 11.3 ($BaTiO_3$/epoxy), at $f = 10$ Hz. Inset depicts the corresponding variation of polarization. Source: Figure reused from Patsidis and Psarras [31] with permission.

range of 110–140 °C forming peaks. Notably that pure epoxy does not exhibit any peak. In this temperature range, the effect of IP phenomenon augments, leading to increased values of (ε'). The presence of peaks in the spectra of the composites cannot be assigned to IP or to the enhanced mobility of the macromolecules. The formed peaks are related to the $BaTiO_3$ particles. Barium titanate is a typical ferroelectric material undergoing a structural transition from the polar tetragonal structure (ferroelectric phase) to the nonpolar cubic structure (paraelectric phase) at a critical temperature (T_C), known as Curie temperature. T_C for $BaTiO_3$ ranges between 120 and 140 °C, depending on the polycrystalline or single crystal structure, the size of particles, etc. The ferroelectric-to-paraelectric transition is considered as a first-order transition [34] leading to the formation of a local maximum. Thus, the broad peak shown in Figure 11.7 is related to the temperature-triggered structural transition of $BaTiO_3$ particles with the overlapping contributions of IP and macromolecular mobility, which are responsible for its broadness. From Figure 11.7, it becomes evident that structural changes and phase transitions can be studied via BDS.

11.4.2 Epoxy/Nonconductive Filler Nanocomposites

Polymer matrix nanocomposites are a new and well-promising class of engineering materials. In this type of composites, the reinforcing inclusions have at least one of their dimensions at the nanoscale level. Epoxy resins are used as matrices in nanocomposites since, besides the other benefits of them, they exhibit good wetting and strong adhesion with many nano-dispersions. The main difference between micro- and nanocomposites is the tremendous increase of interfacial area in the second case. Interactions at the interfacial area are responsible, to a large extent, for the occurring performance of the nanocomposites. It should be noted that nanocomposites achieve or even exceed the micro-composites' performance at much lower reinforcing phase content [35]. Figure 11.8 provides an example upon the difference in reinforcing epoxy resins with ceramic micro- or nanoparticles. In this graph, the variation of the real part of dielectric permittivity vs. frequency, at 30 °C, for micro- and nano-B_4C/epoxy composites is compared. At equal filler content, nanocomposites exhibit higher values of (ε') with respect to the corresponding micro-composites, indicating that nano-reinforcement is more effective [36]. Even more, the 5 phr B_4C/epoxy nanocomposite exhibits significantly higher values from the 20 phr B_4C/epoxy micro-composite. The extensive interfacial area of the dispersed nanoparticles and the occurring interactions at the system's interface are considered as responsible for this performance.

Figure 11.9a gives another example of the dielectric response of ceramic particles/epoxy nanocomposites. The employed nano-filler is $ZnTiO_3$ nanoparticles, and their reinforcing ability becomes evident by the increase of the (ε') values with filler content. It is worth noting that the optimum behavior does not correspond to the nanocomposite with the maximum filler content. At the higher reinforcing phase contents, the formation of clusters and agglomerates modifies the fine dispersion of nanoparticles leading to a decrease of the extent of the constituents' interface and finally to permittivity values decrement. The variation of (ε') with temperature at

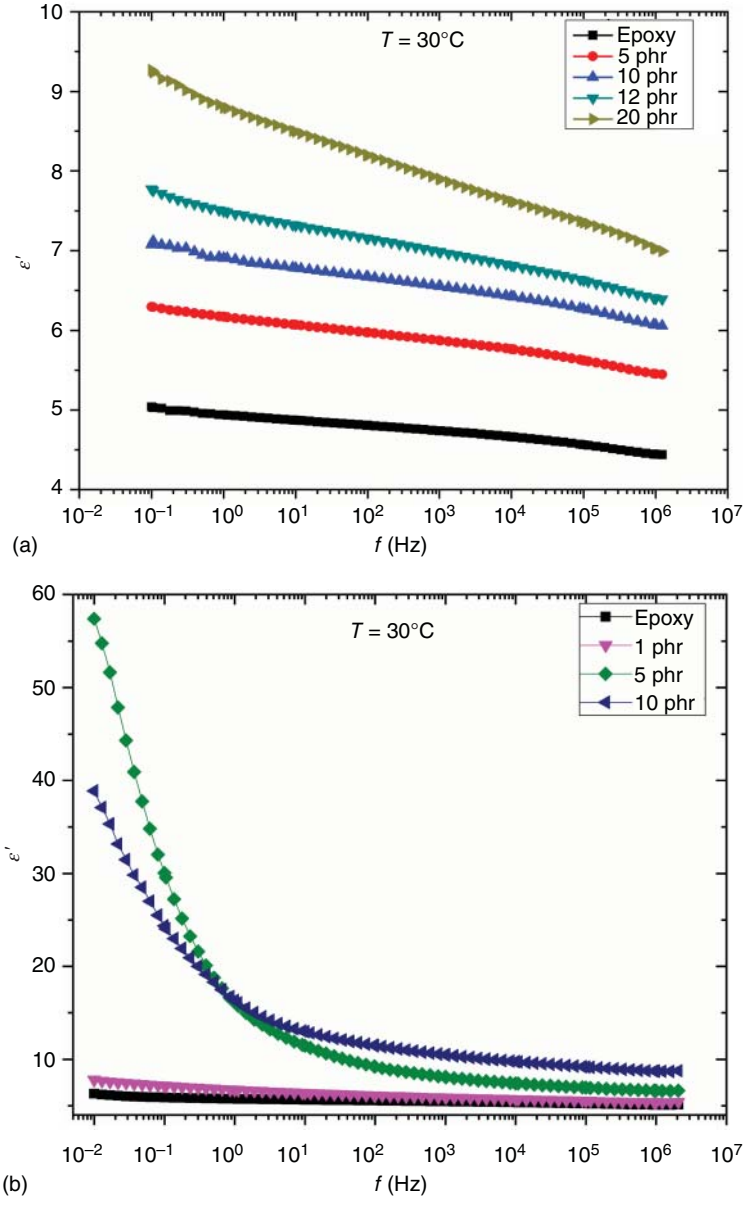

Figure 11.8 The real part of dielectric permittivity as a function of frequency, at 30 °C, for (a) micro- and (b) nano-B_4C/epoxy composites. Source: Senis [36].

1 kHz for the same set of specimens is shown in Figure 11.9b. For a wide range of temperatures, starting at −100 °C and reaching the 50 °C, the effect of filler loading is practically negligible, and only a slight increase of (ε') with temperature is recorded. In the range 50–100 °C, the recorded "hump" corresponds to the glass-to-rubber transition of the epoxy resin, while at higher temperatures, IP effect comes into play

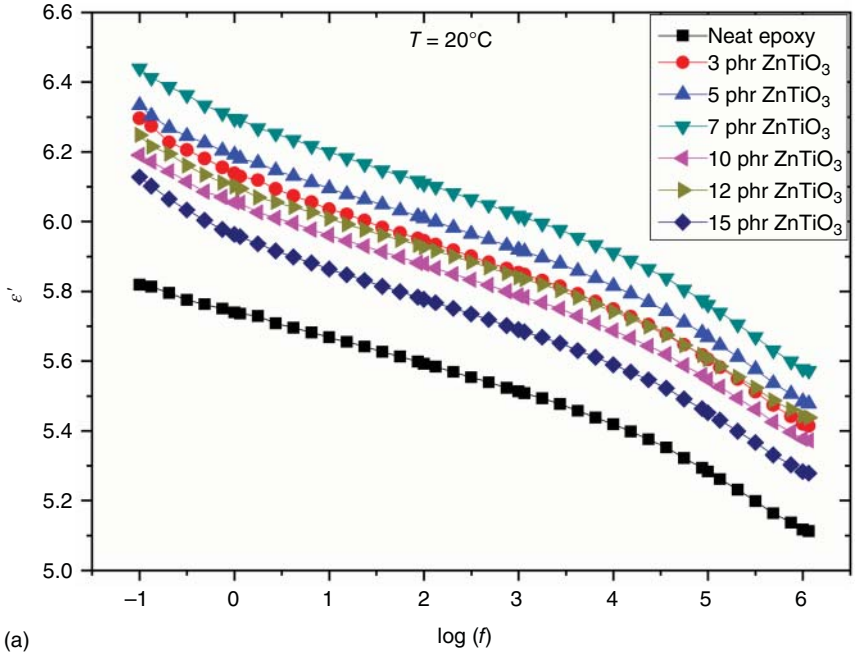

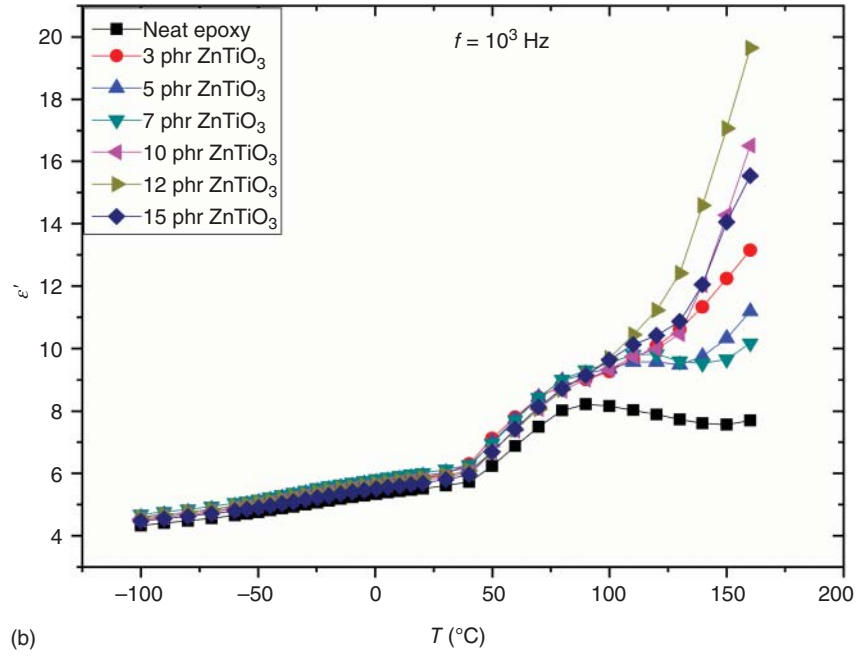

Figure 11.9 Real part of dielectric permittivity as a function of (a) frequency at 20 °C, and (b) temperature at 1 kHz, for $ZnTiO_3$/epoxy nanocomposites. Source: Koufakis et al. [21].

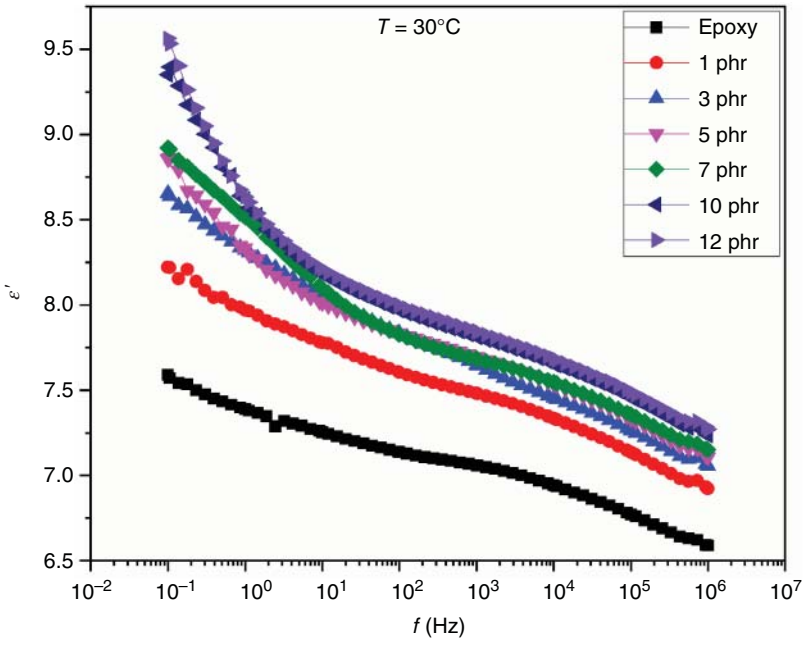

Figure 11.10 Effect of filler loading upon the real part of dielectric permittivity for a TiO_2/epoxy nanocomposite system at 30 °C [37].

giving higher values of permittivity, and the influence of $ZnTiO_3$ content is more pronounced [21].

The effect of filler loading upon the real part of dielectric permittivity for a TiO_2/epoxy nanocomposite system is depicted in Figure 11.10 [37]. The crystal structure of the employed TiO_2 nanoparticles was anatase, and their diameter was less than 25 nm [37]. The observed dielectric performance is in accordance with the previously mentioned comments.

A representative image of the morphology of the $ZnTiO_3$/epoxy nanocomposites and the achieved dispersion of nano-inclusions within the polymer matrix is given in Figure 11.11a for the system with 10 phr zinc titanate [21]. Dispersion of nanoparticles can be characterized as fine although a limited number of small clusters coexist. An additional method for studying the dielectric response and properties of nonconducting materials is given by dielectric reinforcing function (DRF). DRF is defined via Eq. (11.14), as the ratio of the composite's real part of permittivity upon the corresponding value of the neat matrix [32]:

$$G(\omega, T) = \frac{\varepsilon'_{\text{comp}}(\omega, T)}{\varepsilon'_{\text{mat}}(\omega, T)} \tag{11.14}$$

where $\varepsilon'_{\text{comp}}$ and $\varepsilon'_{\text{mat}}$ are the real part of the dielectric permittivity of the composite and the matrix, respectively, while ω is the angular frequency of the field and T the sample's temperature. DRF expresses the measure of the normalized polarization, indicating the dielectric strengthening ability of the reinforcing phase and revealing

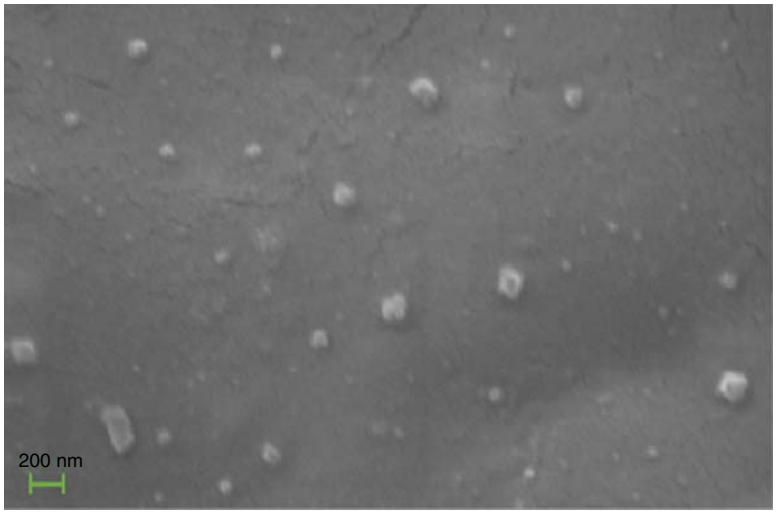

(a)

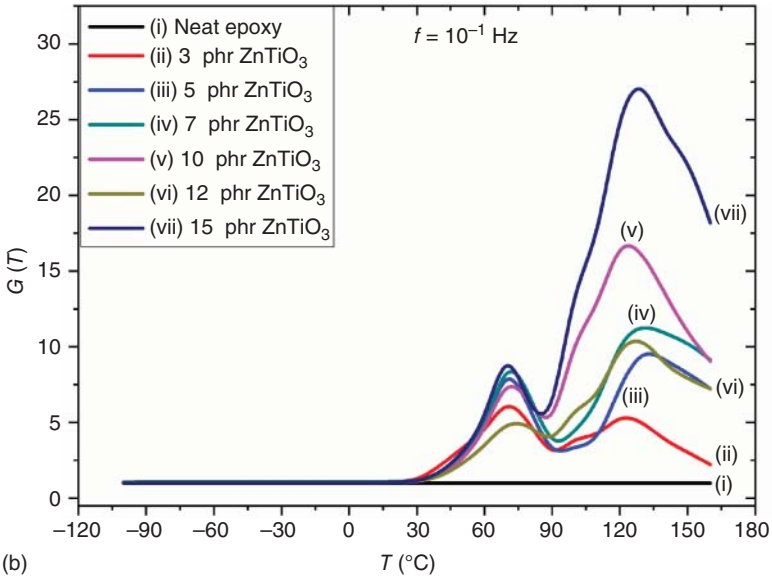

(b)

Figure 11.11 (a) Scanning electron microscopy (SEM) image of the 10 phr $ZnTiO_3$/epoxy nanocomposite and (b) dielectric reinforcing function (DRF) as a function of temperature for $ZnTiO_3$/epoxy nanocomposites at 10^{-1} Hz. Source: Figure reused from Koufakis et al. [21] with permission.

relaxation mechanisms. In addition, it also expresses the level of the energy storing efficiency of the composite at constant applied field.

DRF curves in Figure 11.11b create two sets of peaks located at approximately 70 and 130 °C. These peaks correspond to dielectric relaxation processes and specifically to the glass-to-rubber transition (~70 °C) and to IP (~130 °C). It can be observed

that at the maximum point of the curves, the nanocomposite with the higher reinforcing phase content (15 phr $ZnTiO_3$) has more than 26 times greater energy storing efficiency with respect to the unfilled epoxy matrix.

11.5 Epoxy/Conductive Reinforcing Phase Composites

Conductive reinforcing phase could be metal particles or fibers (such as Cu, Ni, Al, Ag, and other), carbides (like TiC and WC), and different forms of carbon (graphite powder, fibers, etc.). The presence of conductive inclusions within the insulating epoxy resin drastically affects the electrical conductivity of the composites. Epoxy matrix implies the insulating behavior of the composites. However, with the increase of the conductive filler load, a gradual increase of composites' conductivity is observed, and in many cases, at a critical filler content, an abrupt increase of conductivity takes place. The abrupt increment of conductivity is of a few orders of magnitude and happens with a small augment of the conductive filler concentration. At this content, a conductive path is formed through the entire composite allowing charges to flow through it, percolating the whole system. The critical content of the conductive phase, which is responsible for the enhancement of conductivity, is also known as percolation threshold and signifies the transition of the composites from the insulating to the conductive or semi-conductive behavior [38]. This transition is considered as a critical phenomenon and mathematically is described via Eq. (11.15) [39, 40]:

$$\sigma \approx \sigma_0 \left(P - P_C\right)^t \tag{11.15}$$

where P is the concentration of the conductive phase, P_C the critical concentration or percolation threshold, t the critical exponent, and σ_0 a pre-exponential parameter expressing the units of conductivity. In many cases, another term is added in the right-hand side of Eq. (11.15) indicating the conductivity of the composite at the critical concentration [41]. Critical exponent t is a dimensionless constant related to the dimensionality of the conduction path (e.g. 1D, 2D, or 3D). The value of exponent t for a 3D path is very close to 2. Moreover, in Eq. (11.15) concentrations P and P_C are sometimes replaced by the corresponding volume fractions v and v_C. Classical percolation theory regards conductive inclusions as noninteracting perfect spheres, randomly dispersed in the matrix and remaining at fixed positions, surrounded by a frozen insulating medium [28, 38, 39, 42, 43]. By these means, critical concentration is determined at 16% of volume fraction [38]. However, percolation threshold as well as critical exponent is influenced by the inclusions' size and shape, possible interaction between matrix and inclusions, or between inclusions of themselves, conduction mechanism, fabrication method, and rheological properties of the matrix [14, 28, 42, 43].

11.5.1 Epoxy/Conductive Filler Micro-composites

The presence of conductive inclusions within an epoxy resin alters the dielectric permittivity and conductivity of the composites, although does not lead always to the

transition from the insulating to the conductive behavior. Conductive microparticles, such as TiC of iron, randomly dispersed in an epoxy result in altering the real part of dielectric permittivity and dc conductivity. Figure 11.12a shows the dependence of (ε') upon frequency, at 30 °C, varying the filler content for TiC/epoxy composites [44]. As stated previously, permittivity decreases with the frequency of the

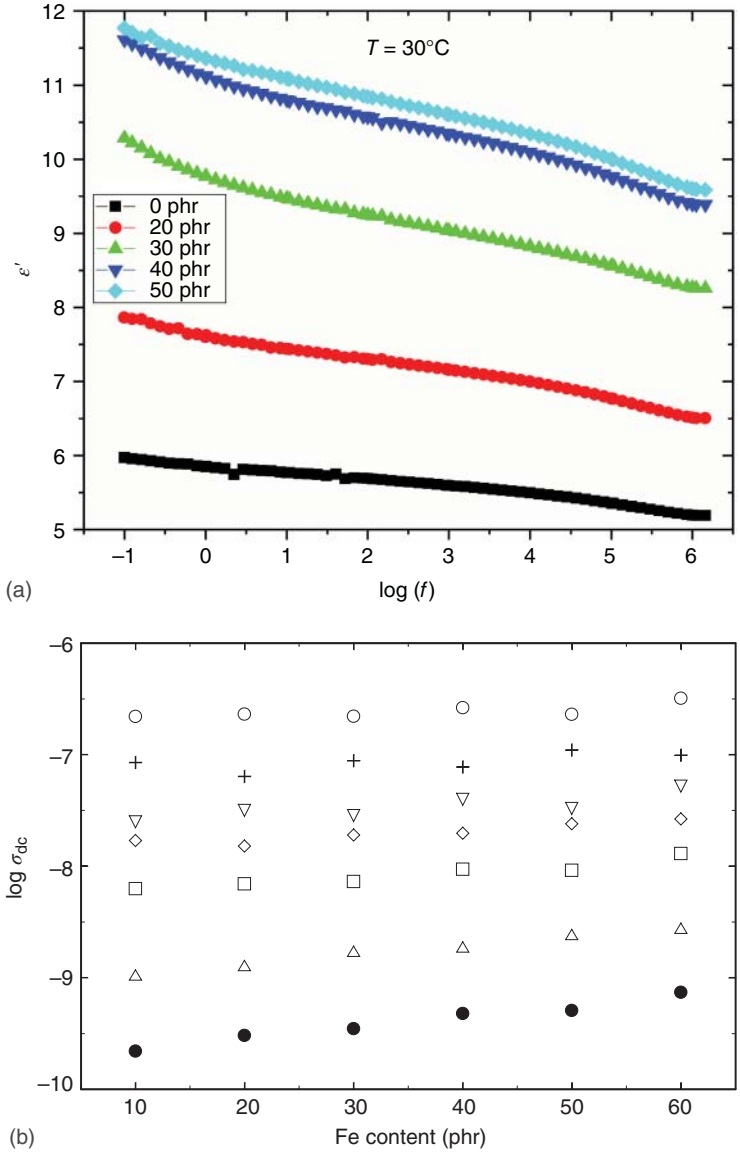

Figure 11.12 (a) The dependence of (ε') upon frequency, at 30 °C, varying the filler content for TiC/epoxy composites [44]. (b) The direct current (dc) conductivity ($\log \sigma_{dc}$) vs. the iron content of composites, at various temperatures: (●) 35 °C, (Δ) 50 °C, (□) 70 °C, (◇) 80 °C, (▽) 90 °C, (+) 100 °C, and (O) 120 °C. Source: Figure reused from [28] with permission.

applied field, due to the inertia of dipoles (permanent and induced) to follow the increasing alternation of the field. The achieved level of polarization lowers, and consequently, values of (ε') diminish. Enhancement of the TiC content results in higher values of the real part of dielectric permittivity because composites' electrical heterogeneity raises. Space charge carriers, present in the composites from the state of their fabrication, accumulate at the interfaces of the constituents forming dipoles strengthening thus IP.

Conductivity under dc conditions of iron particle-reinforced epoxy composites is presented in Figure 11.12b, as a function of the filler content, at various temperatures. Evidently, dc conductivity increases gradually with iron content, at constant temperature, although without achieving an abrupt augment to its values. It can be concluded easily that all composites exhibit dielectric behavior, and no transition from the insulating to the conductive behavior takes place. On the contrary, at constant iron content, a significant alteration of dc conductivity with the increase of temperature is recorded. This enhancement is almost 4 orders of magnitude and implies the presence of a thermally activated charge transport process [28]. In systems exhibiting metallic-type conduction, conductivity diminishes with temperature ($d\sigma/dT < 0$), while dielectric materials acquire higher values of conductivity with increasing temperature ($d\sigma/dT > 0$). In dielectric materials, the dependence of conductivity upon temperature is expressed via Eq. (11.16), which extrapolates conductivity to zero when temperature tends to zero:

$$\sigma_{dc}(T) = \sigma^0 \exp\left[-\frac{E_A}{k_B T}\right] \tag{11.16}$$

where σ^0 is a pre-exponential factor reflecting the conductivity at infinite temperature, E_A the activation energy of the process, k_B the Boltzmann constant, and T the absolute temperature. The dependence of dc conductivity on the reciprocal temperature for various iron particles content is given in Figure 11.13. Data are successfully fitted via the Arrhenius form of Eq. (11.16) in the semi-logarithmic representation of Figure 11.13. For each composite system, activation energy can be determined via the linear fittings of Figure 11.13. Obtained values range between 0.858 and 0.743 eV, from the lower to the higher filler content [28] and diminish systematically as the conductive phase content increases.

Activation energy is considered as a reflection of the composite's microstructure related to the mean size of the metal clusters, their mean interparticle distance, and denoting the minimum required energy for charge transport [28, 42, 43]. Increasing the conductive phase content facilitates the conduction process, since metal particles are getting closer, and subsequently, activation energy diminishes. Considering that Eq. (11.16) is valid in nonconductive materials, its applicability on the data presented in Figure 11.12b indicates the absence of a "metallic-type" contribution to the conductance process.

Aiming to investigate further the occurring conduction mechanism, variable range hopping (VRH) model was applied on the data of Figure 11.12b. VRH has been proposed by Mott [45–47] and is considered applicable to amorphous and disordered materials. According to VRH, charge transport is a phonon-assisted process

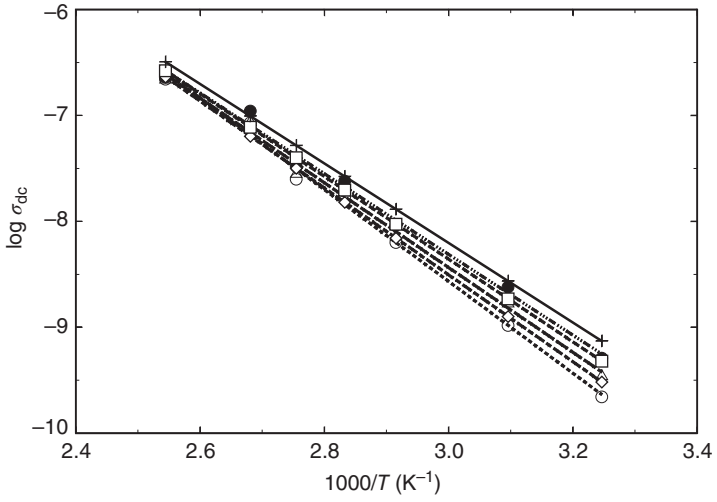

Figure 11.13 The direct current (dc) conductivity (log σ_{dc}) vs. the reciprocal of temperature (1000/T) of the composites with (O) 10, (◇) 20, (Δ) 30, (□) 40, (•) 50, and (+) 60 phr in iron content. Source: Figure reused from Psarras [28] with permission.

and charges move (hop) between nearby localized states with different energies or between spatially separated sites with similar energy. Neglecting the interactions between charge carriers, the temperature dependence of dc conductivity in this process is described by Eq. (11.17):

$$\sigma(T) = \sigma_0 \exp\left[-\left(\frac{T_0}{T}\right)^{\gamma}\right] \tag{11.17}$$

where the pre-exponential factor σ_0 expresses the limiting value of conductivity when temperature tends to infinity, T_0 is a parameter considered as the degree of disorder, T the absolute temperature, and exponent γ expresses the dimensionality of the conduction process. Exponent γ is defined as $\gamma = 1/(1+d)$, where $d = 1,2,3$ represents the dimension of the process.

It is worth mentioning the difference between Eqs. (11.16) and (11.17). The first one describes the temperature dependence of conductivity in dielectric materials (nonconductive materials) and thus is of a more general validity. The second one describes a specific, thermally activated, charge transport mechanism. For this reason, both of them can be applied on the same data, and different information can be extracted by each of them.

The applicability of VRH model upon a set of experimental data is investigated by linear fitting data when plotted in the form of $\log(\sigma \cdot T^{1/2}) = f(T^{-\gamma})$. The quality of produced least square fitting curves provides evidence for the charge transport mechanism as well as for the dimensionality of the conduction process. VRH model has been used, also, for the description of ac conductivity data at constant frequency [28, 48–50].

In Figure 11.14a, the applicability of VRH model upon conductivity data of Figure 11.12b is examined. Linear fitting curves describe very well conductivity

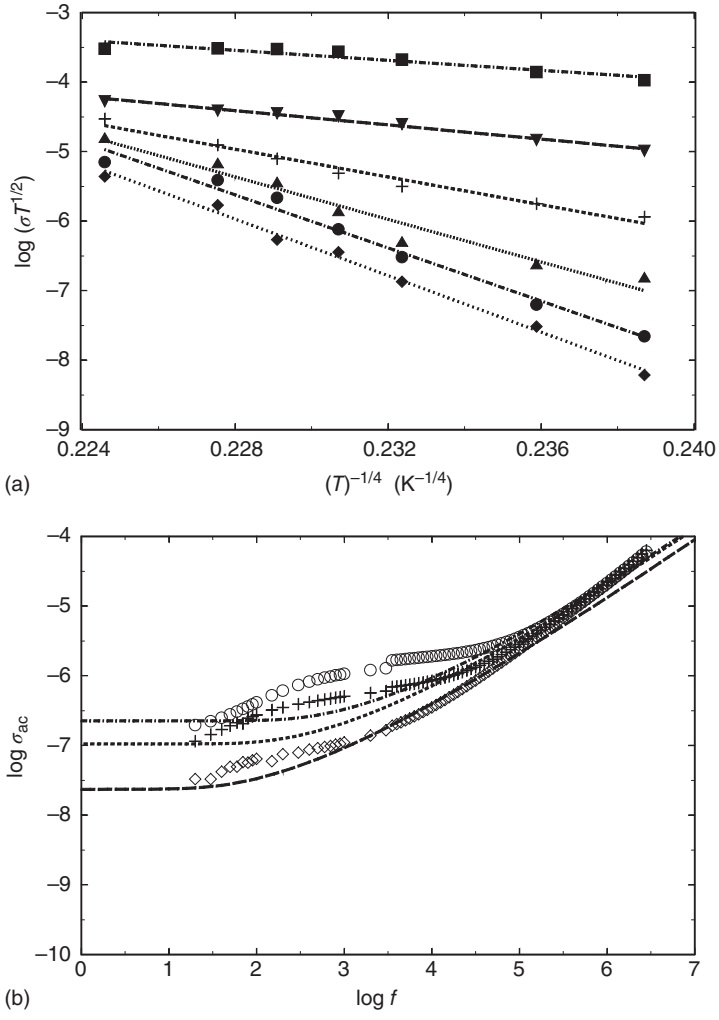

Figure 11.14 (a) Conductivity data of the 50 phr iron/epoxy composite, as described by the variable range hopping model for a three-dimensional (3D) transport mechanism. (♦) dc, (●) 10^2 Hz, (▲) 10^3 Hz, (+) 10^4 Hz, (▼) 10^5 Hz, and (■) 10^6 Hz. (b) The ac conductivity (log σ_{ac}) vs. log f of the 50 phr iron/epoxy composite, at various temperatures: (◇) 80 °C, (+) 100 °C, and (O) 120 °C. Source: Figure reused from Psarras [28] with permission.

data and their variation with temperature, revealing hopping as the occurring charge transport process under dc and ac conditions. Parameter γ is taken as equal to 1/4, for two reasons: (i) specimens are thick (3 mm) and thus a 3D conduction process is expected, and (ii) the fitting quality factor R^2 takes the closest to unity value for $d = 3$. Notably that ac conductivity values increase with frequency since charge carriers execute jumps over adjacent sites, allowing thus the participation of an increased number of carriers. As stated previously, ac conductivity cumulates contributions from all dissipative effects including an actual ohmic conductivity,

caused by migrating charge carriers on isolated metallic clusters, as well as a frequency dielectric dispersion [20]. Although VRH model originally proposed for amorphous semiconductors [24, 46, 47], it has been proved very sufficient in describing conductivity of conducting polymers [51–53] and polymer matrix composites [28, 42, 43, 50, 54]. VRH model describes the thermally assisted dc conduction or ac conductivity at constant frequency.

An additional verification of the hopping transport mechanism is obtained by examining conductivity as a function of frequency at constant temperature. In disordered solids, where conductivity data are typically in accordance with the ac universality law, Eq. (11.11), hopping conduction is the prevailing charge transport mechanism [14]. Random free-energy barrier model, also known as symmetric hopping model, describes the dependence of conductivity on frequency, at constant temperature, in disordered solids [26, 27, 55, 56]. This model, proposed by Dyre, considers dc conductivity as thermally activated according to Eq. (11.16), while ac conductivity is less temperature dependent. The latter suggests that, under ac conditions, conduction processes are determined by lower values of activation energy with respect to the dc ones. Moreover, in this model, it is assumed that charge carriers are not mutually interacting and remain at sites with minimum energy. According to the methodology constructed by Dyre and assuming a continuous-time random walk approximation, the following equation for σ_{ac} is derived [27]:

$$\sigma_{ac}^{*}(\omega) = \sigma_{dc}\left[\frac{i\omega\tau}{\ln(1+i\omega\tau)}\right] \tag{11.18}$$

where σ_{dc} is dc conductivity, ω the angular frequency, and τ the relaxation time. Resolving the complex function of Eq. (11.18) in real and imaginary parts, the following equations are produced:

$$\sigma'(\omega) = \sigma_{ac} = \frac{\sigma_{dc}\omega\tau\arctan(\omega\tau)}{\frac{1}{4}\ln^2\left(1+\omega^2\tau^2\right) + (\arctan\omega\tau)^2} \tag{11.19}$$

$$\sigma''(\omega) = \frac{\sigma_{dc}\omega\tau\ln\left(1+\omega^2\tau^2\right)}{\frac{1}{2}\ln^2\left(1+\omega^2\tau^2\right) + 2(\arctan\omega\tau)^2} \tag{11.20}$$

Figure 11.14b presents ac conductivity data for the 50 phr iron/epoxy composite at three different temperatures [28]. In the low- and high-frequency regions, data follow Eq. (11.11). At high frequencies, the influence of temperature is negligible, while at low frequencies is more pronounced. Lines have been produced by employing Eq. (11.19) in an analytical way with the angular frequency as the independent variable. The agreement of data with predicted values is obvious. The occurring deviations at intermediate frequencies are related to the existence of dielectric relaxation processes. However, the random free-energy barrier model has not been developed to describe/predict dielectric relaxations. With the aforementioned analysis, it can be concluded that below percolation threshold the main charge transport mechanism is hopping conduction. This conclusion leads to the necessity of examining the conduction mechanism in the vicinity and above percolation threshold.

Figure 11.15a depicts dc conductivity as a function of conductive phase content for a carbon black (CB)/epoxy system, at various temperatures [42]. The distribution

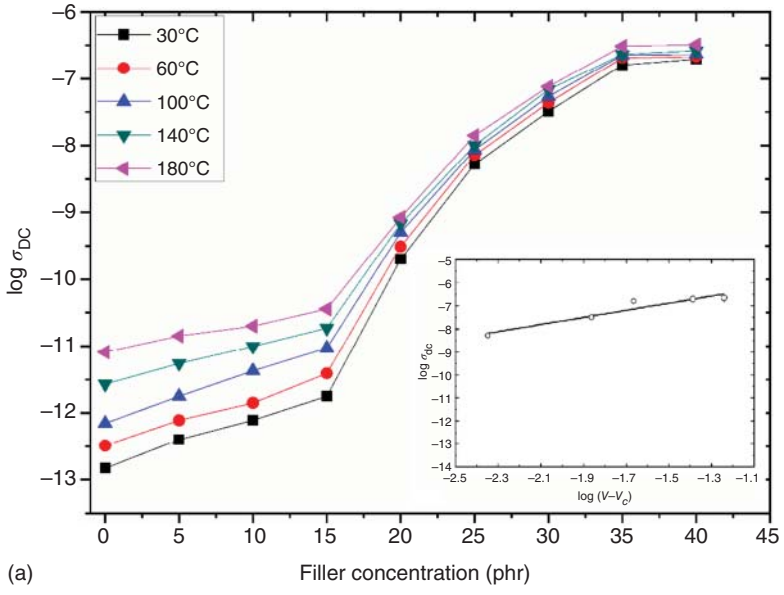

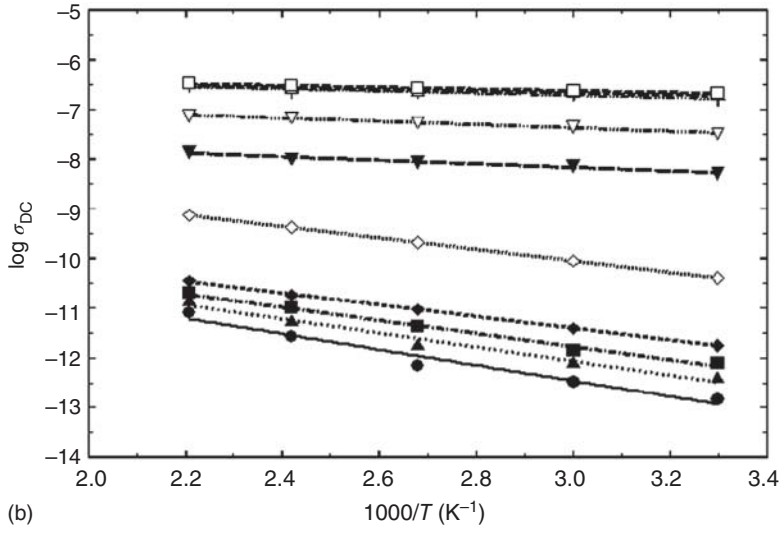

Figure 11.15 (a) dc conductivity of the carbon black (CB)/epoxy composites as a function of filler content at various temperatures. Inset presents an example of the percolation threshold determination at 30 °C. (b) dc conductivity vs. the reciprocal of temperature of the composites with (●) 0, (▲) 5, (■) 10, (♦) 15, (◊) 18, (▼) 20, (▽) 23, (+) 25, (Δ) 30, and (□) 35 phr in CB content. Source: Figure reused from Psarras [42] with permission.

of conductivity values in Figure 11.15a implies the existence of three regions. In the first one, at the lower values of CB content and before the transition zone, conductivity takes low values that gradually increase with filler content. In the same region, the effect of temperature is evident leading to higher σ_{dc} values. The second region is the transition zone, where a sharp and abrupt increase of conductivity values is

present. Conductivity enhances by approximately five orders of magnitude in a very small variation of the conductive phase content (less than 3% in volume fraction). Critical concentration for the transition from the insulating to the conductive behavior should be lying within this region. The third region lies after the transition zone, and conductivity values appear to be affected neither from CB content nor from temperature. In the third region, conductivity values might undergo a small decrease with filler concentration and temperature [42, 43, 54]. The effect of filler concentration is related to the morphology of the composite, the formation of clusters and "dead ends" or self-circuited conductive paths, while the effect of temperature is attributed to the introduction of another conduction mechanism via the physical or geometrical contact of conductive particles. For the determination of percolation threshold and critical exponent, data are plotted in a double logarithmic graph, and scaling law of Eq. (11.15) is employed for fitting data according to the formula $\log\sigma_{dc} \approx t[\log(P - P_C)]$. Interestingly, critical concentration remains unaffected in all examined temperatures taking the value of $P_C = 19$ phr or in volume fraction $v_C = 9.65\%$. Inset in Figure 11.15a presents an example of the percolation threshold determination. Percolation threshold has been found to vary with temperature in polymer composites at temperatures above the glass transition of the matrix, leading to dynamic percolative systems [54]. In the case of data of Figure 11.15a, the employed epoxy matrix has a high glass transition temperature (~195 °C) [42], and in the examined temperature range, all composites remain in the glassy state, resulting in a "frozen" percolation process. Critical exponent (t) appears to decrease systematically with temperature from 1.54 to 1.31 [42]. Its variation should be related to the charge transport mechanisms, reflecting also the possible interactions between the composite's phases. Recalling that conduction process in dielectrics is thermally activated, the applicability of Eq. (11.16) is examined in Figure 11.15b. As it can be seen, conductivity data are well fitted implying Arrhenius-type behavior. Slopes of the straight lines of Figure 11.15b allow the determination of activation energy for each system. Values of activation energy, shown in Figure 11.16a, diminish monotonously with conductive phase content. Activation energy is considered as a function of composites' morphology and microstructure reflecting the mean size of conductive "islands" (particles or clusters) and their mean distance [42, 57]. By these means, the increase of conductive filler content results in the reduction of the interparticle separation and finally in diminishing of activation energy. The variation of parameter (T_0) with CB volume fraction is depicted in Figure 11.16b. T_0 attains high values for CB particles concentration lower than the critical one. As the conductive filler content increases and exceeds the value of the percolation threshold, (T_0) diminishes sharply up to four orders of magnitude. This behavior is in accordance with results from different systems with varying conductivity and expresses the stochastic or disordered character of the investigated composites [28, 49, 50, 58, 59].

In composites with more conductive inclusions, such as silver particles, in the vicinity of percolation threshold, metallic-type conduction occurs via geometrical contacts and Eq. (11.16) becomes not applicable leading to the paradox of negative values for activation energy. The latter simply signifies that the character of the material cannot any longer be considered as dielectric [43].

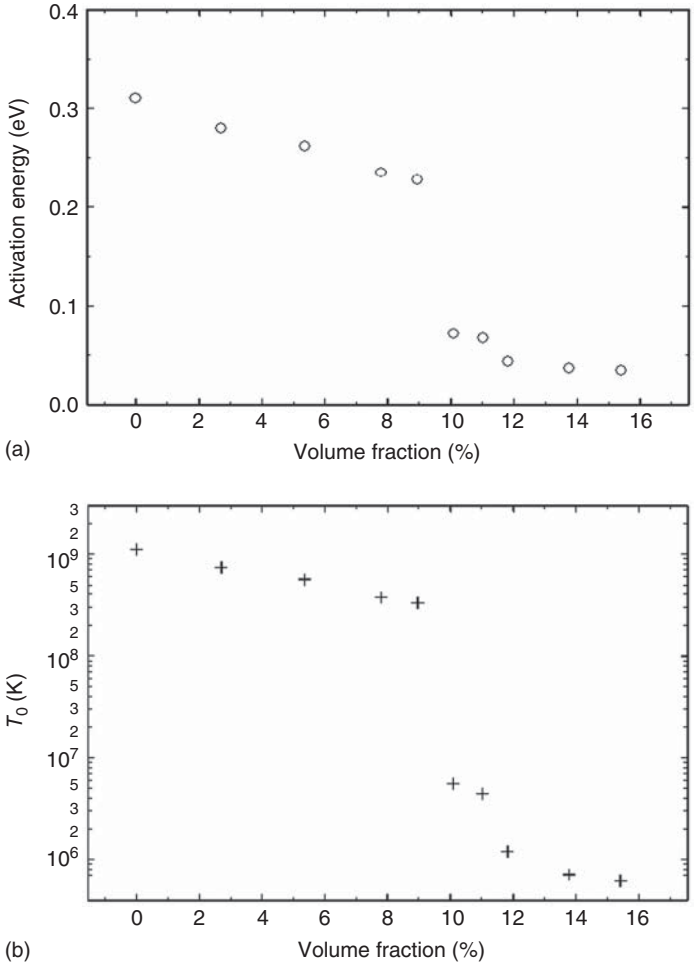

Figure 11.16 (a) Activation energy (E_A) and (b) parameter T_0, as a function of filler content for CB/epoxy composites. Source: Figure reused from Psarras [42] with permission.

11.5.2 Epoxy/Conductive Filler Nanocomposites

Snapshots of the dielectric response of TiC/epoxy nanocomposites are given in Figure 11.17a,b. The dependence of the real part of dielectric permittivity upon frequency follows the typical form that has been already discussed. Moreover, (ε') increases with filler due to the electrical properties of the particles of titanium carbide. The achieved values of (ε') of TiC/epoxy nanocomposites appear to be higher than the corresponding ones of micro-composites at the same or at even higher reinforcing phase concentration (Figure 11.12a). Loss modulus index as a function of frequency for the TiC/epoxy set of nanocomposites, at 100 °C, is presented in Figure 11.17b. The recorded loss peak is attributed to α-relaxation process (glass-to-rubber transition). Loss peak frequency position does not vary significantly with TiC content, indicating good adhesion between the constituents

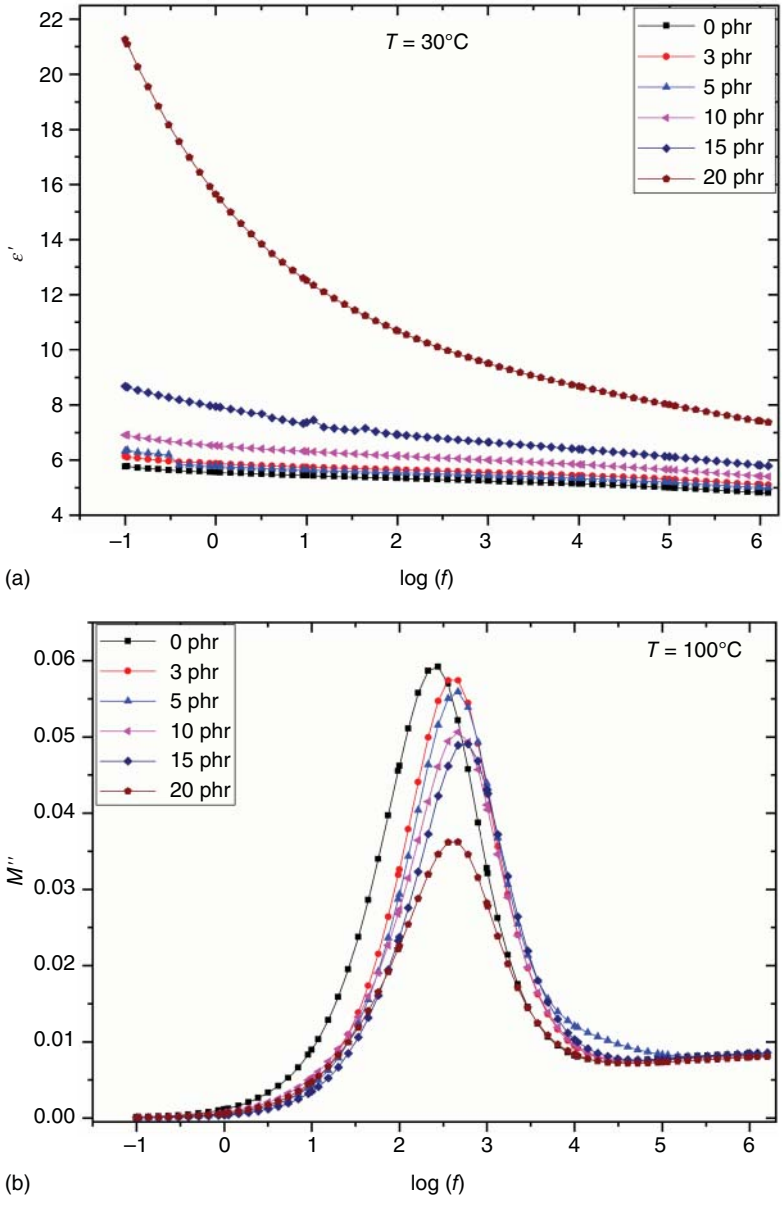

Figure 11.17 (a) The real part of dielectric permittivity (ε') as a function of frequency at 30 °C and (b) the loss modulus index (M'') as a function of frequency at 100 °C, varying the filler content for TiC/epoxy nanocomposites [60].

and sufficient wetting of the nanoparticles by the matrix. A slight shift of the nanocomposites peak at higher frequencies with respect to the neat matrix denotes a small decrease of the glass-to-rubber transition temperature [14, 61].

Nowadays, carbon nanoparticles, such as carbon nanofibers, carbon nanotubes, and exfoliated graphite nano-platelets (GNP), are in the first line from all possible

polymer matrix-reinforcing materials [62–68]. Carbon nano-inclusions are able to improve mechanical performance (i.e. stiffness, tensile strength, etc.), electrical response (dielectric behavior and conductivity), and thermal conductance of the nanocomposites [69]. Exfoliated GNPs consisted of a few stacks of graphite layers. The real part of dielectric permittivity vs. temperature, at constant frequency 1 Hz,

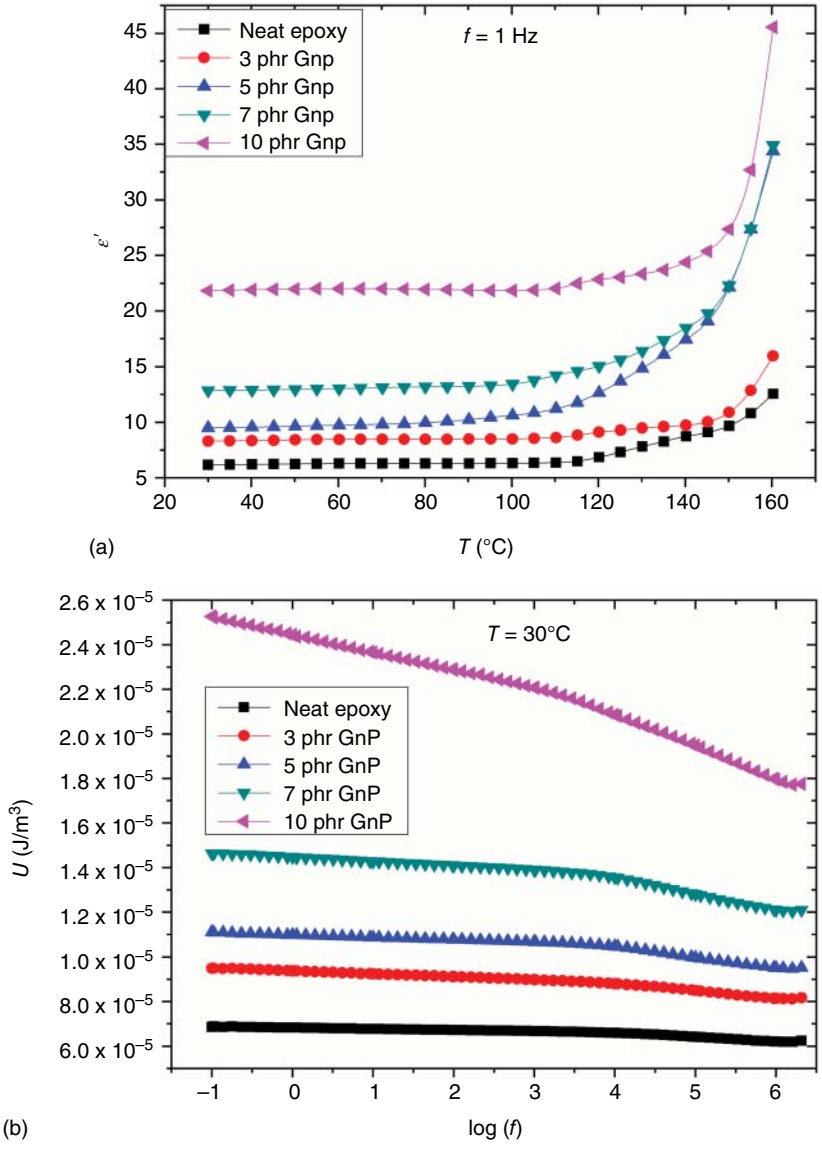

Figure 11.18 (a) Real part of dielectric permittivity vs. temperature, at constant frequency 1 Hz, (b) energy density, at constant field $E = 0.5$ kV/m, as a function of frequency at 30 °C, and (c) energy density, at constant field $E = 0.5$ kV/m, as a function of temperature at 1 Hz, for a set of graphite nano-platelets (GNP)/epoxy nanocomposites. Source: Figure reused from Patsidis et al. [70] with permission.

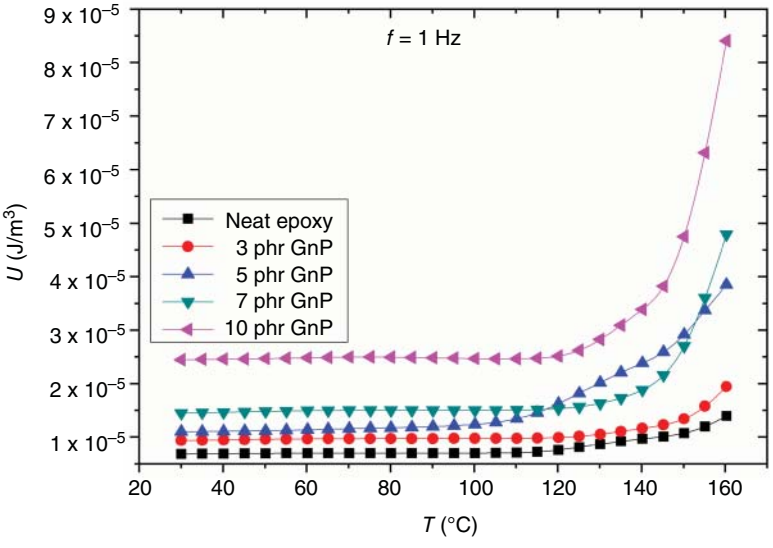

Figure 11.18 (*Continued*)

for a set of GNP/epoxy nanocomposites is presented in Figure. 11.18a [70]. GNP content causes a systematic increase of (ε') in the entire temperature range. In addition, at temperatures higher than T_g values of (ε') augment further because of the enhanced synergetic mobility of large parts of the macromolecular chains. In the same temperature range, the strengthening of the IP process, related to the electrical heterogeneity of the systems, adds another contribution to the permittivity values.

Polymer nanocomposites are considered as suitable materials for the development of electrical energy storing devices. Nano-inclusions alter the system's dielectric permittivity, while polymer matrix offers stability and high dielectric breakdown strength [71–74]. The potential ability of nanocomposites to store electric energy is expressed via the energy density function, which for linear dielectrics and at low applied fields is given by Eq. (11.21) [73, 75]:

$$U = \frac{1}{2}\varepsilon_0 \varepsilon' E^2 \tag{11.21}$$

where ε_0 is the permittivity of free space and E the electric field's intensity. Obviously, the maximum value of energy density is determined by the dielectric breakdown strength, while the only material parameter involved in Eq. (11.21) is the real part of dielectric permittivity. Energy density, at constant field $E = 0.5$ kV/m, as a function of frequency at 30 °C, and temperature at $f = 1$ Hz, for the GNP/epoxy nanocomposites is depicted in Figure 11.18b,c, respectively, [70]. GNP content increase the nanocomposites' dielectric permittivity and energy density in the whole frequency and temperature range up to four times. Optimum performance is exhibited by the nanocomposite with the maximum GNP content.

The variation of ac conductivity vs. frequency at two temperatures (namely 30 and 90 °C) for a set of multi wall carbon nanotubes (MWCNT)/epoxy resin nanocomposites is shown in Figure 11.19. Values of ac conductivity have been determined

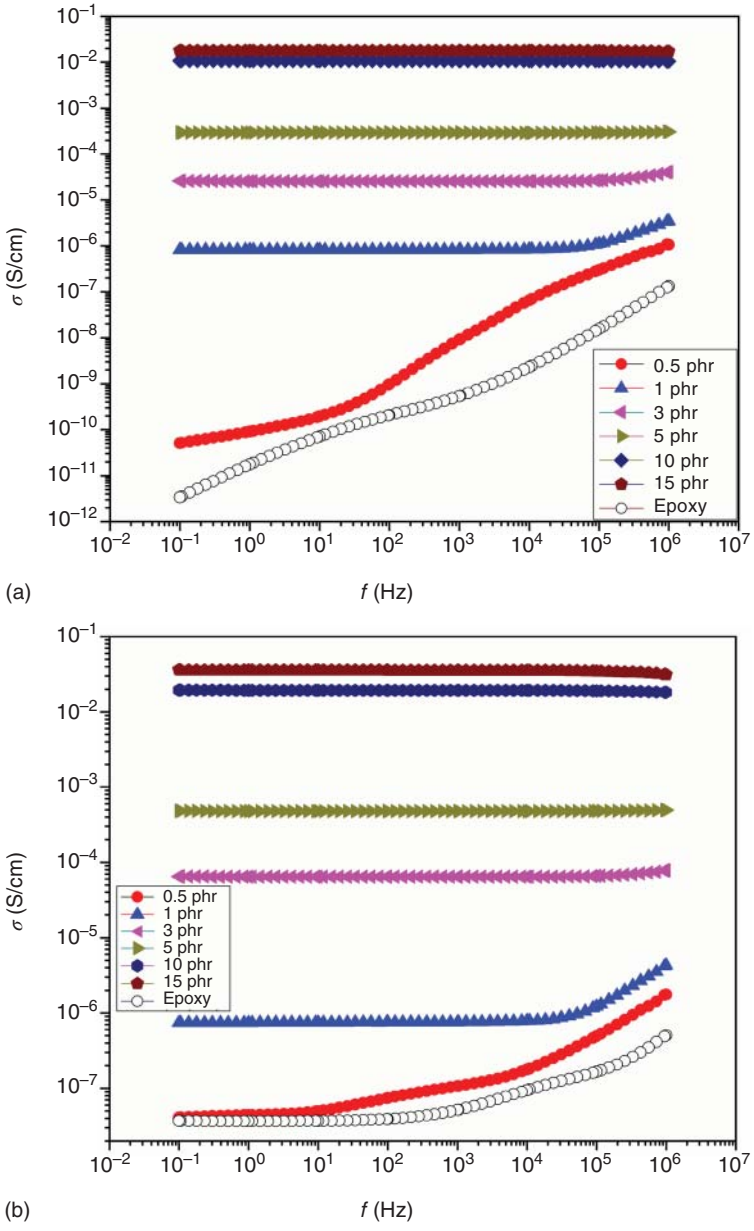

Figure 11.19 Alternating current (ac) conductivity vs. frequency at (a) 30 °C and (b) 90 °C [76] for MWCNT/epoxy nanocomposites.

via Eq. (11.6). Conductive filler content varies from 0.5 to 15 phr, while for comparison reasons, the neat epoxy spectra are also included in the graph. Obviously, σ_{ac} is both frequency and temperature dependent at constant MWCNT content. The influence of frequency is more pronounced in the case of neat epoxy and nanocomposites with low reinforcing phase content (0–1 phr). At MWCNT concentrations higher

than 1 phr, conductivity spectra appear to be frequency independent. However, in the low-frequency edge, all nanocomposites' spectra acquire constant values, which correspond to their dc conductivity value. In this frequency range, charge carriers are forced to migrate over relatively longer distances inside the nanocomposite. The presence and the increase of MWCNT's content facilitate this migration, since it results in the decrement of the "conductive islands" distance. Temperature is another amplifying factor for σ_{ac} due to the applied thermal agitation of charge carriers, which helps them to overcome the potential barriers exerted by the insulating matrix [76].

At the lowest measured frequency (0.1 Hz), which by convention can be considered as the σ_{dc} value, a sharp increase of several orders of magnitude of conductivity is observed between the nanocomposites with 1 and 3 phr in MWCNT content. Figure 11.20a depicts the variation of σ_{ac} with filler content at three different frequencies at 30 °C. The sharp increase of conductivity with a small variation of MWCNT content, present in Figure 11.19, is also apparent in Figure 11.20a. At the lowest frequency, this increase exceeds the seven orders of magnitude, implying that the transition from the insulating to the conductive behavior has been achieved. Percolation threshold or critical concentration should be lying between 1 and 3 phr. The recorded transition can be described via Eq. (11.15). As stated previously, percolation threshold and exponent (t) can be determined by fitting data via the $\log\sigma_{dc} \approx t[\log(P - P_C)]$ formula. Inset in Figure 11.20a gives an example of the determination of critical concentration. At the lowest measured frequency and at 30 °C, critical concentration and exponent (t) take the values of 1.7 and 2.8, respectively [76]. The determined value of critical exponent is higher than the one predicted by the classical percolation theory. According to the classical percolation theory, the value of exponent (t) for a 3D conduction process should be two. However, deviations from the predicted value have been reported often and assigned to the occurring interactions between nano-inclusions or between nano-inclusions and macromolecules, which reflect the dynamic character of the polymer nanocomposites [14, 42, 54]. The dependence of conductivity upon temperature at the lowest measured frequency of 0.1 Hz is shown in the inset of Figure 11.20b. The effect of temperature on conductivity varies below and above the percolation threshold. Below the percolation threshold, conductivity increases with temperature as expressed by the positive value of $d\sigma/dT$, being in accordance with Eq. (11.16), which is valid in dielectric systems. At MWCNT concentrations below the critical content, no complete path has been formed in the composites, through it charges could percolate the whole system. The value of $d\sigma/dT$ above critical content diminishes approaching zero, indicating that the applicability of Eq. (11.16) vanishes. The latter is a strong indication for the existence of a second charge transport mechanism, via physical or geometrical contacts of the conductive inclusions. In this set of nanocomposites, the sign of $d\sigma/dT$ does not become negative implying that "metallic-type" conduction is not the dominating process [76] and that hopping conduction is present above percolation threshold also.

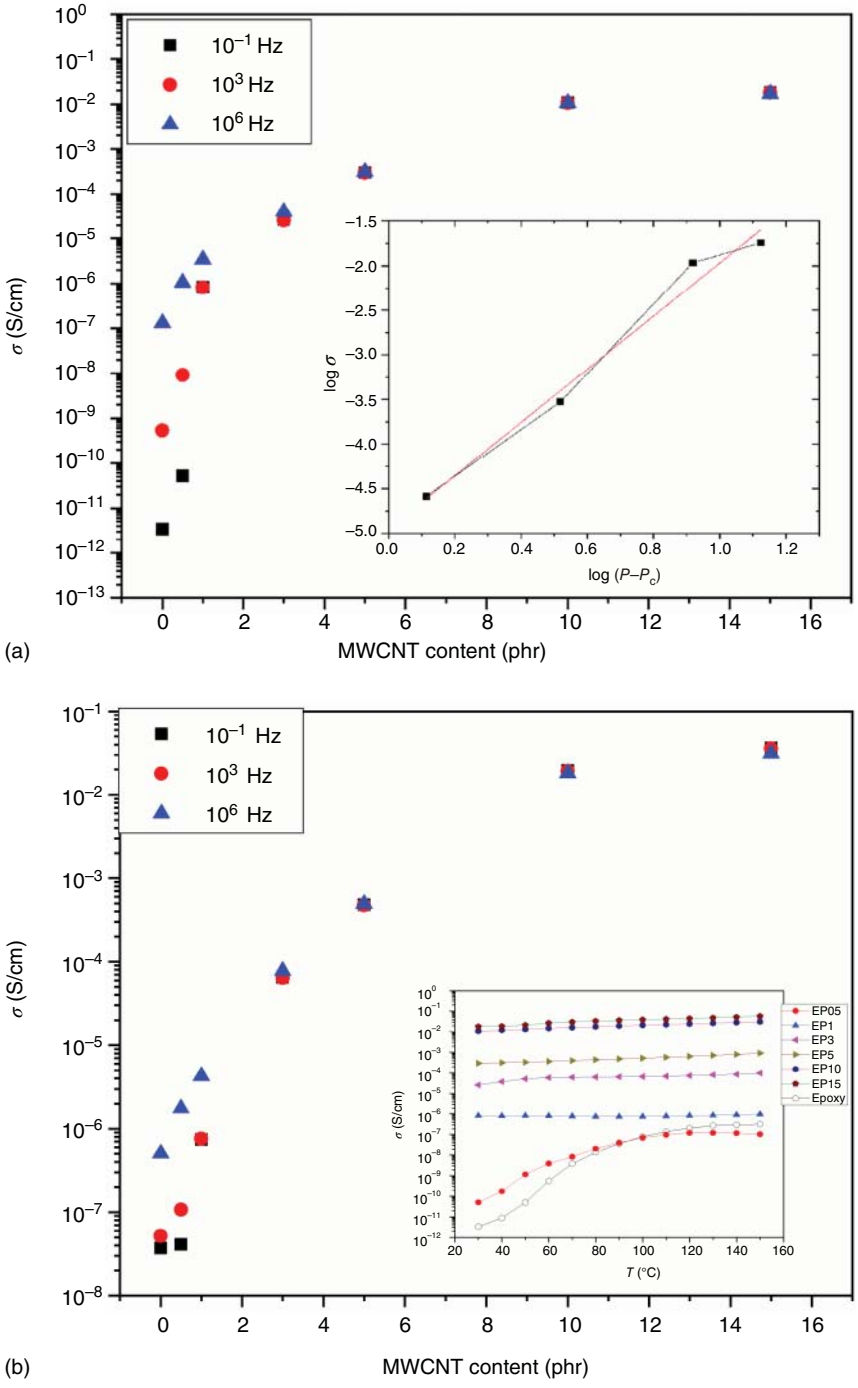

Figure 11.20 Variation of σ_{ac} with MWCNT content at three different frequencies at (a) 30 °C, inset provides an example of percolation threshold determination and (b) 90 °C, inset shows the dependence of conductivity upon temperature at the lowest measured frequency of 0.1 Hz. Source: Trompeta et al. [76].

11.6 Epoxy-Based Hybrid Composites – Targeting Multifunctionality

Epoxy-based hybrid composites or epoxy hybrids are composite materials that incorporate two or more different reinforcing phases. Employed reinforcing materials could differ in various characteristics such as inorganic or organic, conductive or insulating, micro- or nano-inclusions, shape, etc. The incorporation of fillers with various, and sometimes diverting, properties targets the development of composites with multifunctional performance [77, 78]. The term functional materials refers to a class of engineering materials that are able to perform specific functions or operations in response to external stimuli or sign controls [79]. Current requirements of engineering materials include their ability to respond in real time to a rapidly varying working environment. For this reason, in nowadays advanced materials, besides the nominal values of various properties, their controllable behavior under different conditions and stimuli is of great importance. Multifunctional behavior or multifunctional performance is the combination of different desirable properties in a specific material or materials' system. Mechanical sustainability, suitable thermal response, tunable electric conductivity, variable electric polarization and dielectric permittivity, magnetic properties, and thermally induced phase changes are parts of the targeting multifunctional behavior.

Aramid fibers are organic fibers with advanced mechanical properties, which are used as structural reinforcing elements. Electrically, aramid fibers are insulating materials and when they are used as constituents, besides their mechanical reinforcing ability, they also contribute to the dielectric response of the composite. The simultaneous presence of aramid fibers and aluminum microparticles in an epoxy resin results in reinforcing in tandem the mechanical and dielectric performance of the composites. Figure 11.21 presents Cole–Cole plots (M'' vs. M') of aluminum particles/aramid fibers/epoxy resin micro-composites at temperatures varying between 125 and 150 °C [13]. The employed aramid fibers were kevlar 49 aramid pulp of E.I. Du Pont de Nemours, with a mean length of 2 mm, diameter ~14 μm, and density 1.44 g/cm^3. Aluminum microparticles, supplied by Merck,

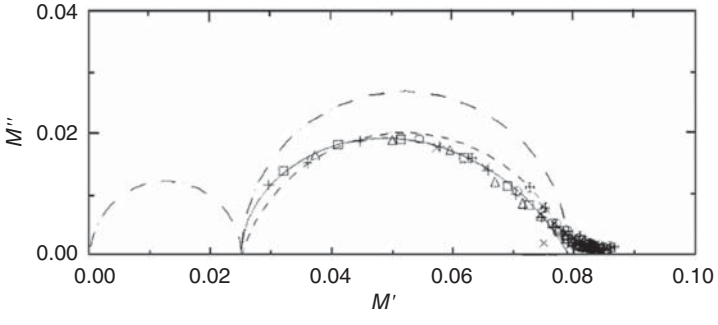

Figure 11.21 Cole–Cole plot of the epoxy system with 25 phr in Al particles and 0.5 phr in aramid fibers. Each line represents a different model function. Source: Figure reused from Tsangaris et al. [13] with permission.

had the form of ellipsoidal with mean axis ratio 0.7 [13]. This ternary hybrid system is characterized by high electrical heterogeneity since in the insulating matrix conductive and dielectric inclusions have been embedded. IP, also known as Maxwell–Wagner–Sillars (MWS) effect, is present at heterogeneous systems and increases with the diversity of their electrical properties [13, 80]. Mobile charges, which are present in the composites from their fabrication stage, move inside the composite and accumulate at the interface of the constituents. At the interface, charges form induced dipoles that have the dimensions of the inclusions. These large dipoles exhibit inertia in responding to the applied ac field, the process is characterized by enhanced relaxation time, and thus, IP is recorded at high temperatures and low frequencies. Low frequencies provide sufficient time for the orientation of dipoles parallel to the field, while high temperatures provide thermal activation. In addition to the dipolar effect, part of the charges at the interfaces achieve to migrate mostly via interface, contributing thus to the system's conductivity. The mathematical description of the phenomenon includes a dipolar and a conductivity term, the influence of which upon the overall process varies according to the constituent materials and the applied conditions (i.e. temperature, frequency, filler content, distribution, etc.) [13, 20, 22, 80]. The real and imaginary part of dielectric permittivity of IP process can be described via Eqs. (11.22) and (11.23):

$$\varepsilon'(\omega) = \varepsilon_\infty + \frac{\left(\varepsilon_s - \varepsilon_\infty\right)\omega\tau}{1+\omega^2\tau^2} \tag{11.22}$$

$$\varepsilon''(\omega) = \frac{\left(\varepsilon_s - \varepsilon_\infty\right)\omega\tau}{1+\omega^2\tau^2} + \frac{\sigma}{\varepsilon_0\omega} \tag{11.23}$$

where ε_s and ε_∞ are the limiting values (at low and high frequencies) of the real part of dielectric permittivity, σ the conductivity of the composite, τ the relaxation time of the process, ω the angular frequency, and ε_0 the dielectric permittivity of free space. The ε_s, ε_∞, and σ parameters are functions of the corresponding permittivities, conductivities, and volume fractions (ε_i, σ_i, v_i), respectively, of the constituent phases as expressed by Eqs. (11.24)–(11.26):

$$\varepsilon_s = \frac{\sum_i v_i \varepsilon_i'/\sigma_i^2}{\left(\sum_i v_i/\sigma_i\right)^2} \tag{11.24}$$

$$\varepsilon_\infty = \frac{1}{\sum_i v_i/\varepsilon_i'} \tag{11.25}$$

$$\sigma = \frac{1}{\sum_i v_i/\sigma_i} \tag{11.26}$$

In the Cole–Cole plots, each formed semicircle corresponds to a relaxation process. Lines in Figure 11.21 are generated by fitting data via the well-known dielectric functions Cole–Cole, Davidson–Cole, and Havriliak–Negami, in their electric modulus representation, varying the skewing factors expressing the symmetric and nonsymmetric distribution of relaxation times [12–14]. The dashed line forming two semicircles in Figure 11.21 is created via Eqs. (11.22) and (11.23) in their electric modulus form [13]. Semicircles correspond to the dipolar and the conductivity terms of Eq. (11.23), with the latter to be formed closer to the origin of the plot. The dipolar

semicircle fails to describe experimental data, since Eq. (11.23) considers a single relaxation time and not a distribution of times. The existence of needle-like and particle-like inclusions as well as possible interactions between composites' phases implies distribution of relaxation times. For this reason, skewing factors in the form of exponents have been proposed for the denominators in the IP formulas.

Epoxy composites incorporating two different polar oxides in the form of ceramic particles are employed for tuning electrical polarization and dielectric permittivity, as well as for inducing functional behavior. Barium titanate is characterized by high values of dielectric permittivity and undergoes a structural transition from the polar ferroelectric phase to the nonpolar paraelectric one in the vicinity of 130 °C. Zinc oxide is a polar ceramic exhibiting piezoelectric [80] and possibly ferroelectric properties. The variation of the imaginary part of electric modulus as a function of frequency at various temperatures for epoxy/20 phr $BaTiO_3$, epoxy/20 phr $BaTiO_3$/50 phr ZnO, and epoxy/50 phr ZnO micro-particles is depicted in Figure 11.22a–c, respectively [81]. In the spectra of pure epoxy (not shown here) and epoxy/20 phr $BaTiO_3$ system (Figure 11.22a), two relaxation processes are evident. Both of them are assigned to the epoxy matrix. The stronger one, occurring at the lower frequencies, is attributed to the glass-to-rubber transition of the matrix (α-mode), while the weak one at high frequencies is related to the reorientation of polar side groups of the macromolecular chains (β-mode) [81]. Loss spectra of the composites with ZnO particles include an additional relaxation, which occurs in the intermediate-frequency zone between the α- and β-relaxations. Evidently, this relaxation is related to the ZnO particles. The intensity of this process is much higher than the respective of β-mode, leading in masking of the latter. This mechanism has been observed also in TiO_2/epoxy, ZnO/epoxy, and Fe_3O_4/epoxy composites [35, 82–84]. Since this process is recorded at the intermediate frequencies, between the relatively slow glass-to-rubber transition mechanism and the fast polar side groups reorientation process, is referred as intermediate dipolar effect (IDE) and is attributed to intrinsic IP effects in parts of the ceramic ZnO [81].

The ability of storing energy in hybrid nanocomposites containing the same micro- and nano-$BaTiO_3$ particles, or nano-$BaTiO_3$ particles and GNP, is depicted in Figure 11.23. The energy storage ability is expressed via the relative energy density, which is defined according to Eq. (11.27), as the ratio of the energy density of the composite upon the energy density of the neat matrix:

$$U_{\text{rel}} = \frac{U_{\text{comp}}}{U_{\text{mat}}} \tag{11.27}$$

Figure 11.23a depicts U_{rel} as a function of temperature at 0.1 Hz for hybrid micro- and nano-$BaTiO_3$ particles/epoxy systems. U_{rel} increases up to 1.45 times relative to unreinforced matrix. Evaluated spectra include two sets of peaks at approximately 105 and 130 °C. The first one corresponds to α-relaxation (glass-to-rubber transition), while the second one is related to IP and to ferroelectric-to-paraelectric transition of barium titanate particles. Both processes occur at close temperatures and thus they superimpose. For comparison reasons, the total concentration, in all presented spectra, is 10 phr, and for the same reasons, spectra from the 10 phr micro-composite and

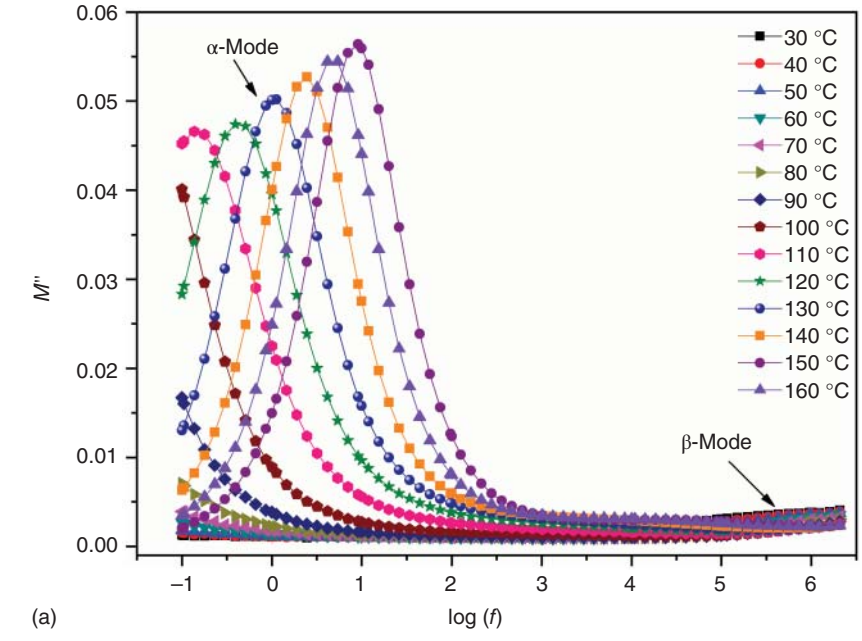

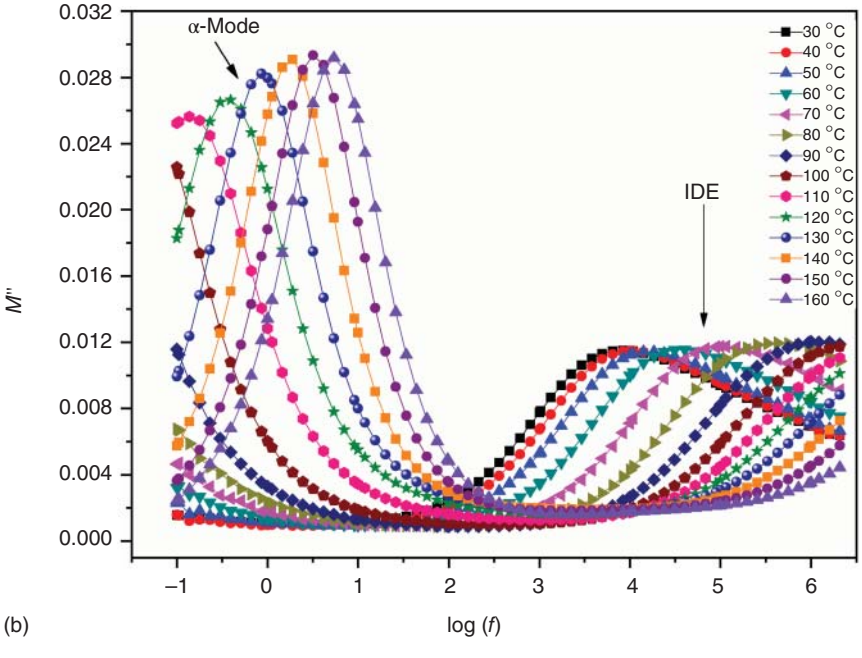

Figure 11.22 The variation of the imaginary part of electric modulus (M'') as a function of frequency at various temperatures for (a) epoxy/20 phr $BaTiO_3$, (b) epoxy/20 phr $BaTiO_3$/50 phr ZnO, and (c) epoxy/50 phr ZnO micro-composites. Source: Figure reused from Ioannou et al. [81] with permission.

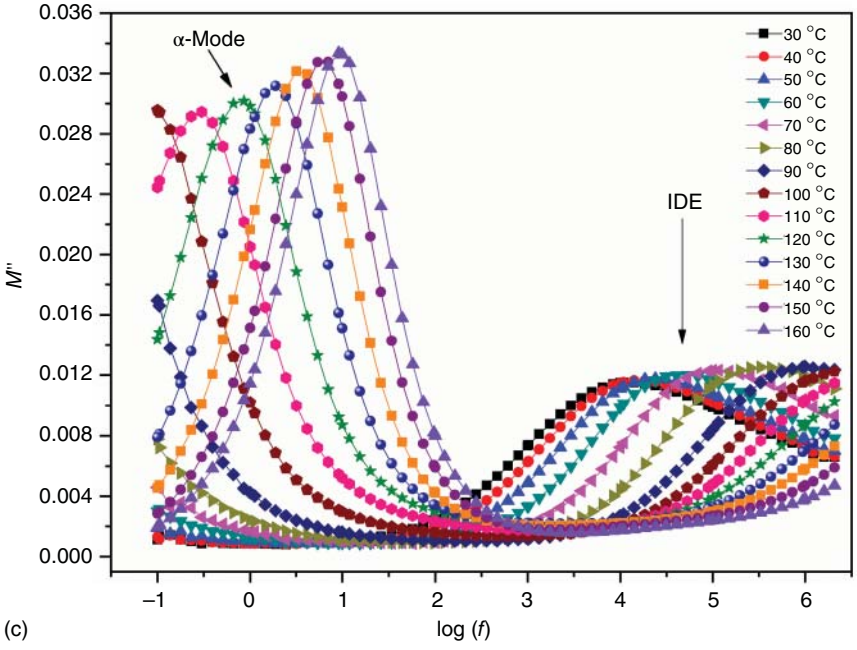

Figure 11.22 (*Continued*)

nanocomposite are also shown. In Figure 11.23b, the variation of U_{rel} vs. temperature, at 0.1 Hz, for hybrid $BaTiO_3$/GNP/epoxy nanocomposites is presented. For reasons of comparison, the spectra of 10 phr GNP/epoxy and 10 phr nano-$BaTiO_3$/epoxy are also shown. The enhancement of energy storing ability exceeds 6.5 times the one of neat epoxy. Energy storing ability increases with GNP content because of their higher conductivity and resulting electrical heterogeneity, as well as due to their elongated 2D morphological form.

Part of the multifunctional performance of nanocomposites is their ability to act as energy storing devices. Dispersed nano-inclusions within an epoxy matrix are regarded as a distributed network of nano-capacitors where electric energy can be stored and retrieved. These systems are also known as nano-dielectrics and their enhanced ability to store energy is related to the extended interfacial area, the high values of permittivity of the filler, and the low dimensions of the inclusions. A schematic representation of a $BaTiO_3$/epoxy nano-dielectric acting as a compact capacitive energy storing device is shown in Figure 11.24 [75]. Nanoparticles are considered as a combination of a capacitive and a resistive element corresponding to the storage and loss of energy, interface has a crucial role, while conduction might occur via interface or between semiconductive particles [75, 85]. To create an energy storing device, it is necessary to establish a procedure where energy can be stored and also retrieved (harvested) in a measurable way and not only calculate the potential ability of storing energy as expressed by the energy density formula of

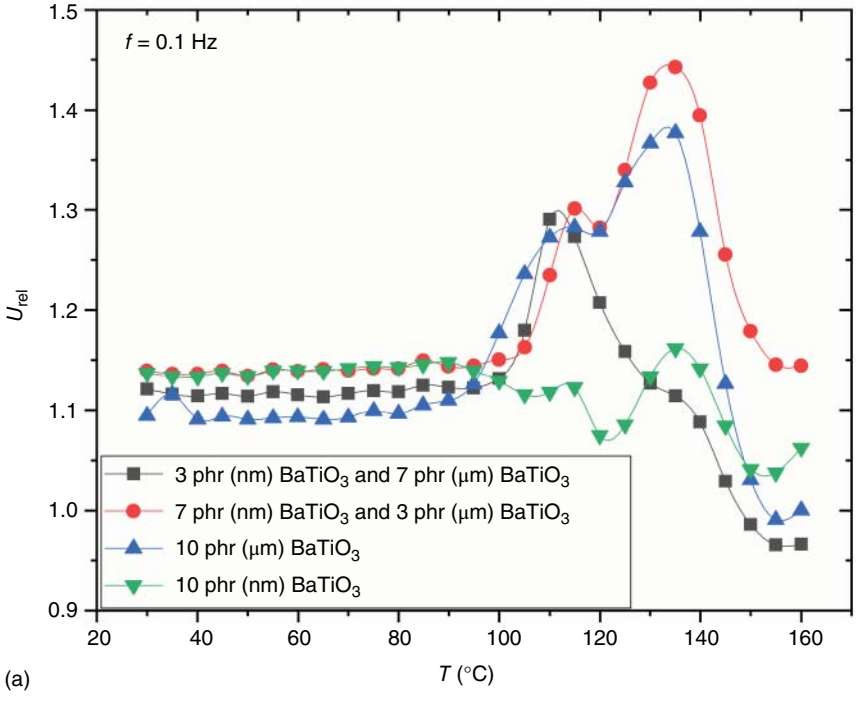

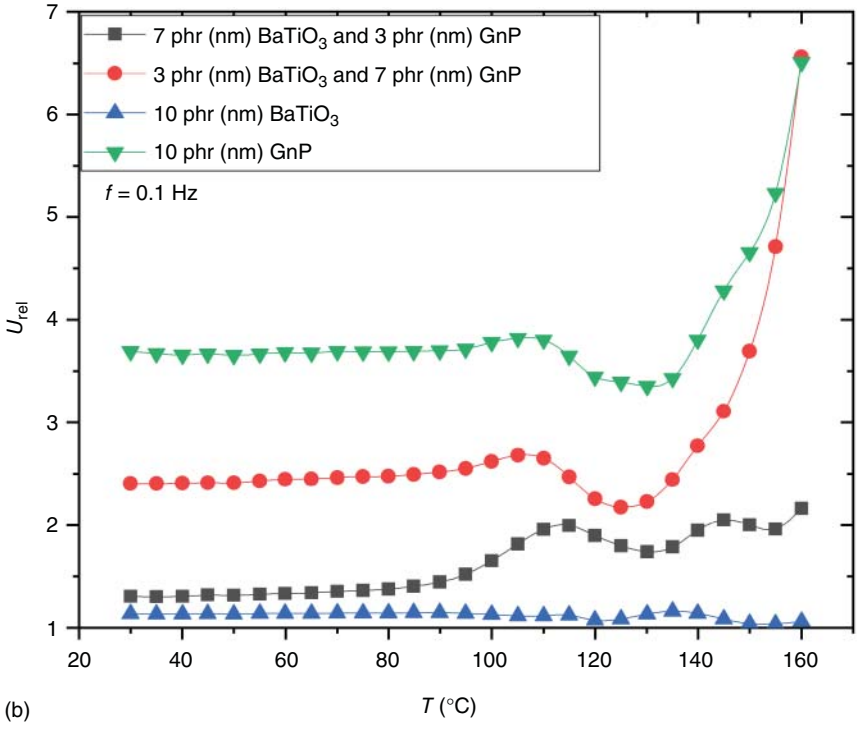

Figure 11.23 (a) U_{rel} as a function of temperature at 0.1 Hz for hybrid micro- and nano-$BaTiO_3$ particles/epoxy systems. (b) U_{rel} vs. temperature, at 0.1 Hz, for hybrid $BaTiO_3$/graphite nano-platelets (GNP)/epoxy nanocomposites.

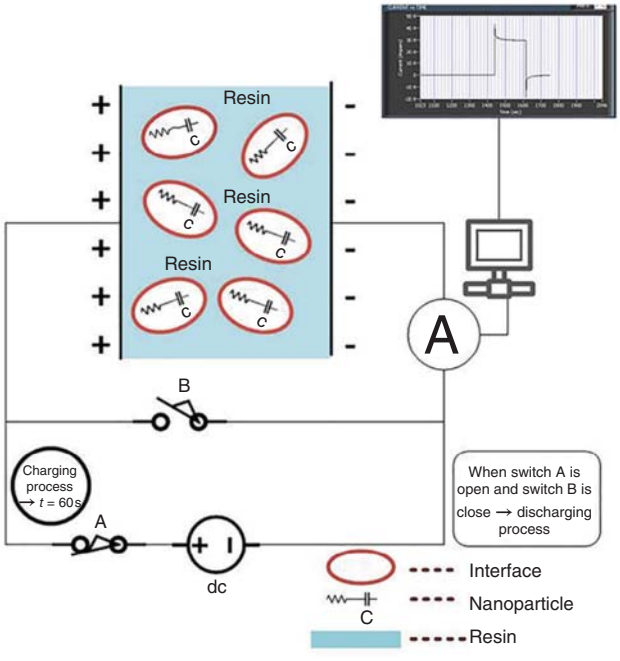

Figure 11.24 Schematic representation of a $BaTiO_3$/epoxy nano-dielectric acting as a compact capacitive energy storing device and experimental setup for dc measurements. Source: Figure reused from Manika and Psarras [75] with permission.

Eq. (11.21). The stored energy under dc conditions can be obtained via Eq. (11.28) [74, 75, 85]:

$$E = \int_0^Q V \cdot \mathrm{d}q = \frac{1}{2}\frac{Q^2}{C} \tag{11.28}$$

where E is the energy of the capacitor, Q the accumulated charge, and C the capacitance. Capacitance is a function of material's dimensions and dielectric permittivity or dielectric constant. Stored and retrieved energy can be determined by integrating the recorded, depending on time, charging and discharging current functions $I = f(t)$ with parameters the applied charging voltage, time, and temperature for each examined composite [74, 75, 85]. Charging (storing) and discharging (retrieving) energies are evaluated via Eq. (11.29):

$$E = \frac{1}{2}\frac{\left[\int I(t) \cdot \mathrm{d}t\right]^2}{C} \tag{11.29}$$

The effectiveness of composite materials as capacitive energy storing devices can be evaluated by introducing the coefficient of energy efficiency (n_{eff}), which is defined as the ratio of the retrieved upon the stored energy, through Eq. (11.30):

$$n_{\mathrm{eff}} = \frac{E_{\mathrm{discharged}}}{E_{\mathrm{charged}}} \tag{11.30}$$

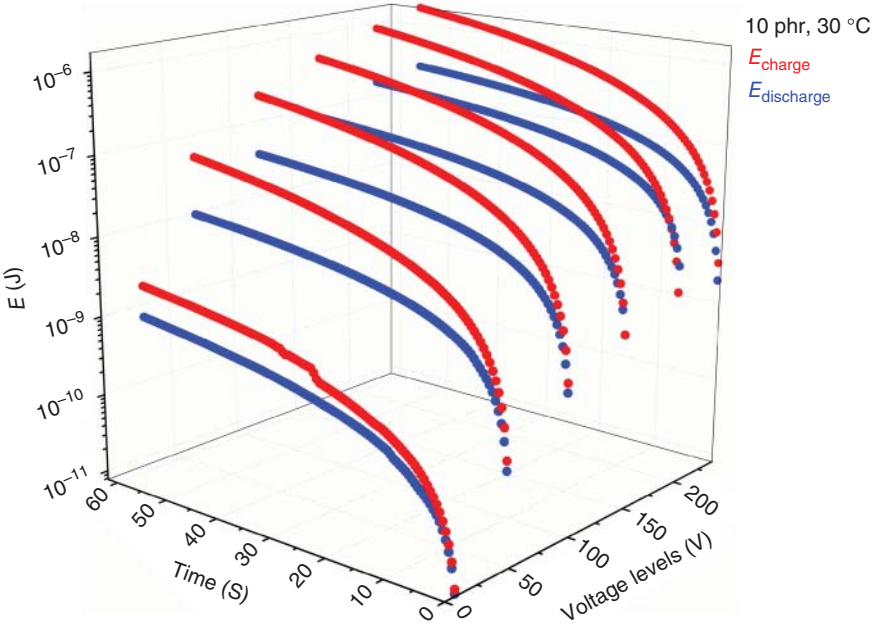

Figure 11.25 Three-dimensional (3D) spectra of the stored and retrieved energy as a function of dc charging voltage and time, at 30 °C, for a 10 phr $BaTiO_3$/epoxy nanocomposite. Source: Figure reused from Manika and Psarras [75] with permission.

Parameters affecting the coefficient of energy efficiency are charging and discharging time, charging voltage, temperature, and composite's filler content.

Figure 11.25 depicts 3D spectra of the stored and retrieved energy as a function of dc charging voltage and time, at 30 °C for a 10 phr $BaTiO_3$/epoxy nanocomposite [75]. Stored and harvested energies increase with charging voltage and time. Table 11.1 summarizes the values of the coefficient of energy efficiency for charging voltages 50, 100, and 200 V, at the time instant 10 seconds, at 30 °C, varying the barium titanate content. Optimum performance corresponds to the 7 phr $BaTiO_3$/epoxy nanocomposite at 200 V.

Coefficient of energy efficiency is a multiparametric quantity exhibiting a non-systematic variation with all four applied parameters (charging voltage/field, time, temperature, filler content). Increasing the intensity of the field results in the injection of an enhanced number of charge carriers by the electrodes to the composite and at the same time facilitates the space charge migration by lowering the intrinsic potential barriers [86]. By these means, charging and discharging currents augment with the applied voltage/field, although the same tendency follows the leakage currents. Increasing of nano-filler content results in strengthening the system's heterogeneity and thus IP effect, which contribute to the dielectric response of the nanocomposites especially at low frequencies and high temperatures. To contribute to the conduction process, the accumulated charge carriers at the interface should

Table 11.1 Coefficient of energy efficiency (n_{eff} (%)) at 50, 100, and 200 V for the time instant $t = 10$ seconds at 30 °C, for all specimens.

$BaTiO_3$ content (phr)	n_{eff}(%)		
	50 V	100 V	200 V
0	17.11	28.02	13.23
1	12.31	43.80	7.06
3	58.16	55.83	54.56
7	49.33	55.72	58.20
10	41.86	39.84	50.42
12	41.85	43.58	48.62
15	38.33	39.68	50.52

Source: Manika and Psarras [75].

overcome the potential barriers by acquiring energy from the applied field and temperature. The variation of dc conductivity with temperature for the $BaTiO_3$/epoxy nanocomposites at 50 V applied voltage is shown in Figure 11.26a [75]. Conductivity for all nanocomposites seems to follow an exponential increase with temperature with positive temperature coefficient, $d\sigma/dT > 0$. Inset of Figure 11.26a shows that the applied voltage has no effect on the form of the conductivity dependence on temperature and the sign of $d\sigma/dT$ is in accordance with the dielectric nature of the nanocomposites. Figure 11.26b presents the variation of ac conductivity as a function of temperature, at 0.1 Hz, varying the $BaTiO_3$ content. Inset shows ac conductivity vs. frequency for the 7 phr $BaTiO_3$/epoxy nanocomposite at various temperatures [75]. The influence of temperature is more noticeable in the low-frequency region, reflecting the thermally activated conduction process. At high frequencies, the effect of temperature is negligible and conductivity varies exponentially with frequency in accordance with Eq. (11.11).

Figure 11.27a,b depicts dc and ac conductivity, at 0.1 Hz, vs. reciprocal temperature for the $BaTiO_3$/epoxy nanocomposites, respectively. In both cases, data can be described via Arrhenius plots. Linear fittings allow the determination of activation energy, which varies between 1.0 and 1.3 eV [75].

Activation energy is related to the structure of the nanocomposites and the occurring interactions between the constituent phases, being a function of the properties of matrix and filler, the mean radius of inclusions or clusters, the mean interparticle separation, and the extend of interface. Insets in Figure 11.27a,b show representative examples of fitting experimental data via Eq. (11.16), for the 10 phr $BaTiO_3$/epoxy nanocomposite, under dc and ac conditions.

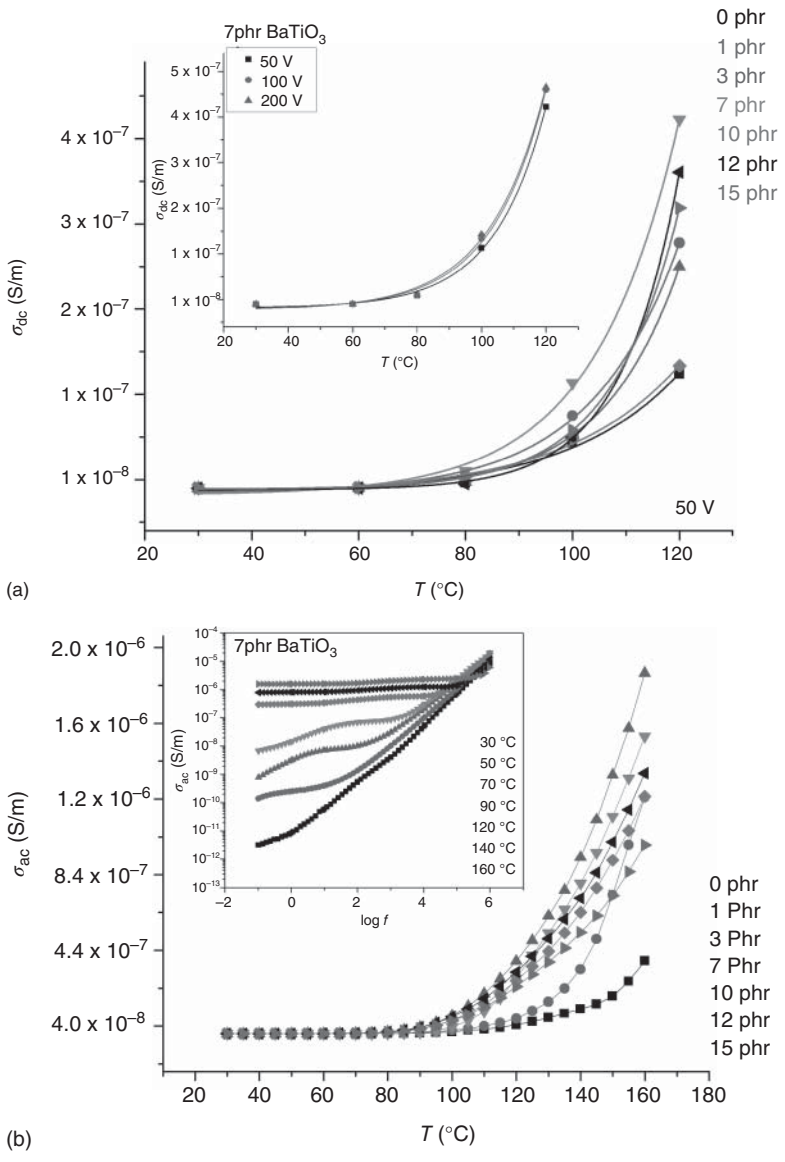

Figure 11.26 (a) Direct current (dc) conductivity as a function of temperature for the $BaTiO_3$/epoxy nanocomposites at 50 V applied voltage. Inset depicts the $\sigma_{dc}(T)$ for the 7 phr $BaTiO_3$/epoxy specimen for various applied dc voltages. (b) ac conductivity as a function of temperature, at 0.1 Hz, varying the $BaTiO_3$ content. Inset shows ac conductivity vs. frequency for the 7 phr $BaTiO_3$/epoxy nanocomposite at various temperatures. Source: Figure reused from Manika and Psarras [75] with permission.

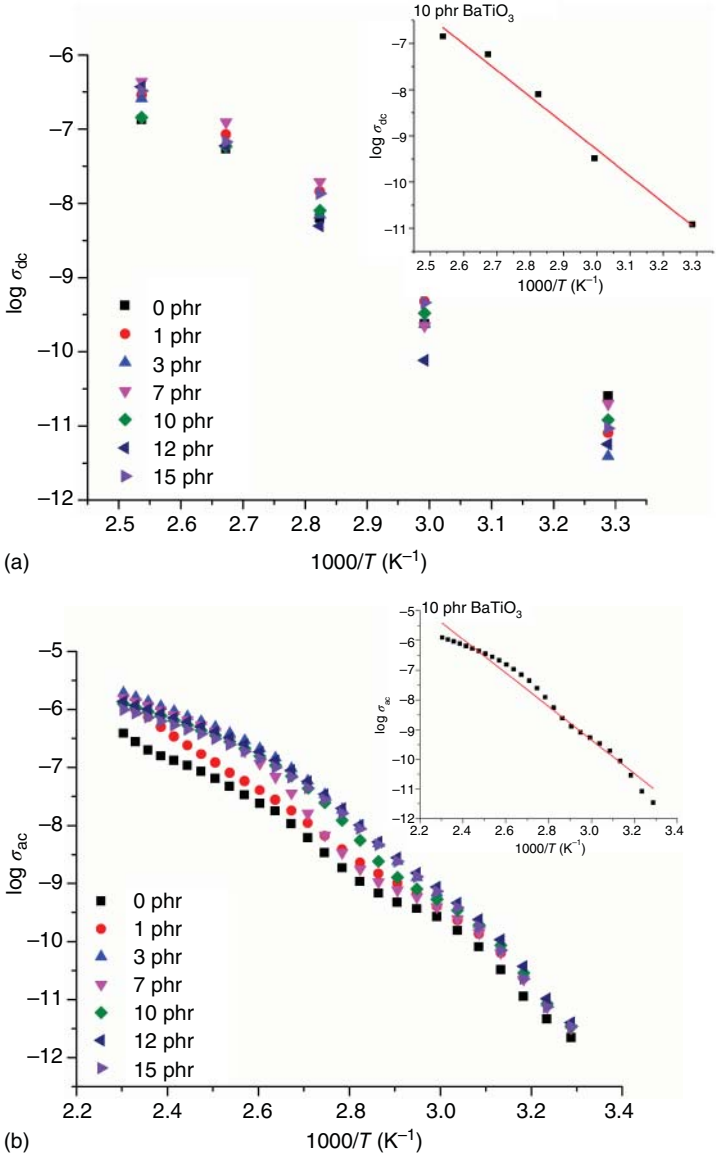

Figure 11.27 (a) Direct current (dc) conductivity and (b) alternating current (ac) conductivity at 0.1 Hz, vs. reciprocal temperature for the $BaTiO_3$/epoxy nanocomposites. Insets show representative examples of fitting experimental data via Eq. (11.16), for the 10 phr $BaTiO_3$/epoxy nanocomposite, under dc and ac conditions. Source: Figure reused from Source: Manika and Psarras [75] with permission.

11.7 Conclusions and Future Trends

Epoxy resin composites became an important class of engineering materials because of their advanced mechanical performance, light weight, and cost-effectiveness. For decades, their electrical performance was staying in backstage. Epoxy-based composites are dielectric materials, that is, materials that can be polarized under the influence of an externally applied field. Electrical properties of polymer matrix composites can be tuned by choosing the constituent materials, the content of the employed reinforcing phase, the method of fabrication, and the achieved type of inclusions' distribution. In the case of nanocomposites, the extent of interface and the interactions at the interfacial area are of pronounced importance. Dielectric response of polymer composites provides valuable information regarding relaxation effects, molecular mobility, interfacial phenomena, conduction mechanisms, interactions between macromolecules/particles or between particles, and phase changes contributing in a deeper insight of the structure–property relationship. Electrical properties of epoxy composites in tandem with their flexibility, thermomechanical stability, corrosion and environmental resistance, light weight, and shock resistance constitute a multifunctional performance leading to the replacement of conventional insulating materials. Multifunctionality can be further increased by integrating conductive inclusions and switching from the insulating to conductive behavior or by embedding magnetic particles and inducing magnetic properties. Moreover, epoxy nanocomposites can be considered as a distributed network of nano-capacitors, where energy can be stored and retrieved on demand.

Current applications based on the electrical properties of epoxy composites include static dissipative members, electromagnetic interference shielding, conductive coatings or adhesives, and current and memory switches. Forthcoming applications are expected to comprise "printing" circuits in nano-electronics, integrated capacitors, transmission lines for electromagnetic signals or information, self-current regulators, self-heating systems, portable energy storing devices, and development of smart materials' systems.

References

1 Hull, D. and Clyne, T.W. (1996). *An Introduction to Composite Materials*. Cambridge University Press.
2 Mathews, F.L. and Rawlings, R.D. (2008). *Composite Materials: Engineering and Science*. CRC, Woodhead Publishing Ltd, Cambridge.
3 Ellis, B. (1993). *Chemistry and Technology of Epoxy Resins*. London, UK: Blackie Academic & Professional, Chapman & Hall.
4 Cowie, J.M.G. (1993). *Polymers: Chemistry and Physics of Modern Materials*, 2e. New York, NY, USA: Blackie Academic & Professional, Chapman & Hall.
5 Kremer, F. and Arndt, M. (1997). Broadband dielectric measurement techniques. In: *Dielectric Spectroscopy of Polymeric Materials* (eds. J.P. Runt and J.J. Fitzgerald), 67–79. Washington, DC: American Chemical Society.

6 Kremer, F. and Schönhals, A. (2003). *Broadband Dielectric Spectroscopy*. Berlin: Spinger.

7 Riande, E. and Díaz-Calleja, R. (2004). *Electrical Properties of Polymers*. New York, NY: Marcel Dekker.

8 Vassilikou-Dova, A. and Kalogeras, M. (2009). Dielectric analysis (DEA). In: *Thermal Analysis of Polymers, Fundamentals and Applications* (eds. J.D. Menczel and R.B. Prime), 497–614. Hoboken, NJ: Wiley.

9 ASTM D257-14 (2014). *Standard Test Methods for DC Resistance or Conductance of Insulating Materials*. West Conshohocken, PA: ASTM International.

10 Blythe, A.R. (1980). *Electrical Properties of Polymers*. Cambridge: Cambridge University Press.

11 Czichos, H., Saito, T., and Smith, L. (2006). *Handbook of Materials Measurement Methods*, 431–484. Leipzig: Springer.

12 Psarras, G.C. (2018). Fundamentals of dielectric theories. In: *Dielectric Polymer Materials for High-Density Energy Storage* (ed. Z.-M. Dang). Elsevier.

13 Tsangaris, G.M., Psarras, G.C., and Kouloumbi, N. (1998). Electric modulus and interfacial polarization in composite polymeric systems. *Journal of Materials Science* 33: 2027–2037.

14 Psarras, G.C. (2010). Conductivity and dielectric characterization of polymer nanocomposites. In: *Polymer Nanocomposites: Physical Properties and Applications* (eds. S.C. Tjong and Y.-M. Mai), 31–69. Cambridge: Woodhead Publishing Limited.

15 Patsidis, A.C. and Psarras, G.C. (2019). Applications of dielectric analysis (DEA) to multi-component polymeric systems. In: *Polymers and Multicomponent Polymeric Systems: Thermal, Thermo-Mechanical and Dielectric Analysis* (ed. S. Thomas), 245–271. CRC Press, Taylor & Francis Group.

16 Salvetat, J.P., Bhattacharyya, S., and Pipes, R.B. (2006). Progress on mechanics of carbon nanotubes and derived materials. *Journal of Nanoscience and Nanotechnology* 6: 1857–1882.

17 Chanmal, C.V. and Jog, J.P. (2008). Dielectric relaxations in PVDF/$BaTiO_3$ nanocomposites. *Express Polymer Letters* 2: 294–301.

18 Hernández, M., Carretero-González, J., Verdejo, R. et al. (2010). Molecular dynamics of natural rubber/layered silicate nanocomposites as studied by dielectric relaxation spectroscopy. *Macromolecules* 43 (2): 643–651.

19 Psarras, G.C., Siengchin, S., Karahaliou, P.K. et al. (2011). Dielectric relaxation phenomena and dynamics in polyoxymethylene/polyurethane/alumina hybrid nanocomposites. *Polymer International* 60: 1715–1721.

20 von Hippel, A.R. (1995). *Dielectrics and Waves*. Boston: Artech.

21 Koufakis, E., Mathioudakis, G.N., Patsidis, A.C., and Psarras, G.C. (2019). $ZnTiO_3$/epoxy resin nanocomposites: development, dielectric behaviour and functionality. *Polymer Testing* 77: 105870.

22 Hedvig, P. (1977). *Dielectric Spectroscopy of Polymers*. Bristol: Adam Hilger Ltd.

23 Korzhenko, A., Tabellout, M., and Emery, J.R. (1999). Influence of a metal–polymer interfacial interaction on dielectric relaxation properties of polyurethane. *Polymer* 40: 7187–7195.

24 Böttger, H. and Bryskin, U.V. (1985). *Hopping Conduction in Solids*. Berlin: Verlag Akademie.

25 Jonscher, A.K. (1992). *Universal Relaxation Law*. London: Chelsea Dielectrics Press.

26 Schrøder, T.B. and Dyre, J.C. (2002). Computer simulations of the random barrier model. *Physical Chemistry Chemical Physics* 4: 3173–3178.

27 Dyre, J.C. (1988). The random free-energy barrier model for ac conduction in disordered solids. *Journal of Applied Physics* 64 (5): 2456–2468.

28 Psarras, G.C. (2006). Hopping conductivity in polymer matrix–metal particles composites. *Composites Part A: Applied Science and Manufacturing* 37: 1545–1553.

29 Gatos, K.G., Martínez Alcázar, J.G., Psarras, G.C., and Karger-Koscis, J. (2007). Polyurethane latex/water dispersible boehmite alumina nanocomposites: thermal, mechanical and dielectrical properties. *Composites Science and Technology* 76: 157–167.

30 Belattar, J., Achour, M.E., and Brosseau, C. (2011). A comparison between the permittivity and electric modulus representations of the microwave response of carbon black loaded polymer composites under uniaxial tension. *Journal of Applied Physics* 110: 054101.

31 Patsidis, A. and Psarras, G.C. (2008). Dielectric behaviour and functionality of polymer matrix–ceramic $BaTiO_3$ composites. *Express Polymer Letters* 2 (10): 718–726.

32 Patsidis, A.C. and Psarras, G.C. (2013). Structural transition, dielectric properties and functionality in epoxy resin–barium titanate nanocompsoites. *Smart Materials and Structures* 22: 115006.

33 Patsidis, A.C., Kalaitzidou, K., and Psarras, G.C. (2012). Dielectric response, functionality and energy storage in epoxy nanocomposites: barium titanate vs exfoliated graphite nanoplatelets. *Materials Chemistry and Physics* 135: 798–805.

34 Kao, K.C. (2004). *Dielectric Phenomena in Solids*. Elsevier.

35 Tomara, G.N., Kerasidou, A.P., Patsidis, A.C. et al. (2015). Dielectric response and energy storage efficiency of low content TiO_2-polymer matrix nanocomposites. *Composites Part A: Applied Science and Manufacturing* 71: 204–211.

36 Senis, E. (2015). Development characterization, and functional behaviour of boron carbide/epoxy resin nanocomposites. MSc thesis. Polymer Science and Technology Interdepartmental Programme, University of Patras, Patras, Greece.

37 Kakarelides, O. (2019). Polymer matrix–TiO_2 composite nanodielectrics. BSc thesis. Department of Materials Science, University of Patras, Patras, Greece.

38 Zallen, R. (2004). *The Physics of Amorphous Solids*. New York, NY: Wiley.

39 Lux, F. (1993). Models proposed to explain the electrical conductivity of mixtures made of conductive and insulating materials. *Journal of Materials Science* 28: 285–301.

40 Roldughin, V.I. and Vysotskii, V.V. (2000). Percolation properties of metal-filled polymer films, structure and mechanisms of conductivity. *Progress in Organic Coating* 39: 81–100.

41 Tsangaris, G.M., Psarras, G.C., and Manolakaki, E. (1999). DC and AC conductivity in polymeric particulate composites of epoxy resin and metal particles. *Advanced Composites Letters* 8 (1): 25–29.

42 Psarras, G.C. (2007). Charge transport properties in carbon black/polymer composites. *Journal of Polymer Science Part B: Polymer Physics* 45: 2535–2545.

43 Psarras, G.C. (2009). Conduction processes in percolative epoxy resin/silver particles composites. *Science of Advanced Materials* 1: 101–106.

44 Raptis, C.G., Patsidis, A., and Psarras, G.C. (2010). Electrical response and functionality of polymer matrix-titanium carbide composites. *Express Polymer Letters* 4 (4): 234–243.

45 Mott, N.F. and Davis, E.A. (1979). *Electronic Conduction in Non-crystalline Materials*. Oxford: Clarenton Press.

46 Mott, N.F. (1987). *Conduction in Non-crystalline Materials*. Oxford: Clarendon Press.

47 Mott, N.F. (1990). *Metal–Insulator Transitions*. London: Taylor & Francis.

48 Epstein, A.J., Rommelmann, H., Bigelow, R. et al. (1983). Role of solitons in nearly metallic polyacetylene. *Physical Review Letters* 50: 1866–1869.

49 Zuo, F., Angelopoulos, M., Macdiarmid, A.G., and Epstein, A.J. (1989). ac conductivity of emeraldine polymer. *Physical Review B* 39: 3570–3578.

50 Aguilar-Hernández, J. and Potje-Kamloth, K. (2001). Evaluation of the electrical conductivity of polypyrrole polymer composites. *Journal of Physics D: Applied Physics* 34: 1700–1711.

51 Reghu, M., Yoon, C.O., Yang, C.Y. et al. (1994). Transport in polyaniline networks near the percolation threshold. *Physical Review B: Condensed Matter* 50 (19): 13931–13941.

52 Capaccioli, S., Lucchesi, M., Rolla, P.A., and Ruggeri, G. (1998). Dielectric response analysis of a conducting polymer dominated by the hopping charge transport. *Journal of Physics: Condensed Matter* 10: 5595–5617.

53 Joo, J., Long, S.M., Pouget, J.P. et al. (1998). Charge transport of the mesoscopic metallic state in partially crystalline polyanilines. *Physical Review B* 57: 9567–9580.

54 Pontikopoulos, P.L. and Psarras, G.C. (2013). Dynamic percolation and dielectric response in multiwall carbon nanotubes/poly(ethylene oxide) composites. *Science of Advanced Materials* 5: 14–20.

55 Dyre, J.C. and Shrøder, T.B. (2000). Universality of ac conduction in disordered solids. *Reviews of Modern Physics* 72 (3): 873–892.

56 Dyre, J.C. and Schrøder, T.B. (2002). Hopping models and ac universality. *Physica Status Solidi B* 230 (1–5): 5–13.

57 Banerjee, S. and Chakravorty, D. (1998). Alternating current conductivity and dielectric dispersion in copper-silica nanocomposites synthesized by electrodeposition. *Journal of Applied Physics* 84: 799–805.

58 Maddison, D.S. and Tansley, T.L.J. (1992). Variable range hopping in polypyrrole films of a range of conductivities and preparation methods. *Applied Physics* 72: 4677–4682.

59 Dutta, P., Biswas, S., Ghosh, M. et al. (2001). The dc and ac conductivity of polyaniline–polyvinyl alcohol blends. *Synthetic Metals* 122: 455–461.

60 Andrikaki, S. (2011). Nanodielectrics: studying the electrical response of polymer matrix composites with embedded titanium carbide nanoparticles. BSc thesis. Department of Materials Science, University of Patras, Patras, Greece.

61 Kalini, A., Gatos, K.G., Karahaliou, P.K. et al. (2010). Probing the dielectric response of polyurethane/alumina nanocomposites. *Journal of Polymer Science Part B: Polymer Physics* 48: 2346–2354.

62 Bryining, M.B., Islam, M.F., Kikkawa, J.M., and Yodh, A.G. (2005). Very low conductivity threshold in bulk isotropic single-walled carbon nanotube–epoxy composites. *Advanced Materials* 17: 1186–11891.

63 Moniruzzaman, M. and Winey, K.I. (2006). Review: polymer nanocomposites containing carbon nanotubes. *Macromolecules* 39: 5194–5205.

64 Liang, J., Wang, Y., Huang, Y. et al. (2009). Electromagnetic interference shielding of graphene/epoxy composites. *Carbon* 47: 922–925.

65 Sengupta, R., Bhattacharya, M., Bandyopadhyay, S., and Bhowmick, A.K. (2011). A review on the mechanical and electrical properties of graphite and modified graphite reinforced polymer composites. *Progress in Polymer Science* 36: 638–670.

66 Singh, V., Joung, D., Zhai, L. et al. (2011). Graphene based materials: past, present and future. *Progress in Materials Science* 56: 1178–1271.

67 Roy, N., Sengupta, N., and Bhowmick, A.K. (2012). Modifications of carbon for polymer composites and nanocomposites. *Progress in Polymer Science* 37: 781–819.

68 Psarras, G.C. (2016). Nanographite-polymer composites. In: *Carbon Nanomaterials Sourcebook: Nanoparticles, Nanocapsules, Nanofibers, Nanoporous Structures and Nanocomposites* (ed. K.D. Sattler), 647–673. Boca Raton, FL: Taylor & Francis.

69 Park, J.K., Do, I.-H., Askeland, P., and Drzal, T. (2008). Electrodeposition of exfoliated graphite nanoplatelets onto carbon fibers and properties of their epoxy composites. *Composites Science and Technology* 68: 1734–1741.

70 Patsidis, A.C., Kalaitzidou, K., and Psarras, G.C. (2014). Graphite nanoplatelets/polymer nanocomposites: thermomechanical, dielectric, and functional behaviour. *Journal of Thermal Analysis and Calorimetry* 116: 41–49.

71 Psarras, G.C. (2016). "Energy materials" … the role of polymers. *Express Polymer Letters* 10: 721–721.

72 Tomer, V., Polizos, G., Manias, E., and Randall, C.A. (2010). Epoxy-based nanocomposites for electrical energy storage. I. effects of montmorillonite and barium titanate nanofillers. *Journal of Applied Physics* 108: 074116.

73 Dang, Z.-M., Yuan, J.-K., Yao, S.-H., and Liao, R.-J. (2013). Flexible nanodielectric materials with high permittivity for power energy storage. *Advanced Materials* 25: 6334–6365.

74 Manika, G.C. and Psarras, G.C. (2016). Energy storage and harvesting in $BaTiO_3$/epoxy nanodielectrics. *High Voltage* 1: 151–157.

75 Manika, G.C. and Psarras, G.C. (2019). Barium titanate/epoxy resin composite nanodielectrics as compact capacitive energy storing systems. *Express Polymer Letters* 13 (8): 749–758.

76 Trompeta, A.-F.A., Koumoulos, E.P., Stavropoulos, S.G. et al. (2019). Assessing the critical multifunctionality threshold for optimal electrical, thermal, and

nanomechanical properties of carbon nanotubes/epoxy nanocomposites for aerospace applications. *Aerospace* 6: 7.

77 Friedrich, K. and Breuer, U. (2015). *Multifunctionality of Polymer Composites*. Elsevier.

78 Krawczak, P. (2019). Polymer composites: evolve towards multifunctionality or perish. *Express Polymer Letters* 3 (9): 771–771.

79 Psarras, G.C. (2011). Smart polymer systems: a journey from imagination to applications. *Express Polymer Letters* 5 (12): 1027–1027.

80 Mathioudakis, G.N., Patsidis, A.C., and Psarras, G.C. (2014). Dynamic electrical thermal analysis on zinc oxide/epoxy resin nanodielectrics. *Journal of Thermal Analysis and Calorimetry* 116: 27–33.

81 Ioannou, G., Patsidis, A.C., and Psarras, G.C. (2011). Dielectric and functional properties of polymer matrix/ZnO/$BaTiO_3$ hybrid composites. *Composites Part A: Applied Science and Manufacturing* 42: 104–110.

82 Kontos, G.A., Soulintzis, A.L., Karahaliou, P.K. et al. (2007). Electrical relaxation dynamics in TiO_2–polymer matrix composites. *Express Polymer Letters* 1 (12): 781–789.

83 Soulintzis, A., Kontos, G., Karahaliou, P.K. et al. (2009). Dielectric relaxation processes in epoxy resin–ZnO composites. *Journal of Polymer Science Part B: Polymer Physics* 47: 445–454.

84 Ramajo, L.A., Cristobal, A.A., Botta, P.M. et al. (2009). Dielectric and magnetic response of Fe_3O_4/epoxy composites. *Composites Part A: Applied Science and Manufacturing* 20: 388–393.

85 Manika, G.C. and Psarras, G.C. (2019). Development, dielectric response and functionality of $SrTiO_3$/epoxy nanocomposites. *Journal of Materials Science: Materials in Electronics* 30: 13740–13748.

86 Dennison, J.R. and Brunson, J. (2008). Temperature and electric field dependence of conduction in low-density polyethylene. *IEEE Transactions on Plasma Science* 36: 2246–2252.

12

Smart Epoxy Composites

Reza Eslami-Farsani and Hossein Ebrahimnezhad-Khaljiri

Faculty of Materials Science and Engineering, K. N. Toosi University of Technology, No. 7, Pardis St., Mollasadra Ave., Vanak Sq., Tehran, Iran

12.1 Introduction

Smart or intelligent materials are often defined as materials, which can respond to the environmentally provocative physical, chemical, and biochemical factors such as light irradiation, presence of specific ions, pH, mechanical forces, magnetic field, solvent, and temperature [1]. But this definition is too general, and each material can be reacted by its environment, namely, the increment of thermal expansion by enhancement of the temperature of matter. Therefore, it is proper to say the smart behavior [2]. Smart materials have special repeatable behavior, which are activated by provocative factors. The idea of fabricating these materials was based on living nature [3]. These materials can have one or combination of the shape memory, self-healing, self-sensing, and self-actuating behaviors [4]. Today, the progress in the different sciences is caused to make the new smart materials. One of the major groups of these materials is the polymeric-based materials. These polymeric materials are included in polyurethane (PU), epoxy, polysaccharides, etc. [5]. The epoxy-based composite materials are one of the interesting major groups, which are used in many industries and applications, due to their excellent properties [6, 7]. The new progressing trend is shown in Figure 12.1, which demonstrates the published documents in the period time of 2010–2019 (https://www.engineeringvillage.com). Based on this figure, it can be said that the smart epoxy and its composites have a remarkable growing rate. The shape memory epoxy (SME) and its composites, self-healing coating, and self-healing composites are the subjects about smart epoxy, which are the most interesting for researchers and inventories.

Today, the smart epoxy composites with the shape memory behavior can be divided into two major groups. In the first group, the epoxy as a matrix has shape memory behavior, whereas in the second group, the shape memory wires as reinforcement are used in the epoxy composites. To comprehend the shape behavior in the first group, the creation of memory behavior into the epoxy matrix

Epoxy Composites: Fabrication, Characterization and Applications,
First Edition. Edited by Jyotishkumar Parameswaranpillai, Harikrishnan Pulikkalparambil, Sanjay M. Rangappa, and Suchart Siengchin.

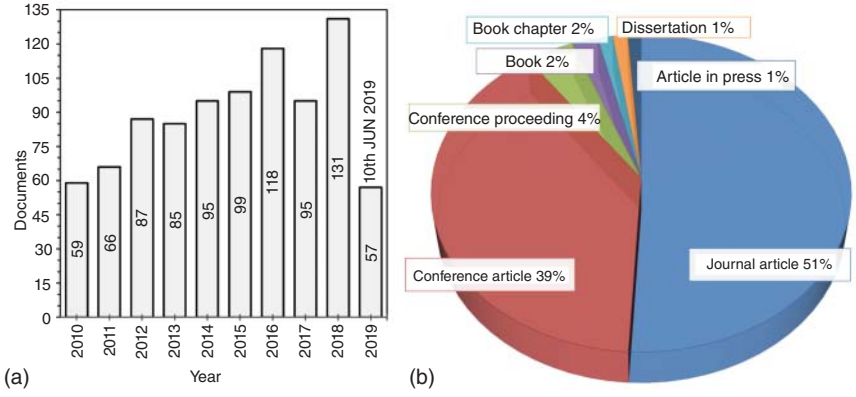

Figure 12.1 The published documents in the field of smart epoxy based on engineering village database (https://www.engineeringvillage.com). (a) Number of published documents in the period time of 2010–2019, (b) Type of documents. Source: Based on Engineeringvillage.com, Smart epoxy based on engineering village database.

is firstly investigated in the Section 12.2. After that, the epoxy nanocomposites and composites are comprehensively surveyed.

One of the important applications of epoxy is using it as a protective coating for different metals, which has grown in the last decade. This coating in the environmental conditions can be scratched, or the corrosion can be occurred between coatings and substrates. To solve these problems, the smart epoxy coating was introduced in the last decade [8]. This smart coating can be healed itself by intrinsic or extrinsic methods or prevented the corrosion of substrate by inhibition. Also, using dual healing and inhibiting mechanisms and promoting them in the smart epoxy coating were investigated by researchers in a few years [9]. It should be noted that in the Section 12.3, the inhibition, self-healing, and dual mechanisms of smart epoxy coatings are reviewed.

Composite materials especially the epoxy composite materials are very sensitive to the microcracks, so that, after the creation of the microcracks, they rapidly propagate and are caused to catastrophic failures. Therefore, the control of the crack behaviors can be helped to stop the failure. One of the simplest ways to that is healing the microcracks before propagation of them [10, 11]. Therefore, the smart epoxy composites have been developed by researchers for healing microcracks, and consequently, controlling the failure of those. Up to now, different methods have been introduced in the inclusion of intrinsic and extrinsic methods [12, 13]. In the Section 12.4, the different healing systems into epoxy composites and structures are investigated.

12.2 Shape Memory Epoxy Polymers and their Composites

12.2.1 The Creation of Shape Memory Behavior into Epoxy

The polymeric materials below the glass transition temperature (T_g) have elastic behaviors, whereas above ones have rubbery or viscous behaviors. Those materials

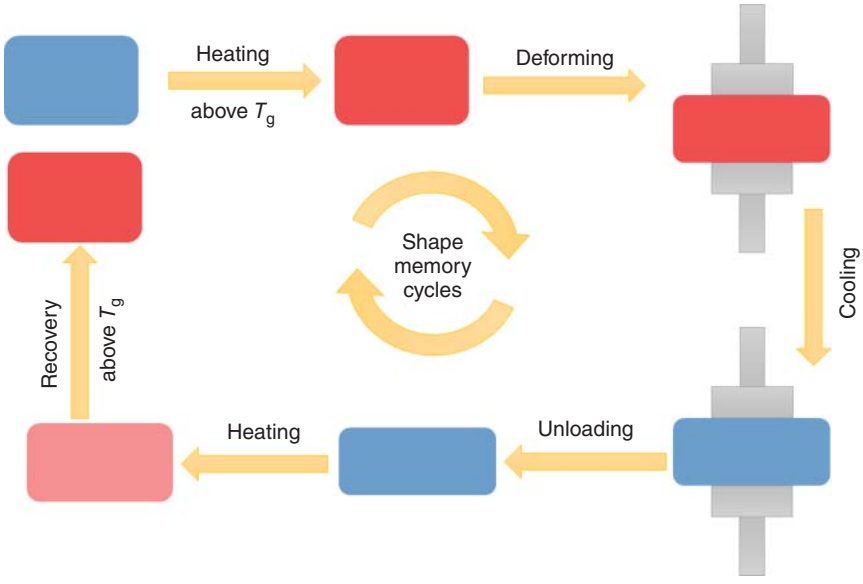

Figure 12.2 The schematic description of shape memory behavior within the polymers.

near the T_g have viscoelastic behaviors, which is the fundamental of shape memory effect of them. The shape memory behaviors are included in four stages (Figure 12.2). In the first stage, the polymeric material has an original shape. In the second stage, above the T_g, the polymer is deformed to have a new shape. In the third stage, the temperature of polymer reduces below T_g and the deformation load is removed. By heating this polymer to the high temperature state, the polymer recovers its original shape [14, 15].

The classification of different phenomena in the shape memory polymers was previously reviewed by Liu et al. [15]. Considering that, the first approach is based on viscoelastic theory, which was studied by Tobushi et al. [16]. In this theory, the shape memory polymer includes spring, dashpot, and frictional basic element, which represent elastic, viscous, and slip mechanisms in the polymer structures, respectively. This theory can be generally used for investigating the shape memory behavior in the thermoplastic polymers like shape memory PU. Another approach was introduced by Liu et al. [17], which was based on the thermomechanical theory and proper for thermoset polymers especially SME. This model was based on the vibration in the polymer structures, which consist of flexible (active) and rigid (frozen) sections in their structures.

The conventional epoxy has rigid sections in its structure because of its thermoset structure. In order to have the epoxy polymer with shape memory behavior, the structure of that should be changed and have the flexible and rigid sections. The whole of the synthesized SME is based on this rule. The simplest ways are that the structures of the epoxy monomer change and create the flexible section into those. Synthesizing diglycidylether of bisphenol-A (DGEBA) from bisphenol A and epichlorohydrin in the presence of NaOH has been shown in the Scheme 12.1. This epoxy structure after curing by conventional hardener creates the rigid structures. To

create the flexible structure, it is necessary to increase the linear structure of bisphenol A. The C—O bond into the bisphenol A can increase the linear structure of epoxy monomer, which had been done by Leng et al. [18]. These researchers added the modified epoxy monomer to the conventional epoxy and reported that the shape was fully recovered, when the temperature was T_g or above that. They stated that if the percentage of the linear monomer is too high, the shape recovery and its speed are decreased. These results had been attributed to the effect of linear monomer to the cross-linking density.

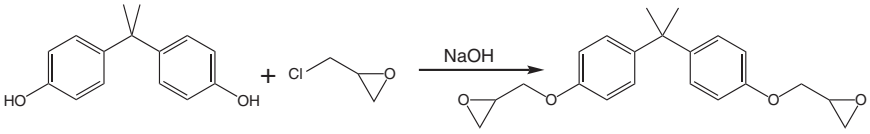

Scheme 12.1 Synthesizing the diglycidylether of bisphenol-A (DGEBA).

Its developed type is the ethoxylation of bisphenol-A, which can be seen in Scheme 12.2. The *m* and *n* show the oxyethylene units. The ethoxylation method was introduced by Yang et al. [19] for fabricating the tough epoxy. They reported that adding 50 wt% ethoxylated DGEBA with six oxyethylene units to the epoxy resin decreases the viscosity, improves the toughness and impact energy, and stabilizes the tensile and flexural strength. By changing the C—O bonds and their units, it can change the SME behavior. Given this point, Fan et al. [20] synthesized DGEBA with two oxypropylene units and investigated its shape memory properties. They reported that the shape recovery and fixity in their research were 96.67% and 98.88%, respectively. This model creation of shape memory effect into the epoxy polymer was named intrinsically toughened network by these researchers.

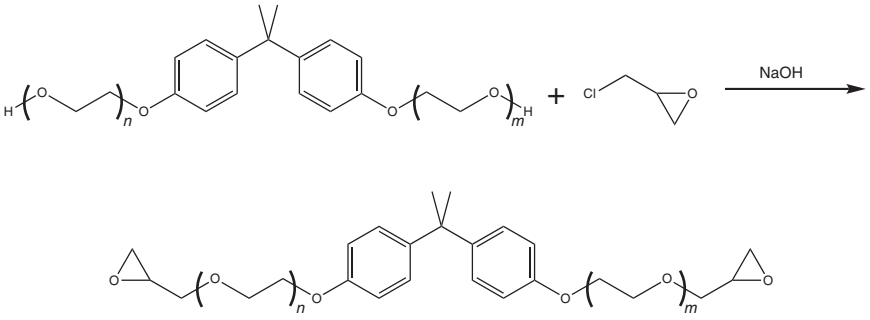

Scheme 12.2 Ethoxylated DGEBA as intrinsically shape memory epoxy, (*m* and *n*: the number of C—O bonds). Source: Yang et al. [19]. © 2012, John Wiley & Sons.

The next generation is the incomplete curing of a tough epoxy monomer. In this method, the linear structure of epoxy is C—C bonds. The commercial epoxy for this method is E51 in which 80% was selected to access the effect of toughening agent [21]. Liu et al. [22] cured E51 with different curing degrees of 60%, 70%, 80%, 90%,

and 100%. They reported that the sample with a curing degree of 60% had the proper shape memory recovery, so that, after nine fold deploy cycles, the tensile strength slightly (about 6%) decreased, which was attributed to the material fatigue.

The second way to create the flexible units is that the used hardener for curing the epoxy has flexible structures. This mentioned approach is introduced as amine-based SME. Rousseau and Xie [23] used two kind of different tough hardeners as trade name of Jeffamine-D400 and Jeffamine T403 (Scheme 12.3). They reported that the shape recovery and fixity of cured epoxy by tough hardeners were approximately 100%. Although the shape recovery and fixity in this research were proper, but it seems that the repeated linear structure (n, a, b, and c in Scheme 12.3) into the hardener can effect and decrease the mechanical strength. It is better to use the tougher hardener with lower repeated linear structures. But, it can reduce the shape recovery and fixity of SME. Therefore, using another amine structure is necessary to solve this problem. Based on the researches, it is found that the researchers use the Jeffamine-D230 as tough hardener and decylamine as a toughening agent (Scheme 12.4). Jeffamine-D230 has the same structure of Jeffamine-D400 with this difference that the repeated linear structure (n) of ones is 2.5. Xie and Rousseau [24] used the Jeffamine-D230 and decylamine to cure the epoxy and investigate its shape memory. The maximum shape recovery and fixity were reached to 99.8% and 102.3% by adding 0.01 and 0.015 mol decylamine to 0.02 mol epoxy resin, respectively.

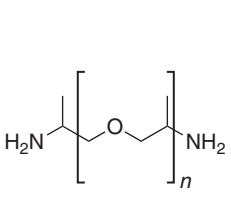

Jeffamine D400, $n \sim 6.1$

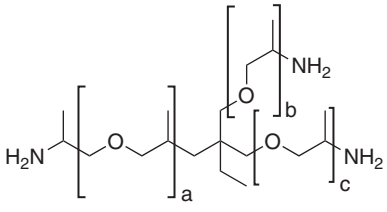

Jeffamine T403, (a+b+c) ~ 5–6

Scheme 12.3 Jeffamine D400 and T403 as commercial tough hardener.

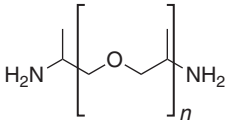

Jeffamine D230, $n \sim 2.5$

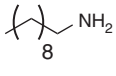

Decylamine

Scheme 12.4 Jeffamine D230 as tough hardener and decylaime as an amine toughening agent.

The third approach is to use the toughening agent. This agent can be amine- or epoxide-based. Decylamine as n-alkylamine was previously introduced, which was used by Xie and Rousseau [24]. The n-alkylamine forms strong physical cross-linking by tail-to-tail associations among alkyl chains [25]. Leonardi et al. [26]

used *n*-dodecylamine as alkylamine to investigate the influence of that on the shape memory behavior of epoxy. Scheme 12.5 shows the neopentyl glycol diglycidyl ether (NGDE), which is an epoxide toughing agent for conventional epoxy resin. By using NGDE, Xie and Rousseau [24] reached the shape memory and recovery of SME to 99.7% and 96.8%, respectively.

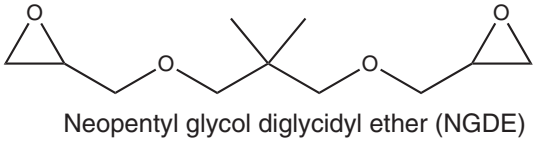

Neopentyl glycol diglycidyl ether (NGDE)

Scheme 12.5 Neopentyl glycol diglycidylether as a toughening agent of epoxy.

The next approach is the grafting agent, where a tough monomer can be grafted to the epoxy monomer. By this method, Dong et al. [27] grafted the polyoxyethylene octyl phenyl ether (TX100) as a tough section by the 2,4-toluene diisocyanate (TDI) to the epoxy monomer and then investigated the shape memory effect of that (Scheme 12.6). The other example of this method was studied by Rajendran et al. [28]. They used the bisphenol A dicyanate ester as a cross-linking agent of epoxy monomer and as a grafting agent for grafting phenol telechelic poly(tetramethylene oxide) to epoxy monomer.

The other approach is to use the second hardener. Song et al. [29] used different percentages of the 4,4′-methylenedianiline (DDM) as the first curing agent and *m*-phenylenediamine (*m*-PDA) as the second curing agent (Scheme 12.7). They reached 99.9% shape fixity and 99.8% shape recovery by adding 9 wt% DDM and 3.6 wt% *m*-PDA. Using the second hardener was also investigated by Konuray et al. [30]. These researchers used the Jeffamine-D400 and 4,4-diamino diphenyl sulfone (DDS) as first and second curing agents, respectively.

The last approach is the blending systems. In this method, the epoxy resin was blended with a thermoplastic system like PU or polycaprolactone [31, 32]. Liu et al. [22] used the active PU into the epoxy matrix and investigated the shape memory behavior of that by fold-deploy test. The obtained results show that the blend of epoxy-PU fully recovered the initial shape after two minutes at T_g. Iregui et al. [33] used the epoxy/poly ε-caprolactone blends to fabricate the mats with the shape memory behavior. They reported that the shape fixity and recovery were more than 95%.

12.2.2 Shape Memory Behavior in Epoxy-Based Nanocomposites

Wang et al. [34] investigated the shape memory effect in the epoxy-reduced graphene oxide (RGO) nanocomposites by electrical actuation. These researchers used the intrinsic SME in their researches. They placed the RGO on the bottom surface of mold and then by the resin transfer molding technique, the RGO–SME nanocomposite was made. The obtained results indicated that by increasing the applied voltage, the shape recovery speed was increased. Also, by using the voltage

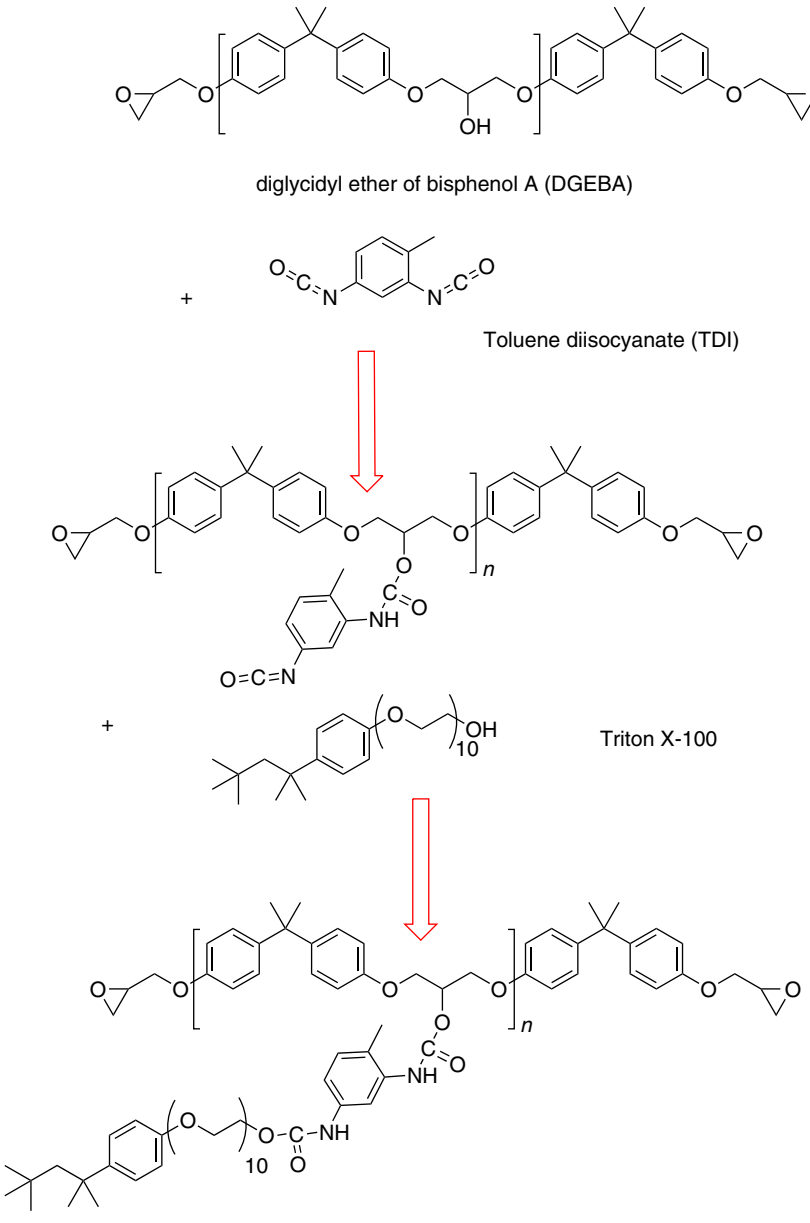

Scheme 12.6 Grafting the polyoxyethylene octyl phenyl ether (TX100) as tough monomer to epoxy monomer by Dong et al. [27]. © 2013, Elsevier.

of 6 V in the 5 seconds, the shape recovery of RGO–SME was reached to 100%. In the similar research, Chen et al. [35] added the 1, 2, and 3 wt% RGO into the SME and investigated the shape memory behavior by thermal actuation. The reported results showed that the elastic modulus, tensile strength, bending modulus, and bending strength were significantly improved by adding the RGO. The thermal stability

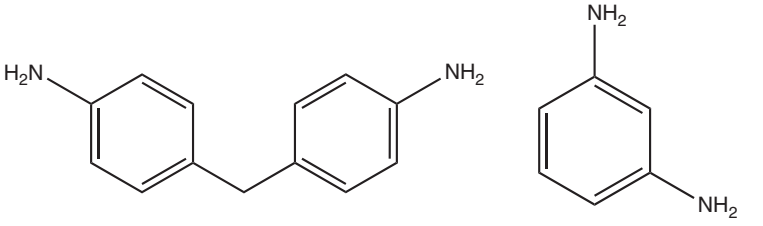

4,4′-methylenedianiline (DDM) *m*-phenylenediamine (*m*-PDA)

Scheme 12.7 The 4,4′-methylenedianiline (DDM) as first curing agent and *m*-phenylenediamine (*m*-PDA) as second curing agent.

and shape fixity in the samples with 1 and 2 wt% RGO were improved. The rate of shape recovery was significantly enhanced by adding 2 wt% RGO, as compared with pristine SME.

Chen et al. [36] in another research fabricated the random dispersed carbon nanotubes (CNTs)–SME and CNT array–SME nanocomposites by using the intrinsic shape memory method and then investigated the shape memory effect by microwave actuation. They reported that the CNT array–SME nanocomposite had higher modulus and hardness, in comparison with the random CNT–SME composite and pure SME, because of CNT alignment. Due to higher contact area with epoxy, the array CNT–SPE had faster shape recovery and shorter recovery temperature than random CNT–SPE.

Liu et al. [37] fabricated the CNT–epoxy nanocomposites with the shape memory behavior. The used system for the creation of shape memory effect was using the amine toughening agent. They used the E51 epoxy, methylhexahydrophthalic anhydride (MHHPA) as a curing agent and *N*,*N*-benzyl dimethyl amine (BDMA) as an amine agent. The CNT content into the epoxy resin was 0, 0.25, and 0.75 wt%. The obtained results revealed that adding CNTs reduced the recovery time to 32 seconds. The mechanical properties such as elastic modulus, maximum stress, and strain at the break near the T_g for the samples containing 0.75 wt% CNTs were significantly increased.

In the study of Ponyrko et al. [38], the tough hardener and amine toughening agents were used in the nanosilica–epoxy nanocomposites. The Jeffamine D400 and 1-butyl-3-methylimidazolium tetrafluoroborate were used as cross-linking agent and ionic liquid, respectively. Also, ethylenediamine (EDA), 4,4′-methylenebis(3-methylcyclohexylamine) (Laromin), and amine-terminated butadiene–acrylonitrile (ATBN) were used as amine agents. In the cross-linked sample with Jeffamine 400, the shape fixity and recovery were 100% and 99.95%, respectively. By adding 5.2 and 15.2 wt% nanosilica, the shape fixity was stable, whereas the shape recovery was 99.5% and 98.2%, respectively. In this research, by adding the ionic liquid into the sample with 5.2 wt% nanosilica, the shape recovery was reached to 99.7%. The cross-linked sample by EDA, Laromin, and ATBN had the 86% shape fixity and 99.9% shape recovery. Adding 5.2 wt% nanosilica into them caused the shape fixity and recovery to be the 95% and 97.9%, respectively.

Dorigato and Pegoretti [39] added silver nanoparticles, carbon black, and carbon nanofibers with the total ratio of 4 wt% to the epoxy and Jeffamine 400. To investigate the shape memory effect, they used the electrical actuation method. Near the T_g, using the carbon black decreased the mechanical properties. Adding silver nanoparticles promoted increasing in the flexural strength. The obtained results showed that the synergistic effects in the electrical and mechanical properties had belonged to the sample with 50/50 ratio of carbon black and nanofibers. By applying voltage of 220 V, this nanocomposite could reach to fully shape recovery after 60 seconds.

Abishera et al. [40] added different percentages of CNTs to SME. The used system in this research was using the NGDE as an epoxy toughening agent with the Jeffamine-230. The sample with 2 wt% had maximum tensile strength, shape recovery, and T_g, which were 32 MPa, 98.5%, and 44.8 °C, respectively. These researcher in the other work investigated the shape recovery under the torsional and bending deformations [41]. They reported that under the torsional deformation, the shape fixity of pure epoxy was 87.5%, whereas that of 1 wt% CNT–epoxy was 94.4%. Under the bending deformations, the shape fixity of neat epoxy and 1 wt% CNT–epoxy were 85.5% and 92.2%, respectively. It is worth noting that the shape recovery of both samples under the both bending and torsion deformation was 100%.

Liu et al. [42] added the carbon black nanoparticles to SME. The used shape memory system in this research was adding the polypropylene glycol diglycidylether as a toughening agent. The shape recovery was done by laser actuation system. The obtained results showed that the maximum shape recovery was above 95.5%. By increasing the carbon black content, the rate of shape recovery was increased. Also, they reported that the high percentage of carbon black is unsuitable, due to improper distribution of that.

Zhang et al. [43] fabricated the graphene oxide (GO)–SME composites by grafting mechanism (Scheme 12.8). They firstly synthesized the functionalized GO. Then grafted the (3-aminopropyl) triethoxysilane (KH-550) to that. The next grafting process was done by a cyanate agent (TDI). The TDI-grafted GO dispersed into the E51 epoxy resin, which can be cross-linked with that during curing process. The aim of this research was to create the progressive bridge between electrical conductivity and shape memory property and fabricate the shape memory nanocomposites with thermoelectric dual-responsive. The obtained results showed that by adding 1 wt% TDI-grafted GO to epoxy, the shape fixity and recovery reached to 96% and 94%, respectively.

As previously mentioned in the Section 12.2.1, grafting a tough agent like TX100 (seen Scheme 12.6) to the epoxy structures is one of the fabricating SMEs. This structure consist of lyophobic and lyophilic blocks. Therefore, carbon-based nanomaterials can strongly react with the TX100-grafted epoxy (water-based epoxy) and backbone of epoxy. The investigated researches about this method are listed in Table 12.1. By comparing different carbon-based nanomaterials, it can be understood that the carbon nanofibers with 98% shape fixity and 100% shape recovery is proper than other carbon-based nanomaterials for shape memory applications.

Wei et al. [48] added the carboxylic nitrile–butadiene nanorubber (CNBNR) to epoxy for creating the shape memory effect to that. The blending ratio of the epoxy

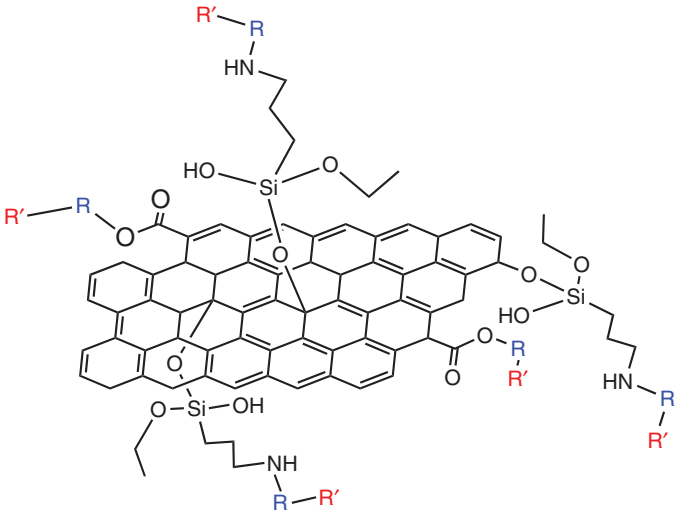

Scheme 12.8 Fabricating the graphene oxide–SME composites by grafting mechanism by Zhang et al. [43]. © 2016, Elsevier.

Table 12.1 Water based shape memory epoxy-carbon-based nanomaterials composites.

Nanomaterials	wt%	Shape fixity (%)	Shape recovery (%)	References
Graphene	1	—	100	[44]
Carbon nanotubes (CNTs)	1	91.2	99.1	[45]
Graphene oxide (GO)	1	93.7	98.6	[45]
CNTs-GO	1	91.4	99	[45]
Reduced graphene oxide (RGO)	1	—	>90	[46]
Carbon nanofibers	1	98	100	[47]

to CNBNR was 5 to 1. The feature of this nanocomposite was highly repeatable shape memory behavior, so that, after the 10 recovery cycles, this nanocomposite had consistency in shape fixity and recovery. The reported shape fixity and recovery of that were 96.3% and 97.6%, respectively.

12.2.3 Shape Memory Behavior in Epoxy-Based Composite Structures

Using the SME in composite structures is one of the interesting subjects for researchers to develop the shape memory composites. Hence, the glass and carbon fibers–SME composites have been developed by different researchers up to now, and this progressive trend in this subject will be continued. Hu et al. [49] fabricated the carbon fibers with satin weave–SME composites. The used epoxy for creating the

shape memory effect was E44, which has similar behavior like E55. This research had been focused on the possibility of fabrication and investigating T_g in the warp and weft of satin weave, which were 29.4 and 29.7 °C, respectively.

Robinson et al. [50] used the shape memory polystyrene between the carbon fibers–epoxy composite to create shape memory effect into that. The full recovery was obtained in the quasi-isotropic and cross-ply laminates, which had 8–9 and 2–3 minutes time recovery, respectively. The effect of CNTs in the carbon fibers–SME composite was studied by Abishera et al. [51]. The used shape memory system was NGDE as tough agent. They mentioned that adding the carbon fibers has caused significant changes in the T_g and cold programmability of composite. Adding 1 wt% CNTs slightly changed the T_g, but had not the effect on the cold programmability and shape fixity of composite. Also, the shape recovery of this structure was 100%. Park et al. [52] made chopped carbon fibers–SME composites with different percentages of chopped carbon fibers. The cross-linked agent of those was DDM. Adding carbon fibers had caused to reduce the recovery rate, in comparison with neat epoxy, due to the difficulty of making heat bridges in composites. This results showed that by controlling the weight percent of carbon fibers, the recovery properties of composites can be controlled for different applications. The interesting research in the shape memory composites is the shape recovery by flexural method as a quasi-static method, which was done by Li et al. [53]. The shape memory method in this work was the intrinsically toughened network. They mentioned that adding the carbon fibers reduced the shape fixity of SME. The obtained results showed that the shape recovery at the 100 °C were 100% after 20 minutes at this temperature.

Jony et al. [54] used the polycaprolactone (PCL) and thermoplastic PU as blending shape memory polymers to investigate the shape memory effect in the carbon fibers–epoxy composite. This method can be used for self-healing applications. The obtained results showed that the optimum time for shape recovery was 30 minutes in 80 °C for both additives. Also, they reached to the healing efficiency of 146% by blending method. As compared with the other shape memory methods, this method is proper for self-healing applications because of highest healing efficiency of that. Liu et al. [55] added the short carbon fibers to the E51 SME. After that, they fabricated the wind blades. The experimental and theoretical results regarding air flow velocity variation showed that the fabricated blades had continues stable mechanical behavior by changing the variation wind speeds. This research introduced the new smart structure with shape memory effect, which can respond to environment variations.

Wei et al. [56] investigated the shape memory effect in the short glass fibers–hydro epoxy (intrinsically tough) composites. The reported results showed that the glass modulus and bending strength initially increased and then decreased by increasing the percentage of short glass fibers. The full shape recovery was obtained for samples <4.5 wt% short glass fibers. If the percentage of that was more than 4.5 wt%, the composites may be destroyed after deformations. This means that adding fibers into the structures with the shape memory behavior is one of the limitations in these structures because of the creation of new rigid sections by fibers, which reduce the deformation capability and consequently the shape memory behavior. Reducing

the shape memory behavior by increasing the percentage of glass fibers was also mentioned by Fejos et al. [57].

12.2.4 Shape Memory Wires in the Epoxy Composites

The shape memory alloys (SMA) like shape memory polymers can recover their initial shapes by heat treatment. Transferring between martensitic and austenitic phases is the basis of shape memory behavior into them. Embedding the SMAs into the epoxy composites changes the mechanical and thermomechanical properties of those [58, 59]. To enhancing the mechanical properties by the SMA, it has firstly been transformed to the martensitic phase and then pre-strain or pre-tension is done and fixed the applied preform during the composite fabrication. When the curing process of polymer like epoxy is done, the SMA returns to the austenitic phase and releases the compressive stress in the composite structure [60, 61]. This created compressive stress influences on the mechanical properties of composites.

Xu et al. [62] investigated the content and position of SMA on the mechanical properties of the glass fibers–epoxy composites. The results showed that in the optimum condition, the flexural modulus was improved about 5.76%, as compared with pristine glass fibers–epoxy composites. Also, the mode I and II interlaminar fracture toughness tests were decreased. The weak adhesion between SMA and epoxy was the influence factor on the mechanical properties. By surface treating like acid treatment or adding nanoparticles, the adhesion between those can be improved [63]. Embedding the SMAs in the smart epoxy composites with capability of shape memory or healing behaviors is the interesting subject, which has been investigated in the last few years. Feng et al. [64] added 1 wt% NiTi in the SME. The results showed the shape fixity and recovery reached 100%. Kirkby et al. [65] embedded the SMA in the self-healable epoxy composites. The SMA improved the healing behavior by crack closure mechanism, which reduces the total crack volume and increases the filling ability of healing agent. Also, by heating the SMA, the curing process and polymerization degree of healing agent increased [66]. Neuser et al. [67] fabricated the SMA–epoxy self-healable composite. The healing mechanism was the solvent-based microcapsules. The reported results showed that, in the equal conditions, the sample without SMA had 24% healing efficacy, whereas adding SMA increased the healing efficiency up to 78%.

12.3 Smart Epoxy Composite Coating

Today, the self-healing and inhibiting behaviors are the interesting subjects in smart epoxy coating. But in the smart epoxy composites in the coating applications, the most focuses of researchers on the inhibition of those, although the simultaneous healing and inhibiting behaviors are investigated by different researchers. The reason for that is the role of used fillers especially nanomaterials in the polymeric coating. In the smart polymeric coating systems, two important organic or inorganic part exist, which the first of that is the polymer matrix as a barrier or passive agent and the

other is the nanocontainers as an active agent [68]. The inhibition molecular agents are immobilized into the nanocontainers. When the substrate stays on the corrosive media, the inhibitor is activated to inhibit the substrate by variations of pH, ultraviolet wavelength, ions, solution, etc. [69]. These nanocontainers should be capable to entrap and hold the inhibitors up to when the substrate will be attacked by the corrosive agent. The most important nanocontainers can be classified based on the kind of inhibitor embedding methods.

The first embedding method is grafting the inhibitor to the nanomaterials. In this method, the inhibitor is attached to the nanomaterials by chemical reactions. Then, the nanomaterials are dispersed into the polymeric matrices like epoxy. When the corrosive agents reach the nanomaterials, the inhibitor is released to create the inhibiting layer on the substrate. Taking this method, Motamedi et al. [70] attached the histamine and Zn on the RGO, which can be seen in the Scheme 12.9.

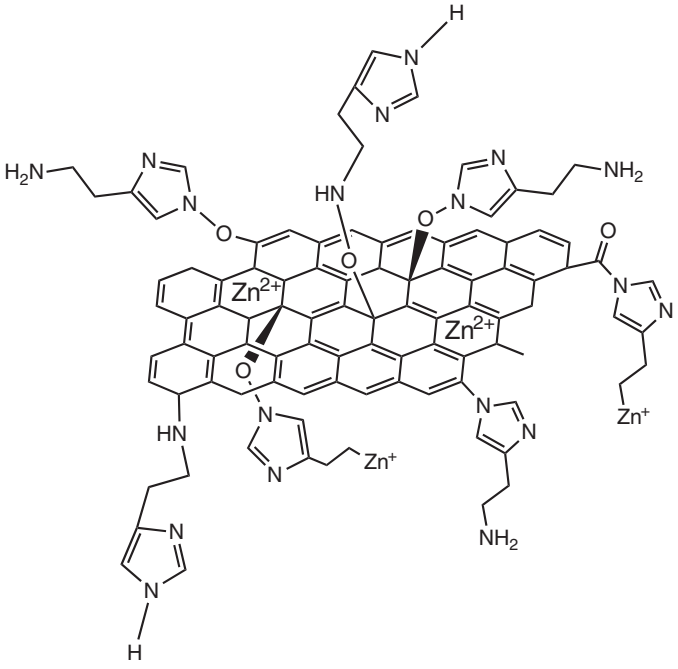

Scheme 12.9 Grafting the histamine and Zn on the reduced graphene oxide, which was done by Motamedi et al. [70]. © 2019, Elsevier.

The second embedding approach is the layer-by-layer method. In this method, the nanomaterials are firstly modified and then inhibitor is embedded on the surface of those. After that, the polymeric shell is coated on the surface of nanomaterials inhibitor to protect them. Following, the nanocontainer is dispersed into the epoxy matrix. When the corrosive agents meet the nanocontainer, firstly the shell is decomposed or solved and then the inhibitor agent is released. Considering that method, Yeole et al. [71] embedded the 2-mercaptobenzothiazole (MBT) on the surface of CNTs and coated those by polyacrylic acid (PAA), which can be seen in Figure 12.3.

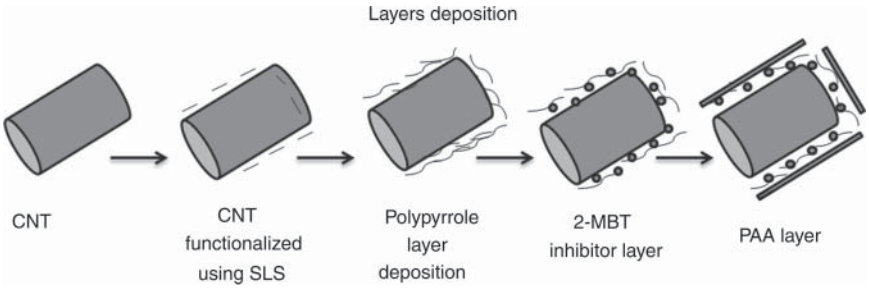

Figure 12.3 The schematic of embedded the 2-mercaptobenzothiazole (MBT) on the surface of CNTs via the layer-by-layer method by Yeole et al. [71]. Reprinted by permission from Springer Nature.

The third generation is loading the inhibitor agent into the nanomaterials. This method is very useful for mesoporous nanomaterials. For this method, a template is firstly used to cover the micro-spheres by nanomaterials. After that, the template is extracted by thermal or chemical extraction method. In the following, the inhibitor agent in the form of solution diffused into the mesoporous structures by a vacuum method or being into the inhibitor solution for long period of time. The template can be polymeric or ceramic materials. The most important of mesoporous nanocontainers is the mesoporous structures of silica, titania, and carbon [72–74]. The example of this method is the research work of Haddadi et al. [75]. These researchers firstly synthesized the carbon hollow spheres using the silica template. After that, the 2- mercaptobenzimidazole (MBI) were loaded into the carbon mesoporous. In the following, the nanocontainer was dispersed into the epoxy coating and used for covering the steel substrate. By reaching the corrosive agent, the MBI diffused the damaged area and created the protective layer by reacting the substrate, which retarded corrosion (Figure 12.4). Although this method was firstly introduced to load the inhibitor agent for inhibition of epoxy coating, but this method can be used for self-healing epoxy coating by loading the epoxy and polyamine agents, which was performed by these researchers in their next research works [76].

The other approach is doping the ions or inhibitors. Although this method is generally used for nanomaterials with plating structures like Na montmorillonite, graphene, zeolite, and layered double hydroxide (LDH) structures [77–79], but some nanotube structures like aluminosilicate halloysite nanotubes have capability for doping the ions or inhibitors [80]. In this method for plating structures, the ions with inhibitor capability such as Co, Ce, and phosphate ions are doped into the gallery spaces through ions exchanging method. When the epoxy coating containing doped inhibitor ions into nanomaterials puts the corrosive media, these ions diffuse the damaged area and entrap the ions like Cl^- or react with substrate (Figure 12.5). This reaction is caused to form the inhibitor layer on the substrate, which retards the corrosion [82].

The newest approach is folding the embedded inhibitor on the surface of graphene layers, which was recognized by Qian et al. [83]. The schematic of this trend is illustrated in Figure 12.6. These researchers firstly synthesized the GO. Then, the GO

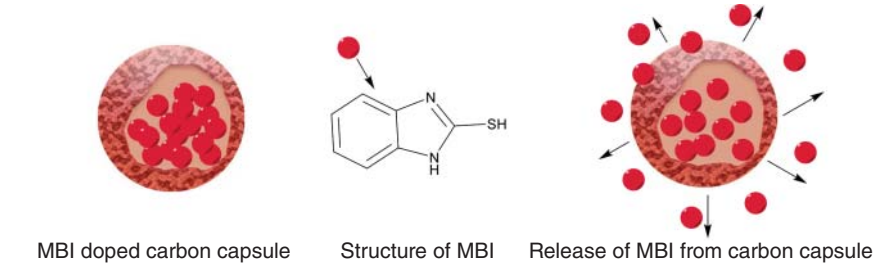

Figure 12.4 Using carbon hollow structure as carrier of inhibition agent, (a) schematic illustration of MBI release from carbon hollow spheres and (b) the consequent adsorption of thiolate and thione configurations of MBI on the mild steel surface. Source: Haddadi et al. [75]. © 2018, Elsevier.

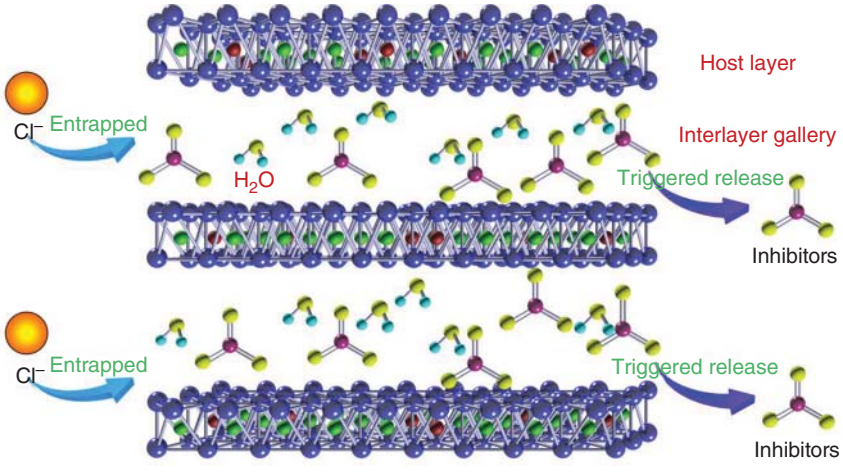

Figure 12.5 The schematic of the entrapment of the aggressive chloride ions and the triggered release of anionic corrosion inhibitors from layered double hydroxide. Source: Zhang et al. [81]. © 2018, Elsevier.

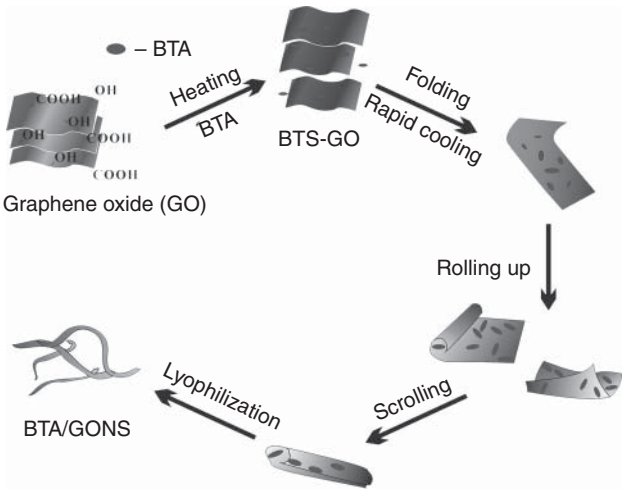

Figure 12.6 The schematic of fabricating the folded graphene oxide containing inhibitor agent. Source: Qian et al. [83]. Reprinted by permission of Springer Nature.

mixed with the benzotriazole (BTA) as an inhibitor agent. After that, this mixture was heated up to 100 °C and then injected to the liquid nitrogen and then followed by lyophilization for two days. The key of the folding is the liquid nitrogen. When the GO was immersed to the liquid nitrogen, the surface tension especially at the edge of that was changed, which caused the edge of GO layer to start the folding or bending to another side. This phenomenon was continued to roll up and form the crumpled scrolls in the nanometer scale, while the BTA trapped into the rolled GO layer. Like the other methods, when the corrosive agent meets the nanocontainers, the inhibitor agent is released and created the inhibiting layer on the surface of substrate.

The other approach is firstly to fabricate the nanocomposite with inhibition behaviors and then disperse into the epoxy matrix for coating the substrates. In this method, the inhibitor can be emended to the nanocomposites or the nanomaterials like nanosilica or nanoclay and inhibitor are composited with together. Sambyal et al. [84] by this approach firstly fabricated the poly(aniline-*co*-phenetidine)/SiO_2 composites and then dispersed into the epoxy matrix for cross-ion protection of mild steel.

12.3.1 Carbon-Based Nanomaterials–Epoxy Coating

The carbon-based nanomaterials can be in the form of CNTs, carbon nanospheres, graphene, and GO sheets [85–87]. In Table 12.2, the different carbon-based nanomaterials as nanocontainer for inhibition of steel substrates were listed. Considering Table 12.2, it can be said that the carbon-based nanomaterials have proper potential to be container for self-inhibiting the polymeric coatings. These nanomaterials can carrier the organic or inorganic inhibitor by different methods such as grafting, layer by layer, loading, doping, and folding, which are the good candidate for using in the epoxy coating.

Table 12.2 Carbon-based nanocontainer for inhibition applications.

Nanocontainer	wt%	Carrier method	Inhibitor agent	References
GO	0.2	Grafting	Metronidazole	[88]
CNTs	1	Layer-by-layer	2-Mercaptobenzothiazole	[71]
Mesoporous carbon	—	Loading	Epoxy and polyamine	[76]
Mesoporous carbon	0.02	Loading	Walnut (green inhibitor)	[89]
GO	0.15	Doping	Ce	[80]
RGO	0.15	Grafting	Histamine + Zn	[70]
GO	0.4	Folding	Benzotriazole	[83]

The CNTs have ability to carrier the inhibitor by grafting, doping, and layer-by-layer methods. The GO, graphene, RGO, and nanographene as well as functionalized nanographene are capable to use as carrier by all methods except the loading method. The mesoporous carbons are the good candidate for loading the inhibitor into them. Also, they have this ability to be carrier the healing agent for self-healing composites especially self-healing coatings. The reason for this ability is the controllable capability of their size during synthesize processing, which is caused to control the healing agent by changing their size. Non-toxicity, chemical stability, and electrical conductivity are other especial features of that for using in the smart epoxy coating [88, 89].

12.3.2 Clay-Based Nanomaterials–Epoxy Coating

One of the interesting nanomaterials for using the smart coatings is nanoclay. The conventional and most famous nanoclay is the sodium montmorillonite (Na^+-MMT), which has a layer structure. The Na^+-MMT has attracted many attentions for using in the epoxy matrix because of the good compatibility of that with the epoxy matrix [90, 91]. The MMT has crystal structure with three sub-layers. Two sub-layers are the tetrahedral silica sheets, and other ones is the octahedral sheet of alumina. This structure gives the ability to MMTs for loading or doping the organic or inorganic inhibitors into them by ions exchanging method. Considering with this feature, Ghazi et al. [92] loaded the benzimidazole into the MMT's layers (Figure 12.7) for fabricating the smart epoxy coating. It is worth noting that the nanoclay can be in the form of nanotube structure. The aluminosilicate halloysite nanotubes (HNT) or nanotube clay with a lumen of 15 nm, external diameter of 50 nm, and length of upto 1 μm is a good candidate for loading or doping the organic or inorganic inhibitors into that for fabricating the smart epoxy coating [79].

In order to better understand the role of nanoclay in the smart epoxy coatings, the newest research works are mentioned in the following. Atta et al. [93] fabricated the nanogel composites from nanoclay and *N*-isopropyl acrylamide as a sensitive monomer with self-healing and inhibiting abilities. Then, the synthesized composites dispersed into the epoxy coating. The obtained results showed that adding the 1 wt% clay *N*-isopropyl acrylamide had the efficient self-healing and

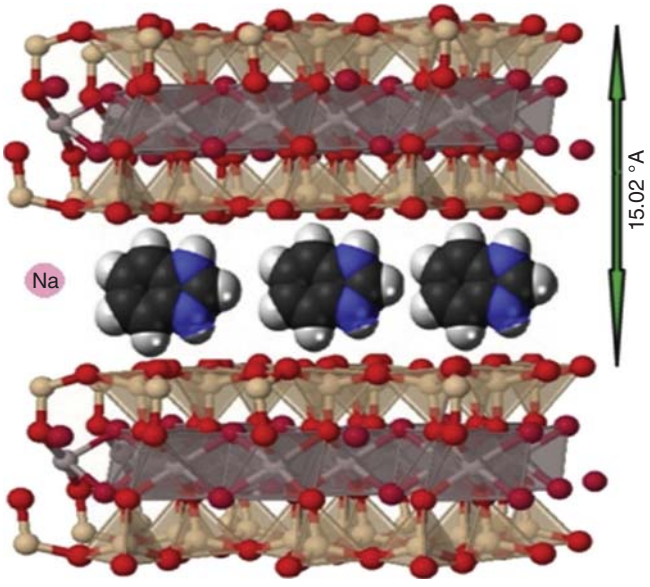

Figure 12.7 The schematic of embedding the inhibitor agent into the sodium montmorillonite layers by ion exchanging method. Source: Ghazi et al. [92]. © 2015, Elsevier.

inhibitor behaviors into the salt spray corrosion test. Njoku et al. [94] loaded the BTA into the HNT and then dispersed into epoxy matrix for coating on the surface of carbon steel. To control the release rate of inhibitor agent, the ends of tubes were capped by Fe^{+} through the dispersing the HNTs into the $FeCl_3.6H_2O$ solution and covering by chitosan. The obtained results indicated that this smart epoxy coating had excellently combined passive, active, and self-healing protective actions. In the study of Truc et al. [95], the 8-hydroxyquinoline as inhibitor was doped into the interlayers of MMT.

12.3.3 Silica-Based Nanomaterials–Epoxy Coating

Some recent researches in the smart coating showed that one of the proper nanomaterials for fabricating the smart epoxy coatings is the nanosilica-based nanomaterials. These nanomaterials can be hold the inhibitor into the epoxy coatings by grafting, coating, and loading methods. In view of the grafting method, Khodabakhshi et al. [96] grafted the MBI and polyethylene glycol (PEG) as an organic inhibitor to the silica nanoparticles for making the epoxy smart composites. The grafted nanosilica by MBI and PEG were dispersed into epoxy with loading ratio 1000, 2500, and 5000 ppm. They mentioned that the MBI-nanosilica with loading ratio 1000 ppm had the best corrosion inhibition, in comparison with 2500 and 5000 ppm loading ratios. They discussed that in the low concentration of nanosilica-MBI, the suppression of anodic reaction and inhibition of metal was occurred, whereas in high concentration of that, the suppression of cathodic and blocking of reduction reactions were happened. Also, the best inhibition efficiency of PEG-nanosilica was reported for samples with 2500 ppm loading ratio.

Taking of the composite method, Gharagozlou et al. [97] fabricated dispersed cobalt ferrite nanoparticles in the silica matrix. After that, this composite was dispersed into the epoxy coating. The obtained results demonstrated that this composite can feel the cavities and block the electrolyte pathway. In this composite by resealing the Co^{2+} cations, the inhibiting behavior and restricting the corrosion phenomenon were seen. It is worth noting that the silica nanoparticles can be in the form of mesoporous silica container, which is one of the especial mesoporous structures for carrying the inhibitor or healing agent [98]. Given this feature, Rahsepar et al. [99] loaded MBT to the mesoporous silica and then 1, 3, and 5 wt% loaded silica dispersed to the epoxy for coating on the carbon steel. The obtained results showed that the 3 wt% loaded mesoporous silica had superior protection performance in the solution of 3.5 wt% NaCl.

12.3.4 Layered Double Hydroxide-Based Nanomaterials–Epoxy Coating

LDH is known as anionic clay or hydrotalcite like compounds [100, 101]. The conventional formula of that is $[M_{II(1-x)}\ M_{IIIx}(OH)^2]^{x+}\ (A^{n-})_{x/n}.mH_2O$, where the M_{II} is a divalent metal like Co, Ca, Cu, Mg, Zn, and Ni; M_{III} is a trivalent metal, namely Ga, Cr, Fe, and Al; A^{n-} is anion with a valency of n; as well as x defined $[M_{III}]/([M_{III}]+[M_{II}]$, which is between 0.25 and 0.33. This nanostructure has anionic exchange feature; therefore, the various organic and inorganic inhibitors can be loaded between intercalated its layers by ion exchanging method [101]. The surveyed researches about the LDH and loading different inhibitors are listed in Table 12.3.

12.3.5 Other Nanoparticles–Epoxy Coating

Although the carbon, clay, silica, and LDH have attracted many attentions as nanocontainers, the other nanomaterials like Fe, Zn, Zr, and Ce have proper

Table 12.3 Various loaded inhibitor into the LDHs.

LDH	Inhibitor agent	Inhibition efficiency (%)	Exposure time (hours)	References
Zn–Al	Nitrate and phosphate	96 (for phosphate) 68 (for nitrate)	24	[102]
Zn–Al	Ethylenediaminetetraacetic acid	42.1	168	[103]
Zn–Al	2-mercaptobenzimidazole	—	—	[77]
Mg–Al	Nitrate and phosphate	57.1 (for phosphate) 47.3 (for nitrate)	24	[101]
Mg–Al	Sodium molybdate	98	3	[104]
Mg–Al	Aminobenzoate	—	—	[105]
Mg–Al	Cerium molibdate	—	—	[106]

potential for using as nanocontainers in the epoxy coating applications. Some of these nanomaterials like Ce nanoparticles can be separately acted as an inhibitor agent. Based on two points of mentioned views, some new researches about other nanocontainers are outlined as follows. ZrO_2 nanoparticles are one of the nanomaterials, which singly increase the corrosion protection of epoxy coatings and ionic resistance [107]. Lv et al. [108] firstly used the RGO for corrosion protection, but some micro-galvanic corrosion were seen as coating defects on the surface of substrate metal. Therefore, they covered the double sites of RGO by ZrO_2 nanoparticles through grafting method. This idea was caused to create micro-galvanic corrosion. Acting the ZrO_2 nanoparticles as insulating spacer and elimination of RGO/metal contact were the explained reasons. The ZrO_2 nanoparticles can be in shape of mesoporous structures for carrying the inhibitor agent, which investigated by Wang et al. [109].

ZnO is another proper nanoparticles as barrier or container of inhibitor agent. In the study of Rostami et al. [110], Co was doped on the ZnO nanoparticles and then were dispersed into epoxy coating. The obtained results indicated that Co-doped ZnO released the inhibitive spaces and restricting the electrochemical reactions, consequently significantly improved the corrosion protection of epoxy coating. Mostafaei and Nasirpouri [78] firstly synthesized the ZnO–PANI nanorods and then dispersed into the epoxy for coating on the steel. The protection mechanism in this work was the passive pin hole by iron oxide and the complex compound between the steel and coating.

Ce is the one of the elements with dual applications, which are inhibitor and carrier agents. Niroumandrad et al. [111] doped Ce on the aluminum nanoparticles and then dispersed into the epoxy for coating on the steel. The obtained results showed that the Ce-doped aluminum had higher corrosion protection, as comparison with aluminum particles. Two mechanisms for this behavior was mentioned. The first is that the Ce blocked the corrosive spaces as a physical barrier. The second mechanism is that Ce(III)/Ce(IV) ions are the metastable and in the present of Cl^- can be converted to each other. This means that Ce/Al can be in the form of Ce–O–Al in the corrosive media. Ce can be in the shape of cerium molybdate and oxide as nanocontainers for barring the MBT, BTA, and imidazole into epoxy coatings [112–114].

12.3.6 Polymer Micro-/Nanocontainer–Epoxy Coating

One of the progressive trends in the smart epoxy coatings is the polymeric micro-/nanocontainers, which have dual application for epoxy coatings. The first application is trapping the inhibitor agent for preventing the corrosion phenomenon, and the second one is trapping the healing agent for healing the epoxy coatings. This method is introduced micro-/nanocapsules. By this method, the inhibiting or healing agents are capsulated by polymeric shell. The famous polymeric shells for capsulation are urea-formaldehyde (UF), melamine formaldehyde, polymethyl methacrylate (PMMA), and etc. [115, 116]. Some researchers considered the epoxy containing the microcapsules as a smart composite, but other researchers introduced as a blending system [117, 118]. Regardless of point of views, the new researches and techniques are outlined as follows. One of the interesting

research about this method is the capsulation the silyl ester. When the scratch on the surface of the epoxy coating is created, the capsules containing the silyl ester are ruptured and diffused the silyl ester into the damage area. By reaching the water in the damage area, the silyl ester reacts to that and creates the hydrophobic shell on the surface of metal. Also, the water is caused to close the broken surface of microcapsules containing silyl ester and can control the releasing rate of that. The advantage of this method is that, the cross-linking agent or catalyst is not necessary and the healing can be done by the available humidity in the atmosphere [119].

Other interesting shell for microcapsulation is using the formaldehyde-based resins especially UF through in situ polymerization. By this method, the used epoxy for coating can be capsulated by UF shell. By using the sonication method, the capsule size can be reached to nanometer. In this method, using another agent for curing the defused epoxy resin from capsules to the damage area is necessary. Grubbs is the first generation of used catalyst for this healing system [13]. The other method is using the hollow glass microspheres (HGM). The HGM firstly are produced and then carried the hardener by using the etching method and diffusing that into HGMs through vacuum method [120]. It seems that this method cannot be used in the sea media because of the solubility of amine hardener in the water media, but in the conventional environment, it is one of the proper candidates as smart epoxy system for coating the metals. Capsulation of the amine agent by polymeric shell was done by Kongparakul et al. through the formation of the polystyrene shell [121]. The other healing agent, which can be capsulated by UF shell, is linseed oil, which was studied by Wang and Zhou [122]. The results showed that the linseed oil creates the thin film on the surface of the substrate and reduces the corrosion phenomenon, but it cannot be completely healed the epoxy coatings.

The capsulation of epoxy resin by EDA is another proposed method. In this method like in situ polymerization by UF, the epoxy is firstly stabilized by emulsifier into the water media and the EDA is added in this media. The epoxy and EDA are reacted together and created the polymeric shell on the surface of epoxy bubbles [123]. Zhang et al. [124] used this method into the epoxy coating containing the polyaniline nanofibers for mild carbon steel. Then, the corrosion behavior of coated mild carbon steel by epoxy was investigated into the NaCl solution. In this method, the second agent was not used. The mentioned mechanisms for curing the epoxy healing agent were reacting the healing agent by residual hardener into the epoxy matrix and alkaline conditions.

One of the biggest problems in the microcapsule systems is the inability of them to multiple healing. For solving this issue, the next generation of microcapsules was synthesized, which introduced as multicore microcapsules, which can be seen in Figure 12.8. To synthesize multi-core capsules, the alginate biopolymer can be used. Hia et al. [117] capsulated the epoxy and polyamine hardener by multi-core encapsulation. The obtained results showed that after four healing cycles, the healing efficiency was between 68% and 85%. Therefore, this method can be a good candidate for smart epoxy coatings for multi-inhibition and healing behaviors [125].

As previously mentioned, achieving the smart epoxy systems with dual applications was the aim of researchers in the last few years. To do so, the new epoxy

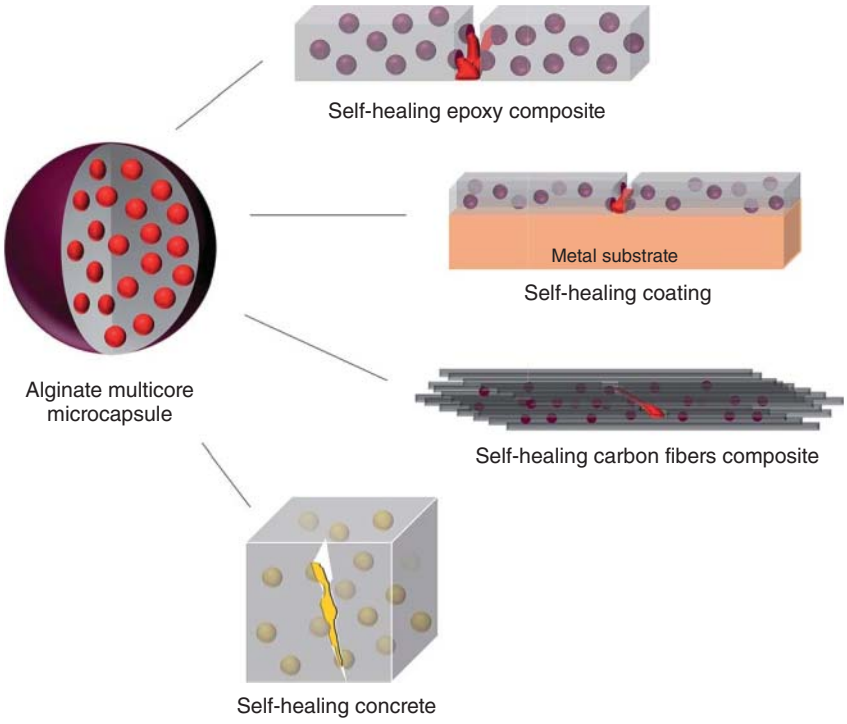

Figure 12.8 Self-healing applications of alginate multicore microcapsules. Source: Lee Hia et al. [117]. © 2018, Royal Society of Chemistry.

coating with dual behaviors was firstly introduced by Khun et al. [126]. They synthesized microcapsules containing the hexamethylene diisocyanate (HDI) and then dispersed them into the epoxy coating. After that, the healing and wear behaviors of fabricated coating were investigated. When the wear test was done, the HDI acted as a lubricant agent in the abrasive media. In other words, the self-lubricating behavior was characterized by this researchers. When the healing test was done, the HDI from the microcapsules diffused into the damage area on the surface of substrate and reacted with water, consequently, healed the microcracks. The self-healing and self-lubricating systems into the epoxy coating was also done by Li et al. [127]. Firstly, these researchers capsulated the tung oil as a healing agent by polysulfone shell through the solvent evaporation method. Then, 10 wt% microcapsules were embedded into epoxy coating. The obtained results showed the excellent anticorrosive behavior in the scratch area, due to the formation of the cross-linked polymeric film. The frictional coefficient and wear rate of smart epoxy coating were decreased by adding the microcapsules containing the tung oil.

12.4 Self-Healing Epoxy Polymers and their Composites

12.4.1 Self-Healing Behavior

One of the nature's smartest features is its ability to heal the created damage by itself. Creating this behavior in the man-made materials as a next-generation technology is one of the topics, which many researchers focused on that over the last decade. This smart feature can be created into the ceramics, metals, and polymers. The self-healing feature had remarkable growing in the polymer and polymer composite materials. The first introduced category of self-healing systems was the intrinsic and extrinsic healing system [128]. But during the last few years, the extrinsic system was grown and divided into the capsule- and vascular-based healing system. Therefore, in the new category, the self-healing systems in the polymer-based materials especially epoxy systems are classified into intrinsic, capsule-based, and vascular systems [129].

The summary of the different systems and subdivision of those is illustrated in Figure 12.9. In the intrinsic method, the polymeric materials have capability to heal or recover the initial properties by using the thermal, ionic, water, UV, etc. activation agents. The intrinsic epoxy system can be divided into three major groups. The first of those is the reversible covalent bonds. The second ones is the supramolecular system, and the last system is the blending with a thermoplastic polymer as a healing agent [130]. In the vascular- and capsule-based healing system, the healing agent is stored into the container in the form of vascular or capsule. When the cracks reach these containers, the healing agent diffuses into the damaged area and by different polymerization methods heals the cracks. The vascular systems are classified into the hollow fibers, microvascular networks, and electrospinning methods [131]. Also, the capsule-based system can be sub-divided based on the polymerization agents, which are catalyst, solvent, and cross-linking agents [132].

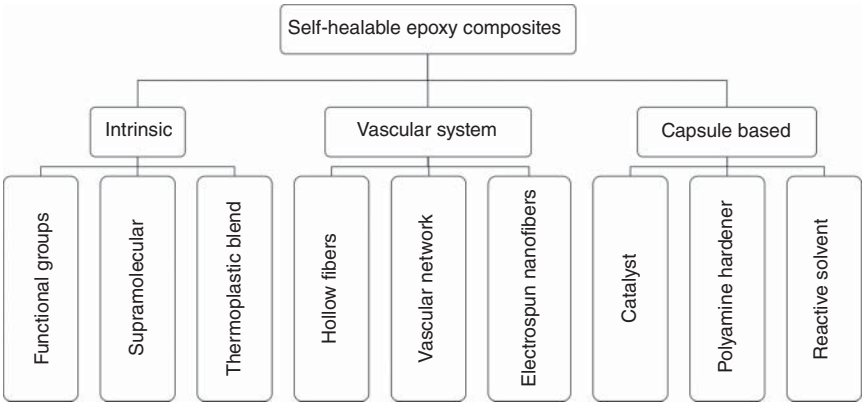

Figure 12.9 The classification of various healing systems in the self-healable epoxy composites.

12.4.2 Intrinsic Healing System

One of the newest strategies in the polymer science is designing the new polymer with functional groups like dynamic covalent bonds in its structures, which can create the new features namely healing ability into that. In the epoxy systems, the various functional groups of Diels–Alder (DA), alkoxyamine moieties, transesterification reaction, and disulfide chemistry have been introduced, up to now [133, 134]. Among the mentioned functional groups, the DA and retro Diels–Alder (rDA) have proper potential for healing applications. In furan/maleimide moieties based, DA reactions are done in the low temperature (50–80 °C), whereas the rDA reactions are taking place at 110–130 °C [134]. The outcome of this method healing mechanism by the thermal activation is demonstrated in Figure 12.10. The number of epoxy composites by this method is limited, and this method has a progressive trend in the near future. Zhang et al. [135] firstly grafted the maleimide agent by surface treatment on the surface of carbon fibers. To do so, the carbon fibers immersed into the acetone, nitric acid, and tetraethylenepentamine solutions for removing the impurity, increasing the acidic groups, and bridging between carbon fibers and maleimide agents, respectively. The epoxy was functionalized by furan agent and then cured by amine agent. The obtained results showed that the epoxy with 20 wt% furan agent had maximum recovery behavior (approximately 80% healing efficiency).

Li et al. [136] fabricated the amino-functionalized CNTs–DA epoxy composites. The applied heat by near-infrared irradiation on the CNTs and the DA network was caused to dissociation/reconstruction of DA network, resulting in healing the damage area. The healing efficiency by this activation agent was 77%. Handique and Dolui [137] modified the CNTs and epoxy by furfuryl (furan group) and then reacted them by bifunctional maleimide (maleimide) as a curing agent for creating the DA bonds. The obtained results showed that the healing efficiencies of first, second, and third healing cycles were 79.82%, 67.91%, and 51.80%, respectively. Oh et al. [138]

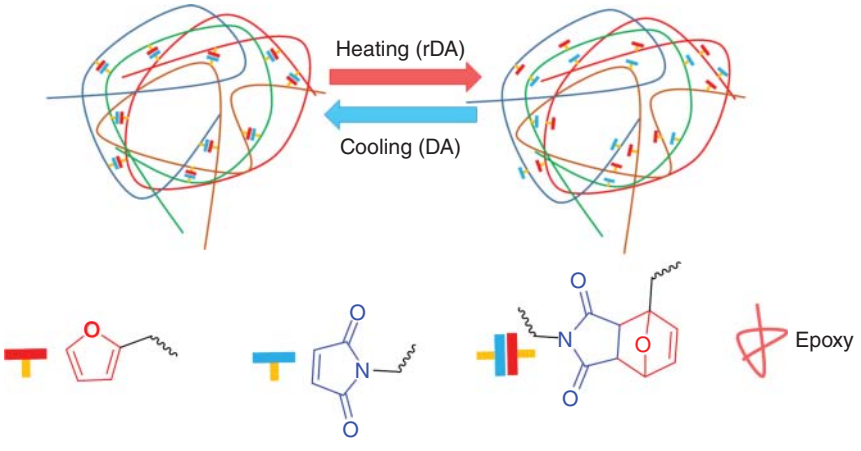

Figure 12.10 The schematic illustration of thermally reversible transition between network and branched molecules in cross-linked epoxy polymer by DA and rDA reactions. Source: Kuang et al. [134]. © 2015, John Wiley & Sons.

grafted the furan group on the epoxy and the graphene nanoplatelets (GNPs) acted as maleimide groups for creating the healing behavior. In the other study, Khan et al. [139] grafted the bismaleimide on the GNPs and dispersed them into the DA epoxy. The obtained results indicated that by adding the 1.5 wt% GNPs, the healing efficiency reached to 87%, whereas the healing efficiency of pristine DA epoxy was 53%.

In the interesting investigation by Li et al. [140], both forum and maleimide agents grafted to the GO and epoxy resin and then the GO–epoxy nanocomposite was fabricated. The healing efficiency of this composite by heating at temperature of 110 °C for 60 seconds was 90%. The calculated healing efficiency by microwave method for 60 seconds was 133%. Also, by infrared light for period time of 5 seconds, the healing efficiency was 106%. In the study of Cai et al. [141], the graphene sheets were dispersed into the DA epoxy and then by the microwave, the healing properties of this composite were investigated. In the light of the above, the carbon-based nanoparticles can have dual actions in the nanocomposites with DA agents. The first of those is the heating agent, due to having the high conductive properties and the second of those is bridging in the DA reactions.

The second strategy in the intrinsic self-healing polymers is using the supramolecular systems. This method generally used for healing the elastomers. This new trend has similar behavior like DA reactions with this difference that the dissociation/reconstruction reactions were done by hydrogen bonds. For this reason, this method may be named as physically healing method. To date, this method into the thermoset polymers especially epoxy system has rarely used. In some researches, the healing behavior of epoxidized elastomers has been investigated [142], where the summary of those is as follows. Nie et al. [143] fabricated the epoxidized natural rubbers (ENR)-chitin nanocrystals composite. By adding 20 wt% chitin nanocrystal, the healing efficiency reached to 83%. Cao et al. [144] synthesized cellulose nanocrystal–ENR composite, which had 80% healing efficiency. Hence, this nanocomposite is very proper for flexible electronic devices. Similar previous research works, Xu et al. [145] fabricated the bentonite–ENR composite, which had 85% healing efficiency.

Guadagno et al. [146] firstly synthesized rubber-toughened epoxy and then the functionalized CNTs added to that and the self-healing capability of this composite was investigated. Embedding the CNTs into the rubber-toughed epoxy leads to reversible CNTs bridging into the epoxy polymer because of the strong interaction between CNTs and rubbery epoxy. By adding 0.5 wt% CNTs into the rubbery epoxy, the healing efficiency reached higher than 50%. The other accomplished approach was modifying the epoxy by hydrogen bonding unit via ureidopyrimidone, which was done by Kostopoulos et al. [147] in carbon fibers–epoxy composite. The healing efficiency after the first damage was approximately 64%, which was obtained by heating in the temperature of 100 °C for 15 minutes under a compressive load of 1 kN. After the seven healing cycles, the healing efficiency dropped to 26%. Although the number of researches about self-healing epoxy by supramolecular is limited, due to lack of elastomeric or rubbery epoxy, but the new synthesized epoxy network including the supramolecular hydrogen bonding cross-links will demonstrate the progressive future about that [148, 149].

The next approach in the intrinsic self-healing epoxy is using the thermoplastic blend into the epoxy. The thermoplastic polymers such as ethylene vinyl acetate (EVA), poly(ethylene-*co*-glycidyl)-methacrylate (PEGMA), poly(vinyl-butyral) (PVB), styrene–ethylene–butadiene copolymer (SEBS), acrylonitrile–butadiene–styrene (ABS), and polyethylene-*co*-methacrylic acid (EMAA) were investigated for healing the epoxy systems by the intrinsic blending system. Varley et al. [150] added 5, 10, and 15 wt% of the mentioned thermoplastic polymers into the epoxy and the healing behavior of them in the four healing cycles was studied. The ability for healing the epoxy by these thermoplastic polymers is as follows: EVA > EMAA > PEGMA > PVB > SEBS ≈ ABS.

Pingkarawat et al. [151] fabricated the carbon fibers–epoxy composites containing one of the EVA, EMAA, PEGMA, and ABS as thermoplastic healing agents. Then, Mode I interlaminar fracture toughness of them was surveyed by a double cantilever beam (DCB) test. The healing process was done in the temperature of 150 °C for 30 minutes. The obtained healing efficiency in the DCB test by EVA, EMAA, PEGMA, and ABS was 103%, 156%, 57%, and 0%, respectively.

The healing of epoxy matrix with EMAA was done by the pressure delivery mechanism. When the EMAA is molten, the acidic group of EMAA and residual hydroxyl group of epoxy react together and create the water in the high pressure. This pressure force squeezes the molten EMAA into the microcracks and fill them. Therefore, after cooling, the damaged epoxy can be healed in the epoxy composites. Similar behavior was seen by PEGMA in the carbon–epoxy composite. The EVA cannot react with the epoxy, but has lower viscosity, as compared with the EMAA and PEGMA. ABS, EVA can easily diffuse into the microcracks and heal the created cracks into the damage area [150, 152].

In view of comparing the mentioned thermoplastic polymers for healing the epoxy composites, the EMAA had highest healing efficiency and compatibility with the epoxy matrix. These features have been caused to attract researchers' attentions for investing the blending intrinsic healing system into epoxy composites. EMAA can be used in the form of micropellet, thin film, or fibers into the epoxy. The healing efficiency of EMAA in the different forms of that into carbon fibers–epoxy is listed in the Table 12.4. By comparing the various shapes of EMAA, it could be understood that the stitch form had the highest healing efficiency in the DCB test. In contrast, the pellet shape had low healing capability in the compressive test.

Table 12.4 Different shapes of used EMAA in the carbon fibers–epoxy composite.

Shape	Content	Test	Healing efficiency (%)	References
Film	23 wt%	DCB	88	[153]
Stich	0.25 stich/cm^2	DCB	250	[154]
Pellet	15 wt%	Compressive	16	[155]
Fibers in the *z* direction	1% weave density fraction	DCB	120	[156]

12.4.3 Vascular Healing System

One of the newest method in the healing system of polymer and polymer composites is the vascular system. In this system, the healing agent is stored into the vascular as a container. When the crack reaches the vascular, the progressive force of crack is caused to destroy a part of vascular. Then, the stored healing agent diffuses into the damage area. After that, the polymerization reactions are caused healing the microcracks. Based on the progressive trend, the vascular system can be classified into the three major groups, which are the hollow fibers, vascular network, and electrospun nanofibers.

The first generation of vascular system was hollow fibers. These fibers can be metallic, ceramic, or polymeric hollow fibers. One of the proper hollow fibers in the epoxy composites is the glass hollow fibers. In this healing system, the healing agent, generally the used epoxy and hardener in the matrix, embedded the hollow fibers by vacuum system. Then, these hollow fibers are added into the epoxy composites. The idea of this method is based on the biomimetic approach. In this method, the illustration of crack and healing behavior is very simple and can be detected by adding UV fluorescent dye [157]. Trask and bond [158] embedded the hollow glass fibers into the E glass fibers–epoxy composites. They reported that the hollow fibers reduced the 16% flexural strength of composite. But this composite can recover 87% of its initial properties. These hollow fibers influence on the ply waviness and create the resin reach zone on the composite structures, which impress on the damage tolerance in the composite structures [159].

The advantage of this method is the capability of multiple healing in the composite structures. Therefore, the hollow fibers have still progressive in trend. Kling and Czigány [160] substituted the hollow glass fibers with hollow polypropylene fibers. Also, they used the polyester as a healing agent for healing the microcracks in the hollow fibers–epoxy composites. The obtained results showed that after the healing process, the bending properties of composite had been improved at least 20%, as compared with undamaged composite. One of the approximately unhealed damages in the composite structures is the fiber breakage and delamination into composites. By combining the healing mechanisms and shape memory strips, it can prevent the catastrophic failure of composite structures. The shape memory strip can close the crack tips, and the healing agent fills the crack area [161]. Embedding the hollow glass fibers and shape memory strip was done by Ghanbari et al. [162]. The obtained results indicated that the structure without the strip had 37.9% healing efficiency, whereas by adding strip with 4% pre-strain, the structure could recover the 78% of initial properties.

In nature, the damaged wound can heal by the vascular network that can carry the healing materials into the damage area. By this concept, the vascular network healing system into the composite materials was born [131]. In the epoxy system, the epoxy monomer and amine hardener can be embedded into the vascular networks. The vascular networks can be produced by different methods like 3D-printed structures, the solid preforms and spontaneous discharge methods [163]. Figure 12.11 represents the 3D structure of vascular network in the epoxy structure, which

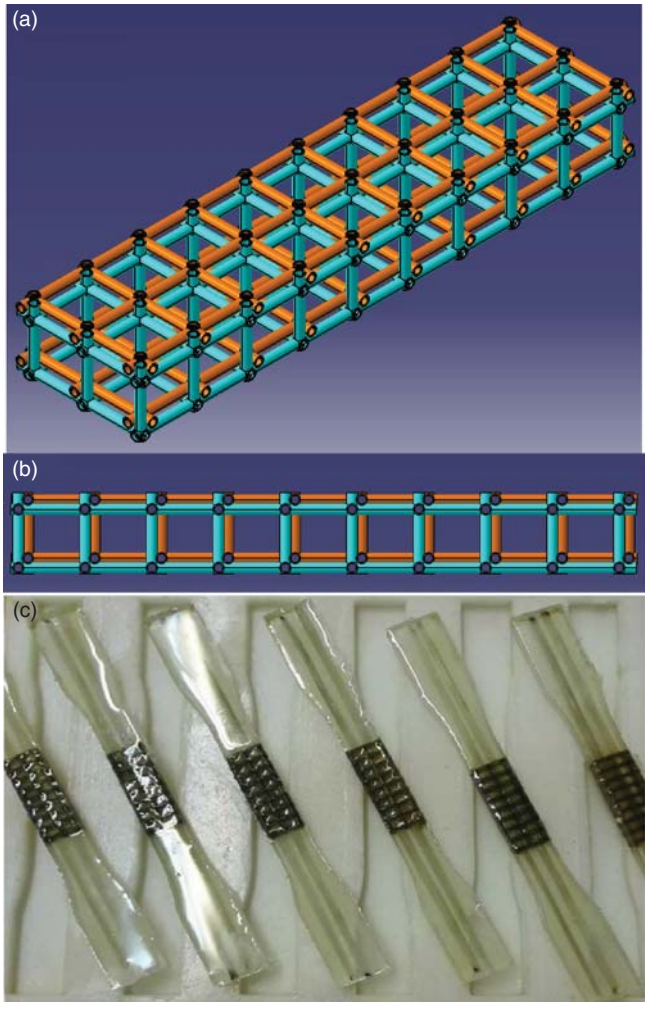

Figure 12.11 The vascular network healing system, (a) schematic of the microvascular network in isometric, (b) schematic of the microvascular network in side view, (c) the self-healable composites for tensile and creep tests. Source: Eslami-Farsani et al. [164] © 2019, Taylor & Francis.

was investigated by Eslami–Farsani et al. [164]. The most influence factors in this method are selecting the suitable hardeners, which was done by Cuvellier et al. [165]. They selected the triethylenetetramine (TETA), trimethylolpropane triglycidylether (TMPTE), Jeffamine D230 polyetheramine and Jeffamine D400 polyetheramine as famous commercial hardeners. They mentioned that the TETA and TMPTE were proper than the other hardeners for using the vascular healing system. The vascular network can be embedded in the *z* direction and create the 3D woven fibers. In this system, the sacrificial fibers are used in the *z* direction. After fabricating the composite structure, the sacrificial fibers are eliminated by thermal or solvent methods. Then, the liquid healing agent is diffused into the created

channels by vacuum method [166]. Coppola et al. [167] fabricated the 3D woven glass fibers–self-healable epoxy composites. These researchers used the polylactic acid (PLA) in the *z* direction for creating the channels. To decrease the degradation temperature of PLA, tin (II) oxalate catalyst was used. After the elimination of PLA, the channels were created in the both longitudinal and transverse orientations.

The promoted fabrication of hollow fibers is the electro-spun methods. In this method, two needles are used. The first one has bigger inner diameter for carrying the solution of polymeric shell and the second that is the healing agent. During the spinning process, the healing agent and polymeric shell flow from nozzle to the collector by loading high voltage. Pending the flowing process, the solvent of polymeric shell is evaporated and consequently, the shell is formed. In the following, these fibers are collected on the surface of collector. The flow rate, distance between nozzle and collector and loaded voltage influence the diameter of final hollow fibers [168]. The fabricated fibers by electrospinning method in addition to using as a container can be used as reinforcement in the epoxy matrix.

Vahedi et al. [169] fabricated the electrospun polyacrylonitrile (PAN) nanofibers containing healing agents (epoxy and amine) and then embedded those into the epoxy matrix. The obtained results showed that this composite is capable to heal itself up to 6 times at the room temperature. Also, the healing efficiency in the temperature of 50 °C had been reported about 75%. Zanjani et al. [170] fabricated tri-axial electrospun fibers with self-healing capability by using PMMA as shell's matter. Then, the electrospun fibers dispersed into the glass fibers–epoxy composites. The results indicated that the healing efficiency for recovery of normalized flexural modulus in the ninth healing cycle was approximately 85%. For fabricating the carbon fibers–epoxy self-healable composites, Neisiany et al. [171] made PAN nanofibers containing healing agents (epoxy and amine hardener) and then embedded those on the surface of carbon fibers during the electrospinning process (Figure 12.12). By adding the electrospun fibers, the tensile strength, short beam shear strength, flexural strength, and impact energy absorption were increased about 11%, 19%, 14%, and 4%, respectively. Also, this composite had capable to recover the 96% of initial flexural strength after 24 hours.

12.4.4 Microcapsule Healing System

The microcapsulation of the healing agent is the other method for healing the composite structures. The healing agent can be capsulated by ceramic or polymeric materials. Generally, the polymeric shell is proper than the ceramic shell for the polymeric composite structures. It is better that the healing agent is the same matrix resin, due to having similar structure. The epoxy as a healing agent can be capsulated by UF, phenol formaldehyde, melamine formaldehyde, PU, PMMA, polysulfone, and porous silica. Among the polymeric shell, the UF and PU and combination of them have attracted many attentions, due to one step polymerization, easy capsulation, and higher capsulation capability. It is worth noting that for curing the epoxy healing agent, the cross-linking agent is so necessary [132]. Therefore, based on the second agent, the microcapsule healing system can be classified into three major groups.

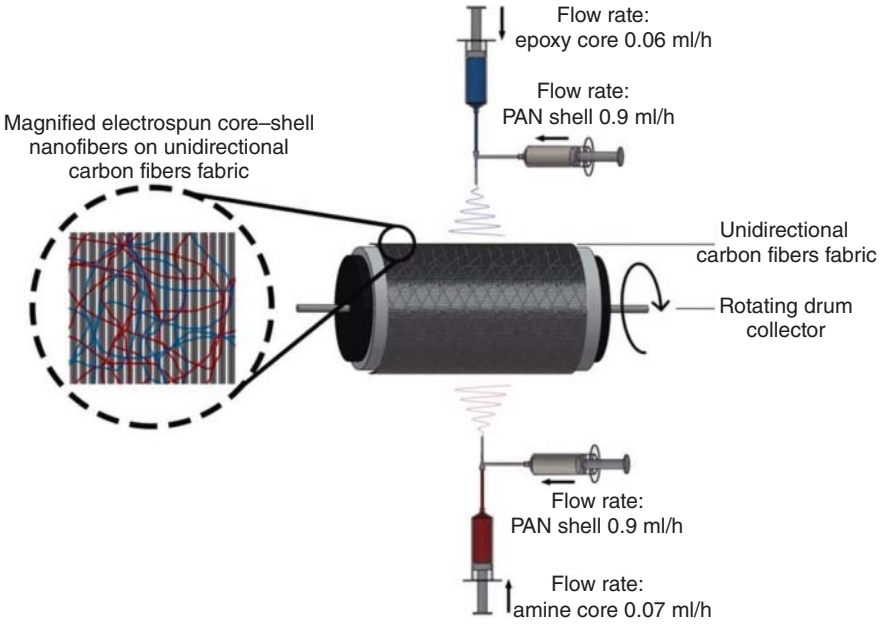

Figure 12.12 The schematic illustration of nanofibers deposition (containing epoxy and hardener as healing agents) on the carbon fibers fabric during coaxial electrospinning. Source: Neisiany et al. [171]. © 2017, John Wiley & Sons.

The first group or trend is dispersing the stable catalyst into the epoxy matrix during the fabrication of composite structure. The first generation of the used catalyst for curing the epoxy healing agent was the Grubbs' catalyst. Although the Grubbs' catalyst had the proper results for healing the epoxy composites, but it had disadvantages like high production cost, difficult synthesis process, and reaction with the epoxy during the fabrication of composite structures. For achieving the higher healing efficiency and reducing the reactivity of that with the epoxy, the Grubbs' catalyst was covered by waxy shell.

The next generation of this catalyst was introduced as Hoveyda–Grubbs' catalyst [132]. The other introduced catalyst was WCl_6 catalyst, which had healing efficiency about 65% [172]. The 5-ethylidene-2-norbornene (ENB) catalyst is the other catalyst, which is proper for using in the low-temperature healing process. But the polymerized structure of healed area by this catalyst had a linear structure. So, the physical properties of healed area was not suitable [173]. One of the important factors during the healing process is the rate of polymerization. Therefore, the SbF_6 was synthesized for healing with high polymerization rate. The gelation, curing, and post curing times for SbF_6 catalyst have been reported 30, 60, and 90 seconds, respectively. The disadvantages of SbF_6 catalyst are the toxicity of that and difficult synthesis process [174].

The new idea for curing by catalyst is using the latent curing agents of epoxy polymer. One of the famous of those is the imidazole-based materials. The first research for using this catalyst was done by Yin et al. [175]. These researchers firstly

synthesized the $CuBr_2$.2-methyl imidazole catalyst. This catalyst does not react with the epoxy polymers during the composite fabrication or post-curing process. The catalyst is activated by thermal in the higher temperature of 130 °C. In the high temperature, the ligand bonds between $CuBr_2$ and 2-methyl imidazole are broken and the 2-methyl imidazole can react with the diffused epoxy monomer in the damage area. The next research about the imidazole-based catalyst was the $NiCl_2$.2-methyl imidazole. Although the broking ligand bonds' temperature of $NiCl_2$.2-methyl imidazole was slightly higher than $CuBr_2$.2-methyl imidazole catalyst, but the toxicity of $NiCl_2$ during the synthesis process is lower than $CuBr_2$ [176].

The other trend for polymerization of the epoxy as healing agent is using the polyamine hardener. One of the simplest ways is capsulating the amine hardener. So, the amine can be capsulated by PMMA through solvent evaporation method, which was done by Li et al. [177]. By adding the 15 wt% combination of epoxy and amine microcapsules, the healing efficiency was reached up to 84.5%. The amine hardener cannot be capsulated by UF method because the pH of amine hardener was higher than seven and the polymerization of UF is done in the pH of 2.5–3.2. Hence, the capsulation of polyamine hardener by UF is not applicable. However, the capsulation of amine was done by Jin et al. [178]. These researches firstly synthesized hollow microcapsules. Then, dispersed them into the amine hardener. By using the vacuum, the hardener diffused into the hollow microcapsules and filled them. The healing efficiency by using this method was reached to the 91% with 7 wt% amine and 10.5 wt% epoxy capsules. Using this method in the glass fibers–epoxy composites was done by Chowdhury et al. [179]. They destroyed the glass fibers–epoxy composites trough low velocity impact test with 30 and 45 J impact energy. The healing efficiencies for 30 and 45 J impact energy were 40% and 29%, respectively.

The most difficult healing process is within the epoxy matrix composite structures, which was completely studied by researchers of Illinois' university. The evolvement flowchart of the healing technology in the composite structures is illustrated in Figure 12.13, which was done by various researchers in the Illinois' university. Firstly, in the year of 2003, the Brown et al. [180] synthesized the UF microcapsules by one stage method. The capsulated healing agent was dicyclopentadiene (DCPD).

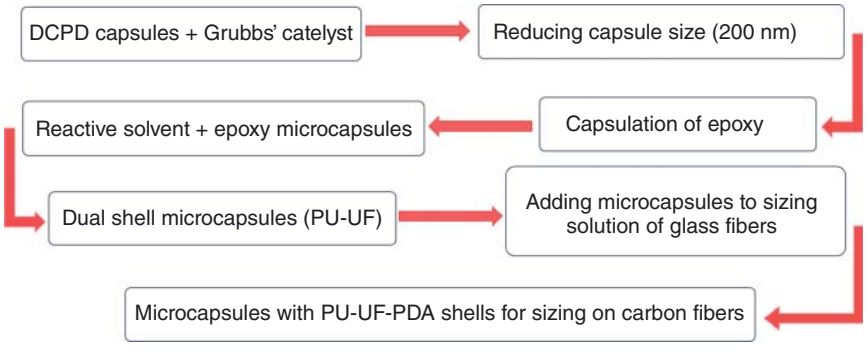

Figure 12.13 The evolvement flowchart of the healing technology in the composite structures in the Illinois' university.

The healing process was done by DCPD microcapsules and Grubbs' catalyst. In the next step, by using the sonication, the size of microcapsules reached to approximately 200 nm, which was done by Blaiszik et al. [181].

In the following, the epoxy was capsulated by UF shell. It is better to eliminate the catalyst and achieve higher healing efficiency. To do so, the idea of using the reactive solvent was born. Based on this idea, the reactive solvent was capsulated and then dispersed into polymeric matrix. When the crack crushes the microcapsules, the active solvent diffuses in the crack area and then solves the matrix. In the following, the polymerization reactions can be re-done by this method. Blaiszik et al. [182] capsulated the epoxy and ethyl phenylacetate (EPA) as reactive solvent by UF capsulation method. This research has been shown that the EPA solved the epoxy matrix in the crack area. The diffused epoxy healing agent from microcapsules was polymerized by released hardener via reactive solvent.

By reducing the microcapsules size down to 200 nm, the shell thickness reduces. Therefore, the microcapsules have not enough strength and rapidly rupture during the fabrication of self-healing composites. In view of this point, the dual shell microcapsules were fabricated in the Illinois' university by Caruso et al. [183]. The modified microcapsulation process was including the interfacial polymerization of PU and in situ polymerization of UF. Kim et al. [184] covered the glass fibers with the sizing solution containing the dual shell microcapsule containing EPA and epoxy. Then, the eight plies of glass fibers–epoxy prepreg were pressed, and the self-healable composite was fabricated. To withstand harsh manufacturing conditions, the microcapsules were modified by coating the polydopamine (PDA), which was done by Kim et al. [185] for using in the sizing process of carbon fibers–epoxy self-healable composites.

12.5 Future Trends

Up to now, the smart epoxy composites have separately grown in the self- healing, shape memory, self-inhibition epoxy composites. Although, some new researches have been published about the epoxy composites with dual smart behaviors. But the number of those is too limited. The new needs or applications lead to fabricate the dual or multiple smart epoxy composites in the next few years. It is worth noting that the most of smart epoxy composites can only activate by one stimulant agent, whereas the events in the nature are too complicated. Hence, the smart materials especially smart epoxy composites must have multiple excitation capabilities in the real nature. Therefore, the new smart epoxy materials with multiple excitation capabilities will be born in the future. In the end, the new hopeful researches indicate that the new applications such as self-senescing or self-actuating epoxy composites will be fabricated in the near future.

12.6 Conclusion

Smart epoxy systems have gained significant interests in the past decade. The SME composites by using the intrinsic SME or shape memory wires like NiTi are used

as smart epoxy composites. In the intrinsic SME by designing the rigid and flexible structure within the epoxy system, the shape recovery or memory properties can be achieved. Whereas using the shape memory strips can increase the mechanical properties of composite structure. Creating the smart coatings with self-inhibition was done in the epoxy composites by using the nanomaterials as inhibitor carrier. The used carrier can be in the form of mesoporous, layer-by-layer structure, nanotube, folding structure, or micro-/nanopolymeric capsules. Also, these nanomaterials can be separately as inhibitor agents. The self-healing epoxy composites were, categorized into the intrinsic, capsule-based and vascular networks. The intrinsic healing system was subdivided into epoxy with functionalized dynamic covalent bonds, supramolecular structures and polymer blending systems. Considering the polymerization reaction into the damage area, the capsule-based healing system can be in the form of reactive solvent, catalyst-based, and capsulated hardener. The vascular system can be embedded into epoxy composites in the form of hollow fibers, electro-spun nanofibers, and 2D–3D vascular networks.

References

1 Cichosz, S., Masek, A., and Zaborski, M. (2018). Polymer-based sensors: a review. *Polymer Testing* 67: 342–348.

2 Bogue, R. (2012). Smart materials: a review of recent developments. *Assembly Automation* 32: 3–7.

3 Hu, J., Meng, H., Li, G., and Ibekwe, S.I. (2012). A review of stimuli-responsive polymers for smart textile applications. *Smart Materials and Structures* 21: 053001.

4 Bogue, R. (2014). Smart materials: a review of capabilities and applications. *Assembly Automation* 34: 16–22.

5 Jochum, F.D. and Theato, P. (2013). Temperature- and light-responsive smart polymer materials. *Chemical Society Reviews* 42: 7468–7483.

6 Ebrahimnezhad-Khaljiri, H. and Eslami-Farsani, R. (2015). The effect of hybridization on thermal and mechanical properties of glass/oxidized PAN fibers-polymer composites. *Fibers and Polymers* 16: 2445–2450.

7 Ebrahimnezhad-Khaljiri, H. and Eslami-Farsani, R. (2017). Thermal and mechanical properties of hybrid carbon/oxidized polyacrylonitrile fibers-epoxy composites. *Polymer Composites* 38: 1412–1417.

8 Meng, Q. and Hu, J. (2009). A review of shape memory polymer composites and blends. *Composites Part A Applied Science and Manufacturing* 40: 1661–1672.

9 Behzadnasab, M., Mirabedini, S.M., Esfandeh, M., and Farnood, R.R. (2017). Evaluation of corrosion performance of a self-healing epoxy-based coating containing linseed oil-filled microcapsules via electrochemical impedance spectroscopy. *Progress in Organic Coatings* 105: 212–224.

10 Hager, B.M.D., Greil, P., Leyens, C. et al. (2010). Self-healing materials. *Advanced Materials* 22: 5424–5430.

11 Thakur, V.K. and Kessler, M.R. (2015). Self-healing polymer nanocomposite materials: a review. *Polymer (Guildf)* 69: 369–383.

12 Zhong, N. and Post, W. (2015). Self-repair of structural and functional composites with intrinsically self-healing polymer matrices: a review. *Composites Part A Applied Science and Manufacturing* 69: 226–239.

13 Syrett, J.A., Becer, C.R., and Haddleton, D.M. (2010). Self-healing and self-mendable polymers. *Polymer Chemistry* 1: 978–987.

14 Karger-Kocsis, J. and Kéki, S. (2017). Review of progress in shape memory epoxies and their composites. *Polymers (Basel)* 10: 1–38.

15 Liu, Y., Du, H., Liu, L., and Leng, J. (2014). Shape memory polymers and their composites in aerospace applications: a review. *Smart Materials and Structures* 23: 023001.

16 Tobushi, H., Okumura, K., Hayashi, S., and Ito, N. (2001). Thermomechanical constitutive model of shape memory polymer. *Mechanics of Materials* 33: 545–554.

17 Liu, Y., Gall, K., Dunn, M.L. et al. (2006). Thermomechanics of shape memory polymers: uniaxial experiments and constitutive modeling. *International Journal of Plasticity* 22: 279–313.

18 Leng, J., Wu, X., and Liu, Y. (2009). Effect of a linear monomer on the thermomechanical properties of epoxy shape-memory polymer. *Smart Materials and Structures* 18: 095031.

19 Yang, X., Huang, W., Wang, W., and Yu, Y. (2012). Epoxy toughening using low viscosity liquid diglycidyl ether of ethoxylated bisphenol-A. *Journal of Applied Polymer Science* 123: 1913–1921.

20 Fan, M., Li, X., Zhang, J., and Cheng, J. (2015). Curing kinetics and shape-memory behavior of an intrinsically toughened epoxy resin system. *Journal of Thermal Analysis and Calorimetry* 119: 537–546.

21 Jing, X., Liu, Y., Liu, Y. et al. (2014). Toughening-modified epoxy-amine system: cure kinetics, mechanical behavior, and shape memory performances. *Journal of Applied Polymer Science* 131: 1–7.

22 Liu, Y., Sun, H., Tan, H., and Du, X. (2013). Modified shape memory epoxy resin composites by blending activity polyurethane. *Journal of Applied Polymer Science* 127: 3152–3158.

23 Rousseau, I.A. and Xie, T. (2009). Relationship between materials properties and shape memory behavior in epoxy-amine polymers. *Materials Research Society Symposium Proceedings* 1190: NN01–NN08.

24 Xie, T. and Rousseau, I.A. (2009). Facile tailoring of thermal transition temperatures of epoxy shape memory polymers. *Polymer (Guildf)* 50: 1852–1856.

25 Puig, J., Zucchi, I.A., Hoppe, C.E. et al. (2009). Epoxy networks with physical cross-links produced by tail-to-tail associations of alkyl chains. *Macromolecules* 42: 9344–9350.

26 Leonardi, A.B., Fasce, L.A., Zucchi, I.A. et al. (2011). Shape memory epoxies based on networks with chemical and physical crosslinks. *European Polymer Journal* 47: 362–369.

27 Dong, Y., Wang, R., Li, S. et al. (2013). Use of TX100-dangled epoxy as a reactive noncovalent dispersant of vapor-grown carbon nanofibers in an aqueous solution. *Journal of Colloid and Interface Science* 391: 8–15.

28 Rajendran, B., Santhosh Kumar, K.S., Rajeev, R.S., and Reghunadhan Nair, C.P. (2013). Epoxy-cyanate ester shape memory thermoset: Some aspects of phase transition, viscoelasticity and shape memory characteristics. *Polymers for Advanced Technologies* 24: 623–629.

29 Song, W.B., Wang, L.Y., and Wang, Z.D. (2011). Synthesis and thermomechanical research of shape memory epoxy systems. *Materials Science and Engineering A* 529: 29–34.

30 Konuray, O., García, A., Morancho, J.M. et al. (2019). Hard epoxy thermosets obtained via two sequential epoxy-amine condensations. *European Polymer Journal* 116: 222–231.

31 Kausar, A. (2016). Nanodiamond tethered epoxy/polyurethane interpenetrating network nanocomposite: physical properties and thermoresponsive shape-memory behavior. *International Journal of Polymer Analysis and Characterization* 21: 348–358.

32 Arnebold, A. and Hartwig, A. (2016). Fast switchable, epoxy based shape-memory polymers with high strength and toughness. *Polymer (Guildf)* 83: 40–49.

33 Iregui, A., Irusta, L., Martin, L., and González, A. (2019). Analysis of the process parameters for obtaining a stable electrospun process in different composition epoxy/poly ε-caprolactone blends with shape memory properties. *Polymers (Basel)* 11: 475.

34 Wang, W., Liu, D., Liu, Y. et al. (2015). Electrical actuation properties of reduced graphene oxide paper/epoxy-based shape memory composites. *Composites Science and Technology* 106: 20–24.

35 Chen, L., Li, W., Liu, Y., and Leng, J. (2016). Nanocomposites of epoxy-based shape memory polymer and thermally reduced graphite oxide: mechanical, thermal and shape memory characterizations. *Composites Part B Engineering* 91: 75–82.

36 Chen, L., Li, W., Liu, X. et al. (2019). Carbon nanotubes array reinforced shape-memory epoxy with fast responses to low-power microwaves. *Journal of Applied Polymer Science* 136: 1–10.

37 Liu, Y., Zhao, J., Zhao, L. et al. (2016). High performance shape memory epoxy/carbon nanotube nanocomposites. *ACS Applied Materials & Interfaces* 8: 311–320.

38 Ponyrko, S., Donato, R.K., and Matějka, L. (2016). Tailored high performance shape memory epoxy-silica nanocomposites. Structure design. *Polymer Chemistry* 7: 560–572.

39 Dorigato, A. and Pegoretti, A. (2019). Shape memory epoxy nanocomposites with carbonaceous fillers and in-situ generated silver nanoparticles. *Polymer Engineering and Science* 59: 694–703.

40 Abishera, R., Velmurugan, R., and Gopal, K.V.N. (2016). Reversible plasticity shape memory effect in carbon nanotubes reinforced epoxy nanocomposites. *Composites Science and Technology* 137: 148–158.

41 Abishera, R., Velmurugan, R., and Gopal, K.V.N. (2018). Reversible plasticity shape memory effect in carbon nanotube/epoxy nanocomposites: shape recovery studies for torsional and bending deformations. *Polymer Engineering and Science* 58: E189–E198.

42 Liu, Y., Zhu, G., Liu, W. et al. (2018). An investigation on laser-triggered shape memory behaviors of hydro-epoxy/carbon black composites. *Smart Materials and Structures* 27: 095008.

43 Zhang, L., Jiao, H., Jiu, H. et al. (2016). Thermal, mechanical and electrical properties of polyurethane/(3-aminopropyl) triethoxysilane functionalized graphene/epoxy resin interpenetrating shape memory polymer composites. *Composites Part A Applied Science and Manufacturing* 90: 286–295.

44 Wang, Y., Tian, W., Xie, J., and Liu, Y. (2016). Thermoelectric responsive shape memory graphene/hydro-epoxy composites for actuators. *Micromachines* 7: 145.

45 Wang, E., Dong, Y., Islam, M.Z. et al. (2019). Effect of graphene oxide-carbon nanotube hybrid filler on the mechanical property and thermal response speed of shape memory epoxy composites. *Composites Science and Technology* 169: 209–216.

46 Wang, E., Wu, Y., Islam, M.Z. et al. (2019). A novel reduced graphene oxide/epoxy sandwich structure composite film with thermo-, electro- and light-responsive shape memory effect. *Materials Letters* 238: 54–57.

47 Dong, Y., Ni, Q.Q., Li, L., and Fu, Y. (2014). Novel vapor-grown carbon nanofiber/epoxy shape memory nanocomposites prepared via latex technology. *Materials Letters* 132: 206–209.

48 Wei, H.Q., Chen, Y., Zhang, T. et al. (2018). Thermal, mechanical, and shape-memory properties of nanorubber-toughened, epoxy-based shape-memory nanocomposites. *Journal of Applied Polymer Science* 135: 1–8.

49 Hu, J., Chen, W., Fan, P. et al. (2017). Uniaxial tensile tests and dynamic mechanical analysis of satin weave reinforced epoxy shape memory polymer composite. *Polymer Testing* 64: 235–241.

50 Robinson, P., Bismarck, A., Zhang, B., and Maples, H.A. (2017). Deployable, shape memory carbon fibre composites without shape memory constituents. *Composites Science and Technology* 145: 96–104.

51 Abishera, R., Velmurugan, R., and Gopal, K.V.N. (2018). Shape memory behavior of cold-programmed carbon fiber reinforced CNT/epoxy composites. *Materials Research Express* 5: 085603.

52 Park, M., Kim, Y., Ok, J. et al. (2019). Shape recovery characteristics of shape memory epoxy composites reinforced with chopped carbon fibers. *Carbon Letters* 29: 219–224.

53 Li, F., Scarpa, F., Lan, X. et al. (2019). Bending shape recovery of unidirectional carbon fiber reinforced epoxy-based shape memory polymer composites. *Composites Part A Applied Science and Manufacturing* 116: 169–179.

54 Jony, B., Thapa, M., Mulani, S.B., and Roy, S. (2019). Experimental characterization of shape memory polymer enhanced thermoplastic self-healing carbon/epoxy composites. *AIAA SciTech Forum*, California, 1112. https://doi.org/10.2514/6.2019-1112.

55 Liu, Y., Guo, Y., Zhao, J. et al. (2019). Carbon fiber reinforced shape memory epoxy composites with superior mechanical performances. *Composites Science and Technology* 177: 49–56.

56 Wei, K., Zhu, G., Tang, Y. et al. (2013). An investigation on shape memory behaviours of hydro-epoxy/glass fibre composites. *Composites Part B Engineering* 51: 169–174.

57 Fejos, M., Romhány, G., and Karger-Kocsis, J. (2012). Shape memory characteristics of woven glass fibre fabric reinforced epoxy composite in flexure. *Journal of Reinforced Plastics and Composites* 31: 1532–1537.

58 Sharifishourabi, G., Alebrahim, R., Sharifi, S. et al. (2014). Mechanical properties of potentially-smart carbon/epoxy composites with asymmetrically embedded shape memory wires. *Materials and Design* 59: 486–493.

59 Wang, Z., Xu, L., Sun, X. et al. (2017). Fatigue behavior of glass-fiber-reinforced epoxy composites embedded with shape memory alloy wires. *Composite Structures* 178: 311–319.

60 Khazaie, M., Eslami-Farsani, R., and Khalili, S.M.R. (2018). Effect of pre-tension on tensile strength of glass fibers-epoxy composite reinforced with shape memory alloy wire. *Polymer Composites* 39: E2454–E2459.

61 Eslami-Farsani, R. and Khazaie, M. (2018). Effect of shape memory alloy wires on high-velocity impact response of basalt fiber metal laminates. *Journal of Reinforced Plastics and Composites* 37: 300–309.

62 Xu, L.D., Shi, M.F., Sun, X.Y. et al. (2018). Mechanical properties and interlaminar fracture toughness of glass-fiber-reinforced epoxy composites embedded with shape memory alloy wires. *Advanced Engineering Materials* 20: 1–10.

63 Zhao, S., Teng, J., Wang, Z. et al. (2018). Investigation on the mechanical properties of SMA/GF/epoxy hybrid composite laminates: flexural, impact, and interfacial shear performance. *Materials (Basel)* 11: 246.

64 Feng, X., Zhao, L., Mi, X. et al. (2013). Improved shape memory composites combined with TiNi wire and shape memory epoxy. *Materials and Design* 50: 724–727.

65 Kirkby, E.L., Rule, J.D., Michaud, V.J. et al. (2008). Embedded shape-memory alloy wires for improved performance of self-healing polymers. *Advanced Functional Materials* 18: 2253–2260.

66 Kirkby, E.L., Michaud, V.J., Månson, J.A.E. et al. (2009). Performance of self-healing epoxy with microencapsulated healing agent and shape memory alloy wires. *Polymer (Guildf)* 50: 5533–5538.

67 Neuser, S., Michaud, V., and White, S.R. (2012). Improving solvent-based self-healing materials through shape memory alloys. *Polymer (Guildf)* 53: 370–378.

68 Keyvani, A., Yeganeh, M., and Rezaeyan, H. (2017). Application of mesoporous silica nanocontainers as an intelligent host of molybdate corrosion inhibitor

embedded in the epoxy coated steel. *Progress in Natural Science: Materials International* 27: 261–267.

69 Grigoriev, D., Shchukina, E., and Shchukin, D.G. (2017). Nanocontainers for self-healing coatings. *Advanced Materials Interfaces* 4: 1600318.

70 Motamedi, M., Ramezanzadeh, M., Ramezanzadeh, B., and Saadatmandi, S. (2019). Enhancement of the active/passive anti-corrosion properties of epoxy coating via inclusion of histamine/zinc modified/reduced graphene oxide nanosheets. *Applied Surface Science* 488: 77–91.

71 Yeole, K.V., Agarwal, I.P., and Mhaske, S.T. (2016). The effect of carbon nanotubes loaded with 2-mercaptobenzothiazole in epoxy-based coatings. *Journal of Coatings Technology and Research* 13: 31–40.

72 Yeganeh, M., Omidi, M., and Rabizadeh, T. (2019). Anti-corrosion behavior of epoxy composite coatings containing molybdate-loaded mesoporous silica. *Progress in Organic Coatings* 126: 18–27.

73 Wang, N., Diao, X., Zhang, J., and Kang, P. (2018). Corrosion resistance of waterborne epoxy coatings by incorporation of dopamine treated mesoporous-TiO_2 particles. *Coatings* 8: 209.

74 Zhang, H., Wang, B., Feng, A. et al. (2019). Mesoporous carbon hollow microspheres with tunable pore size and shell thickness as efficient electromagnetic wave absorbers. *Composites Part B Engineering* 167: 690–699.

75 Haddadi, S.A., Ramazani, S.A.A., Mahdavian, M. et al. (2018). Fabrication and characterization of graphene-based carbon hollow spheres for encapsulation of organic corrosion inhibitors. *Chemical Engineering Journal* 352: 909–922.

76 Haddadi, S.A., Ramazani, S.A., Mahdavian, M. et al. (2019). Mechanical and corrosion protection properties of a smart composite epoxy coating with dual-encapsulated epoxy/polyamine in carbon nanospheres. *Industrial and Engineering Chemistry Research* 58: 3033–3046.

77 Mirzakhanzadeh, Z., Kosari, A., Moayed, M.H. et al. (2018). Enhanced corrosion protection of mild steel by the synergetic effect of zinc aluminum polyphosphate and 2-mercaptobenzimidazole inhibitors incorporated in epoxy-polyamide coatings. *Corrosion Science* 138: 372–379.

78 Mostafaei, A. and Nasirpouri, F. (2014). Epoxy/polyaniline-ZnO nanorods hybrid nanocomposite coatings: synthesis, characterization and corrosion protection performance of conducting paints. *Progress in Organic Coatings* 77: 146–159.

79 Rassouli, L., Naderi, R., and Mahdavian, M. (2018). Study of the active corrosion protection properties of epoxy ester coating with zeolite nanoparticles doped with organic and inorganic inhibitors. *Journal of the Taiwan Institute of Chemical Engineers* 85: 207–220.

80 Asadi, N., Naderi, R., and Mahdavian, M. (2019). Synergistic effect of imidazole dicarboxylic acid and Zn^{2+} simultaneously doped in halloysite nanotubes to improve protection of epoxy ester coating. *Progress in Organic Coatings* 132: 29–40.

81 Zhang, G., Wu, L., Tang, A. et al. (2018). Active corrosion protection by a smart coating based on a MgAl-layered double hydroxide on a cerium-modified

plasma electrolytic oxidation coating on Mg alloy AZ31. *Corrosion Science* 139: 370–382.

82 Javidparvar, A.A., Naderi, R., and Ramezanzadeh, B. (2019). Epoxy-polyamide nanocomposite coating with graphene oxide as cerium nanocontainer generating effective dual active/barrier corrosion protection. *Composites Part B Engineering* 172: 363–375.

83 Qian, B., Ren, J., Song, Z., and Zhou, Y. (2018). One pot graphene-based nanocontainers as effective anticorrosion agents in epoxy-based coatings. *Journal of Materials Science* 53: 14204–14216.

84 Sambyal, P., Ruhi, G., Dhawan, R., and Dhawan, S.K. (2016). Designing of smart coatings of conducting polymer poly(aniline-co-phenetidine)/SiO_2 composites for corrosion protection in marine environment. *Surface and Coatings Technology* 303: 362–371.

85 Khosravi, H. and Eslami-Farsani, R. (2016). On the mechanical characterizations of unidirectional basalt fiber/epoxy laminated composites with 3-glycidoxypropyltrimethoxysilane functionalized multi-walled carbon nanotubes-enhanced matrix. *Journal of Reinforced Plastics and Composites* 35: 421–434.

86 Kazemi-Khasragh, E., Bahari-Sambran, F., Hossein Siadati, M., and Eslami-Farsani, R. (2018). High velocity impact response of basalt fibers/epoxy composites containing graphene nanoplatelets. *Fibers and Polymers* 19: 2388–2393.

87 Rafiee, M., Nitzsche, F., Laliberte, J. et al. (2019). Thermal properties of doubly reinforced fiberglass/epoxy composites with graphene nanoplatelets, graphene oxide and reduced-graphene oxide. *Composites Part B Engineering* 164: 1–9.

88 Yu, Z., Lv, L., Ma, Y. et al. (2016). Covalent modification of graphene oxide by metronidazole for reinforced anti-corrosion properties of epoxy coatings. *RSC Advances* 6: 18217–18226.

89 Haddadi, S.A., Kohlan, T.B., Momeni, S. et al. (2019). Synthesis and application of mesoporous carbon nanospherescontaining walnut extract for fabrication of active protective epoxy coatings. *Progress in Organic Coatings* 133: 206–219.

90 Khalili, S.M.R., Farsani, R.E., Soleimani, N., and Hedayatnasab, Z. (2016). Charpy impact behavior of clay/basalt fiber-reinforced polypropylene nanocomposites at various temperatures. *Journal of Thermoplastic Composite Materials* 29: 1416–1428.

91 Khosravi, H. and Eslami-Farsani, R. (2016). Enhanced mechanical properties of unidirectional basalt fiber/epoxy composites using silane-modified Na+-montmorillonite nanoclay. *Polymer Testing* 55: 135–142.

92 Ghazi, A., Ghasemi, E., Mahdavian, M. et al. (2015). The application of benzimidazole and zinc cations intercalated sodium montmorillonite as smart ion exchange inhibiting pigments in the epoxy ester coating. *Corrosion Science* 94: 207–217.

93 Atta, A.M., Al-Lohedan, H.A., El-Saeed, A.M. et al. (2017). Salt-controlled self-healing nanogel composite embedded with epoxy as environmentally

friendly organic coating. *Journal of Coatings Technology and Research* 14: 1225–1236.

94 Njoku, D.I., Cui, M., Xiao, H. et al. (2017). Understanding the anticorrosive protective mechanisms of modified epoxy coatings with improved barrier, active and self-healing functionalities: EIS and spectroscopic techniques. *Scientific Reports* 7: 1–15.

95 Truc, T.A., Thuy, T.T., Oanh, V.K. et al. (2019). 8-Hydroxyquinoline-modified clay incorporated in an epoxy coating for the corrosion protection of carbon steel. *Surfaces and Interfaces* 14: 26–33.

96 Khodabakhshi, J., Mahdavi, H., and Najafi, F. (2019). Investigation of viscoelastic and active corrosion protection properties of inhibitor modified silica nanoparticles/epoxy nanocomposite coatings on carbon steel. *Corrosion Science* 147: 128–140.

97 Gharagozlou, M., Ramezanzadeh, B., and Baradaran, Z. (2016). Synthesize and characterization of a novel anticorrosive cobalt ferrite nanoparticles dispersed in silica matrix ($CoFe_2O_4$-SiO_2) to improve the corrosion protection performance of epoxy coating. *Applied Surface Science* 377: 86–98.

98 Yeganeh, M., Asadi, N., Omidi, M., and Mahdavian, M. (2019). An investigation on the corrosion behavior of the epoxy coating embedded with mesoporous silica nanocontainer loaded by sulfamethazine inhibitor. *Progress in Organic Coatings* 128: 75–81.

99 Rahsepar, M., Mohebbi, F., and Hayatdavoudi, H. (2017). Synthesis and characterization of inhibitor-loaded silica nanospheres for active corrosion protection of carbon steel substrate. *Journal of Alloys and Compounds* 709: 519–530.

100 Hayatdavoudi, H. and Rahsepar, M. (2017). Smart inhibition action of layered double hydroxide nanocontainers in zinc-rich epoxy coating for active corrosion protection of carbon steel substrate. *Journal of Alloys and Compounds* 711: 560–567.

101 Alibakhshi, E., Ghasemi, E., Mahdavian, M. et al. (2017). Active corrosion protection of Mg-Al-PO_4^{3-} LDH nanoparticle in silane primer coated with epoxy on mild steel. *Journal of the Taiwan Institute of Chemical Engineers* 75: 248–262.

102 Alibakhshi, E., Ghasemi, E., Mahdavian, M., and Ramezanzadeh, B. (2017). A comparative study on corrosion inhibitive effect of nitrate and phosphate intercalated Zn-Al- layered double hydroxides (LDHs) nanocontainers incorporated into a hybrid silane layer and their effect on cathodic delamination of epoxy topcoat. *Corrosion Science* 115: 159–174.

103 Stimpfling, T., Leroux, F., and Hintze-Bruening, H. (2013). Unraveling EDTA corrosion inhibition when interleaved into layered double hydroxide epoxy filler system coated onto aluminum AA 2024. *Applied Clay Science* 83–84: 32–41.

104 Chhetri, S., Samanta, P., Murmu, N., and Kuila, T. (2019). Anticorrosion properties of epoxy composite coating reinforced by molybdate-intercalated functionalized layered double hydroxide. *Journal of Composites Science* 3: 11.

105 Mei, Y., Xu, J., Jiang, L., and Tan, Q. (2019). Enhancing corrosion resistance of epoxy coating on steel reinforcement by aminobenzoate intercalated layered double hydroxides. *Progress in Organic Coatings* 134: 288–296.

106 Montemor, M.F., Snihirova, D.V., Taryba, M.G. et al. (2012). Evaluation of self-healing ability in protective coatings modified with combinations of layered double hydroxides and cerium molibdate nanocontainers filled with corrosion inhibitors. *Electrochimica Acta* 60: 31–40.

107 Behzadnasab, M., Mirabedini, S.M., Kabiri, K., and Jamali, S. (2011). Corrosion performance of epoxy coatings containing silane treated ZrO_2 nanoparticles on mild steel in 3.5% NaCl solution. *Corrosion Science* 53: 89–98.

108 Lv, X., Li, X., Li, N. et al. (2019). ZrO_2 nanoparticle encapsulation of graphene microsheets for enhancing anticorrosion performance of epoxy coatings. *Surface and Coatings Technology* 358: 443–451.

109 Wang, M., Liu, M., and Fu, J. (2015). An intelligent anticorrosion coating based on pH-responsive smart nanocontainers fabricated via a facile method for protection of carbon steel. *Journal of Materials Chemistry A* 3: 6423–6431.

110 Rostami, M., Rasouli, S., Ramezanzadeh, B., and Askari, A. (2014). Electrochemical investigation of the properties of Co doped ZnO nanoparticle as a corrosion inhibitive pigment for modifying corrosion resistance of the epoxy coating. *Corrosion Science* 88: 387–399.

111 Niroumandrad, S., Rostami, M., and Ramezanzadeh, B. (2016). Effects of combined surface treatments of aluminium nanoparticle on its corrosion resistance before and after inclusion into an epoxy coating. *Progress in Organic Coatings* 101: 486–501.

112 Kartsonakis, I.A., Balaskas, A.C., Koumoulos, E.P. et al. (2012). Incorporation of ceramic nanocontainers into epoxy coatings for the corrosion protection of hot dip galvanized steel. *Corrosion Science* 57: 30–41.

113 Hosseini, M.G. and Aboutalebi, K. (2018). Improving the anticorrosive performance of epoxy coatings by embedding various percentages of unmodified and imidazole modified CeO_2 nanoparticles. *Progress in Organic Coatings* 122: 56–63.

114 Liu, X., Gu, C., Wen, Z., and Hou, B. (2018). Improvement of active corrosion protection of carbon steel by water-based epoxy coating with smart CeO_2 nanocontainers. *Progress in Organic Coatings* 115: 195–204.

115 Ullah, H., Azizli, K.A.M., Man, Z.B. et al. (2016). The potential of microencapsulated self-healing materials for microcracks recovery in self-healing composite systems: a review. *Polymer Reviews* 56: 429–485.

116 Hu, J., Chen, H.Q., and Zhang, Z. (2009). Mechanical properties of melamine formaldehyde microcapsules for self-healing materials. *Materials Chemistry and Physics* 118: 63–70.

117 Hia, I.L., Chan, E.S., Chai, S.P., and Pasbakhsh, P. (2018). A novel repeated self-healing epoxy composite with alginate multicore microcapsules. *Journal of Materials Chemistry A* 6: 8470–8478.

118 Yu, H.-C., Zhang, Y.-T., Wang, M.-J., and Li, C.-C. (2019). Dispersion of poly(urea-formaldehyde)-based microcapsules for self-healing and anti-corrosion applications. *Langmuir* 35: 7871–7878.

119 García, S.J., Fischer, H.R., White, P.A. et al. (2011). Self-healing anticorrosive organic coating based on an encapsulated water reactive silyl ester: synthesis and proof of concept. *Progress in Organic Coatings* 70: 142–149.

120 Sadrabadi, T.E., Allahkaram, S.R., and Towhidi, N. (2018). Preparation and property investigation of epoxy/amine micro/nanocapsule based self-healing coatings. *International Polymer Processing* 33: 721–730.

121 Kongparakul, S., Kornprasert, S., Suriya, P. et al. (2017). Self-healing hybrid nanocomposite anticorrosive coating from epoxy/modified nanosilica/perfluorooctyl triethoxysilane. *Progress in Organic Coatings* 104: 173–179.

122 Wang, H. and Zhou, Q. (2018). Evaluation and failure analysis of linseed oil encapsulated self-healing anticorrosive coating. *Progress in Organic Coatings* 118: 108–115.

123 Liu, X., Zhang, H., Wang, J. et al. (2012). Preparation of epoxy microcapsule based self-healing coatings and their behavior. *Surface and Coatings Technology* 206: 4976–4980.

124 Zhang, H., Wang, J., Liu, X. et al. (2013). High performance self-healing epoxy/polyamide protective coating containing epoxy microcapsules and polyaniline nanofibers for mild carbon steel. *Industrial and Engineering Chemistry Research* 52: 10172–10180.

125 Cui, J., Li, X., Pei, Z., and Pei, Y. (2019). A long-term stable and environmental friendly self-healing coating with polyaniline/sodium alginate microcapsule structure for corrosion protection of water-delivery pipelines. *Chemical Engineering Journal* 358: 379–388.

126 Khun, N.W., Sun, D.W., Huang, M.X. et al. (2014). Wear resistant epoxy composites with diisocyanate-based self-healing functionality. *Wear* 313: 19–28.

127 Li, H., Cui, Y., Wang, H. et al. (2017). Preparation and application of polysulfone microcapsules containing tung oil in self-healing and self-lubricating epoxy coating. *Colloids and Surfaces A: Physicochemical and Engineering Aspects* 518: 181–187.

128 Van der Zwaag, S., Grande, A.M., Post, W. et al. (2014). Review of current strategies to induce self-healing behaviour in fibre reinforced polymer based composites. *Materials Science and Technology* 30: 1633–1641.

129 Bekas, D.G., Tsirka, K., Baltzis, D., and Paipetis, A.S. (2016). Self-healing materials: a review of advances in materials, evaluation, characterization and monitoring techniques. *Composites Part B Engineering* 87: 92–119.

130 Cohades, A., Branfoot, C., Rae, S. et al. (2018). Progress in self-healing fiber-reinforced polymer composites. *Advanced Materials Interfaces* 5: 1800177.

131 Lee, M.W., An, S., Yoon, S.S., and Yarin, A.L. (2018). Advances in self-healing materials based on vascular networks with mechanical self-repair characteristics. *Advances in Colloid and Interface Science* 252: 21–37.

132 Zhu, D.Y., Rong, M.Z., and Zhang, M.Q. (2015). Self-healing polymeric materials based on microencapsulated healing agents: From design to preparation. *Progress in Polymer Science* 49–50: 175–220.

133 Bai, N., Saito, K., and Simon, G.P. (2013). Synthesis of a diamine cross-linker containing Diels–Alder adducts to produce self-healing thermosetting epoxy polymer from a widely used epoxy monomer. *Polymer Chemistry* 4: 724–730.

134 Kuang, X., Liu, G., Dong, X. et al. (2015). Facile fabrication of fast recyclable and multiple self-healing epoxy materials through Diels–Alder adduct cross-linker. *Journal of Polymer Science Part A: Polymer Chemistry* 53: 2094–2103.

135 Zhang, W., Duchet, J., and Gérard, J.F. (2016). Effect of epoxy matrix architecture on the self-healing ability of thermo-reversible interfaces based on Diels–Alder reactions: demonstration on a carbon fiber/epoxy microcomposite. *RSC Advances* 6: 114235–114243.

136 Li, Q.T., Jiang, M.J., Wu, G. et al. (2017). Photothermal conversion triggered precisely targeted healing of epoxy resin based on thermoreversible Diels–Alder network and amino-functionalized carbon nanotubes. *ACS Applied Materials & Interfaces* 9: 20797–20807.

137 Handique, J. and Dolui, S.K. (2019). A thermally remendable multiwalled carbon nanotube/epoxy composites via Diels–Alder bonding. *Journal of Polymer Research* 26: 163.

138 Oh, C.-R., Lee, D.-I., Park, J.-H., and Lee, D.-S. (2019). Thermally healable and recyclable graphene-nanoplate/epoxy composites via an in-situ Diels–Alder reaction on the graphene-nanoplate surface. *Polymers (Basel)* 11: 1057.

139 Khan, N.I., Halder, S., and Wang, J. (2019). Diels–Alder based epoxy matrix and interfacial healing of bismaleimide grafted GNP infused hybrid nanocomposites. *Polymer Testing* 74: 138–151.

140 Li, G., Xiao, P., Hou, S., and Huang, Y. (2019). Rapid and efficient polymer/graphene based multichannel self-healing material via Diels–Alder reaction. *Carbon* 147: 398–407.

141 Cai, C., Zhang, Y., Zou, X. et al. (2017). Rapid self-healing and recycling of multiple-responsive mechanically enhanced epoxy resin/graphene nanocomposites. *RSC Advances* 7: 46336–46343.

142 Cheng, B., Lu, X., Zhou, J. et al. (2019). Dual cross-linked self-healing and recyclable epoxidized natural rubber based on multiple reversible effects. *ACS Sustainable Chemistry & Engineering* 7: 4443–4455.

143 Nie, J., Mou, W., Ding, J., and Chen, Y. (2019). Bio-based epoxidized natural rubber/chitin nanocrystals composites: self-healing and enhanced mechanical properties. *Composites Part B Engineering* 172: 152–160.

144 Cao, L., Fan, J., Huang, J., and Chen, Y. (2019). A robust and stretchable cross-linked rubber network with recyclable and self-healable capabilities based on dynamic covalent bonds. *Journal of Materials Chemistry A* 7: 4922–4933.

145 Xu, C., Cui, R., Fu, L., and Lin, B. (2018). Recyclable and heat-healable epoxidized natural rubber/bentonite composites. *Composites Science and Technology* 167: 421–430.

146 Guadagno, L., Vertuccio, L., Naddeo, C. et al. (2019). Self-healing epoxy nanocomposites via reversible hydrogen bonding. *Composites Part B Engineering* 157: 1–13.

147 Kostopoulos, V., Kotrotsos, A., Tsantzalis, S. et al. (2016). Toughening and healing of continuous fibre reinforced composites by supramolecular polymers. *Composites Science and Technology* 128: 84–93.

148 Zhang, P., Kan, L., Zhang, X. et al. (2019). Supramolecularly toughened and elastic epoxy resins by grafting 2-ureido-4[1H]-pyrimidone moieties on the side chain. *European Polymer Journal* 116: 126–133.

149 Montarnal, D., Tournilhac, F., Hidalgo, M., and Leibler, L. (2010). Epoxy-based networks combining chemical and supramolecular hydrogen-bonding crosslinks. *Journal of Polymer Science Part A: Polymer Chemistry* 48: 1133–1141.

150 Varley, R.J., Craze, D.A., Mouritz, A.P., and Wang, C.H. (2013). Thermoplastic healing in epoxy networks: exploring performance and mechanism of alternative healing agents. *Macromolecular Materials and Engineering* 298: 1232–1242.

151 Pingkarawat, K., Bhat, T., Craze, D.A. et al. (2013). Healing of carbon fibre-epoxy composites using thermoplastic additives. *Polymer Chemistry* 4: 5007–5015.

152 Hargou, K., Pingkarawat, K., Mouritz, A.P., and Wang, C.H. (2013). Ultrasonic activation of mendable polymer for self-healing carbon-epoxy laminates. *Composites Part B Engineering* 45: 1031–1039.

153 Wang, C.H., Sidhu, K., Yang, T. et al. (2012). Interlayer self-healing and toughening of carbon fibre/epoxy composites using copolymer films. *Composites Part A Applied Science and Manufacturing* 43: 512–518.

154 Pingkarawat, K., Wang, C.H., Varley, R.J., and Mouritz, A.P. (2013). Effect of mendable polymer stitch density on the toughening and healing of delamination cracks in carbon-epoxy laminates. *Composites Part A Applied Science and Manufacturing* 50: 22–30.

155 Pingkarawat, K., Wang, C.H., Varley, R.J., and Mouritz, A.P. (2014). Mechanical properties of mendable composites containing self-healing thermoplastic agents. *Composites Part A Applied Science and Manufacturing* 65: 10–18.

156 Ladani, R.B., Pingkarawat, K., Nguyen, A.T.T. et al. (2018). Delamination toughening and healing performance of woven composites with hybrid z-fibre reinforcement. *Composites Part A Applied Science and Manufacturing* 110: 258–267.

157 Pang, J.W.C. and Bond, I.P. (2005). A hollow fibre reinforced polymer composite encompassing self-healing and enhanced damage visibility. *Composites Science and Technology* 65: 1791–1799.

158 Trask, R.S. and Bond, I.P. (2006). Biomimetic self-healing of advanced composite structures using hollow glass fibres. *Smart Materials and Structures* 15: 704–710.

159 Kousourakis, A. and Mouritz, A.P. (2010). The effect of self-healing hollow fibres on the mechanical properties of polymer composites. *Smart Materials and Structures* 19: 85021.

160 Kling, S. and Czigány, T. (2014). Damage detection and self-repair in hollow glass fiber fabric-reinforced epoxy composites via fiber filling. *Composites Science and Technology* 99: 82–88.

161 Aghamirzadeh, G.R., Khalili, S.M.R., Eslami-Farsani, R., and Saeedi, A. (2019). Experimental investigation on the smart self-healing composites based on the short hollow glass fibers and shape memory alloy strips. *Polymer Composites* 40: 1883–1889.

162 Ghanbari, H., Khalili, S.M.R., Eslami-Farsani, R. et al. (2019). Experimental investigation on flexural properties of self-healing composites reinforced by shape memory strip. *Mechanics of Advanced Materials and Structures* Published online. https://doi.org/10.1080/15376494.2019.1601311.

163 Saeed, M.-U., Chen, Z.F., and Li, B.B. (2015). Manufacturing strategies for microvascular polymeric composites: a review. *Composites Part A Applied Science and Manufacturing* 78: 327–340.

164 Eslami-Farsani, R., Khalili, S.M.R., Khademoltoliati, A., and Saeedi, A. (2019). Tensile and creep behavior of microvascular based self-healing composites: experimental study. *Mechanics of Advanced Materials and Structures* Published online. https://doi.org/10.1080/15376494.2019.1567882.

165 Cuvellier, A., Torre-Muruzabal, A., Van Assche, G. et al. (2017). Selection of healing agents for a vascular self-healing application. *Polymer Testing* 62: 302–310.

166 Esser-Kahn, A.P., Thakre, P.R., Dong, H. et al. (2011). Three-dimensional microvascular fiber-reinforced composites. *Advanced Materials* 23: 3654–3658.

167 Coppola, A.M., Thakre, P.R., Sottos, N.R., and White, S.R. (2014). Tensile properties and damage evolution in vascular 3D woven glass/epoxy composites. *Composites Part A Applied Science and Manufacturing* 59: 9–17.

168 Neisiany, R.E., Lee, J.K.Y., Khorasani, S.N., and Ramakrishna, S. (2017). Towards the development of self-healing carbon/epoxy composites with improved potential provided by efficient encapsulation of healing agents in core-shell nanofibers. *Polymer Testing* 62: 79–87.

169 Vahedi, V., Pasbakhsh, P., Piao, C.S., and Seng, C.E. (2015). A facile method for preparation of self-healing epoxy composites: using electrospun nanofibers as microchannels. *Journal of Materials Chemistry A* 3: 16005–16012.

170 Zanjani, J.S.M., Okan, B.S., Yilmaz, C. et al. (2017). Monitoring the interface and bulk self-healing capability of tri-axial electrospun fibers in glass fiber reinforced epoxy composites. *Composites Part A Applied Science and Manufacturing* 99: 221–232.

171 Neisiany, R.E., Lee, J.K.Y., Khorasani, S.N., and Ramakrishna, S. (2017). Self-healing and interfacially toughened carbon fibre-epoxy composites based on electrospun core–shell nanofibres. *Journal of Applied Polymer Science* 134: 1–10.

172 Haiyan, L., Rongguo, W., and Wenbo, L. (2012). Preparation and self-healing performance of epoxy composites with microcapsules and tungsten (VI) chloride catalyst. *Journal of Reinforced Plastics and Composites* 31: 924–932.

173 Sheng, X., Lee, J.K., and Kessler, M.R. (2009). Influence of cross-link density on the properties of ROMP thermosets. *Polymer (Guildf)* 50: 1264–1269.

174 Ye, X.J., Zhang, J.L., Zhu, Y. et al. (2014). Ultrafast self-healing of polymer toward strength restoration. *ACS Applied Materials & Interfaces* 6: 3661–3670.

175 Yin, T., Rong, M.Z., Zhang, M.Q., and Yang, G.C. (2007). Self-healing epoxy composites - preparation and effect of the healant consisting of microencapsulated epoxy and latent curing agent. *Composites Science and Technology* 67: 201–212.

176 Tripathi, M., Dwivedi, R., Kumar, D., and Roy, P.K. (2016). Thermal activation of mendable epoxy through inclusion of microcapsules and imidazole complexes. *Polymer-Plastics Technology and Engineering* 55: 129–137.

177 Li, Q., Siddaramaiah, K.N.H., Hui, D., and Lee, J.H. (2013). Effects of dual component microcapsules of resin and curing agent on the self-healing efficiency of epoxy. *Composites Part B Engineering* 55: 79–85.

178 Jin, H., Mangun, C.L., Stradley, D.S. et al. (2012). Self-healing thermoset using encapsulated epoxy-amine healing chemistry. *Polymer (Guildf)* 53: 581–587.

179 Chowdhury, R.A., Hosur, M.V., Nuruddin, M. et al. (2015). Self-healing epoxy composites: preparation, characterization and healing performance. *Journal of Materials Research and Technology* 4: 33–43.

180 Brown, E.N., Kessler, M.R., Sottos, N.R., and White, S.R. (2003). In situ poly(urea-formaldehyde) microencapsulation of dicyclopentadiene. *Journal of Microencapsulation* 20: 719–730.

181 Blaiszik, B.J., Sottos, N.R., and White, S.R. (2008). Nanocapsules for self-healing materials. *Composites Science and Technology* 68: 978–986.

182 Blaiszik, B.J., Caruso, M.M., McIlroy, D.A. et al. (2009). Microcapsules filled with reactive solutions for self-healing materials. *Polymer (Guildf)* 50: 990–997.

183 Caruso, M.M., Blaiszik, B.J., Jin, H. et al. (2010). Robust, double-walled microcapsules for self-healing polymeric materials. *ACS Applied Materials & Interfaces* 2: 1195–1199.

184 Kim, S.Y., Jones, A.R., Sottos, N.R., and White, S.R. (2017). Manufacturing of unidirectional glass/epoxy prepreg with microencapsulated liquid healing agents. *Composites Science and Technology* 153: 190–197.

185 Kim, S.Y., Lim, T.W., Sottos, N.R., and White, S.R. (2019). Manufacture of carbon-fiber prepreg with thermoplastic/epoxy resin blends and microencapsulated solvent healing agents. *Composites Part A Applied Science and Manufacturing* 121: 365–375.

13

Projects Using Composite Epoxy Materials: Applications, Recycling Methods, Environmental Issues, Safety, and Future Directions

Alencar Bravo and Darli Vieira

Université du Québec à Trois-Rivières – UQTR, Research Chair in Management of Aeronautical Projects, Management School, Laboratory of Mechanics and Eco-Materials, 3351, boulevard des Forges, Trois-Rivières, Québec G8Z 4M3, Canada

13.1 Introduction and Context of ECM Projects

In many projects today, epoxy composite materials (ECMs) are generally preferable over other materials. Therefore, this chapter presents an overview of the various parameters associated with sustainable ECM projects. As ECMs are important and useful materials, the widespread utilization of ECMs must progress in an optimal manner, starting from the design phase. Herein, focus will be given to the applications, recycling processes, environmental impacts/issues, and final perspectives associated with ECMs.

The main reason that composites are given credible importance in industries is their high mechanical parameter values, which make these materials much better than their metallic counterparts [1]. Composite materials are unique in the sense that they are made by joining two or more constituents with dissimilar characteristics. It is important to note that composites are not mixtures, as the different constituents remain distinguishable in the final structure (i.e. the constituents do not disband or merge into one another).

The different constituents work together to produce distinctive characteristics of the combined structure. Thus, composites are highly customizable, wherein the overall composite performance can be altered by changing the ratio of matrix to fiber, the type of fiber, or the inclusion of a coupling agent and by varying other parameters [2, 3].

Due to the high customization capabilities of these materials, it is always recommended to perform various types of tests at one point or another in the project life cycle. Tests must be performed thoroughly so that low standard deviations of the properties for the batch are obtained. If any changes to the project material are made (such as a change in the matrix/fiber ratio or even a supplier change in one of the components), it is wise and recommended that the tests be redone. This iteration of tests is even more important in the case of advanced project design.

Epoxy Composites: Fabrication, Characterization and Applications,
First Edition. Edited by Jyotishkumar Parameswaranpillai, Harikrishnan Pulikkalparambil, Sanjay M. Rangappa, and Suchart Siengchin.

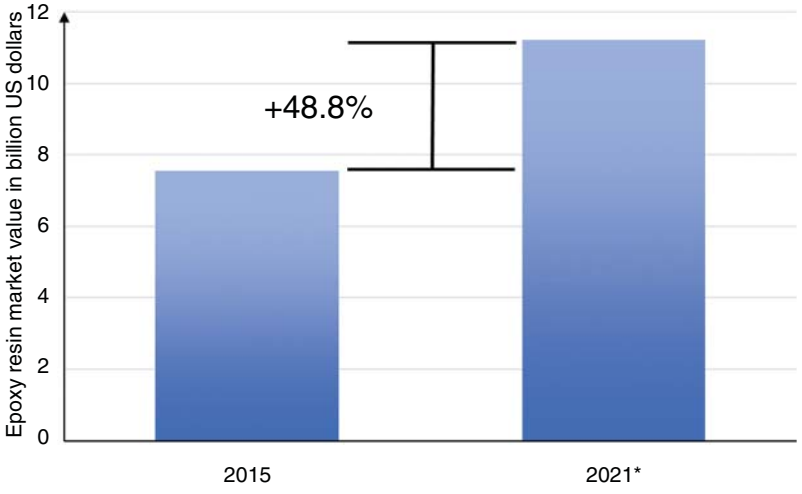

Figure 13.1 Epoxy resin market value worldwide in 2015 and 2021, wherein the * indicates that the market value in year 2021 is a prediction. Source: Data from Zion Market Research [7].

In the early project design of any composite application, it is important to consider that epoxy is one of the most common resins used [4]. The entire global production of epoxy resins is >7 million tons, of which approximately 90% is the diglycidyl ether of bisphenol A (BPA) [5, 6]. As shown in Figure 13.1, the worldwide production of epoxy resins is forecasted to increase 48.8% over the next six years.

ECMs are widely known for having a unique set of interesting properties, such as their durable mechanical qualities, excellent electrical characteristics, caustic fluid and environmental resistance, and excellent high-temperature performance, which is paramount for certain applications [8, 9]. After reading the many chapters in this book, it is apparent why many engineers elect to use ECMs in their projects.

They are often preferable over other materials because ECMs offer other excellent properties, such as the ability to resist shrinkage, the capability to be combined with a diverse selection of products, and the ability to adhere to various substrates [10, 11]. These material properties make it easier and more feasible to start new projects with ECMs than with other materials. At times, these mechanical advantages render ECMs the only available choice in terms of project engineering. Some of the well-known applications of ECMs are flooring, bicycle components, automobiles, pipelines, and biomedical actuators.

As the application of these materials is increasing daily, there are unique opportunities to take advantage of their unique set of properties, such as a higher ultimate strength coupled with excellent weight characteristics, small levels of deformation, and even decreasing prices due to higher availability, leading to the mounting necessity to examine and foresee the deformation and bending of composites made with epoxy under common circumstances [12]. For initial considerations of using different ECM types, the values below are recommended for reference (Table 13.1). They should be used only as guidelines for exploring potential applications in the

Table 13.1 Typical ECMs reinforced with different fibers.

Material	Elastic modulus (GPa)	Ultimate stress (MPa)
Epoxy hardened with E-glass fabric	17.9 (2600 ksi)	248 (36 ksi)
Epoxy hardened with kevlar fabric	34.5 (5000 ksi)	400 (58 ksi)
Epoxy hardened with carbon fabric	59.3 (8600 ksi)	434 (63 ksi)
Epoxy adhesive	2.7 (400 ksi)	69 (10 ksi)

Source: Parvin and Granata [13]. © 2000, Elsevier.

project. It should be noted that ECMs are not a specific material but rather a whole family of materials.

ECM are being utilized in a number of applications, ranging from sporting goods to aerospace products [14]. The **applications section**, as the name indicates, addresses the applications of these materials.

However, the widespread use of ECMs in contemporary projects can be concerning because one of the most important problems in the modern era is pollution. The **environmental issues section** addresses the various issues related to ECM projects and the corresponding impacts these projects have on the environment.

While conceiving a project for the utilization of ECMs, it is important to be aware that the pollution resulting from the misuse of these thermoset composites can cause a variety of diseases and is directly related to global warming. To reduce the overall negative impact from ECM use, one should implement a method, such as life cycle assessment (LCA), to analyze the entire projected utilization of the material. Although material usage is generally fixed in a project (as a consequence of the necessary specific compositions and manufacturing processes), the end-of-life (EoL) options remain open in many scenarios. One of the best options to consider when performing EoL forecasts is the use of recycling techniques at the end of the intended use of a product or project. The **recycling section** provides a brief explanation of the recycling methods used for these composites.

Finally, the end of this chapter presents a **future directions** section, which explains the potential of ECM projects. Furthermore, the future of these materials in industry shall also be forecasted using currently available information.

13.2 Different Applications for ECMs

ECMs have been utilized in numerous applications in many industries due to their possible multifunctional features, such as excellent mechanical characteristics, good moisture and wear resistance, high durability, self-healing capabilities, thermal resistance and outstanding durability [21]. Examples are found in several industries, including gas and oil mining, aerospace, marine, automotive and construction industries [1, 14, 22].

Composites that are reinforced with fibers usually exhibit two basic qualities: high strength and low weight. Fiber-reinforced composites are often tougher

than steel but are very lightweight [15, 16]. For example, the strict corporate average fuel economy standards in the United States and the European Union have imposed restrictions on carbon dioxide emissions and have reduced the limits for passenger car emissions [17, 18]. The automobile industry uses lightweight carbon fiber-reinforced composites, which are one of the best options currently available to increase vehicle efficiency. ECMs reinforced with fibers can provide strength and durability in more than one direction and can be broadly used in weight-bearing applications. These composites can be utilized in the automobile industry to make the vehicles lighter and more energy efficient, thereby helping to reduce environmental pollution [19, 20].

With regard to the excellent mechanical, chemical, and thermal characteristics of epoxy resins along with their dimensional stability and electrical property enhancement provided by the addition of nanocarbons, it is not surprising that ECMs are utilized in a great number of diverse applications [23]. Although ECMs are often utilized in products such as boats, snowboards, aircrafts, bicycles, skis, golf equipment, and automobiles [24], ECMs are also found internally in products, for which a common (but not structural) application is printed circuit boards (PCBs) [25].

Epoxy/nanocarbon materials can be used for semiconductor encapsulation or for hardware component manufacturing. For example, electromagnetic shielding is an added property that makes these materials ideally suited for the production of aircrafts and instrument components operating in the presence of strong electrical fields. This effect can be described theoretically on the basis of Maxwell–Garnett theory in a generalized form [26].

Different proportions of carbon nanotube (CNT)/graphene nanoplatelet (GNP) hybrid fillers are used with other binders in different applications, such as the hybrid permeable electrode required in the new range of supercapacitors, enhancing the process of charge and adsorption recombination in dye-sensitized solar cells, electromagnetic shielding devices, gas barriers, and the latest types of ultrafiltration diaphragms [27].

The impact of the electromagnetic shielding of ECMs can be measured by a useful technique named terahertz time-domain spectroscopy to provide a better understanding of this phenomenon [28]. For example, epoxy is used to mold composites, combine transistors and circuits, and make printed capacitors, circuit boards, and diodes. The dielectric permittivity and electrical conductivity might be set in a certain range of frequencies (e.g. between 8 and 20 GHz) depending on the type of filler.

The properties of ECMs allow them to be used as a potent coating to protect materials from different atmospheric effects, such as temperature, corrosion, and ultraviolet radiation. For this purpose, nanocarbons are the preferential fillers for further extending the properties that favor and enhance fire resistance [29]. ECMs also provide an advantage in terms of chemical resistance, which might be utilized in the design of epoxy impregnation for nuclear reactor waste. Moreover, ECMs are also useful in preventing radionuclides from leaching [30]. ECMs with added nanocarbons can be utilized in applications as a protective coating against blasts, corrosion, and microwaves as well as a tribological coating [31].

Another useful application for ECMs is their use as a binding substance. ECMs can be used for this purpose in projects with several different materials, such as metal, stone, wood, plastic, and glass. Furthermore, the intrinsic brittle nature of epoxy, which hinders the expansion of epoxy applications, might be mitigated by incorporating a second-phase constituent [32]. In fact, ECMs can be used as a structural glue, serving as an alternative to welding, and can be reinforced by the addition of Kevlar, boron, carbon, or glass fibers [13].

ECMs are very interesting for thermal projects because another property of epoxy is its effective heat-resistant nature. The quality-to-cost ratio of epoxy/nanocarbons is excellent in consideration of the heat resistance and conductivity of these materials. Thus, these materials are usually used as a protective layer for applications such as concrete floors and washers or in advanced industrial areas [33].

Furthermore, the addition of specific fibers can increase the flame retardant properties of ECMs. The most commonly used fibers for this purpose are carbon nanofibers, CNTs, montmorillonite (MMT), and polyhedral oligomeric silsesquioxane [34–37]. In these applications, burnable drips of ECMs become inhibited, the melt flow decreases, the total release of heat reduces, the heat resistance increases, and the oxygen index also increases (as a result of the inclusion of nanocarbons). Other fillers that can also be considered for projects where the ECM has a thermal protection role include graphene oxide (GO) functionalized by an organic phosphate, graphene nanosheets, GO functionalized by phenyl-bis phosphamide, MoS_2 or ZnS with graphene material, ammonium polyphosphate or fluorinated MMT with multi-walled CNTs (MWCNTs), and benzalkonium chloride-*N*-methyl pyrrolidine-fullerene.

The combination of GO with calcium carbonate results in a change in the nature of epoxy from water absorbent to water repellent. This type of epoxy offers an improved protective behavior as the formation of a water-repellent surface results in the reduction in surface contact and the time for exposure to the degradation material [38]. Other similar fillers include amino GO functionalized by *p*-phenylenediamine and aromatic diamine, GNP and sodium polyacrylate mixture in water, and metronidazole-modified GO [39].

ECMs with carbon fibers have also been used in orthopedics to imitate natural bone, which has been substantially helpful in bone growth. These materials might also be applied in energy conversion and storage, sensing, and biotechnology [40]. The biodegradable and biocompatible nature of carbon structures, regardless of the additional necessary tests to ascertain certain behaviors of nanomaterials, is helpful for drug targeting and implant design [41, 42].

One of the latest developments in these materials is the reversible plasticity phenomenon called the shape memory effect, which can be utilized as a self-healing mechanism [43, 44]. The utilization of epoxy/MWCNTs is a promising alternative to typical shape memory programming because carbon fillers enhance the response temperature, shape rigidity, and recovery speed [45].

In summary, the inherent mechanical properties of epoxy and the corresponding fracture toughness are increased by the addition of a filler, turning these nanocomposites into an excellent material for maritime, construction, aerospace, and automotive projects [46]. Their high strength-to-weight ratios makes them suitable

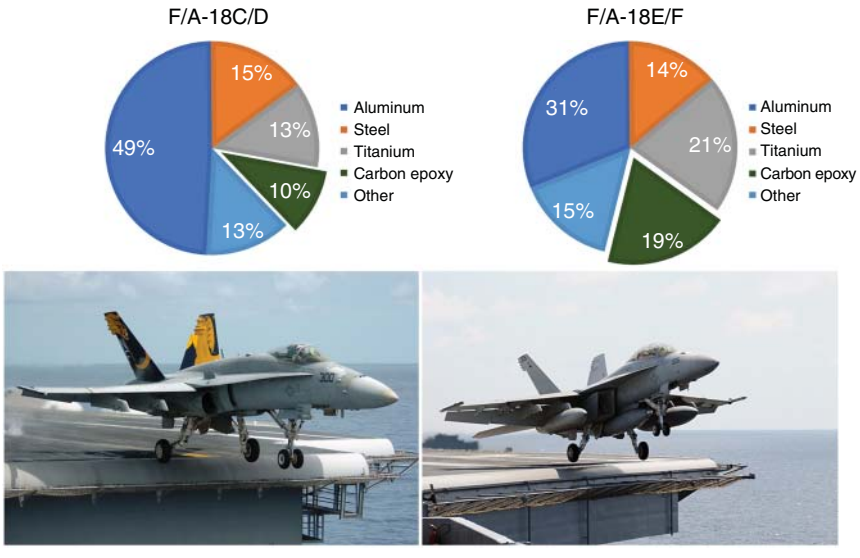

Figure 13.2 Evolution of the same aircraft type and the change in the ECM utilization in the total structure. The version called the "Hornet" is shown on the left, whereas the version called the "Super Hornet" is shown on the right. Source: Data from Deo et al. [48] and images licensed under CC0 1.0.

not only for complex projects but also for projects with smaller scopes, including application in high-performance sporting equipment, such as tennis rackets or individual sailing yacht spars [47].

All the enumerated possibilities explain why the percentage of ECM utilization is increasing in many projects. In complex projects, such as aircraft fighters, these properties are highly required in one product (weight reduction to increase the fighter maneuverability, high structural support for the high loads encountered by the wings, thermal protection for systems close to the engines, electrical protection of the computerized system, and chemical and corrosion protection for aircrafts operated from aircraft carrier ships over the oceans).

Even for existing aircrafts, the use of ECMs can greatly increase the performance. Figure 13.2 shows an example of the evolution of the F-18, called the "Hornet" (up to version "D"), for which the increase in ECM utilization along with other changes in the original project has increased the performance so much that after version "E" the aircraft started to be called the "Super Hornet."

13.3 Safety and Environmental Issues of ECM Projects

From the applications section, it is possible to deduce that a number of items found in daily life are either directly or indirectly linked to ECMs. One of the reasons there is a growing number of projects that preferentially use ECMs is that, in general, epoxy is a relatively safe material. The main issues that can arise from the utilization of epoxy

use involve to sensitivity to the hardener. Certain sensitive individuals can develop severe allergic reactions, and others asthmatic responses. BPA, which is used to make epoxy resin, is a known endocrine disruptor [49]. A number of countries, mainly developed ones, have prohibited the use of BPA in products that contact food. The level of restriction varies from country to country, but in general, the laws tend to be much more strict for the fabrication of products for use by newborn babies, such as baby bottles [50, 51].

BPA has a very bad reputation; it is indeed an endocrine disruptor once in the body and promotes disruptive estrogenic hormonal activity due its similarity to human hormones [52]. Moreover, BPA is an androgen antagonist, a reprotoxic compound that inhibits fertility in men [53].

BPA may possibly be carcinogenic, as it may promote breast cancer precursors, and BPA can affect fetal development [54, 55]. Therefore, BPA is the most controversial compound that should be avoided when possible in ECM applications; furthermore, some studies argue that BPA is used with excessive zeal in many projects and that the economic benefits of using BPA may be overlooked in public debates [56, 57].

Currently, the main concern facing the widespread usage of ECMs in projects is the environmental issues linked to the life cycle of the derived products. Every project or product has a limited lifetime of utilization after which the equipment would be unusable in its original form; these limitations have the potential to cause serious environmental issues.

Many scenarios can occur after parts have reached the end of their intended life. One common assumption in many projects is that the devices are usually disposed of by the user and that no further consideration is needed during project design regarding what should be done with the products of a project at the EoL [22].

As society evolves and environmental awareness increases, other considerations for the EoL aside from dumping has become necessary. There is a list of options that can be foreseen for such cases, and different approaches can be implemented for different projects. Figure 13.3 shows a number of different EoL approaches for projects involving parts made of ECMs.

In terms of their natural decomposition behavior, ECMs can be broadly classified as a subclass of plastics and these materials are known to remain intact for a very long period (centuries) with no decomposition at all. Therefore, the first (and simplest) options are often not acceptable and are placed at the bottom of the hierarchy in Figure 13.3.

The other simple options to consider are disposal via combustion and disposal in landfills. These options are acceptable to some extent. Of course, even if both of these techniques are often considered to be ecological approaches to some extent, they can still have a substantial impact on the environment.

In the process of combustion, ECMs at the EoL are burned at high temperatures, generating two types of pollutants in the process. The first is a black powder solid residue, and the second is a gaseous waste that is released into the air, which requires proper combustion in the incinerators and filters to minimize the potential health risks [58].

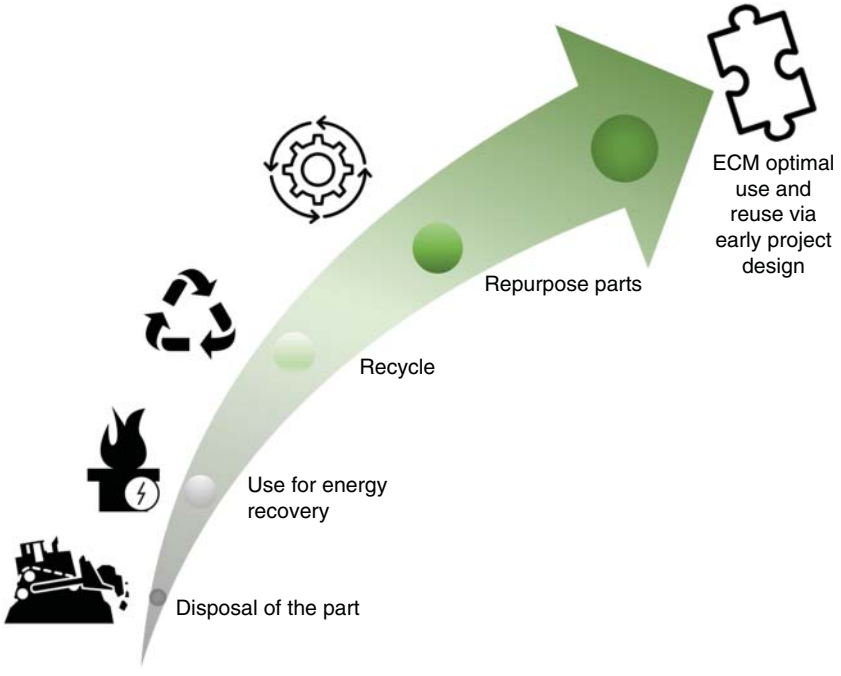

Figure 13.3 Preferable options for counteracting the negative consequences of ECM applications.

In the case of ECMs, most gaseous waste consists of carbon monoxide (CO), which is a very poisonous gas for humans, and carbon dioxide (CO_2), which is better known for the greenhouse effect this gas imposes on the environment. CO is the main reason for a number of diseases and disorders when combustion products from ECMs are inhaled (even in small quantities); the impact of such inhalation includes coughing, breathing problems, and even lung cancer [59, 60]. CO_2, on the other hand, contributes toward more general effects on human health, and it is much more perceptible without any equipment, making it far less dangerous [61, 62].

However, even though CO_2 is a cause of a number of disorders and diseases in humans, the main concern of this gas is global warming. When CO_2 is released from the combustion of epoxy composite-based waste, it diffuses into the atmosphere and migrates upward. Then, a thin layer of carbon dioxide is formed around the surface of earth, affecting people even geographically distant from the original combustion [63, 64]. Although this process is simple, it has profound implications for the natural balance of the environment. This layer of carbon dioxide prevents radiant solar energy from escaping the atmosphere, thereby increasing the overall temperature of the earth; this phenomenon is called "global warming" and is governed by the greenhouse effect [65].

In the incineration process, a considerable amount of CO_2 is produced when ECMs are combusted; moreover, a substantial number of epoxy composites today are combusted at the EoL. Thus, ECMs contribute to global warming [66, 67].

The residue from the combustion process, which occupies considerably less volume than the waste in virgin form, is usually dumped in nature and left unattended. This combustion residue is also a direct cause of land pollution. It is very likely that this residue might end up in bodies of water or underground water supplies. It should be noted that, due to dilution, the effects of combustion residue might be difficult to measure while carrying out an analysis of environmental pollution. However, such contamination is still a form of pollution, and pollution is dangerous even at small levels [67, 68].

Landfills are large holes dug in the surface of the earth for the purpose of disposing waste. In the case of the disposal of ECMs in landfills, it is important to note that there are different landfills that are required for different projects. In most cases, when dealing with ECMs, the landfill location should not be easily accessible by the general population. Moreover, the landfill should have special barriers that prevent any type of leachate from penetrating the ground and polluting underground water sources. Many available landfills are located near industries, and these landfills implement poor control strategies and can be accessed by the general public, which is not suitable for the deposition of potentially toxic products [69–71].

The utilization of the landfills described above is generally not a safe practice and is the cause of many problems, especially the formation of leachate and the subsequent soil and groundwater contamination [72]. Although ECMs do not decompose, it is very likely that potentially toxic materials in composites are introduced during the manufacturing process or at any other stage, and this can be either by the design of the project (on purpose) or by the lack of manufacturing control. These potential toxic ingredients found inside the ECM can be reached and mixed with the water generating a toxic liquid mixture.

Polluted water produced as a result of clean water from precipitation or run-off penetrating and interacting with the materials present in the landfill is the so-called leachate. It is possible that natural underground waterways exist under the landfill. Hence, it is very likely that the leachate leaves the bottom side of the landfill and enters the underground water, which might be used by humans at some stage and can (and, most likely, will) lead to a number of water-borne diseases that can be extremely critical [73]. If the landfill is the chosen option, it is very clear that there are many potential societal issues of this application and strict quality control should be applied throughout to ensure safety and security for local society.

Even if approaches such as incineration or landfilling are chosen to be utilized instead of dumping the ECMs in nature, as seen in Figure 13.4, they still induce a non-negligible negative impact on the surrounding environment. A more ecological and logical way to use landfills and incineration is to try to recover energy from these processes to attenuate some of the generated pollution.

This recovery of energy and the credits gained from this energy recovery will be discussed in Section 13.4. One way of seeing this approach is the recycling of energy but the permanent disposal of the part is created by the project. An even better approach would be to not permanently dispose the part but to recycle the ECM. This ECM recycling can be performed in two stages, either with the generated consumer

(a) (b)

Figure 13.4 Images from the pollution generated by a landfill (a). Source: Pxhere.com, and an incinerator (b). Source: Source: WolfgangBantz/Pixabay.com.

waste or with the consequent generated ECM waste during manufacturing of the designed part.

Figure 13.5 shows a scheme of an ECM application project, the waste and the repurposing of the parts during the entire life cycle. As discussed in the recycling section, even these processes produce substantial pollution and environmental harm. Part of this pollution generated with recycling purposes can be clearly seen in the schema of Figure 13.5, as the recycled material should be remanufactured into a specific part for a given application. The scheme shows that considerable use at the EoL of the ECM part has now become an environmental issue of significant importance and should be considered throughout the project.

Therefore, the best solution would be avoiding any remanufacturing and simply repurpose an ECM for other applications. This repurposing can be accomplished by having a deep knowledge of the specific ECM part; for example, if the time spent in the first structural application is known and the corresponding strength loss caused by fatigue can be determined, the recycled part can be introduced into a less structurally demanding application. It is important to remember that each specific ECM, depending on the mixture, will have a very specific strength vs. number of cycles (S–N) fatigue curve, and under a lower load, one part can be reused for a long period before any catastrophic failure occurs.

Of course, repurposing a part without recycling is not always possible; if possible, this assessment should be defined early in any project considering all possible interactions with external stakeholders. This assessment is a case-specific design and requires much information and brainstorming before any manufacturing begins, but this additional time spent in the early stages of a project can produce the best way to reduce the negative impacts upon EoL in terms of health, safety, and environmental concerns for a particular application. Hence, this process is placed at the top of the most important alternatives to consider, as shown in Figure 13.3.

In the case of ECMs, estimations of the influence made through the LCA technique of dissimilar situations in life have been demonstrated to be useful in project decisions that keep the environment green and this process will continue to be an important trend [22, 74, 75].

When applied to the presented methods of recycling, the LCA shows that in general, techniques of landfilling and combustion do more harm than good over the entire life cycle. Considering that epoxy is a thermoset, these recycling techniques

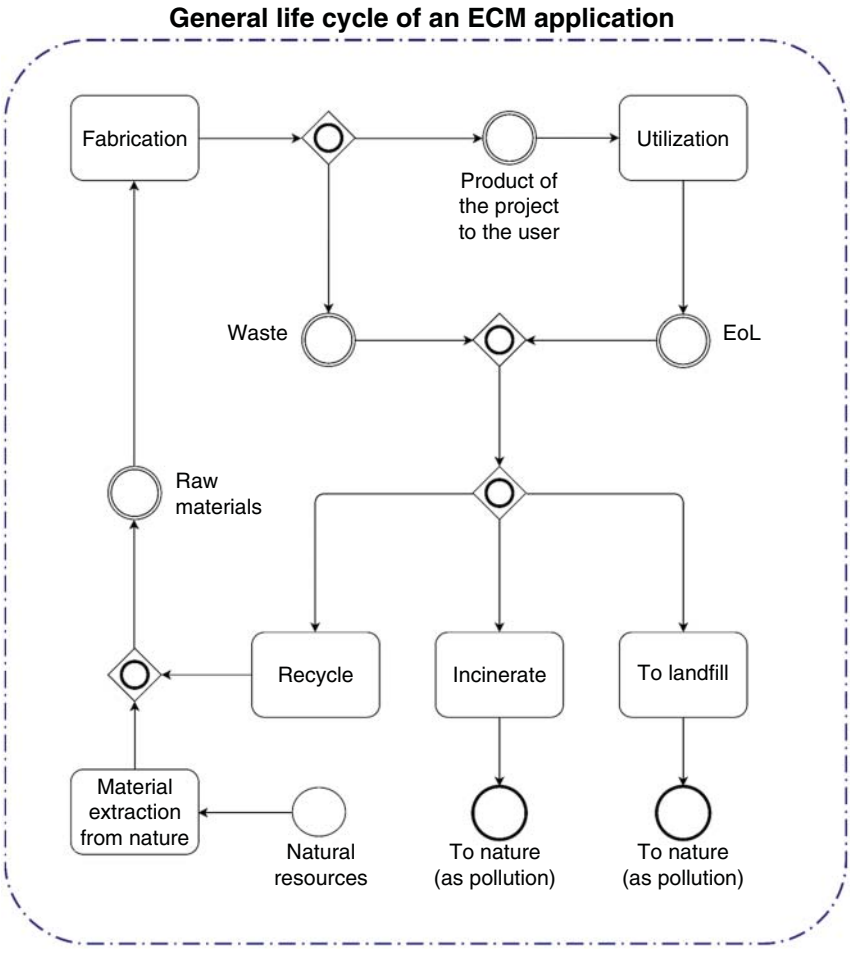

Figure 13.5 A scheme illustrating the processes and phases of the life cycle of ECMs.

are not only damaging to the environment but also yield small profits on the commercial level, especially in consideration of the defective manufactured parts that will be scrapped under this strategy [76].

It is important to consider that a number of countries (mainly in Europe) have established and enforced strict laws and rules that govern the disposal of thermoset resins [77, 78]. For example, the European Union EoL vehicle directive stipulates that 85% of the resources used to construct every light truck and car must be recyclable or reusable, starting with 2015 model vehicles [79].

13.4 Recycling Options for ECMs and Pollution Mitigation by Early Design

It was discussed that ECMs have a number of interesting properties for a number of special applications, including good corrosion resistance, high strength, high

moduli, and low density, which have brought considerable attention and significance to the application of these materials in many projects. These properties are some of the reasons that such composites are gaining increasing significance in the development and production of many high-tech products [80, 81]. Therefore, the use of ECMs has increased because more products that are an integral part of the lifestyle in the current era depend on these composites in one way or another (as discussed in the applications section).

It should be noted that ECMs are a type of thermoset multipurpose material, and common traditional methods of recycling are not very efficient for recycling their derived products [82]. Furthermore, most of the derived products cannot be repaired once their design life is complete [76]. In the absence of more advanced recycling processes, such composites will produce a considerable impact on the environment. In the context of high levels of pollution in the current era, this environmental impact is not acceptable (even though ECMs are used in many fields).

To solve the problem at hand, it is extremely necessary that ECMs are chosen in projects to be converted into valuable products. Furthermore, it is necessary to consider a design in the earlier stages of the project for which the final product can properly close the loop of the life cycle [83, 84]. Increasing the efficiency of such resources by converting the waste into reusable materials is a key problem. This closure of the life cycle loop is shown graphically in Figure 13.6; this concept is in accordance with the ideas presented in this section and Section 13.3. Since the early 1990s, four methods have been traditionally used for recycling ECMs [85]: mechanical recycling, pyrolysis, fluidized bed processing, and chemical recycling.

Powdered subproducts of fibers and fillers are produced in the mechanical recycling technique. In this case, the composites can be ground to create different kinds of reinforcement depending on the characteristics of the original fibers and fillers.

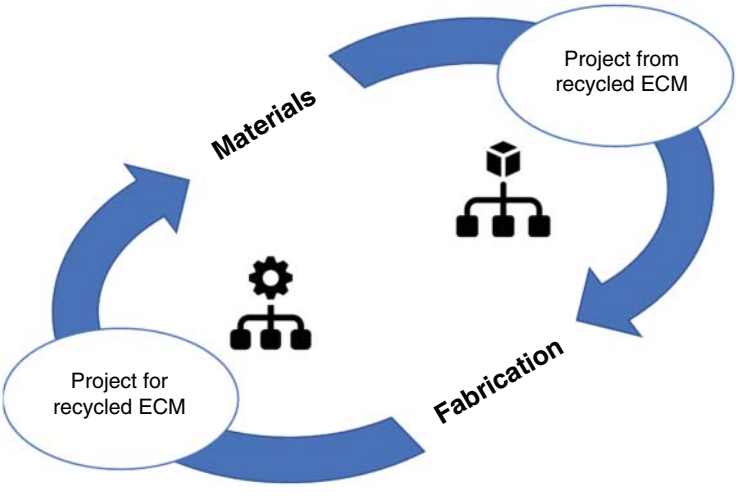

Figure 13.6 A scheme illustrating the complementary roles of the design and recycling in ECM projects.

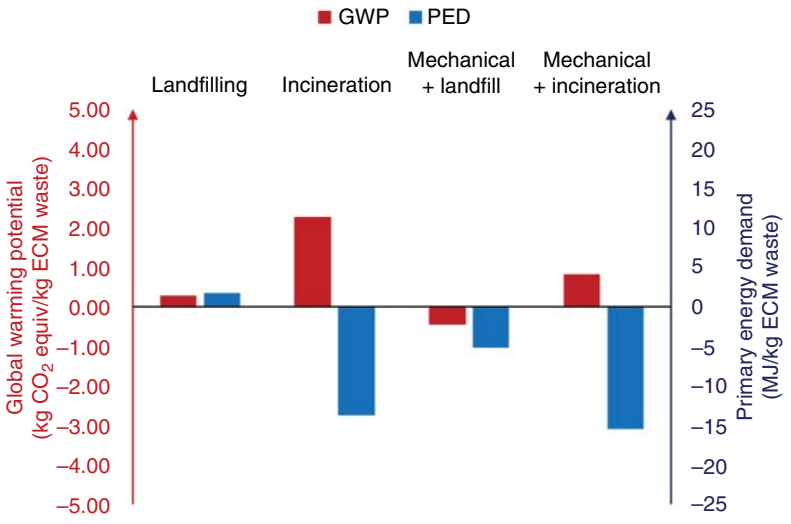

Figure 13.7 Ecological impacts of fiber recovery, including credits from the use of products of recycling processes for landfilling and incineration. Source: Reprinted with permission from Meng et al. [88]. Copyright 2018, American Chemical Society.

Although recycling of composites is possible through this process, it is difficult to obtain high-value subproducts via this technique [86, 87]. Therefore, mechanical recycling is often utilized in conjunction with less advanced methods of handling ECMs, such as incineration and landfilling.

The ecological advantages of combining these methods are shown in Figure 13.7. In this graph, the results of two common measures of environmental harm are shown for a composite consisting of 45 wt% epoxy matrix and 55 wt% carbon fiber. A common measure for the impact that a product will have at the EoL on the environment is kilogram of CO_2. This gas, as previously discussed, is responsible for the global warming effect; therefore, this measure is often called "the global warning potential" (GWP). Another measure that helps elucidate the impact of a part at the EoL on the environment is the "primary energy demand" (PED), which is the amount of energy necessary to process a certain amount of a material through a specific method.

This graph is useful because it quantitatively shows the differences in the environmental performance of landfilling and incineration. Landfilling produces very little GWP and consumes a small amount of energy. On the other hand, incineration produces a much higher volume of GWP, but this approach is compensated by the fact that it has a negative energy demand, i.e. incineration produces a substantial amount of energy rather than consuming energy.

Fillers and fibers are widely produced via a pyrolysis process, which is basically a thermally controlled process of resin degradation that can be used to recover fibers for reuse in another version of the composite. Recycling of such composites via pyrolysis can be conducted at temperatures ranging from 250 to 400 °C [89].

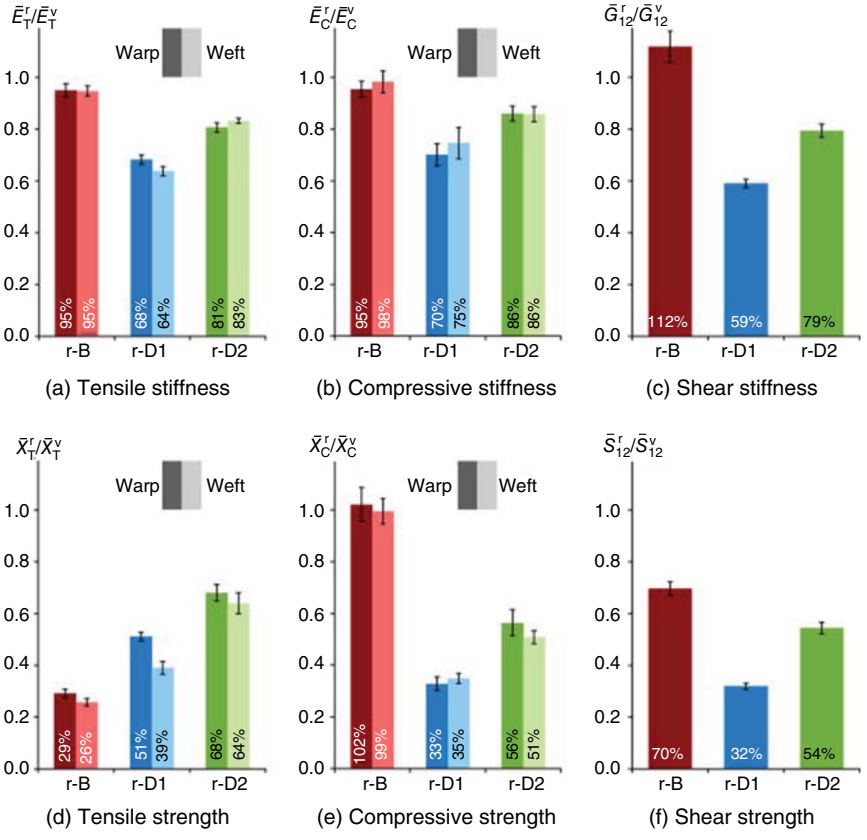

Figure 13.8 Ratios between the mean properties of recycled (by pyrolysis) and virgin composites of carbon–epoxy 2D woven composite, considering true specimen thicknesses. Error bars represent 95% confidence intervals. Parameters: r-B, higher temperature/0 bar pressure; r-D1, lower temperature/0 bar pressure; and r-D2, lower temperature/7 bar pressure. Source: Pimenta and Pinho [90]. © 2012, Elsevier.

The pyrolysis process results in a complex mixture (in liquefied form) of C_5–C_{20} organic compounds; therefore, the output of these processes is fuels in liquefied form and recovered long fibers with relatively high elastic modulus values in solid form. The temperature of the process substantially affects the properties of the recycled composite because exposure to high temperatures can potentially damage the recovered fibers, diminishing their ultimate strength. However, this thermal degradation effect is much less pronounced on the elastic modulus, as illustrated in Figure 13.8. The data in this graph come from an epoxy woven prepreg composite with a fiber volume fraction of 57% [90]. The graph also shows the results of tests performed in the warp and weft directions, which are very similar. Furthermore, the recycled composite was manufactured via resin film infusion, and the results show that applying additional pressure during this remanufacturing process improved the performance of the recycled ECM.

Thermal processing in a fluidized bed is capable of producing clean fillers and fibers by separating fibers from the matrix in a bed of silica sand that is fluidized by hot air at very high temperatures ranging from 400 to 600 °C [91–94]. For example, this process can be used to recover glass fibers from PCBs [95]. However, it should be noted that the reclaimed fibers can be damaged, wherein the mechanical properties of the fibers are reduced in a similar way to the pyrolysis process due to the length of exposure to very high temperatures. The main difference between these approaches is that the fibers reclaimed via fluidized bed processing tend to be very clean because the pyrolytic char formed by the decomposition of the matrix is oxidized [90].

Supercritical fluids are often utilized as a means of chemically recycling ECMs; these fluids have important features in terms of their dissolving power, liquid-like density and diffusivity, and gas-like viscosity [96, 97]. Examples of supercritical fluids that can be used include methanol and propanol. The best recycling technologies for reclaiming carbon fibers from ECMs use supercritical 1-propanol with the addition of 1 wt% potassium hydrate (KOH). The role of KOH is to improve the recovery efficiency of fibers; however, further increasing the content of KOH beyond 1 wt% produces no noticeable change in process performance [97]. An option to treat toxic materials is oxidized epoxy degradation via hydrogen peroxide (H_2O_2) [98]. It should be noted that the services of a strong oxidizer are provided by supercritical water [99].

From the perspective of green chemistry, one of the most suitable oxidants is hydrogen peroxide, since water would be the only side product. H_2O_2 is a very commonly used industrial material and is used at low temperatures and pressures; furthermore, H_2O_2 produces results that are comparable to those for subcritical water at high pressures and temperatures [98, 100]. ECMs containing carbon fibers are normally decomposed with a combination of *N*,*N*-dimethylformamide (DMF) and H_2O_2. The addition of DMF is responsible for the dissolution of the composite structure and to accelerate the decomposition reaction [101]. This approach enables the reutilization of carbon fibers within ECMs while still using low temperatures and pressures. A project can be fine-tuned through certain techniques, such as scanning electron microscopy (SEM), X-ray photoelectron spectroscopy, and thermogravimetric analysis (TGA), to assess the level of remaining impregnated epoxy on the recovered fibers. If the recovered fibers have an important structural role, single fiber mechanical testing can be adopted to determine the tensile strength of the recovered fibers [102].

In terms of environmental performance, these three methods can be compared using the previously discussed measurements of the GWP and PED. All three of these methods exhibited similar and excellent net balances regarding environmental conservation (Figure 13.9) because they recover more pollution than they create according to the credits given from the recycled parts; hence, no energy will be wasted, and no pollution will be generated in the manufacturing of a new part.

However, in terms of applicability, chemical recycling is often considered a more complicated process to optimize in a project because a chemical solution is not suitable for all variations of composites, and a considerable time for tuning the process must be forecasted in the project. Finding chemical methods for recycling thermostat composites and producing useful free carbon fibers and other organic

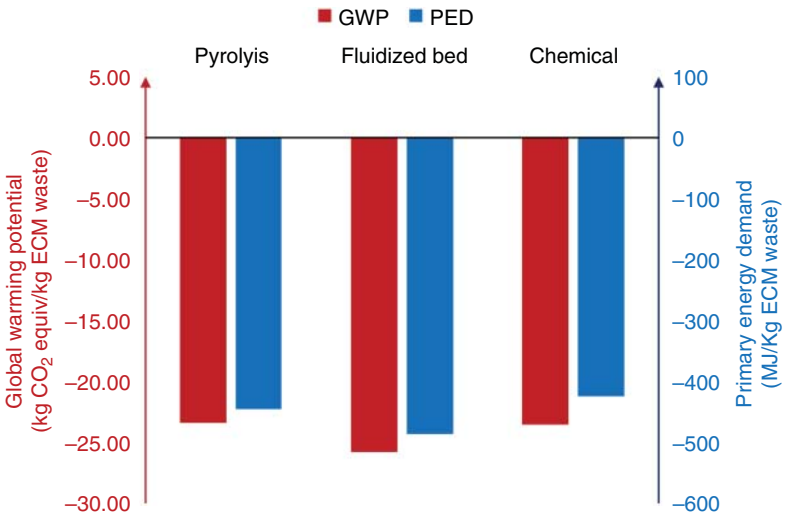

Figure 13.9 Ecological impacts of fiber recovery, including credits from the use of products of recycling processes. Source: Reprinted with permission from Meng et al. [88]. Copyright 2018, American Chemical Society.

compounds for sustainable industrial process is an ongoing field of development [103–105].

These recycling processes mentioned above are the primary methods used for ECMs. There is a new promising technique called electrically driven heterocatalytic decomposition (EHD) that offers many advantages over the traditional methods due to the electrochemical promotion of the catalysis effect in EHD. The results obtained to date indicate that the residual strength of the carbon fibers recycled via EHD is close to that of the virgin carbon fibers [12]. Important features of this method include the promising commercial value and the more general and modest parameters recommended for use in the process. The recommended values and characteristics of all the recycling methods discussed in this section are presented in Table 13.2 for reference.

13.5 The Future for ECM Projects and Conclusions

Society is inevitably developing and progressing, and ECMs play a great part in that progress. The increasing attention and significance given to environmental pollution will surely open doors to better recycling methods for in-use ECMs. Such developments will lead to greater availability of epoxy composites in either virgin or recycled form. The current research and investigations on these materials appear to be quite promising.

As previously stated, ECMs exhibit much better overall performance than their metallic counterparts, which is the reason ECMs are utilized in ultra-high-performance machines, especially when the cost is not the main issue of the project. Figure 13.10 shows that the use of ECMs in combat airplanes has been

Table 13.2 Parameters and characteristics of the main recycling methods for ECMs.

Methods	Mechanical (milling)	Combustion	Pyrolysis	Fluidized bed processing	Chemical (supercritical fluids)	EHD
Temperature	Room temperature	1400–1600 °C	400–1000 °C	450–500 °C	~90 °C	Room temperature
Pressure	Atmospheric pressure	Atmospheric pressure	Atmospheric pressure	10–25 kPa	Atmospheric pressure	Atmospheric pressure
Toxicity	Nontoxic	Nontoxic	Nontoxic	Nontoxic	Toxic	Nontoxic
Waste size limit (length)	10–50 mm	NA	6–25 mm	5–10 mm	1 μm–50 mm	No limit
Residual tensile strength[a)]	50–65%	NA	50–85%	10–75%	85–98%	89.46%
Shear strength[a)]	Unreported	NA	NA	80%	Unreported	120.74%
Important health and environmental issues	Dust	Pollutant gas, dust, high-energy use	Pollutant gas, high-energy use	Pollutant gas, organic solvent, high-energy use	Organic solvent	None[b)]

a) Compared to virgin carbon fibers.
b) According to initial studies (further research is needed).
Source: Ji-Hua Zhu et al. [12]. © 2019, Royal Society of Chemistry, with data from [107–120].

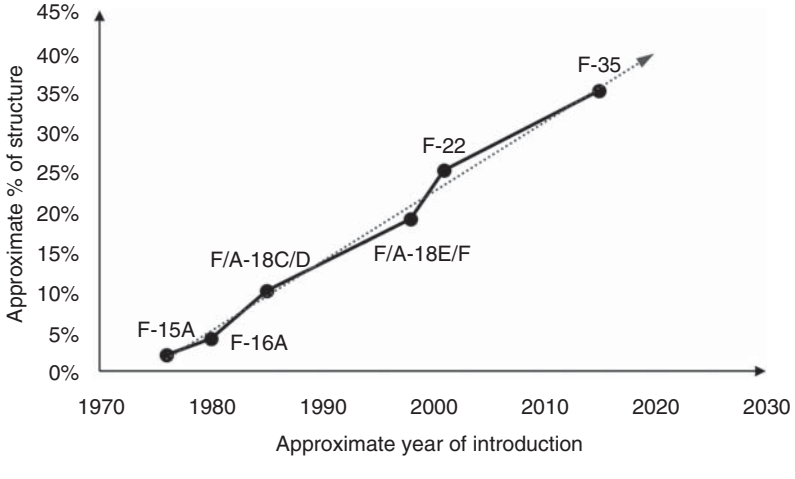

Figure 13.10 Proportion of combat airplane structure composed of ECMs. For each new model, the application of ECMs increases. Source: Data from Dutton et al. [106]. © 2004, American Institute of Aeronautics and Astronautics, Inc.

consistently increasing over time. Considering the historical tendency, it is possible to forecast that this tendency will continue and that this trend will drive the cost of such materials down due to the increase in volume and the optimization of the corresponding production methods. It is a well-known fact that cost is one of the main barriers that prevent materials from being implemented in industrial applications on a large scale.

Since more variations of the material will be available in the future and their produced volume will increase, more investigations can and will be carried out on such materials. As previously mentioned, the main reason ECMs have made it into industry on a large scale is because of their high value as a proposition into a project. The cost of a number of these materials has been decreased by developing cost-effective production or extraction methods. The same developments can enable similar cost reductions for the recycled materials. Further developments in these materials will help realize new machines that were beyond imagining a few decades ago.

References

1 Kausar, A., Rafique, I., and Muhammad, B. (2016). Review of applications of polymer/carbon nanotubes and epoxy/CNT composites. *Polymer-Plastics Technology and Engineering* 55 (11): 1167–1191.

2 Bravo, A., Toubal, L., Koffi, D., and Erchiqui, F. (2015). Damage characterization of bio and green polyethylene–birch composites under creep and cyclic testing with multivariable acoustic emissions. *Materials* 8 (11): 7322–7341.

3 Bravo, A., Toubal, L., Koffi, D., and Erchiqui, F. (2015). Development of novel green and biocomposite materials: tensile and flexural properties and damage analysis using acoustic emission. *Materials and Design (1980–2015)* 66: 16–28.

4 Holbery, J. and Houston, D. (2006). Natural-fiber-reinforced polymer composites in automotive applications. *JOM* 58 (11): 80–86.

5 Giulivo, M., de Alda, M.L., Capri, E., and Barceló, D. (2016). Human exposure to endocrine disrupting compounds: their role in reproductive systems, metabolic syndrome and breast cancer. A review. *Environmental Research* 151: 251–264.

6 Ng, F., Couture, G., Philippe, C. et al. (2017). Bio-based aromatic epoxy monomers for thermoset materials. *Molecules* 22 (1): 149.

7 Zion Market Research. (2016). Epoxy Resin Market Value Worldwide in 2015 and 2021 (in Billion US Dollars). https://www.zionmarketresearch.com/news/global-epoxy-resin-market (Retrieved 26 August 2019).

8 Delamar, M., Desarmot, G., Fagebaume, O. et al. (1997). Modification of carbon fiber surfaces by electrochemical reduction of aryl diazonium salts: application to carbon epoxy composites. *Carbon* 35 (6): 801–807.

9 Ghassemieh, E. (2011). Materials in automotive application, state of the art and prospects. In: *New Trends and Developments in Automotive Industry*, 365–394.

10 Deng, B., Hsu, P.-C., Chen, G. et al. (2015). Roll-to-roll encapsulation of metal nanowires between graphene and plastic substrate for high-performance flexible transparent electrodes. *Nano Letters* 15 (6): 4206–4213.

11 Moghadam, A.D., Omrani, E., Menezes, P.L., and Rohatgi, P.K. (2015). Mechanical and tribological properties of self-lubricating metal matrix nanocomposites reinforced by carbon nanotubes (CNTs) and graphene – a review. *Composites Part B: Engineering* 77: 402–420.

12 Zhu, J.-H., Chen, P.-y., Su, M.-n. et al. (2019). Recycling of carbon fibre reinforced plastics by electrically driven heterogeneous catalytic degradation of epoxy resin. *Green Chemistry* 21 (7): 1635–1647.

13 Parvin, A. and Granata, P. (2000). Investigation on the effects of fiber composites at concrete joints. *Composites Part B: Engineering* 31 (6–7): 499–509.

14 Kausar, A., Rafique, I., and Muhammad, B. (2017). Aerospace application of polymer nanocomposite with carbon nanotube, graphite, graphene oxide, and nanoclay. *Polymer-Plastics Technology and Engineering* 56 (13): 1438–1456.

15 Bhanage, A. and Padmanabhan, K. (2014). Design for fatigue and simulation of glass fibre/epoxy composite automobile leaf spring. *ARPN Journal of Engineering and Applied Sciences* 9 (3): 196–203.

16 Saini, P., Goel, A., and Kumar, D. (2013). Design and analysis of composite leaf spring for light vehicles. *International Journal of Innovative Research in Science, Engineering and Technology* 2 (5).

17 An, F., Earley, R., and Green-Weiskel, L. (2011). Global overview on fuel efficiency and motor vehicle emission standards: policy options and perspectives for international cooperation. United Nations background paper 3.

18 Sharpe, B. and Muncrief, R. (2015). *Literature Review: Real-World Fuel Consumption of Heavy-Duty Vehicles in the United States, China, and the European Union*. Washington, DC: International Council on Clean Transportation.

19 Joost, W.J. (2012). Reducing vehicle weight and improving US energy efficiency using integrated computational materials engineering. *JOM* 64 (9): 1032–1038.

20 Plotkin, S.E. (2009). Examining fuel economy and carbon standards for light vehicles. *Energy Policy* 37 (10): 3843–3853.

21 Du Plessis, H. (2010). *Fibreglass Boats: Construction, Gel Coat, Stressing, Blistering, Repair, Maintenance*. A&C Black.

22 Vieira, D.R. and Bravo, A. (2016). Life cycle carbon emissions assessment using an eco-demonstrator aircraft: the case of an ecological wing design. *Journal of Cleaner Production* 124: 246–257.

23 Laouchedi, D., Bezzazi, B., and Aribi, C. (2017). Elaboration and characterization of composite material based on epoxy resin and clay fillers. *Journal of Applied Research and Technology* 15 (2): 190–204.

24 Kutz, M. (2015). *Mechanical Engineers' Handbook: Materials and Engineering Mechanics*, vol. 1. Wiley.

25 Chen, Z., Yang, F., and Meguid, S. (2014). Multi-level modeling of woven glass/epoxy composite for multilayer printed circuit board applications. *International Journal of Solids and Structures* 51 (21–22): 3679–3688.

26 Liang, J., Wang, Y., Huang, Y. et al. (2009). Electromagnetic interference shielding of graphene/epoxy composites. *Carbon* 47 (3): 922–925.

27 Yen, M.-Y., Hsiao, M.-C., Liao, S.-H. et al. (2011). Preparation of graphene/multi-walled carbon nanotube hybrid and its use as photoanodes of dye-sensitized solar cells. *Carbon* 49 (11): 3597–3606.

28 Macutkevic, J., Seliuta, D., Valusis, G. et al. (2012). Terahertz time domain spectroscopy of epoxy resin composite with various carbon inclusions. *Chemical Physics* 404: 129–135.

29 Liua, S., Fang, Z., Yan, H. et al. (2016). Synergistic flame retardancy effect of graphene nanosheets and traditional retardants on epoxy resin. *Composites Part A: Applied Science and Manufacturing* 89: 26–32.

30 Li, R., Gu, Y., Yang, Z. et al. (2015). Effect of γ irradiation on the properties of basalt fiber reinforced epoxy resin matrix composite. *Journal of Nuclear Materials* 466: 100–107.

31 Bello, S., Agunsoye, J., Hassan, S. et al. (2015). Epoxy resin based composites, mechanical and tribological properties: a review. *Tribology in Industry* 37 (4): 500–524.

32 Prolongo, S.G., del Rosario, G., and Ureña, A. (2006). Comparative study on the adhesive properties of different epoxy resins. *International Journal of Adhesion and Adhesives* 26 (3): 125–132.

33 Khalili, P., Tshai, K., Hui, D., and Kong, I. (2017). Synergistic of ammonium polyphosphate and alumina trihydrate as fire retardants for natural fiber reinforced epoxy composite. *Composites Part B: Engineering* 114: 101–110.

34 Chang, L., Jaafar, M., and Chow, W. (2013). Thermal behavior and flammability of epoxy/glass fiber composites containing clay and decabromodiphenyl oxide. *Journal of Thermal Analysis and Calorimetry* 112 (3): 1157–1164.

35 Hesami, M., Bagheri, R., and Masoomi, M. (2014). Combination effects of carbon nanotubes, MMT and phosphorus flame retardant on fire and thermal resistance of fiber-reinforced epoxy composites. *Iranian Polymer Journal* 23 (6): 469–476.

36 Wu, K., Song, L., Hu, Y. et al. (2009). Synthesis and characterization of a functional polyhedral oligomeric silsesquioxane and its flame retardancy in epoxy resin. *Progress in Organic Coatings* 65 (4): 490–497.

37 Wu, Q., Zhu, W., Zhang, C. et al. (2010). Study of fire retardant behavior of carbon nanotube membranes and carbon nanofiber paper in carbon fiber reinforced epoxy composites. *Carbon* 48 (6): 1799–1806.

38 Tai, R. and Szklarska-Smialowska, Z. (1993). Effect of fillers on the degradation of automotive epoxy adhesives in aqueous solutions. *Journal of Materials Science* 28 (22): 6205–6210.

39 Yu, Z., Lv, L., Ma, Y. et al. (2016). Covalent modification of graphene oxide by metronidazole for reinforced anti-corrosion properties of epoxy coatings. *RSC Advances* 6 (22): 18217–18226.

40 Mittal, V. (2014). *Polymer Nanotubes Nanocomposites: Synthesis, Properties and Applications*. Wiley.

41 Kumbar, S., Laurencin, C., and Deng, M. (2014). *Natural and Synthetic Biomedical Polymers*. Newnes.

42 Reina, G., González-Domínguez, J.M., Criado, A. et al. (2017). Promises, facts and challenges for graphene in biomedical applications. *Chemical Society Reviews* 46 (15): 4400–4416.

43 Wang, C.H., Sidhu, K., Yang, T. et al. (2012). Interlayer self-healing and toughening of carbon fibre/epoxy composites using copolymer films. *Composites Part A: Applied Science and Manufacturing* 43 (3): 512–518.

44 Wu, X.F., Rahman, A., Zhou, Z. et al. (2013). Electrospinning core-shell nanofibers for interfacial toughening and self-healing of carbon-fiber/epoxy composites. *Journal of Applied Polymer Science* 129 (3): 1383–1393.

45 Zhang, J.-X. and Maddison, W.P. (2013). Molecular phylogeny, divergence times and biogeography of spiders of the subfamily Euophryinae (Araneae: Salticidae). *Molecular Phylogenetics and Evolution* 68 (1): 81–92.

46 Higgins, A. (2000). Adhesive bonding of aircraft structures. *International Journal of Adhesion and Adhesives* 20 (5): 367–376.

47 Brown, R.P. (2001). *Polymers in Sport and Leisure*. Citeseer.

48 Deo, R.B., Starnes, J.H. Jr.,, and Holzwarth, R.C. (2003). Low-cost composite materials and structures for aircraft applications. https://ntrs.nasa.gov/citations/20030097981.

49 Kanerva, L., Jolanki, R., Tupasela, O. et al. (1991). Immediate and delayed allergy from epoxy resins based on diglycidyl ether of bisphenol A. *Scandinavian Journal of Work, Environment & Health* 17 (3): 208–215.

50 Boudalia, S. and Oudir, M. (2016). Bisphenol-A: legislation in industrials countries and in algeria. *Research Journal of Environmental Toxicology* 10: 189–192.

51 Scippo, M.-L. (2011). Faut-il interdire le Bisphenol A dans les récipients destinés à contenir des aliments? Culture, le magazine culturel en ligne de l'Université de Liège-DOSSIER/Controverses scientifiques. http://culture.ulg.ac.be/jcms/prod_494506/dossier/-controverses-scientifiques?section= cdu_5047 (accessed 14 October 2020).

52 Wozniak, A.L., Bulayeva, N.N., and Watson, C.S. (2005). Xenoestrogens at picomolar to nanomolar concentrations trigger membrane estrogen receptor-α–mediated Ca^{2+} fluxes and prolactin release in GH3/B6 pituitary tumor cells. *Environmental Health Perspectives* 113 (4): 431–439.

53 Lee, H.J., Chattopadhyay, S., Gong, E.-Y. et al. (2003). Antiandrogenic effects of bisphenol A and nonylphenol on the function of androgen receptor. *Toxicological Sciences* 75 (1): 40–46.

54 European Food Safety Authority (EFSA) (2007). Opinion of the Scientific Panel on food additives, flavourings, processing aids and materials in contact with food (AFC) related to 2,2-bis(4-hydroxyphenyl) propane. *EFSA Journal* 5 (1): 428.

55 Rubin, B.S. and Soto, A.M. (2009). Bisphenol A: perinatal exposure and body weight. *Molecular and Cellular Endocrinology* 304 (1–2): 55–62.

56 Huang, Y., Wong, C., Zheng, J. et al. (2012). Bisphenol A (BPA) in China: a review of sources, environmental levels, and potential human health impacts. *Environment International* 42: 91–99.

57 Petkantchin, V. (2012). Les risques du précautionnisme: le cas de l'interdiction du bisphénol A. In: *The Risks of Precautionism: The Prohibition of Bisphenol A*. Institut économique Molinari. https://www.institutmolinari.org/wp-content/uploads/sites/17/2012/10/note1012_fr.pdf.

58 Reijnders, L. (2005). Disposal, uses and treatments of combustion ashes: a review. *Resources, Conservation and Recycling* 43 (3): 313–336.

59 Antus, B. and Horváth, I. (2007). Exhaled nitric oxide and carbon monoxide in respiratory diseases. *Journal of Breath Research* 1 (2): 024002.

60 Krivoshto, I.N., Richards, J.R., Albertson, T.E., and Derlet, R.W. (2008). The toxicity of diesel exhaust: implications for primary care. *The Journal of the American Board of Family Medicine* 21 (1): 55–62.

61 Hamid, A., Usman, L., Elaigwu, S., and Zubair, M. (2010). Environmental and health risk of bush burning. *Advances in Environmental Biology* 4 (2): 241–249.

62 Rana, S. (2006). *Environmental Pollution: Health and Toxicology*. Alpha Science Int'l Ltd.

63 Pöschl, U. and Shiraiwa, M. (2015). Multiphase chemistry at the atmosphere–biosphere interface influencing climate and public health in the anthropocene. *Chemical Reviews* 115 (10): 4440–4475.

64 Rajeshwar, K. and Ibanez, J.G. (1997). *Environmental Electrochemistry: Fundamentals and Applications in Pollution Sensors and Abatement*. Elsevier.

65 Florides, G.A. and Christodoulides, P. (2009). Global warming and carbon dioxide through sciences. *Environment International* 35 (2): 390–401.

66 Glória, G.O., Teles, M.C.A., Neves, A.C.C. et al. (2017). Bending test in epoxy composites reinforced with continuous and aligned PALF fibers. *Journal of Materials Research and Technology* 6 (4): 411–416.

67 Kolesnikov, A.B. and Kolesnikov, B.Y. (2000). Epoxy polymer gasification under combustion. *Eurasian Chemico-Technological Journal* 2 (2): 191–200.

68 Ehsan Munawer, M. (2018). Human health and environmental impacts of coal combustion and post-combustion wastes. *Journal of Sustainable Mining* 17 (2): 87–96.

69 Dawson, G.W. (1983). Risk management and the landfill in hazardous waste disposal. *Journal of Hazardous Materials* 8 (1): 43–57.

70 Mor, S., Ravindra, K., Dahiya, R., and Chandra, A. (2006). Leachate characterization and assessment of groundwater pollution near municipal solid waste landfill site. *Environmental Monitoring and Assessment* 118 (1–3): 435–456.

71 Westlake, K. (2014). *Landfill Waste Pollution and Control*. Woodhead Publishing.

72 Lisk, D.J. (1991). Environmental effects of landfills. *Science of the Total Environment* 100: 1–521.

73 Erdoğan, A., Gök, M.S., Koç, V., and Günen, A. (2019). Friction and wear behavior of epoxy composite filled with industrial wastes. *Journal of Cleaner Production* (237): 117588.

74 Vieira, D. and Bravo, A. (2016). Life-cycle costing of an aircraft wing project with innovative materials using an eco-demonstrator. *International Journal of Product Development* 21 (5–6): 394–413.

75 Vieira, D.R. and Bravo, A. (2016). Feasibility of green composite aircraft wing projects for unmanned aircraft vehicles. *International Journal of Sustainable Aviation* 2 (3): 248–270.

76 Bai, Y., Wang, Z., and Feng, L. (2010). Chemical recycling of carbon fibers reinforced epoxy resin composites in oxygen in supercritical water. *Materials and Design* 31 (2): 999–1002.

77 Bermejo, R. (2014). Circular economy: materials scarcity, European Union policy and foundations of a circular economy. In: *Handbook for a Sustainable Economy*, 269–287. Springer. springer.com/gp/book/9789401789806.

78 Brems, A., Baeyens, J., and Dewil, R. (2012). Recycling and recovery of post-consumer plastic solid waste in a European context. *Thermal Science* 16 (3): 669–685.

79 Abdellaoui, H., Raji, M., and Bouhfid, R. (2019). Investigation of the deformation behavior of epoxy-based composite materials. In: *Failure Analysis in Biocomposites, Fibre-Reinforced Composites and Hybrid Composites*, 29–49. Woodhead Publishing.

80 May, C. (2018). *Epoxy Resins: Chemistry and Technology*. Routledge.

81 Mittal, V., Saini, R., and Sinha, S. (2016). Natural fiber-mediated epoxy composites – a review. *Composites Part B: Engineering* 99: 425–435.

82 Lu, L., Pan, J., and Li, G. (2017). Recyclable high-performance epoxy based on transesterification reaction. *Journal of Materials Chemistry A* 5 (40): 21505–21513.

83 Bravo, A., Toubal, L., Koffi, D., and Erchiqui, F. (2013). Characterization of tensile damage for a short birch fiber-reinforced polyethylene composite with acoustic emission. *International Journal of Materials Sciences* 3 (3): 79–89.

84 Bravo, A., Toubal, L., Koffi, D., and Erchiqui, F. (2018). Gear fatigue life and thermomechanical behavior of novel green and bio-composite materials vs high-performance thermoplastics. *Polymer Testing* 66: 403–414.

85 Pickering, S.J. (2006). Recycling technologies for thermoset composite materials – current status. *Composites Part A: Applied Science and Manufacturing* 37 (8): 1206–1215.

86 Kouparitsas, C.E., Kartalis, C.N., Varelidis, P.C. et al. (2004). Recycling of the fibrous fraction of reinforced thermoset composites. *Polymer Composites* 23 (4): 682, 689.

87 Palmer, J., Ghita, O.R., Savage, L., and Evans, K.E. (2009). Successful closed-loop recycling of thermoset composites. *Composites Part A: Applied Science and Manufacturing* 40 (4): 490–498.

88 Meng, F., Olivetti, E.A., Zhao, Y. et al. (2018). Comparing life cycle energy and global warming potential of carbon fiber composite recycling technologies and waste management options. *ACS Sustainable Chemistry & Engineering* 6 (8): 9854–9865.

89 Meyer, L.O., Schulte, K., and Grove-Nielsen, E. (2009). CFRP-recycling following a pyrolysis route: process optimization and potentials. *Journal of Composite Materials* 43 (9): 1121–1132.

90 Pimenta, S. and Pinho, S.T. (2012). The effect of recycling on the mechanical response of carbon fibres and their composites. *Composite Structures* 94 (12): 3669–3684.

91 Jiang, G., Pickering, S.J., Walker, G.S. et al. (2008). Surface characterisation of carbon fibre recycled using fluidised bed. *Applied Surface Science* 254 (9): 2588–2593.

92 Yip, H.L.H., Pickering, S.J., and Rudd, C.D. (2002). Characterisation of carbon fibres recycled from scrap composites using fluidised bed process. *Plastics, Rubber and Composites* 31 (6): 278–282.

93 Kennerley, J.R., Fenwick, N.J., Pickering, S.J., and Rudd, C.D. (2004). The properties of glass fibers recycled from the thermal processing of scrap thermoset composites. *Journal of Vinyl and Additive Technology* 3 (1): 58–63.

94 Pickering, S.J., Kelly, R.M., Kennerley, J.R. et al. (2000). A fluidised-bed process for the recovery of glass fibres from scrap thermoset composites. *Composites Science and Technology* 60 (4): 509–523.

95 Xu, P., Li, J. and Ding, J. (2009). A novel approach to recycling of glass fibers from nonmetal materials of waste printed circuit boards. *Composites Science and Technology* 170 (2–3): 978–982.

96 Goto, M. (2009). Chemical recycling of plastics using sub- and supercritical fluids. *The Journal of Supercritical Fluids* 47 (3): 500–507.

97 Yan, H., Lu, C.-x., Jing, D.-q. et al. (2016). Recycling of carbon fibers in epoxy resin composites using supercritical 1-propanol. *New Carbon Materials* 31 (1): 46–54.

98 Chou, S., Sk, M., Sofyan, N. et al. (2009). *Evaluation of the Effects of Hydrogen Peroxide on Common Aviation Structural Materials*. Auburn Univ AL National Air Transportation Center of Excellence for Research.

99 Liu, K., Zhang, Z., and Zhang, F.-S. (2016). Advanced degradation of brominated epoxy resin and simultaneous transformation of glass fiber from waste printed circuit boards by improved supercritical water oxidation processes. *Waste Management* 56: 423–430.

100 Pędziwiatr, P. (2018). Decomposition of hydrogen peroxide-kinetics and review of chosen catalysts. *Acta Innovations* (26): 45–52.

101 Wei, J., Saharudin, M., Vo, T., and Inam, F. (2017). *N*,*N*-Dimethylformamide (DMF) usage in epoxy/graphene nanocomposites: problems associated with reaggregation. *Polymers* 9 (6): 193.

102 Xu, P., Li, J., and Ding, J. (2013). Chemical recycling of carbon fibre/epoxy composites in a mixed solution. *Composites Science and Technology* 66 (Part A): 16–28.

103 Knappich, F., Klotz, M., Schlummer, M. et al. (2019). Recycling process for carbon fiber reinforced plastics with polyamide 6, polyurethane and epoxy matrix by gentle solvent treatment. *Waste Management* 85: 73–81.

104 Kuang, X., Guo, E., Chen, K., and Qi, H.J. (2019). Extraction of biolubricant via chemical recycling of thermosetting polymers. *ACS Sustainable Chemistry & Engineering* 7 (7): 6880–6888.

105 Rahimi, A. and García, J.M. (2017). Chemical recycling of waste plastics for new materials production. *Nature Reviews Chemistry* 1 (6): 0046.

106 Dutton, S., Kelly, D., and Baker, A. (2004). *Composite Materials for Aircraft Structures*. American Institute of Aeronautics and Astronautics.

107 Palmer, J., Ghita, O. R., Savage, L., and Evans, K. E. (2009). Successful closed-loop recycling of thermoset composites. *Composites Part A: Applied Science and Manufacturing* 40 (4): 490–498.

108 Pickering, S. J. (2006). Recycling technologies for thermoset composite materials—current status. *Composites Part A: applied science and manufacturing*, 37(8), 1206–1215.

109 Marsh, G. (2008). Reclaiming value from post-use carbon composite. *Reinforced Plastics*, 52(7), 36–39.

110 Marsh, G. (2009). Carbon recycling: a soluble problem. *Reinforced Plastics*, 53(4), 22–27.

111 Jiang, J., Deng, G., Chen, X. et al. (2017). On the successful chemical recycling of carbon fiber/epoxy resin composites under the mild condition. *Composites Science and Technology*, 151, 243–251.

112 Wang, Y., Cui, X., Ge, H. et al. (2015). Chemical recycling of carbon fiber reinforced epoxy resin composites via selective cleavage of the carbon–nitrogen bond. *ACS Sustainable Chemistry & Engineering*, 3(12), 3332–3337.

113 Nie, W., Liu, J., Liu, W., Wang, J., and Tang, T. (2015). Decomposition of waste carbon fiber reinforced epoxy resin composites in molten potassium hydroxide. *Polymer Degradation and Stability*, 111, 247–256.

114 Li, J., Xu, P. L., Zhu, Y. K. et al. (2012). A promising strategy for chemical recycling of carbon fiber/thermoset composites: self-accelerating decomposition in a mild oxidative system. *Green Chemistry*, 14(12), 3260–3263.

115 Piñero-Hernanz, R., Dodds, C., Hyde, J. et al. (2008). Chemical recycling of carbon fibre reinforced composites in nearcritical and supercritical water. *Composites Part A: Applied Science and Manufacturing*, 39(3), 454–461.

116 Piñero-Hernanz, R., García-Serna, J., Dodds, C. et al. (2008). Chemical recycling of carbon fibre composites using alcohols under subcritical and supercritical conditions. *The Journal of Supercritical Fluids*, 46(1), 83–92.

117 Loppinet-Serani, A., Aymonier, C., and Cansell, F. (2010). Supercritical water for environmental technologies. *Journal of Chemical Technology & Biotechnology*, 85(5), 583–589.

118 Jiang, G., Pickering, S. J., Walker, G. S. et al. (2008). Surface characterisation of carbon fibre recycled using fluidised bed. *Applied Surface Science*, 254(9), 2588–2593.

119 Pickering, S. J., Kelly, R. M., Kennerley, J. R. et al. (2000). A fluidised-bed process for the recovery of glass fibres from scrap thermoset composites. *Composites Science and Technology*, 60(4), 509–523.

120 Yip, H. L. H., Pickering, S. J., and Rudd, C. D. (2002). Characterisation of carbon fibres recycled from scrap composites using fluidised bed process. *Plastics, rubber and composites*, 31(6), 278–282.

Index

Epoxy Composites: Fabrication, Characterization and Applications,
First Edition. Edited by Jyotishkumar Parameswaranpillai, Harikrishnan Pulikkalparambil, Sanjay M. Rangappa, and Suchart Siengchin.